WORLD METEOROLOGICAL ORGANIZATION
GLOBAL OZONE RESEARCH AND MONITORING PROJECT—REPORT NO. 18

Report of the International Ozone Trends Panel 1988

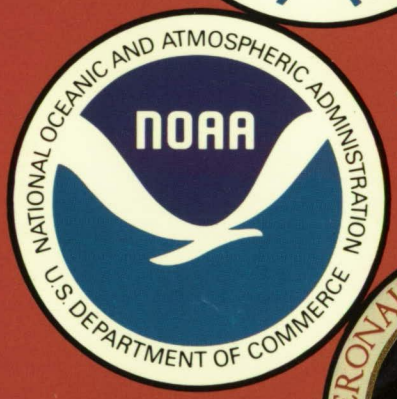

VOLUME I

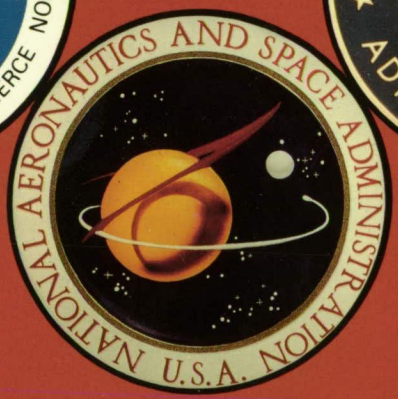

NATIONAL AERONAUTICS AND SPACE ADMINISTRATION
NATIONAL OCEANIC AND ATMOSPHERIC ADMINISTRATION
FEDERAL AVIATION ADMINISTRATION
WORLD METEOROLOGICAL ORGANIZATION
UNITED NATIONS ENVIRONMENT PROGRAM

United Nations Environment Program
United Nations Headquarters
Gigiri
Nairobi, Kenya

World Meteorological Organization
41, Avenue Giuseppe Motta
Case Postale No. 5
CH-1211, Geneva 20, Switzerland

National Aeronautics and Space Administration
Office of Space Science and Applications
Earth Science and Applications Division
600 Independence Avenue, SW
Washington, DC 20546
USA

U.S. Department of Commerce
National Oceanic and Atmospheric Administration
14th Street and Constitution Avenue, NW
Hoover Building, Room 5128
Washington, DC 20230
USA

Federal Aviation Administration
Office of Environment
800 Independence Avenue, SW
Washington, DC 20591
USA

This document was published with the assistance of the Alternative Fluorocarbons Environmental Acceptability Study (AFEAS) as a service to the international science community.

WORLD METEOROLOGICAL ORGANIZATION
GLOBAL OZONE RESEARCH AND MONITORING PROJECT—REPORT NO. 18

Report of the International Ozone Trends Panel – 1988

VOLUME I

NATIONAL AERONAUTICS AND SPACE ADMINISTRATION
NATIONAL OCEANIC AND ATMOSPHERIC ADMINISTRATION
FEDERAL AVIATION ADMINISTRATION
WORLD METEOROLOGICAL ORGANIZATION
UNITED NATIONS ENVIRONMENT PROGRAM

Dedicated to the Memory of
Stephen B. Fels

Steve in the Colorado Rockies, 1986.

This report is dedicated to the memory of Stephen B. Fels, a key member of the Ozone Trends Panel, a senior scientist at the Geophysical Fluid Dynamics Laboratory/NOAA, and a Lecturer with Rank of Professor at Princeton University.

Steve was a central figure in many of the discussions on critical aspects of this Report's conclusions and the evidence supporting them. In particular his deep scientific insights provided essential input toward resolving the serious discrepancies between the apparent trends of ozone and temperature in the upper stratosphere over the past decade. Without his analysis (and some gratifyingly reliable satellite temperature data), the report's conclusions would have been far less robust.

It is a personal privilege to be able to offer this tribute to Steve's impact upon his wide circle of scientific colleagues. First and foremost, Steve was a relentless advocate and devotee of fundamental scientific rigor. He had little use for flimsy handwaving as a substitute for definitive scientific analysis. Conversely though, he had a remarkable ability to initiate and engage in freewheeling, interactive discussions on a prodigious range of scientific (as well as political, economic, and social) problems. Hammering down (or shooting down) his and others' new ideas defined his approach to research.

It was his rare combination of rigor, knowledge, and openness that led to the evolution of Steve as my closest colleague, confidant, and critic. As colleagues, the two of us worked directly together and taught a course together for more than a decade. As confidant, he was the one I first sought out for independent and frank evaluation of many decisions and management issues that plagued me. As a critic, he most likely was not my severest. Almost uniquely, however, his points of disagreement were always completely made known to me. He once said to me after I was "promoted" to management, "I insist on still treating you with the same healthy disrespect you deserve." In his always humorous way, he had that exactly right. I may or may not have "deserved" such a level of unfiltered frankness, but I consider it to have been a gift of priceless value to me.

I submit that it was Steve's combination of rigor, knowledge, frankness, and love of science that made him such an invaluable colleague to the wide range of scientists that knew him, debated with him, and worked with him. I would also submit that these attributes were cemented into something special by his irrepressible sense of humor. Even the most serious of tensions were frequently defused by his humorous comments, invariably peppered by his impeccable linguistic touch.

Because of these things and more, it is singularly appropriate that this report be dedicated to Stephen Fels. Those of us who knew him have become deeper, more creative, and more honest scientists simply because he was with us for that brief interval. I know I speak for many friends and collegues when I say that Steve was a special and irreplaceable friend whose absence I still feel every day.

Jerry D. Mahlman

Table of Contents

VOLUME I

Table of Contents (continued)

Table of Contents (continued)

VOLUME I

CHAPTER 1

Introduction

Robert T. Watson, Chair
Ozone Trends Panel

Ozone Trends Panel

D. Albritton
J. Barnett
P. Bloomfield
R. Bojkov
R. J. Cicerone
D. Ehhalt
S. Fels
P. Fraser
J. Gille
D. Hartmann
R. Hudson
I. S. A. Isaksen
H. Johnston
M. J. Kurylo
J. Mahlman
J. J. Margitan
M. P. McCormick
M. McFarland
M. McIntyre
G. Megie
M. Prather
H. Rodhe
C. Rodgers
F. S. Rowland
A. Schmeltekopf
M. Schoeberl
R. Stolarski
N. Sundararaman
R. Turco
G. Visconti
S. Wofsy

1.0 INTRODUCTION

1.1 BACKGROUND

For more than a decade, scientists have postulated that manmade pollutants, primarily chlorofluorocarbons and halons, could reduce the amount of stratospheric ozone and hence increase the amount of ultraviolet radiation reaching Earth's surface. Consequently, it is recognized that the ozone layer must be protected in order to protect human health and aquatic and terrestrial ecosystems from damage due to enhanced levels of ultraviolet radiation.

Many governments around the world have now acknowledged that the use of chlorine (chlorofluorocarbons [CFC's])- and bromine (halons)-containing chemicals constitutes a potential threat to the stability of the ozone layer and, hence, to human health and ecosystem productivity. More than 20 nations signed the Vienna Convention for the Protection of the Ozone Layer in Vienna, Austria, in March 1985, and the Montreal Protocol on Substances That Deplete the Ozone Layer, in Montreal, Canada, in September 1987. The Vienna Convention and the Montreal Protocol both call for all regulatory decisions to be based on a scientific understanding of the issues. Thus, timely international scientific assessments are needed as a basis for policy formulation when important new information becomes available, as has occurred since the last major international scientific assessment (WMO, 1986).

In 1985, two important reports of changes in atmospheric ozone were released. The first report was of a large, sudden, and unanticipated decrease in the abundance of springtime Antarctic ozone over the last decade. The second report, based on satellite data, was of large global-scale decreases since 1979 in both the total column content of ozone and in its concentration near 50 km altitude. Data from the ground-based Dobson network also indicated that the total column content of ozone had decreased on a global scale significantly since 1979, although to a lesser extent than suggested by the satellite data. Further, there has been a significant amount of new research focussed on understanding the extent and cause of the depletion of ozone in the springtime over the Antarctic.

In October 1986, the National Aeronautics and Space Administration (NASA), in collaboration with the National Oceanic and Atmospheric Administration (NOAA), the Federal Aviation Administration (FAA), the World Meteorological Organization (WMO), and the United Nations Environment Program (UNEP), formed an Ozone Trends Panel, which involved more than 100 scientists, to study the question of whether carefully re-evaluated ground-based and satellite data would support these findings. This report critically assesses our present knowledge of whether the chemical composition and physical structure of the stratosphere have changed over the last few decades and whether our current understanding of the influence of natural phenomena and human activities is consistent with any observed change. This report is different from most previous national and international scientific reviews in that the published literature was not simply reviewed, but a critical reanalysis and interpretation of nearly all ground-based and satellite data for total column and vertical profiles of ozone was performed. To aid in the interpretation of the results of this reanalysis, a series of theoretical calculations was performed for comparison with the reanalyzed ozone data. In addition, a uniform error analysis was applied to all the data sets reviewed that contained information on the vertical ozone distribution.

The *Report of the International Ozone Trends Panel* covers Spacecraft Instrument Calibration and Stability; Information Content of Ozone Retrieval Algorithms; Trends in Total Column Ozone

Measurements; Trends in Ozone Profile Measurements; Trends in Stratospheric Temperature; Theory and Observations; Trends in Source Gases; Trends in Stratospheric Minor Constituents; Trends in Aerosol Abundances and Distributions; Observations and Theories Related to Antarctic Ozone Changes; and Statistical Approaches to Ozone Trend Detection.

1.2 KEY FINDINGS

1.2.1 Source and Trace Gases

There is undisputed observational evidence that the atmospheric concentrations of source gases important in controlling stratospheric ozone levels (chlorofluorocarbons, halons, methane, nitrous oxide, and carbon dioxide) continue to increase on a global scale because of human activities.

1.2.2 Global Ozone

Calculations using two-dimensional photochemical models predict that increasing atmospheric concentrations of trace gases would have caused a small decrease in ozone globally between 1969 and 1986. Predicted decreases between 30 and 60 degrees latitude in the Northern Hemisphere for this period ranged from 0.5 to 1.0 percent in summer and 0.8 to 2.0 percent in winter, where the range reflects the results from most models.

Analysis of data from ground-based Dobson instruments, after allowing for the effects of natural geophysical variability (solar cycle and the quasi-biennial oscillation [QBO]), shows measurable decreases from 1969 to 1986 in the annual average of total column ozone ranging from 1.7 to 3.0 percent, at latitudes between 30 and 64 degrees in the Northern Hemisphere. The decreases are most pronounced, and ranged from 2.3 to 6.2 percent during the winter months, averaged for December through March, inclusive. Dobson data are not currently adequate to determine total column ozone changes in the Tropics, sub-Tropics, or Southern Hemisphere outside Antarctica.

The model calculations are broadly consistent with the observed changes in column ozone, except that the mean values of the observed decreases at mid- and high latitudes in winter are larger than the mean values of the predicted decreases. The observed changes may be due wholly, or in part, to the increased atmospheric abundance of trace gases, primarily CFC's.

Satellite instruments on Nimbus–7 (Solar Backscatter Ultraviolet [SBUV] and Total Ozone Mapping Spectrometer [TOMS]) have provided continuous global records of total column ozone since October 1978. Unfortunately, they suffer from instrumental degradation of the diffuser plate, the rate of which cannot be uniquely determined. Thus, the data archived as of 1987 cannot be used alone to derive reliable trends in global ozone.

The SBUV and TOMS satellite data have been normalized by comparison with nearly coincident ground-based Dobson measurements in the Northern Hemisphere. The resulting column ozone data, averaged between 53°S and 53°N latitudes, show a decrease of about 2 to 3 percent from October 1978 to October 1985. This period is approximately coincident with the decrease in solar activity from the maximum to the minimum in the sunspot cycle.

Theoretical calculations predict that the total column ozone would decrease from solar maximum to solar minimum by an amount varying between 0.7 and 2 percent depending upon

the model assumed for solar ultraviolet variability. Thus, the observed decrease in ozone from the satellite data between late 1978 and late 1985 is predicted to have a significant contribution from the decrease in solar activity during this period.

Theoretical calculations predict that local ozone concentrations near 40 km altitude should have decreased between 1979 and 1985 by 5 to 12 percent in response to the decrease in solar ultraviolet output and the increased atmospheric abundance of trace gases. This range represents the decreases predicted from the different models for the latitude belt 30°N to 60°N for all seasons.

Analyses of satellite (SAGE) and ground-based (Umkehr) data taken since 1979 show small decreases in ozone concentrations; these decreases peak near 40 km altitude with mean values of 3 and 9 percent, respectively. These observational values agree within the range of their errors.

Stratospheric temperatures between 45 and 55 km altitude have decreased globally by about 1.7K since 1979, consistent with decreases in upper stratospheric ozone of less than 10 percent.

Thus, this assessment does not support the previous reports based on SBUV and TOMS data of large global decreases since 1979 in the total column of ozone (about 1 percent per year) or in the ozone concentration near 50 km altitude (about 3 percent per year). These reports used data archived as of 1987, and the trends obtained were erroneously large because of unjustified and incorrect assumptions about the degradation of the diffuser plate common to both the SBUV and TOMS satellite instruments.

1.2.3 Antarctic Ozone

There has been a large, sudden, and unexpected decrease in the abundance of springtime Antarctic ozone over the last decade. Ozone decreases of more than 50 percent in the total column, and 95 percent locally between 15 and 20 km altitude have been observed.

The total column of ozone in the austral spring of 1987 at all latitudes south of 60°S was the lowest since measurements began 30 years ago.

In 1987, a region of low column ozone over Antarctica lasted until late November–early December, which is the longest since the region of low ozone was first detected.

While the column ozone depletion is largest in the Antarctic springtime, ozone appears to have decreased since 1979 by 5 percent or more at all latitudes south of 60°S throughout the year.

The unique meteorology during winter and spring over Antarctica sets up the special conditions of an isolated air mass (polar vortex) with cold temperatures required for the observed perturbed chemical composition.

The weight of evidence strongly indicates that manmade chlorine species are primarily responsible for the observed decrease in ozone within the polar vortex.

CHAPTER 2

Spacecraft Instrument Calibration and Stability

Panel Members

J. Gille, Chair NH 31570a
P. Feldman TRW D(55G, Red, Bldg
R. Hudson — NC999967
J. Lean
R. Madden
L. McMaster
G. Mount
G. Rottman
P. C. Simon

Chapter 2

Spacecraft Instrument Calibration and Stability

Contents

2.1 INTRODUCTION

The advent of artificial Earth satellites has created great possibilities for remotely sounding the atmosphere on a global basis. Ozone was one of the first gases to be proposed for measurement in this way. Its strong and distinct spectral features in the ultraviolet (UV), visible, and infrared (IR) portions of the spectrum, combined with its abundance and distribution, make it a relatively easy gas to detect, and offer the hope of accurate quantitative measurements. Since then, a large number of ozone-measuring experiments has been flown.

The great advantage of regular global observations from satellites is that they provide good information on spatial and short-term temporal variations, and thus allow entirely new types of problems to be addressed. However, soon after the first sounders flew, concern began to be expressed that human activities or natural causes might result in long-term changes in the amount of ozone in the stratosphere. Consequently, attempts have been made to use these sounders to measure long-term changes.

The purpose of this chapter is to review the instruments and techniques that provide the most information on ozone trends, to assess the evidence on the stability of the instrumental calibration, and to reach conclusions on the uncertainties to be associated with any reported trends. Although the Working Group relied heavily on the various experimenters, and could not have done its work without their cooperation, it has attempted to reach independent conclusions and estimates of the errors in the trend determinations.

The trend measurement problem is fraught with great difficulty. In general, when one is interested in trends, it is not the absolute accuracy but the stability of the instrument that is important. However, the measurements must be made over long periods of time in a hostile environment, with no chance to check the instrument in detail or to readjust it. Two strategies for making long-term measurements immediately suggest themselves: making the results insensitive to instrument change, by, for instance, using a ratio technique, or incorporating an in-orbit calibration procedure. Various experiments have used one or both of these approaches.

Different instruments, especially those employing different techniques, generally have different systematic errors. Therefore, it is usually not possible to use measurements by two instruments operating at different times to derive a reliable trend. (It may be possible, however, if the two instruments are very similar and individually reliable.) A discussion of trends, then, must concentrate on those instruments having data records long enough to provide an indication that stands out above seasonal and natural fluctuations. These records must be considered along with others that are simultaneous with them, thereby providing a check on them, or insight into their features.

Figure 2.1 plots the time of operation of several ozone sounders that meet these criteria. They begin with the launch of the Solar Backscatter Ultraviolet/Total Ozone Mapping Spectrometer (SBUV/TOMS) and Limb Infrared Monitor of the Stratosphere Spectrometer (LIMS) on Nimbus–7 late in 1978, and continue to 1987. SBUV measured ozone profiles, while SBUV and TOMS determined total ozone amounts, over virtually the entire period, and thus are central to this discussion. Stratospheric Aerosol and Gas Experiment (SAGE)–I and –II are two very similar instruments, each with an appreciable data record. The two instruments on the Solar Mesospheric Explorer (SME) also have appreciable data records, although their altitude coverage does not greatly overlap that of the others. LIMS has the shortest data record, but has high vertical resolution coupled with temporal and spatial detail. All of these use different measurement

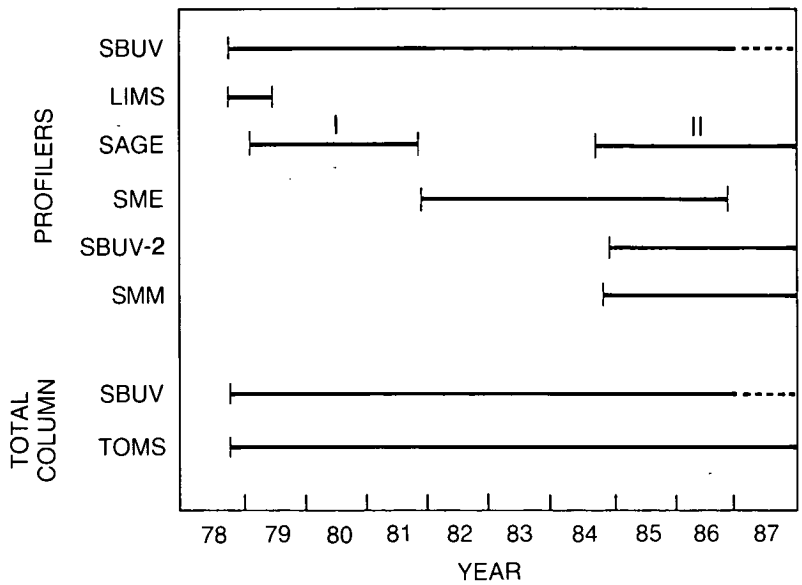

Figure 2.1 Periods of available data for satellite ozone-measuring systems.

techniques than do SBUV/TOMS. SBUV–2 is a National Oceanic and Atmospheric Agency (NOAA) operational version of the SBUV that began collecting data in 1985. However, even with the urgency of this assessment, NOAA has not yet reduced any of the data in a way that would allow comparison with the SBUV results. The SBUV–2 data could have provided an extremely important check on the degradation of the SBUV/TOMS diffuser plate, and indicated ozone trends.

The focus here has been entirely on the internal evidence from the instrument and its test procedures. Ground-based measurements could also serve as a check on calibration changes; this will be discussed in Chapters 4 and 5.

This assessment was greatly assisted by the considerable efforts of several experiment groups to study and reprocess their data to enhance their applicability to trend studies. The SAGE data were reprocessed to take advantage of improvements developed for SAGE–II processing. Similarly, the SME–UVS (ultraviolet spectrometer) and near infrared (NIR) instruments did extensive reanalysis of errors and data reprocessing. Additionally, the TOMS data were reprocessed using new absorption coefficients.

Because of the length of the data record, amount of data, and visibility of the results, more attention was focused on the SBUV experiment than on the others. Additionally, it lent itself to further analysis. However, all experiments were examined critically.

This chapter begins with a general outline of the mechanisms that can cause the performance of a satellite instrument to change with time. Subsequently, Sections 2.3–2.7 discuss each of the relevant techniques and instruments, followed by a review of the evidence for any change of response in orbit, an assessment of its magnitude, and a summary of conclusions about the capabilities of the various instruments. Four instruments that were briefly considered are reviewed in Section 2.8. The last section (2.9) summarizes the conclusions about the ability of the various instruments to determine trends.

2.2 INSTRUMENT DEGRADATION

The fact that the performance of optical instruments changes with time is a well-known phenomenon, both in the laboratory and in space. Overwhelmingly, these changes lead to reduced performance. The causes for the degradation are many, and are discussed in greater detail below:

- Contamination of optical surfaces by thin films.
- Aging of the optical surface of mirrors, diffraction gratings, etc.
- Changes in the transmission of lenses, plates, etc.
- Detector changes.
- Movement or separation of optical elements.

2.2.1 Contaminant Film Formation

The formation of thin films on optical surfaces that are irradiated with ultraviolet radiation is well known in the laboratory, particularly in vacuum systems that use oil pumps and oil diffusion pumps. Much research has been carried out on the nature of the films, and the consensus is that the films arise from the dissociation of oil molecules on the surface of the optical component when it is irradiated (see, e.g., Osantowski, 1983). Figure 2.2 shows the result of exposing an uncoated aluminum surface to 123.6 nm radiation in a vacuum system pumped with

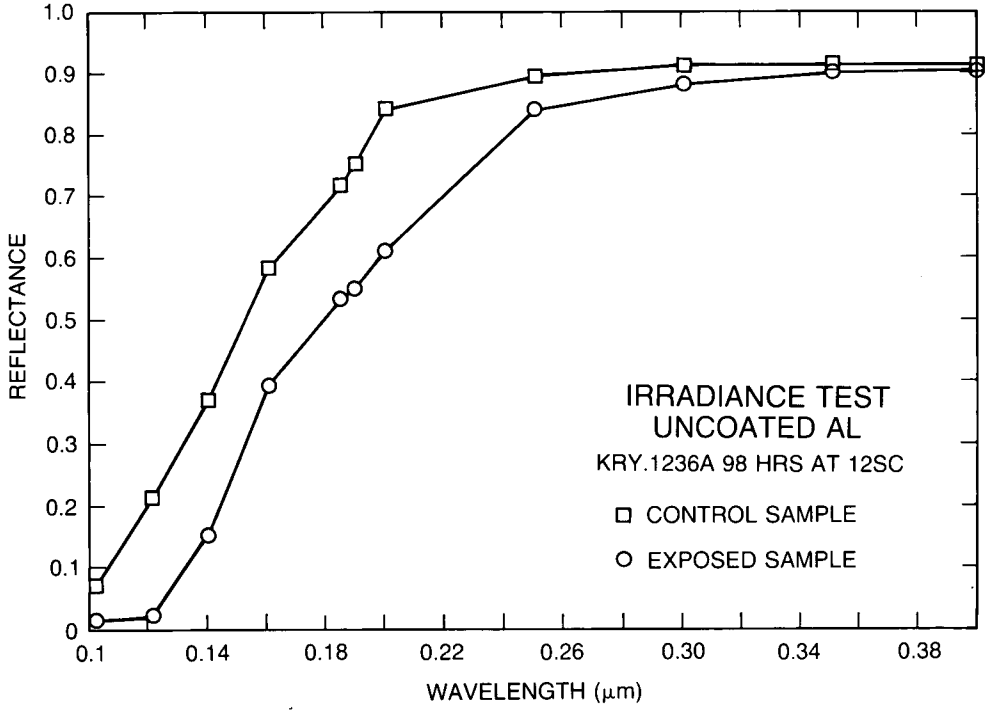

Figure 2.2 Reflectivity as a function of wavelength for uncoated aluminum surfaces, one of which was exposed to an oil-pumped vacuum system, and the other (control sample) not.

oil pumps. There is a considerable change in the reflectivity of the surface even at the longer wavelengths. In some cases, the oil is deposited on the surface in the form of droplets, and then broken down by solar radiation (Figure 2.3). However, the work of Hunter (1977) indicates that the original droplets evaporate quickly if not irradiated. Thus, it is unlikely that an oil film will retain its integrity on a surface in a hard vacuum for longer than a few days.

Figure 2.4 shows results from the SCATHA spacecraft, which carried two quartz microbalances. One of the balances was exposed to the solar irradiance, while the other was not. One can see from this figure that the sunlit sensor shows a steady increase of mass accumulation with

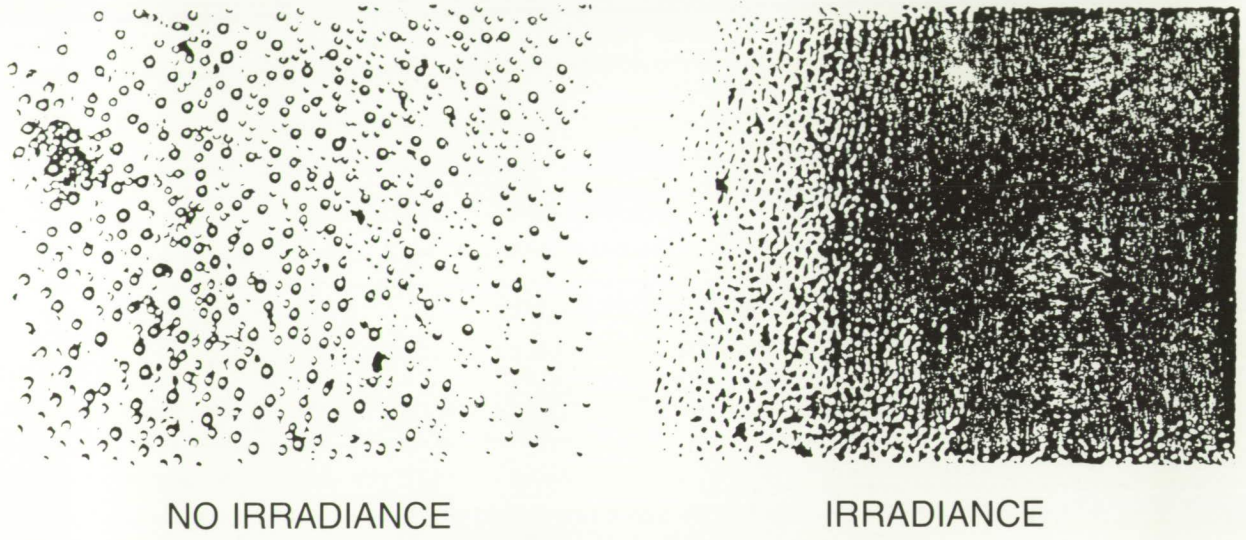

Figure 2.3 Effect of UV irradiation on evaporated DC 705 oil. The effective layer thickness is ≅200Å, evaporated onto an aluminum surface coated with MgF_2 (enlarged 700 times).

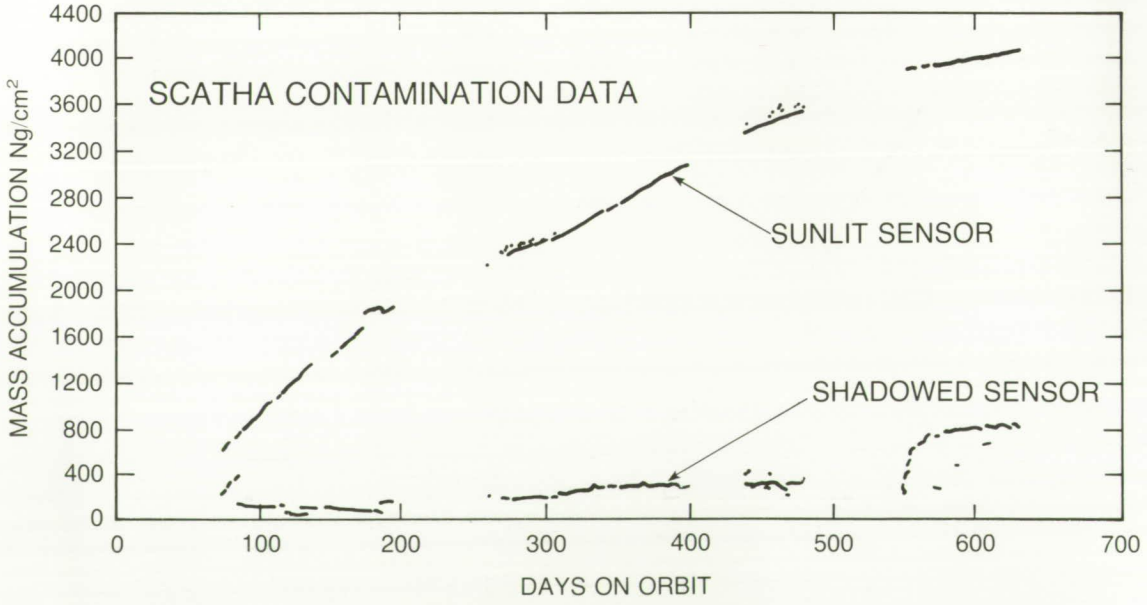

Figure 2.4 Mass accumulation as a function of time in orbit for illuminated and shadowed quartz microbalances on the SCATHA spacecraft.

time while the shadowed balance shows much less of an increase. It is significant, however, that it does show a slight increase, although this could be due to scattered sunlight. The solar wavelengths that can produce the film need not be at the high energies. Figure 2.5 shows the likely points at which the bonds could be broken in the methyl phenyl siloxane (silicon rubber) molecule. The energies correspond to wavelengths in the near ultraviolet.

In the laboratory, the deposited film has many of the characteristics of a carbon film. Figure 2.6 shows the change in the reflectivity at 270 nm for an uncoated oxidized aluminum surface versus the thickness of a carbon film deposited on the surface. It is unlikely, however, that any

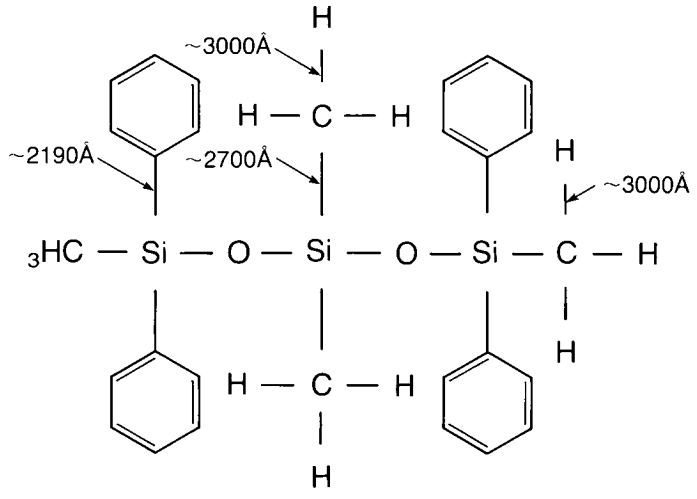

Figure 2.5 Bond energy of likely breaks of methyl phenyl siloxane (silicone rubber).

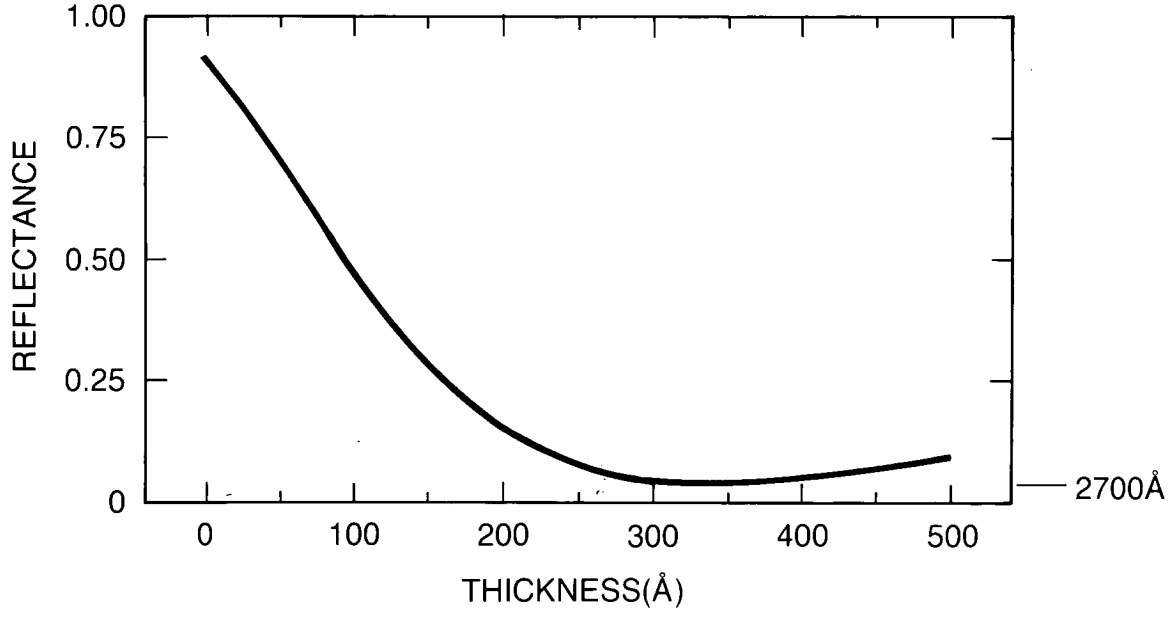

Figure 2.6 Reflectance at 270 nm of an uncoated oxidized aluminum plate as a function of the thickness of a carbon film deposited on its surface.

film deposited in space would be only carbon. The exact nature of the contaminant film will depend on the parent molecule or, in the case of a spacecraft environment, on several parent molecules.

Flight instruments and spacecraft contain many sources of contamination. Potting compounds, conformal coatings, insulation blankets, and attitude control gases are only a few of the possibilities. For most satellite launches, including Nimbus–7, the spacecraft is allowed to outgas for a few days after launch before the instruments are turned on; this should eliminate some of the surface contaminants. However, those sources of contaminants that are deeply rooted in the instruments or spacecraft will take much longer to outgas, and the traditional view that the outgassing will fall off exponentially with time may not hold (or the time constant may be very long).

2.2.2 Aging of Optical Surfaces

Most optical surfaces when incorporated into flight instruments have had a short history of exposure to radiation. There is considerable evidence that uncoated aluminum surfaces continue to lay down a protective layer of aluminum oxide, thus changing the optical properties of the surface. There is some evidence that the surface of replica diffraction gratings flows and changes the reflective properties of the grating. In general, it is usually incorrect to assume that optical surfaces will retain their original properties.

2.2.3 Changes in the Optical Transmission of Lenses, Filters, Etc.

The optical properties of transparent lenses, filters, windows, etc., can change as a result of exposure to radiation. These changes have many causes. Lithium fluoride and magnesium fluoride, for example, form color centers when exposed to ultraviolet radiation.

2.2.4 Detector Changes

Changes in detector response are one of the most common causes of changes in overall instrument responsivity. For this reason, most instruments have some method of monitoring the detector response. For the photomultipliers used in the experiments critiqued, one might expect to encounter:

- Changes in the window transmission.
- Changes in the cathode response.
- Changes in the dynode response. This is coupled with changes in the bleeder voltages to produce changes in the overall gain of the photomultiplier.
- Changes in the electronics.

2.2.5 Movement or Separation of Optical Components

Wearing of the surfaces of grating drive cams, dimension changes due to temperature fluctuations, and relaxation of stressed components are but a few of the mechanical instrument changes that could lead to changes in the optical response of instruments. For example, the SBUV instrument uses a quartz depolarizer at the entrance slit. This consists of a set of thin plates under tension in a holder, with the interfaces filled with an adhesive. During recent tests on one

of the SBUV–2 instruments, the plates were observed to move with respect to one another under thermal stress.

2.3 THE SOLAR BACKSCATTER ULTRAVIOLET (SBUV) EXPERIMENT

2.3.1 Physical Principles

Absorption of sunlight in the Hartley bands and continuum of ozone produces a complete attenuation at Earth's surface of solar radiation between 200 and almost 300 nm. (For a discussion of the spectroscopy of this spectral region, see Brasseur and Solomon, 1984, or Craig, 1965.) Thus, it is not possible to use ground-based absorption spectroscopy of this band system. Absorption spectroscopy is possible in the longer wavelength Huggins and Chappuis bands, but this technique does not provide any information about the vertical distribution of the ozone in the atmosphere. However, since ozone is a minor atmospheric constituent, unit optical depth for absorption in the Hartley continuum occurs at altitudes (wavelength dependent) where significant Rayleigh backscattering of sunlight occurs (despite the seven-order-of-magnitude difference in cross-section). Singer and Wentworth (1957) suggested that observations from above the atmosphere, in which the fraction of sunlight reflected back to space (the planetary albedo) is measured as a function of wavelength, could be used to deduce the concentration of ozone as a function of altitude. This is the principle of the SBUV experiment that flew on Nimbus–7. Other experiments utilizing the same principle have flown on Kosmos–65, OGO–4, Nimbus–4, Atmosphere Explorer–D, and, most recently, TIROS–9 and the Japanese Exos–C. Mathematically, the expression for the backscattered signal can be written as

$$I(\lambda) = F_o(\lambda)A[X(p),\alpha(\lambda),\beta(\lambda),\psi(\mu_o), R(\lambda)] \quad (1)$$

where $I(\lambda)$ is the observed backscattered radiance at wavelength λ, F_0 is the solar irradiance, and A is the albedo of the atmosphere and surface. This latter depends, as indicated, on $X(p)$, the total amount of ozone above a level where the pressure is p, the ozone absorption coefficient α, the Rayleigh scattering coefficient β, the Rayleigh phase function ψ for the solar zenith angle whose cosine is μ_0, and the surface reflectivity R. The full expression is given in Chapter 3 (Algorithms).

It was recognized from the outset that this technique was intrinsically capable of very high accuracy and stability, since the requirement was for a relative measurement of the ratio of Earth's backscattered UV radiance $I(\lambda)$ to the solar UV irradiance $F_0(\lambda)$ at the same wavelength. Because both measurements could be made with the same instrument, the determination of albedo as a function of wavelength over the range 250–340 nm should not depend on either the absolute calibration of the instrument nor on long-term variations in the sensitivity of the instrument.

However, for the SBUV, a major uncertainty is introduced by the use of an optical component not common to both measurements—the diffuser plate—which is used to transform the solar flux (irradiance) into a radiance that is comparable in magnitude to the backscattered Earth radiance, and can be measured instrumentally in exactly the same manner.

The extraction of the ozone profile, depends, then, on two factors: the precision and accuracy of the relative measurement, and the algorithm used to retrieve the information from the measured albedo. The second factor is treated in Chapter 3; the first is our principal concern in this chapter.

The SBUV experimenters recognized the need to achieve as high a measurement precision as possible with the spectrometer, and have devoted much effort to controlling sources of systematic error (e.g., polarization, scattered light, short-term gain changes, etc.). They have also taken care with the absolute calibration procedures, in part to properly address a secondary goal of the SBUV experiment, the long-term monitoring of variability of the solar UV irradiance at the top of Earth's atmosphere. The long-term behavior of the diffuser plate in the Nimbus–7 SBUV instrument remains a crucial area of concern for the evaluation of long-term trends of both ozone and solar irradiance.

The diffuser plate on the earlier Nimbus–4 Backscatter Ultraviolet (BUV) experiment was continually exposed to space, and its reflectivity decreased rapidly. In order to prevent this, the SBUV diffuser was designed to be stored inside the instrument, in a protected position, and deployed only when a measurement of the solar irradiance was made, which was usually once per day.

The plan for maintaining long-term stability was not stated explicitly, but appears to have been based on a belief that the degradation would be slow enough to be negligible. There is no provision for measuring any change of diffuser reflectivity in orbit.

The more recent operational version of SBUV, SBUV–2 (Frederick et al., 1986) has included a reference mercury lamp for evaluating the behavior of the diffuser plate with time. However, to provide a useful calibration, the lamp or other elements that direct its output to the diffuser and spectrometer must be positioned very repeatably, frequently over a long period of time. In addition, the lamp output must be stable over the time period when it illuminates successively the instrument and the diffuser. These conditions were not met for the first SBUV–2 instrument, and the inflight calibration has not been useful. Design changes have been made in an attempt to obtain reliable inflight calibrations on future versions of the SBUV–2 (see also Section 2.8.2).

2.3.2 Instrument

Descriptions of the instrument, together with diagrams, are given in Heath et al. (1975 and 1978, referred to below as User's Guide UG). For ease in following this discussion, a schematic is presented in Figure 2.7. The basic optical system consists of two Ebert–Fastie monochromators used in a double monochromator arrangement to provide twice the dispersion of a single instrument. The use of two monochromators in series, together with a holographically produced diffraction grating, ensures a very low level of instrumental scattering ($<10^{-9}$) in order to eliminate the possibility of contamination of radiance measurements near 250 nm by more intense long-wavelength (400 nm and longer) scattered light in the instrument. The wavelengths used for ozone measurements are, in nm, 255.5, 273.5, 283.0, 287.6, 292.2, 297.5, 301.9, 305.8, 312.5, 317.5, 331.2 and 339.8. The channel at 255.5 nm was measured, but not used because of fluorescence by NO. The next seven are used for extracting profile information, while the latter four are for determining total ozone. The methods by which the ozone profiles and column amounts are retrieved are described in the next chapter.

Another important feature is the use of a depolarizer at the entrance slit to remove the polarization sensitivity of the monochromator to the Rayleigh backscattered radiation. The diffuser plate, used to view the Sun (the field of view FOV of the instrument is normally directed toward the nadir for Earth radiance measurements) is a ground aluminum plate that is rotated into the FOV for the solar measurements.

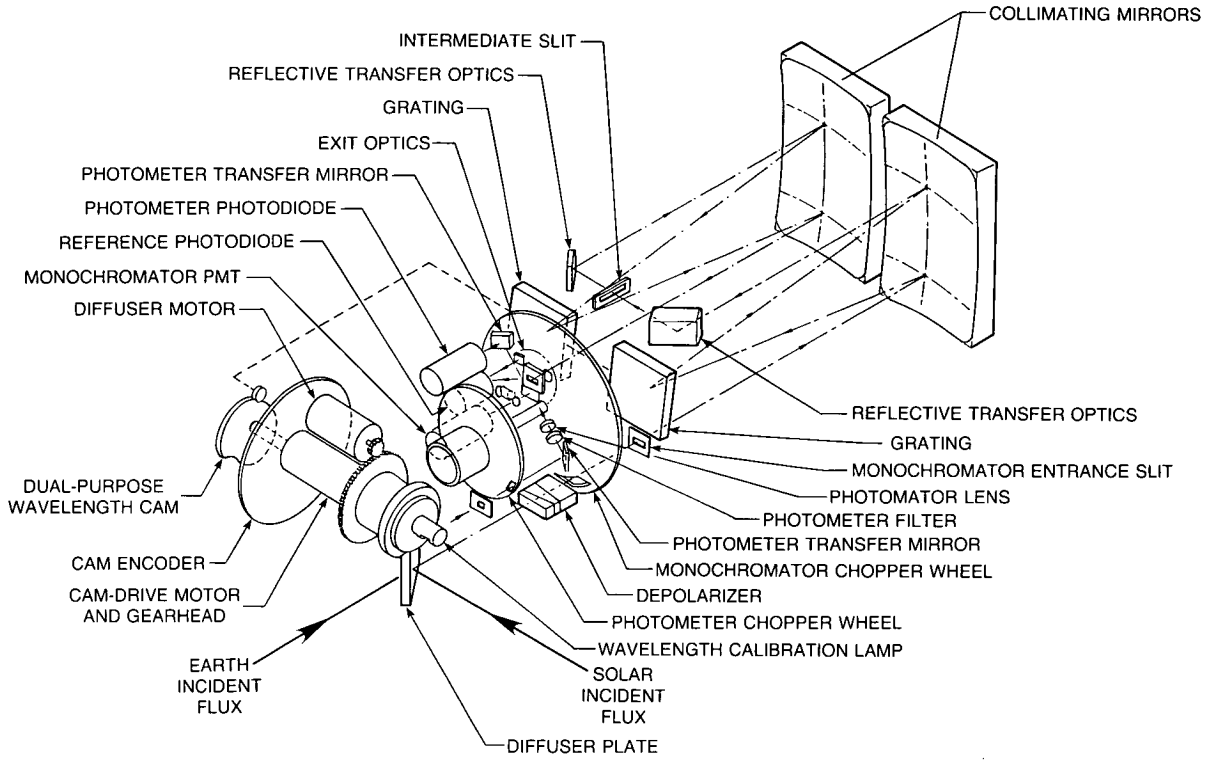

Figure 2.7 Schematic diagram of the SBUV instrument (from Heath et al., 1975).

The various operating modes of the instrument are also described in UG. Unfortunately, much of the material in UG and other reports is not available in the refereed literature, and in any case is difficult to obtain. This lack of available documentation was a serious problem in this investigation.

2.3.3 Prelaunch Calibration

The plan for prelaunch calibration is outlined in UG. Basically, various spectral irradiance sources, traceable to the National Bureau of Standards (NBS), were used, together with several diffusing screens, to produce a source of known radiance as a function of wavelength. The different diffusing screens were both intercompared and measured independently at NBS. The solar irradiance mode is similarly calibrated using the flight diffuser, except that for the spectral region <200 nm, the tests require a clean vacuum system (this region is of no interest for evaluating ozone trends). It should be noted that the quoted uncertainty in the absolute calibration, which is ~3–11 percent using NBS-traceable sources (Heath, private communication, 1987) is considerably larger than the measurement precision (<1 percent) achieved by the instrument itself, which is a measurement only of the reproducibility of a given measurement. In addition, there are two other critical calibration requirements: wavelength knowledge and reproducibility (the grating is coupled to the motor drive through a stepped cam), and electronics system linearity. The prelaunch tests for these parameters are also given in UG. Provisions for inflight calibration checks of the wavelength drive, detector, and the electronics are also described there.

All of the calibrations were performed at Beckman Instruments prior to the thermal–vacuum (T/V) testing that was done at General Electric. One of the goals of the T/V test was to determine

the stability of the instrument after repeated temperature cycles that simulate the expected environment in space. Following these tests, the absolute calibration of the spectrometer was checked at the T/V test site and was found to have changed by ~11 percent in the wavelength band 270–290 nm, 6 percent at 294 nm, 10 percent at 306 nm, and 7 percent at 315 nm and longer. The diffuser plus spectrometer calibration varied similarly with wavelength, so that the albedo change was ~3.5 percent at all wavelengths. This effect introduces an uncertainty of up to 8 percent in the solar output in the 270–290 nm band.

The launch schedule precluded any further measurements to determine possible sources of the change or even a recalibration using the same equipment that was used for the detailed prelaunch calibration. The post-T/V data were used for the initial flight calibration. While the change in absolute calibration does not affect the retrieval of trends in ozone profiles or column amounts, it does lay open the possibility of an undetected change of a similar nature occurring between the post-T/V test and operations in space. During the 7 years of operation of the instrument in orbit, a sudden change of 2 percent would probably be detected. A slow change would be treated as discussed below.

2.3.4 Results in Orbit

The SBUV was launched on Nimbus–7 on October 24, 1978, into a Sun-synchronous polar orbit. The instrument initially operated 3 out of 4 days, beginning on October 31, 1978, and provided an average of 1,200 sets of measurements per day. The observations cover the daylight portion of the globe, and are made close to local noon, except in polar regions. Solar measurements were initially made on one orbit per day, for a period of about 4 minutes.

The most crucial in-orbit observations for the present discussion are those of the time history of the results of the solar observations, shown in Figure 2.8a,b. At all wavelengths, they show a decrease in instrument response with time, with four episodes of rapid decrease interspersed with longer periods of slower decrease. The effect is larger at the shorter wavelengths, reaching a total decrease of about 50 percent after 8 years. There does not appear to be any possibility that more than a small part of this at the shorter wavelengths can be due to changes of the solar output. The response of the spectrometer–diffuser to solar radiation seems to have degraded over the life of the experiment.

The second observation of interest to the question of instrument change is that the response of the photomultiplier tube (PMT) detector changed by about 9 percent relative to a photodiode placed to serve as a check on any PMT changes over the period 1978–1983.

2.3.5 Possible Mechanisms Leading to Change in SBUV Instrument Response During the Mission

In general, instrument response change during orbit will be due to changes in the detection systems (electronics and detector) or in the optical system—including the optical elements, their alignment, and proper deployment (see Section 2.2). This section will point out the large number of mechanisms that are likely sources of change in the SBUV response; it should also discourage us from believing simplistic models of instrument degradation in the absence of independent data. Here we consider how these potential sources of change may affect the response of SBUV.

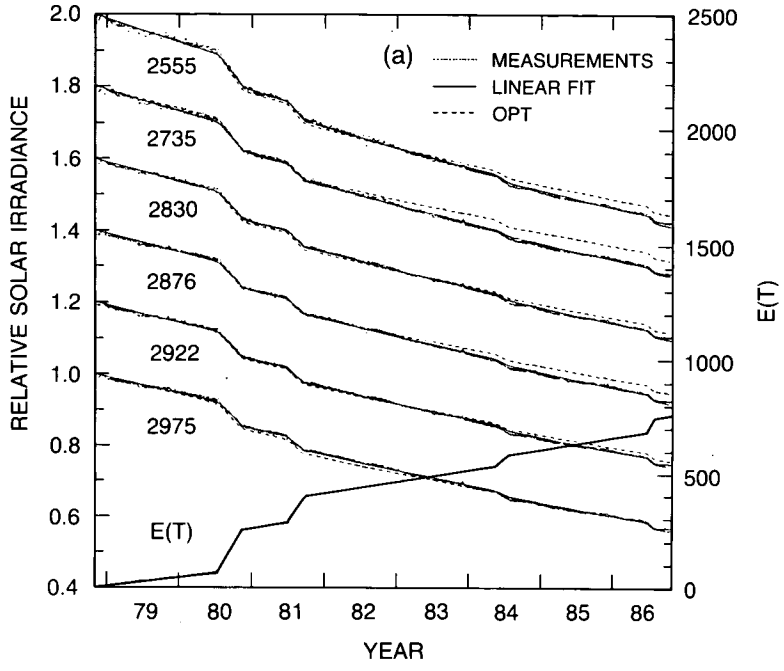

Figure 2.8a The measured degradation of the SBUV instrument, Fm(t)/Fm(0), for 1978–1987. The data, Fm(t), are the solar irradiance viewed by the spectrometer after reflection off the diffuser plate. The data consist of 2,303 measurements taken during one orbit per day. The abrupt inflection regions in 1980, 1981, 1984, and 1986 are for times when the diffuser plate was deployed on each of 14 orbits per day. Also shown are the exponential fit obtained by Cebula et al. (1988) (CPH) and adopted by the OPT (labeled OPT) and the 4-term quasi-linear fit (solid line) passing through the center of the data. The curve labeled E(t) is the accumulated exposure time in hours. The numbers on the left side correspond to the shortest six observing wavelengths. Each wavelength curve is normalized to 1 and displaced by 0.2 units.

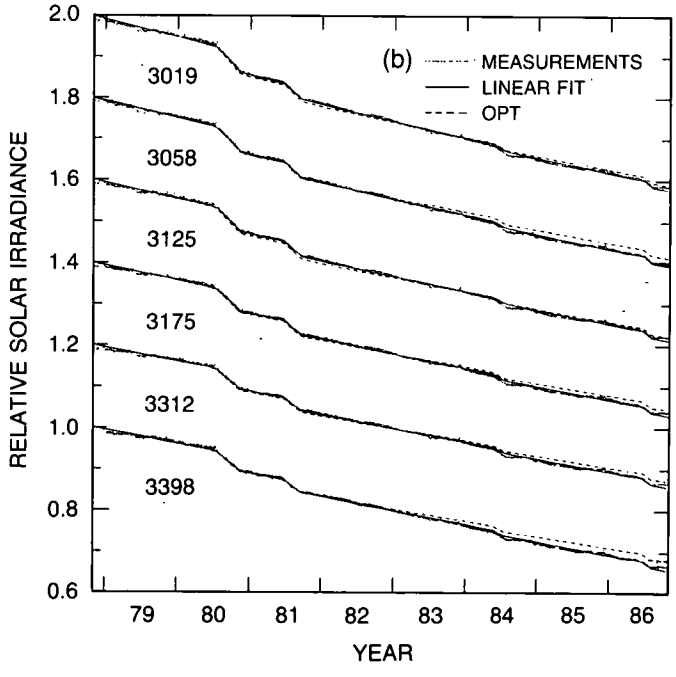

Figure 2.8b The same as for Figure 2.8a, except for the six longest wavelengths.

Detection System

SBUV did not have on board a constant current source often provided (as on TOMS) to check the performance and gain of the amplifier electronics, nor did it have the capability to look at the current from the first dynode of the PMT, which would allow monitoring the gain of the PMT. Rather, SBUV relied on monitoring a "constant" fraction of the light leaving the spectrometer exit slit with a reference vacuum photodiode. On the plus side, this method has the advantage of a "systems" approach, testing the stability of the PMT photocathode response, as well as, simultaneously, the gain of the PMT and the amplifier. On the negative side, it relies on the stability of the optical systems used as well as the diode for its interpretation. The elements involved are a mirror used to select about 10 percent of the light exiting the slit, a second mirror to redirect the selected light to a vacuum diode, and the window and cathode of the diode. In addition there is also a focusing mirror system used to relay the remaining light from the exit slit to the PMT. Changes in the reflectance of any of these mirrors or in the transmission of the diode window or the photoyield of the diode cathode could be misinterpreted as a change in gain of the PMT/amplifier system.

A final factor in evaluating this monitor system is that the light sampled apparently comes from a small portion of the exit slit. Since astigmatism in the spectrometer optical system is reasonably small, the intensity distribution of light along the exit slit would be expected to be proportional to the light distribution along the entrance slit. Any change in this distribution would affect the monitor-to-signal ratio.

In the SBUV data reduction, a change in this monitor signal was interpreted as a gain change. Clearly, this change could also have been due to changes in the relevant optics or the diode, or the intensity distribution along the slit. In their analysis of the observed degradation effects, the Ozone Processing Team (OPT), which is responsible for the operational reduction of SBUV and TOMS data, concluded that a significant degradation of the spectrometer optics has taken place. Thus, it would be logical to assume that some degradation in the detector optics has also taken place, even if the diode is assumed to be completely stable. At least the assignment of the change in monitor signal during the mission as a gain change of the PMT appears to be open to reinterpretation. The effect of a change like this on the ozone trend cannot be quantified without a model of the time history of the change, and of the instrument degradation. For the models described in Section 2.3.6, the effects would probably be small.

Optical Systems

The optical system may be divided into the prespectrometer, spectrometer, and detector (postspectrometer) optics. The prespectrometer optics consist of the reflective scatter (diffuser) plate used in the irradiance measurement (but not in the backscatter radiance measurement), and the depolarizer (used in both). The spectrometer optics consist of six mirror and two grating reflectances in a double Ebert–Fastie mounting. The detector optics consist of a reflector focusing field optic to image the second grating on a field stop in front of the PMT using one or two reflecting surfaces. It should be reiterated at the outset that changes in the spectrometer will affect both solar and ozone measurements, while changes in the diffuser will affect only the solar measurements. However, unless there is a way to unambiguously separate a diffuser change from a spectrometer change in orbit, one kind of change will almost certainly be misidentified, leading to errors in ozone trends.

- Diffuser and Depolarizer—The diffuser is a ground aluminum plate overcoated with evaporated aluminum positioned as the first optical element of the SBUV instrument. The second optical element, the depolarizer, consists of four appropriately oriented and tapered layers of quartz. Since both elements are outside the spectrometer entrance slit, they can receive more UV radiation and higher exposure levels to any contaminants in the vicinity of the spacecraft. The diffuser is the only optical element exposed to the full solar irradiance when deployed. To the extent that the solar radiation contributes to the degradation of the instrument response, it is likely that the diffuser plate is responsible for most of this form of decreased response. On the other hand, the depolarizer is exposed to reflected solar radiation, especially at long wavelengths, for the Earth-viewing period, which is 25 times longer. Even if the reflected solar radiation on the diffuser is only 1 percent of that on the diffuser, its degradation is not negligible.

  In the absence of solar exposure, the optical surfaces should have contamination layers that are at equilibrium with the local low-pressure atmosphere surrounding the spacecraft. Hydrocarbons deposited on a surface exposed to solar UV radiation tend to form strong bonds with the surface and adjacent carbon atoms. The resulting film has a much lower vapor pressure than the original hydrocarbons and so can gradually build up to a considerable thickness at a rate that seems to be proportional to the UV exposure time (for SBUV conditions). The buildup of a permanent film may or may not be proportional to the deposition rate depending on how quickly equilibrium is established during the periods of no solar exposure.

  The presence of a film on the optical surfaces is likely to reduce the reflectance of the scatter plate and, to a lesser extent, the transmission of the depolarizer. If the overall instrumental response can be considered to be a product of the independent degradation of the spectrometer and diffuser plate, then the effect of a film forming on the depolarizer is eliminated when the instrument is used to determine ozone from the measured UV albedo. That is, the effect of spectrometer degradation cancels when calculating the ratio of backscattered radiance to solar irradiance (albedo). The problem is to be able to separate the effects of the diffuser plate and spectrometer degradation when analyzing the measured albedo.

  If a thin film model of the SBUV diffuser plate degradation is correct, then certain characteristics of the film (thickness, real and imaginary parts of the refractive index) must be specified in addition to identifying its bulk characteristics. For example, it can be shown that a nonuniform film thickness across the surface of the optical elements can have an additional effect on the calculated degradation that is comparable to degradation from uniform films of the same average thickness. The radiance–irradiance ratio may be a complex function of the growth rate of a contaminating film of unknown bulk properties, the known rate of solar exposure and total elapsed time since the spacecraft launch, the known number and frequency of diffuser plate deployments, the unknown film geometry, and possible unknown exposure-dependent effects on the depolarizer and other internal spectrometer components. To some extent, the properties contributing to the degradation can be characterized from a series of four experiments performed during 1980 to 1986 (so-called "frequent deployment" experiments), and from the long-wavelength measurements of the radiance and irradiance.

- Spectrometer and Detector Optics—The spectrometer optical system is a double monochromator (Ebert–Fastie), which is a very good design for the reduction of scattered light.

This feature is further enhanced by the field stop in the exit optics to confine radiation reaching the detector to that coming from the second diffraction grating. Thus, only scattering coming from the optical elements themselves can be seen by the detector. In addition, holographic diffraction gratings that are known for low scattered light were employed. The excellence of this overall design in reducing the dangers of scattered light in UV solar measurements was demonstrated by preflight testing. There remains the hazard, however, that the growth of contamination on the spectrometer optics over many years in orbit can increase the scattering from the optical elements and contribute to spectral impurity of the exiting radiation. Also, aging (deterioration of evaporated films) after this long service and UV exposure is a possibility. Regardless of the scattering introduced by contamination and aging of the optics of the spectrometer and detector systems, there is little question that some reduction in specular reflectivity due to contaminants can be expected. Since there are 9 or 10 reflections, a 1 percent average loss per element would result in about a 10 percent overall transmission loss of the system. This "leverage" offsets somewhat the lower level of short-wavelength irradiance existing on the optical elements within the spectrometer. Thus, this is a serious probable change in instrumental response for which there is no method of separate evaluation.

- Other Deleterious Effects—Two other possible sources of change in instrumental response should at least be mentioned. The first is the possible fluorescence of the contaminating layers developing on the optical elements, excited by the UV component of the incident radiation but fluorescing at longer wavelengths. A fluorescence signal from the diffuser or polarizer would add to the intensity arriving at the entrance slit of the spectrometer at the fluorescent wavelengths. Fluorescence from optical elements within the spectrometer would appear similar to scattered light.

  The second possibility relates to the unfortunate change in calibration that was discovered after a thermal vacuum (T/V) test of the SBUV prior to launch. This significant change (radiance 6–11 percent; irradiance 4–8 percent) was most likely due to some contamination during the thermal vacuum test. Credit is due the determined Principal Investigator (PI) who insisted on a post-T/V calibration, which unfortunately was a hurried in-the-field evaluation of the instrument response. This final calibration necessarily was taken to be the initial response of the SBUV in orbit. It is conceivable that some of the contamination that occurred at this time was subject to "cleanup" during the initial flight exposure to high vacuum before exposure to solar UV.

In conclusion, there are many possible sources of change of instrument response during inflight life, with various effects on the solar irradiance and backscatter radiance measurements and the albedo determination. It is not possible to determine which of these effects may be operative to a significant degree in causing the overall instrument degradation observed.

2.3.6 Diffuser Plate Degradation

General Discussion

The problems arising from the SBUV instrument degradation can be understood more easily if $F_{o\lambda}$ and I_λ denote, respectively, the solar irradiance and backscattered radiance determined by applying the values from the prelaunch calibration for diffuser reflectivity and spectrometer sensitivity. Then, denoting the measured quantities, which vary with time t, by subscript M, for each wavelength

$$F_{M\lambda}(t) = F_{o\lambda}(t)D_{\lambda}(t)S_{\lambda}(t) \tag{2}$$

and

$$I_{M\lambda}(t) = I_{\lambda}(t)S_{\lambda}(t) \tag{3}$$

where $F_{o\lambda}(t)$, $D(t)$, and $S(t)$, the solar flux, the diffuser reflectance normalized to its initial (preflight) value and the spectrometer sensitivity normalized to its initial value, are unknown. The quantity related to the atmospheric ozone content is the albedo (radiance–irradiance ratio).

$$A(\lambda,t) = \frac{I_{\lambda}(t)}{F_{o\lambda(t)}} = \frac{I_{M\lambda}(t)}{F_{M\lambda}(t)} D_{\lambda}(t). \tag{4}$$

If $A(\lambda, t)$ increases, it could be due to an increase in I_{λ}, resulting from a decrease in ozone, or an overestimate of $D_{\lambda}(t)$—i.e., an overestimate of diffuser reflectivity, or equivalently an underestimate of its degradation.

From Equation 4, it is clear that a knowledge of $D_{\lambda}(t)$ is critical to deriving the correct albedos, and thus the correct ozone distributions and trends, from the measurements. The SBUV did not include any means to carry out an inflight calibration for evaluating the long-term behavior of either the spectrometer or the diffuser plate, admittedly a difficult task.

The estimation of $D_{\lambda}(t)$ therefore requires the use of other information. Possibilities include making special measurements in orbit to determine $D_{\lambda}(t)$, deriving $D_{\lambda}(t)$ from a comparison with other ozone measurements, or deriving $D_{\lambda}(t)$ from measurements of F_M and I_M. Unfortunately, all of these have problems. There are not enough reliable measurements of the vertical ozone profile to allow $D_{\lambda}(t)$ to be determined at the eight short wavelengths. (Perhaps Dobson measurements could be used for the four long wavelengths, but apparently this was not investigated before the ozone trend studies.) Some inflight measurements will be described below, but they were infrequent, and used only for comparison with other results.

The remaining possibility, which was employed by the OPT, is to use the measurements of I_M and F_M to estimate $D_{\lambda}(t)$. Equations 2 and 3 have four unknowns, since $I_{\lambda}(t)$ may be changing due to a changing ozone distribution. If other information can be used to provide an estimate of the temporal variation of $F_{o\lambda}(t)$, the number of unknowns is reduced to three.

For wavelengths at which the ozone absorption is imperceptible, it is plausible (but not necessarily correct) to assume that the true underlying albedo over a large geographical area (like the Tropics) shows no long-term change. This can be used in Equation 3 to determine $S_{\lambda}(t)$, and thus unambiguously separate the effects of the diffuser from those of the spectrometer.

For wavelengths at which there is measurable ozone absorption, this procedure cannot be followed, because assuming a trend in albedo effectively specifies the ozone trend that is being sought. There is no information that allows one to make this separation with certainty in Equation 3.

Therefore, the approach is to use measurements of $F_{M\lambda}(t)$, expressed by Equation 2, with information on $F_{o\lambda}(t)$ from other data, to estimate the product $D_{\lambda}(t)S_{\lambda}(t)$, and hypothesize the way the product is factored.

The solar irradiance $F_{M\lambda}(t)$ was measured by deploying the diffuser in the direct solar beam for about 4 minutes on at least one orbit per day ("standard" observations) throughout the life of the SBUV instrument. In addition, there were four periods of "frequent" observation, when the diffuser was deployed on each orbit (about 14 per day) for an extended length of time. Figure 2.8a,b shows the measured degradation of the SBUV instrument, $F_{M\lambda}(t)/F_{o\lambda}(=D_\lambda(t)S_\lambda(t))$, for November 1978–November 1986, for the 12 observed wavelengths.

Figure 2.8a also shows the cumulative exposure time E(t) of the diffuser plate to the Sun. From the coincidence between periods of frequent diffuser deployment and rapid decrease of solar signal, it is clear that part of the signal degradation is due to diffuser deployment into the solar beam.

Historically, these are the data on which everything is based. From these, one must first determine how the product DS depends on various factors and, second, separate D from S. Clearly, the solution is not unique. Criteria for assessing the solution are its plausibility and its consistency with the few constraints discussed below. The only physical limits are D = 1 (no degradation on the diffuser) and S = 1 (all degradation on the diffuser).

The Exponential Model (Cebula, Park, and Heath)

Based on the first 6 years of data shown in Figure 2.8, Cebula et al. (1988, referred to as CPH below; see also Park and Heath, 1985) proposed a model of the degradation in which the percentage rate of change of one component was proportional to the total diffuser exposure time E, and the percentage change of the other component was proportional to the total time in orbit, t. Then, after correction for the Sun–Earth distance to 1 AU,

$$\frac{F_{M\lambda}(t)}{F_{o\lambda}} = P(t)e^{-\gamma(\lambda)G(t)}e^{-s(\lambda)t}e^{-r(\lambda)E(t)}. \tag{5}$$

The photomultiplier gain, P(t), is determined from a comparison with the onboard reference diode (which was not stable).

The second term contains the variations in the solar flux, based on the model of Heath and Schlesinger (1984, 1986):

$$\frac{F_{o,\lambda}(t)}{F_{o,\lambda}(0)} = \exp[-\gamma(\lambda)G(t)], \tag{6}$$

where G is the ratio of core to wing radiance of the MgII doublet, and γ are coefficients relating the solar output at λ to G. The γ's were derived from observations of the 27-day rotation period; their use here implicitly assumes that the change in the solar spectrum over the 11-year solar cycle has the same wavelength dependence as the change over a 27-day rotation period. While this is plausible, it neglects the possibility that there could be another component of variation over the longer period (see Lean, 1987). Thus, there is uncertainty in the values used for $F_{o,\lambda}(t)$.

With these assumptions, we have

$$D(t)S(t) = e^{-r(\lambda)E(t)}e^{-s(\lambda)(t)} \tag{7}$$

where the assumptions that $r(\lambda)$ and $s(\lambda)$ do not change with time are included. Thus, to determine the two components, one need only compare time periods in which the ratio E/t

varied substantially. CPH did this by using time spans containing equal periods of nominal and frequent solar observation. Periods of frequent exposure occurred in 1980 and 1981, which were the basis for the original analysis, and again in 1984 and 1986. For those periods, CPH argued that the solar change was small (although they were of several months' duration) and so would not contribute to the variation.

The derived values of $r(\lambda)$ and $s(\lambda)$ are presented for the first two frequent deployment periods in Table 2.1. The values of $r(\lambda)$ were subsequently smoothed in wavelength for use in the OPT processing. The smoothed values are the last column of Table 2.1. The individual values for

Table 2.1 SBUV *r* and *s* Values

Wavelength	*r* (SBUV)	*s* (SBUV)	*r* (smooth)
(nm)	(hr-1)	(dy-1)	(hr-1)
255.5	5.720E–04	1.266E–04	5.8113E–04
273.5	5.090E–04	9.777E–05	4.9232E–04
283.0	4.400E–04	1.096E–04	4.4813E–04
287.6	4.330E–04	9.487E–05	4.2734E–04
292.2	4.090E–04	9.501E–05	4.0737E–04
297.5	3.760E–04	9.708E–05	3.8543E–04
301.9	3.660E–04	8.558E–05	3.6914E–04
305.8	3.620E–04	7.506E–05	3.5619E–04
312.5	3.320E–04	7.554E–05	3.3520E–04
317.5	3.220E–04	6.662E–05	3.2150E–04
331.2	2.880E–04	6.066E–05	2.8983E–04
339.8	2.750E–04	6.181E–05	2.7236E–04

F/F_o = exp (-*r*E(*t*) - *st*) fit to the first two "rapid deployment" periods (1980, 1981). The *r*(smooth) data are the most recent numbers used in SBUV processing.

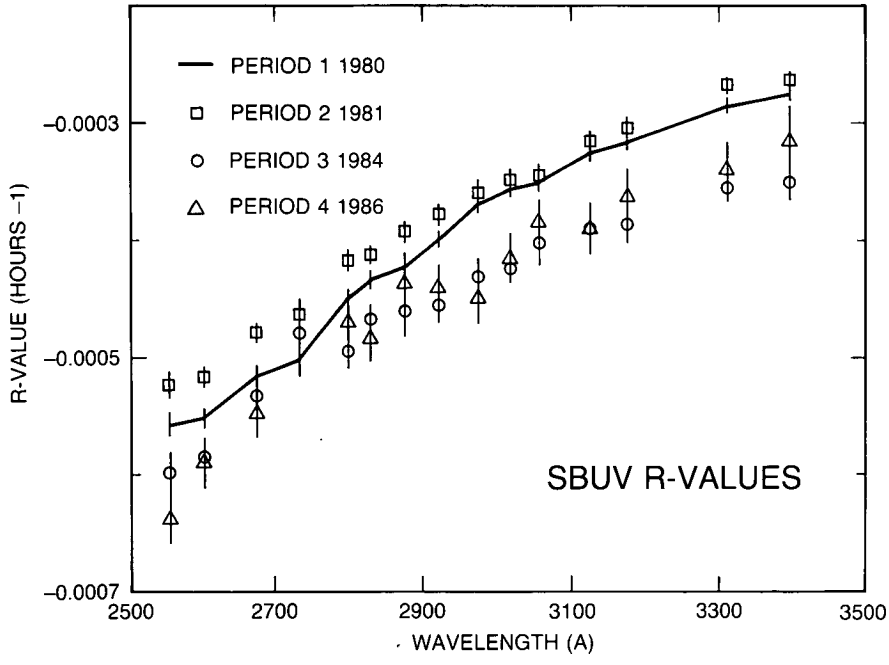

Figure 2.9 Values of $r(\lambda)$ determined during the four frequent deployment periods by CPH.

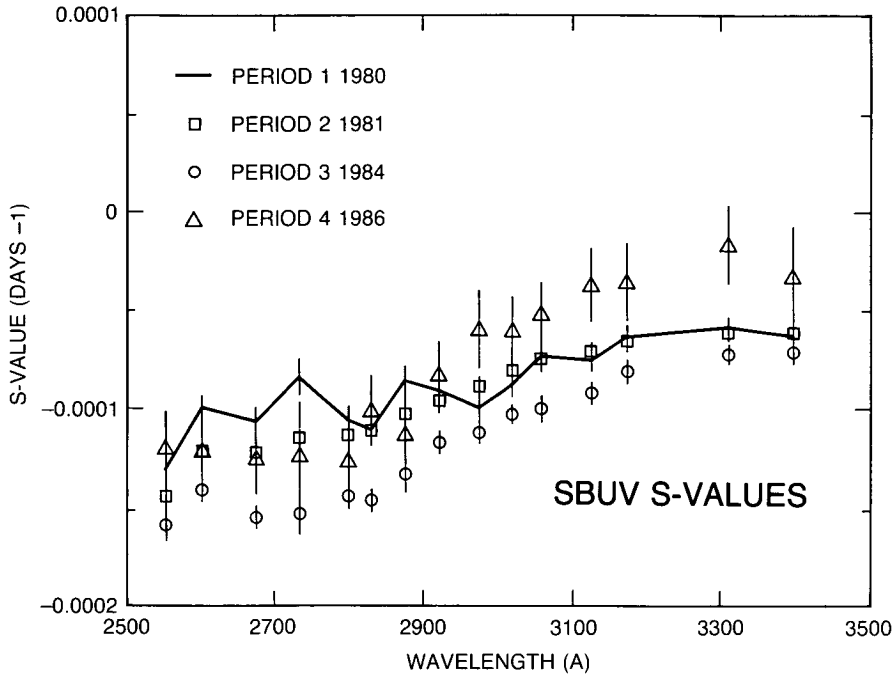

Figure 2.10 Values of $S(\lambda)$ determined during the four frequent deployment periods by CPH.

the four individual determination are shown in Figures 2.9 and 2.10. The formal uncertainty associated with $r(\lambda)$, based on the statistical fit of the solar flux data to the model, has been given as ~2 percent. Thus, at 273.5 nm (the wavelength contributing most to the 1 mb ozone retrieval), the total decrease in diffuser reflectivity over 7 years is 27 percent with a formal uncertainty of ±0.5 percent. Several arguments suggest that this formal error seriously underestimates the true uncertainty in $r(\lambda)$:

- In Figure 2.9, it is clearly seen that the $r(\lambda)$ values, particularly those from 1984 and 1986, differ significantly from the 1980–1981 values. The ozone retrievals use constant $r(\lambda)$ values derived from the 1980–1981 frequent solar observation periods. This is disturbing, as the deviation is largest in 1984–1986, the period of largest purported ozone decrease. The standard deviation of the data points for r at each wavelength is 6–13 percent (depending on wavelength), far greater than the formal 2 percent uncertainty in the 1980–1981 points.

- Values of $r(\lambda)$ derived from the TOMS data (see Table 2.2), are typically 13 percent higher than the SBUV $r(\lambda)$ values for wavelengths in common. This is statistically significant, despite the factor-of-two higher formal error than the SBUV $r(\lambda)$ values. While the TOMS FOV on the diffuser plate is smaller than that of SBUV, it is difficult to imagine an area-sensitive degradation mechanism that is capable of producing such an effect. (It has been suggested that the effect arises because the diffuser reflectivity has an angular dependence and TOMS views the diffuser at a larger angle from the normal, and that the frequent exposure periods were all at times that resulted in extreme angles. A deposit on the diffuser that changed the angular dependence might, in principle, lead to such an effect.)

Table 2.2 Comparison of SBUV and TOMS *r* Values for Combined Periods 1–2

λ	TOMS *r*-value	Sigma *r*	SBUV *r*-value	Sigma *r*
312.5	-3.63E–04	1.11E–05	-3.32E–04	5.04E–06
317.5	-3.76E–04	1.14E–05	-3.22E–04	5.80E–06
331.2	-3.17E–04	1.06E–05	-2.88E–04	4.38E–06
339.8	-3.01E–04	1.06E–05	-2.75E–04	4.92E–06
360.0	-2.50E–04	1.04E–05	-2.38E–04	4.16E–06
380.0	-2.28E–04	1.04E–05	-1.79E–04	4.44E–06

Note: The above uncertainties are based on the formal statistical error of the fit. The TOMS value is at the 65% confidence level, SBUV at the 90% confidence level.

λ	*R*-Value Diff. SBUV–TOMS	Comb. sigma (90% conf.)	Diff./Comb. sigma (90% conf.)
312.5	3.13E–05	1.93E–05	1.62
317.5	5.36E–05	2.00E–05	2.68
331.2	2.87E–05	1.83E–05	1.57
339.8	2.58E–05	1.85E–05	1.39
360.0	1.15E–05	1.80E–05	0.64
380.0	4.84E–05	1.81E–05	2.68
	Average		1.77
	Standard deviation		0.72

λ	Year 6 % Diff. @ E(t) = 600	Uncertainty in % Diff.	Year 8 % Diff. @ E(t) = 761	Uncertainty in % Diff.
312.5	1.90	1.18	2.41	1.50
317.5	3.27	1.24	4.16	1.58
331.2	1.74	1.11	2.21	1.42
339.8	1.56	1.13	1.98	1.44
360.0	0.69	1.09	0.88	1.38
380.0	2.95	1.12	3.75	1.43
Average	2.02	1.14	2.57	1.46
Standard deviation	0.86	0.05	1.10	0.07

Note: Again, the uncertainty in the % difference between the SBUV-based and TOMS-based *r*-values is calculated using only the formal statistical uncertainty in the fit, and does not include any possible systematic error. Specifically, the error in the TOMS *r*-values due to goniometric error is not included.

- The fit (Equation 7) to the degradation data that has been used to convert the SBUV radiance measurements in ozone amounts assumes that *r* and *s* are constants with respect to time. A comparison of this fit with the entire data record is shown by the dashed lines in Figure 2.8 and percent difference plots in Figure 2.11a,b for each wavelength. (Because the OPT adopted the CPU model, values obtained from it are labeled OPT in this and several subsequent figures. The two terms are interchangeable.) CPH argue that only the $\exp(-rE)$ portion of the fit is used in the ozone data reduction, and that the variation of *r*

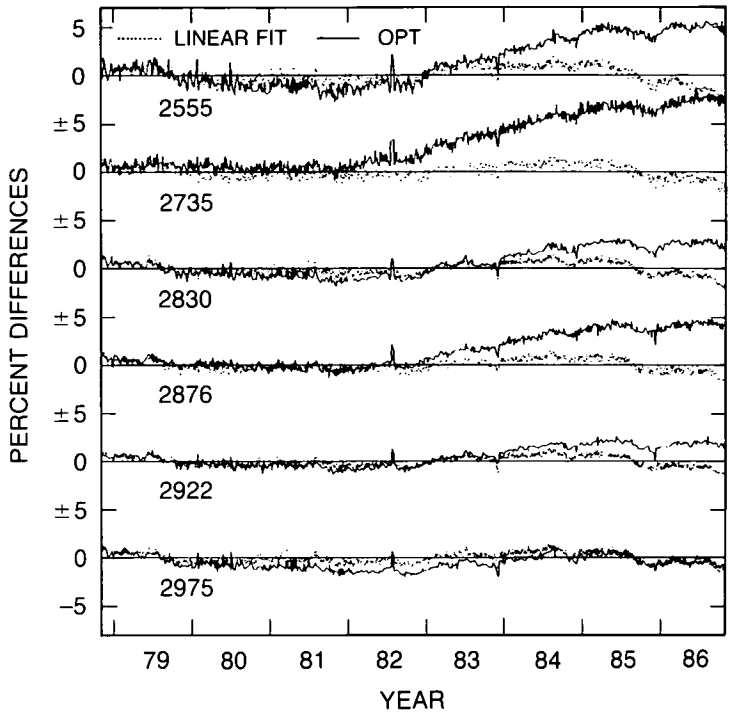

Figure 2.11a Percent difference between solar observation data and models. Horizontal line indicates 0 percent difference, solid line is OPT (CPH) model, and points are quasi-linear model (described below) for the six shortest wavelengths.

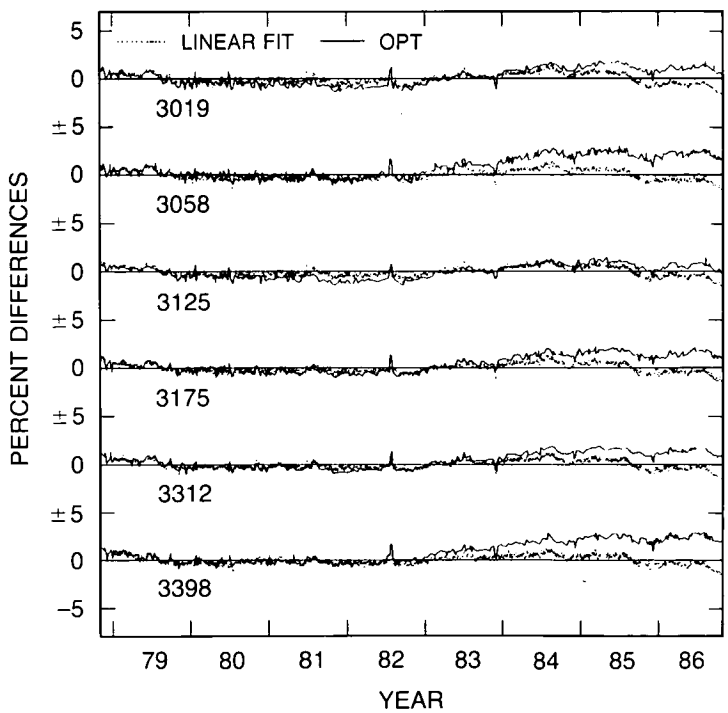

Figure 2.11b As in 2.11a, but for the six longest wavelengths.

calculated at each of the frequent deployment episodes is small. They interpret the small r variation as meaning that the form $\exp(-rE)$ correctly describes the diffuser plate degradation. To obtain an overall fit, they hold r constant in time and force the spectrometer constant, s, to vary. The variation of s with time calls into question the rationale for assuming Equation 7 as a unique form for describing the degradation. At best, it indicates that the formal statistical error given by CPH is probably too small.

The most critical assumption is the separation of the exponential model of the overall degradation into two components. CPH assumed the diffuser plate degradation is described for each wavelength by

$$D_\lambda(t) = e^{-r(\lambda)E(t)} \tag{8}$$

and the spectrometer by

$$S_\lambda(t) = e^{-s(\lambda)t}. \tag{9}$$

The rationale for putting all the exposure effect on the diffuser is that the diffuser plate is the only optical element directly exposed to the solar UV radiance and therefore is most likely to be the element affected by the amount of exposure time. The next element in the optical path, the depolarizer, is exposed to about 1 percent of the solar flux striking the diffuser plate. CPH assume that this amount of exposure would not contribute significantly to the exposure-dependent portion of the observed degradation (although, as noted above, it is continuously exposed). They claim that no exposure-correlated features are seen in the SBUV albedos to within 0.5 percent error. The rationale for assigning all the temporal variation to the spectrometer (Equation 9) is less clear.

The application of Equations 8 and 9 to the 339.8 nm radiance data is illustrated in Figure 2.12. The lower dash–dot line shows the raw solar irradiance, indicating that the SBUV response has decreased by about 28 percent after 8 years. The solid line shows the relative changes in the raw backscattered radiance, averaged from 20°S to 20°N, with seasonal variations removed. If the true backscattered radiance has not changed, the spectrometer has degraded by about 10 percent. The dotted line shows the decrease in F expected from the analysis. The ratio of these, the albedo, shown by the line of short and long dashes, is essentially constant over this period.

This demonstrates that the CPH approximations (including the use of r and s from 1980–1981 only) give reasonable results at this wavelength, but does not establish their applicability at other wavelengths.

One must be cautious about assuming that this approach is general, for at least two reasons:

- While A (340 nm) is sensibly a constant, other data (Cebula, private communication, 1988) indicates that this can vary by ±2 percent. It is not clear how large an uncertainty in D (340 nm) this would permit, and subsequently what part of the time-dependent degradation could be assigned to the diffuser.

- More important, even knowing what fraction of time-dependent degradation could be assigned to the diffuser at 340 nm, where degradation is relatively small, does not necessarily mean that the same fraction is relevant at the shorter wavelengths, where both components of the degradation are greater.

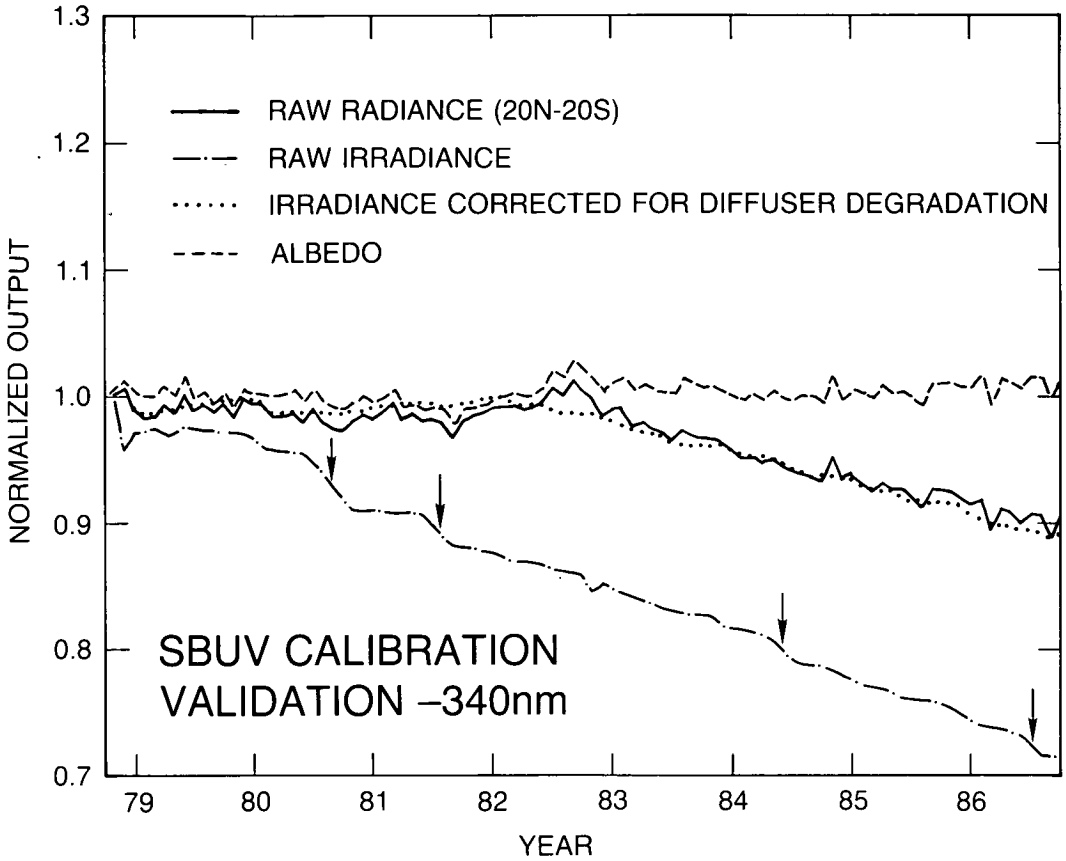

Figure 2.12 Comparison at 340 nm between the measured solar irradiance, irradiance corrected for diffuser degradation, Earth radiance from 20°N–20°S, and albedo, as a function of time.

An Alternate Empirical Model

Alternate empirical models can be derived that accurately describe the observed degradation (Herman and Hudson, private communication, 1988). These are of two types. The first and simplest is the observation that the data between 1978 and 1986 are well fit by linear or quasi-linear functions of the forms

$$D(t)S(t) = a + bt + cE$$

or

$$D(t)S(t) = a + bt + cE + dE(t)t \tag{10}$$

where $E(t)$ is the total accumulated exposure (hours) and t is the total elapsed time (hours) since day 307 of 1978. The linear expression fits quite well, with the largest differences during and after the last frequent deployment period. The second type is more closely based on a physical model of thin film formation on the diffuser plate and its optical effect on reflectivity (Madden, 1963; Smith et al., 1985). In this case, $D(t)$ is a function of the film thickness, real and imaginary parts of the refractive indices of a multilayer film over an aluminum substrate, and film deposition rate. $S(t)$ is an assumed empirical function that could be $\exp(-st)$. For both the quasi-linear and the thin film fits, the four parameters are determined by a least-squares procedure (nonlinear for the

thin film case). The solid line in Figure 2.8 represents Equation 10 plotted over the normalized data F/F_o. The fit is good over the entire period (1978–1986). The region of poorest fit is near the end of the data set, where the last rapid deployment occurred. The same problem occurs with the least-squares fitting procedure if the data are truncated just after the 1984 frequent deployment. If the data were extended into 1988, then the fitting problem would probably disappear. Percentage differences are shown by the solid lines in Figure 2.11.

Although the compressed scale makes the magnitude of the differences hard to see, it is clear that, at all wavelengths, the quasi-linear fit is closer to the data than the exponential model. This is perhaps not surprising in that a four-parameter (or three-parameter) model might be expected to fit better than a two-parameter model. However, it does illustrate the nonuniqueness of the form of the fit. The coefficients derived using Equation 10 are given in Table 2.3.

Table 2.3 Coefficients for the Quasi-Linear Model

Wavelength (nm)	A	B (hr-1)	C (hr-1)	D (hr-2)
255.5	9.900E–01	-5.048E–06	-4.785E–04	2.584E–09
273.5	1.004E+00	-4.623E–06	-4.155E–04	2.110E–09
283.0	1.002E+00	-4.194E–06	-3.907E–04	1.646E–09
287.6	1.007E+00	-4.012E–06	-3.674E–04	1.448E–09
292.2	1.001E+00	-3.683E–06	-3.625E–04	1.417E–09
297.5	1.002E+00	-3.404E–06	-3.542E–04	1.276E–09
301.9	1.001E+00	-3.209E–06	-3.316E–04	1.036E–09
305.8	1.003E+00	-3.009E–06	-3.186E–04	9.008E–10
312.5	1.002E+00	-2.721E–06	-3.042E–04	6.779E–10
317.5	1.006E+00	-2.565E–06	-2.864E–04	5.153E–10
331.2	1.005E+00	-2.235E–06	-2.593E–04	2.312E–10
339.8	1.006E+00	-2.270E–06	-2.498E–04	1.127E–10

$F/F_0 = A + B*t + C*E + D*E*t$ fit to full data set of 2303 points (1978 to 1986).

The quasi-linear fit is not based on any physical model and therefore cannot be extrapolated beyond the domain of the data (1978–1986). Eventually, the degradation data, F/F_o, would have to deviate from the quasi-linear form. Such a deviation might have helped in constructing a physical model based, for example, on thin film optics. In the discussion that follows, different factorization of the quasi-linear model can be shown to yield different rates of degradation for the diffuser plate and spectrometer. One of the many possible cases indicates that the decreasing ozone trend at 1 mb is much smaller (perhaps zero) than that calculated by the OPT using Equation 8, and another case shows a larger decrease than that found by OPT. The point of this exercise is to demonstrate the large uncertainty in any ozone trend analysis based on the presently archived data.

Case M: Diffuser degradation more than exponential model (which will result in higher derived ozone concentration, or more ozone).

Equation 10 can be written as

$$D(t)S(t) = (A + kE)\left(1 + \frac{Bt + DEt + hE}{A + kE}\right) \tag{11}$$

where

$$h = C - k$$

Let

$$k = f\frac{C}{1 + (B/A)t} \tag{12}$$

then assume that

$$D(t) = A + kE$$

and

$$S(t) = 1 + \frac{Bt + DEt + hE}{A + kE} \tag{13}$$

The factor f in Equation 12 is an arbitrary scale factor selected to produce a particular value of the calculated SBUV albedo.

Case L: Diffuser degradation less than the exponential model (which will result in lower derived ozone concentration)

An alternate division of terms is

$$D(t)S(t) = (A + ht)\left(1 + \frac{CE + DEt + kt}{A + ht}\right) \tag{14}$$

where

$$k = B - h.$$

Let

$$h = B \tag{15}$$

then assume the factors can be identified as

$$D(t) = 1 + \frac{CE + DEt + kt}{A + ht} \tag{16}$$

and

$$S(t) = A + ht$$

In Case M, the diffuser and the spectrometer degradation depend on both E and t. In Case L, the diffuser term depends on E and t, while the spectrometer term depends on t alone.

Comparisons between the diffuser degradation using the CPH constant r(smooth) shown in Table 2.1 and the quasi-linear diffuser degradation (Case M $f=1$ is Case M1, $f=0.9$ is M2 and Case L) are shown in Figure 2.13a,b for all 12 wavelengths used in the ozone retrieval algorithm. Figure 2.14a,b shows the corresponding degradation of the spectrometer.

Using Equation 4, the different rates of the diffuser plate degradation can be used to calculate the percent change in albedo relative to the CPH formulation. Results of such a comparison are shown in Figures 2.15a,b. Each line labelled with the wavelength is the zero reference line. Case L generally has a larger albedo at the end of 8 years, while Case M has a smaller one. In terms of ozone, a negative (positive) albedo difference means more (less) ozone than the OPT model based on the CPH exponential fit would predict. (Henceforth, this will be referred to simply as

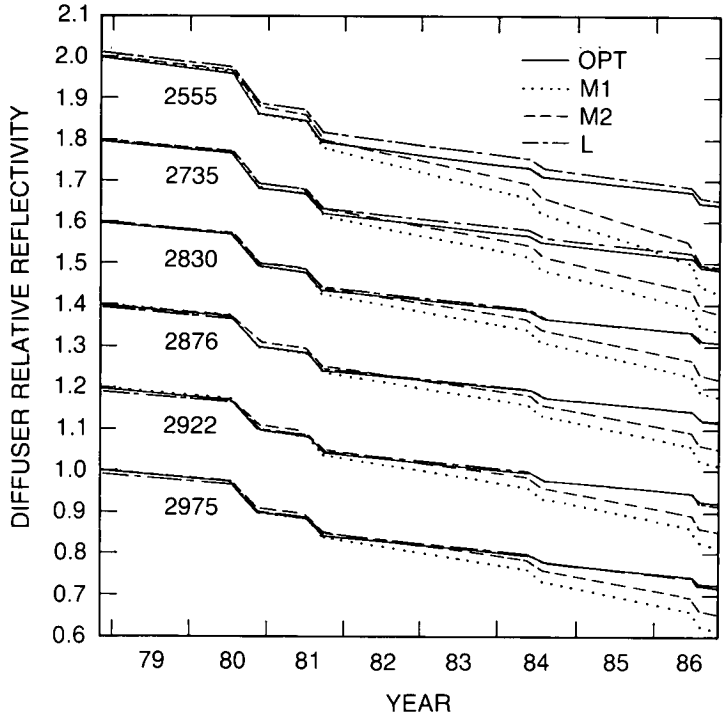

Figure 2.13a Relative diffuser reflectivity as a function of time for the OPT (CPH) and quasi-linear models, for the six shortest wavelengths.

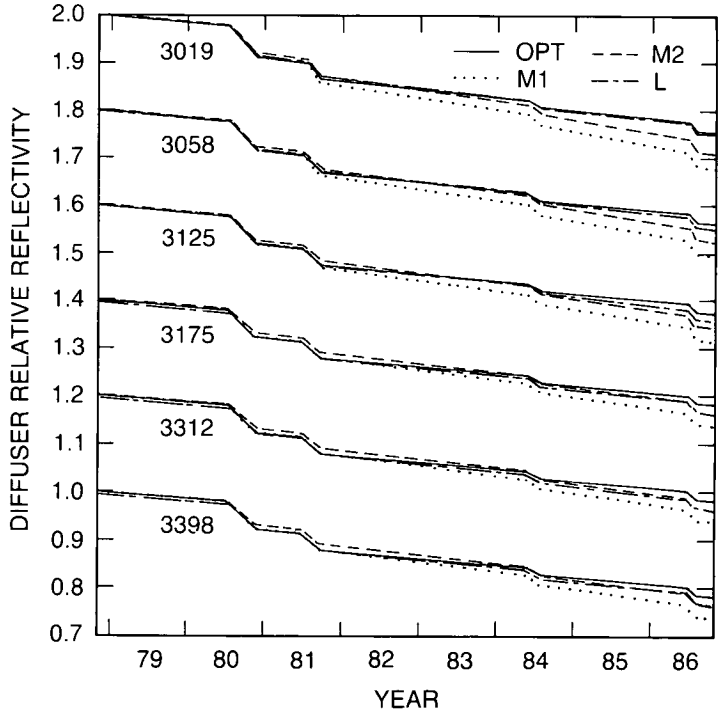

Figure 2.13b As in 13a, but for the six longest wavelengths.

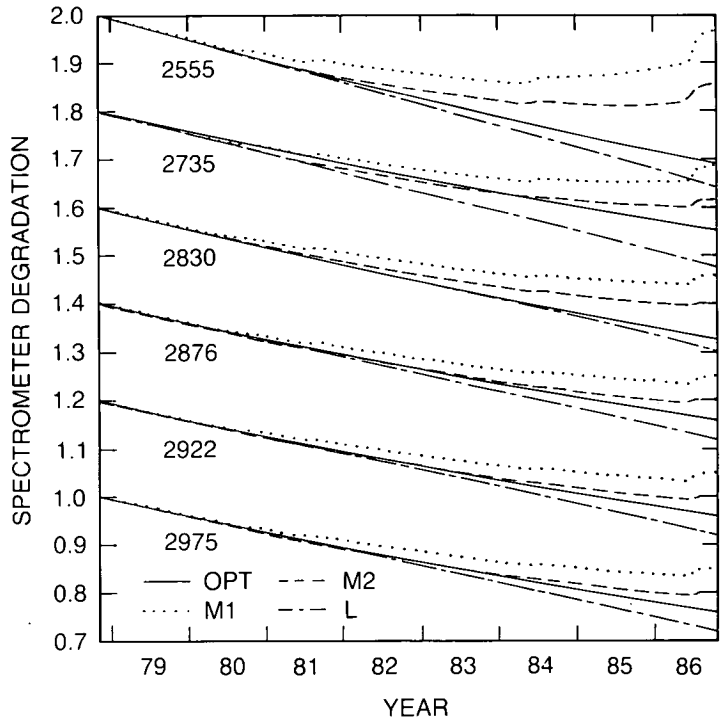

Figure 2.14a Relative spectrometer degradation as a function of time for the OPT (CPH) and quasi-linear models, for the six shortest wavelengths.

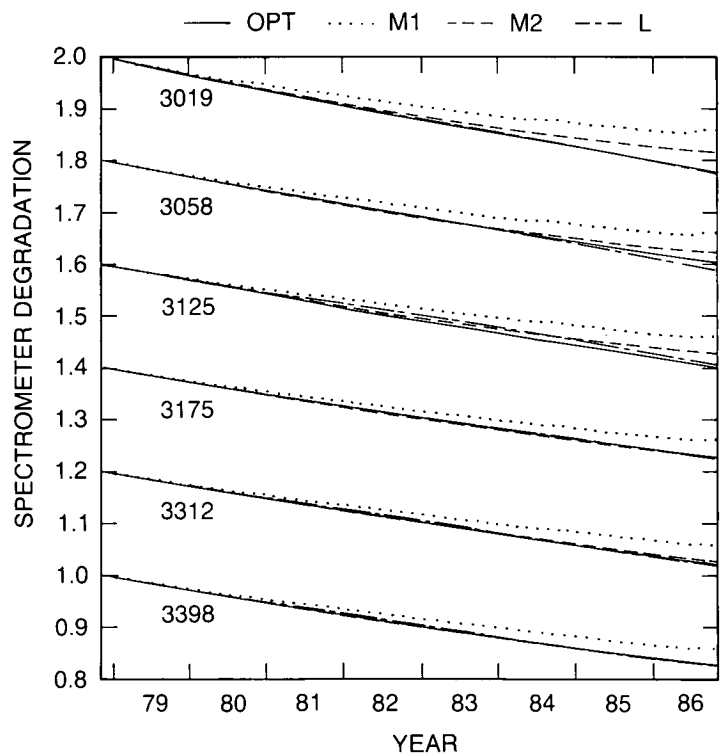

Figure 2.14b As in 14a, but for the six longest wavelengths.

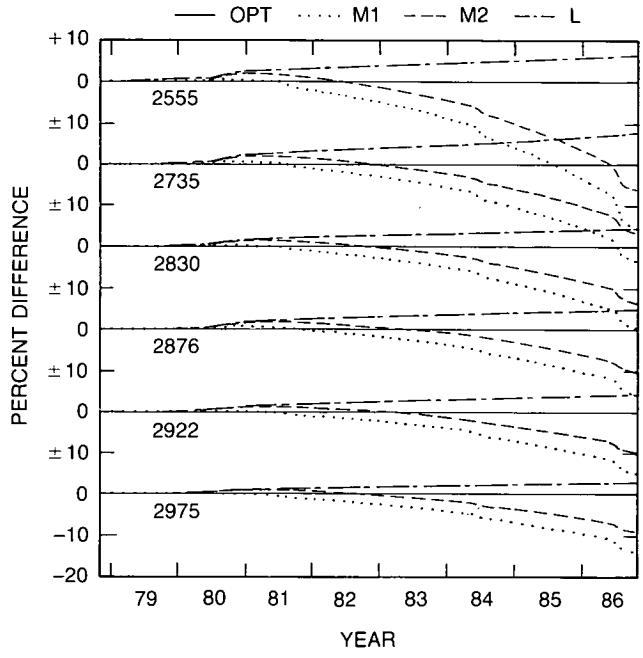

Figure 2.15a The percent difference in the calculated albedo between the quasi-linear models and the exponential (CPH) fits for the six shortest wavelengths. The exponential fit as used in the OPT model is the reference, % diff. = (model - OPT)/OPT. Each line labeled with the wavelength is the zero reference line. In terms of ozone, positive albedo difference means less ozone than the OPT exponential fit would predict. Since 0.1 units = 10%, the 273.5 nm deference for case M2 implies about 14–16% more ozone than OPT. This reduces the reported ozone decrease at 1 mb to about 5% from 1978–1987. Case M1 would yield no decrease over this period, while case L would give a slightly larger decrease than the OPT results.

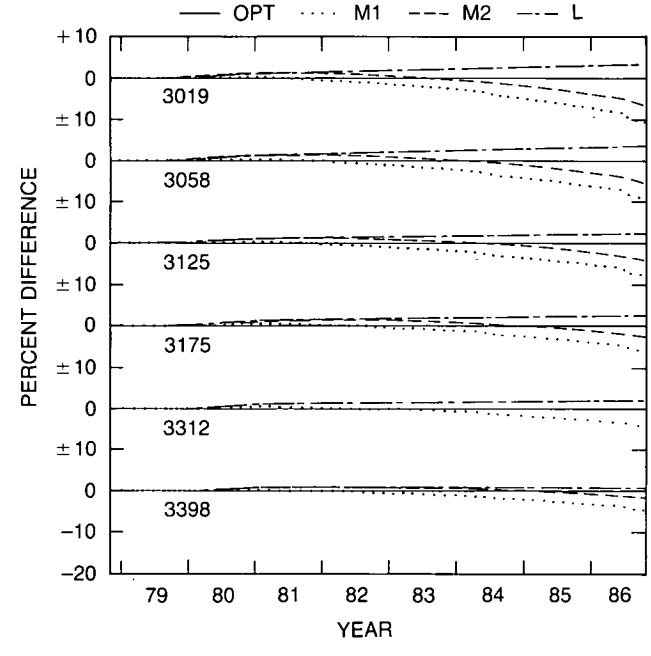

Figure 2.15b The same as 15b, but for the six longest wavelengths. Note that the longest wavelength channel, 339.8 nm, is almost independent of the model chosen to fit the degradation of the instrument or its separation into diffuser plate and spectrometer degradation. This means that the long-wavelength channels cannot be used to determine S(t) and D(t) for the shorter wavelengths (cf. Fig. 2.12).

the OPT model.) Since 0.1 units = 10 percent, the 273.5 nm difference for Case M2 implies about a 14–16 percent smaller albedo than OPT, or about 27 percent more ozone over the 8-year period. The conclusion is that the variation of albedo and ozone amounts can be very large, depending on the way the $D(t)S(t)$ product is factored. Clearly, a critical question is whether there is any way to select one separation over another.

2.3.7 Validation of Diffuser Degradation Models

Comparison With Dobson Network Results

Comparison with the Dobson network results is a way of checking the total ozone results and, therefore, the longer wavelength channels, and will be deferred to the next section, which will discuss TOMS as well. For profile data, i.e., wavelengths shorter than 312.5 nm, it has not been possible to obtain data that would distinguish between the various choices for $D(t)$ and $S(t)$. It might be expected that the inclusion of $E(t)$ in the spectrometer degradation portion of Case M would lead to structure in the radiance observed at 339.8 nm over the tropical regions of Earth. As can be seen from Figure 2.14, no structure corresponding to the frequent deployment periods is present in any of the three forms of $S(t)$, and the magnitudes are sufficiently close as to be within the experimental error. Thus, these data do not point to a preferred model.

Earthshine Data

An additional source of data was critically reviewed. This was the series of diffuser Earth-view studies, during which backscattered radiance of Earth was observed directly, and off the diffuser. The ratio of the diffuser view to the direct view gives a measure of diffuser-relative reflectivity, as other instrument sensitivities and Earth radiance cancel out. By periodically repeating the measurements, it was hoped that a time history of the relative reflectivity could be obtained, and used to compare with and check the model predictions.

The geometry of this experiment is illustrated in Figure 2.16. The diffuser was deployed continuously on December 6 or 7 in the years 1978 and 1983–1987. The data were then ratioed to the average of the direct view on the prior and following days. An example of the results for 1978 in Figure 2.17 illustrates some of the problems. The rapid rise at a subsatellite latitude near 20°N is due to the direct solar illumination of the diffuser, while the drop near 85°S suggests that the FOV is partially in an unilluminated region. However, for the region between, the latitudinal variation is not understood. This is partly because the area of the atmosphere seen by the diffuser is very large and poorly defined. The signal received must include many rays taking long paths at large zenith angles through the atmosphere. The effective backscattered radiance from the atmosphere will thus depend on the ozone amount and distribution. However, neither the complete radiative transfer problem nor the sensitivity to instrumental effects (e.g., the angular dependence of the diffuser reflectivity) has been analyzed in detail. Therefore, there may be systematic errors in the reported values, for which no estimate can now be given. In addition, there are appreciable random errors, due to cloud variability at long wavelengths and to the low signal levels (2.5 percent of the direct signal) and poor signal to noise ratios at the short wavelengths. These are at the 1–2 percent level.

At this time, only data for 1978 and 1983–1985 have been reduced. Figure 2.18a,b,c compares the model used by the OPT and quasi-linear predictions of the degradation from 1978 to 1983–1985 with the "earthshine" results. The rough magnitude and the general trend for greater degradation at shorter wavelengths agree, giving greater confidence in these features. However,

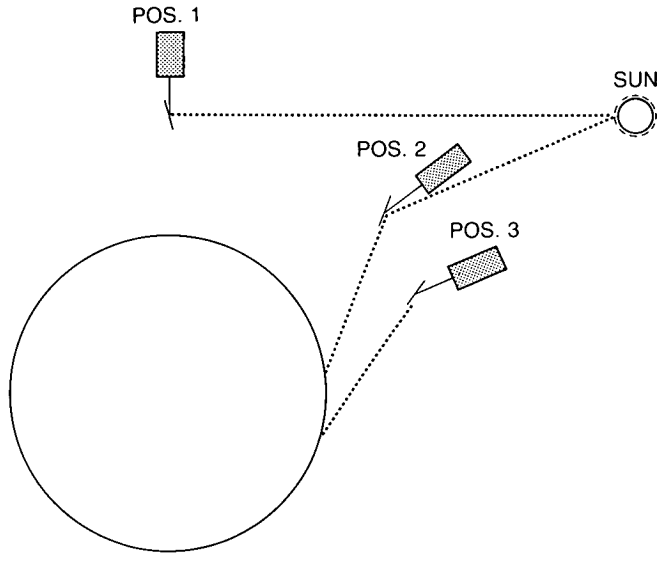

Figure 2.16 Geometry of the earthshine observations.

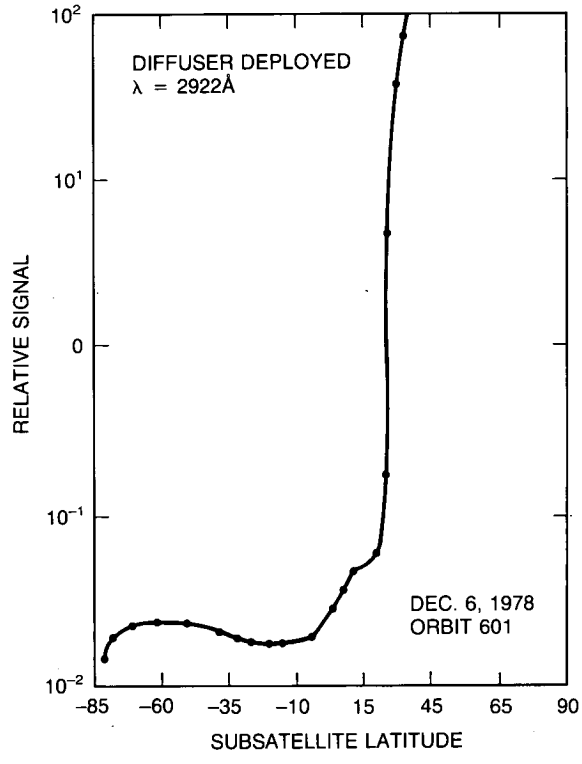

Figure 2.17 Example of ratio of earthshine signal to direct solar irradiance as a function of subsatellite latitude.

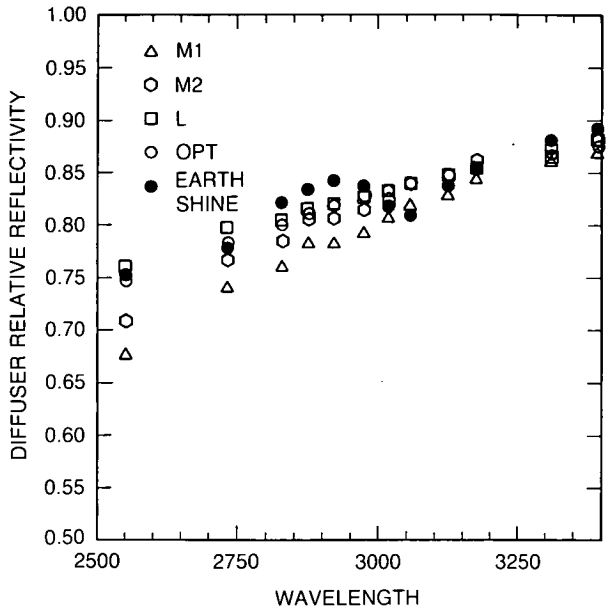

Figure 2.18a Comparison of diffuser reflectivity relative to 1978 versus wavelength, determined from earthshine measurements, and given by the models, for December 1983.

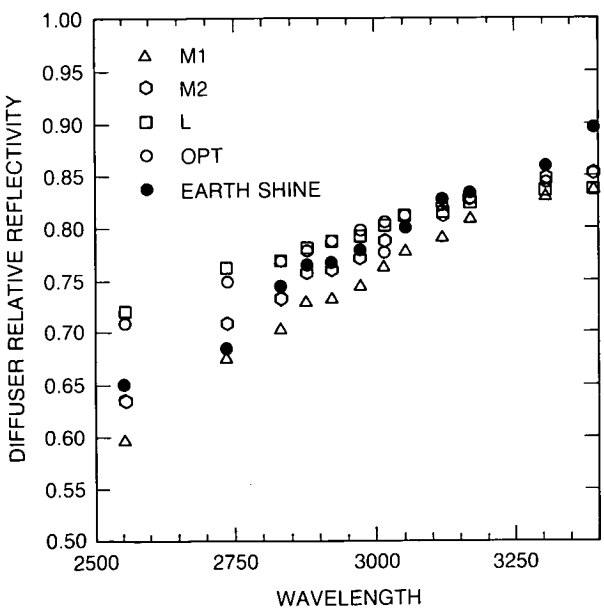

Figure 2.18b As in 18a, but for December 1984.

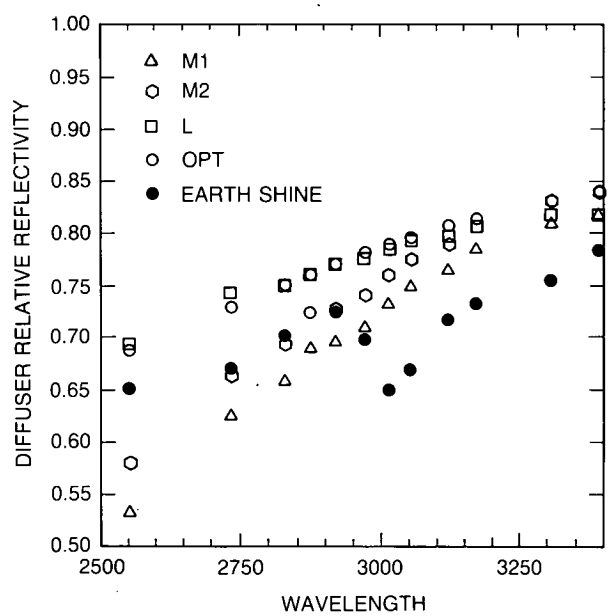

Figure 2.18c As in 18a, but for December 1985.

the earthshine results have a curious local minimum near 303 nm each year that is not suggested by the other results. Taken at face value, the "earthshine" data also indicate a faster degradation with time than either of the models, with greater degradation by 1985 than predicted by the CPH model.

However, because the interpretation of the "earthshine" values is not clear, the only conclusions that can be drawn at this time are that the earthshine data do not consistently or unambiguously favor one model over another, and perhaps disagree with all those discussed here. This could indicate that the assumption that the coefficients are constant with time is not valid. More probably they should be interpreted only as not contradicting the general magnitude and trend with wavelength derived from the models.

Total Ozone Determinations From the D-wavelength Pair

Another piece of internal information from the SBUV experiment indicates strongly that the OPT corrections for the diffuser degradations are not adequate. In a recent study, Bhartia (private communication, 1988) has compared total ozone determined from the D-wavelength pair to archived total ozone in the Tropics. Figure 2.19 shows schematically the SBUV wavelengths involved. Operationally, major reliance is placed on the A and B pairs, with C being used in high latitudes where the solar zenith angle is large and the total ozone amount is large (See Chapter 3).

The D pair uses wavelengths that are only 6.7 nm apart, compared to 18.7 nm for the A pair. Thus, if diffuser degradation is roughly linear in wavelength, the D pair should be $1/2.8 = 0.36$ times as sensitive to diffuser drift as the A pair. In addition, because the difference in ozone absorption coefficients is larger for the D pair than for the other pairs, results then are estimated to be only $1/4.5 (= 0.22)$ times as sensitive to diffuser drift than the archived "best ozone," which is based on a weighted sum of the A, B, and C pairs.

The limitation is that, because the ozone absorption coefficients at the D wavelengths are large, this pair can give results only for the small solar zenith angles, i.e., in the Tropics.

Figure 2.20 shows the difference between the archived "best ozone" and the D pair ozone, between 20°N and 20°S, as a function of time. The points in this plot are monthly averages determined each March and September and show a downward drift of the archived ozone

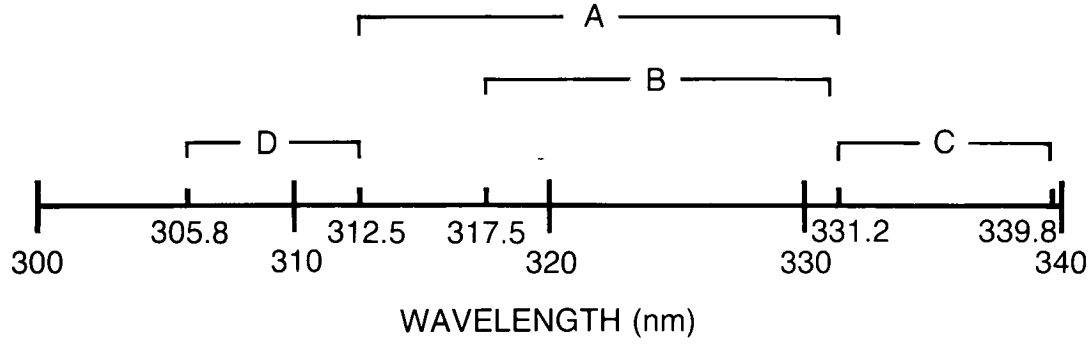

Figure 2.19 Wavelength pairs for total ozone determination.

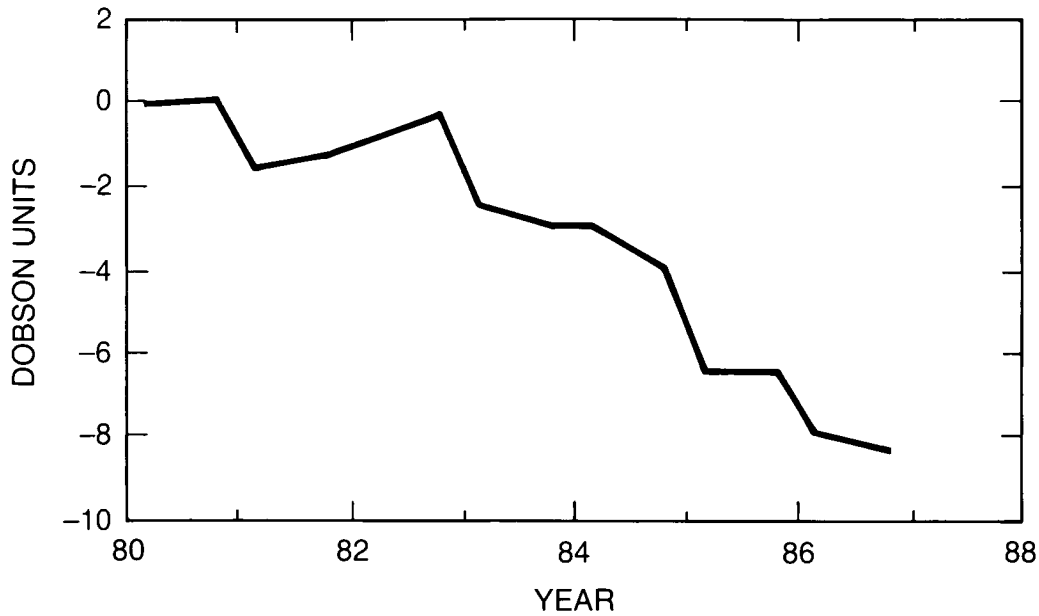

Figure 2.20 Archived SBUV total ozone minus total ozone determined from SBUV D-pair wavelengths, 1980–1987 (from Bhartia, unpublished).

relative to the less sensitive D-pair ozone. The data indicate a small drift, if any, between the archived and D-pair ozone from launch until late 1982, followed by a rapid downward drift of archived ozone. This suggests that the model used to correct for diffuser drift did not display any obvious problems for the first 4 years, but seems to have departed from the actual diffuser thereafter. The change shown in Figure 2.20 is similar to the comparison between SBUV and Dobson results in Chapter 4. This lends further support to the stability of the D-pair ozone, and to the failure of the OPT model to follow diffuser degradation very well after 1982, at least at the longer wavelengths.

2.3.8 Assessment

Section 2.3.6 has shown that a linear or quasi-linear form for the dependence of the degradation on t and E fits the observed degradation of the solar observations somewhat better than an exponential form. The form used by CPH is not only not unique, it is not as good as some others. Section 2.3.6 also pointed out that the product of $D(t)S(t)$ could be factored in an infinite number of ways, leading to large differences in the estimated diffuser reflectivity; again, the form used by CPH is not unique. Section 2.3.7 shows that there are no known data that allow a selection of one factorization over another at the short wavelengths used for ozone profile determination. Thus, the true value of any instrument change (and any ozone trend) is subject to large uncertainty.

Certainly, more complex models of diffuser and spectrometer degradation are possible, but are not amenable to verification from the available data and observing sequences used. The crucial factor is that none of the proposed models has a physical justification for its uniqueness, nor is it possible to show from the data that any one model is the only one compatible with the observations.

Values of D for the quasi-linear and OPT models after 8 years are compared in Table 2.4, along with the percent differences in D between Case M1 or Case M2 and Case L. These percent differences can be used to calculate the uncertainty in ozone change in each Umkehr layer, as described in Chapter 3. These uncertainties are plotted in Figure 2.21. Clearly, the uncertainty in the ozone amounts is quite large after 8 years, as expected from the large uncertainty in the diffuser characteristics. The uncertainties in the trends, or rate of change, are shown in Figure 2.22.

Table 2.4 Model Values of Diffuser D After 8 Years

Wavelength (nm)	M1	M2	OPT	L	Ratio 1*	Ratio 2*
2555	.4276	.4848	.6426	.6508	0.414	0.292
2735	.5349	.5814	.6875	.6977	0.264	0.182
2830	.5800	.6220	.7110	.7020	0.191	0.122
2876	.6147	.6533	.7224	.7162	0.152	0.092
2922	.6286	.6658	.7334	.7297	0.149	0.092
2975	.6469	.6822	.7458	.7346	0.127	0.074
3019	.6748	.7073	.7551	.7453	0.099	0.052
3058	.6939	.7245	.7626	.7523	0.081	0.038
3125	.7146	.7432	.7748	.7577	0.058	0.019
3175	.7362	.7626	.7830	.7649	0.038	0.003
3312	.7674	.7906	.8021	.7780	0.014	-0.016
3398	.7755	.7980	.8128	.7780	0.003	-0.025

*Ratios 1 and 2 are the differences L – M1 and L –2 M2, respectively, divided by their average value.

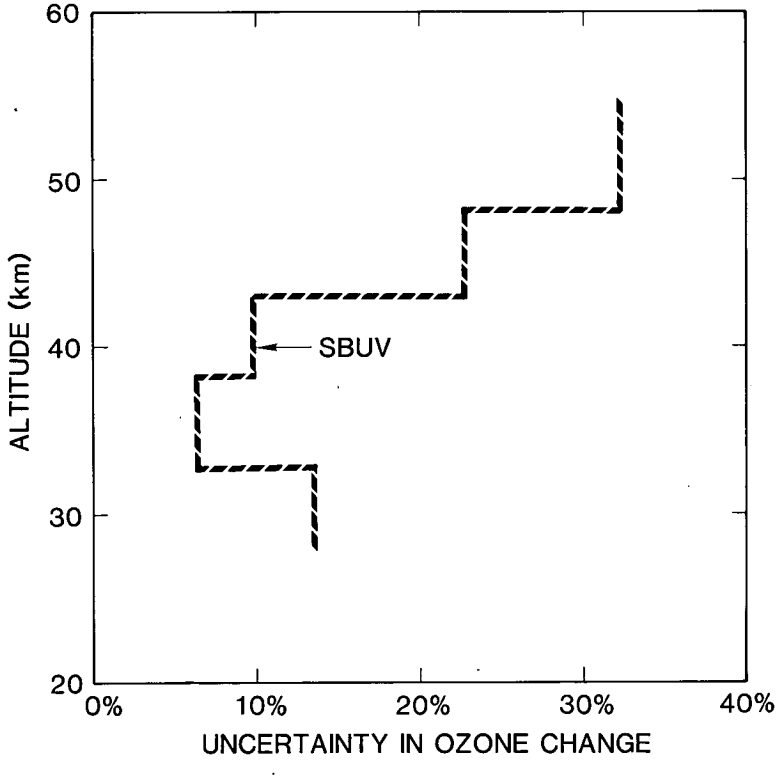

Figure 2.21 Uncertainty in ozone change determined from SBUV data over 8 years.

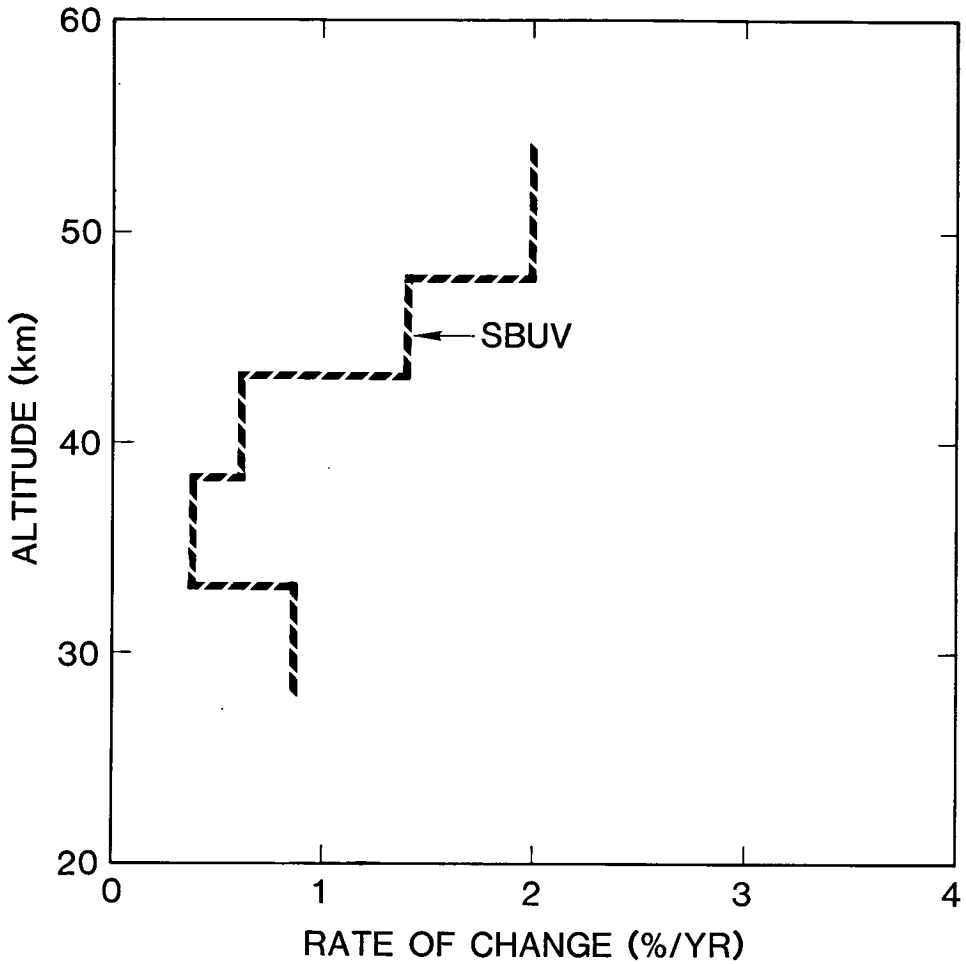

Figure 2.22 Uncertainty in rate of ozone change determined from SBUV data over 8 years.

Table 2.4 and Figure 2.18c also illustrate that the D(OPT) is close to Case L, at the top end of the range, and results in ozone values close to the minimum likely values (i.e., largest decrease). The ozone changes determined using the OPT model, and those determined from cases L, M1, and M2, are compared in Table 2.5 and Figure 2.23. Clearly, the models indicate that the change in ozone is unlikely to have been larger, and may have been considerably smaller, than suggested by the archived OPT data. In fact, there may have been no change or trend at all.

Table 2.5 Midlatitude Ozone Changes (1978–1986) for Different Diffuser Degradation Models

Umkehr Layer	OPT*	L	M2	M1
10	-25	-30	+3	6
9	-22	-24	-3	5
8	-14	-11	-7	-3
7	-9	-8	-4	0

*Different analyses and latitude ranges will lead to slightly different values for the ozone decrease.

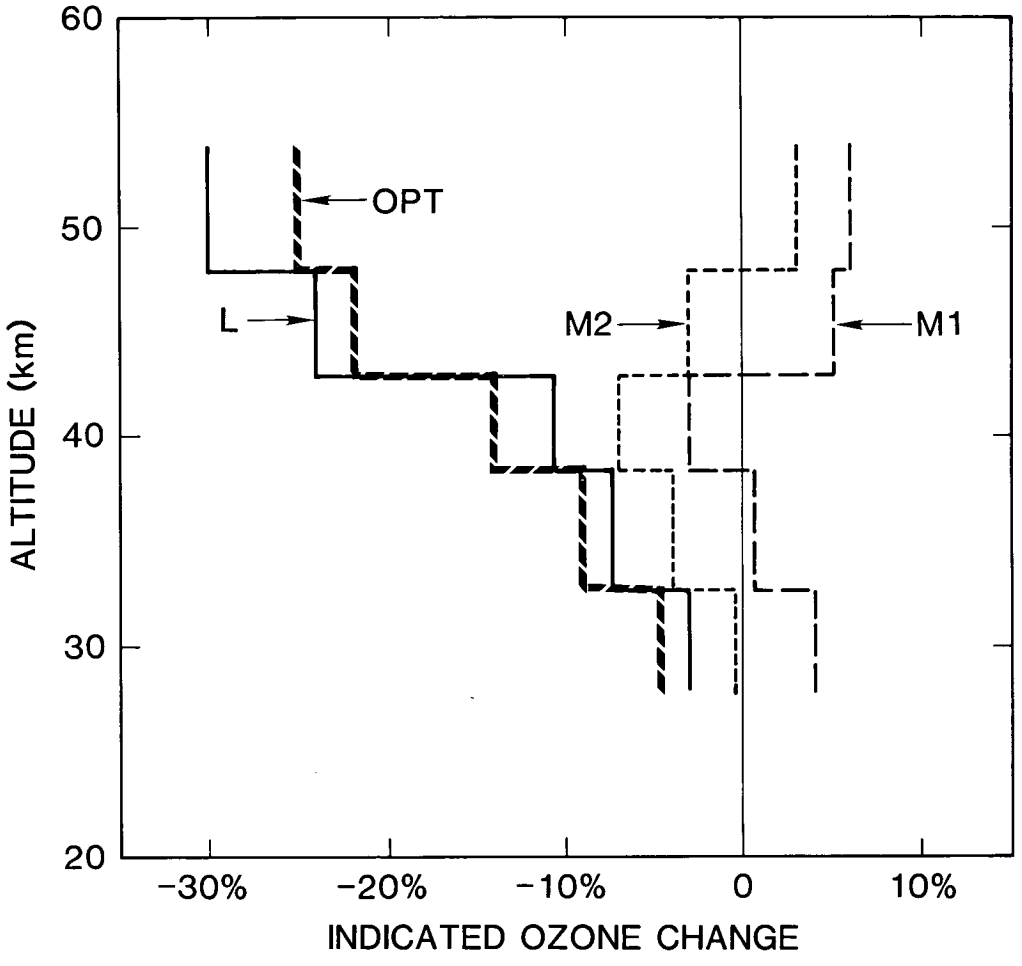

Figure 2.23 Midlatitude vertical distributions of ozone change from 1978–1986 determined from SBUV data, for several models of diffuser degradation. Curve marked OPT used the model employed in producing the data archived as of 1987. Curve L was calculated using a model with less diffuser degradation; M1 and M2 were derived using models with more diffuser degradation than the SBUV archive model.

2.4. THE TOTAL OZONE MAPPING SPECTROMETER (TOMS)

TOMS is an ozone-mapping instrument mounted adjacent to the SBUV instrument on the Nimbus–7 satellite (Heath et al., 1975 and 1978 [UG]). The primary measurement goal of TOMS is to obtain contiguous mapping of the total column ozone density on a latitude–longitude grid on the Earth's surface (Bowman and Krueger, 1985; Schoeberl et al., 1986). To achieve this, TOMS step scans across the orbital track, sampling radiation backscattered from swaths that pass from side to side through the nadir. By comparison, the SBUV observes solar radiation backscattered only in the nadir.

Although TOMS is an independent optical–mechanical ozone sensor, it shares with the SBUV the diffuser that is deployed for direct solar observations. Because the four longest SBUV wavelengths, which are used for total ozone determination, are the same as those used by TOMS, total ozone trend uncertainties for both instruments are treated in this chapter.

2.4.1 Physical Principles

TOMS employs the same measurement principle as the SBUV instrument (see Section 2.3.1). Ozone column amounts are inferred by utilizing the wavelength dependence of Earth's ultraviolet albedo at the wavelengths between 312.5 nm and 380 nm, in the region of the Huggins band of the ozone absorption spectrum. The TOMS raw data, like the SBUV, are measurements of the intensities of direct and backscattered solar UV radiation. TOMS, however, makes measurements in only six fixed wavelength channels (380.0, 360.0, 339.8, 331.2, 317.5, and 312.5 nm), the last four of which are used in pairs to provide three estimates of the total column ozone concentration by the differential absorption method. The remaining two channels, which are free of ozone absorption, are used to determine the effective background albedo. Mathematically, the measurement quantity required for the determination of the total ozone concentrations is (with reference to Equation 1),

$$\frac{I(\lambda_1)}{F_o(\lambda_1)} \Big/ \frac{I(\lambda_2)}{F_o(\lambda_2)} \tag{17}$$

with appropriate corrections for the background albedo and cloud cover. In particular, the so-called A-pair data, which are the ratios of the albedos at 331.2 nm and 312.5 nm, are analyzed to provide low-latitude total ozone concentrations. Since the retrieval of total ozone amounts from the measured raw data is determined from ratios of the albedo of Earth plus atmosphere divided by these wavelengths, the TOMS measurement technique is, in principle, capable of highly reliable determination of the ozone column. The OPT has conducted sensitivity studies that indicate that a 1 percent wavelength-dependent uncertainty in the measured albedos leads to a 1 percent uncertainty in total ozone, whereas a 1 percent wavelength-independent albedo uncertainty results in an uncertainty of only 0.3 percent in total ozone. (For a more complete discussion, see Chapter 3.)

Again, the plan for determining long-term stability is implicit. Most important, as discussed in Section 2.3 with respect to SBUV, no provision was made to monitor the reflectivity of the diffuser during flight. However, the TOMS monochromator wavelengths and the electrometers' gains have been measured during the mission. Unlike the SBUV experiment, the gain of the TOMS photomultiplier has not been monitored, on the assumption that such changes are wavelength independent and therefore cancel in the ratio of the albedos.

2.4.2 Instrument Description

Optical

TOMS measures the direct solar UV irradiance and the UV radiance backscattered by Earth's atmosphere at each of its six fixed wavelengths with a spectral pass band of 1 nm. Four of these wavelengths, those used in ground-based Dobson spectrometer ozone determination, are in common with the SBUV instrument. The principal optical components (Figure 2.24) involved in a TOMS radiance measurement are a depolarizer, mirror system for scanning the Earth "scene," monochromator, and photomultiplier. Radiation backscattered from a given Earth "scene" selected by the scan mirror is depolarized by a calcite Lyot type depolarizer (note that this is different from the SBUV depolarizer), transferred via a mirror to the entrance aperture of a single Ebert–Fastie monochromator (which is a close replica of the first monochromator of the SBUV spectrometer), and dispersed by a fixed grating onto an array of exit slits. A rotating wavelength

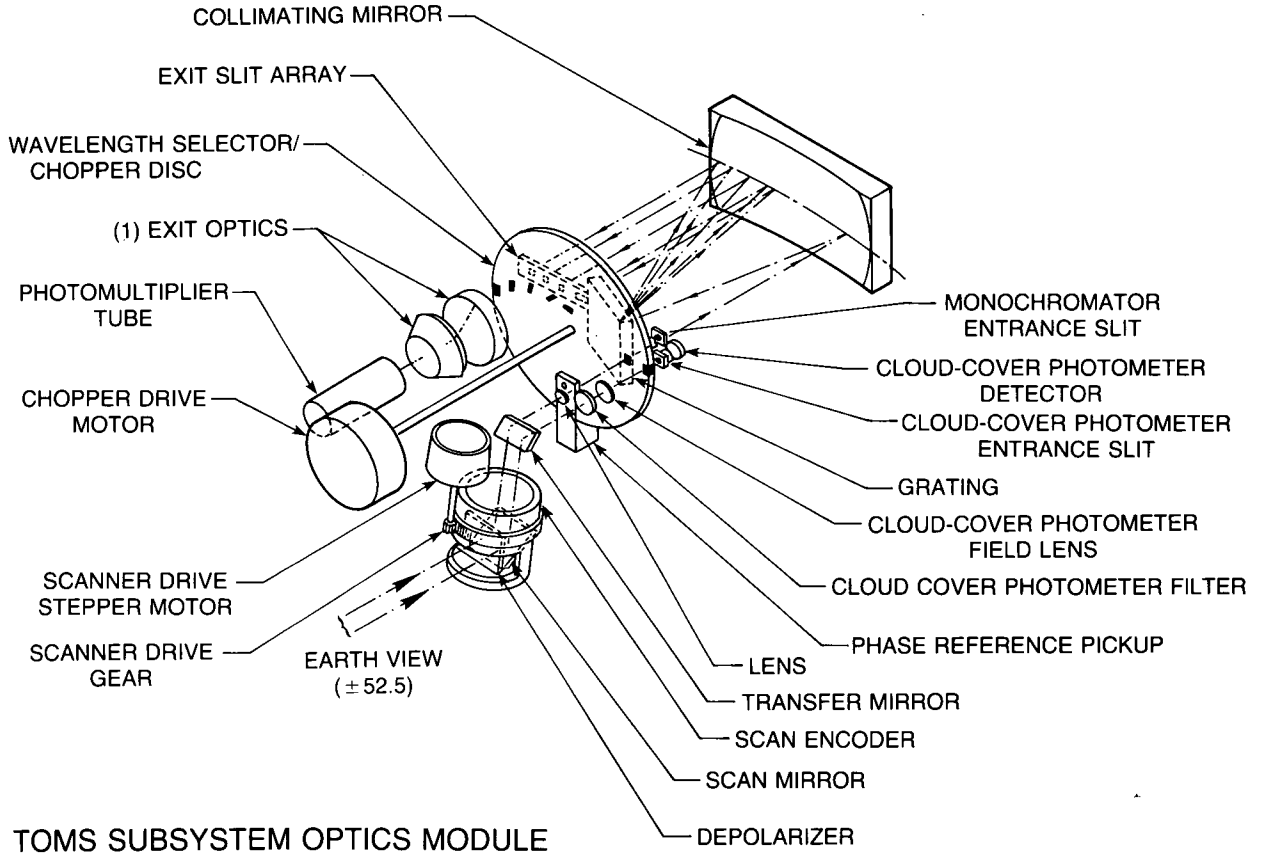

Figure 2.24 TOMS optical diagram (from Heath et al., 1975).

selector is used to gate the dispersed light from the desired exit slit to the detector, which is the same type as that used in the SBUV instrument. This same disc also chops the incident light at the entrance slit to provide dark intervals between the wavelength gates at the exit slit.

When nadir-looking, TOMS, like the SBUV instrument, views radiation backscattered by the underlying atmosphere and Earth along the track of the Nimbus–7 spacecraft. By mechanically scanning its 3° × 3° FOV (by comparison, the SBUV FOV is 11.3° × 11.3°) through the subsatellite point, perpendicular to the orbital plane, TOMS also measures the UV radiation backscattered from along a 105-degree swath (± 52.5 degrees, in 35 sequential steps of 3 degrees each) across the spacecraft track (Figure 2.25). At each scan step, TOMS measures the signal in each of the six wavelength channels. From the data acquired during these scans (achieved by a scan mirror driven by a stepper motor), a contiguous mapping of the total ozone can be created, since the scans of consecutive orbits overlap; the scan geometry provides total Earth coverage somewhat more than once per day. For direct solar irradiance measurements, which TOMS makes once per week, the same diffuser used by SBUV is deployed; TOMS views a central part of this diffuser, which SBUV views in its entirety.

Electronics/Signal Processing

TOMS has its own detector power supply, first-stage signal processing amplifier, and calibration generator. A small bias is designed into the electrometer amplifier that is additive to

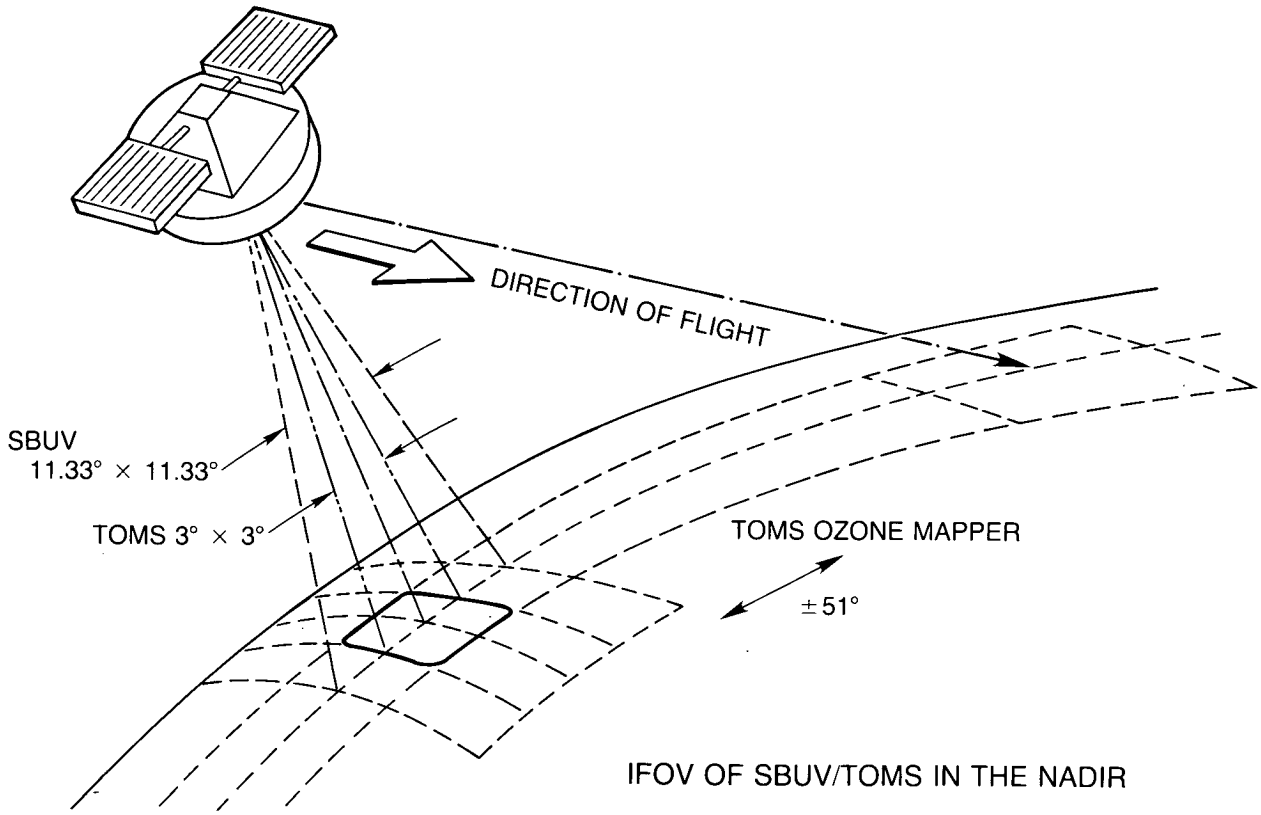

Figure 2.25 Diagram of TOMS scanning swath (from Heath et al., 1978).

the PMT dark current. This bias ensures that the electrometer signal remains onscale during the spacecraft operation lifetime, thus eliminating the need for zero correction circuits. This bias is subtracted along with the dark current by the digital demodulation techniques.

The bulk of TOMS signal processing electronics is performed by the electronics module that TOMS shares with SBUV, and is described in detail in the UG.

Operating Modes

TOMS has five scanner modes: scan off mode, single-step mode, normal scan mode, stowed mode, and view diffuser mode. These are described in the UG.

Inflight Calibration

The techniques used for inflight monitoring of the wavelength calibration of the TOMS monochromator and the gain stability of each electrometer range are described in the UG.

Scientific and Engineering Data Output

The TOMS radiance values at specified wavelengths for each instrument field of view (IFOV) along each orbit, together with housekeeping data such as the PMT bias, temperature, and diode detector bias, as well as the solar, satellite, and Earth reference data, are available on magnetic tape.

2.4.3 Prelaunch Calibration

Analogous to the SBUV prelaunch calibration (see Section 2.3.3 and the UG), TOMS calibration comprises three primary parts: irradiance and radiance radiometric calibrations and system linearity determination. The dynamic range of the TOMS signal is 10^3, and the linearity over this range is assumed to be better than 2 percent (which is the maximum measured SBUV nonlinearity). Stray light rejection is estimated to be better than 10^3, which allows the minimum signal to be measured with 1 percent accuracy. TOMS polarization sensitivity was measured prior to launch, and is discussed in the UG. Unlike the SBUV, TOMS sensitivity to diffuser angle was not determined prior to launch.

2.4.4 Results in Orbit

There is a difference of approximately 3 percent between the absolute total ozone concentrations measured just after launch by TOMS and SBUV, with TOMS data yielding the higher values. The origin of this bias is attributed to differences in the respective prelaunch absolute calibrations of the two instruments, and is not understood by the experimenters.

During the first 7 years of TOMS operation, the drift in the wavelength calibration of its monochromator was less than 0.01 nm. Consequently, the TOMS experimenters do not consider wavelength-drift-induced errors to be a significant source of uncertainty in the TOMS measurements.

The maximum electrical calibration change detected during the first 7 years of operation was less than 0.3 percent, with the typical change being less than 0.1 percent, which is within the measurement noise. Therefore, electrical calibration drift-induced errors are not considered to be a significant source of uncertainty in the TOMS measurements. However, the range 3 to range 4 gain ratio was increased by 0.55 percent after an annual oscillation of 1 percent peak to peak was observed in the ratio of the solar irradiance measurements at the A-pair (331.2 nm, 312.5 nm) wavelengths. This is an effect related to the changing angle of solar illumination of the diffuser. Although this oscillation cancels in the albedo, it compromises the determination of diffuser degradation parameters (the r values discussed in Section 2.3) from the TOMS solar signals for comparison with those determined from the SBUV solar signals (see below). Adjusting the gain ratio removed the A-pair oscillation, but had no impact on the ratios of the B (331.2/317.5 nm) and C (339.8/331.2 nm) pairs.

After the removal of the diffuser degradation, there is an overall increase in the TOMS solar and backscattered signals (e.g., 5 percent at 340 nm). In part, this is considered to be due to an overall increase in photomultiplier gain. However, this does not explain the wavelength dependence of this increased sensitivity.

Since February 1984, the chopper nonsync flag condition has occurred in approximately randomly spaced episodes. This has caused both a relative change and an increase in the scatter in the TOMS-measured solar signal. The B-pair ratio (which is used for high-latitude ozone determination) has been affected more than the A-pair ratio (used for lower latitude ozone determination). In particular, a plot of the B pair ratio vs. time (McPeters, private communication, 1987) shows that since 1984 it has oscillated between two separate values. The nonsync condition is considered to be the cause of drifts in the bias between TOMS and SBUV total ozone concentrations: from launch to 1986, the TOMS A-pair-derived ozone has drifted upwards, from

3 percent to 3.5 percent, compared to SBUV total ozone, and the TOMS B-pair-derived ozone has drifted downward, from 3 percent to less than 1.5 percent. The overall result of this is a downward drift in the bias between TOMS and SBUV total ozone concentrations of 2 percent to 3 percent at high latitudes during winter, and of <1 percent at the Equator.

2.4.5 Mechanisms of Drift

Many of the same kinds of drift mentioned for SBUV (Section 2.3.5) are also relevant to TOMS. Aside from the wavelength dependence of the diffuser degradation, two particular possible sources of wavelength-dependent drifts in the measured TOMS albedos are drifts in the wavelength calibration of the monochromator and in the electrometer gain ratios (since measurements at different wavelengths are made on different gain settings). However, both have been monitored in orbit and are not considered to be major sources of uncertainties in the measured long-term ozone trends.

Changes in instrument throughput (such as PMT gain and reflectance of optical surfaces, which may affect the measured irradiance and radiance) cancel, since the albedo is the ratio of these quantities.

Thus, the primary source of uncertainty in the long-term ozone trends reported by TOMS is the uncertainty in the reflectivity of the diffuser TOMS shares with SBUV. Changes in the wavelength dependence of the diffuser reflectivity (specifically at each of the wavelengths used to form the albedo pairs) affect the measured albedos directly, while uncertainties in the absolute reflectivity at the longer wavelengths (cf. Eck et al., 1987) generate uncertainties in the background albedo that are propagated through the data reduction algorithm (see Chapter 3). Since the diffuser degradation parameters determined from SBUV data are used in the production of total ozone values from TOMS data, the critical evaluation of the diffuser reflectivity degradation parameters, discussed with reference to SBUV in Section 2.3, is also pertinent here.

2.4.6 Estimates of Diffuser Plate Degradation Effects on Total Ozone

Calculations of diffuser degradation at the TOMS wavelengths for the models discussed in Section 2.3 are shown in Figure 2.26 and tabulated in Table 2.6. Since it is clear that the diffuser degradation is wavelength dependent, it is necessary to consider how uncertainties in the spectrum of the change in diffuser reflectivity may affect the total ozone trends derived from the

Table 2.6 Model Values of Diffuser D After 8 Years

Wavelength (nm)	D(OPT)	D (M2)	D (M1)	D (L)%	Diff. D(M1)–D(OPT)	% Diff. D(L)–D(OPT)
312.5	.7767	.7447	.7161	.7592	-8.1	-2.8
317.5	.7827	.7672	.7407	.7695	-5.5	-1.7
331.2	.8032	.7946	.7713	.7820	-4.1	-2.7
339.8	.8112	.8028	.7802	.7827	-3.9	-3.6
360.0	.8343	.8409	.8225	.8105	-1.4	-2.9
380.0	.8727	.8851	.8717	.8241	-0.11	-5.7
Ratio 312.5/ 331.2	0.9670	0.9372	0.9284	0.9708		

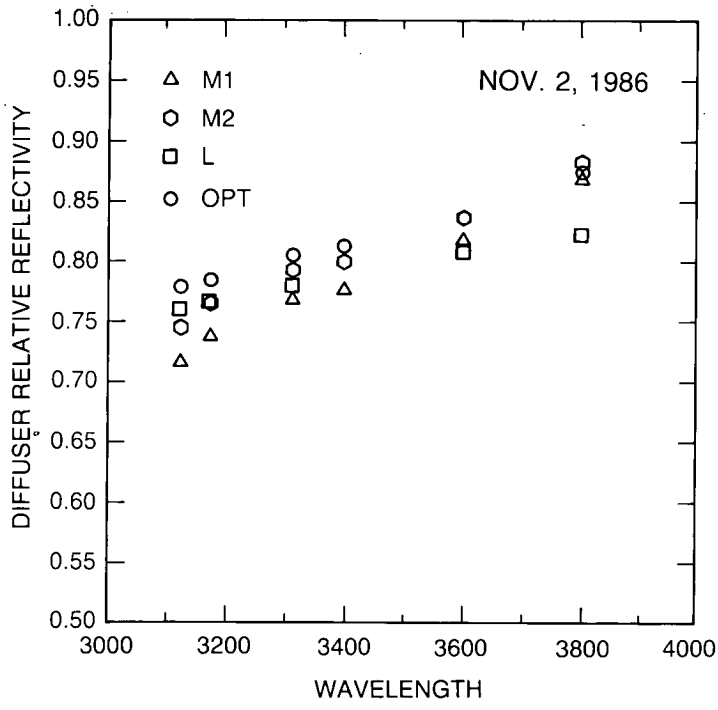

Figure 2.26 Diffuser reflectivity vs. wavelength; comparison of model predictions for TOMS wavelengths.

TOMS data. Three qualitative estimates at the A-pair wavelengths (331 nm and 312 nm) were obtained as follows:

- The diffuser degradation parameters were determined separately for four different frequent deployment periods, using the OPT model. The *r* values are shown in Figure 2.9. For there to be no associated uncertainty in the derived total ozone values, the diffuser degradation at 331 nm must remain the same, relative to the degradation at 312 nm, for each of the four determinations. However, after 650 hours of exposure (i.e., 7 years), the diffuser reflectivity at 331 nm calculated using the 1984 *r* values is 1.1 percent lower than when calculated with the 1981 *r* values (when normalized at 312 nm). This wavelength-dependent uncertainty in the measured albedos would correspond to a similar uncertainty in the derived total ozone.

- Because TOMS views one fifth of the diffuser area seen by SBUV, and does so at a larger angle, the changes in reflectivity determined for the entire diffuser surface from the SBUV data may not be completely appropriate for reduction of TOMS data. The degradation at the center of the diffuser was determined using the OPT diffuser degradation model discussed in Section 2.3.6 and the TOMS raw solar signal. The results were presented in Table 2.2; the TOMS-determined *r* values are about 2 percent higher than the SBUV-determined *r* values. The TOMS-derived values are considered to be less reliable because 1) it was not possible to correct the raw solar signal for changes in the PMT gain because this was not monitored on TOMS and 2) the angle-related annual oscillation noted above interfered with the raw signal during the frequent-deployment time period. Converting the *r* values to D's results in a wavelength-independent shift of 2.3 percent, which translates to an uncertainty of 0.7 percent in the derived total ozone. The wavelength dependence does not differ significantly from the SBUV value.

- Table 2.6 presents the D values for the various total ozone wavelengths for the quasi-linear and OPT models and the A-pair ratios after 8 years. Comparing Cases M1 and M2 with Case L indicates uncertainties of 3.6–4.6 percent in total ozone over the 8 years, or an uncertainty in the rate of change of 0.57 percent per year.

2.4.7 Assessment

Because TOMS views the same diffuser as that used by SBUV, and because the TOMS total ozone values are obtained by using diffuser degradation parameters determined from SBUV data, the long-term total ozone trends measured by TOMS are very similar to those obtained by SBUV. They cannot be considered as independent determinations of the total ozone trends. For the reasons discussed in Section 2.3, there is no information available with which to uniquely determine the partitioning of degradation between the diffuser and the spectrometer. Estimates of the relative D value uncertainties are given in Table 2.6.

An approximate value for the total ozone uncertainty can be obtained by multiplying the D value uncertainties by the sensitivity factors from Chapter 3, Table 3.1. The resulting uncertainty in total ozone, after 8 years of diffuser degradation, is given in Table 2.7.

Table 2.7 Range of Uncertainty in Total Ozone

	Zenith Angle	
	0°	51°
Case M2–Case L	+ 2.2%	+ 2.1%
Case M1–Case L	+ 3.9%	+ 3.3%
Case M1–OPT	+ 4.2%	+ 3.1%

Thus, the range of total ozone, based on the uncertainty in D values, is a few percent. The OPT values suggest the lowest values of total ozone: 4.2 percent below Case M1, or 2.5 percent below Case M2, and even 0.3 percent below Case L for small zenith angles.

Over the 8 years of data, the OPT values are decreasing 0.53 percent per year faster than M1, 0.31 percent faster than M2 and 0.04 percent per year faster than L, again for small zenith angles. Fleig et al. (1986) found OPT TOMS trends lower than the Dobson network by 0.37 percent per year. The Dobson results clearly point toward a larger diffuser degradation than that given by the OPT formula, and suggest values much closer to those given by Case M of the quasi-linear model. This also gives some support to the larger Case M degradation at the shorter profiling wavelengths discussed in Section 2.3.

2.5 THE SAGE–I AND SAGE–II INSTRUMENTS

SAGE–I and SAGE–II are both satelliteborne multiwavelength radiometers employing solar occultation techniques to determine concentrations of stratospheric aerosols and gases. Ozone profiles are determined from measurements of absorption in the most intensely absorbing part of the Chappuis band, at 600 nm. SAGE–I was launched aboard the dedicated Application Explorer Mission–B (AEM–B) spacecraft on February 18, 1979. It operated continuously for 34 months, until November 1981, when the spacecraft power subsystem failed. SAGE–II was launched from shuttle aboard the Earth Radiation Budget Satellite (ERBS) on October 5, 1984. It has operated continuously since that time without problems. Both are in approximately 600 km circular orbits

with inclination angles of 56° and 57° for SAGE–I and SAGE–II, respectively, such that the latitudinal coverage is almost identical.

2.5.1 Physical Principles

In the solar occultation technique, measurements are made of the solar radiation transmitted through the atmosphere as the Sun sets behind it.

Mathematically, the atmospheric transmission value $T_\lambda(h)$ at tangent height h and wavelength λ is expressed as a ratio between the solar radiance observed within the atmosphere to the radiance outside the atmosphere as

$$T_\lambda(h) = I_\lambda(h)/I_{o\lambda} \tag{18}$$

where $I_\lambda(h)$ is the solar radiance at wavelength λ observed at tangent height h and $I_{o\lambda}(h)$ is the measured extraterrestrial solar radiance at λ. Ozone concentration profiles can then be retrieved from the atmospheric transmission profile as described in the algorithm chapter or by Chu and McCormick (1979), Mauldin and Chu (1982), or Chu (1986).

The measured data at the different wavelength channels are converted to transmission values by ratioing a scan across the Sun, obtained when the FOV is transversing the atmosphere, to a reference Sun scan. The reference Sun scan for each channel is obtained from the high-altitude scans with tangent altitudes above 100 km, where no atmospheric attenuation is present. Tangent altitudes of the measured data were previously determined differently for SAGE–I and SAGE–II. The SAGE–II algorithm used spacecraft and solar ephemeris data to calculate tangent altitudes, while the SAGE–I algorithm determined the tangent altitude by fitting the calculated Rayleigh transmission with the short-wavelength channel measurements. For the purpose of these studies of ozone trends, SAGE–I data have been reinterpreted using tangent altitudes determined in the same way as they were for SAGE–II.

It is important to note that the measurements performed by SAGE–I and SAGE–II are self-calibrating, in that only atmospheric transmission or relative radiance measurements are required to determine the concentration of atmospheric species such as ozone, and, therefore, no absolute radiance calibration is performed. The only requirement is that the instrument with all its various components retain constant responsivity for the duration of each measurement event—i.e., a spacecraft sunrise event or sunset event. A typical measurement event duration is about 100 seconds, in which time the instrument configuration is kept nearly constant except for the scan mirror, which views the Sun at an elevation angle that varies slightly with time. The primary consideration is, thus, to keep the instrument at a constant temperature such that no thermal drift can occur during the measurement events.

2.5.2 Instrument Summary

Both the SAGE–I and SAGE–II instruments share the same design, illustrated in Figure 2.27, with similar optical components. Each instrument is composed of three major subsystems, i.e., a scanhead assembly, a telescope, and a spectrometer. The scanhead assembly consists of a scan mirror together with a Sun-presence sensor and an azimuth Sun sensor. The telescope is a spherical Cassegrain with a 152.4 cm effective focal length and an f-number of 30. The telescope is mounted in a graphite–epoxy composite telescope barrel to minimize thermal effect. The spectrometer consists of a concave holographic grating with detector assemblies located at the

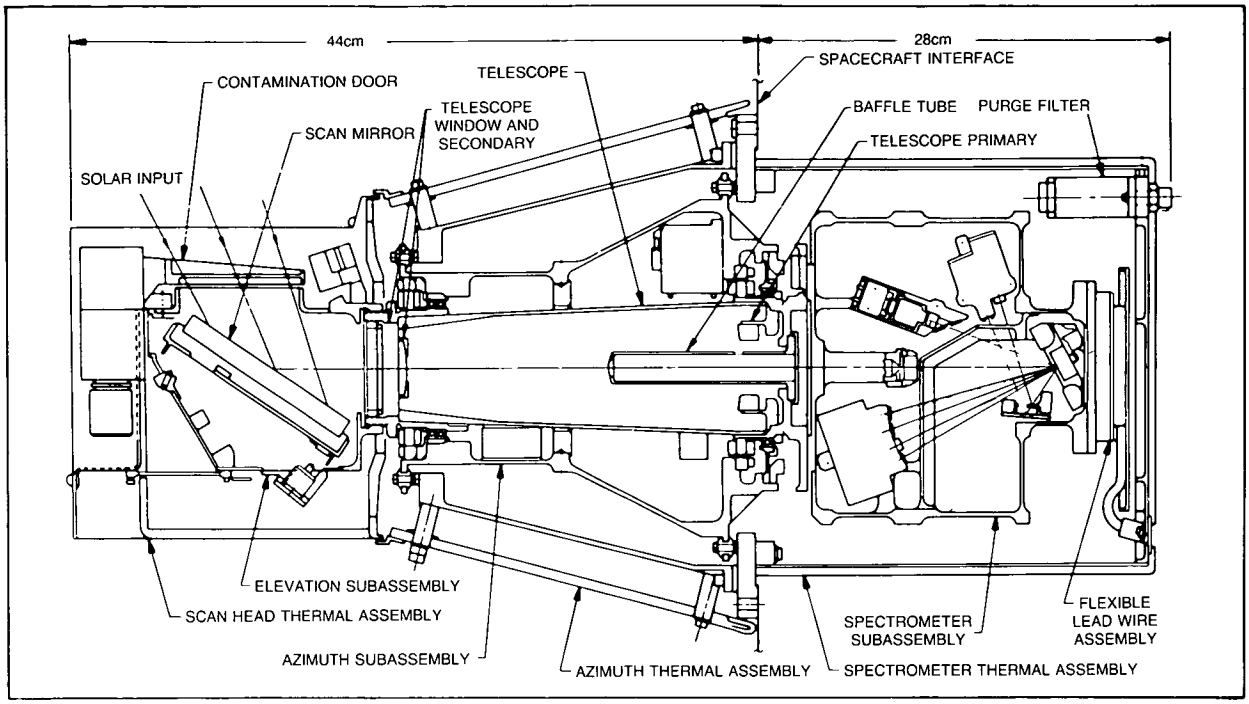

Figure 2.27 SAGE–II sensor assembly (from Mauldin et al., 1985a,b).

zero- and first-order reflection of the grating. The difference between SAGE–I and SAGE–II instruments is primarily in the number of spectral channels employed. For SAGE–I, there were four spectral channels at 1.0, 0.6, 0.45, and 0.385 micron center wavelength, with silicon photodiode detectors located at the first-order reflection of the grating on the Rowland Circle. For SAGE–II, there are seven spectral channels at 1.02, 0.94, 0.6, 0.525, 0.453, 0.448, and 0.385 microns. All of the channels use silicon photodiode detectors, with five located on the Rowland Circle, while the 0.94 and the 0.453 micron channels are situated at the zero-order reflection of the grating. The SAGE–II spectrometer layout is shown in Figure 2.28. The spectral bandwidth for the four channels on SAGE–I was about 30 nm. For SAGE–II, all the channels have a bandwidth of 15 nm except for the 0.448 and 0.453 micron channels which have bandwidths of 2 and 3 nm, respectively.

Another difference between SAGE–I and SAGE–II instruments is the scan mirror coating. SAGE–II uses a simple quartz-coated silver substrate mirror, while SAGE–I used a multilayer dielectric-coated silver mirror that was specially designed for minimizing the change in reflectivity across the scanning angular range. Both coatings were designed to produce changes in reflectivity of not more than 0.1 percent per degree mirror rotation over the operational angular range. Preflight measurements were not sufficiently accurate to verify the designed specifications, but placed an upper bound of 0.5 percent change per degree mirror rotation.

Detailed descriptions of the SAGE–I and SAGE–II instruments have been given elsewhere (McCormick et al., 1979; Mauldin et al., 1985a,b). A comparison of the characteristics of the two instruments is shown in Table 2.8.

During each spacecraft sunrise or sunset event, the instrument is activated when the Sun-presence sensor indicates a Sun intensity of at least 1 percent relative to the unattenuated

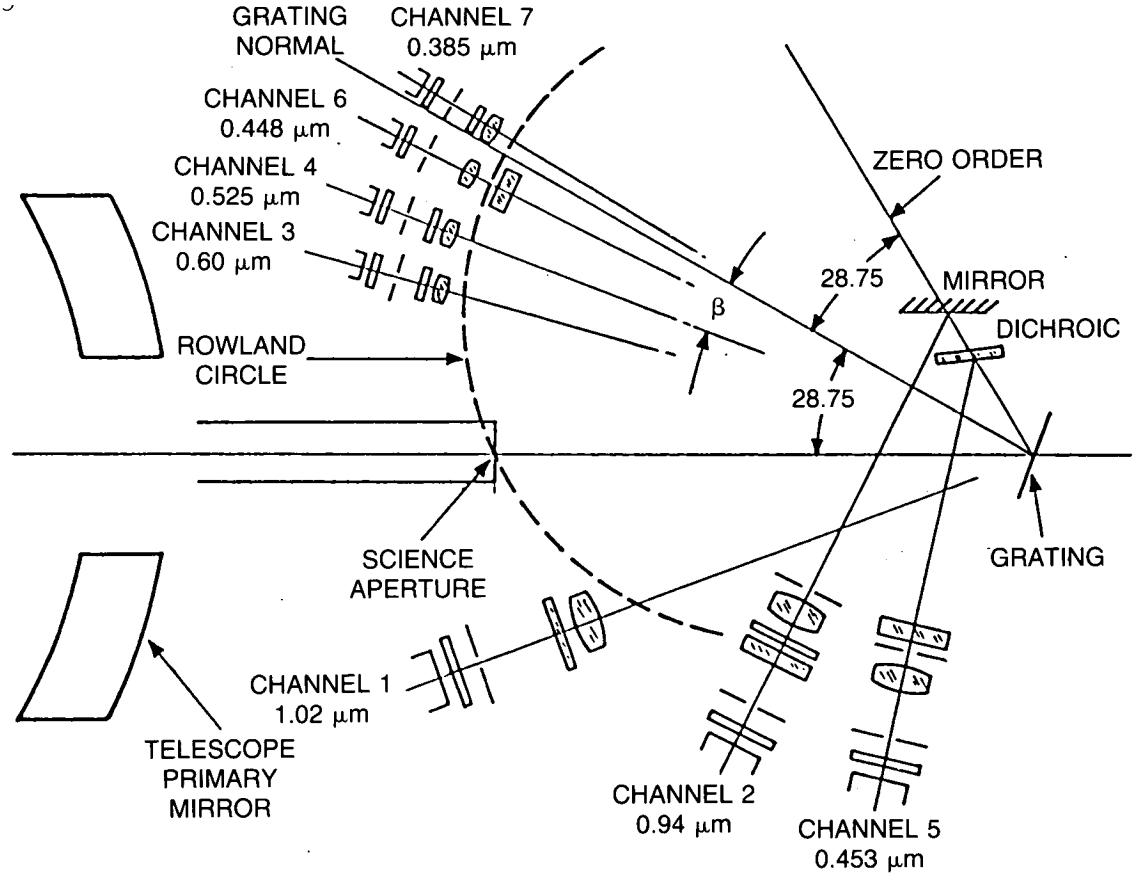

Figure 2.28 SAGE–II spectrometer layout (from Mauldin et al., 1985a,b).

Table 2.8 Sage Instrument Characteristics

Subsystem	SAGE–I	SAGE–II
Telescope	5.1 cm dia F/30 cassegrain	5.1 cm dia F/30 cassegrain
Scan Rate	15′/sec	15′/sec
Instantaneous Field of View	0.5′ dia.	0.5′ elevation 2.5′ azimuth
Azimuthal Pointing Accuracy	0.5′	0.5′
Sample Rate	64/sec (4/km)	64/sec (4/km)
Wavelength Separation (at 600 nm)	Holographic Grating Spectrometer 30 nm	Holographic Grating Spectrometer 15 nm
Detector	Silicon Photodiode	Silicon Photodiode

Sun. The instrument then searches for and locks onto the Sun in azimuth within 1′ of the radiometric centroid. The scan mirror fast scans (3°/s) in elevation until the Sun is acquired in elevation, then it scans vertically across the face of the Sun at a rate of 15′/s, reversing itself each time a Sun limb crossing occurs. Figure 2.29 illustrates a typical data-taking sequence for a sunset event. The two solid lines denote the image position of the top and bottom of the solar disk as viewed from the spacecraft with atmospheric refraction properly included. The left vertical ordinate denotes relative angle measured from the spacecraft coordinate system in arc-minutes, while the right vertical ordinate denotes the corresponding vertical tangent altitude. The horizontal abscissa denotes event time in seconds for nominal orbital geometry. The dashed line represents the up-and-down scan of the IFOV with respect to Earth's horizon. Radiometric data for each channel are sampled at a rate of 64 samples per second.

2.5.3 Prelaunch and Inflight Instrument Characterization

Both SAGE–I and SAGE–II instruments underwent extensive preflight testing. Component and system-level tests that were performed include scan mirror reflectivity, telescope modulation transfer function, grating efficiency, detector spectral response, detector response temperature sensitivity, spectrometer wavelength calibration, individual channel spectral bandpass (in-band and out-of-band) responses, stray light test, scan mirror linearity test, and full-Sun scan on the ground. Considerable effort also went into the setting of the gain for both SAGE–I and SAGE–II instruments to ensure that the full-scale count level for each channel would be neither saturated nor too low.

As stated previously, absolute calibration of the measured radiance is not necessary since all the measurements are nearly self-calibrating. To reduce any thermal change during the measurement, large thermal inertia has been built into the hardware; both instruments have demonstrated less than 0.3 K change in temperature during measurement events.

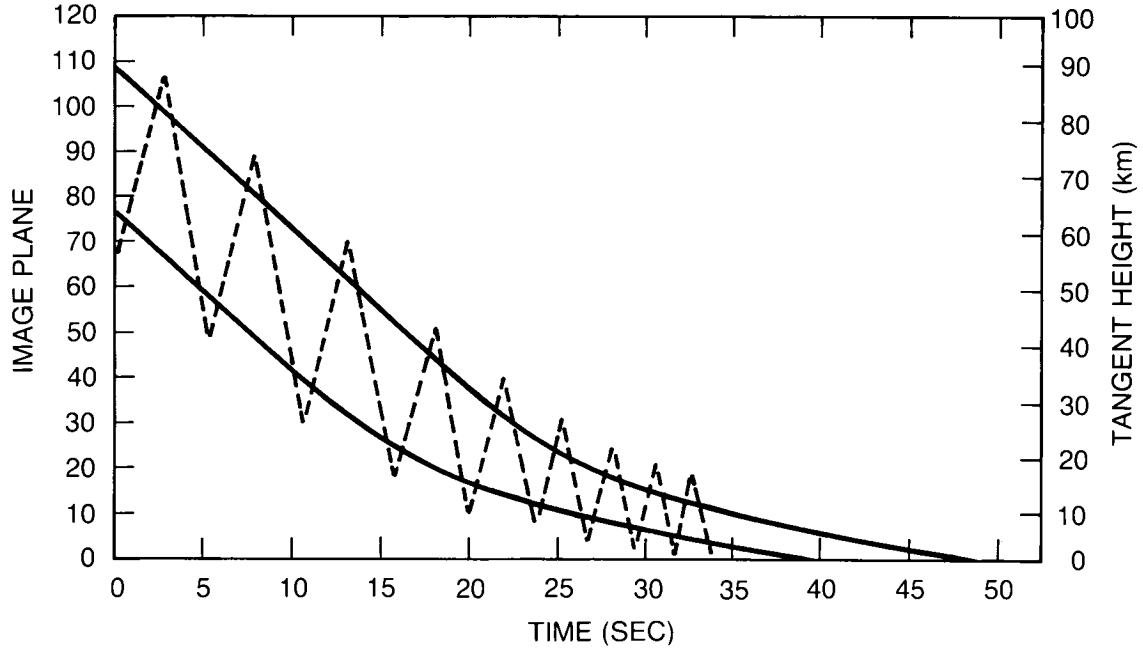

Figure 2.29 Data acquisition mode for solar extinction experiment during sunset event (from Mauldin et al., 1985b).

Changes in mirror reflectivity with angle during the occultation are also a potential source of error. For SAGE–II, a simple quartz coating over a silver substrate was used; the ERBS spacecraft is periodically turned upside down so that the scan mirror reflectivity can be tested across its entire angular range using the unattenuated Sun. Results of the measurements have been used to correct the radiance data for any change in reflectivity with mirror angle. These corrections, however, are very small (between 0.02 to 0.1 percent per degree).

The coating for SAGE–I is a multilayer dielectric over a silver substrate designed to minimize the change in reflection versus scan angle. Inflight testing of the SAGE–I scan mirror over the observing view angles was not possible, however, because the spacecraft could not be maneuvered to view the unattenuated Sun at all scan angles. The SAGE–I scan mirror did measure the unattenuated Sun from tangent height of 100 km to about 250 km. By analyzing the scan mirror reflectivity over the restricted angular range, and assuming linear extrapolation is justified, the results suggest that the SAGE–I scan mirror reflectivity change with angle for the ozone channel is about the same as the SAGE–II scan mirror.

2.5.4 Sources of Error in Ozone Profiles Derived From the SAGE–I and SAGE–II Measurements

This section has been generated from a careful study of all error sources in both the measurement and retrieval processes. Most error sources considered here can be quantified with careful analyses of the known engineering parameters or other measurement parameters. If insufficient information was available for assessing the uncertainty magnitude, then a conservative approach was taken to estimate the error. For error parameters that could be magnified by propagation through the retrieval process, the sensitivity of the retrieved ozone accuracy to those error sources was then determined by a simulation and retrieval study.

The characteristics of the error sources can generally be classified into two distinct categories: systematic and random components. Accuracy in trend determination is usually limited only by the magnitude of any varying part of the total systematic error, and should not be susceptible to the random-error component. However, random-error is unimportant in trends determination only if sufficient sampling of the measurements can be obtained such that the averaging process (or any other statistical means) can be used to reduce the random-error component to an insignificant level. There is also an error component that is partly random and partly systematic. An example of this type of uncertainty is errors with long correlation times. The effect of this type of error for measurements with limited sampling is difficult to assess unless the complete statistic of the error is known. It is possible that the uncertainty in reference height determination for the SAGE–II algorithm belongs to this type of error.

In the following, individual error sources for the SAGE–I and SAGE–II ozone measurements are discussed, and the derivation of the ozone sensitivity factors is explained. The ozone error sensitivity factors discussed here apply only to the retrieved ozone concentration versus geometric height data, and not to any other derived parameters such as ozone-mixing ratio on pressure levels.

Ozone Absorption Cross-Section Error

The ozone Chappuis band absorption coefficient data used in the SAGE–I and SAGE–II processing are those measured by Penney (1979). The precision of the absorption data was estimated by the experimenter to be about 2 percent. However, the room temperature Hg line

measurements in the UV at 296.7 nm and 302.15 nm showed a 6 percent difference from Hearn's (1961) results. Thus, the ozone cross-section values used by SAGE–I and SAGE–II could be associated with a 1σ error of 6 percent.

There is also an uncertainty of 0.5 percent in the Rayleigh cross-section used at 600 nm, which is insignificant compared to the ozone cross-section error. Neither of these varies with time.

Scan Mirror Calibration

Calibration of the SAGE–II scan mirror reflectivity versus angle was possible during the spacecraft pitch 180° exercise (spacecraft titled upside down in orbit). The resulting data have been least-squares fitted to determine the linear coefficients for the correction of mirror reflectivity with scan mirror viewing angle. In all seven channels, the data show small reflectivity changes with angle, and the estimated errors on those coefficients are about the same order of magnitude. To assess the sensitivity of the retrieved ozone to the scan mirror calibration factors, a typical measurement event has been processed with and without the scan mirror reflectivity correction factors. The difference between the two retrievals is illustrated in Figure 2.30, showing a small difference below 40 km altitude and about 1 percent difference above 45 km altitude.

For SAGE–I measurements, scan mirror calibration was impossible to perform in orbit. The only way to assess the scan mirror reflectivity change is by analyzing the mirror reflectivity when the Sun is high above the atmosphere. Using mirror reflectivity data between 160 km and 100 km tangent altitude, no observable change was found. Assuming that one can extrapolate the mirror reflectivity behavior to viewing angles corresponding to atmospheric heights, one should expect very small changes in mirror reflectivity. Therefore, a doubling of the error for SAGE–II scan mirror reflectivity uncertainty has been assigned to the SAGE–I scan mirror reflectivity change.

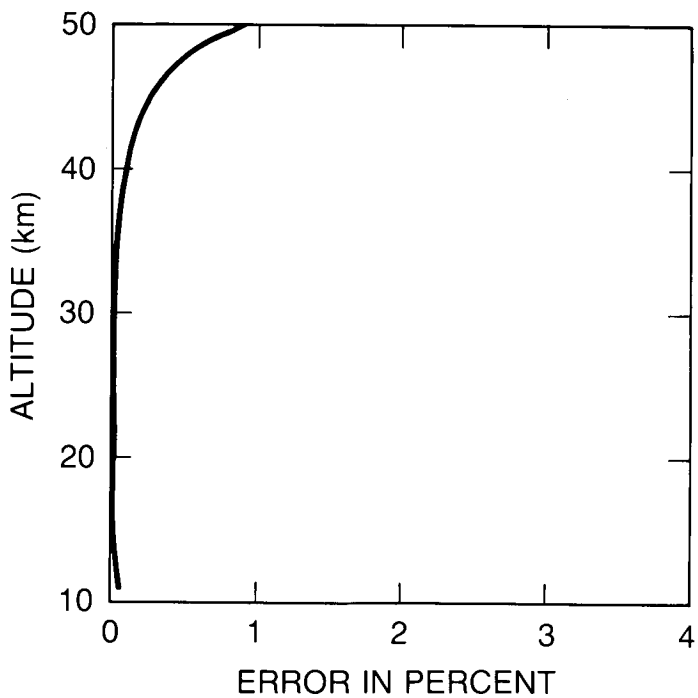

Figure 2.30 Sensitivity of ozone retrieval to variation of scan mirror reflectivity variation with angle.

Aerosol Interference

Due to the overlapping of aerosol signature in the ozone channel at 600 nm, a small residual aerosol contamination of the ozone profile at heights where high aerosol concentrations occur could exist. Error analyses based on simulation and retrieval studies of the aerosol interference in the SAGE–II ozone profile have been performed for typical 1985 aerosol profiles (Chu et al., 1989). The results indicated that, for altitudes above the aerosol (typically above 25 km), aerosol interference in the ozone profile is insignificant. However, for altitudes below 25 km, where the aerosol content is high, up to a 4 percent error in the retrieved ozone could be contributed by the aerosol signature. A similar study on the SAGE–I measurements shows approximately the same size error, even though the aerosol content during 1979–1981 was lower by a factor of five. This is caused by the inaccurate characterization of the aerosol extinction versus wavelength behavior obtained when only SAGE–I's two wavelength channels for determining aerosol properties are available.

Reference Height Uncertainty

Due to the high vertical resolution of the SAGE measurements, the sensitivity of the retrieved ozone profile to height determination becomes important. Figure 2.31 shows a simulation and retrieval study of the ozone profile sensitivity to reference height error. Based on an error study on the determination of reference height from the calculation of orbital and solar ephemeris data (J. Buglia, unpublished report, 1987), it is estimated that the SAGE–II reference height error is approximately 0.2 km, and for SAGE–I it is about 0.35 km. However, the SAGE–I processing algorithm also included a slight adjustment on the reference height by fitting the measured atmospheric airmass data to those computed from the National Meteorological Center (NMC) temperature-versus-height data. Thus, the reference height error on SAGE–I should be approximately the same as the SAGE–II error, even thought the statistic of this error for the two experiments will be very different because of the readjustment process in the SAGE–I algorithm.

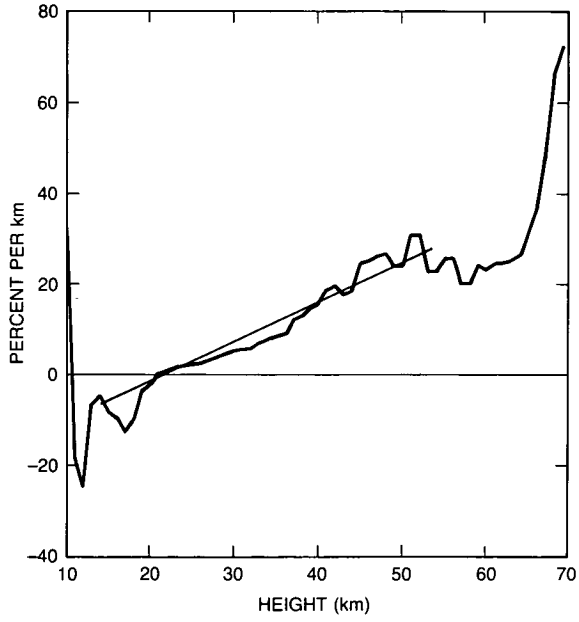

Figure 2.31 Sensitivity of SAGE–II ozone retrieval to reference altitude errors (%/km), as a function of altitude.

In comparing SAGE and SAGE–II ozone data, a possible systematic error component could exist due to the different reference height determination schemes applied to the two satellite systems. These errors arise partly from offsets in the NMC data sets used between the SAGE–I and SAGE–II time frames, and partly from an offset between the NMC data and the ephemeris data. Preliminary results from the analyses of the SAGE–I and SAGE–II data indicated that this error is small and is bounded by a maximum height difference of 60 meters. This would introduce at most a 1 percent systematic error in the SAGE–I to SAGE–II ozone comparison at about 40 km altitude and makes no significant contribution to the total error when root-mean-squared with other error sources. In addition, according to Buglia (unpublished report, 1987), the errors on the SAGE–II reference height calculated from the ephemeris data are generally correlated over a 7-day period coincident with the periodic updating of the spacecraft orbital tracking data. This would imply that the reference height errors on SAGE–II can be treated as systematic errors for ozone data covering spans of approximately 7 days, and can be treated as random errors for data covering spans of several weeks or more.

Random Error

The random errors for the retrieved ozone consist of contributions from the measurement errors of the atmospheric transmission data, the Rayleigh component calculated from the NMC temperature-versus-height data, and random error contributed from the aerosol measurements. Aerosol analyses based on the propagation of uncertainties in the SAGE–I ozone retrieval (Chu et al., 1989) have been used to estimate the precision of the SAGE–I and SAGE–II ozone profiles. It is found that the measurement error is the dominating source of uncertainty in limiting the precision of the SAGE–I and SAGE–II ozone values to a level of about 10 percent between cloud top to 60 km (SAGE–II), and to 50 km (SAGE).

Budget for Trend Errors in SAGE–I and SAGE–II

Combining the independent systematic errors cited above in the first four items results in the total errors shown in Table 2.9 and plotted in Figure 2.32. (The more conservative altitude registration error of 0.35 km is used for SAGE–I.) These are the values relevant in a comparison with other instruments. However, these are dominated by the constant ozone cross-section error. Removing this, and considering that the mirror or altitude registration error could vary by the amounts indicated over 2 years, gives the uncertainty in observed changes, which are also shown in Table 2.9 and in Figure 2.33. These are dominated by altitude registration uncertainties, which seem more likely to be random than characterized by a trend, so these errors, too, are probably conservative.

It should be emphasized that these errors do not necessarily represent the changes that could be seen by SAGE–I and SAGE–II over their 2-year periods of operation. To determine such a change requires a sufficiently large number of observations at a given location under similar seasonal conditions, with a meteorological situation that allows a representative longitudinal average to be obtained. The limited data taken by SAGE–I or SAGE–II do not necessarily fulfill these conditions. The numbers in Figure 2.33 should be regarded as suggestive. However, as SAGE–II continues in operation, the same total errors will apply over a longer period with more data and, presumably, improved sampling, allowing it to observe any changes of this magnitude.

Table 2.9 Errors of SAGE–I and SAGE–II (all errors in percent)

Altitude	Ozone Abs. Cross-Section	Mirror	Altitude Registration	Aerosols	Total Error	Error in Changes
			SAGE–I			
20	6	0	0	4	7.2	4
25	6	0	1.5	1	6.3	1.9
30	6	0	2.9	.5	6.7	2.9
35	6	.1	4.4	.2	7.4	4.4
40	6	.2	5.8	0	8.3	5.8
45	6	.5	7.3	0	9.5	7.3
50	6	2	8.8	0	10.8	9.0
			SAGE–II			
20	6	0	0	4	7.2	4
25	6	0	.8	1	6.1	1.3
30	6	0	1.7	.5	6.3	1.8
35	6	.05	2.5	.2	6.5	2.5
40	6	.1	3.3	0	6.8	3.3
45	6	.25	4.2	0	7.4	4.2
50	6	1	5.0	0	7.9	5.1

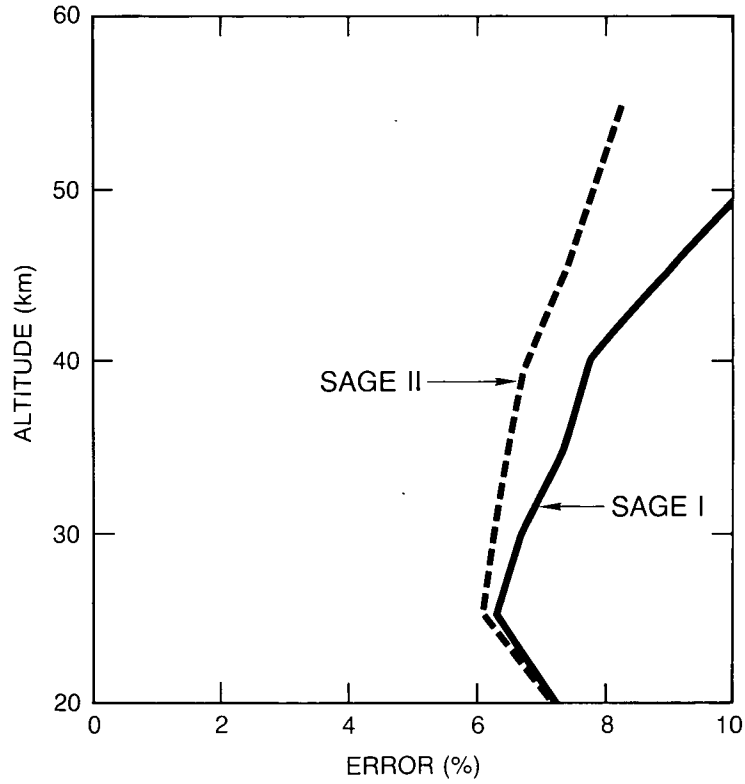

Figure 2.32 Combined systematic errors in SAGE ozone profiles.

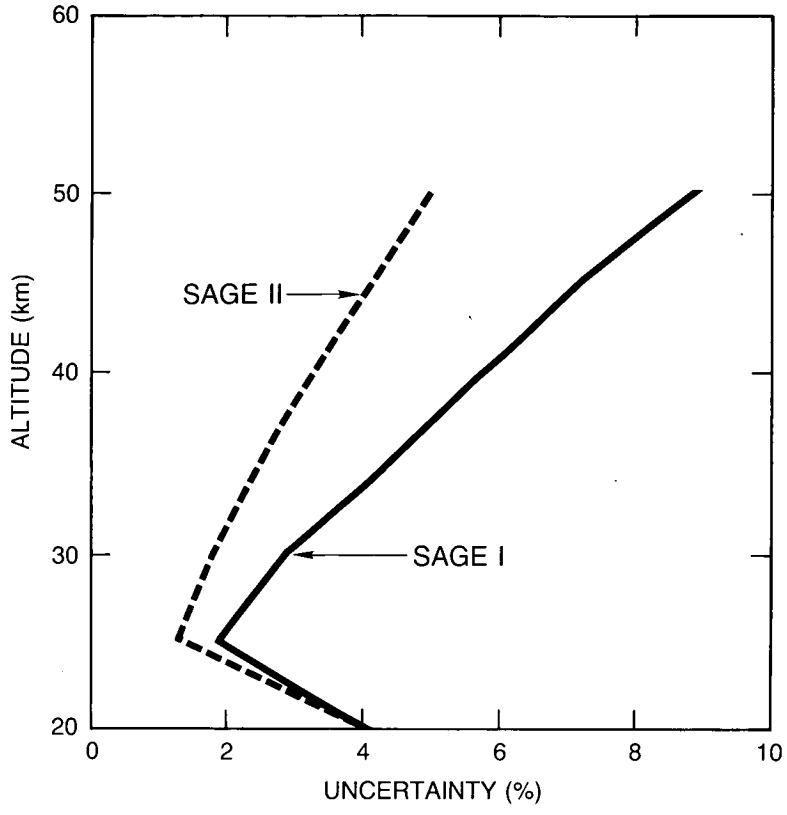

Figure 2.33 Uncertainty in SAGE ozone changes.

2.5.5 Error Budget of the Difference Between SAGE–I and SAGE–II Ozone Retrievals

There are three error sources that can produce a consistent difference between SAGE–I and SAGE–II ozone results besides the aerosol interference, which is transient in nature. These error sources are the relative uncertainties in the mean ozone absorption cross-sections for the two instruments, the scan mirror calibrations, and any systematic difference in the reference height.

Relative Uncertainty in the Mean Ozone Absorption Cross-Section

The ozone channels for SAGE–I and SAGE–II are both nominally centered at 600 nm, with nominal widths of 30 nm and 15 nm, respectively. The factor that affects the ratio of SAGE–I to SAGE–II ozone determinations is the ratio of the two mean absorption cross-section values R, defined as

$$R = \bar{\sigma}_1/\bar{\sigma}_2 \tag{19}$$

$$= \frac{\int_{w_1}\sigma(\lambda)d\lambda/w_1}{\int_{w_2}\sigma(\lambda)d\lambda/w_2}$$

where σ_1 and σ_2 are the mean ozone absorption cross-sections over the bandwidths w_1 and w_2 for SAGE–I and SAGE–II, and $\sigma(\lambda)$ is the ozone absorption cross-section.

By partitioning w_1 into regions w_2, w_S, and w_L, where the latter are regions within w_1 at wavelengths shorter and longer than w_2, respectively, and introducing δ for the uncertainty in the absorption cross-section, Equation 19 may be written

$$R + \delta R = \tag{20}$$

$$\frac{\frac{1}{w_1}\int_S[\sigma(\lambda) \pm \delta(\lambda)]d\lambda + \frac{w_2}{w_1}\cdot\frac{1}{w_2}\int[\sigma(\lambda) \pm \delta(\lambda)]d\lambda + \frac{1}{w_1}\int_L[\sigma(\lambda) \pm \delta(\lambda)]d\lambda}{\frac{1}{w_2}\int_S[\sigma(\lambda) \pm \delta(\lambda)]d\lambda}$$

$$= \frac{1}{\bar{\sigma}_2}\left[\frac{w_2}{w_1}\bar{\sigma}_2 + \frac{1}{w_1}\int_{w_S}\sigma(\lambda)d\lambda + \frac{1}{w_1}\int_{w_L}\sigma(\lambda)d\lambda \pm \frac{1}{w_1}\int_{w_S}\delta(\lambda)d\lambda \pm \int_{w_L}\delta(\lambda)d\lambda\right]$$

Note that any uncertainty in the $\sigma(\lambda)$ that is used in w_2 has no effect, because the identical values are used in that part of w_1.

In $w_{S,L}$ we can define

$$\bar{\sigma}_{S,L} \equiv \frac{1}{w_{S,L}}\int_{S,L}\sigma(\lambda)d\lambda \equiv a_{S,L}\bar{\sigma}_2 \tag{20a}$$

In the last two terms in Equation 20, expressing the uncertainty, if δ has the same sign at all frequencies in S or L (a worst case), then

$$R = \frac{w_2}{w_1} + \frac{w_S}{w_1}a_S + \frac{w_L}{w_1}a_L \tag{20b}$$

and

$$\delta R^1 = \pm\frac{\delta_S}{\bar{\sigma}_2}\frac{w_S}{w_1} \pm \frac{\delta_L}{\bar{\sigma}^2}\frac{w_L}{w_1} \tag{20c}$$

Since $w_{S,L}/w_1 \simeq 0.25$, and Penney (1979) indicates that $\delta/\delta_2 \simeq 0.02$, then, very conservatively, $\delta R^1 = 0.01$.

There is another uncertainty, δR^2, because the widths w_1, w_2, w_S, and w_L are not known exactly, but subject to the constraint that $w_2 + w_S + w_L \equiv w_1$. Evaluating the relevant expression gives $\delta R^2 = 0.0045$.

The errors δR^1 and δR^2 are independent; their RSS is 1.1 percent. To be conservative and allow for other possible small terms, we take 1.2 percent as the uncertainty in the relative cross-sections in Table 2.10 below.

Uncertainty in the Scan Mirror Calibration

The systematic retrieval errors due to the mirror for SAGE–II are shown in Figure 2.30. The mirror reflectivity effects for SAGE–I are estimated to be about twice as large. These values are presented again in Table 2.10.

Table 2.10 Errors in the Difference Between SAGE–I and SAGE–II (all errors in percent)

Altitude (km)	Ozone abs. Cross-section Difference	Mirror SAGE–II	Mirror SAGE–I	Alt. Registration Difference	SAGE–I Aerosol	SAGE–II Aerosol	Root Sum Square
20	1.2	0	0	0	4	4	5.8
25	1.2	0	0	.25	1	1	1.9
30	1.2	0	0	.50	.5	.5	1.5
35	1.2	.05	.1	.75	.2	.2	1.5
40	1.2	.1	.2	1.0	0	0	1.6
45	1.2	.25	.50	1.25	0	0	1.8
50	1.2	1	2	1.5	0	0	3.0

Systematic Differences in SAGE–I/SAGE–II Reference Height

As noted above, there may be a maximum error between the reference heights of SAGE–I and SAGE–II of 60 m. Combining this with the sensitivity curve in Figure 2.31 results in the uncertainties given in Table 2.10.

Combined Instrumental Error of SAGE–I/SAGE–II Differences

The errors noted in the three items above, plus contributions due to aerosols, are given in Table 2.10. Their combined value, treating the errors as independent, is given in the last column, and plotted in Figure 2.34. It should be noted again that there may be errors resulting from the sampling and data sparseness.

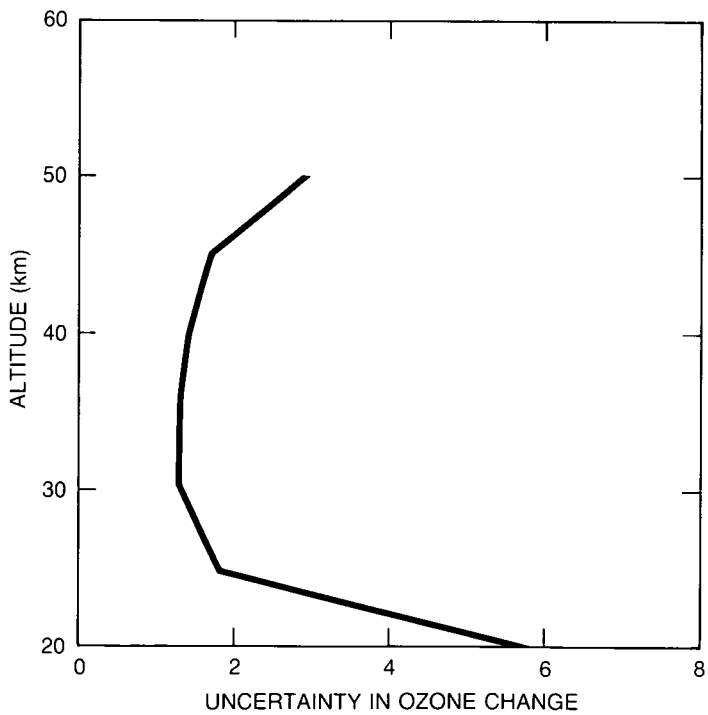

Figure 2.34 Uncertainty in ozone change determined from SAGE–I/SAGE–II differences.

The differences reported in Chapter 5 were obtained by pairing soundings taken at the same latitude and season during 2 years of operation of each instrument. This does not entirely eliminate the possibility of a systematic error due to the interaction of the sampling and the interannual variability, but the magnitude of such an effect has not been quantified at this time. The errors given in Table 2.10 and Figure 2.34 are the instrumental errors associated with the differences.

2.6. SOLAR MESOSPHERE EXPLORER (SME) UV OZONE AND NEAR INFRARED (NIR) AIRGLOW INSTRUMENTS

The SME UV Ozone and Near Infrared Airglow instruments were launched aboard the SME satellite on October 6, 1981. The satellite is in a polar orbit that is Sun synchronous and spins once every 12 seconds. The instruments take data from sunrise to sunset when the IFOV's are at the limb. Ozone data are recovered from 48–70 km from the UVS and from 50–90 km from the NIR. The two instruments overlap their altitude coverage by approximately 20 km, allowing an internal comparison of the ozone trend to be made. Data are taken at Earth's limb with an altitude resolution of about 4 km over a slant path hundreds of kilometers long. Figure 2.35 shows the observing geometry of both instruments. Ozone is deduced by independent physical means from the two instruments; however, satellite parameters, such as altitude of the observations, are common to both instruments.

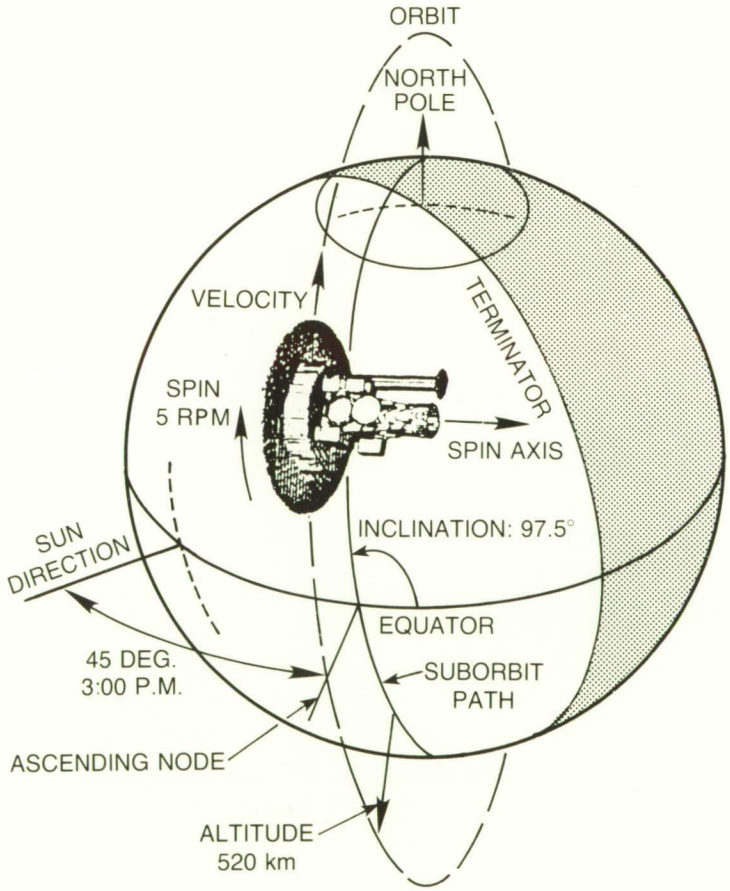

Figure 2.35 SME orbit and scan geometry.

SME experienced two problems after launch that had an unplanned effect on the two ozone instruments. First, the operating temperature of the instruments was approximately 40°C less than was anticipated. This resulted in operational problems with the diffraction grating drives, and the decision was made early on not to move them more than was necessary. This did not cause serious problems for the NIR as it was designed to work mainly at a single wavelength. The UV instrument science was restricted however, since the atmospheric altitude band of the ozone retrieval is very wavelength dependent. The instrument operates over the Hartley ozone region. Wavelengths with large ozone cross-section give good ozone retrievals at high altitudes where the ozone abundance is small, and wavelengths with small ozone cross-section give good results where the ozone abundance is large. It had been hoped to move the wavelengths over the entire Hartley band to give full altitude coverage. Instead, the mission was accomplished at a single wavelength pair that corresponded to ozone recovery in the 1.0–0.1 mb (48–70 km) altitude regions.

The second problem was the inability of the passive cooling device on the long wavelength infrared radiometer to reduce the detector temperatures to the point where they could provide an accurate pressure altitude for the coaligned instruments on board. This resulted in a serious problem in recovery of the all the IFOV altitudes at the limb. The altitudes are now derived approximately from the spacecraft bus IR horizon sensors that are part of the spacecraft attitude control system and then further refined using the actual data from each horizon scan from the UV ozone instrument. Final determination of altitude accuracy of the FOV at the limb is stated to be approximately 1 km. The derived altitude of the FOV of the UV ozone instrument was used for all the instruments on board the satellite. The UV ozone and NIR instruments were turned off in December 1986.

2.6.1. UV Spectrometer

2.6.1.1 Physical Principles

The technique is described by Rusch et al. (1984) and in User's Manual (Mount, 1982). Figure 2.36 illustrates the geometry and the physical processes. The radiance measured by the UVS at wavelength λ, I_λ, looking at an altitude z_0, can be written as

$$I_\lambda(z_o) = F_\lambda \sigma_\lambda \phi(\psi) \int_{-\infty}^{\infty} T_{\lambda s}(s)[T_{O_3}(s,\infty)]N[z(s)]ds \qquad (21)$$

where F_λ is the solar flux, and σ and $\phi(\psi)$ are the Rayleigh scattering cross-sections and phase function for scattering angle ψ. $T_s(s)$ is the transmittance of solar radiance to the scattering point s, $N(s)$ is the volume density of Rayleigh scatters at s, and T_{O_3} and T_R are the transmittances after attenuation by ozone absorption and Rayleigh scattering, respectively, between the scattering point and SME, taken to be at $+\infty$. Only single scattering is included for the altitudes of interest.

As the data are now reduced, data from the long wavelength channel (296.4 nm) are used to determine the density at a level where ozone absorption is negligible ($T_{O_3}(s,a) = 1$). In this case, I/F depends only on the number of scatterers (i.e., the density) that can be related to an approximate height using the proposed COSPAR International Reference Atmosphere (CIRA) model atmosphere (Barnett and Corney, 1985). This incorporates climatological latitudinal and seasonal variations, but not the effects of short-period disturbances or systematic longitudinal variations. The density level selected corresponds to an altitude of about 65 km. The exact altitude depends on the ratio of the absolute calibrations of the UVS and the separate solar instrument (Rottman et al., 1982) as well as on meteorological effects.

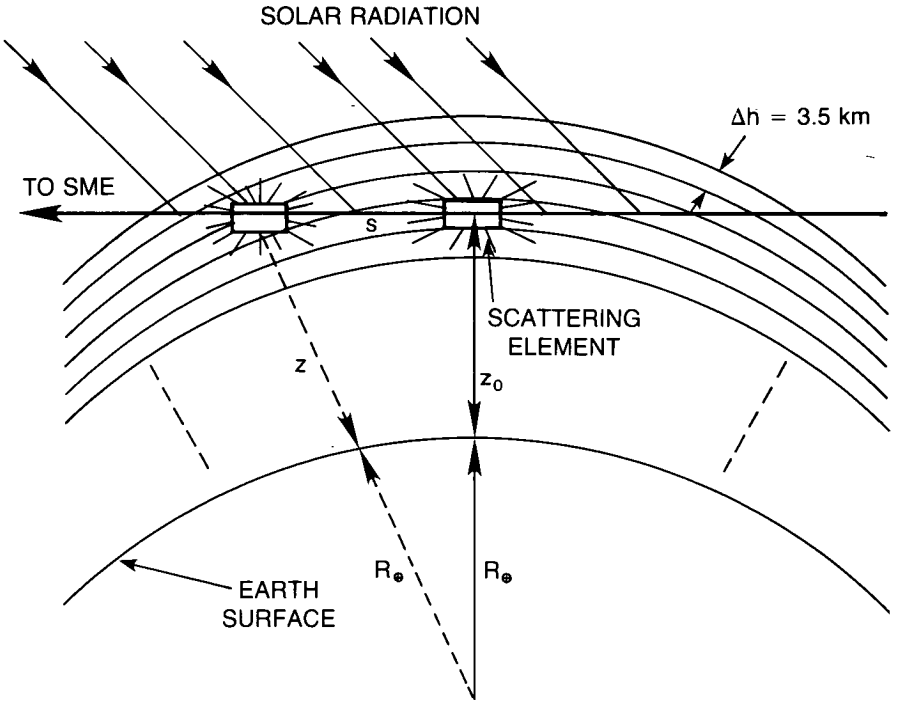

Figure 2.36 The geometry of limb viewing with the UVS on SME. Z_o is the minimum ray height of the 3.5 km vertical resolution of the measurement (from Rusch et al., 1984).

With the density and altitude point determined from the long wavelength channel, the short wavelength channel (265.0 nm) radiance profile is then adjusted in magnitude to force agreement with the model Rayleigh scattering at 76 km altitude where the short wavelength channel ozone absorption is negligible. Only the relative shapes of the radiance profiles from the short wavelength channel are needed to deduce ozone abundance once these shifts are made, and the shapes depend only on atmospheric Rayleigh scattering and ozone abundance. It is very important to note that the absolute calibration of only the long-wavelength channel is required in the determination of ozone abundance. Neither the absolute nor the relative calibration of the short wavelength channel plays a role.

There was no plan for long-term calibration, since the mission was originally specified to last for 1 year. The expectation, apparently, was that there would be no serious degradation over this period, and the experimenters were directed not to plan for longer instrument life. The UV instrument did not incorporate an internal calibration lamp. Two features helped to reduce degradation over the 5 years in orbit. First, the SME was a very clean spacecraft, resulting in less outgassing that could contaminate the optical surfaces. Second, the UVS did not view the Sun, so solar dissociation and fixing of contaminants on the optics could not occur.

2.6.1.2. Instrument Description and Prelaunch Testing

The instrument and its testing have been described by Rusch et al. (1984) and in User's Manual (Mount, 1982). The collecting telescope is a nonobscured f/5, 250-mm focal length off-axis parabola. The telescope feeds an f/5, 125-mm Ebert–Fastie spectrometer employing a 3600 l/mm diffraction grating. Spectral resolution is approximately 1.5 nm. Dual channel detectors are EMR 510–F–06 photomultiplier tubes. Figure 2.37 shows a schematic diagram of the

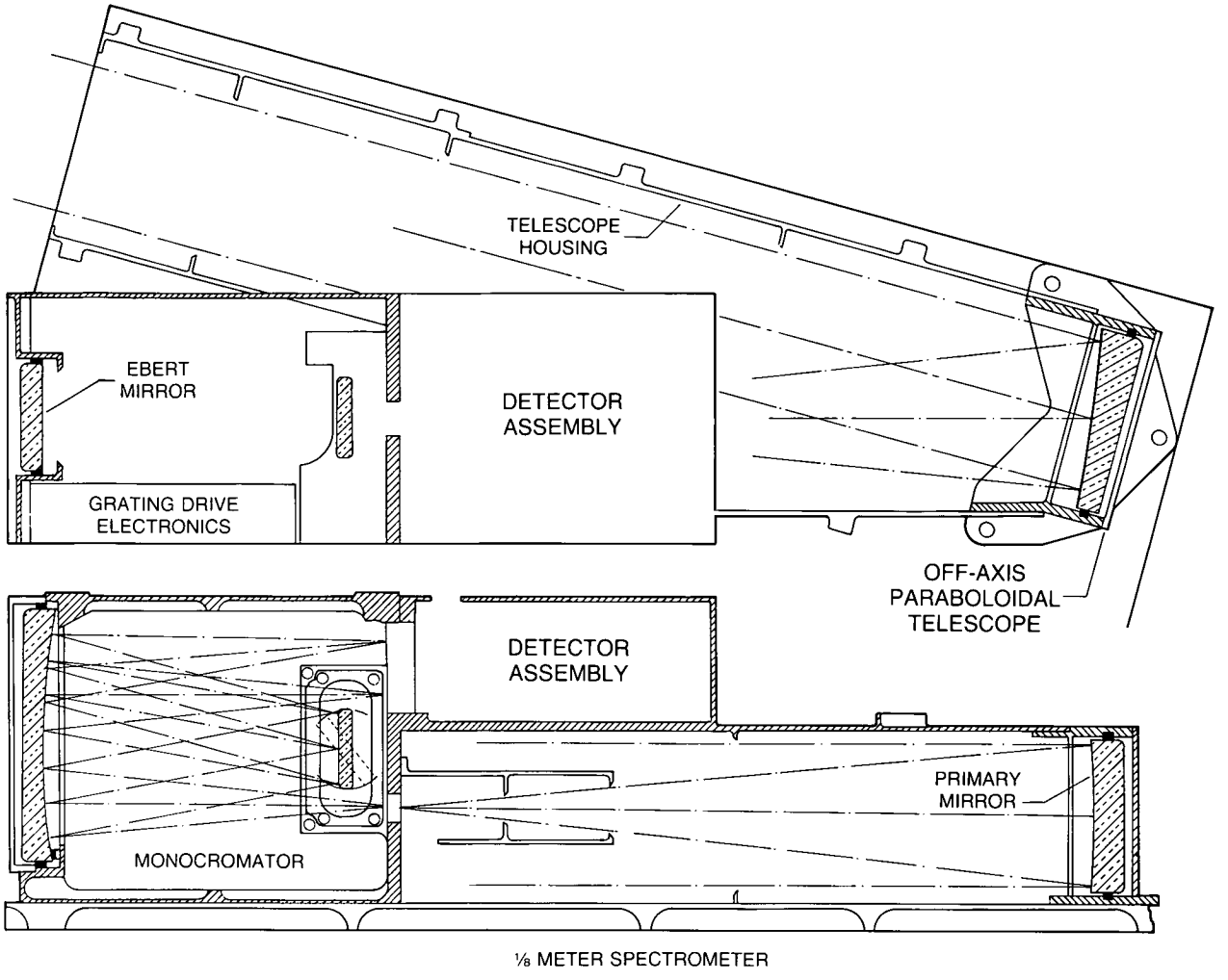

Figure 2.37 Schematic drawing of the SME UV spectrophotometer. Two views are shown rotated 90° with respect to each other. The detector assembly houses two photomultiplier tubes and pulse-counting electronics (from Rusch et al., 1984).

UV ozone instrument. Calibration tests performed on the instrument and its components were grating efficiency, grating scatter and ghosts, grating polarization, mirror efficiency, mirror off-axis scatter, mirror RMS surface roughness, detector dead time, detector efficiency, detector sensitivity maps, absolute instrument efficiency, instrument off-axis scatter, instrument wavelength calibration, instrument polarization, FOV sensitivity variation, and spectral bandpass.

The instrument absolute calibration for wavelengths of less than 260 nm was made using a system similar to the Johns Hopkins CTE, which utilizes NBS photodiodes and transfer photomultiplier tubes as the standards. For wavelengths greater than 240 nm, NBS standard tungsten strip filament lamps were used, either focused directly onto the ozone spectrometer entrance slit (with telescope removed) or onto a $BaSO_4$ scattering screen with the telescope on the instrument. The resulting (one sigma) error budget was wavelength less than 240 nm: ±25 percent; 240–270 nm: ±12 percent; 270–320 nm: ±10 percent; and greater than 320 nm: ±15 percent. Wavelengths used in flight were 265.0 nm and 296.4 nm, and so the absolute calibration for the retrieval wavelength pair was about ±10 percent (one sigma). These wavelengths provide

information on ozone from about 1 mb–0.1 mb. A relative sensitivity shift of the two channels, noted after launch, results in an absolute sensitivity determination of about 20 percent (one sigma).

Figure 2.38 shows the altitude-dependent errors resulting from the inversion process for each indicated calibration measurement. The UV ozone instrument retrieves the ozone abundance in

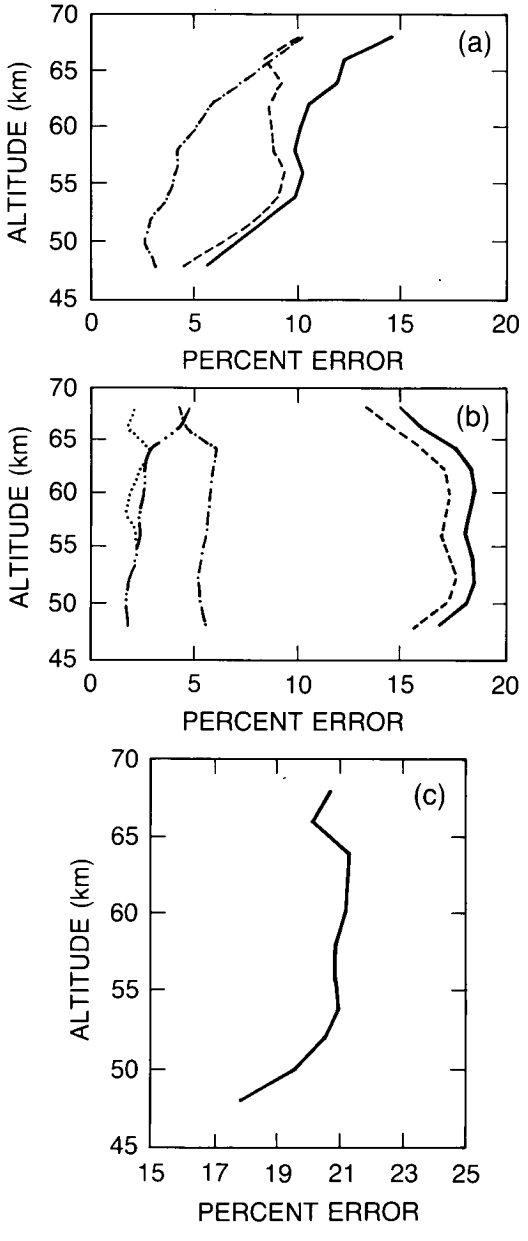

Figure 2.38 (a) Random altitude-dependent errors associated with noise and data compression (dashed dot line) and temperature and pressure (dashed line). The solid line is the rms sum. (b) Systematic altitude-dependent errors associated with uncertainties in instrument sensitivity (dashed line), instrument polarization (dash-dot-dot-dash), dead-time constants (dotted line), and ozone cross-sections (dash-dot-dash). The solid line is the rms sum. (c) The altitude-dependent error from combined random and systematic errors (from Rusch et al., 1984).

the 1–0.1 mb region with an overall accuracy of approximately 21 percent (one sigma), which includes errors caused by using model atmosphere that may differ from the real atmosphere, although the differences are not expected to be significant from year to year. The use of temperatures determined from Wallops Island (U.S.) rockets fired during satellite overpasses results in insignificant changes in the retrieved ozone from the model assumption.

FOV limb altitudes are determined by comparison of the Rayleigh-scattered radiance measured with that calculated from modeling this signal using the relevant solar fluxes, cross-sections, and the proposed CIRA model. The normalization in altitude is done at 65 km in the long-wavelength channel (296.4 nm), where no ozone absorption is detectable and the Rayleigh scattering is optically thin. The altitude is then considered by the SME science team to be determined with an accuracy of approximately 1 kilometer, based on uncertainty in the absolute calibration, with a repeatability of 0.3 km. Figure 2.39b (taken from Barth, Rusch, Clancy, and Thomas [BRCT], unpublished report, 1987) shows the required corrections to the spacecraft IR horizon sensors for a particular orbit and the limb sensor altitude determinations themselves (Figure 2.39a). Sensitivity to the long-wavelength channel absolute calibration is about 1 km per 15 percent change in long-wavelength channel calibration.

Several factors affect the ability of the UV ozone instrument to detect ozone abundance trends: changes in the absolute calibration of the long-wavelength channel of the instrument, since it determines the model normalization at 65 km, which in turn determines the absolute altitude of the FOV; reliance on a model atmosphere that has seasonal and latitudinal changes, but that is assumed to be the same every year and has no local spatial or rapid temporal variability; drift in the wavelength drive, resulting in incorrect use of ozone cross-sections and solar fluxes; changes in the solar flux at the long-wavelength (296.4 nm); and changes in instrument polarization as a function of time.

2.6.1.3 Performance in Orbit

The UV ozone instrument incorporated no internal calibration lamp. The tropical background radiance was monitored for about a year after launch; there was no apparent change in either of the two channel radiances, other than the expected seasonal changes, to a level of about 10 percent.

The wavelength drive has been checked regularly since launch, and shows a very small and easily corrected change that is known to a very high degree of accuracy from wavelength scans of the scattered solar light. Based on the SME solar instrument measurements of solar flux, no correction is applied for a time-dependent solar flux.

Since launch, there has been an observed time-dependent trend in the altitude correction deduced from the UV instrument relative to the spacecraft IR limb sensors that can be explained by a 9 percent per year change in total instrument sensitivity. Observation of the altitude shifts over time since launch indicate that these shifts are correlated with the roll angle of the spacecraft and with the resulting tilt of the entrance apertures of the instruments, which were designed to operate on a tangent to Earth's limb. The orbit was optimized for operation during the first year after launch, and orbit precession has increasingly tilted the projected slits relative to the tangent. Determination of the altitude shifts during June of each year, when the roll angle is near zero, indicates a 6 percent per year change in the instrument sensitivity. Thus, 3 percent can be removed as having been caused by the changing roll angle of the spacecraft.

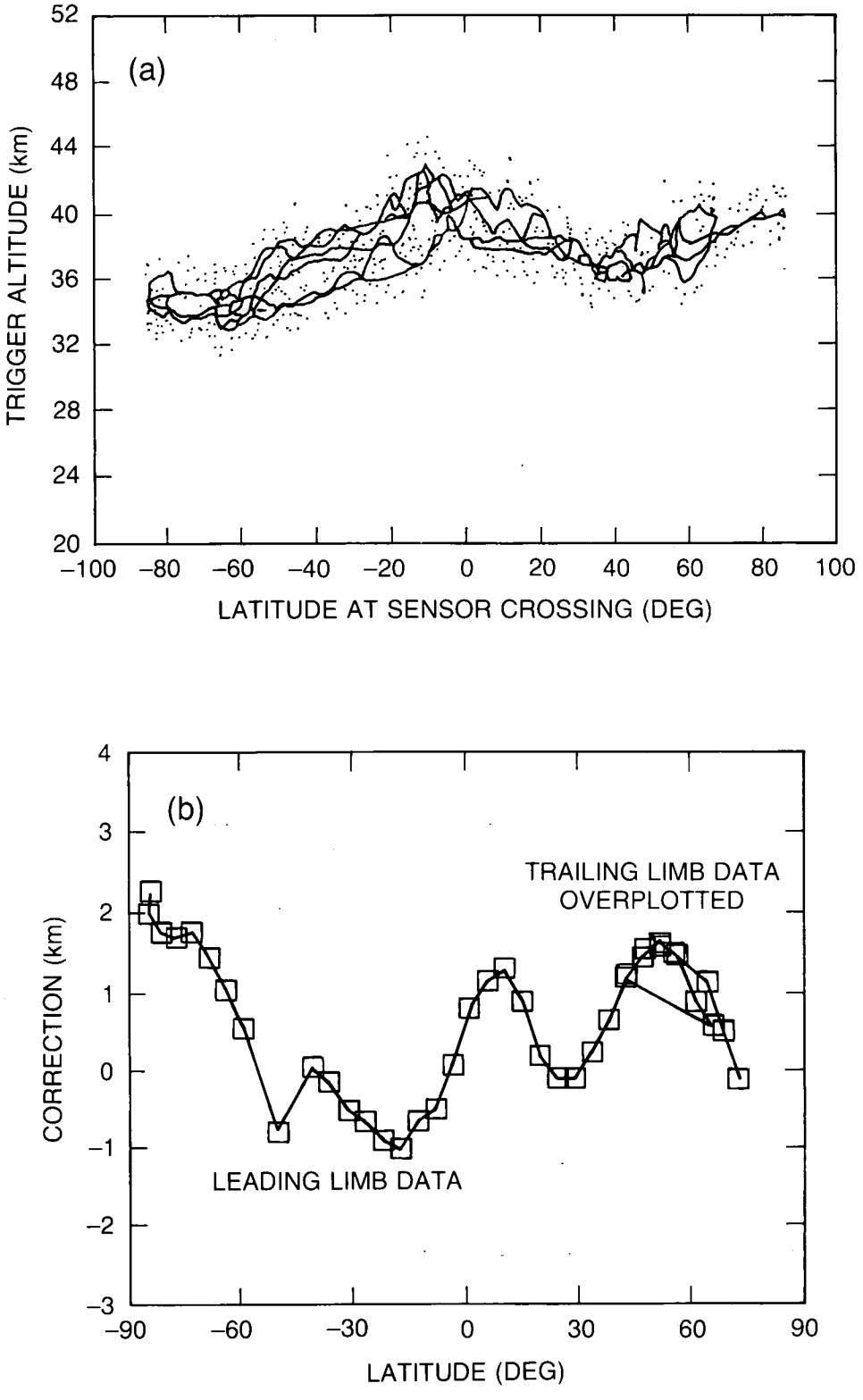

Figure 2.39 (a) Example of IR horizon sensor trigger altitudes vs. latitude. (b) Altitude corrections vs. latitude (from BRCT).

There is a dual channel visible light spectrometer (VIS) on board SME that measures NO_2 near 440 nm (Mount et al., 1984). The detectors used are dual silicon photodiodes, which are etched in the same active material in the rectangular shape of the "exit slits." The instrument scans the altitude range from about 100 km above to 20 km below the horizon. Assuming that the wavelength-dependent scattering properties of the atmosphere at 48 km have not changed since launch and that there is no measurable NO_2 absorption in the visible spectrum at 48 km (a good assumption), then it is determined that the relative drift of the diodes with respect to each other is 0.4 percent/year. This is quite reasonable, since the diodes are physically located only a few millimeters apart. The absolute calibration of the diodes and the associated analog electronics is not known, but the relative drift of the two diode channels relative to each other is expected to be small since the diodes are from the same piece of silicon. No onboard electronics test of standard current levels was provided. There is evidence that the electronics drift is less than 1 percent per year, since the electronic offset added to the electrical signal from the photodiodes has remained very stable over the 5-year life of the mission.

2.6.1.4 Assessment of Instrument Drift and Its Effects

The following discussion is based in part on BRCT. Assuming that the VIS diodes have not drifted in absolute calibration, and ratioing their observed signal near 440 nm at 48 km to the observed signal from the UV spectrometer long-wavelength channel at 76 km altitude (where ozone absorption should be negligible), leads to a deduced change in the UV instrument long-wavelength channel sensitivity at 296 nm of -4.8 percent/year ± 1.4 percent/yr. This change in sensitivity then translates into an ozone change at 0.75 mb (53 km) averaged over 0–60°N latitudes in the summers of $+1.6$ percent/year since launch, with a range from $+4.1$ percent/year (for smaller instrument degradation) to -0.7 percent/year (greater instrument degradation). These error bars are a measure of the statistical variation in the summer data from each year and do not include algorithm-related errors in the ozone retrieval. The SME UVS shows an ozone trend bounded by a range $+4.1$ percent/year to -0.7 percent/year assuming no change in the absolute calibration of the visible spectrometer photodiodes.

The ozone trend determined from this method depends on the assumptions that there will be:

- No change in the absolute calibration of the visible instrument photodiodes.
- No change in the calibration of the analog electronics that convert the photodiode signals to data numbers.
- No shift in the positions of the two instrument fields of view in relation to each other.
- No nonseasonal changes in atmospheric albedo and temperature effects between 48 and 76 km between 1982 and the present.
- No nonseasonal systematic drifts of atmospheric shape with time.

While changes in the VIS photodiode sensitivity are expected to be small, there is no way to verify that this is, indeed, the case. The SME science team feels that it would detect changes in the diode sensitivities of the order of several percent per year since this would change the response to NO_2. There is also no way to measure changes in the analog electronics. The relative sensitivity drift of the two photodiode channels is 0.4 percent/year, indicating that the diodes

and their absolute sensitivity could well be changing in a similar manner. There has been very little stress on the diodes, since the operating current is six decades below the nonlinear operating point. The diodes are operated in photovoltaic mode, so there is no voltage stress on them. No increase in noise level has been observed. Measurements of polar albedo (which is expected to remain fairly constant) taken in the nadir indicate approximately a 10 percent change in 5 years. Assuming no change in albedo due to aerosols (El Chichón) and other factors, this gives a 2 percent/year photodiode sensitivity change. There is no reason to expect that the FOV's have shifted relative to each other. Atmospheric effects should be small, but are again not verifiable. Therefore, the SME science team has set a limit on the change of the photodiode calibration at 1 percent per year ±1 percent per year; in this assessment, the worst case value of 2 percent per year has been used.

There is evidence from the SME solar instrument that SME is a particularly clean satellite because there is no evidence of significant degradation of the optical surfaces in that instrument. It is reasonable to conclude that it has not occurred in other instruments. Thus, any sensitivity degradation in the UV spectrometer is assumed to be mostly in the photomultiplier tubes. The tubes were used in the pulse-counting mode, which makes them initially insensitive to changes in gain with increasing total count rate. The tubes were used in orbit at rates of several hundred thousand counts per second, which are conservative rates. The long-wavelength channel photomultiplier would suffer count-rate degradation first, since its count rate is more than twice that of the other channel. This is in agreement with the determination above. The changes in solar flux have been negligible at these wavelengths, and there is no reason to suspect that the polarization of the optics has changed. It is important to repeat that only the long-wavelength channel absolute calibration is required for the altitude determination, and even the relative calibration between the two channels is not needed for ozone determination.

2.6.2. Near Infrared (NIR) Instrument

2.6.2.1 Physical Principles

The physics of the ozone retrieval on the NIR instrument is quite different from the UV instrument, which measured relative absorption in two channels. The approach is described by Thomas et al. (1984). The most important processes are indicated in Figure 2.40. Photodissociation of ozone by solar radiation

$$O_3 + h\nu(210 < \lambda < 310\text{nm}) \rightarrow O_2(^1\Delta_g) + O(^1D) \tag{22}$$

and other processes lead to the formation of $O_2(^1\Delta_g)$. Some of these molecules are quenched, while others radiate. The NIR measures the emission by $O_2(^1\Delta_g)$ at 1.27μm. Deduction of the ozone from the $O_2(^1\Delta_g)$ emission depends on ozone absorption, O_2 absorption, ozone photodissociation, the solar flux in the UV and visible/red, and quenching of excited oxygen. Rate constants and cross-sections must be known, photochemistry must be correct, and a correct background atmosphere must be used.

In particular, the signal will depend on solar radiation and its spectral variations and on atmospheric temperature. The retrieval is made from approximately 50–90 km. The retrieval requires that the absolute radiance at 1.27μm emerging from the atmosphere be measured. Again, planning for long-term operations was not part of the preflight strategy, but the NIR included an inflight calibration source to allow measurement of, and correction for, instrument drift.

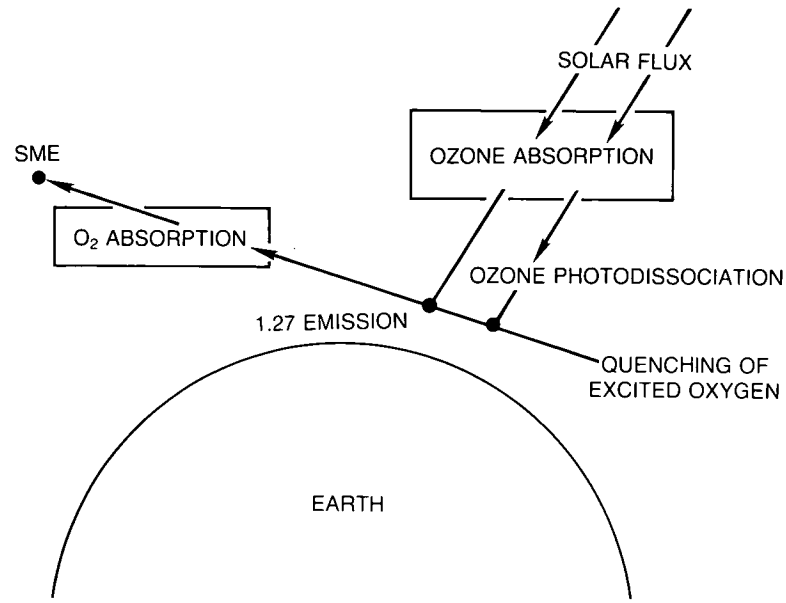

Figure 2.40 NIR physical processes (from Thomas et al., 1984).

2.6.2.2 Instrument Description and Prelaunch Testing

The optics of the NIR instrument are very similar to those of the UV spectrometer; Figure 2.41 shows a schematic diagram of the NIR. The detectors are chopped lead sulfide photoconductors with immersion lenses cooled by radiation to space. The following quantities were measured during calibration: absolute sensitivity, spectral bandpass, polarization, wavelength scale, FOV, off-axis scatter, time response, out-of-band leakage, linearity, and thermal characteristics. The absolute sensitivity was determined with an NBS-calibrated tungsten strip filament lamp. The filament was focused on a barium sulfate screen producing a diffuse light of known intensity. Absolute calibration was accurate to about 20 percent.

The NIR spectrometer had an onboard calibration source. A small tungsten lamp, a silicon photodiode, and a thermistor were placed at the edge of the f/5 telescope beam near the entrance slit of the spectrometer (Figure 2.41). Light scattered from the baffles enters the spectrometer, and, if the time-dependent calibration of the system is understood, the relative time-dependent response of the instrument (not including telescope) can be deduced. The brightness of the lamp depends on its operating conditions (such as temperature and voltage) and changes as it ages. The photodiode measures the lamp brightness; since it is temperature sensitive, a thermistor is placed next to the diode. The system is not a precise calibration for short-term use, but should detect major short-term changes. For long-term changes it is very useful.

2.6.2.3 Performance in Orbit

One hundred forty-nine calibrations were performed after launch. The following conclusions have been drawn from the calibrations: comparison of the two NIR detector channels indicate that the brightness changes of the lamp are changes in the black-body temperature of its filament, and the photodiode output has been determined and shows that the change in its sensitivity over the mission is small. Normalized sensitivity of the 1.27μm detector is shown in Figure 2.42. The result is an increasing sensitivity of only 0.28 percent ±0.15 percent per year.

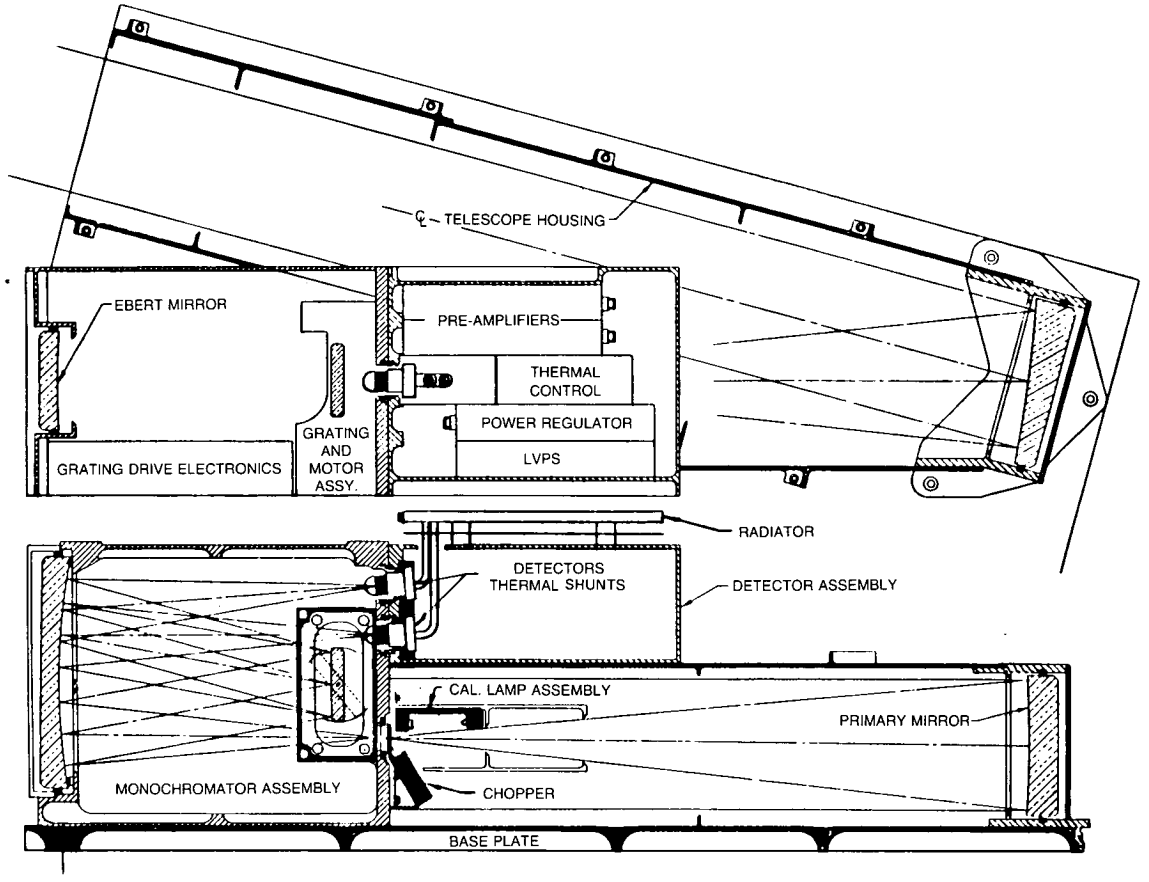

Figure 2.41 Optical scheme of the near-infrared spectrometer. Light enters the telescope through a baffle assembly. The light is focused onto the entrance slit and chopper. In the monochromator, the chopped light is collimated by the Ebert mirror onto the grating. The Ebert mirror then focuses the dispersed light onto the detectors, which define the exit slit. The detectors are passively cooled by a radiator on the outside of the instrument (from Thomas et al., 1984).

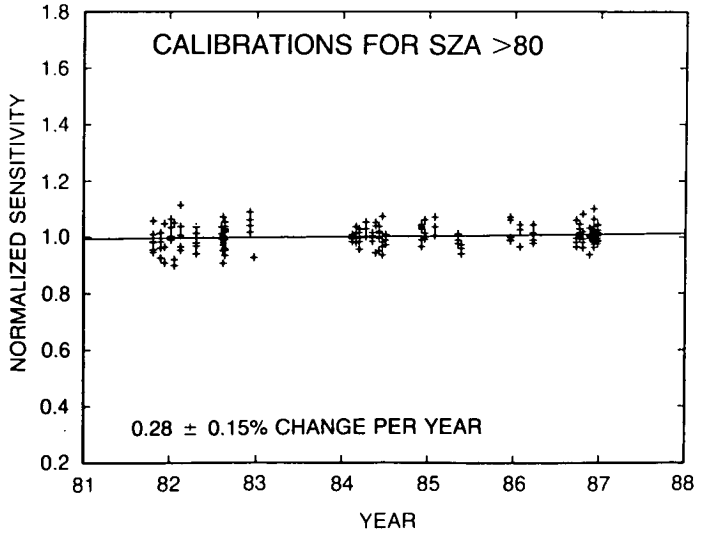

Figure 2.42 Normalized NIR photodiode sensitivity through the mission (from BRCT).

Thus, from the inflight calibration checks it appears that the instrument was very stable over time.

The derived ozone profiles from the NIR spectrometer overlap those determined from the UV ozone instrument in the 50–65 km region. The NIR results were adjusted by 10 percent to force a match between the two instruments for the time period immediately after launch. This adjustment has been used since then without change. The trends from the two instruments have diverged since launch if the preflight calibration values are assumed.

2.6.2.4 Sources of Instrument Drift

Systematic errors due to errors in rate or cross-sections, poor background atmospheric models, and instrument calibration errors result in a 50 percent error near 1 mb and a 30 percent error near 0.001 mb. Total systematic errors are shown in Figure 2.43 as a function of altitude.

Although the systematic errors are large, they will not change with time and will not introduce drifts in the inferred ozone. A detailed discussion is contained in Chapter 3. Errors that introduce trends into the data are changing instrument calibration, drifts between the real and model background atmosphere, changes in the assumed solar irradiance in the UV and the red, and dependence on the UV instrument for the altitude determination of the FOV. In this chapter, only the effects of changing calibration and altitude determination are addressed.

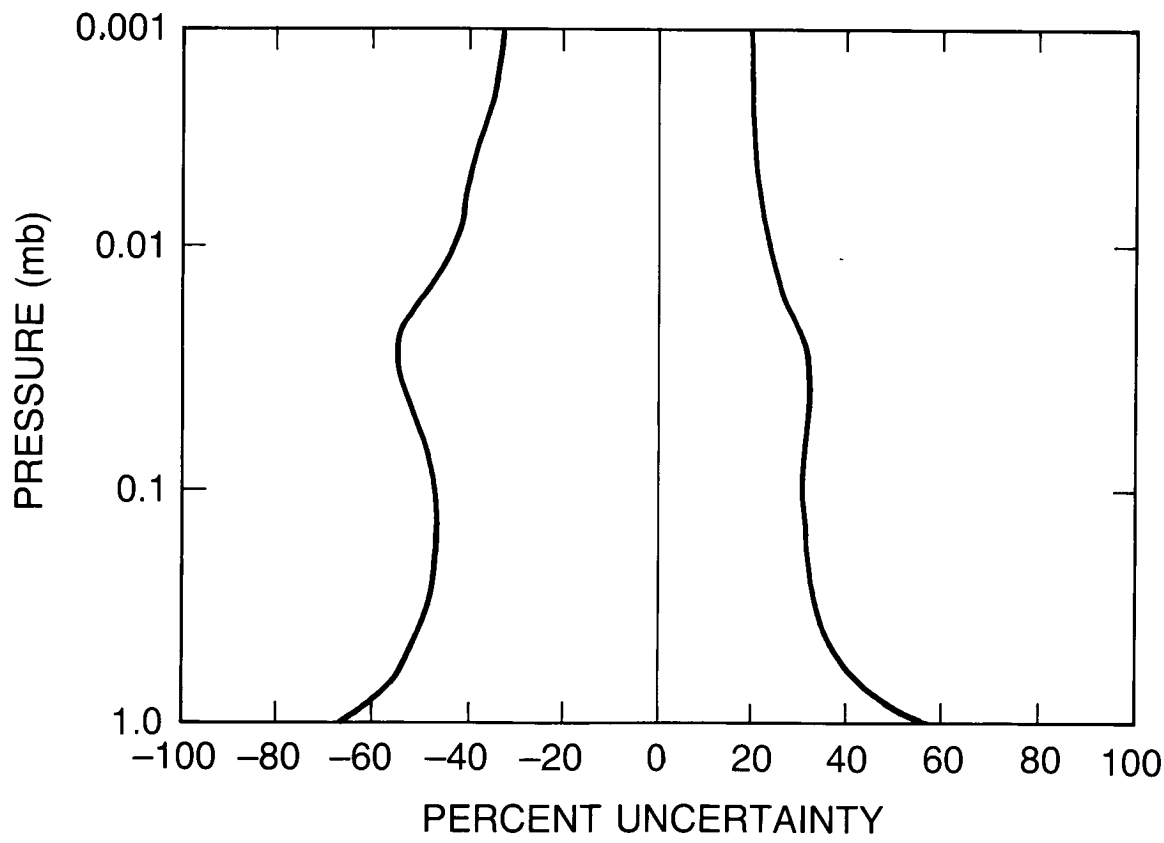

Figure 2.43 Total systematic error on ozone data estimated from input errors (from Thomas et al., 1984).

2.6.3 UVS and NIR

2.6.3.1 Comparison of Ozone Trends From the Two Instruments

Using the standard UVS altitude corrections for both the UVS and NIR instruments with no allowance for any changes in UV sensitivity produces the ozone trends for June shown in Figure 2.44a,b for 0.75mb averaged over 0°–60°N latitude. These changes are +13.2 percent per year for the UV instrument and +2.4 percent per year for the NIR instrument. These are the data in the NSSDC data base as of September 1987.

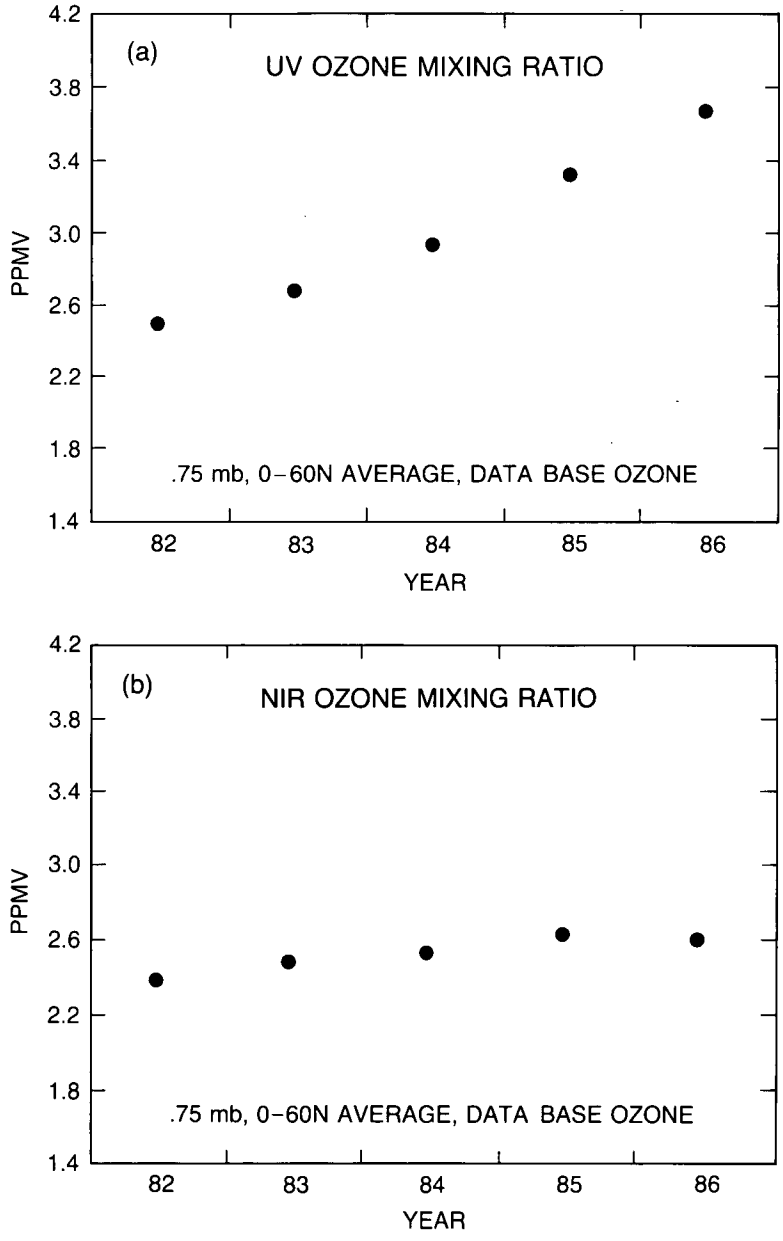

Figure 2.44 UV and NIR 0.75 mb mixing ratio with time. No correction for sensitivity drift of UV LW channel (from BRCT).

Figure 2.45a,b shows plots of the 0.75mb data for the derived change in UV instrument long-wavelength channel sensitivity of -4.8 percent per year as described earlier (assuming no degradation of the visible spectrometer photodiodes). The NIR data are calculated using the altitude shifts derived from the changed long-wavelength channel UV sensitivity. The calculated ozone changes, 1.57 percent per year for the UV and 1.6 percent per year for the NIR, are in close agreement.

Using the spacecraft bus IR CO_2 horizon sensors, an FOV determination independent of the UV instrument can be made for the NIR Airglow instrument. The altitude pointing determined this way is noisier, but provides a useful check on ozone that is independent of the UV instrument. Figure 2.46 shows the trends in ozone for the NIR instrument using this technique.

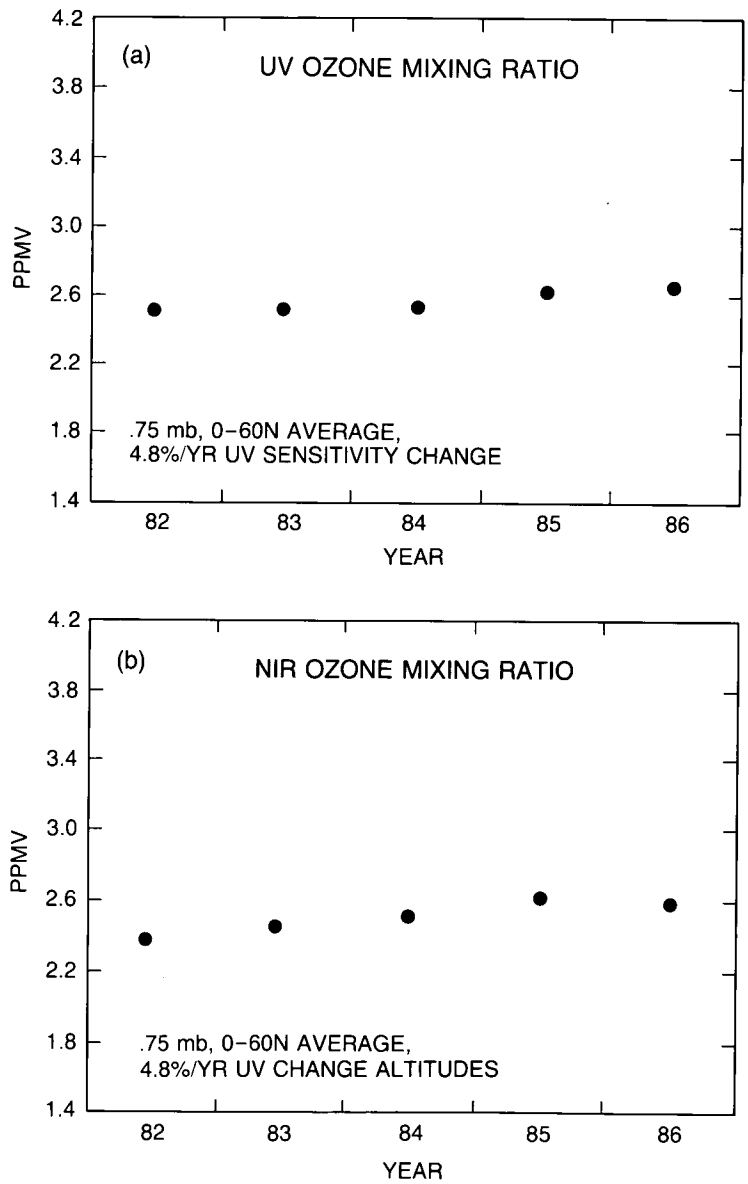

Figure 2.45 UV and NIR 0.75 mb mixing ratio with time. Correction for sensitivity drift of UV LW channel (from BRCT).

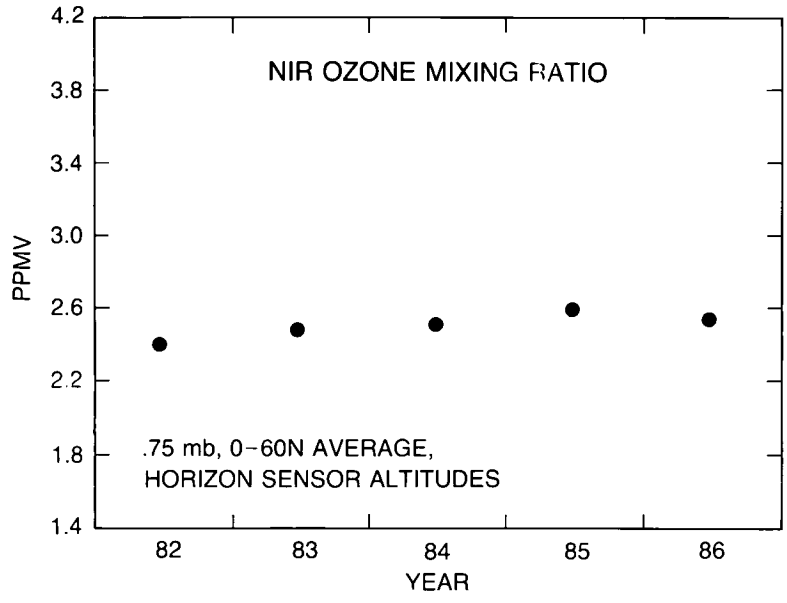

Figure 2.46 NIR 0.75 mb mixing ratio with time using the bus horizon sensors (from BRCT).

Note that the trend in ozone derived from this method (1.8 percent per year) is very nearly equal to that derived from using the UV altitude shifts shown in the previous figure. The 0.75 mb ozone-mixing ratios from the NIR instrument are only slightly affected by changes in the altitude determinations, since the broad maximum of the 1.27μm airglow is near this altitude.

Figure 2.47 shows the range in the trends for 0°–60°N for June 1982–1986 that results from inverting the UV data using two standard deviation uncertainties in the UV long-wavelength

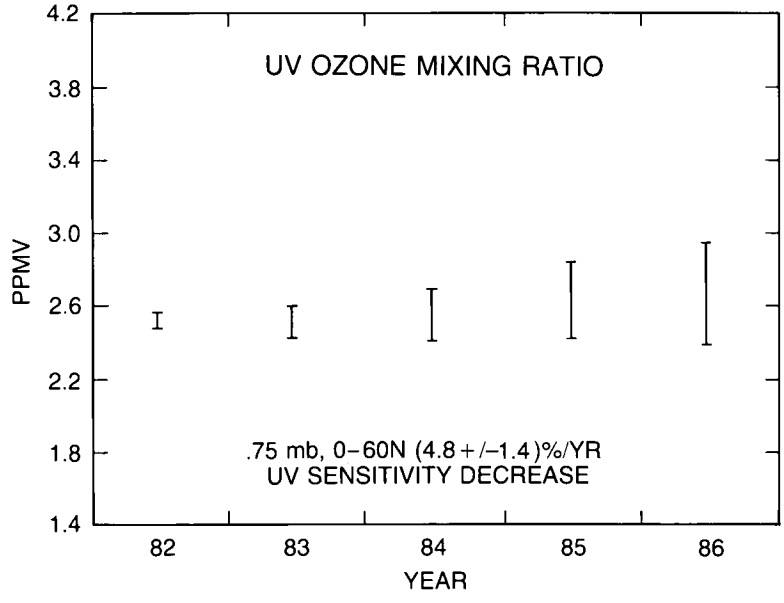

Figure 2.47 Ozone mixing ratios for June 1982–1986 for the UV instrument. The error bars denote the range of the data resulting from the uncertainty in the determination of the UV sensitivity change as a function of time assuming no algorithm retrieval error and no visible spectrometer photodiode drift with time (from BRCT).

channel sensitivity, assuming the algorithm physics is correct and assuming the visible photodiodes have not drifted with time. The values for the ozone change at the extremes of the sensitivity changes are -0.7 percent per year and +4.1 percent per year. When the possibility of visible spectrometer photodiode degradation of 2 percent per year is taken into account, the range of possible ozone trend is +4.1 percent per year to -3 percent per year for 0°–60°N in June.

2.6.3.2 Assessment

The accuracy of the absolute calibration of the SME UVS long-wavelength channel determines the accuracy to which the altitude of the FOV of this instrument can be determined. The ozone abundance and ozone trend depend crucially on this determination. The SME science team has used the photodiode channels on the SME visible spectrometer to correct the absolute calibration of the UV long-wavelength channel for drift over the 5-year period in orbit. The change in the UVS absolute calibration relative to the visible instrument photodiodes is -4.8 percent per year ±1.4 percent per year*. An observable limit to the degradation of the visible instrument photodiodes, on which the UV calibration is based, is 2 percent per year. Including this limit in the absolute calibration uncertainty, the ozone trend derived from the SME UV instrument is +4 percent per year to -3 percent per year.

A detailed analysis of the long-term drift of the NIR instrument was presented, and a convincing case for only small calibration drifts during the 5 years in orbit was made. However, although the NIR instrument has a reasonably determined calibration drift, which is small, the altitude of its FOV, and hence its ozone determination, is dependent upon the absolute calibration of the UV ozone instrument, which determines the altitude used in its inversion. This dependence is very small at the 0.75 mb pressure level. The range of uncertainties, including uncertainties in both calibration and altitude, is ±0.7 percent per year. Thus, the ozone trend determination from this instrument at the 0.75 mb level is +2 percent per year ±0.7 percent per year.

A determination independent of the UVS altitude corrections was made from the NIR instrument using the altitude determination from the spacecraft bus IR horizon sensors; this analysis gave a trend of +1.8 percent per year.

2.7 THE LIMB INFRARED MONITOR OF THE STRATOSPHERE (LIMS)

LIMS is a six-channel infrared limb scanning radiometer on the Nimbus–7 spacecraft. The experiment and its calibration have been described in detail by Gille and Russell (1984); previous discussions are contained in Russell and Gille (1978) and Gille et al. (1980).

*Note added in proof. Subsequently, Rusch and Clancy (1988) have claimed an accuracy in trends of ±1.3%/year. These authors reference an *oral* presentation by Barth, Rusch, and Thomas at the 1987 spring AGU meetings as the source of the ±1.3%/year trend determination accuracy. However, it was clearly stated in the meetings that this report is based on the ±1.3%/year number reported at AGU *assumed* that the visible diode instrument experienced no drift in sensitivity. In fact, it experienced a 0± 1% drift as described in Figure 2.47 above, which must be included in the total trend error budget, as has been carefully done in this report.

2.7.1 Principles of the Technique

The viewing geometry is the same as that shown in Figures 2.36 and 2.40, except that LIMS measures the infrared radiation emitted by the atmosphere as it scans across the limb. At any given measurement during the scan, when the instrument is viewing tangent altitude h above the surface, it receives a radiance in the ith channel given by

$$N_i(h) = \int_{-\infty}^{\infty} B_i(T,x)\frac{d\tau_i(\mu_i)}{dx}\,dx \tag{23}$$

where

B is the Planck function,
T is the temperature,
τ is the transmittance, and
x is the distance along the line of sight from the instrument through the tangent altitude h.
μ_i is the mixing ratio of the gas that absorbs in this channel.

The general strategy is to measure N_i for channels in which CO_2 is the emitting gas. Because its mixing ratio is known, τ and $d\tau/dx$ may be calculated, allowing B and thus the temperature T to be derived. This temperature is then used to calculate B for the ozone channel (indicated by subscript 3); from N_3 and B_3, the distribution of the ozone-mixing ratio, μ_3, can be derived through the dependence of τ_3 on μ_3.

From this discussion it is clear that the solution depends on the absolute value of the N_i, resulting in a requirement for accurate calibration of the measurements.

More exactly, Equation 23 should be written

$$N_i(h_j) = C_i \int_{h_i}^{h_2}\int_{\nu_{i_1}}^{\nu_{i_2}}\int_{-\infty}^{\infty} \phi(h - h_j)\psi_i(\nu)B(\nu,T(x)) \times \frac{d\tau}{dx}(\nu,x,h_j)dx\,d\nu\,dh \tag{24}$$

where h_j denotes the jth tangent height,
C_i is a calibration constant, relating the output from the instrument to the input radiance,
$\phi(h\text{-}h_j)$ is the relative spatial response,
$\psi_i(\nu)$ is the relative spectral response.

In addition, we note that

$$h_o + j\cdot\Delta h$$

where h_0 is an (initially) unknown reference height, and measurements spaced Δh apart are made on a vertical scale relative to it.

Thus, the quantities C, ϕ, and ψ must be known in order to determine the absolute radiance, and the spacing Δh must be known to perform the retrievals.

2.7.2 Instrument Description

The instrument has been described by Gille and Russell (1984), referred to below as GR. Here, a very brief summary is given, with emphasis on those features most important for determining the calibration and its stability during orbital operation.

A schematic of the optical train is shown in Figure 2.48. Radiation from the limb is reflected off the scan mirror to the primary mirror, an off-axis parabola that brings the light to a focus where it is chopped. A parabolic secondary recollimates the beam and directs it through a Lyot stop to a folding mirror, from which it passes through relay optics, interference filters that define the spectral response of the channels, and an FOV-defining mask, and onto mercury–cadmium–telluride detectors. The optics from the Irtran 6 lens through the detectors are cooled to about 61 K by the primary cryogen, solid methane. The optical train out to the thermal mask was maintained at about 152 K by the solid ammonia second-stage cryogen. The amount of methane in the cooler limited the experiment life to 7 months.

In operation, the scan mirror caused the line of sight (LOS) to traverse the limb at a rate of 0.25 degree per second. The mirror position is controlled by a low-resolution sensor, but accurate relative positions are obtained from a 15-bit optical encoder on the scan mirror shaft, which nominally puts a pulse into the data stream for every 79.1 arc seconds of LOS motion, or approximately every 1.4 km. The encoder was used to determine Δh.

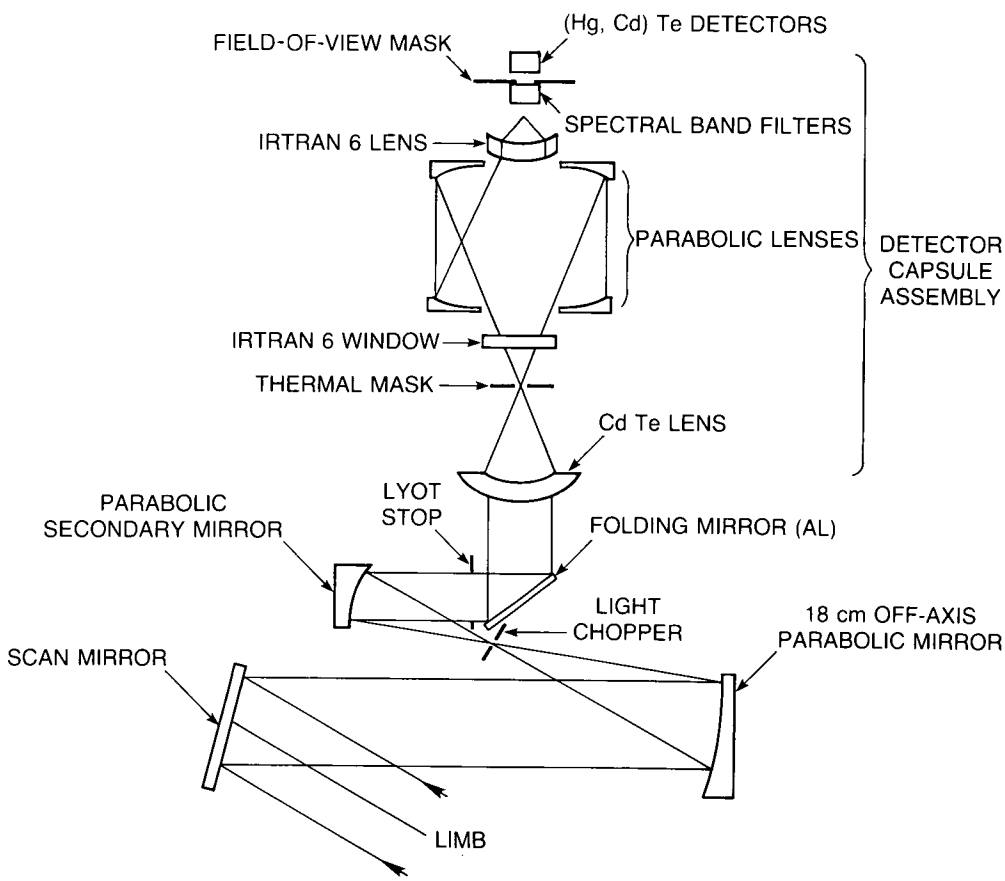

Figure 2.48 Schematic drawing of LIMS optical train (from Gille and Russell, 1984).

To ensure that all channels scanned high enough to see cold space and low enough to view the hard Earth, the total scan was 3 degrees, making each down or up scan 12 seconds. After every second up-down scan pair, the scan mirror scanned up so that a small off-axis blackbody cavity in the focal plane adjacent to the chopper, at the focus of the primary, was reflected from the scan mirror back through the optics, in the same way a signal would be. The temperature of the cavity was held at 308 K, and its temperature was monitored by a platinum resistance thermometer and a backup thermistor. The cavity design should be relatively insensitive to changes in the condition of its surface. The calibration of this inflight calibrator (IFC) will be discussed further below.

After viewing the source for ~2 seconds, the mirror scanned down to a position in which all channels were viewing above the detectably emitting atmosphere, and viewed space for 1 second, to get a cold radiometric calibration point. The scan sequence then began again.

2.7.3 Preflight Calibration

The ability to obtain retrievals required that the absolute radiances be measured, which in turn required that the instrument characteristics defined by Δh, $\phi(h)$, $\psi(\nu)$, and C(N) be known accurately. The first three are not expected to change from the laboratory to orbit, and were measured on the ground. The radiometric response depends on a number of factors, including detector temperature and possible degradation in the optics, which require inflight calibration. The latter requires that the characteristics of the IFC under different instrument conditions be known.

Encoder Spacing

The repeatability of a given pulse position was determined to be 1–2 arc seconds. The average pulse spacing, 80.4 arc seconds, was slightly larger than the nominal 79.1 arc seconds, and there was an unexpected small oscillation of the mean spacing of the pulse positions (these deviations were subsequently used in the data calibration software to get a better relative vertical registration of the radiance samples).

Field of View

The instrument was mounted in a protected enclosure purged with dry nitrogen for most of the optical tests. The FOV shape was measured by scanning the radiometer very slowly across a hot wire, which had an angular width about 0.1 that of the CO_2 and O_3 channels. The normalized results of these scans are shown in Figure 2.49. For reference, one milliradian translates to ~3.6 km at the limb.

The major peaks correspond to the positions of the channels on the FOV mask. The response of one channel seen at the position of another channel is an unwanted side lobe feature. Other tests showed that these side lobes were not caused by radiation outside the spectral passband of the channel, but are believed to be due to internal reflections between the interference filters and the concave rear side of the final lens; the negative values result from the 180° phase difference in chopping of the narrow and wide channels. These are extremely important for interpreting the measurements, since when a main lobe is viewing weak radiance at 50 km, even a small side lobe viewing the large tropospheric radiance can provide a significant fraction of the received signal.

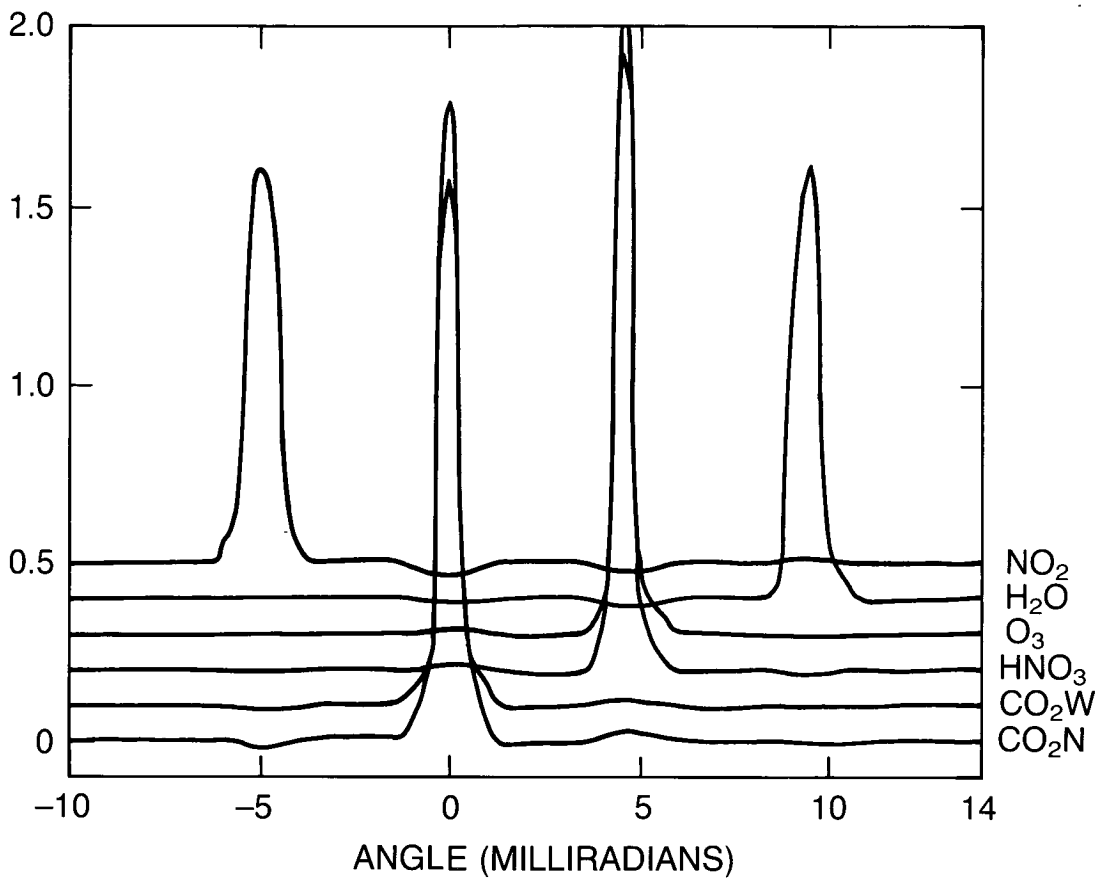

Figure 2.49 Normalized instantaneous FOV functions for the six LIMS channels. The response of a channel at the position of another channel is a side lobe. Toward the left is the downward (Earthward) direction on a scan (from Gille and Russell, 1984).

To correct for this effect, the shapes of the side lobes were taken from the hot wire scans, but the magnitudes were determined from scans across a knife-edge target, for which there was a better signal-to-noise ratio. The corrected spatial response function was Fourier transformed (to yield the transfer function of the optics and FOV mask) and multiplied by the electronics frequency response to give the system modulation transfer function. This was used in the spatial frequency domain to remove side lobe effects and to partially deconvolve the effects of the FOV on the radiance scan, as outlined in GR and described by Bailey and Gille (1986).

Spectral Response

The relative spectral response $\phi(\nu)$ of the instrument was determined by aligning a monochromator having 1–2 cm^{-1} resolution on a given detector and measuring the response of the instrument as the monochromator scanned in frequency. Three in-band measurements of spectral response were made at two perpendicular orientations of a polarizing screen, and the resulting values were averaged. Individual runs generally differed by less than 0.01 at a given frequency. Monochromator output was calibrated against a thermocouple bolometer that was traceable to a spectrally flat, black standard.

Wavelength calibration of the monochromator was performed, using a HeNe laser line seen in high-order reflection from the grating, with CO_2 and H_2O lines from the small amount of room air in the protective enclosure, to define the frequency scale, estimated to be known to be ≤ 0.7 cm^{-1}.

The shapes of the relative spectral responses are shown in Figure 2.50, while the cuton and cutoff points (5 percent response) are tabulated in Table 2.11.

Table 2.11 Characteristics of LIMS Channels*

Channel	Emitting Gas	Bandpass 5% Relative Response Points cm^{-1}	Field of View at Limb, km Vertical	Horizontal	Noise Equivalent Radiance (W/m^2sr)
1	NO_2	1560–1630	3.6	28	0.00055
2	H_2O	1370–1560	3.6	28	0.0023
3	O_3	926–1141	1.8	18	0.0037
4	HNO_3	844–917	1.8	18	0.0015
5	CO_2W	579–755	1.8	18	0.0055
6	CO_2N	637–673	1.8	18	0.0014

*From Gille and Russell, 1984

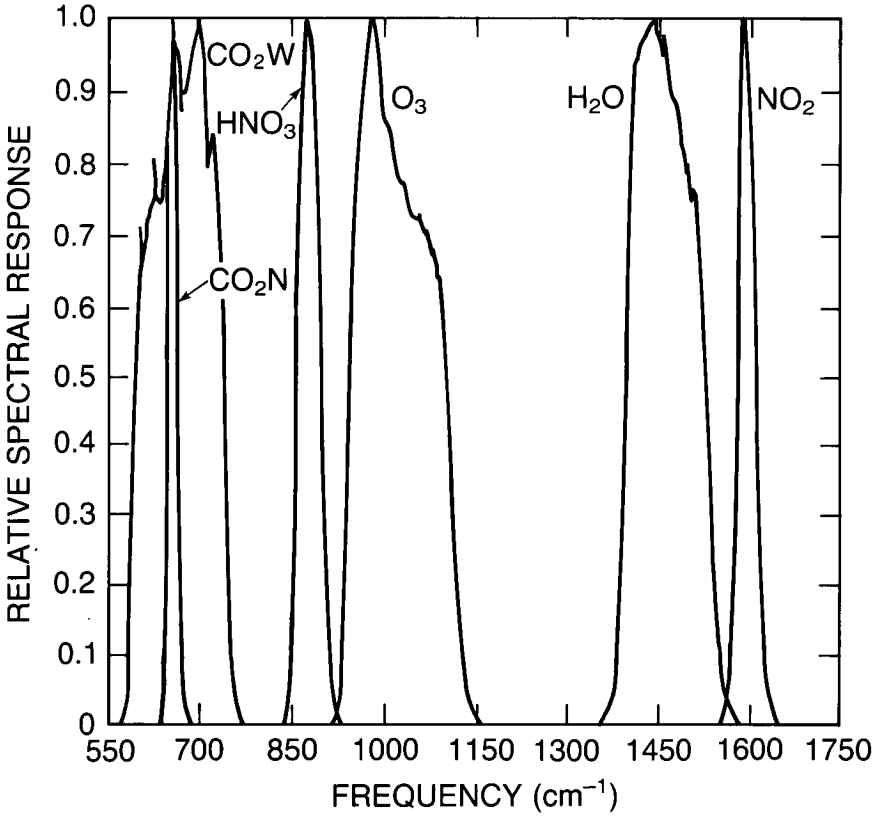

Figure 2.50 Normalized spectral response curves for LIMS channels (from Gille and Russell, 1984).

In addition to the in-band scans, slow scans with lower spectral resolution were performed to look for out-of-spectral-band leaks. The requirement of <0.2 percent of full response in the out-of-band regions was met for all channels from 2 to 20μm, beyond which other optical elements effectively reduced the response to zero.

Finally, the output signal from each channel was measured when every other channel was irradiated with radiance at its center frequency. Responses were $\lesssim$ 1 percent in all cases, with many being zero.

Radiometric Calibrations

This test was carried out in the vacuum chamber while the instrument was being exposed to the range of thermal conditions expected to be encountered in orbit. The radiometer viewed a honeycomb blackbody target (emissivity $\geq$ 0.997) at a series of known, uniform temperatures, so that the radiation reaching the detectors could be calculated accurately and related to the instrument output. The two major functions of this test were to measure any nonlinearity in the radiometer response and to calibrate the IFC so that it could function in orbit as a transfer standard.

The target blackbody radiances (estimated accuracy $\leq$ 0.6 percent) were then convolved with the measured spectral response curves to give the relative signal that each channel was expected to see. Calibrations were performed at three instrument temperatures near 288, 298, and 308 K.

A typical calibration curve at 298 K is shown in Figure 2.51a, which compares the target observation to the IFC, but which does not allow any departures from linearity to be seen easily. Figure 2.51b shows the same results, after the least-squares straight-line fit has been removed. The departures from linearity are consistent, although they are small compared to the requirements, and could be due to problems with the test setup. The radiometer response was taken to be nearly linear, with a slight quadratic component.

The IFC signal does not lie on the same line as the calibration target. This is primarily because the IFC has an emissivity <1 and thus reflects some lower temperature radiation from the surrounding instrument onto the detectors. In addition, there is one more reflection off the primary mirror during calibration than during atmospheric observations (or target calibration). By using the calibration results at all three instrument temperatures, the target and mirror emissivities were determined. These values were used to correct the IFC radiances measured in orbit. The random noise did not depend on target or instrument temperature.

2.7.4 Instrument Calibration and Performance in Orbit

LIMS instrument activation took place on October 24, 1978, during the first few orbits, when pyrotechnic valves were fired, allowing the methane and ammonia to begin subliming to space. The methane temperature, which is very close to the detector temperature, immediately began to drop from the prelaunch value (~70 K) to its expected operating level near 61 K. The subsequent methane temperature history is shown in Figure 2.52. As methane depletion approached, the temperature rose, very slowly at first, then more rapidly. (Small downward spikes indicate the temperature drop when the instrument was turned off.)

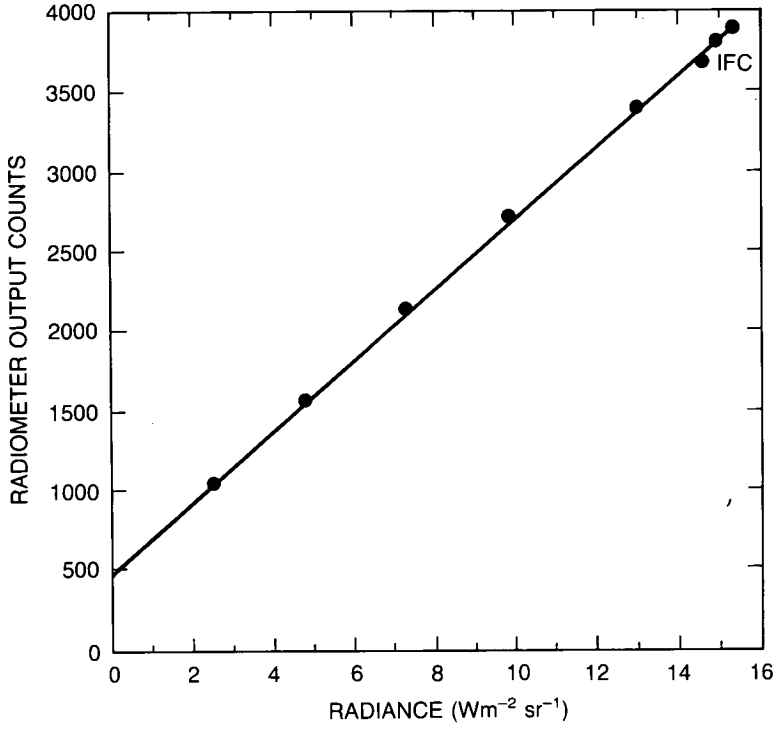

Figure 2.51a LIMS primary calibration curve for ozone channel; • • • indicate measured points; line is least-squares fit.

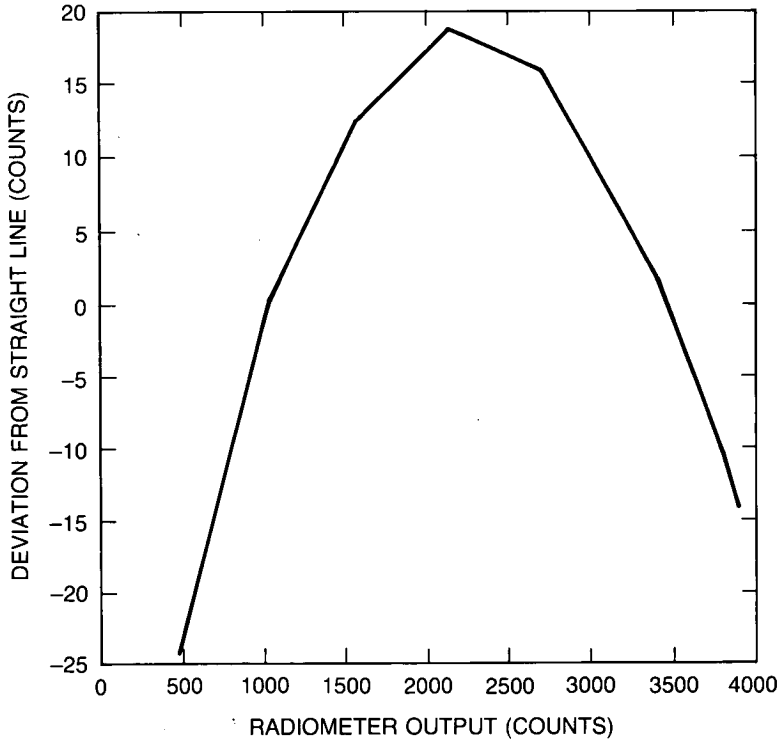

Figure 2.51b Departure of curve in 2.51a from linearity.

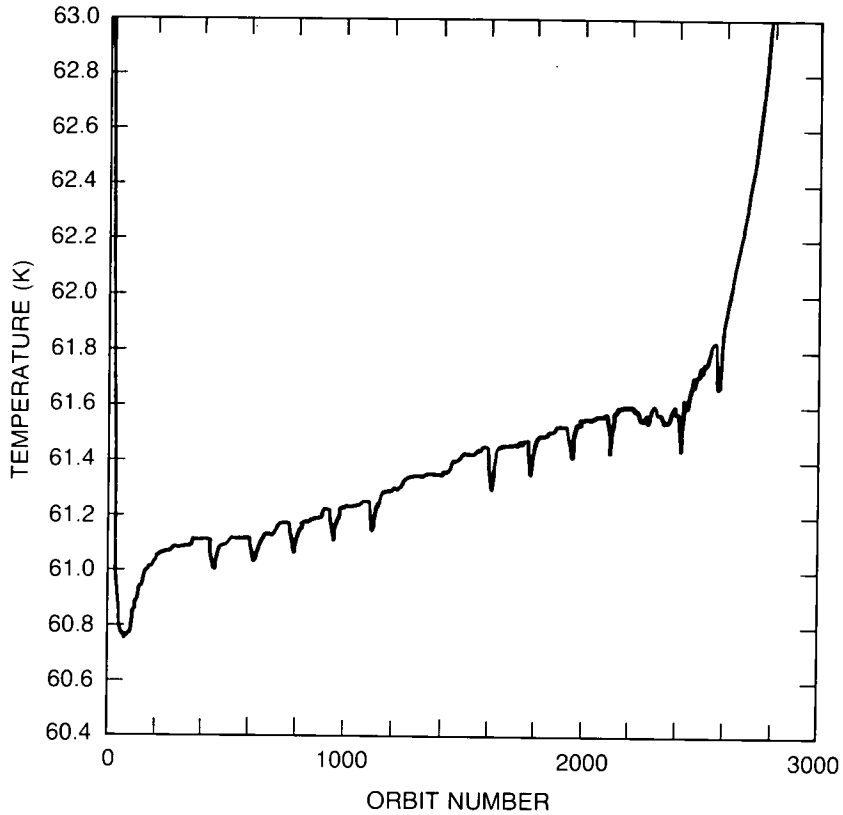

Figure 2.52 LIMS detector temperature vs. time (expressed in orbit number). One week is approximately 100 orbits.

The radiometer performed according to expectations when it was turned on during the first day and whenever it was turned on later. A wide-angle scan located the desired part of the limb, which was tracked by the adaptive scan thereafter.

The operation of the instrument under orbital conditions can be assessed by studying the results of the inflight calibration sequence. The stability of the IFC temperature over the mission is discussed in GR; it was constant to ± 1 bit (0.023°) during an orbit and close to that for the mission. GR also shows the variation of several instrument temperatures around a typical orbit. The temperatures of the outer baffles, primary mirror, and chopper plane drop during the southward (night) part of the orbit, then rise on the northgoing (day) portion. The temperature variation is slightly larger for the outer baffles and the primary mirror than for the focal plane, further inside the instrument. Although the variations are small, their effects must be carefully removed to interpret the small signals in some channels, as well as to take full advantage of the low noise levels of the radiometer.

The IFC and space view signals vary around an orbit, due to radiation reaching the detectors from parts of the radiometer where temperatures vary. The IFC and space signals follow each other closely, although the scale factors between radiance and voltage, which would be constant if the signals varied by the same amount, do show small (~0.5–0.7 percent) variations around the orbit. These are shown for the CO_2 and O_3 channels in Figure 2.53. These variations may be due to a residual and unexplained temperature dependence of the instrument response that had

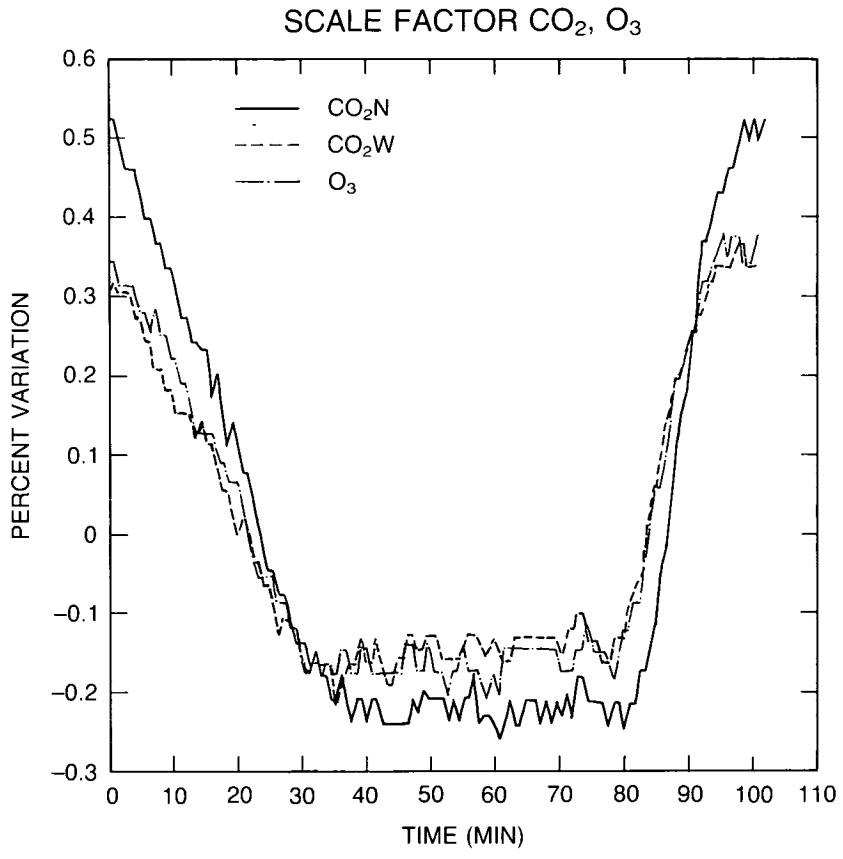

Figure 2.53 Percent variation of indicated scale factor around an orbit for LIMS carbon dioxide (temperature) and ozone channels.

been observed earlier in the laboratory, or may indicate the sizes of residual uncertainties in the inflight calibration.

The long-term stability of the scale factors over the mission is illustrated in Figure 2.54a,b,c, by the performance of the O_3 and CO_2 channels, as well as the similarity to the preflight calibration values. Note that changes in scale factor or offset are not a problem, as they are measured frequently in space.

The noise level may be determined as it was in the laboratory, by calculating the standard deviation of the output radiance when the radiometer is viewing the steady signal from space or the IFC target. These two determinations are quite close, with the IFC giving figures slightly larger, presumably due to tiny variations in temperatures in the IFC cavity or slight movement of the LOS across the target.

The noise behavior determined from the orbital data is illustrated in Figure 2.54d by results from the O_3 channel. There is no change, even at the end of the mission. The noise levels shown in Table 2.11 are based on the more conservative computer calculations.

These figures, taken together, clearly indicate instrument performance that is very close to design levels, stable, and in agreement with values measured on the ground.

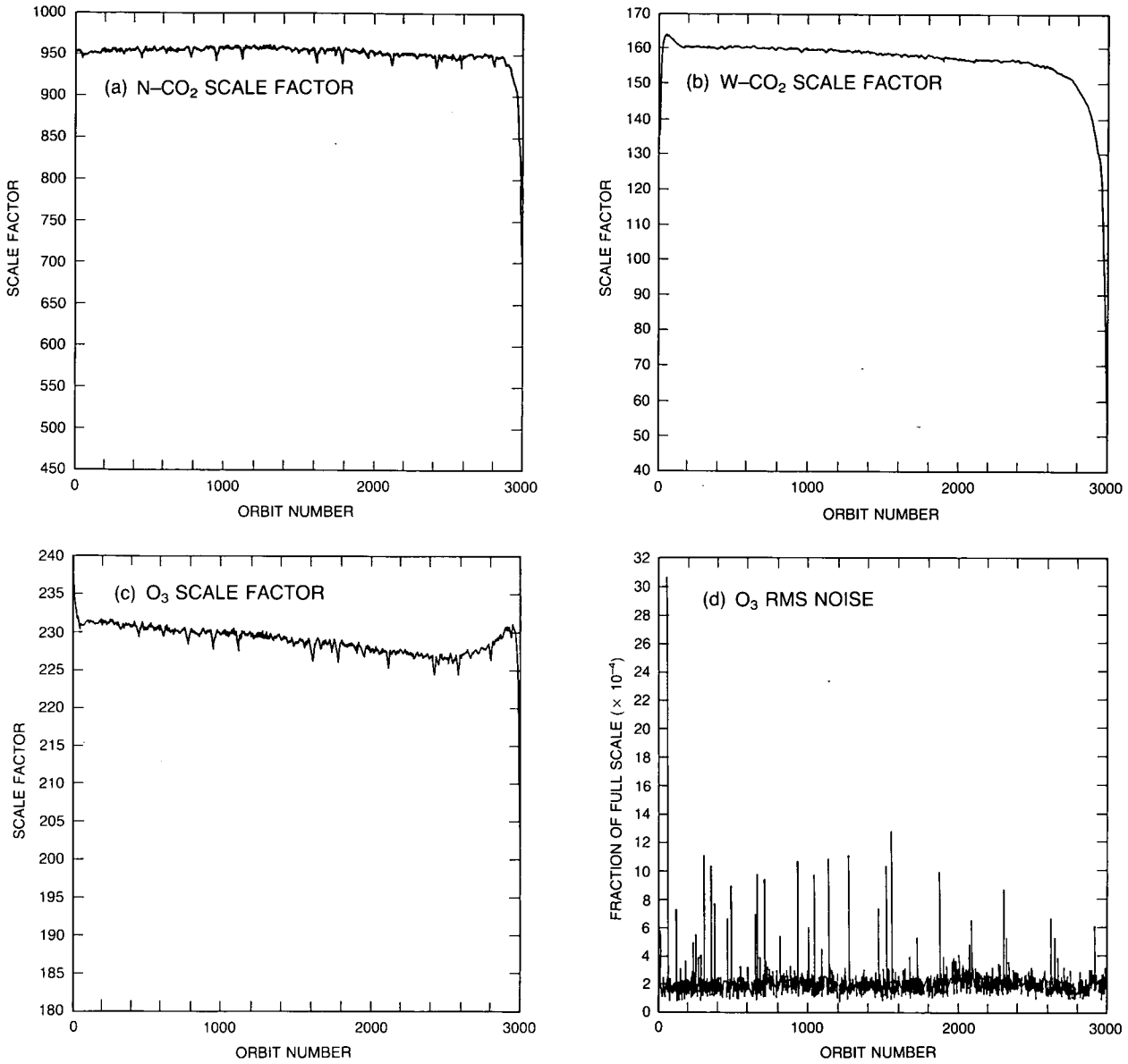

Figure 2.54 (a) Scale factor for narrow CO_2 channel as a function of time during LIMS missions. (b) Scale factor for wide CO_2 channel as a function of time during LIMS missions. (c) Scale factor for wide O_3 channel as a function of time during LIMS missions. (d) RMS noise in O_3 channel as a function of time during LIMS missions.

2.7.5 Instrumental Factors That Could Lead to Measurement Trends

At this point, the instrumental characteristics are discussed in light of possible changes that could take place and result in long-term changes.

Encoder Spacing

The design of the encoder resulted in four series of encoder pulses. These might shift relative to one another, but the spacing in each string should be nearly constant at about 320 arc seconds.

C-2

The spacing of the pulses could be roughly assessed on the assumption that the scan rate was constant, and knowing the time of the pulses to 0.25 ms. This showed no evidence of changes with time over the life of the experiment.

Electronic Filter Response

The chopper frequency was carefully controlled with a feedback loop. The response is determined by the electronics. The low frequency response is determined essentially by the inflight calibration. No evidence of a change in high-frequency response was seen, but it would have been difficult to detect. In the unlikely event that this or a phase shift occurred, it would have affected only the spatial components with higher frequencies and not those on which a long-term mean would have been primarily based.

Field of View

This is determined by a physical mask. It is possible to imagine a mechanical shift of the whole mask, which would have affected all channels. If it were small, it would not matter; if it were large, it would be catastrophic, and impossible to overlook. No evidence for a change was seen.

Spectral Response

It is possible to imagine the filters having a sudden failure, such as a partial delamination, but it seems very unlikely once the filters had been mounted in the detector capsule assembly (which had been evacuated). Similarly, they are not exposed to contaminant buildup from spacecraft outgassing. Outgassing from the interior of the detector capsule assembly (DCA) should be small at those temperatures. In addition, the DCA had been assembled and evacuated for several months when the spectral response measurements were made. Any residual outgassing in the DCA would have been included in the measured spectral response values.

Radiometric Calibration

The radiometric response should depend strongly on detector temperature. As Figure 2.51 shows, the detectors were nearly constant in temperature for both long- and short-term variations. The temperature of the IFC was very constant over the entire life of the mission, as indicated by both readouts. It is possible that the surface emissivity of the material lining the cavity of the IFC changed, but the cavity design requires incident radiation to make several reflections on the average before it reemerges, making the output of the cavity less dependent on the details of the surface state, and more like that of a blackbody.

Because the same optical train is used for calibration and for making atmospheric measurements, the results should be insensitive to changes in instrument response. However, the primary enters into the optical train twice on the calibration, and only once on the measurement. A change in its emissivity would result in some change in response. There is some evidence that something like this might have occurred, as the size of the variation of the calibration around an orbit grew larger with time in orbit. However, the variation was from a peak amplitude of 0.3 percent on orbit 100 to 0.7 percent on orbit 2850. The effect of any such change was clearly quite small, as the regular long-term change of the calibration factor shown in Figure 2.54 indicates. In addition, because of its location well inside the instrument housing, the primary should be relatively protected from the general spacecraft outgassing. This possibility cannot be neglected, however, nor can the effects of outgassing by the instrument baffle material or insulating wraps.

2.7.6 Conclusions

The evidence suggests that the LIMS, because of its design and inflight calibration, operated in a very stable manner from shortly after activation on October 24, 1978, until after May 20, 1979, when its solid cryogen was nearly depleted. The data over this time should not exhibit any spurious trends of more than a few tenths of a percent.

2.8 OTHER INSTRUMENTS

Four other measurement systems that have not been treated in detail are relevant to the present discussion. These are briefly described here.

2.8.1 The Backscatter Ultraviolet (BUV) Experiment

The BUV, which flew on Nimbus–4, was the forerunner of the SBUV. It was launched in April 1970, and operated for 7 years. The experiment is described by Heath et al. (1970, 1973, 1975). Basically it was very similar to the SBUV, but differed in that the input radiance was not chopped and the diffuser was continuously exposed. In addition, power and tape recorder limitations on the spacecraft limited the amount of data collected.

Thus, the data from the BUV are poorer and fewer than those from the SBUV. The BUV diffuser degraded faster than that on SBUV, and the technique to determine degradation constants on SBUV cannot be applied. Some ingenious attempts have been made to correct the instrument drift based on ground-based observations of ozone profiles, and the albedo of the Sahara. All wavelengths show large drifts, but the accuracy and validity are hard to characterize. It appears that effort is better spent trying to understand the SBUV and its degradation. At that point, it may be possible to apply this knowledge to the BUV, but it seems somewhat unlikely at the moment that much additional information on trends can be extracted from BUV.

2.8.2 The SBUV–2 Operational Instrument

The SBUV–2 instrument was designed for flight on the NOAA series of satellites as part of its operational meteorological satellite program. The first instrument was launched in December 1984, and began making operational measurements in April 1985. The design is based largely on that of the Nimbus–7 instrument, and thus only the major differences will be discussed in this section. These are summarized in Table 2.12. A detailed description of the instrument has been given by Ball Aerospace Systems Division (1981).

The largest difference between the two instruments is that the onboard mercury lamp, which was used on Nimbus–7 for wavelength calibration only, can be repositioned on SBUV–2 so that light from the lamp can be either reflected off the diffuser into the instrument, or reflected directly into the instrument. This enables the reflectivity of the diffuser plate to be monitored. A second difference has to do with the photomultiplier output. In SBUV, all three ranges of the electrometer amplifier are taken from the anode; thus, the ratios of the three ranges will be independent of the gain of the photomultiplier. In the SBUV–2 instrument, the least sensitive range of the electrometer (corresponding to the higher photon flux measurements) is taken directly from the cathode of the photomultiplier, while the other two ranges are taken from the anode. The ratio between the anode and the cathode signals is the gain of the photomultiplier. The gain change mechanism has been changed on models after the first one launched. A third

Table 2.12 Comparison of Important Features Between SBUV–2 and SBUV

Features	SBUV–2	SBUV
Monochromator mode	4 (discrete, sweep wavelength, and position)	4 step (continuous wavelength, and cage cam)
Control of monochromator mode	FIX System FLEX System (wavelengths can be changed by command)	One fixed system
Scene mode	4 (Earth, Sun, wavelength calibrate, diffuser check)	2 (Earth and Sun)
Diffuser position	4 (stow, Sun, wavelength calibration or diffuser check, & decontamination	2 (stow and Sun)
Mercury lamp position	2 (stowed and deployed)	1
CCR wavelength	379 nm	343 nm
Shortest wavelength of discrete mode (other 11 wavelengths match)	252 nm (in FIX system)	255.5 nm
Wavelength calibration steps	12	5
Electronic calibration	Every scan in retrace	By command
Scanning discrete mode sweep mode	 32 seconds 192 seconds	 32 seconds 112 seconds
Sampling time discrete sweep	 1.25 seconds 0.1 second	 1 second 0.08 second
Diffuser check	Yes	No
Diffuser decontamination	Yes	No
Gain Range	2 from PMT anode 1 from PMT cathode	3 from PMT 1 from ref. diode
IFOV	11.3° × 11.3°	11.3° × 11.3°
Discrete (step scan) scanning direction	From short to long wavelengths	From long to short wavelengths

difference is that the grating drive on SBUV–2 is direct, through a stepping motor on the grating shaft, and not cam driven as on SBUV.

Although SBUV–2 is an operational instrument, and data collection began 2 years before this study, no data have been available for evaluation of the stability of its calibration, the degradation of its diffuser, or its simultaneous ozone measurements. In addition, it appears that many of the lessons learned by SBUV have not been incorporated by NOAA in the processing of SBUV–2 data. An analysis of the instrument performance of Flight Model 1 during the first 3 months of operation is given in a paper by Frederick et al. (1986), which also contains a fuller overview of the instrument. As is to be expected, the analysis uncovered several aspects of instrument behaviour not expected prior to launch. Recommendations for software changes were made and are now included in the latest engineering algorithm used in the data reduction.

By October 1985, the reflectivity of the diffuser plate, as measured by the onboard mercury lamp, had apparently decreased by 15 percent, yet the solar flux signal at 273.5 nm showed no such degradation. An enhanced deployment of the diffuser plate carried out in August 1986 suggests that the diffuser plate had degraded by no more than 2 percent by that time. Thus, it appeared that the onboard diffuser calibration was in error. The problem was traced to a design error. The lamp is viewed directly when placed in front of the slit, and, as the lamp is in the form of a narrow folded discharge, only a portion of the IFOV is filled. On the other hand, the entire FOV is filled when the lamp is reflected off the diffuser plate. The throughput of the instrument is not constant across the FOV, and, thus, changes in the characteristics of the discharge could manifest themselves as apparent changes in the diffuser reflectivity. In a new design, to be used in all future flight models, the lamp is reflected off a small diffuser before it is used in either mode.

It is interesting to note that the inferred diffuser plate degradation of less than 2 percent by August 1986 is considerably smaller than that for the SBUV instrument for the same period of exposure. This suggests that either the NOAA spacecraft or the SBUV–2 instrument is much cleaner than Nimbus–7 or SBUV. NOAA's failure to process these data for use in this and other aspects of the ozone trend studies has made them much more difficult. NOAA is strongly encouraged to process and understand the SBUV–2 data, which are critical to a continued measurement of ozone trends.

2.8.3 The Solar Maximum Mission (SMM) Ultraviolet Spectrometer Polarimeter (UVSP)

This occultation experiment utilizes the Tanberg–Hanssen ultraviolet spectrometer polarimeter on the SMM spacecraft. Launch occurred in early 1980, but solar pointing was lost in late 1980. In-orbit spacecraft repairs were effected in 1984, and operations have continued since that time. Details of the instrument and its performance have been described elsewhere (Woodgate et al., 1980). Briefly, the instrument consists of a Gregorian telescope having a geometric aperture of 66.4 cm, followed by a 1-m Ebert–Fastie spectrometer and five detectors. The spectrometer is equipped with a 3600-line/mm grating. Rotation of the grating provides wavelength coverage between 1150Å and 1800Å in second order and 1750Å and 3600Å in first order. Areas of the Sun as small as 3 arc seconds can be studied.

The experiment shares with SAGE the advantages and disadvantages of occultation measurements for long-term trend determinations. Because of the wavelengths used, ozone profiles are obtained over the altitude range from 50 to 70 km. Appreciable amounts of data are now

being collected and reduced, but the record with appreciable data is not long, and the profiles barely extend down to levels where they can be compared to other experiments. It could provide data for future studies of trends of mesospheric ozone.

Further details of the experiment may be noted. In conducting the ozone experiment, the entrance slit size is set at 1 × 180 arc seconds and the exit slit width is 0.01Å. Spectral resolution is 0.02Å in second order and 0.04Å in first order. The wavelength drive is fixed at a single wavelength. The experiment is conducted by observing the attenuation of a narrow-wavelength region within the Hartley ozone absorption bands during satellite crossing of the terminator. The resulting intensity during any time of the occultation is given by the Lambert–Beer law relating the observed and unattenuated intensities, respectively, at the tangent height h and the height where no attenuation occurs. The solar intensity is attenuated exponentially by the optical depth. The optical depth is equal to the product of the ozone absorption cross-section and an integral giving the total amount of ozone between the Sun and the satellite. The resulting integral equation is solved for the ozone concentration, making use of the fact that it is a linear Voltera integral equation of the first kind. The atmosphere is divided into a series of concentric shells at altitudes defined by the tangent heights corresponding to averages of the measured points. The integral equation is then represented by a sum over the number of shells so that the equation is now a matrix equation that can be inverted. Complete details are given in a publication by Aikin et al. (1982).

Two observing wavelengths were employed. The first was at 2765Å near the MgII line. In this experiment, the spectrometer wavelength range was 1Å and the maximum intensity in this range was detected. This wavelength was then employed for the occultation. The experiment was performed between November 1984 and March 1985. The remainder of the data from August 1985 until May 1987 were also collected while performing the experiment at a single wavelength. Due to an instrument malfunction caused by a broken wavelength drive, there is some uncertainty in the wavelength utilized in the experiment. This is reflected in the absolute cross-section to be employed in analyzing the ozone data. The final wavelength position was at 1379.528Å in second order. To convert this to first order the wavelength is doubled. In addition, it is necessary to correct for the offset between the different slits employed for experiments in first and second orders. This offset amounts to +4.586Å as determined by prelaunch calibration. The wavelength used for ozone measurements is 2764 with an uncertainty of ±10Å. Using the cross-section data of Molina and Molina (1986), this translates into an uncertainty of +5.25Å percent and -8.33 percent.

In addition to the error introduced by uncertainty in wavelength, there are other sources of error due to pointing uncertainty, photon counting noise, and ephemeris error (Aikin et al., 1982). Pointing introduces ±0.36 km. An ephemeris error in orbital track of 100 to 200 meters will introduce an altitude uncertainty of 0.14 to 0.28 km.

2.8.4 The ROCOZ–A Ozonesonde

The ROCOZ–A ozonesonde (Barnes and Simeth, 1986) is a four-filter, sequential-sampling, ultraviolet radiometer. The instrument is propelled aloft by a Super–Loki booster rocket. At rocket burnout, the instrument and its carrier coast to a nominal apogee of 70 km, where the payload is ejected for deployment on a parachute. The instrument measures the solar irradiance over its filter wavelengths as it descends through the atmosphere. Using the Beer–Lambert law, the amount of ozone in the path between the radiometer and the Sun is calculated from the

attenuation of solar irradiance as the instrument comes down. In addition, radar from the launch site measures the height of the payload throughout its descent. This allows calculation of the fundamental ozone values measured by the radiometer, ozone column amount versus geometric altitude (Barnes et al., 1986). Ozone number density is the derivative of ozone column amount with respect to altitude.

Combined with auxiliary atmospheric soundings for pressure and temperature, ROCOZ–A results can duplicate the fundamental ozone values from all satellite ozone instruments. Details of the performance characteristics of the auxiliary pressure and temperature instruments are given in Barnes et al. (1986, 1987). Auxiliary ozone soundings are made with balloonborne electrochemical concentration cell (ECC) ozonesondes (Komhyr, 1969; Komhyr and Harris, 1971). Analyses of the accuracy and precision of the ECC ozonesonde have been published (Torres and Bandy, 1978; Barnes et al., 1985). ROCOZ–A flights are also accompanied by total ozone measurements with the Dobson spectrophotometer. A preliminary intercomparison with the Dobson, showing no bias at the 1 percent level, has been published (Holland et al., 1985). A complete Dobson intercomparison, again showing no bias between instruments, has been submitted for publication as part of a description of ROCOZ–A measurements at northern midlatitudes.

Measurements of the precision (profile-to-profile repeatability) of ROCOZ–A ozone column amounts and number densities are in the literature (Holland et al., 1985; Barnes et al., 1986). For both column amount and density, the precision of the measurements is 3–4 percent (one sigma). Additionally, the published results of an equatorial ozone measurement campaign (Barnes et al., 1987) showed very low variability in stratospheric ozone, pressure, and temperature. From the results of that campaign, the precision of ROCOZ–A ozone-mixing ratios is estimated to be 3–4 percent. The campaign also produced estimates of the precision of temperature measurements as 1 percent; pressure measurements as 2–2.5 percent; and atmospheric density measurements as 2–3 percent.

The accuracy estimates for ROCOZ–A ozone measurements come from an internal, unpublished error analysis. The analysis is based on errors in the effective ozone absorption coefficients used to convert the radiometer readings into ozone profiles, plus the differences between the ozone values at altitudes where two ROCOZ–A channels give simultaneous readings (Barnes et al., 1986). A laboratory flight simulator, based on long pathlength photometry (DeMore and Patapoff, 1976; Torres and Bandy, 1978), has been constructed to measure the accuracy of ROCOZ–A ozone measurements. Publication of a detailed error analysis will follow the conclusion of experiments with the flight simulator and will complete the primary characterization of the ROCOZ–A ozonesonde. The accuracy of ROCOZ–A ozone column and number density measurements is estimated to be 5–7 percent. For ozone-mixing ratios, the accuracy is estimated as 6–8 percent (Barnes et al., 1986).

Since individual ROCOZ–A radiometers are not recovered after flight, the long-term repeatability of measurements from the instrument is determined by the consistency of the calibrations of the radiometers with time. To ensure this consistency, the calibration facility for ROCOZ–A ozonesondes (Holland et al., 1985) incorporates physical standards that are periodically recertified at NBS. The dominant factor in the response of the four ROCOZ–A radiometer channels is the transmission of the ultraviolet filters. Measurements of the transmission of the optical components within the instrument are made with a Cary model 17–D double-beam spectrophotometer.

The wavelength readings of the spectrophotometer are calibrated in the ultraviolet with a low-pressure mercury discharge lamp. The linearity of the transmittance measurements from the Cary is checked with respect to the high-precision reference spectrophotometer at NBS (Mielenz et al., 1973; Eckerle, 1976). Details of the intercomparison of the spectrophotometers are given in Holland et al. (1985).

The electronic gains for the instrument channels are adjusted to provide output signals that are 80 percent of full scale at the top of the atmosphere. Gains are set with an argon maxi-arc, a somewhat larger version of the previously reported argon mini-arc (Bridges and Ott, 1977). The NBS certification of the maxi-arc is described in Holland et al. (1985). In addition to periodic certification at NBS, the maxi-arc is checked in the laboratory to assess the changes in the arc's output. The NBS certification of the maxi-arc is given as good to within 5 percent. This calibration is typically duplicated in the laboratory at the 3 percent level (Holland et al., 1985).

2.9 CONCLUSIONS

2.9.1 General Comments

It is difficult to design any instrument or system to measure ozone changes to 1 percent or less per year over a period of a few years. This is especially true if one requires that the instrument operate unattended, a condition that severely constrains the amount of recalibration, testing, and adjustment that can be carried out, and usually limits the length of the measurement series to a few years. The difficulties become truly formidable if one further demands that the instrument operate under the harsh conditions in space.

Among the problems in space are the vacuum that allows contaminant molecules to outgas from instruments and spacecraft, and the strong solar ultraviolet radiation. When the contaminants deposit on optical surfaces and are dissociated by the radiation, the optical characteristics change, and the throughput decreases by unpredictable amounts.

Nonetheless, satellite instruments are indispensable for the determination of trends of ozone on a global basis. In spite of the difficulties and the relatively early stages of development of most of the methods and measurement technologies, they have already made enormous contributions to our knowledge of the global distribution of ozone, including its spatial and temporal variations.

Since 1978, seven instruments have collected large amounts of data that have been reduced and are clearly relevant to the problem of ozone trends.

However, none of these instruments was specifically designed for trend measurements. Only two of the experiment descriptions mentioned long-term trends as a goal, but even these instruments did not take measures to ensure that reliable data for trend detection were obtained. Some were designed under cost constraints that precluded planning for extended operations. The operational SBUV–2 instrument was launched for trend measurements in 1984, but data are only now becoming available in sufficient amounts for careful evaluation. Thus, at this time reliance must be placed on instruments for which trend detection is an afterthought. In this situation, it is necessary to make the best use of available data. In most cases, under the impetus of this study, the data were extensively reanalyzed. All available information has been critically evaluated to establish the accuracy and long-term stability of these instruments. In some cases,

the uncertainties in trend-determining capabilities resulting from the present analysis are different from those reported by the experimenters.

It should be pointed out that, to compare the ability of each instrument to determine trends, it is necessary to compare derived ozone amounts. Some of the differences in reported trends may result from effects introduced by the retrieval algorithms.

2.9.2 Instruments and Techniques

This section summarizes some general comments on the measurement characteristics and problems of the different instruments, and reviews the features of their coverage.

The various techniques for measuring ozone are affected to some extent by changes in instrument sensitivity. Some techniques rely to first order on relative measurements or ratios obtained over a short time; from an instrument point of view, these are less susceptible to drift than those that require an absolute radiance measurement. In either case, greater confidence is obtained by monitoring the inflight sensitivity of the instrument, generally through measuring the response of the instrument to a known calibration signal. It is easier to be sure of the output of an inflight calibration source in the infrared than in the visible, where, in turn, more stable sources are available than in the UV. In addition, the effects of instrument degradation are generally more pronounced in the UV than in the visible and infrared.

The SAGE–I and SAGE–II instruments fall into the relative measurement category. They measure infrared solar radiation during the occultation periods at sunrise and sunset; ozone is deduced from the relative attenuation of the solar signal over a period of tens of seconds. For both SAGE instruments, additional information suggests that other instrumental contributions to errors of trend determination are small. The principal limitation in occultation techniques is that only two profiles are obtained per orbit, at two latitudes that depend on spacecraft orbit and astronomical factors, and thus the coverage is sparse compared to other techniques.

A characteristic of these (and other) limb-viewing techniques is that they require very accurate knowledge of the direction of the line of sight or, equivalently, the tangent height of the ray path through the atmosphere. For SAGE–I and SAGE–II, these have now been calculated from the ephemerides of the Sun and the spacecraft. To do this requires accurate spacecraft tracking and accurate timing data, but these problems appear to have been solved satisfactorily for the SAGE instruments.

The SME UVS experiment also makes use of a relative measurement technique. The instrument measures the solar UV radiation scattered by Earth's limb as the IFOV scans across it. The presence of ozone alters the limb radiance profile from that of a purely Rayleigh-scattering atmosphere, and it is the shape of the radiance profile measured by the short-wavelength channel during a single limb scan (fraction of a second) that provides information on the absolute ozone concentration. In this case, measurements are possible anywhere along the orbit on the daylight hemisphere.

However, independent information on SME pointing directions is not available with sufficient accuracy, forcing the use of the UVS itself to determine those directions. In this case, the absolute calibration of the long-wavelength channel enters, making it sensitive to first order to changes in instrument sensitivity and model inaccuracies. This has apparently been several percent; additional information from the visible spectrometer, with some reasonable assump-

tions about the drift of its visible diodes, has been used to establish limits on the drift of the long-wavelength UVS calibration.

Other methods of measuring ozone are directly related to the photometric calibration of the instrument, and trends in ozone can be known only as well as the trends in the instrument response. These can be determined best by using an inflight calibration device. Two such instruments have been included in this study, the SME NIR and LIMS. The NIR measures the 1.27 μm emission from the $^1\Delta_g$ state of molecular oxygen, a product of ozone photodissociation. The instrument has an internal calibration lamp that suggests that the NIR has been quite stable over the 5-year SME mission. Again, the NIR is a limb-viewing instrument, and the pointing direction had to be determined externally from the UVS observations or from the SME horizon sensors. However, the signal is relatively insensitive to altitude at the signal maximum, near 0.75 mb. The technique derives values at the stratopause and in the mesosphere along the orbit over the daylight hemisphere.

LIMS measured the thermal emission of ozone in the 9.6 μm bands in the middle infrared. It carried a small blackbody as an inflight calibration device, so that its output can be calculated from basic physical principles. These have been used with good results in long-lived operational infrared temperature sounders. All inflight calibration data, as well as external comparisons, indicate that LIMS was very stable and well characterized over its short mission. The pointing direction toward the limb was determined from measurements from the LIMS CO_2 channels, and can be done quite accurately. Coverage is possible from any point in the orbit, on the day or night side.

The SBUV and TOMS instruments almost fall in the category of devices making relative measurements. They compare the signals of solar radiation backscattered from Earth's atmosphere to solar radiation directly scattered from an instrument diffuser plate. Unfortunately, the reliability of their ozone determinations is directly related to the knowledge of the scattering efficiency of the diffuser throughout their missions. While there is information on the degradation of the entire optical train, there is no independent information at wavelengths at which ozone absorbs to allow the separation of the degradation in the diffuser reflectivity (which is the only part that affects the determination of the albedo, and thus ozone amounts) from degradation elsewhere in the optical system. While plausible models of the partitioning can be made, they cannot be proven to be correct. These are nadir measurements, and so are insensitive to pointing direction; measurements are possible along the orbit on the daylight hemisphere.

2.9.3 Trend Measurement Capabilities

The findings may be summarized and compared to show the altitude ranges and capabilities of the data now available. Two related quantities are compared: the minimum detectable ozone change over the life of the experiment, and the minimum detectable ozone trend, which is usually the minimum detectable change divided by the life of the experiment.

Measurements of the Vertical Distribution

- SAGE–I and –II—Of the error sources discussed in this chapter, it is apparent that for either instrument the ozone and Rayleigh cross-sections will remain constant. Taking the root sum square of the other error sources leads to the conclusion that SAGE–I can discern an ozone change of 2 percent near 25 km, 4 percent at 20 and 6 percent near 40 km. Similarly, for SAGE–II, the values are 1.3 percent, 4 percent, and 3 percent, respectively. However,

because of the difficulties of sampling the same latitudes at the same seasons and under the same atmospheric conditions, in general it is not possible to detect changes of this size unambiguously. On the other hand, the instrumental uncertainty in the differences between SAGE–I and SAGE–II (for situations carefully matched in latitude and season) is ±1.5–2 percent between 25 and 45 km; this value is plotted in Figure 2.55. This does not include the effects of errors resulting from systematic geophysical variations between the matched pairs of situations that are sampled. At present, these have not been quantified.

To make a rough estimate of the annual rates of ozone decrease that can be determined, it is necessary to consider the time period over which a change might be sought. Although SAGE–I operated for 34 months, only 2 complete years of operation are used because of the sampling problems. A SAGE–II data record of the same length is now available. Dividing the detectable changes mentioned above by their 2 years of operation indicates that, near 40 km, trends of the order of 1.5–3 percent per year are detectable (in principle). Again, the interaction of measurement sampling with natural variability requires that these numbers be regarded as no more than suggestive. It should be pointed out that, as the SAGE–II mission extends to 3 and more years, in principle it will be able to detect correspondingly smaller trends.

There are roughly 5 years between the midpoints of the SAGE–I and SAGE–II data. Dividing this into the ±1.5–2 percent minimum detectable total change based on instrumental factors suggests a minimum detectable trend of ±0.3–0.4 percent per year, which is shown in Figure 2.56.

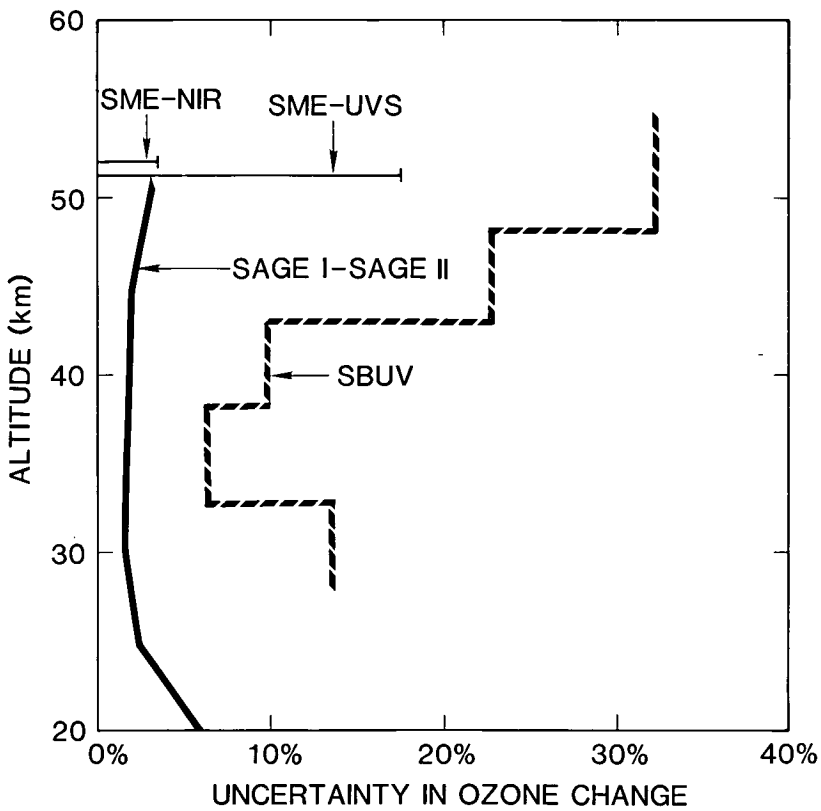

Figure 2.55 Uncertainty in total change determined by the various experiments over their lifetimes, as functions of altitude. For SBUV, the uncertainty is half of the range between models of high and low diffuser degradation.

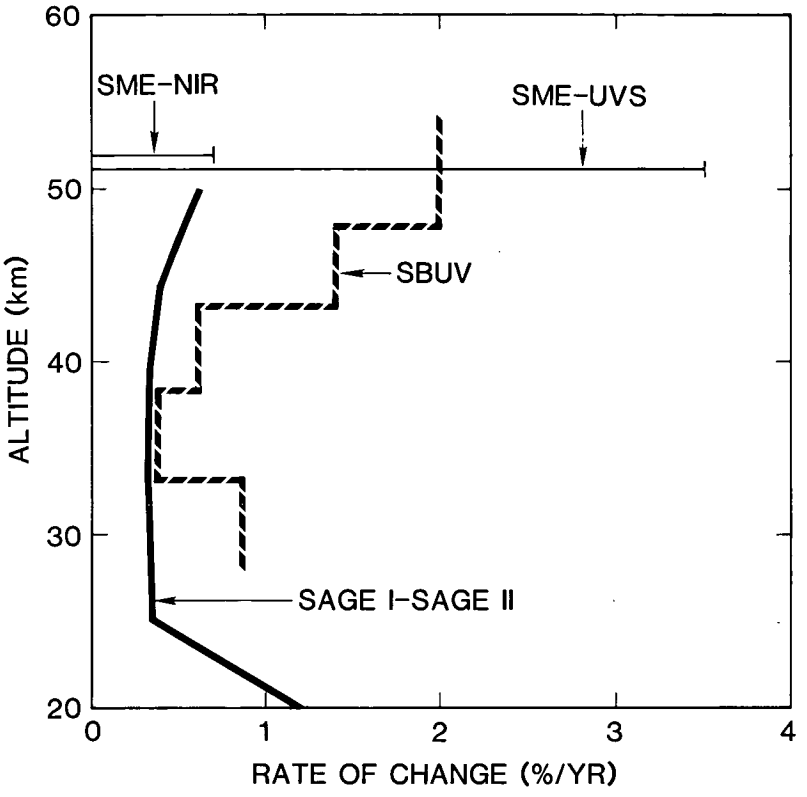

Figure 2.56 Uncertainties of trends determined by various experiments over their lifetimes, as functions of altitude. For SBUV, the uncertainty is half of the range between models of high and low diffuser degradation.

- SBUV—The major instrumental uncertainty in the SBUV results is due to lack of knowledge of the way the diffuser plate has degraded with time. There are no measurements from the instrument that provide this information unambiguously. A family of models was introduced to provide a plausible range of values for the degradation. Based on differences in the model values after 8 years, the range of ozone content was calculated. One half of this range is plotted for Umkehr layers 6–10 in Figure 2.55. Thus, in layer 10, the range is 64 percent, or ±32 percent around the central value. Clearly, the range of ozone content based on these models is very large at all levels. It must be emphasized that the bounding values are rather arbitrary, and the actual values could even be outside this range, although this is felt to be unlikely for reasons mentioned below.

The range of detectable trends is presented in Figure 2.56 in the same way—i.e., in layer 10 the trend range of the models is 4 percent per year, or ±2 percent per year around the midpoint of the model results.

These models assume that the coefficients relating the degradation to the exposure time and the elapsed time are constant over the 8 years, which is not necessarily true, adding another degree of uncertainty.

The change in vertical ozone distribution (in Umkehr layers) from November 1978 to November 1986 is shown in Figure 2.57 for several different diffuser degradation models. The curve labeled OPT is based on the data in the archives in 1987. They show a large decrease near 50

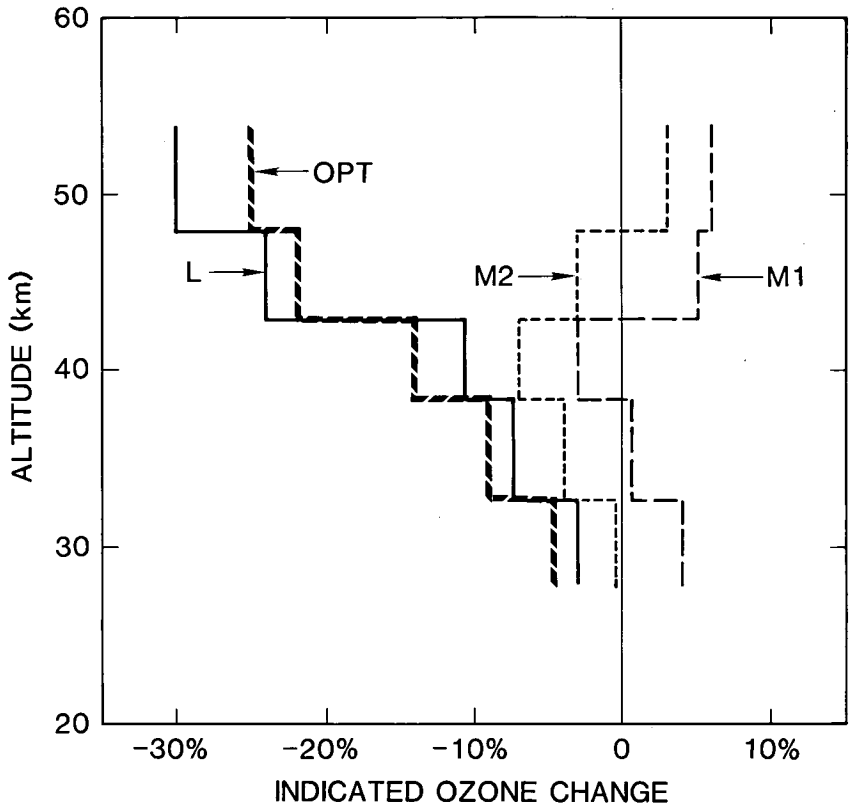

Figure 2.57 Midlatitude vertical distributions of ozone change from 1978–1986 determined from SBUV data, for several models of diffuser degradation. Curve marked OPT used the model employed in producing the data archived as of 1987. Curve L was calculated using a model with less diffuser degradation; M1 and M2 were derived using models with more diffuser degradation than the SBUV archive model.

km, which was reported by the principal investigator (Heath) to the Congress in 1987. The curve labeled L shows the same measurements, interpreted by means of a diffuser model with low degradation, while M1 and M2 indicate results obtained using two models with more degradation than the one used to create the archived data. These illustrate the nonuniqueness of the results, their strong dependence on the diffuser model, and the position of the archived values close to the low extreme of this family of models. M1 and M2 indicate small changes, or a slight increase in ozone near 50 km, with a small decrease near 40 km, similar to that indicated by the SAGE–I/SAGE–II differences. As noted below, total ozone derived using M1 or M2 agrees better with Dobson total ozone than do the archived (OPT) data. The wavelengths that provide information on the vertical distribution at 30–50 km are shorter than those that determine the total ozone, so the shape of the stratospheric profile depends only on the assumptions in the diffuser degradation model. The present results give weak support to the decrease at 40 km. It is possible to construct a reasonable model of the diffuser degradation that causes the vertical distribution of the SBUV rate of ozone decrease to agree with the SAGE–I/SAGE–II rate, and the SBUV change in total ozone to agree with the change in Dobson total ozone, but this provides no additional independent information.

These results indicate that the uncertainties in the diffuser degradation model, and the resulting uncertainties in ozone column amounts and vertical distributions, are much greater than has been stated previously. The weight of evidence also suggests that the diffuser degradation model used in producing the archived data has underestimated the diffuser

degradation, and thereby systematically underestimated the vertical ozone distribution, resulting in a large, but false, decrease.

- SME–UVS—The arguments presented in the report indicate that the SME–UVS instrument can determine an ozone trend at 0.75 mb to ±3.5 percent per year, or detect a ±17.5 percent change over the 5-year lifetime of the SME spacecraft.

- SME–NIR—From the considerations in the report, the trends at 0.75 mb apparently can be determined to be ±0.7 percent per year, or ±3.5 percent over the SME lifetime. However, this technique is very different from those that have been used before, and relies on an involved set of photochemical reactions. Until the underlying chemistry is understood more completely, the possibility exists that additional reactions are involved, or that there are unrecognized sensitivities to other factors. Thus, the instrumental error bars shown here may be unrepresentative of the true variation.

- LIMS—Because of its short lifetime, no attempt has been made to evaluate the LIMS capability to measure long-term trends. In this study, LIMS has served as a useful check and source of comparisons with measurements by other techniques.

As infrared limb scanning uses a stable onboard blackbody for calibration, this technique should be a good candidate for long-term trend measurements. The major difficulty is the requirement that detectors with sufficient sensitivity operate over a period of a few years. This will probably require cooling the detectors well below spacecraft ambient temperatures.

Comparison of Trend Detection Capabilities for the Vertical Distribution

Figure 2.55 shows that, at present, the SAGE–I/SAGE–II difference sets the most sensitive limits on the detection of a change in the stratosphere, followed by the SME–NIR (in the lower mesosphere). Similarly, Figure 2.56 compares trend detection capabilities. The SAGE–I/SAGE–II difference is capable of detecting trends of less than 0.5 percent per year in the stratosphere above 25 km. As noted above, as the SAGE–II record becomes longer, it should be able to detect smaller trends, but this must be evaluated in light of its sparse coverage and of the problems of obtaining comparisons under similar seasonal, latitudinal, and atmospheric conditions.

In the future, if the SBUV–2 results can be proven to be highly accurate, it should be possible to use them with the SBUV measurements to determine long-term changes to better than 1 percent per year. Determining the time history of the changes will be a more difficult task.

Total Ozone Determinations from SBUV and TOMS

Because SBUV and TOMS employ the same wavelengths and share the same diffuser plate, they show the same trends and have the same sensitivity to diffuser degradation. The uncertainties in total ozone were calculated, using a range of diffuser degradation models for wavelengths of 312.5 nm and longer. This leads to a range of about 4 percent in total ozone change over 8 years, and a consequent range of total ozone trends of 0.3–0.5 percent per year.

In this case, the diffuser model used to obtain the archived data results in ozone amounts near the minimum of the range. The true total ozone values could be 4 percent higher than those suggested by the archived TOMS data, and the downward trend could be smaller than that of the

archived data by ≈ 0.4 percent per year. Diffuser models M1 and M2 thus give total ozone changes that are in good agreement with the changes observed by the Dobson network.

A Final Observation on SBUV and TOMS Results

The evidence indicates that the uncertainties in the total ozone changes and in the changes in the vertical distributions are considerably larger than has been stated previously. The preponderance of evidence suggests that the model adopted in producing the archived data has underestimated the diffuser degradation, and thereby underestimated total column ozone and ozone profile amounts in recent years. Within the uncertainties, the total amounts could have changed by the amounts indicated by the Dobson network, while the vertical profiles could have remained nearly unchanged, or had a small decrease near 40 km with a small increase near 50 km.

2.9.4 Ongoing Work

Many studies were carried out as part of this investigation. Two in particular that were not completed at the time of this writing should be brought to completion:

- A comparison of SBUV and SBUV–2 results during the period of overlap.
- A comparison of the SBUV, SME, and other solar measurements.

2.9.5 Future Satellite Measurements of Ozone Trends

The analyses discussed here have shown that the measurement of long-term ozone trends from satellites is a difficult but viable task. Results to date, with data that, for the most part, were not taken for this purpose, have proven to be very instructive, and such a measurement program should continue. The measurement system should be based on a careful scientific analysis of the capabilities of the techniques with a view to optimizing them. Of necessity, this will need to be tightly linked with studies on the best methods of implementation to define the instruments employed by such a system. The methods for demonstrating the stability of the systems results will also need to be addressed. This study suggests that a measurement program should include the following features:

- The instruments should be designed for long life and stable operation. All instruments should include provisions for monitoring their operations and characteristics in space, preferably by including a stable inflight calibration source.
- Attempts should be made to reduce the amount of contamination to which the instruments are subject. This applies most strongly to instruments making measurements in the UV, but is relevant for all instruments. It should begin with concerted efforts to reduce the amount of outgassing from the spacecraft. Additional attention should be paid to the cleanliness of the individual instruments. Testing should not be carried out in vacuum systems that are oil pumped, since this often results in traces of the pump oil being adsorbed by the spacecraft materials. As noted above, degradation effects are most noticeable on surfaces that are exposed to solar UV radiation. Such surfaces and the amount of exposure should be minimized. Strategies of heating such surfaces before solar exposure, to drive off adsorbed contaminants before they are fixed on the surface, should also be investigated.

- Ideally, the program should consist of more than one satellite instrument, employing different experimental techniques. If a sequence of instruments is used over time, then adequate overlap between instruments must be made, such that differences in trends (or lack thereof) can be firmly established. Thus, for the present SBUV–2 series of instruments on the NOAA operational spacecraft, the ideal arrangement would be to collect data from each instrument for its life, without being governed by the operational need for the instrument, which would have an instrument turned off as soon as its successor is put in operation. While the SBUV–2 system is in operation, the shuttle SBUV is an extremely desirable component of the overall program.

- The system should also consist of a continuous long-term set of ground-based measurements, carefully maintained at a high level of accuracy. Such systems are the proposed Global Network for the Early Detection of Stratospheric Change, for the vertical distribution of ozone, and the Dobson network for total ozone. It is important for the stations to be accurate and very stable. Only a limited number of such stations is needed, but they should be capable of obtaining data on a nearly daily basis, preferably under all weather conditions.

CHAPTER 3

Information Content of Ozone Retrieval Algorithms

Panel Members

C. Rodgers, Chair

P. K. Bhartia
W. P. Chu NDZ10491
R. Curran
J. DeLuisi NJ9209 44
J. Gille NH315709
R. Hudson NC999967
C. Mateer A6530300
D. Rusch
R. J. Thomas
R. Turco
W. Wiscombe

Chapter 3

Information Content of Ozone Retrieval Algorithms

Contents

3.0 INTRODUCTION

All practical methods of measuring atmospheric ozone that are useful for monitoring trends are indirect in some way. The quantity that an instrument measures directly is related, in some more or less complicated way, to the ozone distribution. Deriving the ozone distribution from the measurement involves the numerical solution of the equations expressing this relationship by a process generally known as "retrieval." The error analysis of the retrieval algorithm is an important part of evaluating the performance of the overall observing system.

The total ozone measurements made by the Dobson spectrophotometer and the Total Ozone Mapping Spectrometer (TOMS) and Solar Backscatter Ultraviolet (SBUV) instruments on Nimbus–7 are relatively simply related to the total ozone, so that the retrieval error analysis is straightforward. However, the profile measurements made by instruments such as the SBUV are very indirect. In some cases, the retrieval problem is "ill-posed" and needs a great deal of care.

We note that because the measurements are indirect, data from different observing systems will have different characteristics; this must be taken into account when comparing data from different sources. Consequently, the primary aim of this chapter is to characterise the algorithms that have been used for production processing by the major suppliers of ozone data to show quantitatively:

- How the retrieved profile is related to the actual profile. This characterises the altitude range and vertical resolution of the data.
- The nature of systematic errors in the retrieved profiles, including their vertical structure and relation to uncertain instrumental parameters.
- How trends in the real ozone are reflected in trends in the retrieved ozone profile.
- How trends in other quantities (both instrumental and atmospheric) might appear as trends in the ozone profile.

Error analyses for the ozone data that we have considered have, in general, been published in the open literature. Unfortunately, they have not been performed in a uniform and comparable way. We therefore decided to define a uniform error analysis and to apply it to all the data sources. At the request of the Ozone Trends Panel, these error analyses have been carried out by the experimenters.

Because it may be possible to largely eliminate random error in the long-term averages required for trends, retrieval methods appropriate to trend estimation are not necessarily the same as those appropriate to estimation of single profiles. However, the retrieval methods used for the data now available are designed for single profiles. It has become clear in the course of this study that data from some sources would be improved by reprocessing with improved methods; some data suppliers (e.g., Umkehr) are planning to do this. As our primary task is not to discuss the efficacy of the inverse methods used, but to characterise the ozone trend information currently available, we only consider in detail the algorithms that have been used to produce these data. However, we will make suggestions about retrieval methods suitable for trend estimation.

3.1 PROFILE RETRIEVAL CONCEPTS

The relationship between the ozone distribution and the quantity measured by a remote-sounding instrument is usually complicated and difficult to solve explicitly. The experimenters providing ozone data have used a wide range of retrieval methods to deal with the problem. In this section, we survey the types of methods used, as a background for our error analysis.

Any retrieval method uses some mathematical or numerical model of the relationship between the unknown profile and the quantity measured. We denote the quantities measured by an instrument in relation to any one profile by a vector $\mathbf{y}$, and the unknown ozone profile by a vector $\mathbf{x}$, which could be, for example, the mixing ratio at a set of altitudes. We describe the measurement algebraically or algorithmically by a *forward model* or *measurement model*, $F(\mathbf{x})$. The retrieval method will adjust the retrieved profile in some way so that the computed measurement corresponding to the retrieval agrees to some extent with the actual measurement. We describe this process by an *inverse model*, $I(\mathbf{y})$. Three classes of retrieval method have been used to produce the data studied here: onion peeling, relaxation, and linearisation with constraints.

The problem is fundamentally ill posed because the profile will always have structure on a scale finer than that on which it is possible to measure. Thus, all methods must use some explicit or implicit constraint on the solution. This usually takes the form of a profile representation that has finite vertical resolution.

A limb sounder measures a quantity that depends on the ozone profile only above the tangent height. If the profile is determined sequentially, starting at the top, then to find the ozone amount in the next layer down, it is only necessary to find the amount that matches the measured radiance (or transmittance, etc.) from that layer. Thus, onion peeling needs only to be able to solve a sequence of one-dimensional problems.

Relaxation methods solve the problem at all levels simultaneously by adjusting the profile according to a relaxation equation to improve the match between the measurement and the quantity computed by the forward model. The version of the Chahine method developed by Twomey et al. (1977) uses the following relaxation equation:

$$x_i^{n+1} = x_i^n \left[1 + \tilde{K}_{ij}(\mathbf{x}^n) \left(\frac{y_j^m}{F_j(\mathbf{x}^n)} - 1 \right) \right] \tag{1}$$

where n is an iteration index, i is a height index, $\tilde{K}$ is the weighting function (defined by Equation 2 below) normalised so that its maximum value is unity, and y_j^m is the measurement in channel j. The iteration is carried out for each channel in turn (i.e., for each j), and then repeated until convergence. The iteration modifies the profile in the region where the weighting function is nonzero by an amount that depends on the ratio of the measurement to the forward model.

If the forward model is linearised about some standard profile $\mathbf{x}_0$,

$$\mathbf{y} = F(\mathbf{x}_0) + \mathbf{K}_0(\mathbf{x} - \mathbf{x}_0) + O(\mathbf{x} - \mathbf{x}_0)^2 \tag{2}$$

where $\mathbf{K}_0$ is the Fréchet derivative $\partial F(\mathbf{x})/\partial \mathbf{x}$ evaluated at $\mathbf{x}_0$, then a Newtonian iteration can be used. Unfortunately, this relationship is usually ill posed; i.e., $\mathbf{x}$ has more elements than $\mathbf{y}$, so further constraints are required on $\mathbf{x}$. If we use a quadratic form constraint, and jointly minimise $(\mathbf{x}-\mathbf{x}_0)^T\mathbf{S}_x(\mathbf{x}-\mathbf{x}_0)$ and $(\mathbf{y}_l(\mathbf{x})-\mathbf{y}_m)^T\mathbf{S}_y(\mathbf{y}_l(\mathbf{x})-\mathbf{y}_m)$, where the matrices $\mathbf{S}$ express the nature of

the constant, y_l is the linearised forward model, and $\mathbf{y}_m$ is the measurement, then the iteration is of the form:

$$\mathbf{x}_{n+1} = \mathbf{x}_0 + \mathbf{S}_x\mathbf{K}_n^T(\mathbf{K}_n\mathbf{S}_x\mathbf{K}_n^T + \mathbf{S}_y)^{-1}[\mathbf{y}_m - F(\mathbf{x}_n) - \mathbf{K}_n(\mathbf{x}_0 - \mathbf{x}_n)] \quad (3)$$

Both the Twomey (1963) "minimum information" method and the optimal estimation approach reviewed by Rodgers (1976) are of this kind, with different interpretations for the constraint matrices.

3.2. ERROR ANALYSIS CONCEPTS

Many sources contribute to errors in retrieved ozone data sets. Those that lead to constant offsets or purely random errors are of minor importance when studying trends, as random errors will average out in the long run, and constant offsets make no difference to the trend. There are sources of error that distort the profile in some way, for example, by smoothing it. These are important because the derived trend profile will be similarly distorted. The most important sources of error are those that have trends themselves, which might appear as false trends in ozone.

To understand the nature of the retrieved data, we have carried out a formal error analysis of each observing system, including the instrument and the retrieval method. This will tell us how the retrieved data are related to the true profile and how the various sources of uncertainty affect the result. The error analysis must be general enough to apply to a wide variety of systems and to deal with various kinds of systematic errors. We generalise the forward and inverse model definitions to include some other parameters. The forward model becomes:

$$\mathbf{y} = F(\mathbf{x},\mathbf{b}) + \epsilon_y \quad (4)$$

The vector $\mathbf{b}$ represents any other parameters that the measurement might depend on, such as instrumental calibration or atmospheric temperature, and that may affect the derived ozone profile if not perfectly known. It may also be used to describe forward model deficiencies. The vector ϵ_y is the direct measurement error in $\mathbf{y}$. Note that, in principle, the measurement vector is in units of volts or telemetry counts, and not in scientific units. Calibration and retrieval are usually treated as separate processes operationally, but the boundary between them is often ill defined; they must be considered together for the error analysis.

The retrieved profile $\hat{\mathbf{x}}$ is related to the measurement in a way described by a slightly generalised inverse model:

$$\hat{\mathbf{x}} = I(\mathbf{y},\mathbf{b},\mathbf{c}) \quad (5)$$

where $\mathbf{c}$ represents any quantities that are used in the inverse model and subject to error or variability, but that do not appear in the forward model. The primary example is an a priori profile and its covariance, or an instrumental noise covariance assumed for the retrieval.

We can now formally relate the retrieved profile to the true profile. To carry out an error analysis with respect to the uncertain quantities $\mathbf{b}$, $\mathbf{c}$, and $\mathbf{y}$,

$$\begin{aligned}\hat{\mathbf{x}} &= I(F(\mathbf{x},\mathbf{b}) + \epsilon_y, \mathbf{b} + \epsilon_b, \mathbf{c} + \epsilon_c) \\ &= I(F(\mathbf{x},\mathbf{b}) + \epsilon_y, \hat{\mathbf{b}}, \hat{\mathbf{c}})\end{aligned} \quad (6)$$

where $\hat{\mathbf{b}}$ and $\hat{\mathbf{c}}$ are our best estimates of these parameters, but include errors ϵ_b and ϵ_c. This can be expressed in the form $\hat{\mathbf{x}} = T(\mathbf{x}, \mathbf{b}, \mathbf{c}) +$ *error terms*, where T is a *transfer function* relating $\mathbf{x}$ to $\hat{\mathbf{x}}$. Characterising the transfer function is one way of understanding how the retrieved profile is related to the true profile.

For the error analysis, we linearise about some ensemble mean $\bar{\mathbf{x}}$ and our best estimate of the forward model parameters, $\hat{\mathbf{b}}$ and $\hat{\mathbf{c}}$. We cannot use the true values of the model parameters, as they are not known.

$$\begin{aligned}\hat{\mathbf{x}} &= T(\bar{\mathbf{x}},\hat{\mathbf{b}},\hat{\mathbf{c}}) + \frac{\partial T}{\partial \mathbf{x}}(\mathbf{x}-\bar{\mathbf{x}}) + \frac{\partial T}{\partial \mathbf{b}}\epsilon_b + \frac{\partial I}{\partial \mathbf{c}}\epsilon_c + \frac{\partial I}{\partial \mathbf{y}}\epsilon_y \\ &= T(\bar{\mathbf{x}},\hat{\mathbf{b}},\hat{\mathbf{c}}) + \mathbf{A}(\mathbf{x}-\bar{\mathbf{x}}) + \mathbf{A}_b\epsilon_b + \mathbf{A}_c\epsilon_c + \mathbf{D}_y\epsilon_y\end{aligned} \tag{7}$$

thus defining the matrices $\mathbf{A}$, $\mathbf{A_b}$, $\mathbf{A_c}$, and $\mathbf{D_y}$. The first term is the transfer function operating on the ensemble mean $\bar{\mathbf{x}}$. Ideally, we might expect this to yield $\bar{\mathbf{x}}$, i.e.,

$$T(\bar{\mathbf{x}},\hat{\mathbf{b}},\hat{\mathbf{c}}) = \bar{\mathbf{x}} \tag{8}$$

but this is not necessarily true for the general retrieval algorithm. Any difference contributes to systematic error in the observing system.

The term $\mathbf{A}(\mathbf{x}-\bar{\mathbf{x}})$ is equivalent to the integral in a relation of the form

$$\hat{x}(z) = \bar{x}(z) + \int A(z,z')[x(z') - \bar{x}(z')]dz' + \text{other terms} \tag{9}$$

Thus, the rows of matrix $\mathbf{A}$ show how the observing system smooths the profile. Ideally, $\mathbf{A}$ would be the unit matrix $\mathbf{I}$, but in practise it is not, nor is it symmetric. We call the rows the *averaging kernels*. In regions where the retrieval is valid, they will be peaked functions centered on the appropriate altitude, having approximately unit area. They indicate the altitude range over which the observing system is sensitive to changes in the actual profile and give an indication of its vertical resolution. As an alternative to thinking of the averaging kernels' smoothing effect on the profile, we can consider the error in the solution contributed by structure on the vertical profile that is orthogonal to the averaging kernels. This is called the *null space* error. However, its size can be estimated only if the statistical behaviour of the true profile is known.

The columns of $\mathbf{A}$ differ from the rows and show the response of the retrieval to a δ-function perturbation in $\mathbf{x}$. Insofar as the linear expansion for $\mathbf{A}$ is valid, trends derived from retrieved data will have the same vertical resolution and range of validity as individual profiles.

Sensitivity of the observing system to forward model parameter errors is expressed by $\mathbf{A}_b$, and contributes to both systematic and random error, according to the nature of the errors in $\mathbf{b}$. Sensitivity to inverse model parameters is likewise given by $\mathbf{A}_c$. $\mathbf{D}_y$ expresses the sensitivity to instrumental noise. For the analysis of trends, the effect of the instrumental noise terms and the random components of the error in $\mathbf{b}$ is reduced by averaging. The important terms are the systematic errors in $\mathbf{b}$ and $\mathbf{c}$, especially those components that may have unrecognised, or unmodeled, trends themselves.

A full description of this approach to profile retrieval error analysis is being prepared for publication (Rodgers, 1988).

3.3 RETRIEVAL ANALYSIS FOR INDIVIDUAL INSTRUMENTS

In the following sections, we discuss the characteristics of the data supplied by instruments with a relatively long-term data record. These include SBUV, TOMS, Dobson, Stratospheric Aerosol and Gas Experiment (SAGE) –I and –II, the Solar Mesospheric Explorer (SME) Ultraviolet Spectrometer (UVS), and Near Infrared Spectrometer (NIRS). The Limb Infrared Monitor of the Stratosphere (LIMS) has been included as a source of validation data. The TIROS–N Operational Vertical Sounder (TOVS) has not been included, as the retrieval is by regression against Dobson measurements and it will have nothing of its own to say about trends.

We present a brief description of the forward and inverse models for each data source, and graphically display the averaging kernels and the major components of the systematic error. These diagnostics are used to assess the effect of the retrieval on the estimation of trends and the aliassing of trends in other quantities into apparent trends in ozone. Errors are 1σ, unless otherwise stated. For detailed descriptions of the instruments, see Chapter 2 of this report.

3.3.1 TOMS and SBUV Total Ozone

The TOMS instrument on Nimbus–7 consists of a monochromator whose narrow (3° × 3°) field of view (FOV) is scanned through the subsatellite point in a plane perpendicular to the orbital plane. Backscattered radiation is sampled at the six wavelengths—313, 318, 331, 340, 360, and 380 nm—sequentially in 3-degree steps in a ±51 degree cross-scan from the nadir. This scanning creates a contiguous mapping of the total ozone, since the scans of consecutive orbits overlap.

All TOMS data currently available from the archives (National Space Science Data Center—NSSDC) have been reprocessed using a new algorithm (Version 5) that uses a revised set of ozone absorption cross-section and instrument calibration parameters. The reprocessing started in December 1986 and was completed in July 1987.

The SBUV instrument (see Section 3.3.3) on Nimbus–7 measures total ozone by the same method, with a larger field of view (11.3 degrees square), and without the cross-track scanning. The wavelengths used for total ozone are 340, 331, 318, and 313 nm, a subset of the TOMS wavelengths. Both instruments are calibrated by viewing solar radiation reflected by the same diffuser plate, but with slightly different geometries.

3.3.1.1 Forward Model

The forward model used for analysis of the TOMS and SBUV data expresses the diffuse reflection of solar radiation by a multiple-scattering/absorbing atmosphere, bounded at the bottom by a diffusely reflecting surface. The physical basis of this forward model has been discussed by Dave and Mateer (1967) and reviewed subsequently by Klenk et al. (1982). The observational approach uses measurements at wavelengths near the long-wavelength end of the Hartley–Huggins O_3 absorption band. The wavelengths are chosen so that most of the radiance reaching the satellite instrument has passed through the ozone layer and has been backscattered from within the troposphere.

The absorption optical thicknesses for typical amounts of stratospheric ozone at the wavelengths used for ozone determination range from 0.05 to 0.5. The Rayleigh-scattering optical thicknesses for the entire atmosphere at these same wavelengths are around unity; about 90

percent of the scattering occurs in the troposphere. Thus, the backscattered radiance at the satellite depends on (1) the attenuation of the direct solar beam on its slant path through the ozone layer; (2) the reflecting power of the troposphere (molecular and aerosol scattering and surface and cloud reflections), and (3) the attenuation of the diffusely reflected radiation as it passes upward through the ozone layer.

If $\mu 0$ is the cosine of the Sun's zenith angle for the solar ray incident on Earth's surface at the view point, and μ is the cosine of the zenith angle of the line of sight to the satellite at the view point, then the total attenuation path of backscattered photons through the ozone layer, from (1) and (3), is approximately proportional to $1/\mu_0 + 1/\mu$. This proportionality is modified by the effects of the sphericity of Earth (important when μ or μ_0 are small) and by the presence of ozone in the tropospheric scattering layer.

An important aspect of the evaluation method is the treatment of cloud and surface reflections and backscattering by tropospheric aerosols. It is assumed that the average of these effects, over the instantaneous field of view, is that the atmosphere acts as if there were a Lambertian surface with equivalent albedo or reflectivity R. For a given wavelength, the forward model may then be written:

$$I(\Omega,\mu,\mu_0,R) = I(\Omega,\mu,\mu_0,0) + T(\Omega\mu,\mu_0)\ \frac{R}{[1 - RS(\Omega)]} \qquad (10)$$

where Ω is the total ozone, $I(\Omega, \mu, \mu_0,R)$ is the measured backscattered radiance, $I(\Omega, \mu, \mu_0,0)$ is the Rayleigh backscattered radiance from the atmosphere alone, $T(\Omega, \mu, \mu_0)$ is the direct plus diffuse radiance reaching the surface times the transmittance of the atmosphere for radiation reflected isotropically by the surface, and $S(\Omega)$ is the albedo of the atmosphere seen from below by the reflected surface radiance.

Precomputed tables of I, T, and S are used to evaluate the terms of the forward model. These data cover the full range of possible solar zenith angles and view angles. All orders of molecular scattering are accounted for by successive iteration of the auxiliary equation (Dave, 1964) in a pseudospherical atmosphere (DeLuisi and Mateer, 1971). The computations were carried out for 17 standard O_3 profiles, including 3 for a latitude of 15°, 7 for 45°, and 7 for 75°. Two sets of tables were computed: one for a surface pressure of 1.0 atm, the other for 0.4 atm. The ozone absorption coefficients are based on the measurements of Bass and Paur (1985). The effect of atmospheric temperature on ozone cross-sections is accounted for by using the three standard temperature profiles, one for each latitude. The computation of the band-averaged coefficients is described by Klenk (1980).

3.3.1.2 The Inverse Method

The surface albedo R is determined from the radiance measurements at 360 nm and 380 nm for TOMS and at 340 nm for SBUV, using Equation 10. All of these are outside the ozone absorption band, for which the Ω dependence drops out. This determination is dependent on tabulated values for $I(\mu, \mu_0,0)$, $T(\mu, \mu_0)$, and S. It is assumed that R is independent of wavelength.

Total ozone is inferred from the relative logarithmic attenuation N for absorbing wavelength pairs (λ_1, λ_2). The quantity N is related to the observations through the equation

$$N(\lambda_1, \lambda_2) = 100 \times [\log_{10}(I/F_0)_2 - \log_{10}(I/F_0)_1] \qquad (11)$$

where F_0 is the solar irradiance and I the measured backscattered Earth radiance, each at the wavelengths indicated. In the ideal case of a nonscattering atmosphere bounded by a Lambertian reflector, this quantity would be proportional to the total ozone in the optical path. When scattering is present, the relationship is nonlinear, and depends on the angles, the surface reflectivity, and the vertical distribution of ozone.

For TOMS, there are 12 separate estimates of total ozone: 4 from each of the 3 pairs—the A-pair (313/331), the B-pair (318/331), and the C-pair (331/340); for each pair from the two pressure tables (1.0 and 0.4 atm); and for each pressure from the two sets of standard ozone profiles from the latitudes nearest to the measurement latitude. The total ozone is linearly interpolated in latitude, except that between 0° and 15° latitude, only the 15° profile set is used, and polewards of 75°, the 75° profile set is used.

To combine the ozone values from the two pressures, an estimate is made of the effective surface pressure using the following procedure:

$$\bar{p} = wp_t + (1-w)p_c \tag{12}$$

where p_t is the terrain pressure, p_c is the estimated cloud-top pressure, and w varies from 0 to 1 based on surface reflectivity. It is unity for $R \leq 0.2$, zero for $R \geq 0.6$, and linearly interpolated for intermediate reflectivity. The cloud-top pressure is estimated in two ways: based on an empirically derived relationship that gives the cloud-top height as a function of latitude, and on an estimate based on the collocated infrared measurements from the THIR (temperature humidity infrared) sensor on Nimbus–7. The relationships used are "tuned" so that, on average, both estimates give the same total ozone amount.

The above rule is modified when snow or ice is known to be present (based on daily snow/ice maps from the U.S. Air Force). In such cases, it is assumed that there is only a 50 percent probability that clouds are present, despite the higher reflectivity, and the surface pressure ($\bar{p}$) derived above is averaged with the terrain pressure.

Finally, the three estimates of total ozone from the three pairs are combined using a weighting scheme that takes into account the varying sensitivities of the three pairs (with total ozone, solar zenith angle, view angle, and reflectivity) to total ozone amount and to errors in the retrieval. The combined estimate is reported as "best ozone."

3.3.1.3 Forward Model Assessment

The forward model scattering atmosphere is assumed to be Rayleigh; the lower boundary reflecting surface is assumed to be opaque and Lambertian. Simulation results (Dave, 1978) show that this assumption works well for aerosol optical thickness up to 1.0 except in unusual scattering situations, such as when two layers of thick clouds, separated by several kilometers of absorbing atmosphere, may be present.

The effects of the sphericity of Earth are accounted for only in the direct-beam and first-order scattering, but not in multiple scattering. The error in total ozone caused by this uncertainty is likely to be small.

Absorption by volcanic SO_2 has not been included in the forward model and the retrieval. This can clearly be seen as a perturbation in the retrieved total ozone for a short period after major eruptions, but it is quickly converted to H_2SO_4, and is unimportant for long-term studies.

3.3.1.4 Inverse Model Assessment

The primary source of error in deriving total ozone from the TOMS and SBUV measurements is the presence of tropospheric ozone. In the presence of thick clouds, the instruments obviously cannot measure the ozone column below the cloud layer. In effect, the algorithm adds an amount based on climatology. For a typical dark reflecting surface, even in the absence of clouds, variations in the total ozone column caused by changes in the ozone near the surface have relatively little effect on the measurement, because some backscattering takes place above this ozone. Therefore, effects of such variations will be underestimated in the TOMS- and SBUV-derived total ozone. A detailed discussion of this effect is given by Klenk et al. (1982).

Another possible source of error is the assumption that the surface reflectivity is wavelength independent. The TOMS instrument was designed with three reflectivity wavelengths (380, 360, and 340 nm) that can be used to study any possible wavelength dependence of the reflectivity. Early studies indicated no systematic wavelength dependence over different surfaces; therefore, the algorithm was designed to use a simple average of 380 nm and 360 nm reflectivities, whilst in the case of the SBUV, only 340 nm is used.

3.3.1.5 Error Analysis

Sensitivity to Diffuser Plate Reflectivity

The wavelength dependence of the sensitivity of retrieved total ozone to diffuser plate reflectivity D_λ is given in Table 3.1 for both TOMS and SBUV. On the basis of the discussion of diffuser plates in Chapter 2, we have carried out several tests (a–e, below) of the sensitivity of the retrieved total ozone to possible variations of diffuser plate reflectivity.

Table 3.1 Sensitivity of Retrieved Total Ozone to Diffuser Plate Reflectivity, $d \ln \Omega / d \ln D_\lambda$, for TOMS at Two View Angles, θ, and for SBUV. The Reference Atmosphere Contains 280 Dobson Units (DU) of Ozone, Surface Reflectivity is 0.3, and the Solar Zenith Angle is 45°.

λ (nm)	TOMS, $\theta = 0°$	TOMS, $\theta = 51°$	SBUV
313	0.71	0.53	0.58
318	0.71	0.62	0.72
331	−1.41	−0.85	−1.3
340	0.0	−0.34	0.24
360	0.13	0.11	—
380	0.12	0.10	—

(a) A random error of 1 percent in D_λ, uncorrelated between wavelengths, but constant in time. This gives a contribution to the formal random error in the total ozone, but should have no effect on the measured trend. The root mean square (rms) caused by this error source is given in row (a) of Table 3.2.

(b) A constant error of 1 percent in D_λ at all wavelengths. Thus, a drift of 1 percent per year in the error in D_λ would lead to an annual drift in total ozone given by row (b) of Table 3.2.

(c) A random error of 2 percent in $r(\lambda)$, the formal uncertainty quoted in Chapter 2. This is assumed to be uncorrelated between wavelengths, but constant in time. It leads to a scale error proportional to exposure time, whose value is random with an rms value given by row (c) of Table 3.2 at $E = 761$ hours (the end of the data set, after 8 years of measurements).

(d) A constant error of 5 percent in $r(\lambda)$. Five percent is roughly the scatter of the values of r given in Chapter 2, Figure 2.10. Row (d) of Table 3.2 gives the percentage error in total ozone from this source after an exposure time $E = 761$ hours.

(e) We have also considered the alternate diffuser plate models M1, M2, and L of Chapter 2. The change that these make to the retrieved total ozone relative to the model assumed by the OPT at an exposure time of 761 hours is given in Table 3.2.

Table 3.2 Sensitivity of Retrieved Total Ozone to Diffuser Plate Model Error Scenarios. The Basic State Is as for Table 3.1. The Details of the Scenarios Are Discussed in the Text.

λ (nm)	TOMS, $\theta = 0°$	TOMS, $\theta = 51°$	SBUV
(a) D_λ ±1%	1.7	1.2	1.6
(b) D_λ +1%	0.3	0.2	0.2
(c) $r(\lambda)$ ±2%	0.8	0.6	0.7
(d) $r(\lambda)$ +5%	0.4	0.3	0.4
M1 after 8 yrs	4.5	3.3	4.8
M2 after 8 yrs	2.9	2.0	3.1
L after 8 yrs	−0.6	−0.8	−0.8

Averaging Kernel

The "total ozone" measured by TOMS and SBUV is not the true total. It can be described as a weighted mean of the ozone density profile, plus an a priori contribution to allow for the tropospheric ozone not seen. The weighting function is close to unity for layers above the scattering layer, and smaller for layers below. For the tropospheric layers, the value of the weight can vary from zero (for thick clouds with tops near the tropopause) to near unity (for cloud-free scenes with a brightly reflecting surface). Typical weights for SBUV measurements with a solar zenith angle of 45° are <15 mb: 1.06; 15–30mb: 1.00; 30–100mb: 0.97; surface–100mb (cloud free): 0.7; cloud top–100mb (opaque cloud): 1.1–1.3; cloud top–ground: 0.0. These weights are appropriate for solar zenith angles up to about 70°, but will decrease considerably at low levels closer to the terminator.

A nominal value of 0.6 may be used for determining the error in the long-term trend due to changes in the tropospheric ozone.

Sensitivity to Atmospheric Temperature

The sensitivity of total ozone to atmospheric temperature is relatively small. At a nominal ozone density weighted atmospheric temperature of −46°C, the sensitivities are A-pair: 0.16 %/K; B-pair: 0.14 %/K; C-pair: 0.2 %/K. Note that the C-pair is used only near the terminator. The temperature dependence becomes even smaller at temperatures below −65°C. Thus, a temperature change of around 6–7K would be needed to produce a fictitious ozone change of 1 percent.

3.3.1.6 Trend Estimation Assessment

The primary source of error in TOMS and SBUV total ozone is the relative drift of the calibration of the diffuser plate reflectivity over the 20 nm intervals between the wavelength pairs. The range of possible models of the time change of the reflectivity leads to a drift in TOMS and SBUV total ozone of between −4.8 percent and +0.8 percent over the period 1978 to 1986. This could account for a large fraction of the drift relative to the Dobson network, discussed in Chapter 4.

The ozonesonde data indicate that tropospheric ozone may be increasing by about 1 percent per year (Logan, 1985; Tiao et al., 1986). The contribution to the column trend would be around 0.1 percent per year; about half of this would not be seen by SBUV and TOMS because these instruments are not sensitive to lower tropospheric ozone, but all of it would be seen by the Dobson instrument.

Although 8½ years' worth of TOMS ozone data are currently available, the TOMS instrument has had problems with its chopper electronics since April 1984. The best current estimates (Fleig et al., 1986) are that the error in total ozone data due to this problem has both positive and negative signs, with no more than 10 matm-cm error in any single measurement, no more than 5 matm-cm in the zonal mean of any given day, and no significant effect in deriving long-term trends.

3.3.2 Dobson Ozone Spectrophotometer: Total Ozone

The basic references for the Dobson Ozone Spectrophotometer are the *Observers' Handbook* (Dobson, 1957a, hereinafter BR1) and the *Adjustment and Calibration Manual* (Dobson, 1957b, hereinafter BR2). The instrument is used to measure the relative logarithmic attenuation of two wavelengths in the Hartley–Huggins ozone bands, one strongly and one weakly absorbed by ozone. These measurements may be made in either the direct sun (DS) or zenith sky (clear blue, ZB; or cloudy, ZC) modes of observation.

In some countries, the measurements are processed centrally and in others, at the individual instrument sites, but in all cases according to the process described in BR1.

3.3.2.1 Forward Model

For DS observations, the forward model for the relative logarithmic attenuation for a wavelength pair may be derived trivially from Beer's Law as

$$\begin{aligned} N &= \log_{10}(I/F_0) - \log_{10}(I'/F'_0) \\ &= (\alpha - \alpha')\mu\Omega + (\beta - \beta')mp + (\delta - \delta')\mu_0 + C_0 \end{aligned} \tag{13}$$

where I, I' are the solar irradiances for the short and long wavelengths, respectively,
F_0, F'_0 are the extraterrestrial solar irradiances,
α,α' are the decadic ozone absorption coefficients, atm-cm^{-1},
μ is the relative slant path of the Sun's rays through the ozone layer, $\simeq \mu_0$ for small solar zenith angles,
μ_0 is the relative slant path of the Sun's rays through the aerosols, generally mostly tropospheric,

Ω is the total ozone amount (atm-cm),
β,β' are the decadic Rayleigh scattering coefficients, atm^{-1},
m is Bemporad's optical air mass,
p is the station pressure, atm,
δ,δ' are the decadic optical depths for atmospheric aerosol,
C_0 is a constant including some instrumental effects and the log-ratio of the extra-terrestrial solar fluxes.

There is no provision in the standard forward model for absorption by other atmospheric gases such as SO_2, which is the main interfering gas.

The standard DS total ozone observation recommended by the International Ozone Commission and adopted by WMO is for the AD double pair (A-pair: 305.5, 325.4 nm; D-pair: 317.6, 339.8 nm), for which the forward model becomes

$$N_{AD} = N_A - N_D = 1.388\mu\Omega + 0.012mp \tag{14}$$

where 1.388 is the decadic ozone absorption coefficient difference for the double pair and 0.012 is the decadic Rayleigh-scattering coefficient difference for the double pair.

It is assumed that $(\delta-\delta')_A - (\delta-\delta')_D \simeq 0$ for the double pair measurements. Observations may also be made on the BD and CD double pairs (B-pair: 318.8, 329.1 nm; C-pair: 311.45, 332.4 nm).

There is no forward model for ZB or ZC observations.

3.3.2.2 Inverse Method

The inverse method for the DS observation follows directly from the forward model for the AD double pair as

$$\Omega = \frac{N_{AD}}{1.388\mu} - 0.009\frac{mp}{\mu} \tag{15}$$

The inverse method for ZB and ZC observations is entirely empirical. It is embodied in so-called zenith sky charts, that are developed from near-simultaneous DS and ZB observations. For further details, see BR1.

3.3.2.3 Forward Model and Inverse Method Assessment

The forward model for the double pair neglects the relative attenuation by atmospheric aerosol scattering and by absorption of atmospheric gases other than ozone, primarily SO_2 (see Komhyr and Evans, 1980, for example). It can be shown by Mie-scattering calculations for reasonable aerosol size distributions that the aerosol error in AD/DS total ozone observations is extremely small (for example, less than 1 matm-cm for the maximum aerosol optical depth over Mauna Loa following the El Chichón eruption). For SO_2 interference in urban areas, AD/DS total ozone observations will be approximately l matm-cm too high for each matm-cm of SO_2 present.

The forward model parameters include the ozone absorption coefficients and the Rayleigh-scattering coefficients. These are discussed in Section 3.3.4 on Umkehr measurements.

For DS observations, the forward and inverse models are essentially the same. The empirical ZB sky charts must be derived empirically and will represent average conditions. Their main deficiencies stem from the effects of aerosols on observations and the effects of differences in the ozone profile (for the same total ozone) on the observations. For ZC observations, the optical effects of the clouds will introduce additional errors.

3.3.2.4 Error Analysis

Ozone Absorption and Rayleigh-Scattering Coefficients

Errors in the absorption coefficient difference produce a change of scale in the total ozone measurements. The present standard IOC/WMO absorption coefficients give total ozone values 3–4 percent higher than the Bass-Paur (1985) coefficients. Rayleigh-scattering coefficients in current use may be in error by 1–2 percent; this will produce an insignificant bias in double-pair total ozone observations.

Absorption by SO_2

Absorption by SO_2 will produce erroneously high values of total ozone, as noted earlier. According to Komhyr and Evans (1980), the AD pair coefficient is 2.13, so that 1 matm-cm of SO_2 would appear as $2.13/1.388 = 1.53$ matm-cm of O_3. Evans et al. (1980) give 1.06 for this ratio. There may be errors due to SO_2 as great as 20–30 matm-cm in extreme cases (Kerr, private communication).

Instrumental Effects

Instrumental effects that may affect the total ozone measurements include optical alignment errors and wedge calibration errors. It is convenient to include errors in C_0 in this group. Interstation comparisons, using TOMS as a transfer standard, suggest that the above-noted errors produce a 2–3 percent variation in total ozone over the network.

Temperature Dependence

The temperature dependence of the derived total ozone is 0.13 %/K for AD pair measurements. This is unlikely to be significant.

Zenith Sky Measurements

ZB and ZC total ozone measurements have considerably greater errors than the DS measurements because of the empiricism in the inverse model and because of cloud effects. Errors as large as 20 percent may occur in extreme cases (thick clouds). These errors are discussed in Chapter 4, Ground-Based Measurements of Ozone.

3.3.2.5 Trend Estimation Assessment

Instrumental calibration changes produce errors in total ozone trend estimates made from a single instrument. How these are reflected in errors in the trend seen by the network is discussed in Appendix 1, Statistical Issues, and in Chapter 4.

Absorption and scattering coefficient errors are constant and will, therefore, have no impact on trend estimation.

Local (urban or regional) trends in tropospheric ozone are not strictly errors in total ozone measurements, but may serve to confuse the determination of "global" trends of total ozone. Trends in tropospheric SO_2 in urban areas will also introduce spurious trends in total ozone.

Only measurements taken by the direct sun (DS) method should be used for trends studies.

3.3.3 Solar Backscatter Ultraviolet Spectrometer

The SBUV data from November 1978 to February 1987 have been archived with the NSSDC. Instrument problems have arisen such that data collected after that date may be unsuitable for trend analysis. SBUV–2 data will be processed with the same algorithms as SBUV data.

3.3.3.1 Forward Model

The SBUV measures solar radiation that has been Rayleigh scattered by the atmosphere into the zenith direction and partially absorbed by ozone in the process. Ignoring the algebraic complication of sphericity, the observed backscattered UV radiance I_{obs} is given by

$$I_{obs}(\lambda) = \frac{F_0(\lambda)\beta(\lambda)P(\theta)}{4\pi} \int_0^{p_s} \exp[-(1 + \sec\theta)(\alpha(\lambda,T)X(p) + \beta(\lambda)p)]dp + I_{msr}(\lambda) \quad (16)$$

where F_0 is the direct solar irradiance, β is the Rayleigh-scattering coefficient per atmosphere, $P(\theta)$ is the Rayleigh phase function at solar zenith angle θ, α is the ozone absorption coefficient, $X(p)$ is the integrated ozone amount from the top of the atmosphere down to pressure level p, p_s is the surface pressure, and I_{msr} is the contribution to the measured radiance from photons multiply scattered by the atmosphere and reflected by the surface.

The primary unknown is $X(p)$; all the other variables apart from F_0, in Equation 16 are known, in principle. F_0 is measured by periodically viewing a diffuser plate of known reflectance, illuminated by direct solar radiation. The accuracy of this measurement and the degradation of the diffuser plate are critical and are discussed in detail in Chapter 2. The natural vertical coordinate system for this problem is pressure, rather than height, so SBUV measures ozone amount as a function of pressure.

The profile retrieval is carried out in terms of the quantity

$$Q_j = \frac{4\pi[I(\lambda_j) - I_{msr}(\lambda_j)]}{F_0(\lambda_j)\beta(\lambda_j)P(\theta)} \quad (17)$$

i.e., the integral in Equation 16. The penetration of solar UV radiation is primarily governed by the strength of the ozone absorption, which varies with wavelength. The Q-value has the dimensions of pressure, and in strongly absorbing regions (shorter wavelengths) it can be thought of as the pressure in the atmosphere at which the optical depth between the Sun and the instrument via this scattering level is about unity. In weakly absorbing regions (longer wavelengths), the solar radiation is scattered mainly from below the ozone layer, so the albedo is essentially a transmittance measurement depending largely on total ozone.

At the shorter wavelengths, the expression for single scattering (the integral in Equation 16) is sufficient. However, as the radiation at longer wavelengths penetrates to deeper levels (below about 15–20 km), multiple scattering and surface reflection become important and must be accounted for. I_{msr} depends on wavelength, surface reflectivity (cloud, ground, water, or snow), solar zenith angle, and the ozone profile. Fortunately, Taylor et al. (1980) have shown that it depends primarily on total ozone amount, and relatively little on ozone profile shape. Tables of I_{msr} have been calculated using the method of iteration of the auxiliary equation of radiative transfer (Dave, 1964; Dave and Furukawa, 1966), where the primary scattering is calculated for a spherical atmosphere, and higher orders assume a flat atmosphere. I_{msr} is pretabulated in terms of total ozone amount and surface reflectivity.

3.3.3.2 The Inverse Method

The retrieval approach is based on the optimal statistical estimation method (Strand and Westwater, 1968) as formulated by Rodgers (1976).

Three Retrieval Stages

The atmosphere is divided into 12 layers, based on the Umkehr layers (see Table 3.3); the ozone amount x_i in each layer is sought. The retrieval is formulated in terms of a profile vector $\mathbf{x}$ with elements $\ln(x_i)$ because of the wide range of possible values of x_i and to avoid negative quantities. To give more closely spaced layers needed to evaluate the forward model, the logarithm of total ozone X_j above each level, i.e., $\ln(\Sigma_{i=j}^{12} x_i)$, is interpolated in $\ln p$ using a cubic spline. Details of the sublayers are given in the same table.

Table 3.3 Layer Numbers Used by SBUV and Umkehr Retrievals

Layer Number	Pressure Range	Approx Km.*	No. of SBUV Sublayers
1	1013–253	0–10	14
2	253–127	10–14.5	7
3	127–63.3	14.5–19	7
4	63.3–31.7	19–23.5	7
5	31.7–15.8	23.5–28	7
6	15.8–7.92	28–33	7
7	7.92–3.96	33–38.5	7
8	3.96–1.98	38.5–43	7
9	1.98–0.990	43–48	7
10	0.990–0.494	48–54	7
11	0.494–0.247	54–59	7
12	0.247–0.127	59–64	7
	0.127–0	64–∞	1

*Using a midlatitude equinox temperature profile.

In practise, the SBUV retrieval is carried out in three stages. First, the three or four longest wavelength channels (depending on the solar zenith angle) are used to derive total ozone X_1 and surface reflectivity R using the algorithm described in Section 3.3.1.

In the second stage, a linearisation point is derived using latitude, day of year, and total ozone X_1 as a guide. For layers 6 through 12, the ozone amount in layer k is given by an equation of the form

$$x_k^a = A_k + B_k cos\{2\pi/365(J - J_{0k})\} \tag{18}$$

For layers 1 through 3, x_k^a is given by a quadratic function of total ozone, with coefficients independent of latitude and date. The coefficients used are given in the *SBUV Users Guide.* Layers 4 and 5 are fitted by assuming that the total ozone X_k above the base of layer k is cubic through levels 3, 4, 6, and 7, where *level* number n corresponds to the base of *layer* number n.

The third stage of the retrieval uses optimal estimation. The measurement vector $\mathbf{y}$ consists of $\ln(Q_j)$ for each channel together with the total ozone estimate X_1 from stage one. The a priori is taken to be the same as the linearisation point determined in stage two, together with a covariance matrix $\mathbf{S}_x$, which is independent of time and place.

The forward model linearised about a vector $\mathbf{x}_n$ is

$$\mathbf{y} = Q(\mathbf{x}_n) + \frac{\partial Q}{\partial \mathbf{x}}(\mathbf{x} - \mathbf{x}_n) = \mathbf{y}_n + \mathbf{K}_n(\mathbf{x} - \mathbf{x}_n) \tag{19}$$

thus defining the weighting functions $\mathbf{K}_n$, which are obtained by numerically integrating the algebraic derivative of $\mathbf{Q}$ with respect to each of the x_i in turn. The linearisation of the forward model for the total ozone measurement (i.e., $X_1 = \Sigma_1^{12} x_i$) is trivial.

The iteration to obtain x_{n+1} from x_n is

$$\mathbf{x}_{n+1} = \mathbf{x}^a + \mathbf{S}_x\mathbf{K}_n^T[\mathbf{K}_n\mathbf{S}_x\mathbf{K}_n^T + \mathbf{S}_\epsilon]^{-1}[\mathbf{y} - \mathbf{y_n} - \mathbf{K}_n(\mathbf{x}^a - \mathbf{x}_n)] \tag{20}$$

starting with $x_1 = \mathbf{x}^a$. Convergence is determined by the size of $\mathbf{x}_{n+1} - \mathbf{x}_n$.

The term $Q_{msr} = 4\pi I_{msr}/F_0\beta P(\theta)$ in Equation 17 depends primarily on total ozone amount, surface (or cloud top) reflectivity and pressure, zenith angle, and wavelength. It is found from a lookup table, using the retrieved total ozone, reflectivity, and a surface pressure estimated in the same way as for the TOMS and SBUV total ozone measurement (Section 3.3.1).

A Priori Assumptions

The a priori profile/linearisation point $\mathbf{x}^a$, used in the estimation equation, has a complicated history. The antecedent a priori profiles used in the original BUV algorithm (Bhartia et al., 1981) were based on a statistical analysis of ozonesonde data (Hilsenrath et al., 1977; Mateer et al., 1980) at levels below about 20 mb; the BUV observations at 274 and 283 nm were used to derive an exponential form for the profile at levels well above the mixing ratio maximum. The "upper" and "lower" profiles were joined by a cubic spline.

A priori profiles for the original processing of SBUV data were based on the World Ozone Data Center ozonesonde data archives for layers 1 through 5, and on the original BUV data set for layers 6 through 12. The profiles were fitted to an equation of the form

$$x_k^a = A_k + [1 - \cos(2\theta)][B_k + C_k \cos\{2\pi/365(J - J_{0k})\}] \tag{21}$$

where k is a layer index, θ is latitude, J is day of year, and A_k, B_k, C_k, and J_{0k} are regression coefficients.

The a priori profiles for the current SBUV algorithm (Bhartia et al., 1985) use the total ozone to estimate the layer 1, 2, and 3 amounts, using a quadratic relationship based on soundings at Natal, Brazil (5.9°S); Hohenpeissenberg, FRG (47.8°N); Churchill, Canada (58.8°N); and Resolute, Canada (74.7°N). For layers 6 through 12, the original processing of SBUV was fitted to an equation of the form of Equation 18.

The a priori profile error covariance matrix, $\mathbf{S}_x$, was developed for layers 1 through 5 as the covariance of the Hohenpeissenberg data set about the fitted values. The same process was used for layers 6 through 12 using the original SBUV data set, but with the subjective modifications to allow for the difference between the covariance of an ensemble of real profiles and that of an ensemble of retrieved profiles. Off-diagonal elements linking the two sets of layers were estimated subjectively. The same matrix is used for all latitudes and seasons.

Measurement Error Covariance

The measurement error $\mathbf{S}_\epsilon$ for stage three includes not only the errors in the measured radiance (0.5 percent) and total ozone (1.5 percent), but also the errors that enter into the calculation of y_n in Equation 19 and the calculation of the multiple-scattering correction. Thus, allowance is made for contributions to the measurement error covariance from errors in ozone absorption coefficients due to atmospheric temperature variations (0.5 percent). Surface reflectivity and surface pressure errors are not accounted for, but are believed to be small.

3.3.3.3 Forward Model Assessment

Single-Scattering Model

The method of calculating single scattering is considered to be highly precise for a molecular atmosphere because the coefficient for scattering by molecules is known to be better than 1 percent, and ozone absorption is believed to be 1 percent relatively and better than 2 percent absolutely. We have found no serious deficiencies in the integral in Equation 16.

Multiple-Scattering Corrections

The method used for calculating the multiple-scattering contribution involves the iteration of the auxiliary equation of radiative transfer in a pseudospherical atmosphere, in which only the primary scattered source photons for multiple scattering are calculated for a spherical-shell atmosphere. Higher order scattering is calculated for a flat atmosphere. This is considered to be a "reasonably good approximation" for SBUV out to a solar zenith angle of 88°, which is the maximum processed by the algorithm. The accuracy of this has not been checked, and we recommend that it should be. However, there should be no impact on trend estimates.

The lookup tables used for estimating I_{msr} are calculated from standard profiles; this approach is reasonable when I_{msr} is not a large correction. The error covariance matrix includes terms caused by the error in looking up the tables, but there is no numerical estimate of the accuracy of the parameterisation itself, particularly the dependence on the ozone profile.

Aerosols and Other Trace Gases

The effects of aerosol scattering and absorption, absorption by molecules other than ozone, fluorescence (both resonance and Raman), and scattering by other atmospheric gases are omitted in the forward model.

Fluorescence from nitric oxide has been detected in the continuous scan data from the SBUV (McPeters, 1986, 1989). Indeed, the decision not to use the 255 nm wavelength in the profiling algorithm was made because of interference from a strong NO fluorescence band resulting from absorption of solar radiation near 200 nm. The observed fluorescence is small (<4 percent of the Rayleigh scattering at 255 nm for the strongest bands), and is probably smaller above 260 nm.

O_2 is another molecule that is observed to fluoresce above 250 nm because of excitation by wavelengths near 200 nm (in the Schumann Runge Bands). In addition, O_2 can resonantly scatter in the Herzberg Bands between 250 and 300 nm. The analysis of the continuous scan data from SBUV by McPeters and Bass (1982) shows no peaks above 260 nm, but the superposition of the many fluorescent and resonant peaks could produce a quasi-continuum above 260 nm. No estimate of this continuum has been made.

Effects of the UV-absorbing gases NO_2 and SO_2 have been examined as possible sources of error; they were found to be insignificant under most circumstances. An exception to this is SO_2 from volcanic eruptions, but these are infrequent and short-lived phenomena, after which the SO_2 is rapidly converted to nonabsorbing sulphate compounds that produce stratospheric aerosol.

Scattering by stratospheric aerosols causes an increase in the measured albedo for the SBUV profiling wavelengths. For a normal stratospheric aerosol profile, this albedo change is strongly wavelength dependent. Figure 3.1 is a SAGE–I average aerosol profile for 5°S latitude for

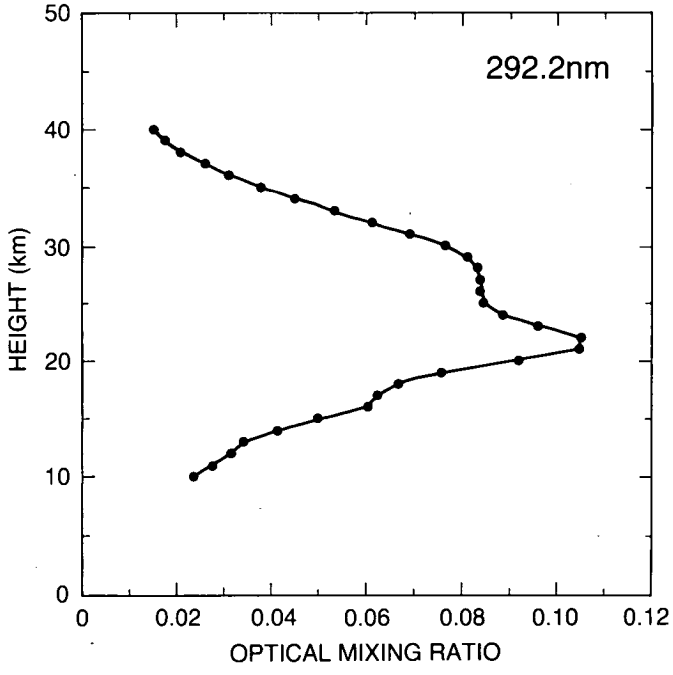

Figure 3.1. Aerosol profile from SAGE–I: average ratio of aerosol to Rayleigh extinction at 292 nm, for 5°S in summer 1980.

summer 1980, plotted as the scattering optical mixing ratio (aerosol extinction/Rayleigh extinction) as a function of altitude. The impact of this profile on the SBUV albedo is plotted in Figure 3.2 for the following case. The aerosol optical properties were defined by a real index of refraction of 1.435 and by taking the average of the properties for two size distributions of spherical Mie particles: modal radius 0.1 μm, standard deviation 0.4 μm, and modal radius 0.2 μm, standard deviation 0.4 μm. The calculations were made for a low-latitude ozone profile of 250 matm-cm, an effective surface reflectivity of 0.3, and a solar zenith angle of 0°. The SBUV albedo change has a rather sharp peak at 297.5 nm because the aerosol profile peak has a best match with the Rayleigh-scattering source function (or scattering layer) producing the backscattered albedo for this wavelength. The scattering layers for the other wavelengths are either above (λ<297.5) or below (λ>297.5), and the impact on these wavelengths is substantially reduced.

The effect of this albedo change "signature" on the retrieved profile is illustrated in Figure 3.3. Note the profile decrease in layers 6 and 7 and the increase in layers 5 and below. The reason for this decrease–increase pattern is that the total ozone is unaffected by these aerosols, so that the ozone removed from layers 6 and 7 has to be replaced because of the constraint that the retrieved profile should have approximately the measured total ozone.

This is only one example, intended to illustrate the impact of stratospheric aerosols on SBUV retrievals. In any particular case, the impact will depend on the aerosol optical properties (a function of index of refraction and aerosol size distribution) and on the aerosol profile. The effect will increase with aerosol amount; the retrieved profile distortion (level of the increase–decrease pattern) will depend on the aerosol profile shape (level of maximum optical mixing ratio).

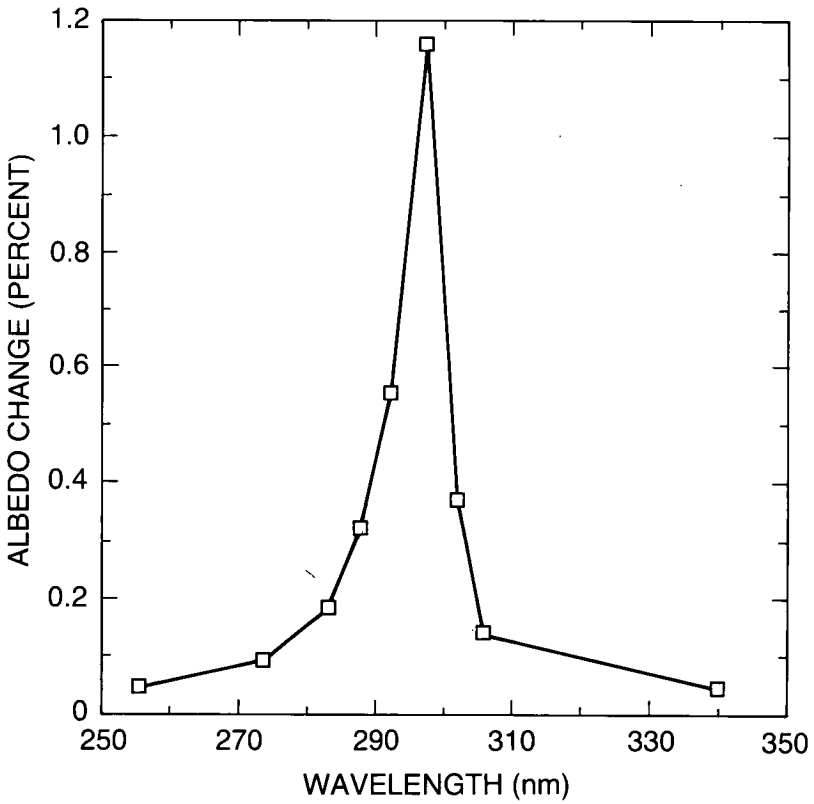

Figure 3.2. Calculated SBUV spectral signature for the Figure 3.1 aerosol profile. The assumed atmosphere contains 250 DU of ozone, the surface reflectivity is 0.3, and the solar zenith angle is 0°. Assumed aerosol optical properties are given in the text.

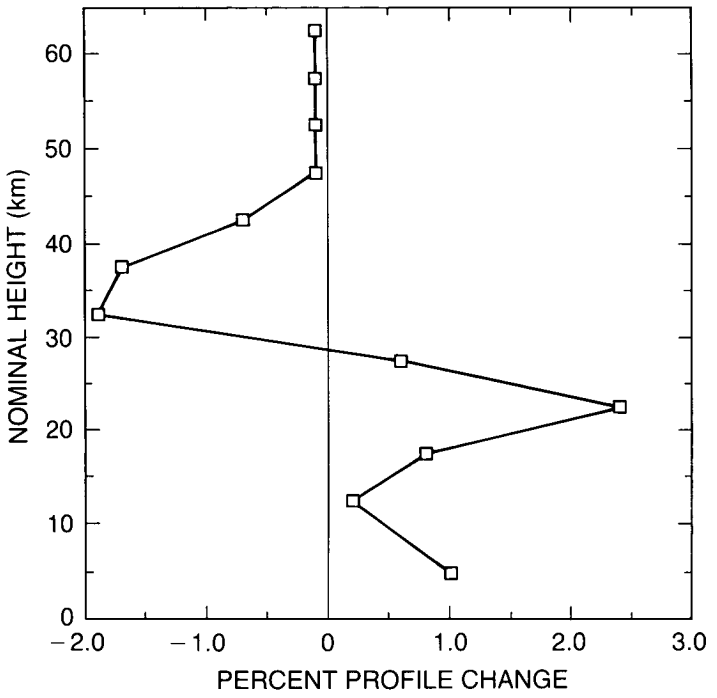

Figure 3.3. The effect of the Fig. 3.1 aerosol on the SBUV-retrieved ozone profile.

The climatology of aerosol optical properties and aerosol profiles is discussed in Chapter 10, on aerosols. Calculations using preliminary estimates of properties and profiles suggest that the large observed changes in SBUV albedo in the months immediately following the El Chichón eruption can be explained by calculations similar to those illustrated here.

Ozone Absorption and Rayleigh-Scattering Coefficients

The band-averaged ozone absorption coefficients for the SBUV wavelength bands are obtained using the procedure described by Klenk (1980), using Bass and Paur (1985) measurements of the ozone absorption spectrum in the ultraviolet and their reported temperature dependence.

For the computation of single-scatter radiances, the ozone absorption coefficients are computed at a nominal atmospheric temperature that varies with wavelength, determined by the altitude at which the weighting function peaks for that wavelength.

Since the atmospheric temperature effects are more important for the computation of I_{msr}, 3 standard temperature profiles are used, along with the 17 standard ozone profiles described in Section 3.3.1.1. The scattering coefficients are based on data from Bates (1984).

Instrument Attitude Errors

The instrument views the atmosphere nominally in the nadir direction. Any error in pointing knowledge will appear primarily as solar zenith angle errors. However, with a field of view of 11.3 degrees, the expected variations of spacecraft attitude of a few tenths of a degree will not seriously affect the measurement. No significant bias error is expected from attitude errors.

3.3.3.4 Inverse Method Assessment

We have found no significant problems with the inverse method. To the extent that the forward model is correct, the retrieval will reproduce the measurements within experimental error.

The constant a priori covariance used in the retrieval is based in part on the subjective modification of an earlier set of SBUV and BUV retrievals. As such, it may represent an ensemble of profiles that are too smooth at higher altitudes and, hence, constrain the retrieval too tightly.

The second-stage retrieval leads to difficulties in extreme situations, such as the Antarctic ozone hole (McPeters et al., 1986), where the algebraic forms described in Section 3.3.3.2 are used outside their region of validity, giving rise to unrealistic initial profiles that are reflected in the final retrieval. However, the error analysis below shows that the profiles are unsuitable for trend studies in this altitude range for other reasons.

Apart from the ozone hole problem, however, most of these comments are not of immediate significance for trend measurement as they do not introduce spurious trends and are taken into account in the retrieval characterisation presented in the next section.

3.3.3.5 Error Analysis

Forward model parameters include the absorption coefficient, α, the Rayleigh scattering coefficient, β, the diffuser plate reflectivity and its wavelength dependence, and the surface/cloud albedo and pressure. Inverse model parameters include the a priori regression coefficients and the a priori and measurement error covariances.

Averaging Kernels

The averaging kernels show how the retrieved ozone profile is related to the true profile. In an ideal observing system, the averaging kernel for *layer i* would be unity within *layer i* and zero outside. They have been computed for a range of cases, including midlatitude conditions with total ozone of 325 and 525 matm-cm, a low-latitude case, and a high-latitude case representative of the ozone hole.

Figure 3.4 shows the averaging kernels for a midlatitude case. These curves are partial derivatives $\partial \ln \hat{x} / \partial \ln x$ of the log of the retrieved layer amount, with respect to the log of each of the sublayer amounts.

We note that layers 6 to 9 or 10 give averaging kernels (ak's) centered at approximately the correct nominal level and with a full width at half maximum of about 1.6–2 Umkehr layers (8–10 km). The layer 10, 11, and 12 ak's are all centered on layer 10, with significant negative excursions at layer 8. The layer 5 ak is very broad, whilst the layer 1 to 4 ak's are generally peaked in the wrong place, have significant negative excursions, and are found to vary considerably from one case to the next.

We must conclude that only the retrievals from layer 6 to layers 9 or 10 are of value for trend estimation as they stand. Trends derived from layers 1 to 5, 11, and 12 may be misleading because the retrievals depend on the ozone variations at other levels. It may be that the retrievals for these layers are reasonable estimates of ozone in those layers on a single profile basis, but that

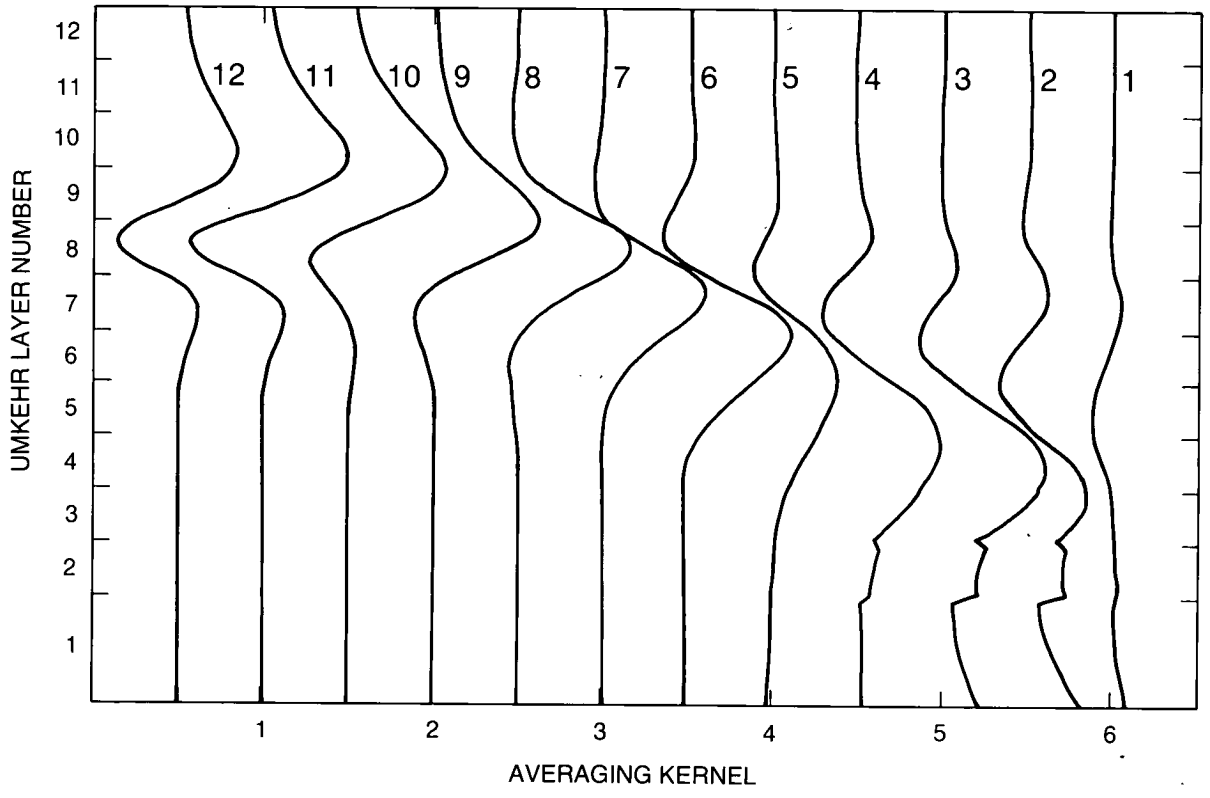

Figure 3.4. SBUV averaging kernels for retrieved layer amounts. The reference profile is at a midlatitude (45°), solar zenith angle is 45°, and a total ozone amount is 325 DU. The curves are labeled with layer numbers and offset by multiples of 0.5 for clarity.

is because there are correlations between levels in the ozone climatology. This is not appropriate for trend estimation, where past climatology of individual profiles may not be a good estimate of the climatology of future changes.

Sensitivity to Diffuser Plate Reflectivity

If the measured value of the diffuser plate reflectivity D_λ is in error by δD_λ, then the measured Q-value will be in error such that $\delta \ln(Q_\lambda) = \delta \ln(D_\lambda) = \delta D_\lambda / D_\lambda$. Thus, the sensitivity of the retrieved profile to diffuser plate errors is the same as its sensitivity to the measured Q-value. On the basis of the discussion of diffuser plates in Chapter 2, we have carried out several tests of the sensitivity of the retrieved profile to diffuser plate reflectivity:

(a) A random error of 1 percent in D_λ, uncorrelated between wavelengths, but constant in time. This gives a contribution to the formal random error in the profile, but should have no effect on the measured trend. The rms of this error source is curve (a) in Figure 3.5.

(b) A constant error of 1 percent in D_λ at all wavelengths. Thus a drift of 1 percent per year in the error in D_λ would lead to an annual drift in profile given by curve (b).

(c) A random error of 2 percent in $r(\lambda)$, the formal uncertainty quoted in Chapter 2. This is assumed to be uncorrelated between wavelengths, but constant in time. It leads to a scale error proportional to exposure time, whose value is random with an rms value given by curve (c) in Figure 3.5 for $E = 761$ hours (8 years).

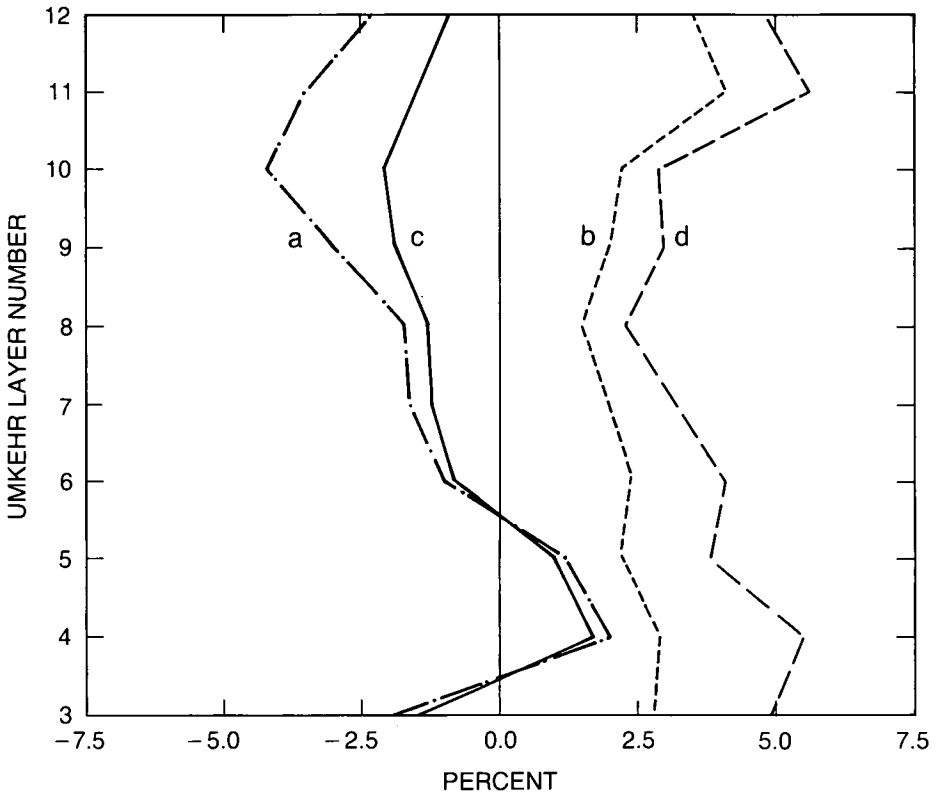

Figure 3.5. (a) rms error in the SBUV profile due to a 1 percent random error in D_λ. (b) increase in ozone due to an increase in D_λ of 1 percent at all wavelengths. (c) rms scale error due to a 2 percent random error in $r(\lambda)$, after 8 years' operation. (d) increase in ozone due to a 5 percent increase in $r(\lambda)$ at all wavelengths.

(d) A constant error of 5 percent in $r(\lambda)$. Five percent is roughly the scatter of the values of r given in Chapter 2, Figure 2.10. Curve (d) shows the effect of this error at $E = 761$ hours.

(e) We have also considered the alternate diffuser plate models M1, M2, and L of Chapter 2. The change that these make to a retrieved midlatitude profile is shown in Figure 3.6, for a profile measured at the end of the data set, after 8 years. The change here is so large that it is probably outside the bounds of this linear error analysis, but this should give a guide to the magnitude of the error.

Sensitivity to Atmospheric Temperature

The retrieved ozone profile will depend on atmospheric temperature through the temperature dependence of absorption coefficient. Figure 3.7 shows the percentage change in the retrieved profile to a temperature perturbation of 1K in each layer. We note that, to produce a 1 percent change in ozone at level 6, we would need about a 10K change in temperature in layers 6 and 7.

Sensitivity to Surface or Cloud Top Reflectivity and Pressure

The sensitivities of the profile to surface or cloud top reflectivity and pressure are shown in Figure 3.8. Except at levels 1 to 3, both are very small and are unlikely to be significant.

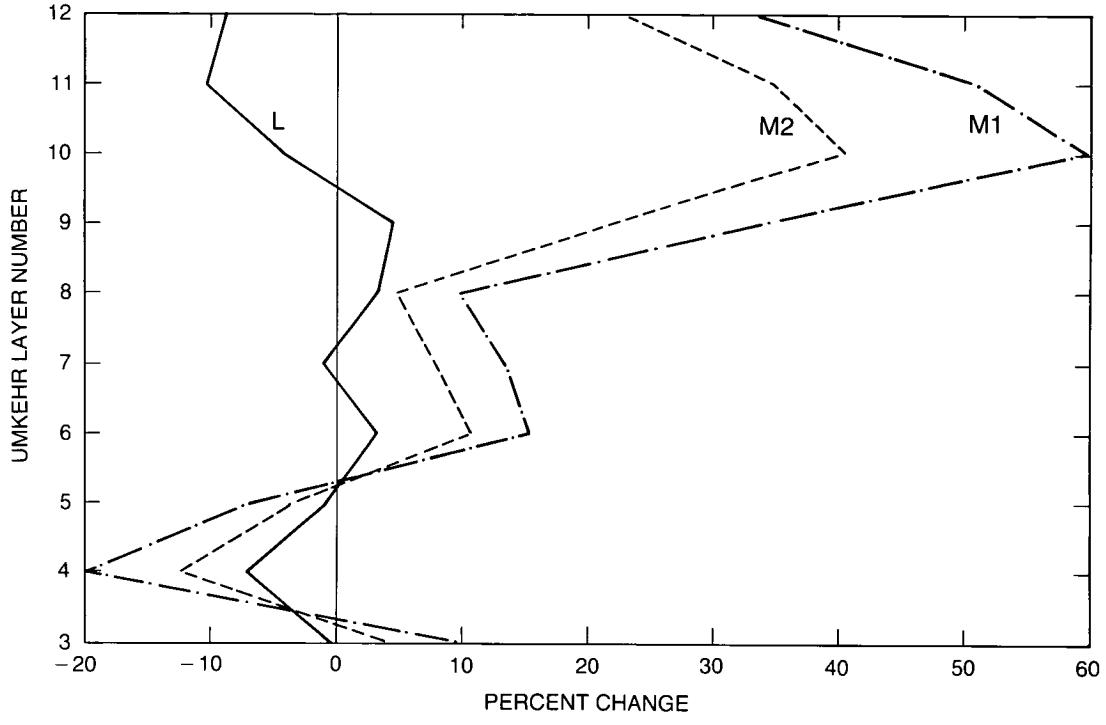

Figure 3.6. Change in ozone relative to the SBUV archived data, due to the diffuser degradation models M1, M2, and L, as defined in Chapter 2.

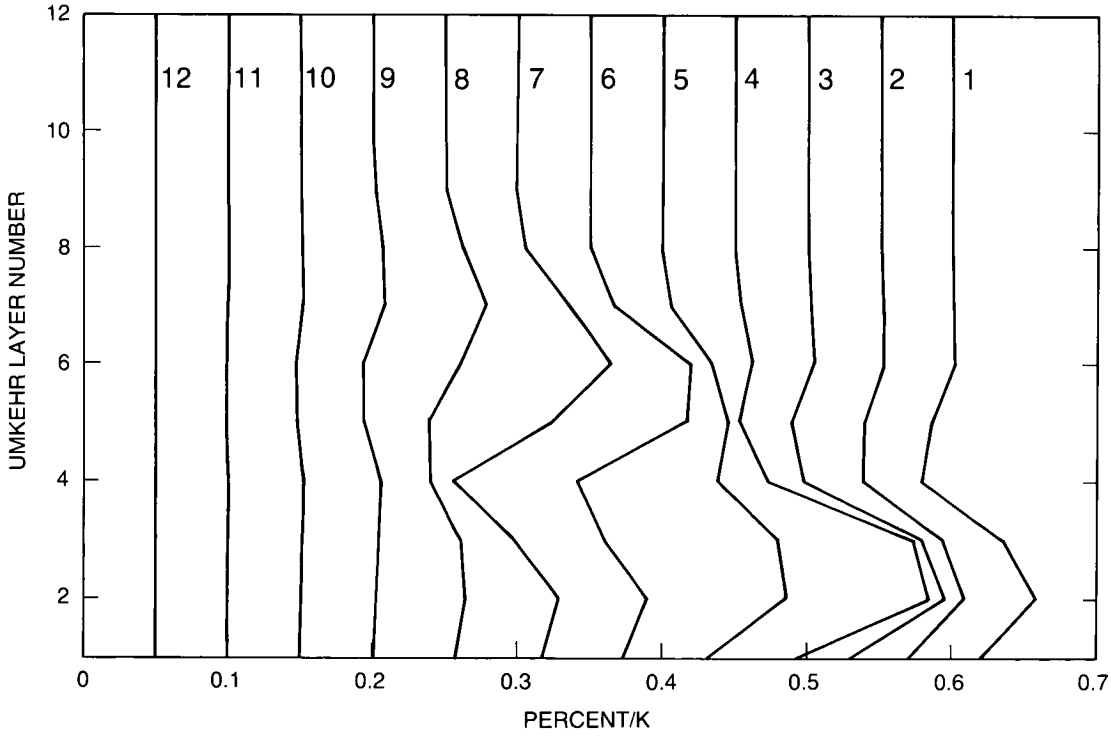

Figure 3.7. Sensitivity of the SBUV retrieved layer amounts to errors in the mean layer temperatures. The curves are labeled with the layer in which the temperature is perturbed and are offset by multiples of 0.05%/K for clarity.

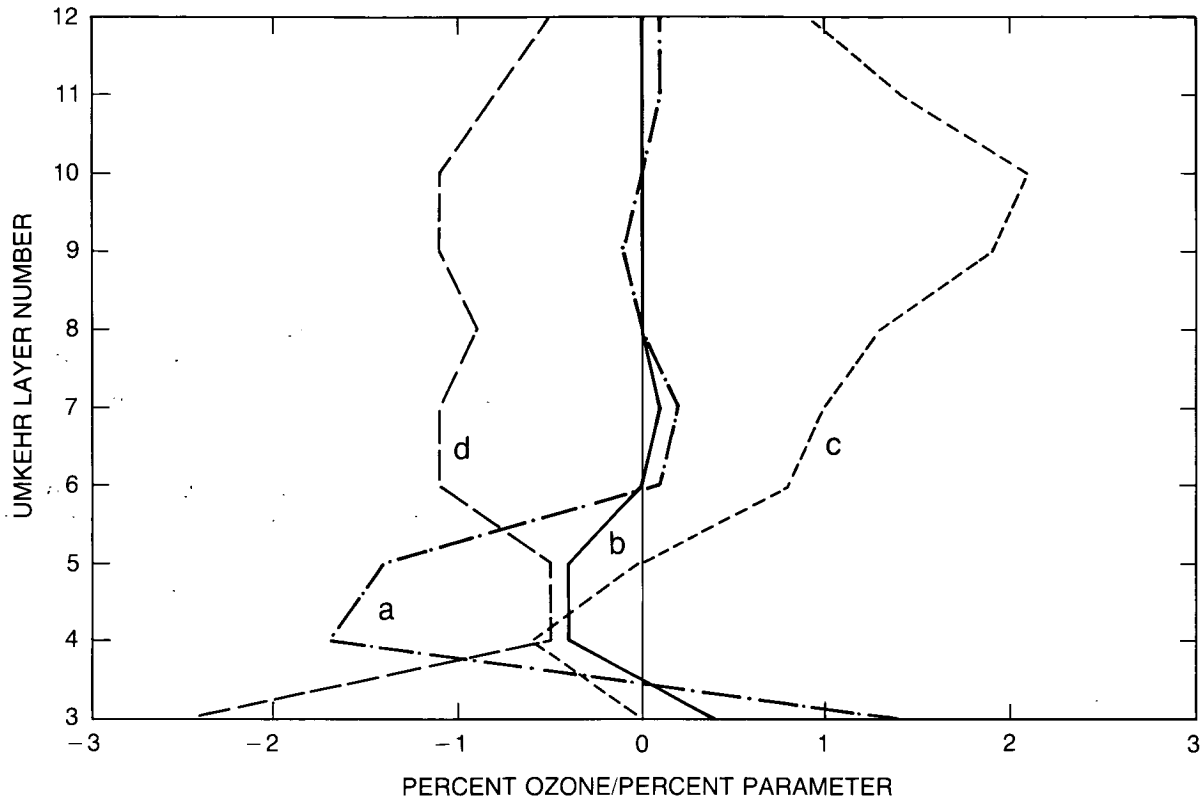

Figure 3.8. Sensitivities of the SBUV-retrieved layer amounts to errors in (a) surface reflectivity (b) surface pressure (c) Rayleigh-scattering coefficient (d) ozone absorption coefficient.

Sensitivity to Ozone Absorption and Rayleigh-Scattering Coefficients

The ozone absorption coefficients and Rayleigh-scattering coefficients, or their errors, will not change with time. Therefore, errors due to this cause will not contribute to trend errors. The sensitivities shown due to these causes are given in Figure 3.8 for completeness.

Sensitivity to Aerosol

A formal error analysis of the sensitivity to aerosol is complex, and has not been carried out by us. A case study giving a typical impact is discussed in Section 3.3.3.3 above; further discussion will be found in Chapter 10.

3.3.3.6 Trend Estimation Assessment

The averaging kernel plots indicate that SBUV data should be capable of representing the ozone profile between Umkehr layers 6 and 9 or 10 (16–0.7mb, 28–51 km) with a vertical resolution of 1.6–2 layers (8–10 km). Trends should be measurable in the same range with the same resolution, except insofar as they are aliased by trends in other quantities involved in the retrieval. The most important uncertainties, which may introduce unreal trends into the data, are diffuser plate reflectivity and atmospheric aerosol. Our best estimate of the diffuser plate uncertainty leads to the conclusion that the apparent trends in currently archived SBUV ozone profiles (Chapter 5) are not significantly different from zero, and that SBUV measurements are not capable of definitively identifying the ozone depletion due to chlorofluorocarbons (CFC's)

that is predicted by the chemical models (Chapter 7). This position may change if further information on the diffuser degradation becomes available. This does not, of course, apply to SBUV–2, for which an archival data set is not yet available.

Atmospheric temperature, as well as surface or cloud-top reflectivity and pressure, have the potential of introducing apparent trends, but these effects are small.

The problem with the second stage of the retrieval mentioned in (d) above implies that current SBUV profile data below about 20 km cannot be used for ozone hole studies. However, the averaging kernels analysis implies that the retrievals in that altitude range are dubious for other reasons.

3.3.4 Dobson Ozone Spectrophotometer: Umkehr

The Dobson spectrophotometer measures the ratio of zenith sky or direct Sun radiance at two wavelengths in the ultraviolet. An Umkehr observation consists of a series of zenith sky measurements taken as the solar zenith angle changes from 60° to 90°. The observation includes a concurrent measurement of the total ozone column with the same instrument (Section 3.3.2). In the standard technique, as reported in the World Ozone Data Center archives, the C-pair of wavelengths centered at 311.45 and 332.4 nm is used. The present standard algorithm, which is described and assessed in this section, was developed by Mateer and Dütsch (1964).

3.3.4.1 Forward Model

The solar radiation received by the instrument is scattered mainly by the gaseous atmosphere and absorbed mainly by ozone. The physics of the measurement is basically the same as that for SBUV (Section 3.3.3), but the geometry is different.

The forward model used in Umkehr retrieval accounts for scattering only by the gaseous atmosphere (assumed to obey the Rayleigh scattering law) and for absorption only by ozone. For this idealized atmosphere, computation of zenith sky light is relatively straightforward, although somewhat tedious, especially at solar zenith angles near 90°, where the effects of the sphericity of Earth need to be accounted for precisely. Since the scattering optical depth of the atmosphere at the Umkehr wavelengths is near unity, multiple-scattering effects are also important.

In the real atmosphere, there is also scattering by the dust and aerosols suspended in the atmosphere at different altitudes. Other gases, such as SO_2, are also sometimes present in sufficient quantities to provide significant absorption.

Determination of Ozone Absorption Coefficient

The Dobson instrument has a band-pass of about 1 nm at the shorter wavelength and close to 4 nm at the longer wavelength of the C-pair. Therefore, the instrument is sensitive to the radiation received in a range of wavelengths over which the scattering and absorption properties of the atmosphere may vary. For forward model calculations, however, it is convenient to assume that the instrument is sensitive to a pseudo-monochromatic radiation, having both an effective ozone absorption value and an effective scattering cross-section. The effective ozone cross-sections used in the standard Umkehr algorithm were obtained by convolving the meas-

urements of Vigroux (1953) (at −44°C) with the nominal instrument band-passes for each wavelength (for band-passes, see Vigroux, 1967). These cross-sections are published in the Dobson instrument manual (Dobson, 1957b).

Computation of N-Value Tables and Derivatives

The full forward model is too complicated for efficient use in standard retrievals, so it is approximated for this purpose by a set of second order Taylor series expansions of the full model about a set of three standard profiles.

The N-value tables and first-order partial derivatives used in the standard algorithm are calculated in a manner that accounts for the sphericity of Earth for the primary and second-order scattering. A flat-atmosphere multiple-scattering code was used to calculate the ratio of total multiple scattering to secondary scattering. Each spherical-shell secondary scattering radiance was then multiplied by the appropriate ratio to obtain an equivalent spherical-shell total multiple scattering. For the first-order partial derivatives, this same radiance ratio was used to obtain an equivalent spherical-shell multiple-scattering partial derivative. The calculation of the second-order partial derivatives involved only primary scattering in a spherical-shell atmosphere. The effects of atmospheric refraction were not included in these calculations.

3.3.4.2 The Inverse Method

The inverse method is based on the "minimum information" method of Twomey (1963).

$$N(\mathbf{x},\theta) = 100\log_{10}\left[\frac{I(\mathbf{x},\theta,\lambda_1)}{I(\mathbf{x},\theta,\lambda_2)}\right] + C_0 \tag{22}$$

where $\mathbf{x}$ is the profile to be estimated, θ is the solar zenith angle, $I(\mathbf{x},\theta,\lambda)$ is the zenith sky radiance at wavelength λ, and C_0 is the "extraterrestrial constant," a combination of the solar spectrum and the instrumental response. The measurement vector $\mathbf{y}$ comprises the Dobson total ozone X_{obs} and the quantities $N'(\mathbf{x},\theta_i)$, obtained by subtracting $N(\mathbf{x},60°)$ from each of the other N-values.

The elements of the profile vector $\mathbf{x}$ are $-\ln(x_i)$, where x_i is the ozone amount in Umkehr layer i.

The second-order expansion of the forward model is written

$$\mathbf{y} = \mathbf{y}_{std} + \mathbf{K}(\mathbf{x} - \mathbf{x}_{std}) + (\mathbf{x} - \mathbf{x}_{std})^T\mathbf{L}(\mathbf{x} - \mathbf{x}_{std}) \tag{23}$$

where $\mathbf{K}$ is the first-order derivative and $\mathbf{L}$ is the second-order derivative, both evaluated at $\mathbf{x}_{std}$. For the retrieval, the vector $\mathbf{u}$ is defined

$$\mathbf{u} = \mathbf{K}(\mathbf{x} - \mathbf{x}_{std}) = \mathbf{y} - \mathbf{y}_{std} - (\mathbf{x} - \mathbf{x}_{std})^T\mathbf{L}(\mathbf{x} - \mathbf{x}_{std}) \tag{24}$$

An ozone conservation equation is added to the set as the forward model for X_{obs}. The retrieval iteration is

$$\hat{\mathbf{x}}^n = \mathbf{x}_{std} + (\mathbf{K}^T\mathbf{K} + \gamma\mathbf{I})^{-1}\mathbf{K}^T\mathbf{u}^{n-1} + \gamma(\mathbf{x}_{fg} - \mathbf{x}_{std}) \tag{25}$$

where $\mathbf{x}^{n-1}$ is used in evaluating the quadratic term in $\mathbf{u}^{n-1}$, $\mathbf{x}_{fg}$ is a first-guess profile, and γ is

Twomey's smoothing constant. The convergence criterion is based on the change in size of the quadratic term between iterations.

Three standard profiles are used, each containing different amounts of total ozone. The linearisation point is chosen to be one of the three, on the basis of the total ozone amount. The first-guess profile is also chosen to be one of the standard profiles on the same basis, except that for total ozone amounts near the changeover points, a linear interpolation is used so that there are no discontinuities in the first guess as a function of total ozone. No seasonal or latitudinal variation is used in the standard profiles.

3.3.4.3 Forward Model Assessment

Ozone Absorption Coefficient Calculation

The spectral characteristics of the received radiation depend on the extraterrestrial spectrum, the solar zenith angle, the ozone profile, the temperature profile, and the scattering and absorbing constituents of the atmosphere. Consequently, strictly speaking, for a given effective ozone cross-section, agreement between calculated and "true" band-pass-averaged radiation can occur only for a limited range of conditions. Fortunately, simulation studies suggest that this error is less than 1 percent for a broad range of atmospheric conditions.

The algorithm is based on the assumption that all instruments in the Umkehr network have essentially the same band-pass. Actual instrument band-passes have been measured for only one instrument (Komhyr, unpublished), and these were generally broader than the nominal band-passes used by Dobson (1957a,b). However, interstation total ozone intercomparisons, using TOMS as a transfer standard, suggest that the standard error in total ozone measurements arising from both absorption coefficients (via band-pass and spectral alignment problems) and from extraterrestrial constant (C_0) errors combined does not exceed about 2 percent (Bojkov and Mateer, 1985; conclusion from data in their Table 1). This may be considered an indication of interstation precision.

Insofar as absolute errors in the effective absorption coefficients are concerned, Table 3.4 is relevant.

Table 3.4. Effective Ozone Absorption Coefficients for Dobson C-Pair

Source	T(°C)	Short	Long	Diff.	Ratio
[a]1. Dobson, 1957, Vigroux, 1953	−44	2.100	0.108	1.992	19.4
2. Vigroux, 1967	−50	1.957	0.099	1.858	19.8
[b]3. IOC–WMO, 1968	—	(1.941)	(0.099)	1.842	(19.6)
4. Bass & Paur, 1985	−45	2.0044	0.0917	1.9127	21.86
[c]5. Error Tests	—	1.9303	0.0883	1.842	21.86
% Range excl. (5)		8.2	17.8	8.1	12.7

[a]Standard Algorithm
[b]Effective 1/1/68
[c]Section 3.3.4.5

The absorption coefficient difference in line 3 was adopted by WMO in 1968 for use in total ozone measurements, but values were not specified for the individual wavelengths. The values in parentheses were estimated for use in the assessment of the sensitivity to errors in absorption coefficient and spectral alignment in Section 3.3.4.5. The values in line 1, used in the standard algorithm, are considerably in error, due at least in part to the spectral sparseness of the early Vigroux measurements. The Bass–Paur data are stated to have a precision of 1 percent between 245 and 330 nm. The precision at the long C wavelength is not this good—perhaps 2 percent. The absolute accuracy is related to the measurement of Hearn (1961) of the ozone cross-section at 253.65 nm, which is believed to be accurate to about 2–3 percent. The assumption in the standard algorithm of an isothermal atmosphere (−44°C) introduces distortion in the retrieved profiles, due to temperature dependence of the absorption coefficient.

Calculation of N-Value Tables and Derivatives

The quadrature for the spherical-shell part of the N-value and partial derivative calculations should be accurate to better than 0.5 percent for primary scattering and to 1 percent for secondary scattering. The quadrature for the flat-atmosphere multiple-scattering calculations should also be accurate to better than 1 percent. The extension of the flat atmosphere calculations to third and higher orders of scattering in a spherical atmosphere may lead to errors as great as 3 percent (estimated) in the radiance ratio (1.3 N-units) for a solar zenith angle of 90°, where the error is greatest. Errors in the first-order partial derivatives may be somewhat greater.

The application of the second-order partial derivatives, which are calculated for primary scattering only, involves some empirical adjustments developed by Dütsch (unpublished). This process should not involve significant errors for ozone profiles close to one of the standard profiles. Errors for profiles that are not close to one of the standard profiles have not been determined; they may be significant.

Aerosol and Other Scattering

The forward model used in the Umkehr retrieval does not account for the scattering by dust, aerosols, and thin clouds sometimes present during the measurement. The main reason for this is that the quantity of suspended matter is extremely variable from day to day, and its optical properties are rarely known accurately enough to include it correctly in the forward model. Consequently, the error introduced by aerosol scattering remains the most significant source of error in Umkehr retrievals over the short term, as well as in determining seasonal and long-term variations of ozone.

With the present-day theoretical capability of calculating radiative transfer for a molecular medium, including large-particle scatters, it is possible, in principle, to include aerosol effects directly into an Umkehr forward model. This would be valuable only if the aerosol properties were known a priori for each observation. However, the Umkehr inverse model is not capable of separating aerosol information from ozone information. Aerosol properties that must be known are phase function, albedo of single scattering, and vertical profile. It is not practical to measure these properties, which can be quite variable with time, at all Umkehr stations on a regular basis.

A detailed discussion of the effect of aerosols on Umkehr retrievals, and on possible approaches to making corrections, is found in Chapter 10.

Absorbers Other Than Ozone

The only known absorber of any significance that has been omitted from the forward model is SO_2, which may occur in highly polluted urban environments (see Section 3.3.2) and in the stratosphere as a short-lived species immediately after major volcanic eruptions.

3.3.4.4 Inverse Method Assessment

Accuracy of the Second-Order Expansion

The standard algorithm starts with a known linearisation-point profile and a precomputed table of *N*-values. As the estimated profile is modified during the iteration process, the table values are adjusted to account for the change. This adjustment is calculated using precomputed coefficients of a truncated (after second order) Taylor series expansion of the *N*-values around the a priori profile.

As discussed in Section 3.3.4.3, the calculation of these coefficients is not sufficiently accurate and may introduce error in the forward model calculation. The impact of error in the coefficients will be insignificant when the atmospheric ozone profile is close to the a priori, but could be significant when it is not.

Ozone Above Layer 9

The retrieval method solves for the ozone amount in layers 1 to 9. However, there is enough ozone above layer 9 to cause significant absorption of the strongly absorbing wavelength at large solar zenith angles. The Umkehr retrieval assumes an a priori value of 2.07 matm-cm above layer 9, and that this amount is always 54 percent of the layer 9 amount. These figures are derived primarily from photochemical calculations carried out in the early 1950's. Recent satellite and rocket measurements indicate that 2.07 is too large, by about 50 percent, and that the value varies seasonally.

3.3.4.5 Error Analysis

Averaging Kernels

Averaging kernels have been computed for a range of cases, showing how the retrieved layer ozone is related to the true ozone profile. In an ideal observing system, the averaging kernel for *layer i* would be constant within *layer i*, and zero elsewhere. Figure 3.9 shows that is by no means the case. Only one example is shown; the others gave results that were qualitatively similar but that differed in detail. A summary of the peak heights and widths of the averaging kernels is given in Table 3.5.

We note that, for layers 4 through 8, the averaging kernels are peaked at approximately the right level, with a full width at half maximum of around 2.5 layers. The kernels for layers 3 and 9 have significant negative excursions; they are peaked about one layer too high and low, respectively. The kernels for layers 1 and 2 are more complicated functions of the true profile; they appear to be unrelated to the ozone in those layers. The averaging kernel also describes the relationship between the measured trend profile and the true trend profile, so trends with a broad vertical structure between layers 4 and 8 would be reasonably well measured, but retrieved trends in layers 1, 2, 3, and 9 should be treated with caution.

Table 3.5. Averaging Kernel Peak Heights and Widths

Layer	Level of Maximum			Full Width Half Height	
	Layer	p(mb)	H (km)	Layers	H (km)
1	—	1013	0	2.4*	12
2	3.56	60.6	19.4	2.9	14.5
3	4.06	42.9	21.6	2.4	12
4	4.56	30.3	23.8	2.8	14
5	5.31	18.0	27.2	2.9	14.5
6	6.19	9.84	31.2	2.6	13
7	6.69	6.96	33.5	2.3	11.5
8	7.69	3.48	38.3	2.2	11
9	7.94	2.92	39.6	2.0	10

*One-sided

Absorption Coefficient and Spectral Alignment

Errors in the ozone absorption coefficients used in the algorithm have been discussed in Section 3.3.4.3. A spectral alignment problem may be considered equivalent to an absorption coefficient error for an individual instrument.

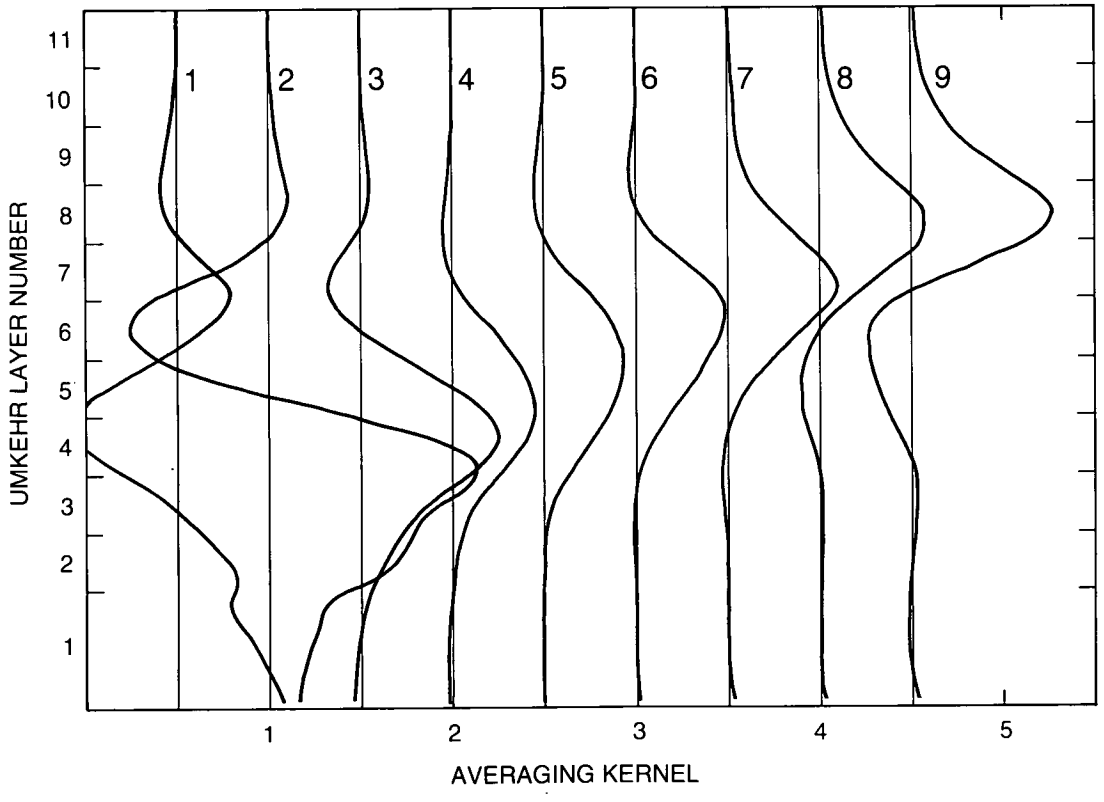

Figure 3.9. Umkehr averaging kernels for retrieved layer amounts. The reference profile is a midlatitude profile with a total ozone amount of 340 DU. The curves are labeled with layer number and offset by multiples of 0.5 for clarity.

Umkehr retrievals are sensitive to the difference in the absorption coefficients for the short- and long-wavelength channels and to their ratio. An error in the difference produces, primarily, an error in scale, accompanied by some profile distortion. An error in the ratio of the coefficients produces profile distortion in the retrievals. The sensitivity of the retrieval to errors in the coefficients for the individual channels is shown in Figure 3.10. This result has been obtained by perturbing the standard algorithm.

Additional results have been obtained using another algorithm in the following manner. First, the values in line 3 of Table 3.4 were used to obtain an average Umkehr retrieval for 20 Umkehr observations at Arosa (Switzerland) in 1980. Second, the values in line 5 were used to obtain an average retrieval for the same 20 Umkehrs. This retrieval, shown as a percentage difference from the first one in curve (a) of Figure 3.11, illustrates the effect of changing the coefficient ratio to the Bass–Paur value while holding the coefficient difference unchanged. This coefficient change produces very little profile change in layers 1 and 6, increases up to 1 percent in layers 2–5, and decreases as much as 4.5 percent above layer 6, i.e., a profile distortion. Curve (b) in Figure 3.11 is obtained using the Bass–Paur values in line 4 of the table. As noted above, comparing curve (b) with curve (a), this has produced primarily a scale change of between 3 and 4 percent, except in layer 1 where there is little change. Roughly similar results would apply if this procedure could be applied to the standard algorithm.

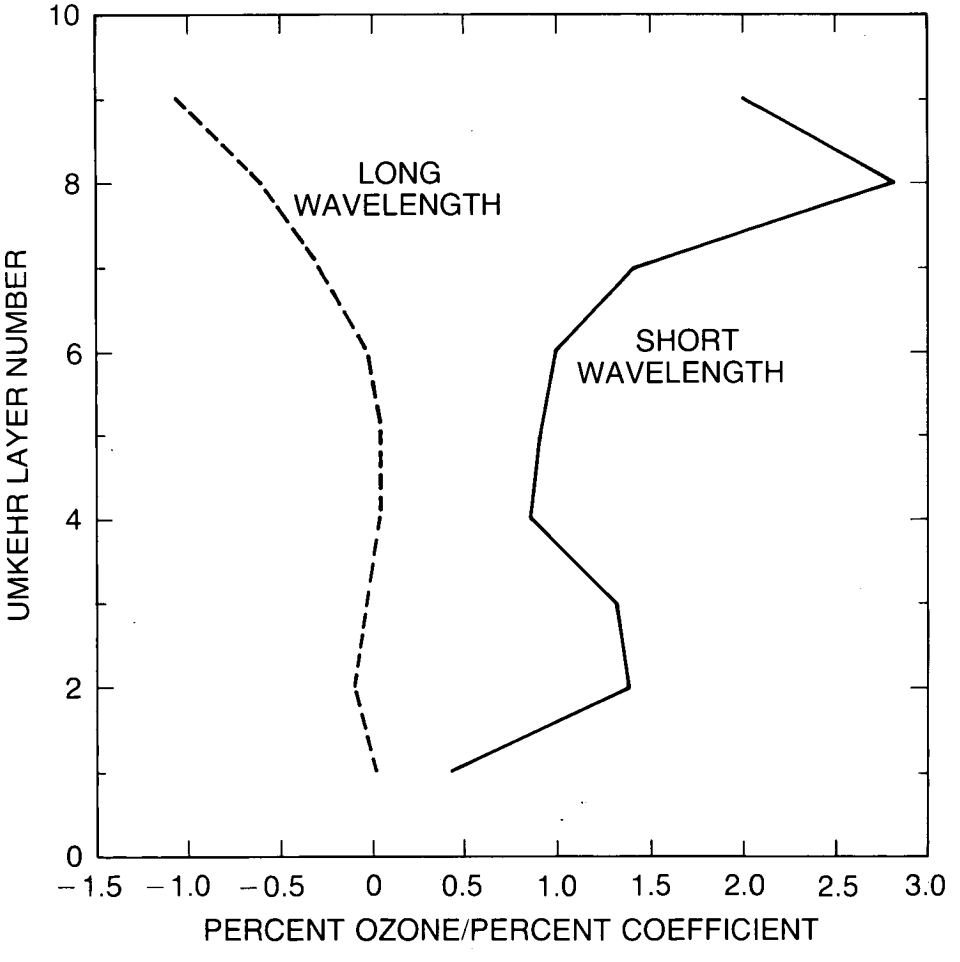

Figure 3.10. Sensitivity of the Umkehr retrieval to absorption coefficient errors.

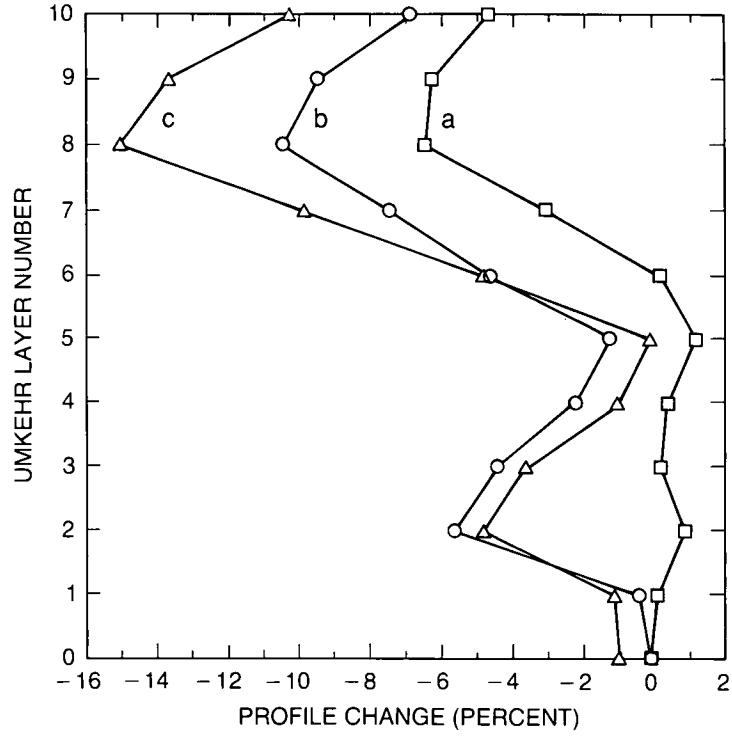

Figure 3.11. Changes in Umkehr retrievals due to the following absorption coefficient assumptions: (a) changing the coefficient ratio to the Bass–Paur value, keeping the difference unchanged. (b) Bass–Paur values at −44°C. (c) Bass–Paur values, including temperature dependence.

Finally, we must explain how the change in 1968 in the scale of C-pair total ozone has been handled in the standard algorithm. First, the observed total ozone value on the 1968 scale is multiplied by 0.925 (= 1.842/1.992) to reduce it to the scale implied by the coefficients used in the algorithm. The inversion is then carried out using the algorithm. Finally, all layer amounts in the retrieved profile are divided by 0.925 to convert them back to the 1968 ozone scale. This procedure introduces some profile distortion (similar to curve (b) minus curve (a) in Figure 3.11), but should have little effect on ozone trends derived from Umkehr profiles. Curve (b) alone gives an idea of the overall profile bias (distortion) caused by the use of the incorrect coefficients.

Temperature

Umkehr profile retrievals are also sensitive to atmospheric temperature through the temperature dependence of the ozone absorption coefficients. The short wavelength coefficient of the C-pair has a temperature sensitivity of 0.15%/K, while the long wavelength sensitivity is 0.37%/K. Failure to include this temperature dependence, as in the standard algorithm, which assumes a constant temperature of −44°C, produces an additional profile distortion. This distortion is such that atmospheric layers that are warmer than −44°C will have too much ozone in the retrieved profile, and vice versa. The result of adding the temperature dependence for an average midlatitude temperature profile is illustrated by comparing curve (c) with curve (b) (isothermal atmosphere at −44°C). The greatest effect is seen in the 40–50 km region, where the temperature is significantly warmer than −44°C.

It is evident that real temperature trends will introduce fictitious ozone trends in Umkehr profiles. Figure 3.12 illustrates the effect of a 20K temperature change in each layer. For this

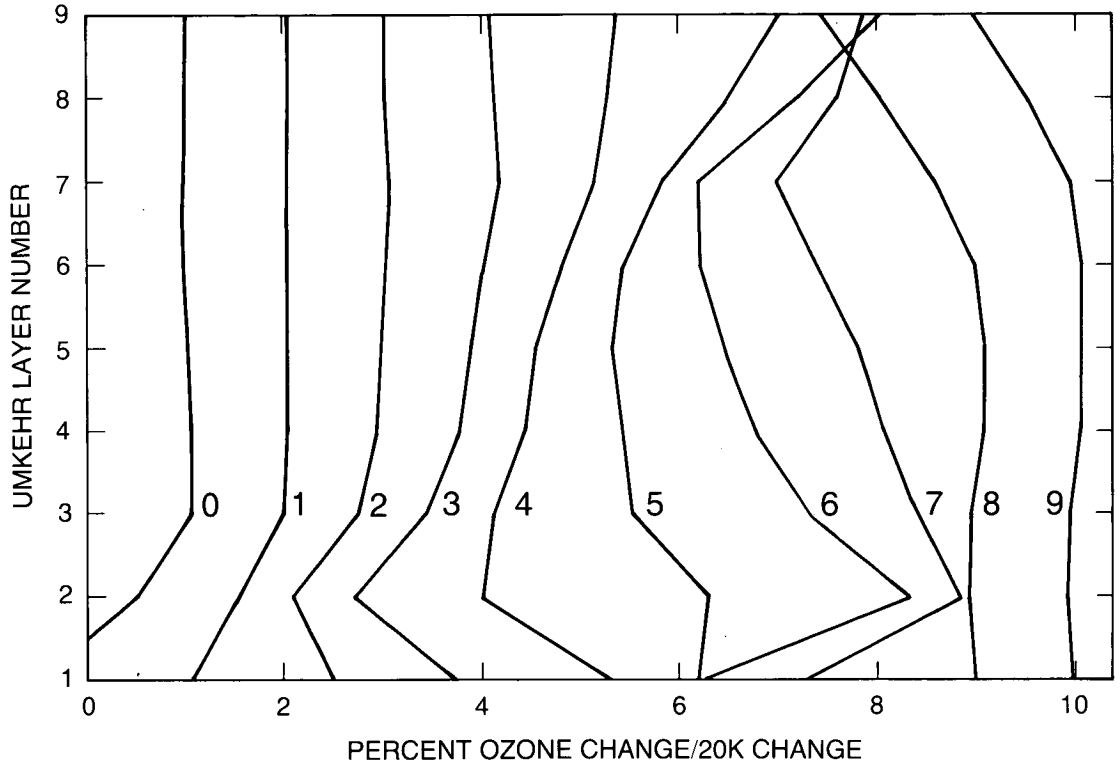

Figure 3.12. Sensitivity of Umkehr-retrieved ozone to atmospheric temperature changes. The curves are labeled with the number of the layer in which the temperature is perturbed by 20K and are offset by 1%/20K for clarity.

particular test, the troposphere (layer 1) has been divided into two layers (curves 0 and 1). We may conclude that realistic atmospheric temperature trends will have a rather small effect.

Rayleigh-Scattering Coefficients

The Rayleigh-scattering coefficients β are known to better than 1 percent. The change in the retrieved profile for a change in β of 1 percent is shown in Figure 3.13. This is a small but constant systematic error.

Total Ozone Measurement

An error in the extraterrestrial constant C_0 has no effect on the N-values, but affects the total ozone measurement. As noted in Section 3.3.4.3, this error combined with others does not exceed about 2 percent over the Dobson network. Sensitivity of the retrieved profile to the total ozone measurement is given in Figure 3.14. This sensitivity is small, except for layer 1.

Surface Reflectivity

The standard algorithm assumes zero surface reflectivity, whereas typical reflectivities might be around 20 percent, approaching 100 percent in the case of snow cover. Sensitivity to assumed surface reflectivity is given in Figure 3.15. The error in retrieved ozone is unlikely to be more than about 1 percent, except in layer 1. This is unlikely to contribute to errors in trends.

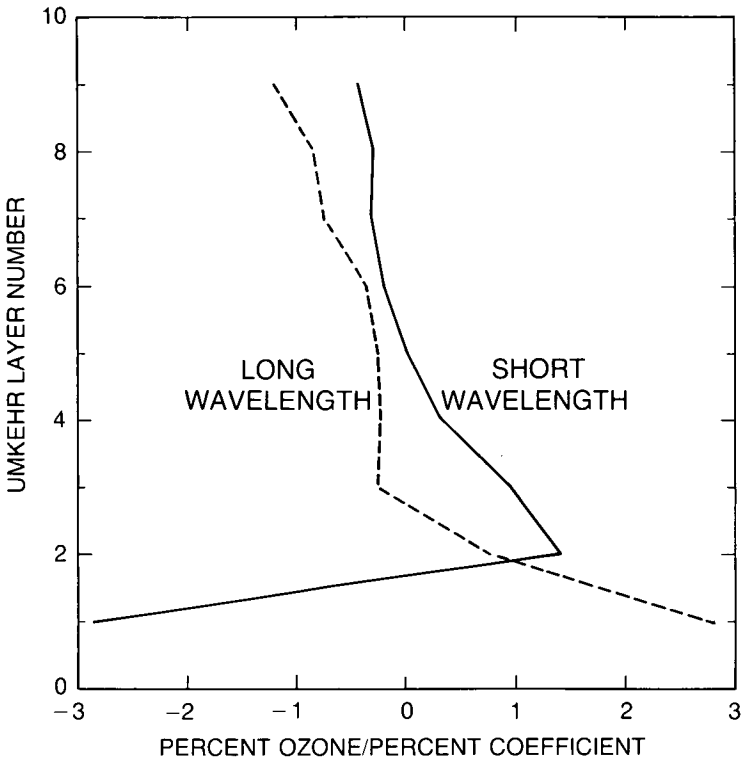

Figure 3.13. Sensitivity of Umkehr-retrieved ozone to Rayleigh-scattering coefficient errors.

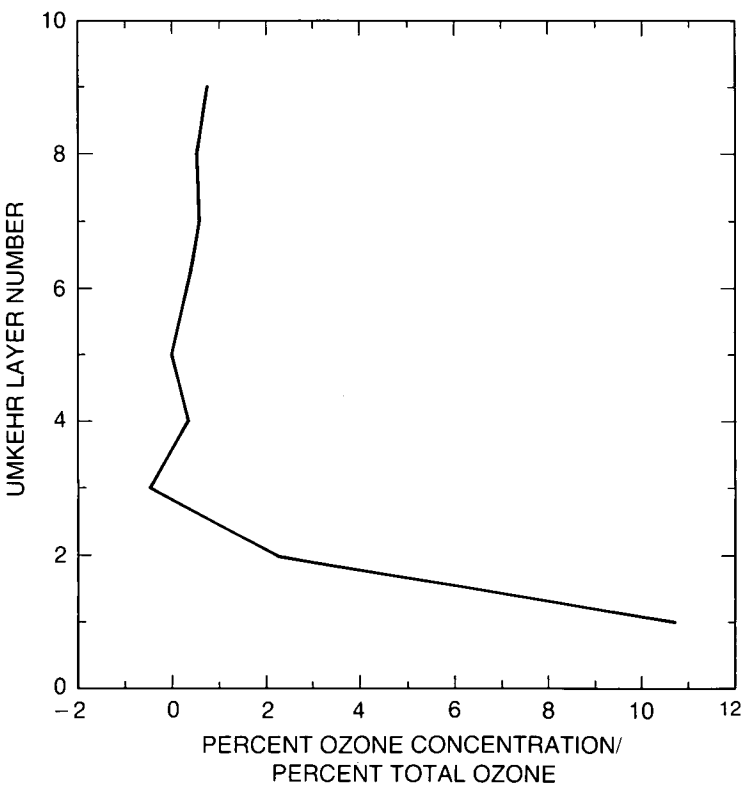

Figure 3.14. Sensitivity of the Umkehr-retrieved profile to errors in the total ozone measurement.

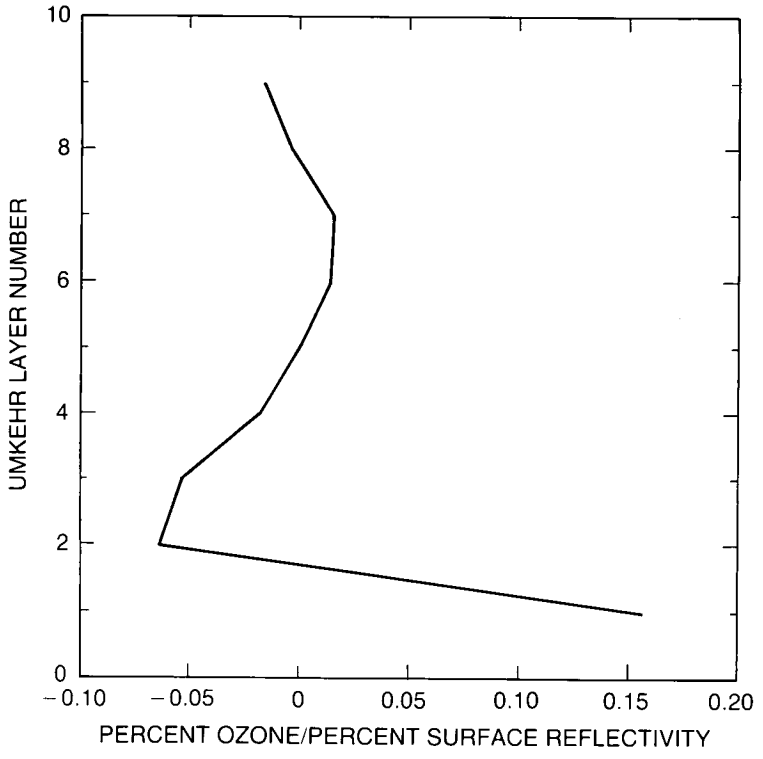

Figure 3.15. Sensitivity of the Umkehr-retrieved profile to surface reflectivity errors.

Multiple-Scattering Correction

The error in the multiple-scattering correction has not been determined. An estimate of this error has been obtained by computing the corrections, using the pseudospherical atmosphere method for one of the standard profiles, and taking the difference between these corrections and those used in the standard algorithm. The effect of this difference on the retrieved profile is shown in Figure 3.16. The profile changes are small for layer 4, with roughly a 5 percent increase for higher layers, and decreases below layer 4 with a maximum 20 percent decrease in layer 2. These errors should be primarily systematic and have little effect on trends.

Other Absorbers

The effect of unaccounted SO_2 absorption on the retrieved profile, for 1 matm-cm in the lower half of layer 1, corresponding to a typical background (i.e., low pollution level) urban troposphere (Kerr, private communication), is shown in Figure 3.17. Also shown is the effect of a moderately heavily polluted troposphere, with 10 matm-cm. This is significant for quality control, but should not be for trends, unless a significant number of stations are in polluted areas.

Volcanic SO_2 is very short lived and has not been considered here.

Other Effects

Wedge calibration and other similar discontinuities in the record may be corrected if the information is available (it has been done for Belsk, Poland). This has nothing to do with the

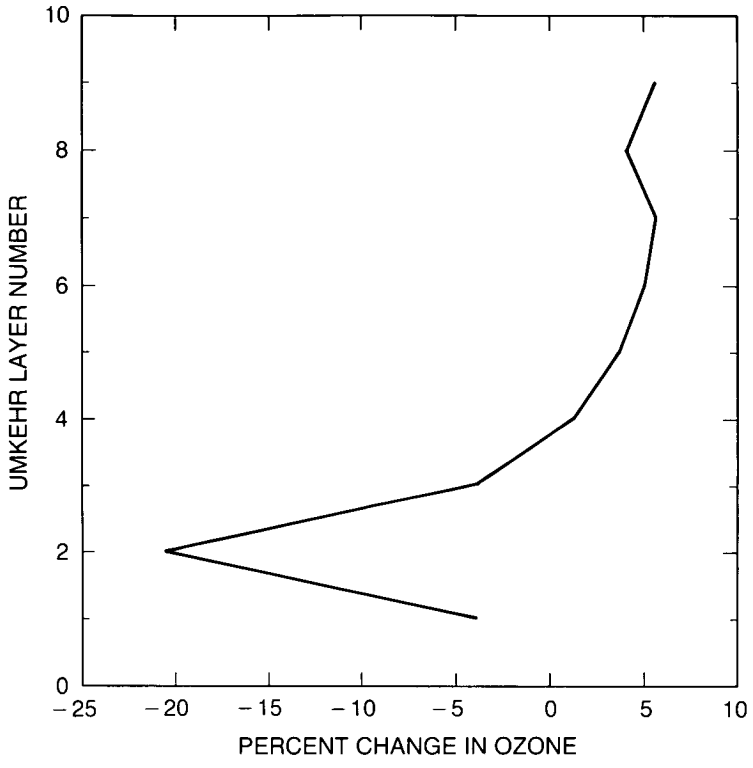

Figure 3.16. Effect on the ozone profile of changing the method of calculating the multiple-scattering correction.

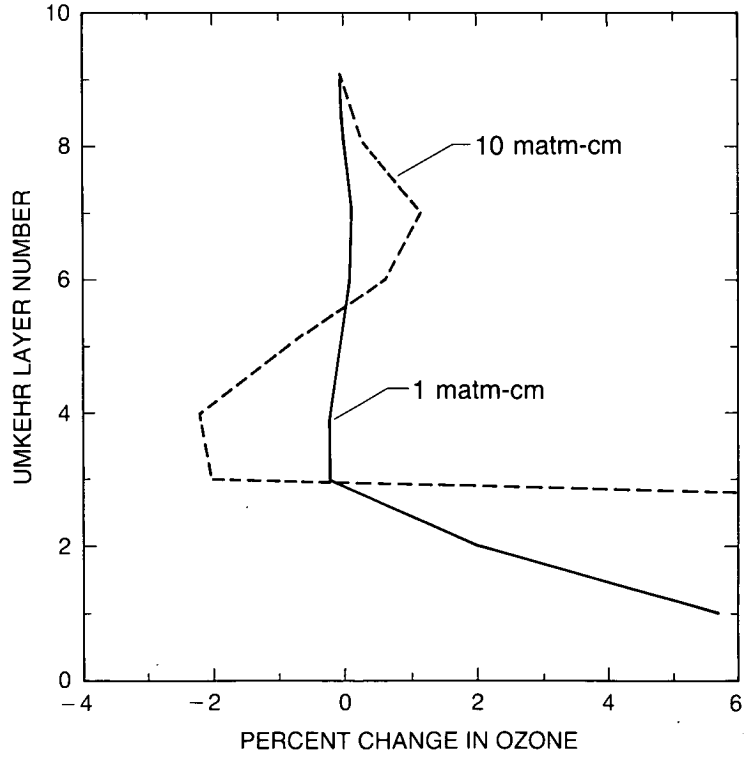

Figure 3.17. Sensitivity of the Umkehr-retrieved profile to SO_2 in the lower half of layer 1.

algorithm. If the necessary information is not available, then the problem is best handled by statistical methods; again, not a problem to be discussed in this chapter.

Nonlinearity errors have been discussed in Sections 3.3.4.3 and 3.3.4.4. Although such errors are not systematic in individual cases, they should average out to a roughly systematic error in trend estimation.

The "no refraction" assumption will lead to a systematic error such that derived ozone amounts in the uppermost layers are too low. This is understandable because the slant path attenuation is always decreased when refraction is added, and the scattering layer is always lower in the atmosphere for the longer wavelength of the pair, leading to a higher N-value at the larger zenith angles where the effect is greatest. The error is probably small, but it may depend, to some extent, on the amount of ozone at upper levels, thereby leading to an over- or underestimation of 40 km trends. This trend impact should be very small.

3.3.4.6 Trend Estimation Assessment

Many of the sources of error are unimportant for trend estimation because they should average out over the network, or over time, as instruments are periodically recalibrated, or if they have constant systematic errors. The important error sources are the sensitivities to atmospheric quantities that may have their own trends. It is unlikely that any instrumental parameter will have a trend that is repeated across the network. However, we should always be aware of sampling problems with a small network.

It is important to understand how true trends are reflected in the retrieved trend quantified by the averaging kernels, which indicate that the Umkehr retrievals for layers 4 through 8 (63–2 mb, 19–43 km) correspond to means over layers ~2.5 layers (12.5 km) thick, centered on approximately the correct nominal altitude. Outside this altitude range, and at higher vertical resolution, information about trends should be treated with caution. This is important, since the postulated chlorofluoromethane (CFM) effect will occur in layer 8 of the atmosphere. Retrievals from the standard Umkehr algorithm may show ozone being displaced upward in the atmosphere.

The most important quantities that may have trends unaccounted for in the Umkehr retrieval scheme are stratospheric aerosol, tropospheric pollution, and temperature.

Amounts of stratospheric aerosols, which vary with time, are undoubtedly the most important source of error in the long-term trend determination from Umkehr. Attempts have been made to do a first-order correction using the Mauna Loa Sun-sensor data. More recently, lidar measurement results are being used to obtain better corrections for the time period following the El Chichón eruption. However, the accuracy of the correction schemes used so far is still an open question.

Background urban tropospheric SO_2 levels (1 matm-cm) will cause negligible error in layers 4 to 8, but moderately heavy pollution (10 matm-cm) may cause errors of about 1 percent. As this is likely to be confined to a few heavily polluted urban areas, it is unlikely to be important for global trends, unless a significant number of stations are in polluted areas.

A false change of 1 percent in ozone in layers 4 to 8 would require a change of 10–15K in stratospheric temperature. This is unlikely to be a source of significant uncertainty.

3.3.5 Stratospheric Aerosol and Gas Experiment

The SAGE measures extinction of solar radiation in a limb path in the wavelength region from 380–1,020 nm. SAGE–II, currently in operation, measures sunrise and sunset extinction at seven wavelengths: 1,020, 936, 600, 525, 452, 448, and 385 nm. Those important for determining the altitude distribution of ozone are the aerosol-sensitive wavelengths of 1,020, 525, and 385 nm, and the ozone-sensitive wavelength of 600 nm. It is important to note that other measured constituents, such as NO_2, also contribute to the extinction at these wavelengths, if only slightly.

SAGE–II data have not yet been archived with NSSDC, but have been made available to the Ozone Trends Panel; it is the algorithm by which this data set was processed that is discussed here. SAGE–I was an instrument similar to SAGE–II, but with only four spectral channels, at 1,000, 600, 450, and 385 nm. The original inversion algorithm (Chu and McCormick, 1979), corresponding to the data in the NSSDC archive, is significantly different from that used in the SAGE–II data reduction. Because of the recent effort in ozone trend work, SAGE–I data have been reprocessed using an algorithm similar to the one used for SAGE–II; the reprocessed data are used in this report for comparison with other ozone data. The following discussions about the SAGE–I inversion algorithm will be understood to refer to the reprocessing algorithm.

The instrument has a field of view of 0.5 minutes of arc, which corresponds to 0.5 km at the limb. The instrument scans the solar disk during each measurement sequence to produce vertical profiles of constituent extinction. During a measurement sequence, the SAGE radiometer scans the Sun from top to bottom, as viewed from the spacecraft, at a scan rate of 15 minutes of arc per second. The Sun is scanned about 20 times for a normal sunset or sunrise event. Each channel is sampled 64 times per second and digitized to 12 bits.

Neither SAGE–I nor SAGE–II produces complete global data sets; thus, it is difficult to separate seasonal and long-term trends from the respective data sets. The first use of the SAGE data, therefore, is in a comparison with SBUV when both instruments observe the same ozone field. This comparison yields the long-term differences in calibration or changes in the relative bias between the two instruments.

3.3.5.1 Forward Model

The irradiance H_λ measured by the instrument at a given time t is given by

$$H_\lambda = \int_{\Delta\lambda}\int_{\Delta\Omega} I_{0\lambda} W_\lambda(\theta,\phi) F_\lambda(\theta,\phi,t) T_\lambda(\theta) d\Omega d\lambda \tag{26}$$

where $I_{0\lambda}$ is the incoming solar spectral radiance, W is the radiometer's FOV function, ϕ is the azimuthal angle, Ω is the solid angle, T is the transmittance of the atmosphere as a function of view angle θ, and F is the extraterrestrial solar radiance for wavelength λ. The mean transmittance over the spectral bandwidth and instrument field of view is obtained by dividing the irradiance measurements by those for a solar scan above the atmosphere. The transmittance function in terms of the minimum ray height is given by

$$T_\lambda(h) = \exp\left[-\int \beta_\lambda(h) dl_\lambda(h)\right] \tag{27}$$

where β is the total extinction coefficient of the atmosphere as a function of altitude h, and l is the geometric path length corrected for refraction.

The total extinction at each altitude is a linear combination of the extinctions of each constituent measured.

$$\beta_\lambda = \beta_R(\lambda) + \beta_{O_3}(\lambda) + \beta_{NO_2}(\lambda) + \beta_A(\lambda) \tag{28}$$

where $\beta_R(\lambda)$ is the extinction coefficient for Rayleigh scattering, $\beta_{O_3}(\lambda)$, $\beta_{NO_2}(\lambda)$, and $\beta_A(\lambda)$ are the extinction coefficients for ozone, nitrogen dioxide, and aerosol, respectively. It is assumed that there are no other constituents contributing to the extinction. For ozone and nitrogen dioxide, the extinction coefficient is given by the product of the number density and the absorption cross-section at the given wavelength.

The aerosol extinction coefficient is a function of aerosol size distribution, shape, and index of refraction. The following formula applies to homogeneous, spherical particles:

$$\beta_A(\lambda) = \int_0^\infty \sigma(n,r,\lambda)N(r)dr \tag{29}$$

where $N(r)$ is the size distribution function and $\sigma(n,r,\lambda)$ is the extinction cross-section for a particle with refractive index n and radius r, as computed from Mie theory. Because of the finite number of spectral channels being used, only a limited amount of information on either the aerosol size distribution or the wavelength-dependent extinction coefficient can be deduced. The refractive index is assumed to be 1.43, corresponding to sulfuric acid aerosol.

3.3.5.2 The Inverse Method

The procedure for inverting the SAGE–II data follows the approach taken in the inversion of the SAGE data, the basic algorithm for which is discussed by Chu and McCormick (1979). A two-step technique is used. The line-of-sight transmission measurements at the seven wavelengths are first separated into optical depths for each species, separately for each tangent altitude. These line-of-sight optical depths are then inverted for each species to give vertical profiles, assuming horizontal homogeneity.

After calibration, the data consist of optical depths at each wavelength, for each tangent height. Each is a linear combination of the line-of-sight absorber amounts of O_3, NO_2, the aerosol optical depth at each wavelength, and the Rayleigh-scattering optical depth. The tangent heights for the measurements are calculated from the satellite ephemeris and time in the case of SAGE–II. In the case of SAGE–I, this is not accurate enough; the height reference is obtained by matching the retrieved density profile with that calculated from the U.S. National Meteorological Center (NMC) data. The Rayleigh-scattering optical depth is calculated for each tangent ray using atmospheric temperature, pressure, and height data supplied by NMC, based on both radiosonde and satellite measurements. It is then removed from the measurements. The NO_2 component is calculated from the differential measurement supplied by the 448 nm and 453 nm data and removed from the measurements. The resulting five channels (ignoring the 954 nm water vapor channel, which is dealt with separately) are then used to solve for the ozone optical depth at 600 nm and for the four aerosol optical depths at 1020, 525, 453, and 385 nm.

The procedure for separating the ozone optical depth at 600 nm from the aerosol contribution is as follows: representing the aerosol size distribution $N(r)$ at a finite number of sizes $r_j, j = 1...m$, the aerosol extinction at the four wavelengths can be written as

$$\beta_i = \sum_{j=1}^{m} \sigma_{ij}(n)N_j \qquad i = 1...4 \tag{30}$$

which is an underconstrained set of linear equations for N_j. These can be solved using Twomey's minimum information solution (1963)

$$\mathbf{N} = \mathbf{K}^T(\mathbf{K}\mathbf{K}^T + \Gamma)^{-1}\beta \tag{31}$$

where $\mathbf{K}$ is a matrix with elements σ_{ij}, $\mathbf{N}$ is a vector with elements N_j, and Γ is a diagonal matrix with elements proportional to the estimated noise level at each aerosol wavelength. The aerosol extinction at 600 nm can then be expressed as a linear function of the retrieved $\mathbf{N}$, and hence as a combination of the extinction values at the other four wavelengths:

$$\begin{aligned} \beta_{600} &= \mathbf{K}_{600}\mathbf{N} \\ &= \mathbf{K}_{600}\mathbf{K}^T(\mathbf{K}\mathbf{K}^T + \Gamma)^{-1}\beta \\ &= \mathbf{a}\beta \end{aligned} \tag{32}$$

The four coefficients a_i can be precomputed, assuming only that the scattering is due to Mie particles with given refractive index. The aerosol extinction cross-section is calculated with the anomalous diffraction approximation.

The line-of-sight optical depth profile for each species is inverted using Twomey's modified Chahine algorithm (Twomey et al., 1977). The vertical profile for each species is represented by its averaged extinction in homogeneous slabs of 1 km thickness. Therefore, the line-of-sight optical depth for each species can be expressed as the product of a path-length matrix with each extinction profile. Since the measured signals for all channels decrease at a higher altitude, a 5 km vertical smoothing of the retrieved profile at high-altitude level is performed during each updating cycle in the inversion algorithm. Iteration is stopped when the residue between the measurement and the calculated optical depth approaches the estimated measurement uncertainty.

The primary difference between the SAGE–I and the SAGE–II inversion algorithms is the separation of optical depth values for aerosol, ozone, and NO_2. Because of the limited number of channels on SAGE–I, insufficient information is available to give a good description of aerosol optical depth versus wavelength behavior. In addition, the aerosol has almost the same spectral variation as NO_2 between 450 and 385 nm, thus making their separation impossible if only the measured data are used. In the SAGE–I algorithm, aerosol optical depth values at 450 and 385 nm are assumed to be a constant multiple of the values at 1,000 nm for altitudes above 27 km. The constants are determined assuming the aerosols are log normal distributed with refractive index $n = 1.43$, mean radius $r = 0.07\ \mu$m, and spread $\sigma = 1.8$ ($\log \sigma = 0.59$). Similarly, the NO_2 optical depth values below 27 km are calculated assuming constant NO_2 density. The aerosol optical depth values at 600 and 385 nm are then estimated with the same method as in the case of SAGE–II.

3.3.5.3 Forward Model Assessment

The aerosol representation is restricted to spherical Mie particles with a uniform index of refraction. Effects due to nonspherical shapes and nonuniform refractive index or composition are not included.

Ozone absorption cross-section measurements from Penney (1979) are used here. In the UV, these differ from those of Hearn (1961) by about 5 percent, which could lead to a bias in the ozone values. For NO_2, the unpublished data by Johnston and Graham (1977) are used. The accuracy of

ozone absorption cross-section at 600 nm is probably within 5 percent, while the accuracy at wavelengths other than 600 nm is probably not better than 10 percent. For NO_2, the accuracy of the absorption cross-section at all wavelengths is not better than 10 percent. However, this will produce only a constant systematic error and will have little effect on trend studies.

Measurements by Penney (1979) and by Vigroux (1953) indicate that the ozone Chappuis band centered at 600 nm showed no temperature dependence, while data from Vassey and Vassey (1948) showed some variation with temperature. It is likely that the temperature dependence of the ozone absorption cross-section at the SAGE–II spectral region is small and insignificant for ozone trend estimation. For the NO_2 absorption spectrum, Bass's et al. measurements (1976) for wavelengths below 400 nm indicated about a 10 percent change between room temperature and −40°C. However, there are no measurements of temperature effect at the wavelengths used by SAGE–II (448 and 453 nm). Due to the small effect of NO_2 on SAGE–II ozone determination, it is unlikely to affect ozone trend studies.

3.3.5.4 Inverse Method Assessment

NMC Temperature Field

The Rayleigh contributions at all seven channels are calculated from the NMC temperature and pressure data. The NMC temperature data are derived mainly from rawinsonde data at altitudes of 30 km and below and from satellite soundings above 30 km altitude. The accuracy of the NMC temperature data being used by the SAGE–II inversion algorithm is believed to be about 1 percent at or below 10 mb, degrading to 6–7 percent at 0.4 mb pressure level. However, due to the small contribution of Rayleigh extinction at 600 nm, the basic SAGE–II inverted product—ozone number density versus geometric height—is not sensitive to temperature error. Large error could be introduced if the results were converted to an ozone-mixing ratio at fixed pressure levels, as is needed for carrying out intercomparisons with instruments (such as SBUV) that measure ozone on a pressure scale.

Aerosol Representation

Because of the location of the spectral channels on SAGE–II, the aerosol extinction values at 600 nm will be most sensitive to size distributions that are multimodal in nature. This would affect the ozone retrieval up to about 20 to 25 km in altitude, depending on latitude and the amount of volcanic dust in the stratosphere.

In the case of SAGE–I, this problem is much worse because there are fewer channels. The only compensating factor is that the aerosol content of the atmosphere during SAGE–I lifetime (pre-El Chichón) was lower by a factor of 5 to 10 compared to SAGE–II measurements.

Horizontal Inhomogeneity

Since SAGE uses a solar occultation technique, measurements are performed at a solar zenith angle of 90°. Horizontal inhomogeneity on a scale of a few hundred kilometers becomes an important issue for constituents exhibiting strong photochemical reactions. This will be true for ozone above 50 km altitude during the sunrise and sunset measurement events. Other short-term, transient events that can lead to horizontal inhomogeneity in the ozone distributions could occur during sudden warming events. Similarly, cirrus clouds and Polar Stratospheric Clouds (PSC's) are likely to be horizontally inhomogeneous.

SAGE–I NO_2

The assumption of constant NO_2 density below 27 km restricts the available NO_2 information to 30 km or above. The effect on the aerosol data at 450 nm is not great because of the large differences in signal levels.

3.3.5.5 Error Analysis

The fundamental vertical resolution of SAGE is very high, as illustrated by the SAGE–II averaging kernels in Figure 3.18. These are very close to ideal—i.e., unity at the nominal altitude and zero elsewhere, from 20 km to 50 km. Below 20 km, the response to real changes in the atmosphere is somewhat reduced and broadened. Above 50 km, the noise on an individual profile is poor, so the vertical resolution has been deliberately reduced.

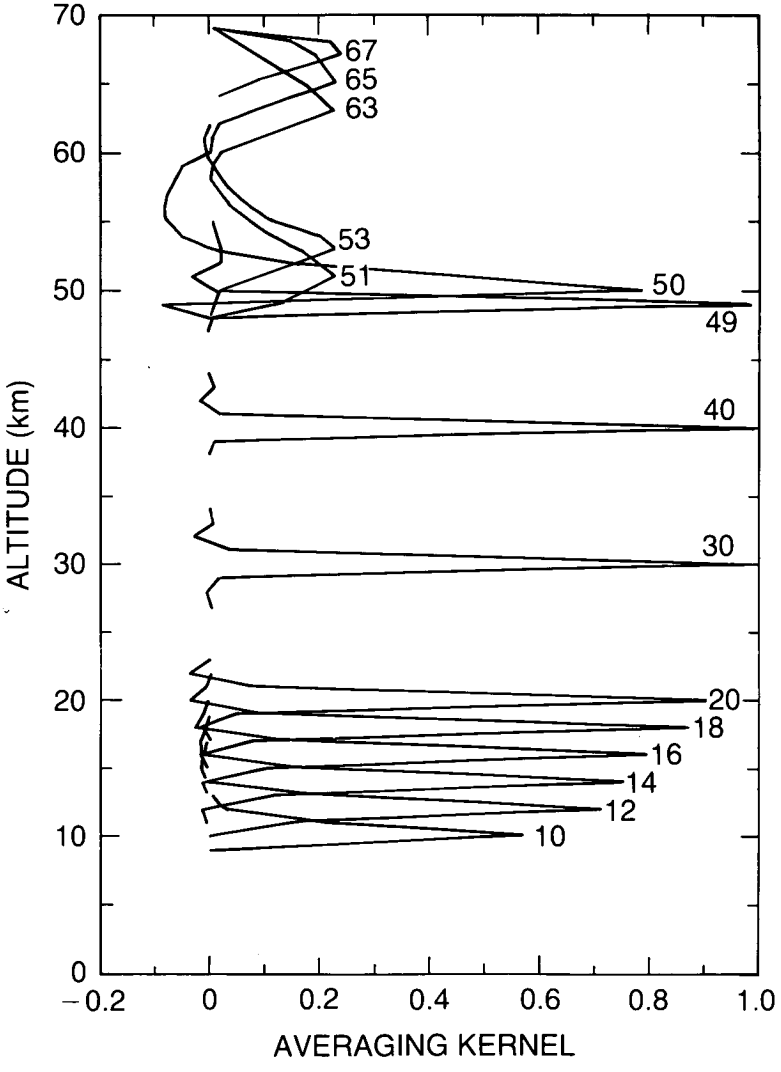

Figure 3.18. Averaging kernels for SAGE–II. Curves are not plotted for all altitudes.

For SAGE, the random error in the profile may be significant for trend estimation because it is a solar occultation measurement, and there are a maximum of two measurements per orbit. An estimate of this quantity, using only measurement error as sources of noise, is given in Figure 3.19. It is necessary to average more than 100 profiles for this source of error to become unimportant at the level of accuracy required for trend estimation.

The forward model parameters that may lead to profile errors include the extinction coefficients, the NMC temperature profile, and the registration of the profile in altitude. There is no opportunity for drift in radiometric calibration because a good zero and full-scale measurements are obtained at every occultation (see Chapter 2). Extinction coefficient errors may lead to trends in NO_2 or aerosol being aliased into trends in ozone. Temperature profile errors will lead to retrieval errors through both the Rayleigh correction and the temperature dependence of absorption coefficients.

Sensitivity of the retrieved profile to altitude registration is shown in Figure 3.20. Typical accuracy of the registration of SAGE–II is believed to be 100 m; it is not subject to long-term drift errors (unless there is unaccounted drift in the spacecraft clock and tracking), and thus will not contribute to trend estimation errors. The altitude registration accuracy for SAGE–I is believed to be about 150 to 200 m.

Sensitivity to the temperature profile is shown in Figure 3.21. One curve is shown for temperature at each of the standard levels from 300 mb to 0.4 mb. Above 20 km, the effect is very small and would not contribute to ozone trend errors, even for large trends in the error of the NMC temperature profile.

An error in the NO_2 differential absorption coefficient could lead to an incorrect NO_2 correction, and hence to an error in the O_3, which depends on the NO_2 amount. However, the NO_2 cross-section at 600 nm is only 5.5 percent of that at 448 nm, so this effect will be small.

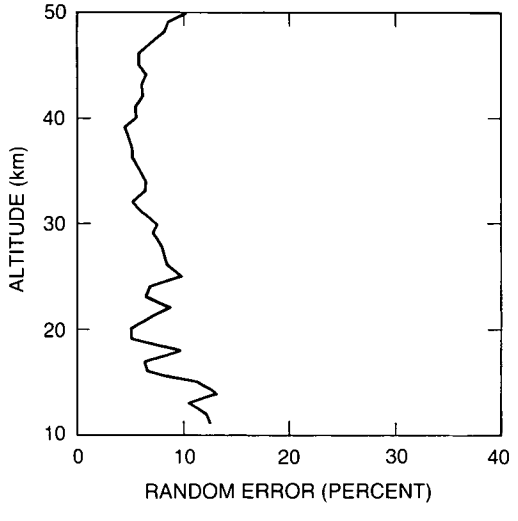

Figure 3.19. Random error of a single SAGE–II profile due to instrument noise only.

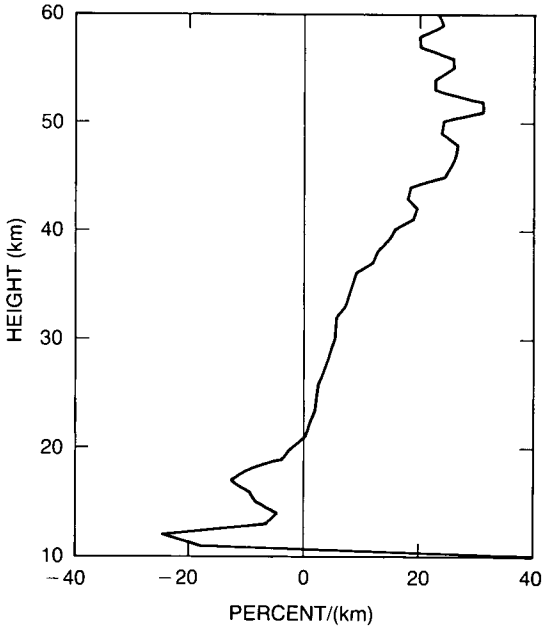

Figure 3.20. Sensitivity of the SAGE retrieval to altitude reference error.

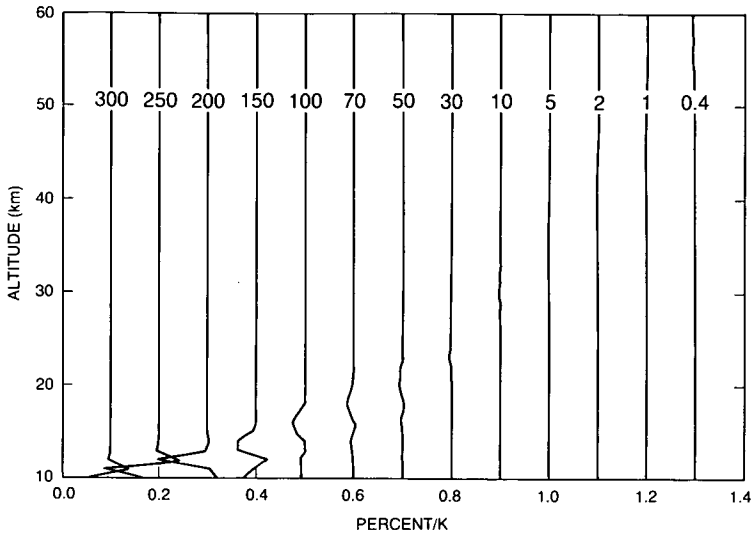

Figure 3.21. Sensitivity of the SAGE retrieval to atmospheric temperature errors. Curves are labeled with the pressure level (mb) at which the NMC temperature is perturbed and are offset by multiples of 0.1%/K for clarity.

3.3.5.6 Trend Estimation Assessment

SAGE–II data sampling is limited to 2 events per orbit, or 30 events per day. A latitudinal sweep in coverage for each event (sunrise or sunset) from about 80°S to 80°N takes about 3 weeks. The sampling frequency varies with latitude, with most sampling occurring at 80°N or 80°S, and less in between. With such a low and irregular sampling rate, SAGE data cannot easily be used for trend estimation, but can be used to assess the drift in other instruments, primarily the SBUV. Once a statistically meaningful sample is obtained, the SAGE–II data can be used for investigating trends.

The altitude range over which SAGE–II ozone data are relatively insensitive to other perturbations (i.e., aerosol correction at low altitude and photochemical correction at high altitude) is between 25 km and 50 km. Typical altitude resolution is about 1 km. The precision for each ozone profile in this altitude range is about 10 percent, while the systematic error (primarily the absorption cross-section uncertainty plus knowledge of the SAGE–II spectral filter response) could be up to 8 percent.

Other trends that can alias into the ozone include aerosol and temperature trends. Aerosol has been seen by the SAGE–II data processing team to alias into ozone in preliminary retrievals, when the aerosol correction for the ozone channel was not done correctly. This aliasing was evident in altitudes up to about 25 km at the low-latitude region from 1984 to 1985 because of remnant from El Chichón. The effect of a temperature trend is probably not significant when the SAGE–II ozone profile is restricted to altitudes below 50 km.

It is possible to estimate a trend from the difference between the SAGE–I and SAGE–II climatologies (for example, see Chapter 5). The accuracy of this trend will depend on the difference in systematic errors between the two instruments, the most important one probably being the treatment of the altitude reference. A preliminary analysis shows that SAGE–I heights may be around 90 m greater than those of SAGE–II, leading to a 2.5 percent error in the SAGE–I/SAGE–II ozone difference at 50 km.

3.3.6 Solar Mesosphere Explorer UV Spectrometer

A data set from the SME UV Spectrometer (SME–UVS) for 1982 to 1985 has been archived with NSSDC; however, it suffers from a drift in the sensitivity of the UVS, which leads to a drift in altitude registration, and hence a false trend in ozone. This section refers to a reprocessing, the results of which have been made available to the Ozone Trends Panel and will be placed in the archive in the near future.

3.3.6.1 Forward Model

As described in Rusch et al. (1984), hereinafter referred to as the Basic Reference (BR), and in Chapter 2 of this report, this experiment involved the measurement of the radiance of solar ultraviolet radiation scattered by Earth's limb in two channels (265 and 296.4 nm) with a half-width of approximately 1.5 nm. As the satellite spins, the radiances are measured for a series of lines of sight that have tangent heights, at the limb, ranging from 0 to 100 km. The response function for the measurement has a full width at half maximum of 3.5 km in the vertical. The radiance measurements are sensitive to ozone density changes within the altitude range from about 48 to 68 km, varying somewhat with solar zenith angle.

The limb-viewing geometry is illustrated in Figure 2.33 in Chapter 2. The forward model (see Equations (1), (2a), (2b), (2c) in BR) involves a numerical quadrature calculation of primary Rayleigh scattering in a thin-shell, horizontally homogeneous, spherical atmosphere containing absorbing ozone and scattering air molecules, but no aerosols. This is similar to SBUV and Umkehr, but with a different geometry.

The ozone absorption cross-sections of Bass and Paur (1985) are convolved with the instrument slit functions to obtain effective absorption cross-sections for each channel. The temperature effect is very small at 265 nm (.03%/°C) and small at 296.4 nm (0.1%/°C). The molecular-scattering cross-sections of Penndorf (1957) and Bates (1984) were convolved with the instrument slit functions to obtain effective cross-sections for each channel. The effects of aerosol scattering and absorption by molecules other than ozone, resonance fluorescence, and scattering by other atmospheric gases are omitted (see Section 3.3.3 on SBUV for a discussion of this effect).

The solar flux values measured in a separate experiment on SME (Rottman et al., 1982) were used in the calculation of radiances. Absolute error of these fluxes is estimated to be ± 10 percent, with relative error of ± 1 percent.

The MAP model atmosphere (Barnett and Corney, 1985) was used for the air density profile. This model specifies monthly averages of temperature, pressure, and density as a function of altitude; the algorithm uses a cubic spline fit to obtain data for any specific day, assuming the monthly averages apply to the middle of the month.

As with any limb experiment, a critical phase of the data evaluation is the assignment of an altitude or pressure to each measurement point in a scan. The following (updated) quotation from BR (p. 11684) describes the procedure used in the UVS experiment.

The absolute direction of the line of sight of the scientific instruments is determined from an analysis of averaged pitch angles derived from the four horizon sensor crossings each spin. This analysis leads to limb altitude determinations with residuals of the order of 1 km at a slant distance of 2,550 km (Cowley and

Lawrence, 1983). The limb altitudes are further refined by comparisons of the Rayleigh-scattered radiance measured by the UVS with that calculated from modeling this signal using the relevant solar fluxes, cross-sections, and the MAP model atmosphere. The normalization in altitude is done at 65 km in the long wavelength channel (296.4 nm), where no ozone absorption is detectable and the Rayleigh-scattering signal is optically thin.

Rusch advises that, in fact, one or two radiances above 65 km may be included in the normalization procedure for improved accuracy. In a sense, this procedure could be considered a direct measurement of the pressure at the tangent point.

The radiance quadrature is carried out over the field of view of the instrument by assuming horizontal homogeneity and integrating in the vertical at 3.5 km intervals, using a four-point Lagrangian interpolation. The variation of the instrument sensitivity over the FOV is included in the quadrature. In addition, the polarization sensitivity of the long-wavelength channel is applied in the radiance calculation for that channel. The short wavelength channel has no measured polarization sensitivity (Figure 6 of BR). With the tilting of the FOV, the quadrature becomes slightly more complex because the sum for each 3.5 km interval has a different weight, depending on the amount of the tilt.

In preparing observed data for inversion, a minimum of five and a maximum of six radiance profiles are averaged to ensure "adequate counting statistics." This is consistent with a latitude resolution of about 5°. In addition, there is an inherent "smearing" along the line of sight in the limb technique.

3.3.6.2 The Inverse Method

The equations to be inverted are linearized in terms of a departure from a first-guess ozone profile (Krueger and Minzner, 1976), computing radiances, and first-order partial derivatives of radiance with respect to layer ozone density. Since the radiative transfer equation is nonlinear, the problem is solved iteratively. The solution involves Twomey's (1963) minimum departure from the first-guess profile.

We define the matrix of first order partial derivatives, $\mathbf{K}$, by

$$K_{ij}^{n} = \frac{\partial y_i^n}{\partial x_j^n} \tag{33}$$

where n refers to the iteration number, y_i^n is the calculated radiance at a wavelength and tangent height indexed by i, and x_j^n is the ozone density at layer number j.

The solution is given by

$$\mathbf{x}^n = \mathbf{x}^{n-1} + (\mathbf{K}^T\mathbf{K} + \Gamma)^{-1}\mathbf{K}^T(\mathbf{y}_{obs} - \mathbf{y}_{cal}^{n-1}) + \Gamma(\mathbf{x}^0 - \mathbf{x}^{n-1}) \tag{34}$$

where $\mathbf{K}$ is calculated at $\mathbf{x}^{n-1}$, $\mathbf{y}_{obs}$ is the measured radiance vector, $\mathbf{y}_{cal}^{n-1}$ is the radiance calculated using $\mathbf{x}^{n-1}$, and Γ is a diagonal matrix with Twomey's smoothing vector on the diagonal. The iterative procedure is terminated when the elements of the residual vector $(\mathbf{y}_{obs} - \mathbf{y}_{cal}^{n-1})$ are reduced below the measurement noise level. This convergence criterion is not strictly correct, but it will lead only to random errors and occasional failures to converge, and does not matter for trends studies.

The SME–UVS radiance measurements are sensitive to ozone density changes within the approximate altitude range of 46 to 68 km. For tangent heights above about 68 km, there is insufficient ozone to affect the measurement at 265 nm. For tangent heights below about 46 km, 296.4 nm photons received at the satellite have been scattered mostly from altitudes above the tangent height; the radiances, therefore, contain no information about ozone at the tangent height. The elements of the smoothing vector are set to zero in the central part of the good information region and are increased sufficiently beyond the boundaries to ensure that the first-guess profile is returned outside the good information range and to avoid instabilities in the solution.

The algorithm solves for the mean ozone densities in 2 km layers centered at heights of 48, 50, . . . 68 km. The lower altitude information limit for the 265 nm channel and the upper altitude information limit for the 296.4 nm channel roughly coincide at about 58 km.

A second algorithm was developed to reduce the data taken after the beginning of 1987 because fewer independent pieces of information were available in the measurements, as a result of the poorer resolution with the spin axis tilting (we note that a similar end result could have been achieved by an increase in the elements of the smoothing vector). In the new algorithm, both the first-guess $x^0(z)$ and the iterated solution $x^n(z)$ are specified as the exponential of a polynomial

$$x^n(z) = \exp[a_1^n + a_2^n(z - z_0) + a_3^n(z - z_0)^2 + a_4^n(z - z_0)^3] \tag{35}$$

where z is altitude, $z_0 = 48$ km is a reference altitude, and a_i^n $(n>0)$ are the unknown polynomial coefficients to be determined at iteration n. As a first guess, a_3^0 and a_4^0 are taken to be zero. For calculating the radiances and the partial derivatives, the profile is taken to be a linear combination of the first guess and the solution profile on the last iteration.

$$x^{*n}(z) = B(z)x^n(z) + [1 - B(z)]x^0(z) \tag{36}$$

where $B(z)=1$ for $48<z<69$ and tends to zero smoothly outside this range. The procedure is exactly as before but with all elements of the smoothing vector set to zero

$$K_{ij}^n = \frac{\partial y_i^n}{\partial a_j^n} \sum_k \frac{\partial y_i^n}{\partial x_k^n} \frac{\partial x_k^n}{\partial a_j^n} \tag{37}$$

$$\mathbf{a}^n = \mathbf{a}^{n-1} + [\mathbf{K}^T\mathbf{K}]^{-1}\mathbf{K}^T(\mathbf{y}_{obs} + \mathbf{y}_{cal}^{n-1}) \tag{38}$$

and the iteration procedure is stopped using the same criterion as before. This is an ordinary least-squares solution.

3.3.6.3 Forward Model Assessment

Single Scattering Approximation

The worst case error in calculated radiances is probably less than 1 percent due to neglect of multiple scattering. The quadrature error in this calculation does not appear to have been directly assessed in the BR.

Neglect of Refraction

This is negligible at these altitudes.

Ozone Cross-Sections

Experimenters estimate the uncertainty at 5 percent, although, at these wavelengths, the error is likely to be less than 3 percent. Bass and Paur (1985) estimate their measurement error to be less than 1 percent. However, their measurements are relative to that of Hearn (1961) at 253.7 nm, which is believed to be within 2–3 percent (Hudson, private communication).

Rayleigh Scattering Cross-Sections

Bates (1984) estimates that his values are within 1 percent.

Omission of Aerosols

Polar mesospheric clouds produce obvious anomalous effects; these cases are discarded in the data evaluation. The possible effects of background mesospheric aerosols at heights at and above 48 km are difficult to assess. There are no measurements of particle size distribution at these levels, and the presence of aerosols is very difficult to detect. If such background aerosols do exist, they are likely to be variable; derived ozone densities may be too low and exhibit spurious variability. Aerosols have been detected at altitudes below 48 km (Clancy, 1986). Such aerosols could affect results by increasing the small multiple-scattering error.

Other Scattering Mechanisms

Resonant and Raman scattering and scattering by other atmospheric gases have not been included in the forward model; see Section 3.3.3.3 for a discussion of this effect.

3.3.6.4 Inverse Method Assessment

This assessment refers primarily to the original algorithm.

The first-guess profile is the Krueger–Minzner (1976) midlatitude Northern Hemisphere profile. The choice of first guess should not affect the retrieved profile within the validity range of altitude of the experiment. However, this is not specifically stated by the experimenters.

The customary $\mathbf{S}_x$ and $\mathbf{S}_\epsilon$ covariance matrices are not used explicitly in the inversion procedure, although their implied general characteristics may be inferred from the smoothing vector elements. The smoothing vector is designed empirically to retrieve the first-guess profile outside the information range and the true profile (within error bounds) within the information range, and to have a smooth transition in between.

3.3.6.5 Error Analysis

The SME–UVS team has not been able to provide the standard diagnostics at the time of writing this chapter; therefore, we summarise here the analysis of random and systematic errors in the retrieved profiles from the BR. We have not confirmed this analysis.

Random errors include photon counting errors (noise), data compression before transmission to ground, real atmosphere differences from the model atmosphere, and errors arising from altitude–radiance normalization. In the analysis, the first two and last two of these are considered together. The first two combined produce errors in the retrieved profiles ranging from about 3 percent at 48 km to about 10 percent at 68 km, while the second two combined produce 4 and 10 percent at the lower and upper levels, respectively. When all four are combined, the total random error ranges from about 6 percent at 48 km to about 14 percent at 68 km (See BR Table 2 and Figure 10a).

The systematic errors include absolute instrument calibration (but solar flux error has not been included here), measurement of instrument polarization, measurement of PMT dead time, and ozone cross-section. The first of these, assumed to be 10 percent for instrument calibration, produces the dominating systematic error component of about 17 percent from 50 to 62 km, decreasing somewhat above and below this range. Since solar flux instrument calibration error was not included, this result really applies to the (radiance–irradiance) ratio. This error results from the dependence of the reference density level, nominally at 65 km, on the instrument gain. If the true gain is larger than that given by the calibration (positive error), the scattered UV radiance calculated for the reference level in the model atmosphere will be sensed from a lower density level (higher altitude). Because ozone density decreases more rapidly with height than atmospheric density, the ozone error is larger than the calibration error, as well as being of opposite sign. When the remaining error components are included, assuming no correlation between the different error types, the total systematic error is just over 18 percent from 50 to 62 km (see BR, Table 3, Figure 10b, and Chapter 2).

3.3.6.6 Implications for Trend Estimation

Trend estimation will be compromised by the total relative in-flight drift of UVS and Solar Flux instrument calibrations (PMT sensitivity and dead-time constant). In each case, this includes any relative drift of calibration between the two wavelength channels. A +1 percent per year drift in the (radiance–irradiance) ratio will produce a fictitious ozone trend of −1.7 percent per year.

Real trends in atmospheric temperature within the 48–68 km altitude range will produce only small effects in this range through the absorption cross-section temperature dependence in the 296.4 nm channel (+1°C per year produces +0.1 percent per year fictitious ozone trend). A more important contribution may arise through temperature changes at any altitude below 68 km, as this affects the pressure–height relationship through the hydrostatic equation. It would then be possible for derived ozone densities to be assigned to the wrong altitude. A symptom of this effect could be a drift in the radiance–height matchup at 65 km. This symptom, however, would apply also to a net relative calibration drift as described above. Monitoring this matchup could be a good first-order diagnostic of possible problems.

A change in background mesospheric aerosol may introduce a fictitious ozone trend of a sign that depends on optical properties. We assume that obvious cases of polar mesospheric clouds are correctly detected, then rejected from processing.

3.3.7 Solar Mesospheric Explorer Near Infrared Spectrometer

The Solar Mesospheric Explorer Near Infrared Spectrometer (SME–NIRS) measures infrared limb emission by excited oxygen ($O_2(^1\Delta_g)$) at 1.27 μm—the result of photodissociation of ozone

by ultraviolet radiation and subsequent photochemical reactions. The analysis of the data is complicated by the fact that some of the $O_2(^1\Delta_g)$ molecules are quenched by collisions with the major atmospheric molecules, and that the other product of the photodissociation of ozone, $O(^1D)$, can produce $O_2(^1\Delta_g)$ indirectly by collision with molecular oxygen.

The SME–NIRS data set for 1982–1985 has been archived with the NSSDC. However, this data set suffers from a drift in the sensitivity of the SME–UV spectrometer, which leads to a drift in altitude registration, and hence a false trend in ozone. The data are being reprocessed with better values for the altitude registration and will be placed in the archive in the near future. The description below applies to both data sets.

3.3.7.1 Forward Model

The complete forward model has been described by Thomas et al. (1984) and will not be reproduced here in detail. It is assumed that the only reactions that occur are

$$\begin{aligned}
O_3 + h\nu(210<\lambda<310\text{nm}) &\rightarrow O_2(^1\Delta_g) + O(^1D) && \epsilon J_3 \\
O_2(^1\Delta_g) + O_2 &\rightarrow 2O_2 && k_D \\
O(^1D) + O_2 &\rightarrow O(^3P) + O_2(^1\Sigma) && k_O \\
O(^1D) + N_2 &\rightarrow O(^3P) + N_2 && k_N \\
O_2 + h\nu(\lambda = 762\text{nm}) &\rightarrow O_2(^1\Sigma) && J_s \\
O_2(^1\Sigma) + M &\rightarrow O_2(^1\Delta_g) + M && k_s
\end{aligned} \tag{39}$$

It should be noted that the J's are altitude dependent due to absorption of incoming solar radiation, and that the k's may be temperature and, therefore, altitude dependent. By solving the kinetic equations associated with these reactions, it can be shown that the volume emission rate V at an altitude h is given by

$$V(h) = \left\{ \frac{P_s k_s[M]}{A_s + k_s[M]} + \epsilon J_3[O_3] \right\} \frac{A_D}{A_D + k_D[O_2]} \tag{40}$$

where A_s and A_D are the spontaneous emission coefficients for the $O_2(^1\Sigma)$ and $O_2(^1\Delta_g)$ levels, respectively, and the $O_2(^1\Sigma)$ production rate P_s is given by

$$P_s = J_s[O_2] + \epsilon J_3[O_3] \frac{k_O[O_2]}{k_O[O_2] + k_N[N_2]} \tag{41}$$

Thus, the volume emission rate is a linear function of $J_3[O_3]$. The observed slant intensity for tangent height h_0 is related to the volume emission rate by an integral along the line of sight

$$S(h_0) = \int_{FOV} W(\theta - \theta_0) \int_0^\infty V(l,\theta) T(l,\theta) dl d\theta \tag{42}$$

where θ is scan angle, $W(\theta)$ is the FOV profile, and $T(l)$ is the transmittance along the line of sight from the emission at position l to the instrument, accounting for absorption by the O_2 ground-state molecules.

3.3.7.2 The Inverse Method

In preparing observed data for inversion, the good profiles are averaged together in sets of six. This merging reduces the latitude resolution to about 5°.

The instrument's line of sight is determined by relating the Rayleigh-scattered radiance near 70 km, measured by the SME–UV spectrometer, to that calculated from a model atmosphere, thus relating the altitude scale to a pressure reference. In the long term, the ultraviolet spectrometer sensitivity is tied to that of the visible spectrometer (see Chapter 2). Any degradation of the visible spectrometer will therefore be manifested as an altitude error. The inverse method is carried out in two parts. First, the observed line-of-sight radiances are inverted to yield volume emission rates as a function of altitude. Second, the volume emission rates are reduced to ozone profiles using the MAP model atmospheric temperature and pressure distribution (Barnett and Corney, 1985) and the assumed photochemistry.

The present inversion scheme uses a constrained linear matrix equation to solve for the volume emission rates. The constraint weighting for each layer is obtained from an empirical relation chosen to give a stable solution with the least possible constraint. It should be noted that the present scheme differs from the onion-peel approach described by Thomas et al. (1984).

The volume emission rate $V(h)$ is represented by a four-point Lagrangian interpolation between values at a set of levels spaced at 3.5 km intervals, expressed as a vector $\mathbf{v}$. The integral in Equation 42 for the line of sight radiance becomes a matrix product of the form $\mathbf{I} = \mathbf{F}\mathbf{v}$, where $\mathbf{F}$ depends on W and T. This equation is solved for $\mathbf{v}$ by least squares with the smoothing constraint that the vertical derivative of $V(h)$ is close to an average volume emission rate vertical derivative, $\overline{\Delta \mathbf{v}}$, by minimising

$$|\mathbf{I} - \mathbf{F}\mathbf{v}|^2 + w^2 |\overline{\Delta \mathbf{v}} - \mathbf{D}\mathbf{v}|^2 \tag{43}$$

where $\mathbf{D}$ is a matrix operator expressing vertical differentiation. The empirically determined weight w determines the relative importance of the smoothness constraint, increasing with α, the absolute value of the slit tilt angle

$$w(\alpha) = \frac{c|\mathbf{I}|}{2\overline{\Delta \mathbf{v}}\sqrt{n}} (1 + \tanh(b(\alpha/a - a/\alpha))) \tag{44}$$

The constants a, b, and c were chosen to give a stable solution with minimum constraint. Note that no constraint is placed on the value of the volume emission rate itself, only on its derivative.

The ozone profile is then derived from the volume emission rate according to Equations 40 and 41, using the assumed photochemistry and the climatological atmospheric temperature profile. This is not linear in O_3, as J_3 depends on the ozone above h, but it is straightforward.

3.3.7.3 Forward Model Assessment

The relationship between the measured quantity and the ozone profile is complicated; it depends on a complete understanding of the photochemistry involved. It is always possible that some significant constituent or reaction has not been considered, although we are not aware of any. The rate constants used in the SME analysis appear sound, but there are some concerns that can be raised.

$O_2(^1\Delta_g)$ Formation in the O_3 Photolysis

Not all of the photodissociation of O_3 leads to the production of $O_2(^1\Delta_g)$. The ratio used by SME is 0.9, based on the work of Fairchild et al. (1978). This ratio was not measured by observing

the $O_2(^1\Delta_g)$ emission, but by measuring the production of the $O(^1D)$ atom. There is some evidence that this may not give the same answer (Valentini et al., 1987). However, no explanation of the discrepancy has yet been given.

O_3 Photolysis Rate

The rate of 8×10^{-3} mols/sec given in Thomas et al. (1984) is a misprint. It should read 9×10^{-3} mols/sec, in agreement with other derivations.

Quenching of $O(^1D)$

The rates given in Thomas et al. (1984) for the quenching of $O(^1D)$ by N_2 and O_2 have the wrong temperature dependence, according to the original reference (Streit et al., 1976). The forward model also does not include the fact that not all quenching of $O(^1D)$ by O_2 leads to the production of $O_2(^1\Sigma)$; some of the reactions lead to a ground-state molecule. Harris and Adams (1983) give a branching ratio for the production of $O_2(^1\Sigma)$ of 0.77 ± 0.2. This branching ratio was obtained at room temperature, but it could be temperature dependent, and therefore different at mesospheric temperatures.

To test the sensitivity to temperature dependence, the correct temperature dependence has been put in the inversion; a 6 percent decrease in ozone resulted in most of the region. Adjusting the rates and adding the branching ratio was not done but would cause a small ($\sim$ 3 percent) increase in ozone.

Quenching of $O_2(^1\Delta_g)$ by O_2

The value chosen for the forward model for the quenching rate of $O_2(^1\Delta_g)$ by O_2 is that of Findlay and Snelling (1971). Wayne (1985) recently reviewed the measurements for this reaction. His preferred room temperature value for the rate is 1.56×10^{-18} compared with 2.22×10^{-18} used by SME. The temperature dependence of the reaction has been measured by Findlay and Snelling over a limited temperature range (285–322K), all above mesospheric temperatures. Thus, the values used by SME are from an extrapolation outside the measurement range. A decrease in quenching results in a corresponding decrease in the ozone by the same amount; this change would give a significant decrease (30 percent) in ozone.

Quenching of $O_2(^1\Sigma)$

The error bars assigned by SME to the quenching rate of the $O_2(^1\Sigma)$ by N_2 seem too large. Wayne (1985) recommends a value of 2.2×10^{-15}, which is close to the value of 2.0×10^{-15} used by SME.

3.3.7.4 Inverse Method Assessment

We have found no significant problems with the inverse method that might lead to errors in trend analyses based on SME–NIRS data. The only minor point is the use of a rather ad hoc constraint, which might be too loose or too tight. The averaging kernels in Figure 3.22a indicate that the constraint is probably too loose for single-profile retrievals at $\theta = 0$.

3.3.7.5 Error Analysis

The averaging kernels for the ozone mixing ratio on a pressure scale are shown in Figure 3.22a–c for three values of the slit tilt, θ, and for a set of levels spaced at intervals of 0.5 in $\log_{10} p$. The resolution is comparable with the FOV width (3.5 km) for $\theta = 0$, about 5 km at $\theta = 10°$, and about 10 km at $\theta = 25°$. We note that the resolution varies only slightly with altitude. There are significant negative excursions in all cases, although for $\theta = 0°$ they lie close to the main peak and may not be significant for trend estimation. For higher altitudes at $\theta = 25°$ (above about 0.005 mb), the negative excursions are serious; these data should not be used for trend studies.

Sensitivities to the forward model parameters are shown in Figures 3.23 and 3.24. The primary sources of random error are detector noise, digitization errors, and variations of the atmospheric temperature. Systematic errors include errors in the rates, cross-sections, the chemical reaction scheme, errors in the temperature climatology, and instrument calibration errors. Of these, the quantities that may be subject to trend errors are atmospheric temperature, altitude reference, and calibration (gain). The solar input $\epsilon J_{3\infty}$ will vary slightly with solar cycle, but with insignificant effect.

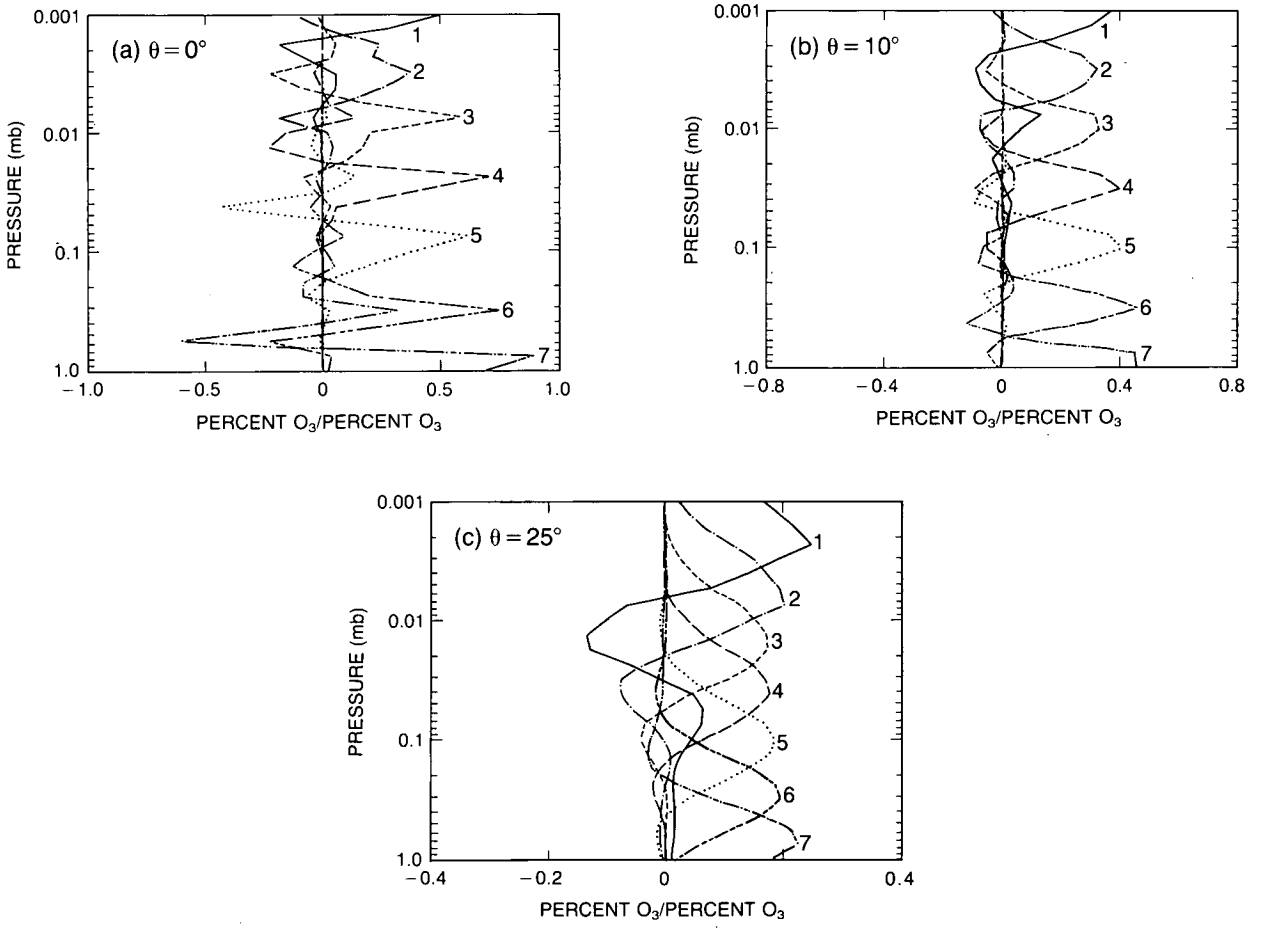

Figure 3.22. Averaging kernels for SME–NIRS at selected altitudes. (a) Slit tilt = 0°. (b) Slit tilt = 10°. (c) Slit tilt = 25°. The curves are labeled (1) 0.001 mb, (2) 0.0032 mb, (3) 0.01 mb, (4) 0.032 mb, (5) 0.1 mb, (6) 0.316 mb, and (7) 1 mb.

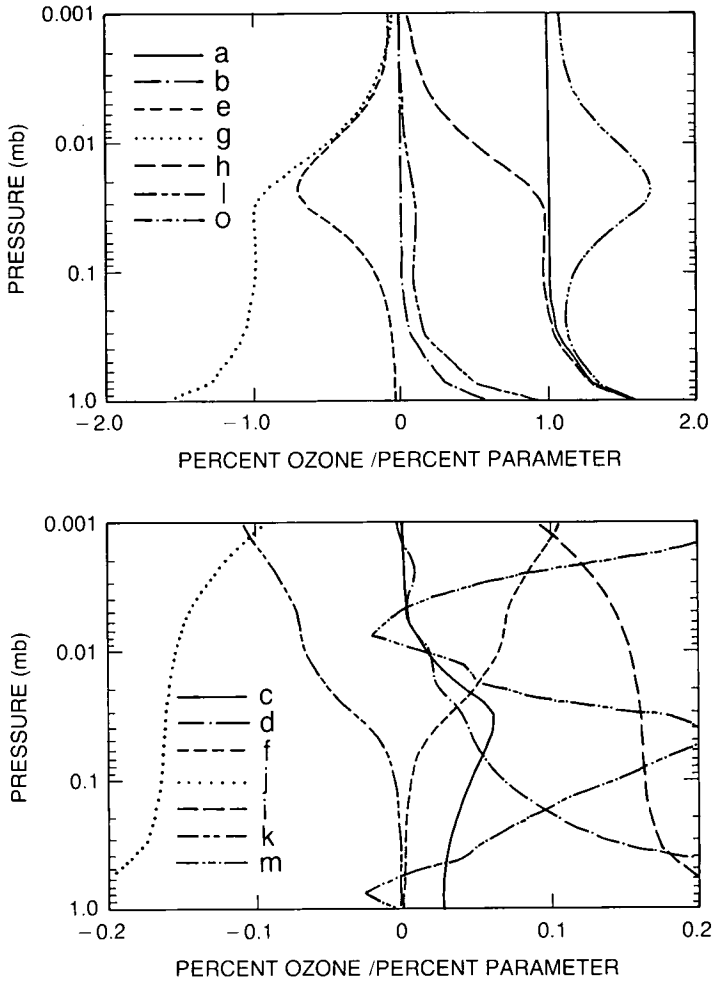

Figure 3.23. SME–NIRS sensitivities to model parameters at slit tilt = 0°. Units are percent ozone per percent parameter, except where stated. (a) $J_{3,\infty}$ (b) τ_{UV} (c) τ_{762} (d) $\tau_{1.27}$ (e) $J_{S,\infty}$ (f) A_S (g) A_D (h) k_D (i) k_N (j) k_O (k) k_S (l) Cal (m) Altitude reference (percent ozone per 0.01 km) (o) Solar zenith angle (percent ozone per 0.01 radian).

3.3.7.6 Trend Estimation Assessment

The SME–NIRS method is somewhat indirect, relying on a complete understanding of the relevant ozone photochemistry, including its temperature dependence. We have found no significant errors in the photochemistry, but it is always possible that some reactions have been omitted or misunderstood.

The SME–NIRS should be capable of measuring trends from around 50 km to around 90 km with a vertical resolution of about 4 km at the start of the mission, and then 10 km at the end, as a result of slit tilt. The averaging kernels at zero slit tilt are rather oscillatory and could be improved.

Drift in the retrieval caused by drift (around ± 0.18 km/year) in the reference altitude will be small at 1 mb, rising to about 4 percent per year at 0.05 mb. This is the largest source of uncertainty.

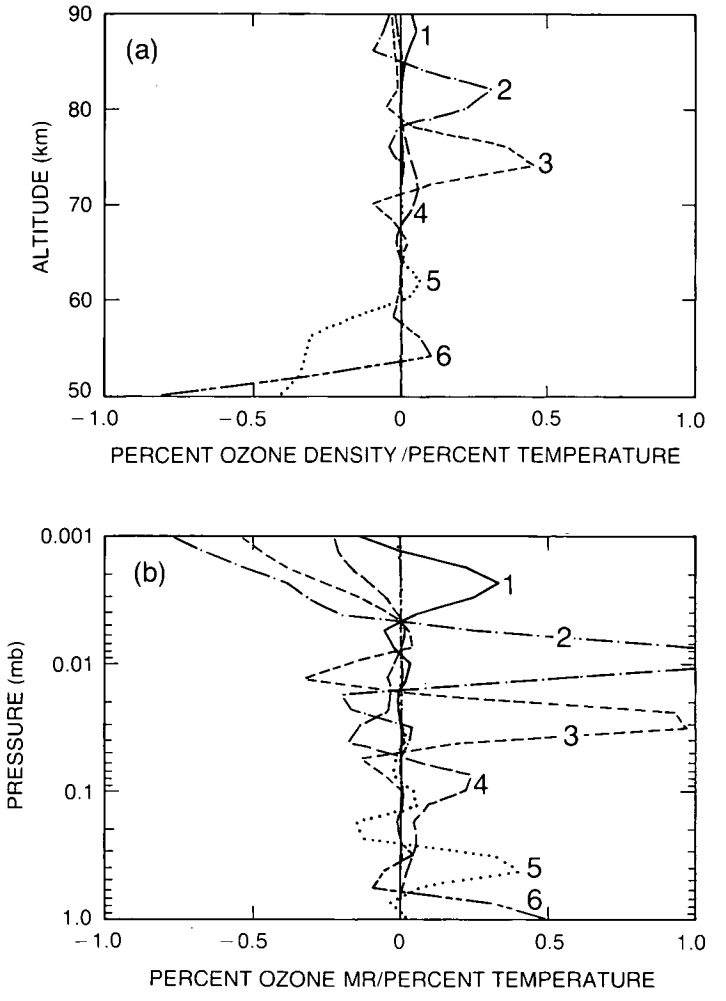

Figure 3.24. Sensitivity of SME–NIRS retrievals to temperature errors. (a) Density on a height scale (b) Mixing ratio on a log pressure scale. Plotted are the perturbations in the profile due to a 1K temperature change at (1) 90 km, (2) 82 km, (3) 74 km, (4) 66 km, (5) 58 km, and (6) 50 km.

Changing instrument calibration (<1%/yr) may lead to drifts of a similar magnitude in ozone.

Drift caused by real temperature changes, relative to the climatology used, would have to be 3–5K/yr to explain the +1.6%/yr change seen by the SME–NIRS measurements. Real temperature changes are likely to be rather less than this.

3.3.8 The Limb Infrared Monitor of the Stratosphere

The Limb Infrared Monitor of the Stratosphere (LIMS) experiment was launched on the Nimbus–7 spacecraft in October 1978, and produced data until May 1979. It measured concentrations of ozone and other gases in the stratosphere by measuring the limb-emitted radiation in selected spectral regions in the infrared (Gille and Russell, 1984). The spectral region covered by the LIMS radiometer ranged from 6 to 16 μm wavelength. Ozone measurements were obtained from the spectral channel centered at 9.6 μm. Two CO_2 channels, one wideband and one narrowband, centered at the 15 μm, were used to generate stratospheric temperature

profiles. The temperature profiles were then used in the reduction of data from all the other channels for the calculation of the Planck function term.

The LIMS radiometer scanned vertically at a rate of 0.25° per second. The data were sampled at a rate of one per 24 msec and digitized with a 12-bit A-to-D converter. The vertical instrument FOV for the ozone channel was 1.8 km when projected to the atmosphere at the tangent point location.

This discussion applies to the LIMS Version 5 algorithm, the results of which have been archived with NSSDC.

3.3.8.1 Forward Model

The limb radiance $I(h)$ measured by the LIMS instrument at a fixed tangent height h is given by (Gille and Russell, 1984)

$$I(h) = \int_{h-\Delta z}^{h+\Delta z} dz \int_{\upsilon_1}^{\upsilon_2} d\upsilon \int_{-\infty}^{\infty} dl B(\upsilon,\Theta(l))\phi(\upsilon)W(h-z)\frac{dT(\upsilon,l,h)}{dl} \qquad (45)$$

where $B(\upsilon,\Theta)$ is the Planck function at wavenumber υ and temperature Θ, l is distance along the line of sight, T is the infrared transmittance between l and the spacecraft, $\phi(\upsilon)$ is the instrument spectral response function, and $W(h-z)$ is the instrument field of view (IFOV) function.

The forward model for LIMS data retrieval is a numerical integration of Equation 45. Radiances are computed appropriate to the LIMS measurement geometry, at 1.5 km intervals (the same altitude interval as the homogeneous shell thickness used in the inversion). The Planck function is calculated from the temperature profile retrieved from the LIMS's two CO_2 channels (Gille et al., 1984a). The atmosphere is assumed to be in local thermodynamic equilibrium.

Limb path transmittance values are calculated with the emissivity growth approximation (EGA) scheme (Gordley and Russell, 1981). The most up-to-date line parameters for the ozone 9.6 μm band were used in the calculation of transmittance tabulation. The isotope line parameters of Drayson et al. (1984) were also included. No interfering species were included. The calculated $I(h)$ was smoothed with a Gaussian filter of width 1.1 km, to match the preconditioning applied to the measured radiances.

3.3.8.2 The Inverse Method

Preconditioning of the Radiances

The radiances subject to inversion were obtained from the radiometer measurements through a series of steps, the most important of which are discussed below.

The radiometer measurements were calibrated using the preflight data on the linearity of the radiometer and the black body source as described in Chapter 2. A correction for spacecraft rotation during the scan is inferred from a pair of up and down scans. The correction results in an effective change of the scan rate. Data are discarded if the required correction is larger than 4 percent of the nominal scan rate.

The radiance scan, with samples nominally every 0.375 km, were Fourier transformed and multiplied by the inverse transform of the IFOV and electronic filter. Thus, a correction for the effect of the IFOV sidelobes and the amplitude and phase rates of the electronic filter was applied in the frequency domain. In addition, the measurements in the different channels were co-aligned by this process; high frequencies were removed with a Gaussian apodization filter. These steps are described in Gille and Russell (1984) and Bailey and Gille (1986), although the details of the apodization in this paper differ slightly from that applied to the archived data.

The final filtered radiances were sampled at 1.5 km intervals for input into the inversion procedure.

The Inversion Procedure

The inversion procedure is basically an onion-peeling approach in which the solution profile is sought from the top to lower layers. In each layer, the solution is updated in an iterative manner, as described by Russell and Drayson (1972) and Bailey and Gille (1986). The radiances are compared to the calculated forward radiances at each layer. The first-guess solution for the top level is from the solution obtained from the previous scan, while for the lower levels, the first-guess solution is always from the previous higher level. During the iteration cycle, the solution at a particular level is updated with a partial derivative computed from the previous iteration. The convergence criterion for each level is that the relative difference between the filtered and the synthetic radiances is less than 0.1 percent.

The inversion procedure does not explicitly use a priori information, except for the smoothing implied by the preconditioning described above and a zero vertical derivative in ozone above the topmost level.

3.3.8.3 Forward Model Assessment

Ozone Line Parameters

The ozone 9.6 μm band strength is known to better than 8 percent. However, there are a large number of weak lines within the band with less accurate line parameters. Because of the limb geometry, the uncertainty of the calculated transmittance values due to line parameter errors is about 8 to 10 percent for altitudes above the ozone peak, increasing to 15 to 20 percent for altitudes below the ozone peak, due to the significant contributions from the less well-known weak lines (Drayson et al. 1984). However, emission errors can be larger when this effect is coupled with a steep positive lapse rate and optically thick paths, as in the equatorial lower stratosphere.

Transmittance

The accuracy of the emissivity growth approximation for calculating the limb transmittance is generally within a few percent, and the errors are smaller for weak and strong absorption.

Temperature

The error in the temperature values used is less than 2K, based on the retrieval of the two 15 μm CO_2 channels (Gille et al. 1984a). The inclusion of horizontal temperature gradient correction in calculating the limb transmittance is important.

Horizontal Gradients

Roewe et al. (1982) showed that horizontal gradients along the line of sight could have a large effect on the outgoing radiance at altitudes for which the optical depth from space to the tangent point along the limb viewing path is of order 1 or more. This paper further showed that gradients in trace constituents concentrations had a considerably smaller effect than temperature gradients. The LIMS forward radiance model allowed a first approximation to the horizontal temperature gradient to be used to lead to improved temperature and constituent retrievals.

Local Thermodynamic Equilibrium (LTE)

The model assumes that CO_2 and O_3 are in LTE; that is, their energy levels are populated according to a Boltzmann distribution, so that the source function is given by the Planck function. On theoretical grounds (Houghton, 1969), and from ATMOS observations (Muggeridge, private communication), there appears to be no reason to question this for the 15 μm bands of CO_2 at altitudes below 80 km that materially affect LIMS radiances. However, O_3 may be photochemically formed in a vibrationally excited state, with several excess 9.6 μm quanta. This energy can be removed through quenching or radiation. Solomon et al. (1986b) have suggested that quenching is sufficiently slow that the source function is significantly greater than the LTE value above 0.5 mb. The various rates for these processes are uncertain, so the quantitative size of this effect is not precisely known. However, the calculations of Solomon et al. indicate that LIMS ozone is around 30 percent too large at 0.1 mb.

3.3.8.4 Inverse Method Assessment

The inversion procedure does not require a first-guessed profile; thus, the solutions are not biased to some a priori profile.

No noise covariance matrices are used in the inversion procedure. The solutions are derived exactly from the measured radiances, thus propagating any measurement error directly into the retrieved solution.

Retrieval Errors

A detailed error analysis on the LIMS ozone retrieval was performed through model simulations and retrievals (Remsberg et al., 1984). Table 2 in the referenced paper summarized the various error components and their magnitudes. The two dominating factors in the LIMS ozone retrieval uncertainty are the temperature uncertainty and the ozone line parameters uncertainty, which can (conservatively) produce retrieved ozone mixing ratio errors as high as 10–30 percent and 8–15 percent, respectively. The total retrieved ozone upper limit uncertainties were estimated to be 15 percent between 5 and 1 mb, and to increase to 40 percent at 100 mb and 0.1 mb.

Aerosols, PSC's, and high-altitude cloud interference should, in principle, affect LIMS data only at the height of the atmospheric perturbation. Most of these occurrences are removed by identifying their signatures in the moderately transparent ozone channel. The corrections in the frequency domain for sidelobe effects should remove the effects of high, cold, tropospheric clouds, but a small residual effect may be present. Volcanic aerosols were particularly low during the LIMS observing period.

3.3.8.5 Error Analysis

For LIMS, the state vector **x** is the ozone mixing ratio at levels spaced every 1.5 km on a grid for which the temperatures and pressures are known from the temperature–pressure retrieval. Correspondingly, the measurement vector **y** has as elements the emitted radiances on the same grid, smoothed and filtered as described above.

Averaging kernels for several altitudes are shown in Figure 3.25. The full width at half maximum is about 2.5 km.

Sensitivity to temperature errors at individual levels is shown in Figure 3.26. Figure 3.27 illustrates the total effect of a 1K temperature error at all levels, where the signs are opposite; i.e., a temperature that is low will result in a high ozone concentration. The temperature channels are used to derive a registration pressure; the effect of a 1 percent error in this quantity is also shown. Finally, the effect of a 1 percent calibration error is given. It should be emphasised that the error cases are somewhat simplified in that a calibration error probably would affect the temperature (and pressure) channels as well, and some cancellation of errors would result. The temperature and pressure errors here should be thought of as those that are not due to calibration errors and, because this relationship is not included, are illustrative rather than exact.

3.3.8.6 Trend Estimation Assessment

Trend estimation from the LIMS measurements will not be discussed here because of the short lifetime of LIMS operation (operated from October 1978 to May 1979), and because the retrieval algorithm is tailored to handle the particular engineering problems of LIMS, such as the

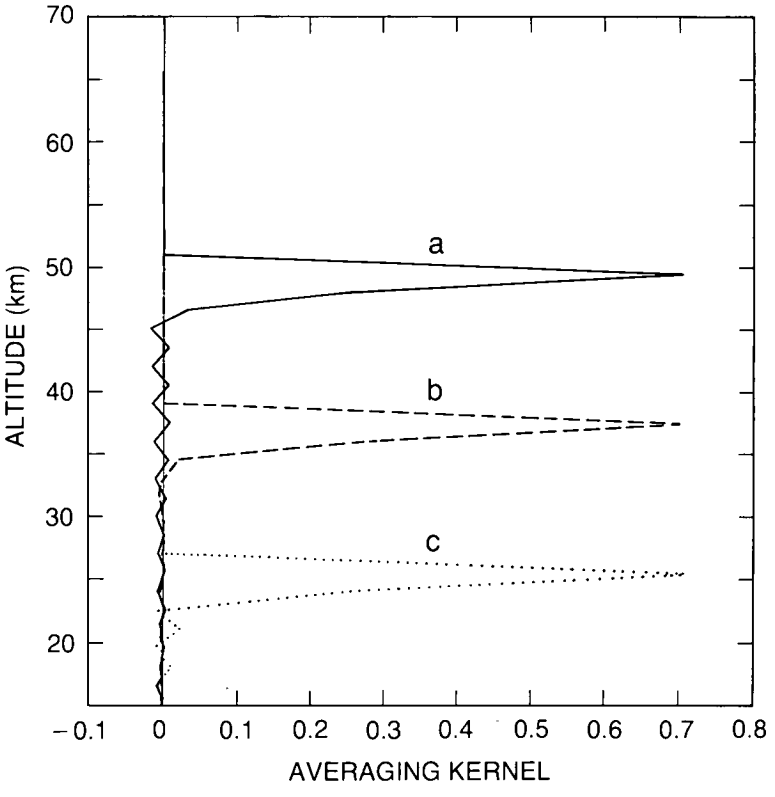

Figure 3.25. LIMS ozone averaging kernels at three selected altitudes.

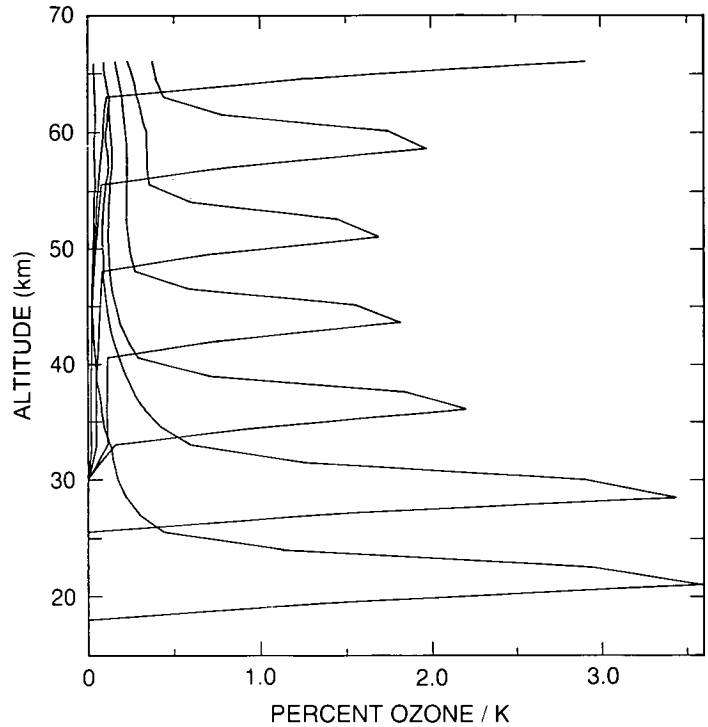

Figure 3.26. Sensitivity of LIMS-retrieved ozone to temperature errors at selected altitudes.

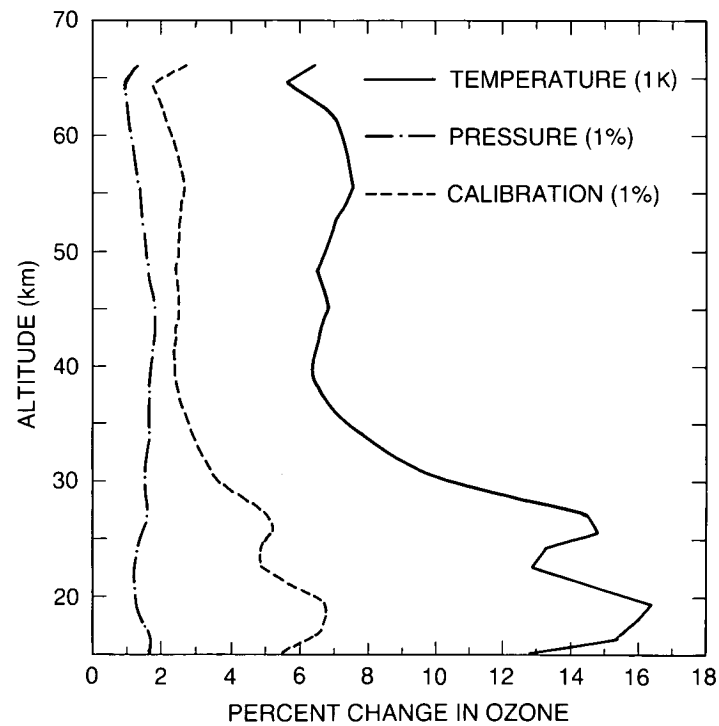

Figure 3.27. Sensitivity of LIMS-retrieved ozone to a 1K temperature change at all levels, a 1 percent radiance calibration error, and a 1 percent registration pressure error.

IFOV sidelobe problem, compounded with the spacecraft attitude uncertainty. As with most other measurement schemes, ozone trends sensed with a LIMS-type instrument would be susceptible to problems of instrument degradation; these can, in principle, be corrected for by in-flight calibration. However, for the LIMS type of measurement, temperature sensitivity is its biggest drawback since the source function and the species line parameters are dependent on the exact value of the atmospheric temperature. Thus, an undetected or wrongly retrieved temperature drift would lead to an erroneous ozone trend.

3.4 ALTERNATIVE STRATEGIES FOR OZONE PROFILE TREND DETECTION

The traditional method for looking for trends in remotely sensed ozone profiles has been the direct statistical analysis of the retrieved profiles on a layer-by-layer basis (e.g., see Reinsel et al., 1984). The retrieval methods generally have been designed to give the best results for individual profiles and may not produce optimal results for trend studies as a result of the relative weight given to a priori and measurement, for example.

In this section, we discuss possible alternative approaches for the detection of trends in ozone profiles. These include methods that involve the statistical analysis of the actual physical measurements, without direct recourse to a retrieval algorithm, and methods involving retrieval, but designed to retrieve trend profiles.

3.4.1 Analysis of Directly Measured Quantities

3.4.1.1 SBUV and Umkehr Measurements

We have examined the signature, in measurement space, of the postulated CFM ozone depletion centered near 40 km. Figure 3.28 shows the SBUV spectral signature, in terms of

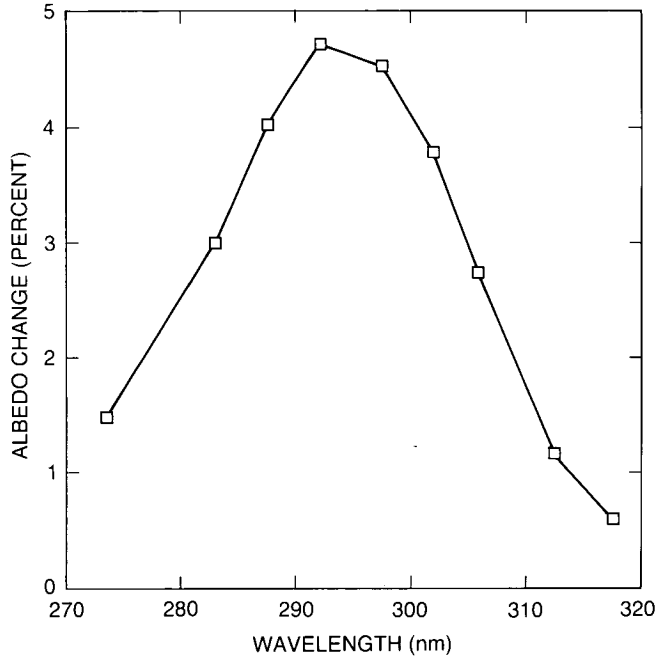

Figure 3.28. SBUV spectral signature for a Gaussian ozone depletion of 10 percent centered at 3 mb, with a width of 10 km at half maximum.

percentage albedo change, for a Gaussian shape percentage depletion centered at 3 mb, with a peak depletion of 10 percent and a width of 10 km at half maximum. This is a distinctive signature that is unlikely to be produced by either a wavelength-dependent drift in the reflectivity of the SBUV diffuser plate or by a small drift in the wavelength calibration (see Chapter 2). Since the overall shape of the SBUV spectral albedo curve depends on such factors as total ozone, season, latitude, solar zenith angle, and the multiple scattering and reflectivity "correction" to the observations, the analysis is not trivial. Moreover, the spectral signature of the profile depletion will also be somewhat dependent on these same factors. Finally, it would be necessary to distinguish between the spectral signature of this depletion and the stratospheric aerosols (Figure 3.2). Fortunately, this particular aerosol signature has a much narrower peak than the depletion signature. It is beyond the scope of this section to explore this potential method in full detail. However, it is evident that a good place to start would be with the initial preinversion, forcing residuals of the present SBUV algorithm, since the factors listed above are already largely removed from these residuals.

The curves joining the small squares in Figure 3.29 illustrate the Umkehr measurement-space signature of a similar Gaussian shape percentage depletion with, however, a maximum depletion of 25 percent and a half-width of about 14 km. Unfortunately, this signature is very similar to the stratospheric aerosol signature given by the curves joining the small triangles. Figure 3.29a is for a stratospheric aerosol optical depth of 0.0348, and for midlatitude ozone profiles with 200 matm-cm total ozone. The aerosol curve is taken from the data of Dave et al., 1979. Figures 3.29b and c show similar curves for midlatitude ozone profiles with total ozone of 300 and 400 matm-cm, respectively. For both the depletion and haze signature curves, the width of the signature increases and the amplitude decreases (only very slightly in the case of the depletion signatures) as the total ozone increases. It follows that any attempt to use this signature technique for the trend analysis of the Umkehr observations must deal appropriately with the problem of stratospheric aerosol contamination of the measurements, when such contamination exists.

With respect to calibration problems with the Dobson instrument, this alternative method appears to offer no particular advantage over the traditional method, because a wedge calibration error might very well have a signature similar to those in Figure 3.29.

In summary, this trend approach may offer some advantage when applied to SBUV data, but appears to offer little if any advantage with the Umkehr data. Only the broad, 40 km depletion has been examined here because other features of model-predicted ozone changes will be more difficult to find with either SBUV or Umkehr data.

3.4.1.2 SME–NIRS

An alternate method of obtaining ozone trends from the NIRS experiment on SME is to examine the airglow layer itself. This layer, which has a peak near 1 mb, is approximately a Chapman layer following the absorption of ultraviolet solar radiation. The radiance at the peak is primarily a function of the ozone density profile. With all other conditions being constant, long-term trends in its intensity would indicate ozone trends. The other parameters that influence the airglow peak intensity, and hence the peak radiance observed from the spacecraft, are solar zenith angle, tilt angle, and the ozone distribution. With a simple model, effects of solar zenith angle and tilt angle can be accounted for. Although a long-term change in the ozone distribution would be seen as a trend, it is, of course, an ozone trend—that is, there may be some ambiguity about the exact nature of the observed ozone trend. A remaining uncertainty is any

change in the sensitivity that has been measured by the inflight calibration. This method removes the largest source of uncertainty in SME–NIRS ozone, the altitude determination.

3.4.2 Trend Retrieval

Some of the observing systems use "optimal" retrieval methods. These are methods that attempt to minimise the error terms in the error analysis described in Section 3.2 on the basis of assumptions about the statistical behaviour of the instrument noise and the atmospheric profile.

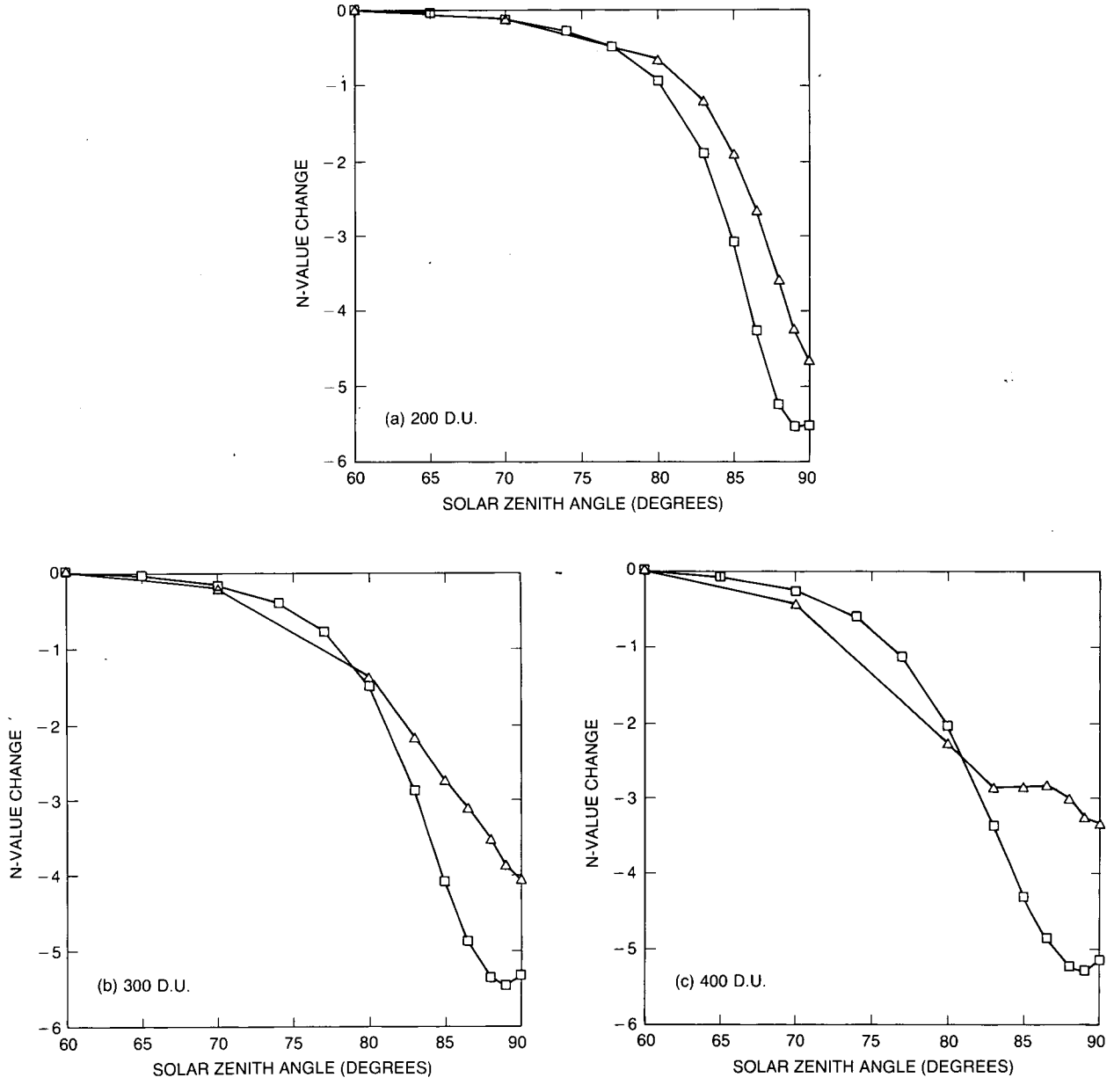

Figure 3.29. Umkehr measurement signature for a Gaussian-shaped depletion with a maximum of 25 percent and a half width of about 14 km centered at 3 mb (squares). Stratospheric aerosol signature (triangles). (a) Total ozone 200 DU. (b) Total ozone 300 DU. (c) Total ozone 400 DU.

These methods are usually designed to give optimal results for single profiles; consequently, they do not necessarily give optimal estimates when the retrieved profiles are used for long-term means or trend analysis. The user must be aware of the nature of optimal retrievals when carrying out statistical analyses.

Qualitatively, the optimal retrieval is a weighted mean of the true profile and an a priori profile, with the weighting depending on the measurement error

$$\hat{\mathbf{x}} = \mathbf{A}\mathbf{x} + (\mathbf{I} - \mathbf{A})\mathbf{x}^a \tag{46}$$

If the measurement error can be reduced, for example, by averaging, then the weighting should lean more toward the true profile and less toward the a priori.

The quoted error on a profile may include components from the error in $\mathbf{x}^a$ as well as those due to experimental error. Only the latter varies from one profile to the next.

It should be possible, in principle, to retrieve trends over a greater height range and with better resolution than that obtainable from individual retrievals because random errors in the data are reduced by averaging. This is straightforward in the case of linear forward models because the measurements can be averaged directly to remove noise. In the nonlinear case, it is more difficult; further research is needed to set up a sound basis for trend retrieval.

We note that, as random errors are reduced, systematic errors with trends become more important and need more careful treatment.

3.5 SUMMARY AND CONCLUSIONS

We have found no serious deficiencies in the algorithms used in generating the major available ozone data sets. As the measurements are all indirect in some way, and the retrieved profiles have different characteristics, data from different instruments are not directly comparable. Thus, the primary aim of this chapter has been to characterise the algorithms to show quantitatively:

- How the retrieved vertical profile is related to the actual profile. This characterises the vertical resolution and altitude range of the data.
- How trends in the real ozone are reflected in trends in the retrieved-ozone profile.
- How trends in other quantities, both instrumental and atmospheric, might appear as trends in the ozone profile.

3.5.1. Error Analysis Concepts

Error analyses for the ozone data sets that we have considered have, in general, been published in the open literature, but not in a uniform and comparable way. We have, therefore, defined a uniform error analysis approach and applied it to all of the data sources. The formal error analysis shows that the retrieved vertical profile $\hat{x}(z)$ can be expressed as an explicit function of the true profile $x(z)$, plus error terms due to instrument noise and systematic errors. This

function can be thought of as a smoothing of the true profile with a smoothing function we call the *averaging kernel* $A(z, z')$:

$$\hat{x}(z) = \bar{x}(z) + \int A(z, z')(x(z') - \bar{x}(z'))dz' + \text{error terms} \quad (47)$$

The range of height z over which the averaging kernel has a well-defined peak determines the height range of validity of the retrieved profile, while the width of the peak defines the vertical resolution of the profile. The error terms due to various sources can be examined independently. Those leading to constant offsets, or purely random errors, are of minor importance when studying trends, as random errors will average out in the long run and constant offsets make no difference to trend estimates. The most important sources of error are those that have trends themselves, which might appear as false trends in ozone.

The range of validity and vertical resolution of the ozone data sets that have been available to the Ozone Trends Panel are given in Table 3.6. Also listed are the primary sources of systematic error that may introduce incorrect trends into the retrieved data.

Table 3.6 Summary of Retrieval Characteristics

Instrument	Altitude Range*		Resolution	Sources of Trend Error
	mb	km	km	
SBUV	16-1	(28-50)	8-10	Diffuser plate reflectivity, aerosol.
Umkehr	64-2	(19-43)	11-14	Aerosol, sampling.
SAGE–I	(250-1)	10-50	1	Aerosol below 25 km, sampling.
SAGE–II	(250-1)	10-50	1	Aerosol below 25 km, sampling.
	(1-0.1)	50-65	5	
SAGE–II/–I	(250-1)	10-50	1	Altitude reference, filter placement.
SME–UVS†	(1-0.05)	48-68	4	UVS and Solar Flux instrument calibration, pressure at 68 km, mesospheric aerosol?
SME–NIRS	0.3-0.003	(55-85)	4-10‡	Altitude reference, calibration, atmospheric temperature.
LIMS	100-0.1	(15-64)	2.5	(short record)

*Brackets indicate approximate equivalent
†Experimenters assessment.
‡Varying with time

3.5.2 Individual Data Sources

3.5.2.1 Dobson Total Ozone

The only algorithmic source of trend error is the omission of the effects of SO_2, which itself has a trend. Stratospheric aerosol, which has variability on a long time scale, is also omitted.

3.5.2.2 TOMS and SBUV Total Ozone

The primary source of error here is the spectral variation of the drift in diffuser plate reflectivity. The range of reasonable models of this drift presented in the calibration chapter leads to a possible overestimate of around 3–4 percent in the ozone depletion over the 8-year data period. A minor source of trend error is an underassessment of tropospheric ozone by a factor of about two.

3.5.2.3 SBUV

Although the archival data cover Umkehr layers 1 to 12 (altitude range approximately 0–64 km), we find that only layers 6 to 9 or 10 (28–50 km) are suitable for trend analysis. The sensitivity of the retrieval to diffuser plate reflectivity errors has a similar vertical profile to the global trend seen in SBUV Version 5 data. Uncertainty in this trend due to errors in the diffuser plate reflectivity within experimental error is comparable with the trend itself.

3.5.2.4 Umkehr

The archival data cover an altitude range of layers 1 to 9 (0–48 km). We find that only layers 4 to 8 (19–43 km) are suitable for trend analysis. There are many sources of systematic error that affect an individual instrument in a way that varies with time, such as recalibration and operator competence. The network is not large enough to rely on these effects averaging out in the long run. We note also that aerosol effects and temperature dependence are not allowed for in the retrieval.

3.5.2.5 SAGE

SAGE has an excellent vertical resolution, but a poor sampling frequency. This means that care must be taken in deriving statistically valid trends. We have found no problems that might lead to trend errors when using data from one instrument, other than its sensitivity to aerosols below about 25 km. When comparing SAGE–I with SAGE–II, it must be remembered that the systematic errors in the two data sets are likely to be different. Specifically, the different treatment of the reference altitude can lead to a systematic difference increasing with height; errors in filter placement can lead to scale errors, differing between the two instruments. It should also be noted that, as SAGE measures on a height scale, while SBUV measures on a pressure scale, temperature trends must be correctly modeled when comparing trends from these two instruments.

3.5.2.6 SME

The vertical resolution of the retrieval from both the UVS and the NIRS degraded with time as the attitude of the spacecraft changed. The primary source of trend errors for both instruments is the altitude reference. The NIRS retrieval relies on a complete understanding of the relevant photochemistry, including its temperature dependence. We have found no errors, but it is quite possible that some chemistry has been omitted or misunderstood.

3.5.2.7 LIMS

We have found no significant sensitivities that might influence trend assessment. However, the measurement period is rather short, so that LIMS has little to say about trends. Its main value here is to validate other data sources.

3.5.3 Discussion

In view of the above characterisation of the various sources of data, it is clear that comparisons should be made only over the range of validity of the individual data sets, at comparable vertical resolutions, degrading the higher resolution data as necessary. It would be helpful for

future exercises of this kind if data suppliers could present a standard set of observing system characteristics, perhaps based on those developed for this report.

Retrieval methods appropriate to trend estimation are not necessarily the same as methods appropriate to estimation of single profiles because it may be possible to largely eliminate random error in the long-term averages required for trends. However, the retrieval methods used for the data now available are designed for single profiles. Further research is needed to design trend profile retrieval methods.

An alternative approach to trend detection is to look for changes in the quantity actually measured, without retrieving a profile. Modeled changes in the ozone distribution can be used with the forward model for a particular instrument to determine whether the resulting perturbation in the quantity measured is detectable.

CHAPTER 4

Trends in Total Column Ozone Measurements

Panel Members

F. S. Rowland, Chair

J. Angell
W. Attmannspacher
P. Bloomfield
R. Bojkov
N. Harris
W. Komhyr
M. McFarland
R. McPeters
R. Stolarski

Chapter 4

Trends in Total Column Ozone Measurements

Contents

4.0 INTRODUCTION

A century ago, Hartley (1881a) explained the observed sharp 293-nm cutoff in ultraviolet (UV) radiation at Earth's surface as caused by ozone whose UV spectrum he had measured in the laboratory. By finding the same cutoff in mountaintop measurements, Hartley later showed that most of the ozone existed in the atmosphere at still higher altitudes (1881b). The initial quantitative measurements of the total ozone content in the vertical column were made with optical instruments at ground level about 75 years ago by Fabry and Buisson (1913, 1921). The subsequent discovery that concentrations of ozone in the vertical column varied with local weather conditions inspired several scientists, including G.M.B. Dobson, to begin systematic ozone measurements in the 1920's, largely with the hope of improving the capabilities of weather forecasting (Dobson and Harrison, 1926; Dobson et al., 1927, 1929; Dobson, 1930; Cabannes and Dufay, 1927; Fowle, 1929). The basic ultraviolet double monochromator spectrophotometer system developed then by Dobson is still the instrument used in the ground-based observational network for the determination of the total ozone content of the atmosphere, and the standard instrument is now known as a Dobson spectrophotometer (Dobson, 1931, 1957a,b, 1973).

Total ozone is defined as being equal to the amount of ozone contained in a vertical column with a base of 1 cm^2 at standard pressure and temperature, and can be expressed in units of pressure with a typical value of about 0.3 atmosphere cm. The more frequently used unit is milliatmosphere centimeters, commonly known as the Dobson Unit (DU). One DU represents an average atmospheric concentration of approximately one part per billion (ppb) by volume of O3, but the ozone is not distributed uniformly through the vertical column. Typical amounts of ozone vary from 230 to 500 DU's, with a world average of about 300 DU. About 90 percent of atmospheric ozone lies in the stratosphere, a fact already well known during the 1930's.

Several other instruments used to measure ozone are based on principles similar to those of the spectrophotometer designed by Dobson. These instruments include the M–83 filter ozonometers in use for the last 30 years at as many as 45 stations in the U.S.S.R., the Brewer spectrophotometers recently introduced chiefly in Canada, and the new M–124 filter ozonometers in the U.S.S.R. (Gustin, 1963, 1978; Brewer, 1973; Gustin et al., 1985). The principles of operation of these ground-based instruments, the length of their record, and their locations are described in Section 4.1 of this chapter. Several satellite-based instruments measure ozone; for the purposes of this chapter only the results from the Total Ozone Mapping Spectrometer (TOMS) are extensively discussed. Section 4.2 contains a description of this instrument as well as brief descriptions of the other satelliteborne instruments; Chapter 2 contains a fuller discussion of the satellite instruments.

If one is to have faith in the trends versus time calculated from a long time series of measurements, it is extremely important that the quality of the data is high. Critical examination of the data from the individual Dobson stations and from the TOMS satellite instrument has been carried out, and the diagnostic tools used are described in Sections 4.3 and 4.4, respectively. In both cases, the data needed some revision; the Dobson data have been corrected using information available in the records of the individual stations. Because of time and labor constraints, the process of revision treated only the monthly average ozone values from the Dobson stations, and the improved and recommended data set is, therefore, referred to as "Provisionally Revised." A full review of the Dobson data requires that each reading be examined and that the review is carried out on a station-by-station basis, with full access to all of the daily log books and records. It is hoped that individual stations will do this and that their fully revised data sets can, in time, take the place of the provisionally revised data sets presented in Appendix A to this chapter.

Sections 4.5 and 4.6 describe the statistical analysis of this provisionally revised data set; the results are presented in Appendix B to this chapter.

A drift in the calibration of the TOMS instrument was found relative to both the network of Dobson instruments and to the Dobson Primary Standard instrument. The likely cause of this drift is an imperfect correction for the known slow degradation of the TOMS diffuser plate from cumulative direct Sun exposure, as discussed in detail in Chapter 2. The TOMS data set has, therefore, been normalized to the results of the network of Dobson instruments. This continuing normalization over the whole time period provides a time-dependent correction for the diffuser plate. Because TOMS has global coverage, this procedure allows an analysis of the changes in total ozone that occurred anywhere in the world between 1979 and 1987, as described in Section 4.7.

In summary, the basic intent and philosophy of this chapter has been a very careful examination of all of the available total ozone data. Preliminary data analyses have been carried out on data sets as recorded in the archives for both the ground-based Dobson and TOMS satellite instruments. More sophisticated statistical calculations were carried out on data sets corrected by the procedures described in this chapter. The scope of these statistical analyses has also been widened in a search for any seasonal and latitudinal effects in the trends in total ozone.

4.1 GROUND-BASED MEASUREMENTS OF OZONE

Three instruments are routinely used to measure total ozone from Earth's surface: the Dobson spectrophotometer, the M–83 filter ozonometer, and the Brewer grating spectrophotometer. The Dobson and M–83 stations have data sets that are long enough for meaningful trend analysis. However, the Dobson instruments constitute the backbone of the ground-based network, as the number of stations is greater and the records are typically longer. The Brewer instrument has been in regular use for a much shorter time and currently has no long-term records suitable for such analysis. Total ozone data are routinely reported to the World Meteorological Organization–World Ozone Data Center (WMO–WODC) in Toronto, Canada, and printed regularly in a series of publications entitled *Ozone Data for the World* (ODW).

4.1.1 Dobson Spectrophotometer

4.1.1.1 Operation

The standard instrument in the Global Ozone Observing System is the Dobson spectrophotometer, containing a double quartz-prism monochromator that permits comparison of the radiances at two different wavelengths in the ultraviolet (UV). The basic design has been described by Dobson (1931) and has undergone many improvements in its optics and in the electronic evaluation of its signals. Detailed descriptions of its operation and physical accuracy have been given by Dobson (1957a,b; Dobson and Normand, 1962) and, more recently, in WMO Ozone Project Report Nos. 6 (Komhyr, 1980) and 13 (Basher, 1982). The operational principle of the Dobson spectrophotometer is based upon the knowledge that the absorption coefficient of ozone for ultraviolet radiation decreases rapidly with increasing wavelength across the Huggins absorption band (300–350 nm), providing a range in Earth's atmosphere from nearly complete to only minor absorption of incoming solar radiation. The technique utilizes the relative absorption of solar radiation from two wavelengths, one absorbed moderately strongly by ozone and one absorbed slightly. The basic measurement of ozone relies on the ratio of the intensities of UV

radiation at two standard wavelengths. Measurements are made looking directly at the Sun near noontime, or symmetrically before and after noon. (At local noon the path length of the solar radiation through the atmosphere is shortest, and the air mass, μ, defined as the actual path length of the solar beam divided by the vertical path through the atmosphere, is also smallest. Measurements are made most accurately when the air mass is low because the intensity of UV light reaching Earth's surface is greatest.) The individual measurements are averaged to form the daily value. Four UV wavelength pairs have been established by the International Ozone Commission (Table 4.1), and recommended for universal use by the WMO.

Table 4.1 Ultraviolet Wavelength Pairs Used for Atmospheric Ozone Measurements With Dobson Spectrophotometers (Wavelengths in Nanometers).

Pair	Wavelength	Wavelength	O_3 Absorption Coefficient (a)
Designation			
A	305.5	325.4	1.748
B	308.8	329.1	1.140
C	311.45	332.4	0.800
D	317.6	339.8	0.360
C′	332.4	453.6	

(a) Difference in ozone absorption coefficients (in units of atm $^{-1}$cm) for the shorter wavelength minus longer wavelength (according to the 1968 recommendations by IOC and WMO based on the Vigroux coefficients (1967).

The most widely used combination, recommended as the international standard, is the pair of wavelength pairs listed as A and D in Table 4.1. The combined absorption for this "AD pair" is $(\alpha_A - \alpha_D) = 1.388$. Measurements of most physical quantities exhibit changes in the "best" or "accepted" values over time as equipment is improved or minor errors are discovered; the values for the absorption coefficients of ozone have changed several times in this manner over the last half century. The value of $(\alpha_A - \alpha_D)$ for the AD pair was defined in July 1957 for the International Geophysical Year to have the value 1.388, based upon the absorption coefficient measurements of Vigroux (1953, 1967), and has not been changed since, even though additional careful evaluations have been carried out. In this arrangement, the amount of atmospheric ozone is calculated from the UV radiation received at the two shorter wavelengths, and separately from the two longer wavelengths from the AD pair. The reported ozone content is obtained from the combined results of the four wavelengths. As the slant path of sunlight becomes longer, as in high-latitude stations in midwinter, so much light is absorbed at 305.5 nm that measurements with the A pair become very difficult and inaccurate, and observations tend to be made with the CD double wavelength pairs for which sufficient UV light is still arriving at 311.45 nm and 317.6 nm. At very low Sun angles and very long slant paths, it can become necessary to use the C′ wavelength pair for higher accuracy.

While the observation of the ratio of received UV light for standard wavelength pairs from direct sunlight is preferred, such observations are not always practicable or even feasible. In the winter months at very high latitude stations, little or no direct sunlight is received. In this situation, observations are possible using direct moonlight—but are clearly much more difficult because of the much lower UV light intensity reflected by the Moon. At other latitudes, measurements are also desirable on days in which direct sunlight is intermittent or absent. These observational data are based upon the measurement (at the same standard wavelengths) of scattered sunlight from either the clear or cloudy zenith sky, converted to the standard

AD–direct-Sun measurement by an empirically established transfer table. The accuracy of this transfer depends upon numerous carefully taken, nearly simultaneous, direct-Sun and zenith-sky observations. These are performed by alternating sequential measurements of the ratios of radiation received from the direct Sun and from either the clear or cloudy zenith sky on days when such experiments are possible. Empirical zenith sky charts must be constructed for each station as functions of the total ozone content; of the air mass (μ), i.e., the slant angle of the Sun; and of the instrument readings themselves. Sky charts are further constructed for the various kinds of cloud layers found over the particular station. Accurate sky charts require a very substantial amount of careful scientific work, and individual stations frequently use charts of less than optimum reliability, as for instance one constructed for another, geographically distant station with different average vertical ozone distributions and with different cloud conditions. The direct-Sun measurements are more straightforward than any of the others and are normally of higher accuracy. For some purposes, calculations can be carried out using only the direct Sun-data, but in most locations this may limit the information to only half or fewer of the days in some months.

No completely satisfactory method is available for estimating the scattering of ultraviolet radiation by aerosol or dust particles. In practice, because most ozone observations are made on the double AD pair of wavelengths and because both A and D pairs are approximately equally affected by aerosol scattering, any aerosol effect on UV penetration is assumed to cancel. The absorption by ozone then remains the overwhelmingly major factor causing differential removal of the different UV wavelengths from the direct path of sunlight. The effects of aerosol scattering in the presence of very large quantities of such particles, as in the aftermath of large volcanic explosions, requires careful separate consideration, but the effects of even large amounts of volcanic dust on measurements of total column ozone are very small. Such scattering from volcanic aerosol is of primary importance for attempts to determine the vertical distribution of ozone from Umkehr measurements made as the Sun approaches the horizon (see Section 4.1.4).

For the purposes of the standard observation of absorption of radiation by ozone, the altitude at which this absorption occurs is of relatively minor importance. An ozone molecule is capable of absorbing ultraviolet radiation at about 300 nm with approximately equal efficiency at all altitudes, and the net effect is the same at the arrival slit of the ground-based instrument. However, the ability of ozone to absorb ultraviolet radiation does exhibit a small temperature dependence (varying by about 0.13 percent per °C at the average temperature of the ozone layer) so that the conversion of a measured fractional UV absorption into number of molecules of ozone has a slight temperature dependence. No corrections are made in the standard Dobson measurements for these temperature effects, and the amounts of ozone are calculated as though all of the ozone molecules in the atmosphere were present at a temperature of -44°C, chosen as generally appropriate for the lower stratospheric location of most of the ozone molecules. Small errors can thus be introduced into the relative comparison of total ozone columns measured with different average stratospheric temperatures. Comparisons for the same months in different years are affected only if the average temperature of the stratosphere has changed significantly, and then only to a slight extent.

The reported amounts of ozone are also dependent upon the measured absorption cross-sections of ozone at the various wavelengths used with the Dobson instrument. These absorption coefficients have been determined more and more accurately by various research groups over the years, with the most recent being the measurements of Bass and Paur (1985) and the closely concurrent results of Molina and Molina (1986). By international convention, the world-wide Dobson network has reported all data subsequent to July 1, 1957, as calculated with the

ozone absorption coefficients measured by Vigroux, and this procedure, amended in 1968, is still in force. The (α_D - α_D) value for the AD pair is 1.388 with the Vigroux coefficients and 1.428 with the Bass–Paur coefficients. A systematic bias of several percent therefore exists in any evaluation of the absolute amounts of ozone with a Dobson instrument using the Vigroux coefficients relative to the same data interpreted with the newer Bass–Paur absorption coefficients. (The instrument readings from the Nimbus–7 satellite are converted into ozone with the Bass–Paur coefficients.) Although the absolute amounts of ozone as evaluated with the Vigroux coefficients are presumably slightly in error, no bias exists in any trend measurements with the Dobson system for AD data collected from 1957 on and uniformly interpreted with the same (Vigroux) absorption coefficients. Prior to 1957, a different set of absorption coefficients (Ny and Choong, 1932, 1933) was in use as the standard, and comparisons of pre-1957 and post-1957 data with Dobson instruments must be made with correction for this change of absorption cross-sections assumed in the ozone calculations. The AD wavelength pair was adopted as the standard for ozone measurement in 1957, with the agreement that measurements made with other wavelengths should be transferred to the AD standard to eliminate systematic biases related to the absorption coefficients. The number of ozone stations operating before 1957 was relatively small, and no data taken prior to 1957 have been used in the statistical evaluations reported later in this chapter.

4.1.1.2 Sources of Errors and Ozone Data Quality

In order to determine the accuracy of ozone measurements, one needs to consider possible errors related to single-station measurements as well as potential sampling errors in the event that geographical averaging of the data is attempted. There is no simple method for combining the various error estimates into a single "accuracy" value. Most of the individual sources of error and theoretical estimates of their values are considered in detail by Basher (1982) in WMO Ozone Report No. 13. Our brief discussion here attempts incorporation of pertinent information from some other sources (WMO Ozone Report Nos. 9, 11, 12) as well as rough estimation of the accuracy of the data set used in this report.

The precision of long-term total ozone measurement from a Dobson spectrophotometer is estimated for annual means at ± 1 percent (at the 2 δ level), based on the standard deviation (δ) from the mean analysis of individual stations. However, attainment of this precision requires consideration of a number of error sources, described in detail in WMO Ozone Reports 9 and 13. These include absolute instrument calibration at various times during a solar cycle; observational and instrumental errors; aerosol effects; ozone absorption coefficient uncertainties, including temperature dependence; interfering trace gas absorbing species; ozone produced in the troposphere; and uncertainties in the empirically derived relations between direct and clear or cloudy zenith-sky observations.

The accuracy of the Dobson instrument is strongly dependent on the quality of the instrument's calibration and operation. Unfortunately, this quality can vary widely during an instrument's history, and only through the availability of periodic recalibrations can the ozone data be reevaluated.

Until 1973, instrument calibrations at different stations were conducted randomly and independently. In some cases, only the manufacturer's original calibrations were used. Theoretical error studies and field intercomparisons show that such instruments may exhibit systematic errors as large as 10 percent in the direct Sun ozone measurements at the AD wavelengths, with mean biases for the worst cases in the order of 5 percent. From 1974 on, increasing numbers of

instruments have been modernized, refurbished, and calibrated by direct intercomparison with the WMO-designated World Primary Standard (Dobson No. 83) located at the World Dobson Spectrophotometer Central Laboratory at Boulder, Colorado. In subsequent intercomparisons, these instruments show typical calibration changes of 1 percent to 2 percent in AD-wavelength direct-Sun measurement, which is close to the limit of accuracy expected on the basis of theoretical and experimental studies. It should be noted immediately that, following recalibration, a step change in the ozone calculated from the instrument can appear comparable to the percentage change in the recalibration. However, in the present study, the required mean corrections were considered in reevaluation of the station data.

Instrument errors are generally not fixed percentages valid for all conditions throughout the year, but may vary with solar altitude and ozone amount and, therefore, with latitude and season. The AD wavelength ozone absorption coefficient, and therefore the absolute values of AD estimated total ozone, may have bias errors of up to 3 percent and will vary by about ± 2 percent for the maximum seasonal and latitudinal variations of about 15°C, in ozone-layer-weighted mean temperature. Actual stratospheric temperature observations indicate any long-term changes in temperature vertical profiles could contribute less than 0.5 percent per decade to any trends in total ozone data because neither season nor latitude is a variable in data sets used for evaluation of specific trends.

Errors originating from aerosol scattering are usually much less than ± 1 percent, but may rise to ± 3 percent during occasional extremely hazy conditions or nearby volcanic eruptions. Errors from interfering tropospheric absorbers (mainly SO_2, NO_2, and locally produced ozone) are usually negligible, but may raise the background error to about 1 percent. Solar irradiance changes around 300 nm are considered negligible, and therefore have no effect on instrument calibrations.

The international protocol calls, where possible, for a report of the total ozone measured for each day by each Dobson station, together with coded information indicating the wavelengths used and the technique involved—i.e., direct Sun, moonlight, clear zenith sky, etc. The daily Dobson total ozone data stored at the WMO–WODC are usually means of three or more measurements taken within a period of several hours centered on local solar noon. These individual daily ozone values are combined to form a monthly average, also reported to the WMO–WODC, and the monthly averages can, in turn, be combined to provide a yearly average ozone value. Not infrequently, weather conditions or other difficulties may prevent a successful measurement on a given day, or for several days in a row, or the measurement may be successfully made at a time not near solar noon at the station. Monthly averages are then calculated as the average of the daily values for the days with measurements, no attempt being made to interpolate or estimate the ozone values for the days without measurements. This inclusion of some days for which the data are not noontime measurements and the complete omission of other days raises the general problem of sampling errors for individual stations. Mean diurnal variations are thought to be less than 1 percent and contribute negligible sampling error. The size of day-to-day variations increases poleward with latitude, and seasonally from summer/autumn to winter/spring.

These seasonal variations range from a minimum of about 5 percent in the Tropics to about 30 percent in high-latitude winters and springs. Weather conditions and operational factors that cause great losses of data (e.g., fewer than 13 daily readings in a month) may cause biases of perhaps 5 percent in the mean ozone for some months, especially since total ozone amounts are strongly correlated with the synoptic weather conditions. Special care must be taken when

analyzing winter data from high latitude stations for which the limited data may not be representative of the actual average monthly ozone amount. The uneven geographical distribution of the global Dobson spectrophotometer network is a further spatial source of sampling error when attempts are made to determine global ozone content and trends. The limited number of existing Dobson stations, their scarcity south of 30°N latitude, and the low-frequency variations of large-scale planetary waves should be accounted for in attempts for global total ozone analyses.

It is clear that the reliability of ozone measurements depends on random as well as systematic (or bias) errors. The latter are important for determination of ozone trends. If the period of variation of a systematic error is much shorter than the length of ozone record under consideration, it is treated as a random error. Sources that can promote errors with trendlike behavior are listed in Table 4.2, expressed in percent per decade.

Table 4.2 Possible Causes of Error in Ozone Trends From Dobson Stations; Estimates of the Effects on the Determined Trends Due to Instrumental and Other Experimental Causes.

Potential Error	Good case (%)	Bad case (%)	Note
Optical calibrations	0.4	2.0	(a)
Uncorrected instrument drift	<1.0	2.0	(b)
Trend in ozone layer "mean" temperature	0.2	<0.5	(c)
Extraterrestrial constant	0.1	2.0	(d)
Aerosol extinction	0.1	<1.0	(e)
Interfering absorption	0.1	<0.5	(f)
Increasing tropospheric ozone	0.2	1.0	(g)

The first number is an estimate applicable to "good" stations with reevaluated data records, as those used in the present report, while the second number refers to the "worst" conditions, occurring as exceptions.

(a) May create step-changes if the data record prior to calibration is not reevaluated using the calibration. The experience with the published data indicates an error on the order of 1 to 2 percent and, only in a few isolated cases, up to 5 percent.

(b) Can be positive or negative depending on the cause. A number of instruments have been compared with the World Primary Standard on a few occasions during the last 14 years and have shown either no drift or a drift of <1 percent.

(c) A 5°C change per decade is required to introduce a 0.5 percent error. There is no evidence for such stratospheric temperature changes except in the Antarctic in springtime in the past decade. Our statistical procedures have not been applied to these Antarctic data.

(d) The "extraterrestrial constant" is the ratio of solar intensities for each standard wavelength pair, and is, in principle, identical for all locations, being a function only of solar conditions. In practice, however, the instrument accepts a band centered on each standard wavelength, and minor variations can exist in these band passes, requiring calibration for each specific instrumental construction. Transfers from the Primary Standard through direct comparisons have assured <1 percent error, although there are isolated cases with much higher potential error.

(e) May influence the AD measured ozone only in the event of a continuous extreme increase (or decrease) of aerosol pollution.

(f) Gases such as SO_2 and NO_2 can have an effect only if measurements are carried out in the immediate vicinity of the source and if their concentrations are steadily increasing.

(g) An increase in tropospheric ozone is not a potential error in measurement of total column ozone, but a possible contributor to a trend in total ozone. Such tropospheric ozone changes only become a "potential error" when, as is often done, measurements of total ozone are used as direct estimates of possible trends in the stratospheric contribution to total ozone.

(h) The combination of biases due to bandwidth effect, airmass calculation, solar irradiance variability, and sampling practices is likely to be negligible.

C-3

Despite the difficulty in estimation and the need to use individual judgment, one can attempt to determine the potential error, giving an overall indication of the accuracy of the Dobson data used in this report. These systematic errors are believed to be uncorrelated, with some positive and others negative, and the bounds of the accuracy can then be estimated as the square root of the sum of the squares of the individual error terms above, or from about 1.2 percent for stations with reevaluated records to 3.8 percent for the "worst" station case.

An important point is that statistical trend analyses of historical data series, if properly done, can show any substantial step changes in the data record, together with any systematic variations or excesses in the quasi-random components of the record. Clearly, in order to extract the most information from any Dobson ozone data set, it is essential for statisticians and instrument specialists to examine the data set together, preferably on a station-by-station basis. Typical error estimates, such as those given here, may result in large overestimates or underestimates of errors for a particular instrument, as well as a missed opportunity to detect, and hence correct, obvious data errors.

4.1.1.3 Geographical Distribution of Dobson Stations

For historical and geographical reasons, the Dobson stations with the longest records are spread unevenly around the world, with the greatest number located in Europe and North America. Figure 4.1 displays a global map of the location of the ground-based ozone stations

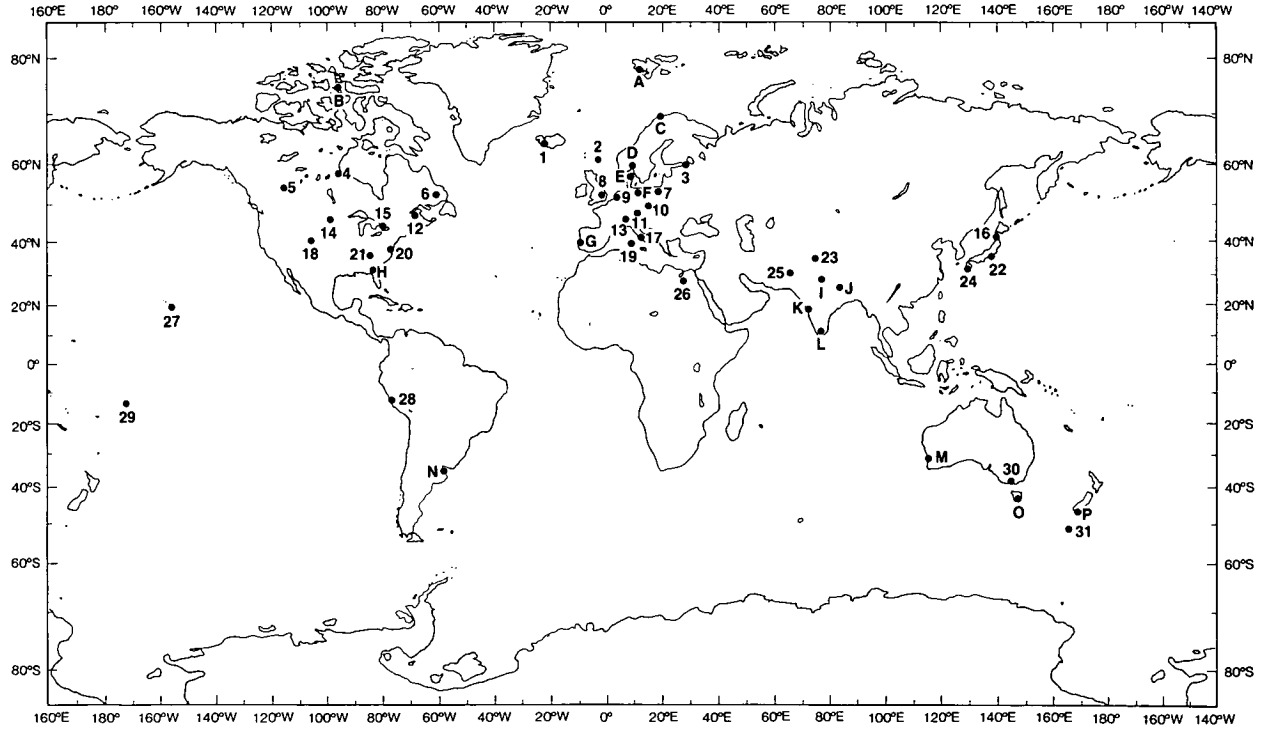

Figure 4.1 Geographical distribution of Dobson stations with long records. Revisions needed in some cases before the data are suitable for trend analysis (the letters shown correspond to those given in Tables 4.3 and 4.4).

with records over a substantial period of time. Table 4.3 provides a list of Dobson stations for which revised ozone data are available; Table 4.4 lists some additional Dobson stations whose data are mentioned in this report. More stations are now in operation, especially in the Tropics, but the coverage of the Southern Hemisphere outside the Antarctic continent is still poor. The most recent index of *Ozone Data for the World* contains a detailed listing of all of the ozone stations that have been in operation at any time during the period from 1957 to 1988.

Table 4.3 Dobson Stations for Which Preliminary Revised Ozone Data Are Available Over Time Periods Long Enough for Trend Analysis.

Station	Country	Latitude	Longitude	Altitude Meters	Dates Measured Start	Through
Northern Hemisphere						
1 Reykjavik	Iceland	64°08′	21°54′W	60	6/57	10/86**
2 Lerwick	U.K.	60°08′	1°11′W	80	1/57	11/86*
3 Leningrad	U.S.S.R.	59°58′	30°18′E	74	8/68	12/86
4 Churchill	Canada	58°45′	94°04′W	35	1/65	12/86
5 Edmonton	Canada	53°34′	113°31′W	668	7/57	11/86
6 Goose	Canada	53°19′	60°23′W	44	1/62	10/86
7 Belsk	Poland	51°50′	20°47′E	180	1/63	12/86
8 Bracknell	U.K.	51°23′	0°47′W	70	5/69	12/86*
9 Uccle	Belgium	50°48′	4°21′E	100	2/71	12/86
10 Hradec Kralove	Czechoslovakia	50°11′	15°50′E	285	1/62	12/86
11 Hohenpeissenberg	F.R.G.	47°48′	11°01′E	975	1/67	12/86
12 Caribou	U.S.A.	46°52′	68°01′W	192	6/62	12/86
13 Arosa	Switzerland	46°46′	9°40′E	1860	1/57	12/86
14 Bismarck	U.S.A.	46°46′	100°45′W	511	1/63	12/86
15 Toronto	Canada	43°47′	79°28′W	198	1/60	12/86
16 Sapporo	Japan	43°03′	141°20′E	19	1/58	12/86
17 Rome	Italy	42°05′	12°13′E	262	4/54	12/86*
18 Boulder	U.S.A.	40°01′	105°15′W	1634	1/64	12/86
19 Cagliari	Italy	39°15′	9°03′E	4	1/56	12/86**
20 Wallops Is.	U.S.A.	37°51′	75°31′W	4	1/70	12/86
21 Nashville	U.S.A.	36°15′	86°34′W	182	1/63	12/86
22 Tateno	Japan	36°03′	140°08′E	31	7/55	12/86
23 Srinagar	India	34°05′	74°50′E	1586	7/57	5/86**
24 Kagoshima	Japan	31°38′	130°36′E	283	4/61	12/86*
25 Quetta	Pakistan	30°11′	66°57′E	1799	7/57	12/86
26 Cairo	Egypt	30°05′	31°17′E	35	11/74	10/86
27 Mauna Loa	U.S.A.	19°32′	155°35′W	3397	1/64	12/86
Southern Hemisphere						
28 Huancayo	Peru	12°03′	75°19′W	3313	2/64	6/86
29 Samoa	U.S.A.	14°15′	170°34′W	82	1/76	12/86
30 Aspendale	Australia	38°02′	145°06′E	0	7/57	12/86
31 MacQuarie Is.	Australia	54°50′	158°57′E	6	8/62	12/86

*Stations for which further reassessment of the ozone data is recommended, with evaluation of the detailed station records.
**Interruptions in the record.

Table 4.4 Other Dobson Stations for Which the Records Are Too Short for Trend Analysis, Have Major Interruptions in Their Records, or Are Otherwise Unsuitable at the Present Time for Analysis on an Individual Basis.

Station	Country	Latitude	Longitude	Altitude Meters	Dates Measured Start	Through
Northern Hemisphere						
A Spitzbergen	Norway	78°56′	11°53′E	0	50	86
B Resolute	Canada	74°43′	94°59′W	64	57	86
Point Barrow	U.S.A.	71°19′	156°36′W	973	82	
C Tromso	Norway	69°39′	18°57′E	100	35	86
D Oslo	Norway	59°54′	10°43′E	50	57	86
Uppsala	Sweden	59°51′	17°37′E	15	57	66
E Aarhus	Denmark	56°10′	10°12′E	53	41	86
Eskdalemuir	U.K.	55°19′	3°12′W	242	57	63
F Potsdam	G.D.R.	52°22′	13°05′E	89	57	86
Oxford	U.K.	51°45′	1°11′W	140	28	67
Moosonee	Canada	51°16′	80°39′W	10	57	61
Camborne	U.K.	50°13′	5°19′W	88	57	67
Mont-Louis	France	42°30′	2°08′E	1650	62	79
Shiangher	China	39°46′	117°00′E	13	79	86
G Lisbon	Portugal	38°46′	9°08′W	105	60	86
Messina	Italy	38°12′	15°33′E	51	57	75
White Sands	U.S.A.	32°23′	106°29′W	1224	72	81
Torishima	Japan	30°29′	140°18′E	83	57	65
H Tallahassee	U.S.A.	30°26′	84°20′W	53	64	86
I New Delhi	India	28°38′	77°13′E	216	57	86
Naha	Japan	26°12′	127°41′E	27	74	86
J Varanasi	India	25°18′	83°01′E	76	63	86
Kunming	China	25°01′	102°41′E	1917	80	86
K Ahmedabad	India	23°01′	72°39′E	55	51	86
with Mt. Abu	India	24°36′	72°43′E	1220	69	84
Mexico City	Mexico	19°20′	99°11′W	2268	74	86
Poona	India	18°32′	73°51′E	559	73	86
Bangkok	Thailand	13°44′	100°34′E	2	78	86
K Kodaikanal	India	10°14′	77°28′E	2343	57	86
Singapore	Singapore	1°20′	103°53′E	14	79	86
Southern Hemisphere						
Cairns	Australia	16°53′	145°45′E	3		
Cachoeira Pau.	Brazil	22°41′	45°00′W	573	74	86
Brisbane	Australia	27°25′	153°05′E	5	57	86
M Perth	Australia	31°55′	115°57′E	2	69	86
N Buenos Aires	Argentina	34°35′	58°29′W	25	65	86
O Hobart	Australia	42°49′	147°30′E	4	67	86
P Invercargill	New Zealand	46°25′	168°19′E	1	71	86
Argentine Is.	U.K.	65°15′	64°16′W	10	57	86
Syowa	Japan	69°00′	39°35′E	21	61	86
Halley Bay	U.K.	75°31′	26°44′W	31	56	86
Amundsen–Scott	U.S.A.	89°59′	24°48′W	2835	61	86

4.1.1.4 Instrument No. 83: The Role of the Dobson Primary Standard in Long-Term Calibration

With the realization in recent years of the potential for partial destruction of the atmospheric ozone layer by manmade trace gas pollutants, the task of accurate, long-term measurement of total ozone has grown in importance. Temporal fluctuations in ozone also occur naturally—as a result of changes in circulation patterns that transport ozone, variations in solar ultraviolet intensity over the 11-year solar sunspot cycle, etc. To separate man-induced from natural changes in ozone, long-term ozone measurement precision of ± 0.5 percent is desirable. Additionally, global coverage for total ozone measurements, as provided by satellite ozone instrumentation, is highly desirable. Among the currently available ground-based instruments for measurement of total ozone, only Dobson spectrophotometers have been used for long-term calibration of satellite ozone instrumentation.

The maintenance of a Dobson spectrophotometer in calibration requires that observations with the instrument are always made on correct wavelengths (to within 0.04 nm); that the instrument's optical wedge (adjusted to provide a null signal between the two wavelengths of the measurement) is calibrated to a high degree of accuracy; that temporal changes in the instrument's spectral response are monitored routinely with standard ultraviolet lamps; and that the extraterrestrial constants (the ratio of the solar intensities of the wavelengths as they reach Earth before any atmospheric attenuation) for the instrument are known with high accuracy at the various pairs of wavelengths. Procedures for establishing correct Dobson spectrometer wavelength settings and for calibrating the optical wedge have been standardized (Dobson, 1957b).

In principle, any spectrophotometer within the global Dobson instrument station network can be maintained in calibration by the established procedures. However, scattered light within an instrument can present a problem. If the light scattering is appreciable for observations on low Sun (μ = 2.5–3.2), then the absolute calibration determined for the instrument can be significantly in error. Furthermore, should the light scattering gradually increase with time, a fictitious trend can be introduced into the measured total ozone amounts. Significant absolute calibration errors can also occur with the Dobson spectrophotometer if the measurements are made at sites where observing conditions for calibration are not ideal—i.e., where atmospheric turbidity is appreciable and large day-to-day changes occur in total ozone. Calibration of the extraterrestrial constants for the various wavelength pairs is most favorable under conditions of directly overhead Sun, clear sky, and negligible variation over the course of a day in the amount of ozone in the atmosphere. The U.S. tropical site at 3,400 meters altitude on Mauna Loa, Hawaii, provides an especially favorable location for such calibrations.

To achieve compatibility in ozone data from the global Dobson spectrophotometer station network, a procedure was established in 1976 by the Atmospheric Ozone Research Project of the WMO whereby a set of regional secondary standard Dobson spectrophotometers are calibrated at periodic intervals relative to a primary standard Dobson instrument. The secondary standard instruments serve to calibrate fieldstation Dobson spectrophotometers within their respective regions. Dobson spectrophotometer No. 83 was established in 1962 as the standard U.S. instrument for measurements of total ozone. In August 1977, Dobson No. 83 served as the reference spectrophotometer during an international intercomparison of regional secondary standard Dobson instruments held in Boulder, Colorado. In 1980, instrument No. 83 was designated by the WMO as the Primary Standard Dobson Ozone Spectrophotometer for the world. Table 4.5 lists the regional secondary standard Dobson instruments, and the dates when they were calibrated relative to instrument No. 83.

Table 4.5 Primary and Secondary Standard Dobson Ozone Spectrophotometers.

Instrument Number	Country	Calibration Dates
83**	U.S.	1962, 1972, 1976, 1978, 1979, 1980, 1981, 1984, 1986, 1987, 1988
41	U.K.	1977, 1981, 1985
64	G.D.R.	1981, 1986
71	G.D.R.	1977, 1986
77	Canada	1977, 1981, 1986*
96	Egypt	1977, 1986
105	Australia	1977, 1984, 1988
108	U.S.S.R.	1977, 1988
112	India	1977, 1984
116	Japan	1977, 1984, 1988

*Indirect calibration in 1986, involving a Brewer ozone spectrophotometer.

**Designated by WMO in 1980 as World Standard Dobson Spectrophotometer; calibrations performed at Mauna Loa Observatory, except at Sterling, Virginia, in 1962.

While calibrations of this kind ideally should occur at 3- to 4-year intervals, national or international funding for such a routine program has not been established. Nevertheless, nearly all Dobson instruments in the global Dobson spectrophotometer station network now have calibrations traceable either directly or indirectly to World Standard Dobson Instrument No. 83 (Komhyr, 1987, 1988). The conclusions drawn in this chapter and in the full report are strongly based on the provisionally revised ground-based data, and these in turn are traceable to the calibration record for instrument No. 83. The TOMS satellite data have been normalized to the Dobson network, and therefore also to the calibration record of instrument No. 83. The integrity of the conclusions concerning any trends in total ozone depend critically, therefore, on the calibration and maintenance record of instrument No. 83, for which a detailed description is now presented.

The normal calibration procedure depends on sequential total ozone observations made on the direct Sun during clear-sky half-days (i.e., A.M. or P.M.) when $1.15 < \mu < 3.2$, and total ozone remains fixed or varies only slowly with time. Graphical analysis of the changing ratios of UV light received versus path length through the atmosphere permits accurate evaluation of the ratios received at the top of the atmosphere—i.e., the extraterrestrial constant. A comprehensive series of such calibration observations was obtained over a period of many days with instrument No. 83 at Mauna Loa Observatory (MLO) in 1976. This series established, on August 26, 1976, a calibration scale according to which all other domestic and foreign spectrophotometers have been calibrated. The N values determined for a series of standard lamps at that time defined an essentially independent 1976 standard lamp calibration scale for Dobson instrument No. 83. Absolute calibrations of instrument No. 83 were also conducted at MLO in 1972, 1978, 1979, 1980, 1981, 1984, 1986, and 1987. A similar calibration was performed on the instrument at Sterling, Virginia, in 1962. Differences among the recorded values for any of these separate absolute calibrations represent a composite estimate of the precision with which such observations can be made and the stability of the instrument itself over a 25-year period.

The results of these absolute calibrations are summarized in Table 4.6. Column 4 of the table lists the mean total ozone amounts measured during each of the calibration time intervals using the August 16, 1976, calibration scale for data processing.

Table 4.6 Summary of Results of Calibrations of World Standard Dobson Spectrophotometer No. 83 With Standard Lamps and by Means of Direct-Sun Observations at Mauna Loa Observatory.

Times of Calibrations	No. Obs. Used/ Made	Wavelengths λλ	Reference: 1976 MLO Calib.† x (1976 MLO calib.)	S	Adj. x (1970 MLO calib.)	Reference: Std. Lamp Calib.†† x (Std. Lamp calib.)	S	S.e. (New MLO calib.)	x	% Error in x (Std. Lamp calib.)	% Error in x (1976 MLO calib.)	Notes
		AD	280	0.001	280	280	−0.002	±0.004	280	+0.2	−0.1	
May 14	9/12	A		−0.001	280		−0.003	±0.005	281			
to		CD	279	−0.001	277	277	−0.002	±0.003	274	+0.9	+1.6	Very clear sky.
June 22		C		−0.001	281		−0.001	±0.002	281			
1972		D		−0.001	283		0.000	±0.004	287			
		AD	274	0.000	274	—	−0.001	±0.001	274	0.0	0.0	Very clear sky
June 16	86/90	A	275	0.000	275	—	−0.001	±0.002	275	0.0	0.0	Sunspot cycle
to		CD	278	0.000	278	—	0.000	±0.001	278	0.0	0.0	minimum.
Aug. 25		C	278	0.000	278	—	0.000	±0.001	278	0.0	0.0	*Aug. 26, 1978
1976		D	278	0.000	278	—	0.000	±0.001	278	0.0	0.0	Calibration Scale
		AD	273	0.000	273	273	0.006	±0.002	275	−0.7	−0.5	
July 13	29/33	A		−0.002	274		0.001	±0.002	274			
to		CD	274	0.002	276	272	0.004	±0.001	276	−1.6	−0.8	Very clear sky.
Aug. 23		C		0.000	276		0.000	±0.001	274			
1978		D		−0.002	276		−0.005	±0.001	271			
		AD	282	0.002	282	282	0.006	±0.002	284	−0.7	−0.7	Very clear sky.
June 8	43/51	A		0.001	284		0.003	±0.002	284			Sunspot cycle
to		CD	282	0.002	284	282	0.003	±0.001	285	−1.0	−0.9	maximum.
Aug. 14		C		0.002	288		0.001	±0.001	284			
1979		D		0.000	289		−0.002	±0.001	283			
		AD	272	−0.002	271	272	0.004	±0.005	273	−0.4	−0.4	Poor-quality
June 20	19/23	A		0.006	277		0.009	±0.009	277			observations.
to		BD	282	−0.008	277	283	−0.007	±0.004	270	+1.4	+1.0	Sky clear,
Aug. 4		B		0.003	283		−0.003	±0.006	283			hazy, and
1980		CD	276	−0.007	266	274	−0.005	±0.002	260	+2.0	+2.5	very hazy.
		C		−0.003	277		−0.004	±0.004	274			Sunspot cycle
		D		0.006	293		0.004	±0.004	288			maximum.
		AD	274	0.002	275	274	0.004	±0.002	276	−0.5	−0.6	Clear sky.
June 8	36/47	A		−0.001	276		0.000	±0.002	276			Near sunspot
to		BD	280	−0.002	279	281	−0.001	±0.002	281	+0.1	−0.4	cycle maximum.
Aug. 7		B		−0.003	281		−0.003	±0.002	281			Discarded obs.
1981		CD	271	0.003	275	271	0.006	±0.002	277	−2.3	−2.1	made during
		C		−0.004	277		−0.002	±0.002	276			increased solar
		D		−0.004	282		−0.005	±0.002	278			activity (see text).
		AD	270	−0.004	269	271	0.001	±0.003	271	−0.2	−0.3	Sky hazy.
July 31	11/13	A		−0.011	268		−0.008	±0.003	288			
to		BD	277	0.000	277	279	0.002	±0.002	280	−0.3	−1.1	Observation
Oct. 23		B		−0.007	274		−0.007	±0.003	273			quality
1984		CD	271	0.005	276	273	0.008	±0.003	281	−2.9	−3.5	good.
		C		−0.002	272		−0.001	±0.002	271			Near sunspot
		D		0.007	266		−0.009	±0.003	259			cycle minimum.
		AD	276	−0.001	276	277	0.000	±0.002	277	0.0	−0.5	Generally clear
June 10	13/14	A		−0.008	276		−0.007	±0.004	276			but some
to		BD	281	0.000	281	284	−0.002	±0.002	283	+0.4	−1.0	haze.
July 11		B		−0.007	279		−0.009	±0.003	280			
1986		CD	276	0.001	277	277	0.002	±0.001	279	−0.9	−1.0	Sunspot cycle
		C		−0.006	277		−0.005	±0.002	277			minimum.
		D		−0.007	276		−0.007	±0.002	273			
		AD	292	−0.001	291	292	0.000	±0.002	292	0.0	0.2	Generally clear
May 20	36/40	A		−0.002	292		−0.002	±0.002	292			sky.
to		BD	297	−0.002	296	300	−0.003	±0.001	299	+0.6	−0.4	Excellent
July 9		B		−0.003	296		−0.004	±0.002	297			quality obs.
1987		CD	292	0.000	292	293	0.000	±0.001	294	−0.2	−0.5	Sunspot cycle
		C		−0.002	293		−0.002	±0.001	293			July 10, 1987
		D		−0.001	296		−0.002	±0.001	293			Calibration scale.

*Percent errors in x are expressed for indicated x and $\mu - 2.2$

†Provisional N-tables used were those of August 26, 1976.

††Provisional N-tables used were derived from instrument 83 standard lamp readings. N values assigned to the lamps August 28, 1976, and current wedge density tables.

Column 6 gives corresponding adjusted mean total ozone amounts, deduced after application of the calibration corrections S of column 5. Note that, for direct Sun observations on AD wavelengths—the standard procedure—the ozone values in columns 4 and 6 do not differ by more than 1 DU. Columns 7 to 10 present ozone data obtained from calibrating by means of standard lamps. In deriving the ozone values in column 7, the provisional N tables used were those established from the optical wedge densities of instrument No. 83 current at the time of calibration, and standard lamp N values assigned to the lamps on August 26, 1976. The ozone amounts in column 10 are the corrected values, determined by application of the corrections S given in column 8. For observations on AD wavelengths, the mean total ozone values in columns 4, 6, 7, and 10 of Table 4.6 do not differ by more than 2 DU.

The percentage errors in total ozone relative to the 1976 standard lamp calibration scale and to the Dobson instrument August 26, 1976, calibration scale are given, respectively, in columns 11 and 12 of the table for indicated total ozone and for $\mu = 2.2$, approximately the mean μ for the series of observations. As indicated earlier, the August 26, 1976, calibration scale for instrument No. 83 and the 1976 standard lamp calibration scale are essentially independent. From the percentage error data given in columns 11 and 12, we conclude that the Dobson instrument No. 83 calibration scale for direct Sun observations on AD wavelengths has remained unchanged between June 1972 and July 1987 to within about ± 0.5 percent.

A calibration scale established on June 18, 1962, for Dobson spectrophotometer No. 83 at Sterling, Virginia, based on direct Sun observations, yields $N_A - N_D$ values that differ by only 0.003 from those given by a corresponding calibration scales based on N values for the standard lamps of instrument No. 83 on August 26, 1976. This difference corresponds to a difference of 0.4 percent in total ozone for $\mu = 2$ and an ozone content of 300 DU, or about 1 DU between the two calibration scales. Either of the scales is, therefore, suitable for use, with an uncertainty of less than about ± 1 percent relative to the August 26, 1976, calibration scale.

An analysis of errors associated with Dobson spectrophotometer calibration observations indicates a collective uncertainty of not more than several tenths of 1 percent corresponding to uncertainties in the air mass, the ratio of the actual and vertical path lengths of the solar beam through the ozone layer, the solar zenith angle, the Rayleigh-scattering coefficients, and the particle-scattering coefficients used for observations on AD wavelengths. Ozone absorption coefficients specified for use with Dobson spectrophotometers are applicable at -44°C. At MLO, the mean temperature in the region of the ozone maximum, determined from radiosonde observations conducted during June–August 1958–1987, was about -48.4°C. Because ozone absorption coefficients for the AD wavelengths increase with increasing temperature at a rate of 0.13%/°C, total ozone values computed at MLO must be increased by about 0.57 percent. The radiosonde data also indicate a long-term temperature trend at Mauna Loa of about 0.05%/year, which translates into a trend in effective ozone absorption coefficients, and therefore in total ozone, of only about 0.006 percent per year. Shorter (3- to 6-year) time-interval temperature variations, unaccounted for, lead to errors in ozone trend calculations of up to about 0.1 percent.

In an attempt to ascertain whether the extraterrestrial constants for the Dobson instrument wavelengths vary during the course of the 11-year solar cycle, calibration observations were scheduled at times of maxima and minima in sunspot numbers. No significant difference in results (Table 4.6) was obtained for observations on AD wavelengths. Data obtained for the A and D wavelengths in 1980, at the time of a maximum in sunspots, indicated an apparent need for N-value corrections of about S + 0.006, but this result has been discarded because of known systematic observer errors. In 1981, 9 half-days of calibration observations (of 47) were discarded

following a marked temporary increase in solar activity about July 17. N-value corrections for AD wavelengths computed for these observations were about ± 0.035. Because the need was indicated for both positive and negative corrections that roughly cancelled, it is likely that the required assumption of constant ozone for the half-days during which observations were made was not valid in those periods. We tentatively conclude that if variations in the extraterrestrial constants occur during the course of a solar cycle, the assumption of constant value over the cycle most likely leads to errors in total column ozone not exceeding a few tenths of a percent, as determined from observations on AD wavelengths.

The Dobson instrument No. 83 calibration observations made at MLO during 1972–1987 have yielded a unique, precise total ozone data set that is separately useful for testing the calibration of satellite instrumentation for the measurement of total ozone. These data have been used (see Section 4.4) for the calibration of ozone measurements by TOMS aboard Nimbus–7 (McPeters and Komhyr, 1988).

4.1.1.5 Reporting Procedures to Ozone Data for the World

The daily total ozone column measurements are reported by the individual stations to the WMO–WODC and have been published since 1960 in ODW. The standard data report provides the value of the total ozone content for that day, the local time of the measurement, the wavelengths used (usually AD), and the radiation source: direct Sun, direct Moon, blue zenith sky, or one of five classifications of zenith cloud cover. In most cases, the data submitted by the stations for publication in ODW do not include corrections for periodic instrument calibrations or for intercomparisons with the world primary or regional standards, despite repeated recommendations by WMO (e.g., Ozone Report Nos. 9 and 12). Retroactive revisions of station data in ODW are very rare, even though later recalibration has demonstrated instrumental drift. (In almost all instances, essentially no budgetary provision has been made for personnel to carry out such reevaluations.) The uncritical use of published data can result in erroneous statements and major disagreements in apparent trends, even between stations located in the same macrocirculational region. As one of many examples, Figure 4.2 shows a sharp disruption in 1976–1977 in the Mauna Loa data published in ODW. (The regular Mauna Loa data are not recorded with instrument No. 83, which is normally in Boulder, Colorado, and is sent to Mauna Loa for periodic recalibration.)

The Dobson spectrophotometers are intended to be checked at least monthly with mercury-lamp tests, which monitor the spectral sensitivity response to a standardized exposure to UV radiation. The hoped-for result is that these monthly lamp tests indicate constancy of sensitivity; otherwise, the tests should catch any problems or mishaps that might have occurred, such as a change in the wavelength selection by the instrument slits. The extended series of monthly lamp tests can provide information pointing either to an abrupt change or to a steady change in instrument response to the UV test. However, the lamp response is not necessarily linearly related to the absolute sensitivity of the Dobson instrument for ozone, so that while the lamp test is a test of stability, the changing lamp values alone do not provide a quantitative correction when some change is indicated to have occurred. The quantitative aspect is resolved through recalibration. There is no set pattern to the frequency with which the instruments are calibrated, with some stations performing regular calibrations and some not. The individual Dobson instruments are also occasionally recalibrated by direct comparison at a common location with either the world primary standard (instrument No. 83) or with one of the secondary standards. Sometimes, recalibration produces only a small adjustment, but, occasionally, a correction of several percent is indicated. International comparisons of a few dozen Dobson instruments in 1974, 1977, 1978, 1979, 1984, and 1986 indicate average deviations of the order of only 2 percent.

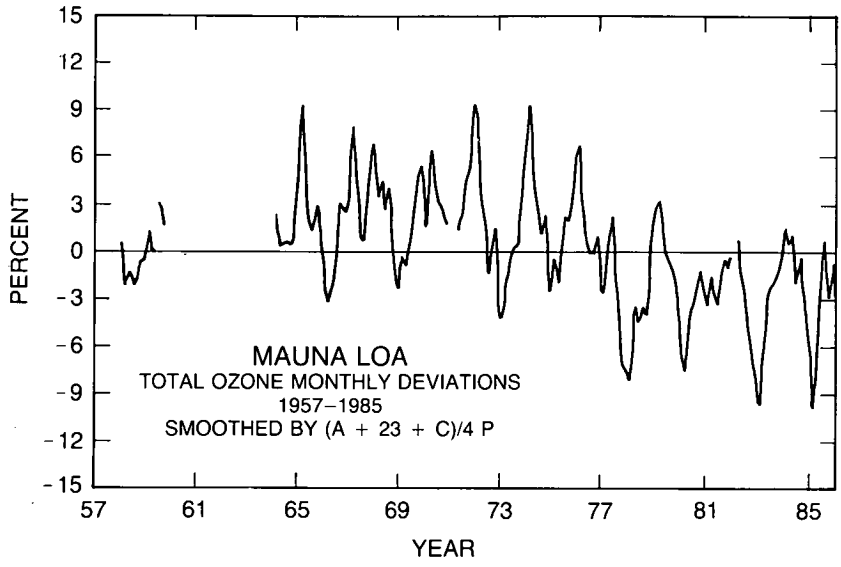

Figure 4.2 Total ozone monthly deviations at Mauna Loa (1957–1986). Calculated from the data published in *Ozone Data for the World*, showing the apparent disruption in the data in 1976–1977.

The usual procedure after calibration is the immediate installation of the new N-values, with no retrospective reevaluation of any earlier data—including the measurements made according to the old calibration scale only a short time before. In principle, such reevaluation is done by the individual stations and reported for printing in ODW. In practice, however, such published reevaluations are rare. It is worth emphasizing that, in accordance with the International Council of Scientific Unions (ICSU) principles governing the world data centers, the authority for any data adjustment resides with the individual reporting stations. Accordingly, no attempt is now made by the WMO–WODC to adjust data taken prior to recalibration, and the data are left as originally reported by the stations, with any such discontinuity intact. In almost all instances, such apparently obvious corrections are not routinely applied in the ozone data submitted for publication in ODW because the heavy workloads for other duties supersede in priority such reevaluations. Such corrections can be done if personnel time is available for such recalculations, but most ozone stations have not, in practice, been able to do any reevaluation of previously published data.

Furthermore, not all recalibrations are communicated for publication in ODW, and the information contained in routine lamp tests or other instrumental checks typically remains with the individual station records and is available only with difficulty to anyone else. Questions can then arise about the possible influence of such calibration changes upon trends in ozone concentrations inferred from the published data. The simplest question follows from the statement that, in most instances, the instrumental change that brought about the discrepancy noted during recalibration probably did not occur abruptly just prior to the recalibration. We have attempted in this chapter to revise the ozone data as published in ODW to take into account the corrections needed for these data, but not yet carried out by the individual stations. The bases for our corrections are outlined in Section 4.3.

4.1.2 Filter Ozonometer (M–83)

Since 1957, routine ground-based total column ozone measurements have been made at more than 40 stations in the USSR (see Table 4.7 and Figure 4.3) using a filter ozonometer instrument

Table 4.7 USSR M–83 Ozone Stations.

No.	WMO Index	Station	Latitude (°N)	Longitude (°E)
1	37500	Abastumani	41.45	42.50[a]
2	36870	Alma–Ata	43.14	76.56[a]
3	35746	Aralskoe More	46.47	61.40
4	22550	Archangelsk	64.35	40.30
5	38880	Ashkhabad	37.58	58.20[a]
6	32150	Bolshaya Elan (Sakhalin)	46.55	142.44[a]
7	30054	Vitim	59.27	112.35
8	31960	Vladivostok	43.07	131.54[a]
9	34560	Volgograd	48.35	45.43
10	34122	Voronez	51.42	39.10
11	35700	Gurev	47.01	51.51
12	20674	Dikson Island	73.30	80.14[a]
13	38836	Dushanbe	38.35	68.47[a]
14	23274	Igarka	67.28	86.34
15	30710	Irkutsk	52.16	104.21[a]
16	35394	Karaganda	49.48	73.08
17	33347	Kiev	50.24	30.27[a]
18	21432	Kotelnyj Island	76.00	137.54
19	29574	Krasnoyarsk	56.00	92.53[a]
20	28900	Kuibyshev	53.15	50.27[a]
21	26063	Leningrad	59.58	30.18[a,b]
22	33393	Lwow	49.49	23.57
23	25551	Markovo	64.41	170.25
24	27612	Moscow	55.45	37.34[a]
25	22113	Murmansk	68.58	33.03[a]
26	25913	Nagaevo	59.35	150.47[a]
27	31369	Nikolaevsk–Na–Amure	53.09	140.42
28	33837	Odessa	46.29	30.38[a]
29	24125	Olenek	68.30	112.26
30	28698	Omsk	54.56	73.24[a]
31	32540	Petropavlovsk–Kamchatskii	52.58	158.45
32	23418	Pechora	65.07	57.06
33	26422	Riga	56.58	24.04[a]
34	28440	Sverdlovsk	56.48	60.38[a]
35	36177	Semipalatinsk	50.21	80.15
36	30692	Skovorodino	54.00	125.58
37	37545	Tbilisi	41.41	44.57
38	21825	Tiksi	71.35	128.55
39	24507	Tura	64.10	100.04
40	33976	Feodosija	45.02	35.23[a]
41	23933	Hanty–Mansijsk	60.58	69.04
42	20046	Heiss Island	80.37	58.03[a]
43	34646	Cimljansk	47.44	42.15
44	38687	Cardzou	39.05	63.36
45	24959	Yakutsk	62.05	129.45[a]

[a] Data published and used in the formation of regional averages
[b] Dobson station

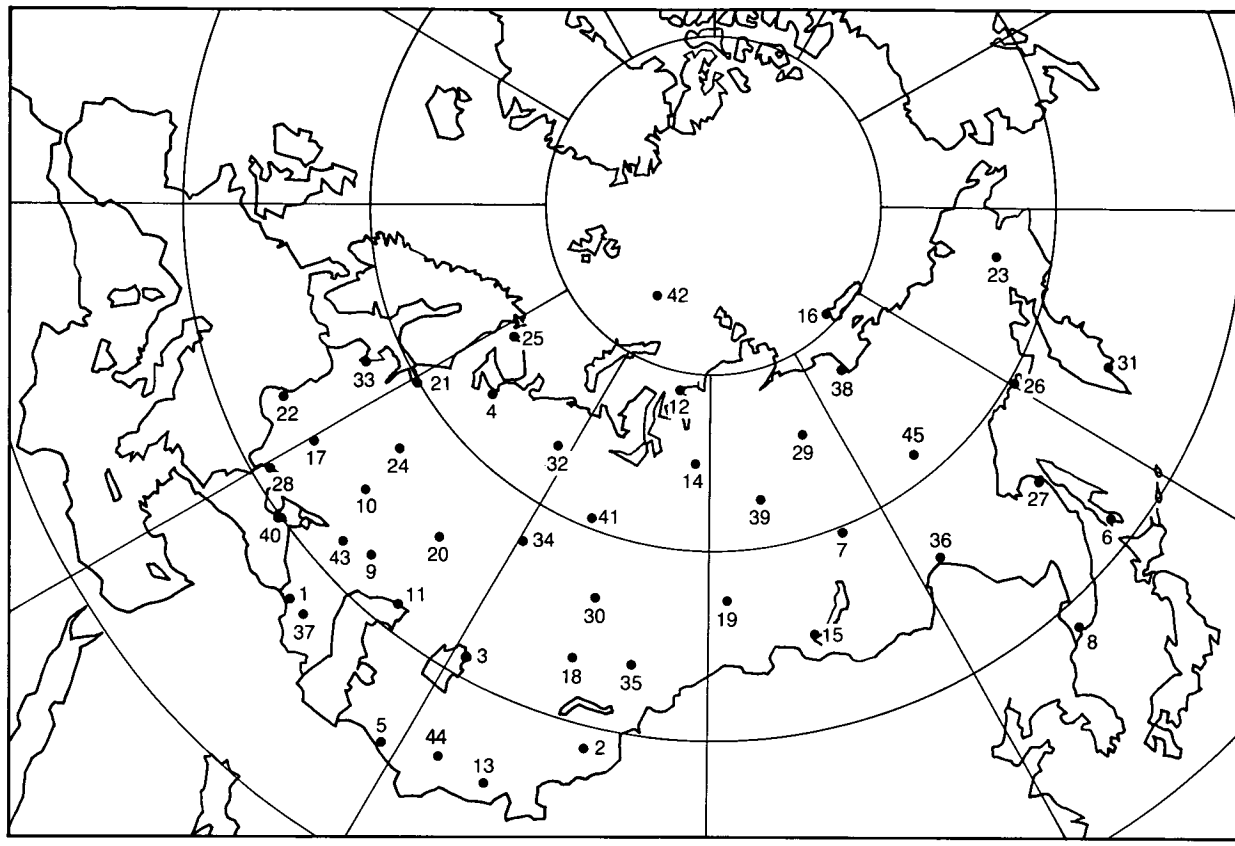

Figure 4.3 Geographical distribution of the M–83 filter ozonometers in the USSR (the numbers correspond to those given in Table 4.7).

designated as type M–83 (and not to be confused with the Standard Dobson ozone spectrophotometer, which was the 83rd instrument manufactured of the Dobson type). The filter-type instrument is based upon the same principle as the Dobson spectrophotometer in using differential absorption of UV radiation in the 300–350 nm Huggins band of ozone. The M–83 instrument, however, uses two broadband filters and measures the relative attenuation of the solar UV radiances either directly from the Sun or indirectly from the zenith sky (Gustin, 1963).

Direct intercomparisons between M–83 filter instruments and Dobson spectrophotometers prior to 1971 (Bojkov, 1969b) revealed that the M–83 recorded 6 percent less ozone when the observations were restricted to $\mu < 1.5$, and 20 percent to 30 percent more ozone when data were taken for $\mu > 2.0$. A strong dependence on turbidity was also detected, with 9 percent to 14 percent higher ozone readings when the surface visibility was less than 5 km. These strong deviations for $\mu > 2.0$ make very uncertain many of the high-latitude measurements in the USSR.

Improved filters were introduced into the M–83 instrument starting in 1972–1973 (Gustin, 1978). The new filters have maximum transmittance at 301 nm and 326 nm, and their bandpasses are less than those in the earlier version: 22 nm (291–312 nm) and 15 nm (319–334 nm). Comparison of Nimbus–4 BUV satellite overpasses over M–83 stations in the USSR demonstrated a standard deviation of about 50 DU before 1973 and about 25 DU afterward. The Nimbus–4 BUV overpasses of Dobson stations maintained a standard deviation of about 17 DU during the 1970–1977 lifetime of the satellite.

A much newer, reportedly improved instrument designated as M–124 has been installed in many stations since 1986 (Gustin et al., 1985), but no ozone data have been reported yet for this instrument. No trend data with the M–124 can be expected for about a decade unless the data can be satisfactorily cross-calibrated with the M–83 data from the same location.

4.1.3 Brewer Grating Spectrophotometer

An improved optical and electronic scheme for observations of total ozone was proposed by Brewer (1973) based in part on earlier developments by Wardle et al. (1963). The instrument has one diffraction grating (1,800 lines per mm) and five slits corresponding to five wavelengths in the 306–320 nm spectral band. The resolution is 0.6 nm as compared to 0.9–3.0 nm in the Dobson instrument. Combination of the data from all five wavelengths provides information about the total column content of SO_2, a potential interference for the Dobson measurements in SO_2-polluted air.

The Atmospheric Environment Service of Canada has been developing and testing the Brewer ozone spectrophotometer for the purpose either of replacing or supplementing the current Dobson network. Intercomparisons between the Brewer and Dobson instruments at Toronto have shown a difference in total ozone within ± 1 percent for direct-Sun observations. However, some questions about the stability of the Brewer instrument with respect to calibration and spectral sensitivity have been raised following comparisons of the Dobson and Brewer instruments in the Federal Republic of Germany at Hohenpeissenberg (Köhler and Attmann-spacher, 1986) and in the USA at Wallops Island (Parsons et al., 1982). At this time, no plans for the worldwide utilization of the Brewer instrument have been announced, pending further field tests of the instrument in several regions of the globe. Brewer instruments are currently known to be operated at several Canadian stations (Kerr et al., 1988, 1988a), Salonika (Greece), Norshopping (Sweden), and Hohenpeissenberg. Only the data from Hohenpeissenberg have been published in ODW. The longest Brewer record commenced in 1983, so a long-term "Brewer-only" analysis cannot yet be carried out.

4.1.4 Measurements of Vertical Ozone Distributions: Umkehr and Ozonesondes

The measurements with the Dobson spectrophotometer are based entirely upon the ability of molecular ozone to absorb UV radiation in the Huggins band, and have produced the only long-term record of total ozone in the atmosphere measured by ground-based stations. The vertical distribution of ozone within the atmosphere can be deduced through the Umkehr technique with the Dobson spectrophotometer, and has been routinely applied at about a dozen Dobson stations. The preferred time of day for Dobson instrument measurements of total ozone is local noon, for which the slant path of the solar radiation is the shortest. For directly overhead Sun ($\mu = 1.0$) and for angles corresponding to $\mu = 2$ or 3, the radiation reaching the instrument is overwhelmingly the direct radiation from the solar source. However, as the Sun approaches the horizon, the importance of scattered radiation relative to direct radiation continues to increase. Under these conditions, the altitude of the scattering process relative to the altitude of absorption of ozone becomes important, and the ratio of wavelengths reaching the Dobson instrument begins to carry information about the altitude distribution of the ozone within the stratosphere. The ratio of radiation intensity (longer wavelength divided by shorter wavelength, e.g., 332.4 nm and 311.45 nm for the C pair) is expected to increase steadily with increasing slant path for the direct radiation because of the larger number of molecules of ozone available for absorption along the path. The radiation received from the zenith sky presents a mixture of scattering from various altitudes. When the Sun reaches a zenith angle of about 86°, the altitude dependence of

the scattering process causes the intensity ratio to pass through a maximum and then to decrease again. Continued measurement beyond a zenith angle of 90° can lead to a minimum in the radiation intensity for the two wavelengths, and then an increase again. Careful evaluation of the detailed shape of such graphs of ratios of radiation intensity versus solar zenith angle provides information about the vertical distribution of the ozone in the stratosphere. The technique was developed in 1931 by Götz (1934); it is known as the Umkehr procedure from the German word for reversal because of the existence of a maximum in the graph of intensity versus zenith angle.

Entirely separate data on the vertical distribution of ozone over particular stations have also been obtained through the use of ozonesondes, balloonborne devices that utilize the oxidizing capability of ozone to cause a measurable chemical change. Under the usual operating conditions, the reliability of the ozone measurements by the sondes is checked by its degree of agreement, when integrated, with the total amount of ozone measured nearly simultaneously by a nearby Dobson instrument (Brewer and Milford, 1960; Komhyr, 1965; Kobayashi and Toyama, 1966).

Ozone profile data are covered more fully in Chapter 2.

4.2 SATELLITE MEASUREMENTS OF TOTAL OZONE

The first long series of measurements of total ozone from space were made in 1970 from the Nimbus–4 satellite by the BUV spectrometer. This instrument was capable of daily measurements covering the entire sunlit portion of the globe—i.e., all but the area within the 24-hour polar darkness. The Backscatter Ultraviolet (BUV) instrument worked well for about 2 years; it then encountered problems that permitted far fewer daily ozone readings, which continued into 1977.

The Nimbus–7 satellite was launched on October 23, 1978, with two instruments on board, each capable of monitoring total ozone from all of the sunlit globe. TOMS and the SBUV spectrometer are briefly described here. A detailed description of the TOMS instrument is given in Chapter 2. The SBUV instrument provides measurements of both total ozone and the ozone vertical profile up to 50 km altitude, but only in the nadir (i.e., along the satellite groundtrack). The TOMS instrument measures only total ozone, but it is not limited to the nadir and, by sweeping through a series of slant angles, it provides a much denser pattern of daily measurements of total ozone. Data from the other satellite instruments that measure ozone are not presently suitable for a discussion of possible changes in total ozone concentrations. Some instruments measure only ozone profiles, while others had only a few months of good data at the time of this report.

4.2.1. Total Ozone Mapping Spectrometer (TOMS)

The Total Ozone Mapping Spectrometer on the Nimbus–7 satellite is designed to provide daily global maps of Earth's total ozone by measuring sunlight backscattered from the Earth-atmosphere system in six wavelength bands, each with a 1.0 nm bandpass: 312.5, 317.5, 331.2, 339.8, 360, and 380 nm. The two longest wavelengths are insensitive to atmospheric ozone and are used to measure surface reflectivity, while the remaining wavelengths are used in the inference of total ozone concentrations. TOMS contains a single monochromator with a scanning

mirror to measure backscattered radiation at 35 observation angles perpendicular to the orbital plane every 8 seconds—i.e., as many as 378,000 ozone data points per day. The angular swath from each satellite orbital track extends far enough to provide overlap with both the preceding and succeeding orbital tracks, and provides a complete global map of total ozone daily, omitting only the area of complete polar night.

Dave and Mateer (1967) demonstrated the feasibility of determining atmospheric ozone from measurements of backscattered solar UV radiation. The UV radiation received by the TOMS instrument in the total ozone wavelength bands consists of solar radiation that has penetrated the stratosphere and has been either scattered back by the dense tropospheric air or reflected by Earth's surface. Ozone, concentrated mostly in the lower stratosphere, lies above the region in which the radiation is backscattered, and acts as an attenuator of this radiation. By determining the differential attenuation as a function of wavelength, the amount of ozone above the reflecting surface can be accurately determined. More than 90 percent of the ozone is located above the tropopause, while all the clouds, most of the aerosols, and 80–90 percent of the atmosphere are located below it. This almost complete separation of the ozone above the scatterers and reflectors minimizes errors caused by the ozone vertical profile shape or by clouds, aerosols, and other tropospheric variables. However, the instrument has a lessened sensitivity to that fraction of ozone that lies in the troposphere in the midst of the scattering agents. The standard algorithm (see Chapter 3) for calculation of total ozone from the recorded satellite data includes the addition of a small amount of ozone to compensate for this lessened sensitivity to tropospheric ozone. The magnitude of this computed tropospheric correction is fixed from the average of other, non-satellite ozone observations, and has been assumed to be invariant between 1978 and 1988. Further, no allowance is made in the correction term for possible seasonal or latitudinal differences in tropospheric ozone. The satellite instrument is, therefore, relatively insensitive to any trends in ozone concentration with time that might occur in the lowest levels of the atmosphere.

Accurate ozone measurement is facilitated by the availability of simultaneous measurements with several wavelength pairs. Both TOMS and SBUV are programmed to infer total ozone using an A wavelength pair (312.5/331.2 nm), a somewhat less sensitive B wavelength pair (317.5/331.2 nm), and, at very large solar zenith angles, a C wavelength pair (331.2/339.8 nm). The use of wavelength pairs completely removes the effect of any wavelength-independent component of errors such as instrument calibration or aerosol scattering. The conversion of relative radiances at two different wavelengths into total ozone depends upon the differences in ozone absorption coefficients, as described earlier for the Dobson instruments. However, the total ozone data from the two instruments on Nimbus–7 have been calculated with the more recent Bass–Paur (1985) ozone absorption cross-sections. (The initially reported ozone data inferred from Nimbus–7 preceded the Bass–Paur coefficients and were calculated differently, but all of the data have now been calculated with a consistent algorithm based on the Bass–Paur coefficients, and the archived data set now contains only the data from this algorithm.)

Ozone is inferred from the UV backscattered albedo, which is defined as the ratio of the backscattered radiance to the extraterrestrial solar irradiance. The backscattered radiance is measured at each of the six wavelengths for each observation. The solar flux at each of these wavelengths is recorded once each week by measuring the solar radiation arriving from a ground aluminum diffuser plate deployed into direct view of the Sun. The use of the ratio of intensities from Earth and from the diffuser plate eliminates the effects of the solar spectrum, and the weekly remeasurement of solar irradiance tracks any changes in instrument throughput during the life of TOMS. One of the most significant instrumental changes in the 10-year life of

Nimbus–7 has been the degradation of this aluminum diffuser plate from its intermittent exposure to direct solar UV bombardment (see Chapter 2).

The orbit of Nimbus–7 determines the possible ozone coverage by TOMS. The satellite is in a Sun-synchronous retrograde polar orbit that crosses the Equator at approximately local noon on each orbit. The orbital inclination necessary to provide Sun-synchronous precession is such that the satellite reaches a maximum latitude of 80 degrees in each hemisphere. However, the cross-track scanning of the TOMS instrument permits ozone measurements all the way to the pole as long as it is sunlit. True pole-to-pole ozone measurements are not obtained except near equinox because scattered sunlight is necessary for the measurement of ozone, and data cannot be obtained in winter at high latitudes. Total ozone is measured to a maximum solar zenith angle of 88 degrees.

Total ozone data from TOMS are available continuously since November 1978. The processing of the recorded UV radiances into measurements of total ozone is currently on a near-real-time basis, with daily global maps available approximately 3 weeks after measurement. The data are archived at the National Space Science Data Center (NSSDC) at the Goddard Space Flight Center (GSFC).

4.2.2 Solar Backscatter Ultraviolet Spectrometer (SBUV)

The Solar Backscatter Ultraviolet Spectrometer, also on the Nimbus–7 satellite, is similar to TOMS but is designed to measure ozone profiles as well as total ozone. The instrument is an improved version of the BUV, flown on Nimbus–4 in 1970. It contains a double monochromator with a highly linear detector system that allows it to measure UV radiation over a dynamic range of seven orders of magnitude. SBUV and TOMS share the same ground aluminum diffuser plate for the weekly measurement of the solar irradiance, although the instruments do not look at precisely the same areas of the diffuser plate. Both SBUV and TOMS incorporate two important improvements over the BUV. First, a mechanical chopper allows accurate subtraction of any dark current signal so that measurements can be made even in the presence of energetic particles. Second, the diffuser plate is protected except during solar flux measurement in order to reduce the rate of degradation. Finally, SBUV has an additional improvement over BUV through a continuous scan mode that measures the complete UV spectrum from 160 nm to 400 nm in 0.2 nm steps.

The important difference in the total ozone measurements provided by TOMS and SBUV is that SBUV measures ozone only along the orbital track, while TOMS scans between tracks. The TOMS field of view (FOV) is 40 km $\times$ 40 km at nadir, while the SBUV FOV is 200 km $\times$ 200 km.

SBUV measures the solar backscattered radiance every 32 seconds (i.e., as many as 2,700 data points per day) at 12 wavelengths, with a bandpass of 1.1 nm: 255.5, 273.5, 283.0, 287.6, 292.2, 297.5, 301.9, 305.8, 312.5, 317.5, 331.2, and 339.8 nm. The wavelengths from 255.5 nm to 305.8 nm are used to infer an ozone profile, while the four longer wavelengths, which are identical to those in TOMS, are used to infer total ozone. Instead of separate, and still longer, wavelength channels to determine scene reflectivity, SBUV uses a photometer set at 343 nm to measure reflectivity coincident with each monochromator scene in order to compensate for satellite motion. Except for differences caused by these slight instrument variations, the algorithms used to infer total ozone for TOMS and SBUV are identical.

Total ozone and ozone profile data are available from SBUV for November 1978 through March 1988. In February 1987, the SBUV began to experience a high rate of loss of chopper synchronization—i.e., a lack of coincidence between the insertion of the dark current chopper and the recording of the signals into the correct time bins. The effect of this loss was to introduce an apparently random 2 percent noise into the radiance measurement, degrading the accuracy of the inferred ozone profiles in particular. The SBUV data are also archived at the NSSDC.

4.3 USE OF EXTERNAL DATA TO DIAGNOSE PROBLEMS AT GROUNDSTATIONS

Examination of the published ozone data from a particular ground-based station sometimes brings to light apparent incongruities within the full time series. For instance, the total ozone values recorded in ODW for Mauna Loa have been deseasonalized and plotted in Figure 4.2; a step in the mean ozone level appears sometime during 1976 or 1977. For this report, the total ozone records of about 30 stations have been examined for internal consistency and for external consistency with data from other sources. For the period from November 1978 to December 1986, every ground-based total ozone measurement can be compared with the total ozone measured by TOMS when the satellite was overhead on that same day. The search for data incongruities is more difficult prior to November 1978, but comparisons with total ozone data from proximate stations and with the recorded local stratospheric temperatures at the 100 millibar level have revealed numerous instances when Dobson recalibrations have occurred but have not been reported to the ODW. The approximate dates of such discrepancies were noted, and the stations were asked whether a recalibration had taken place at that time and, if so, the magnitude of the calibration change. The total ozone data were revised only when information regarding the operation of the instruments was available. These diagnostic tests of the quality of the total ozone data brought to light many more recalibrations than would have been detectable by examining each ozone record in isolation.

4.3.1 Comparisons of Ground-Based and Satellite Measurements

The existence of two entirely separate systems that simultaneously measure total ozone provides an excellent opportunity for the detection of flaws in either system through the comparison of overlapping observations. Because the satellites orbit Earth in less than 2 hours, an overpass not too far from each groundstation occurs daily. Such satellite overpasses of groundstations took place during 1970–1972 with the BUV ozone detector on Nimbus–4, and since November 1978 with the TOMS and SBUV instruments on Nimbus–7. The nearest daily overpass is geographically much closer with the TOMS system because, unlike SBUV, which measures total ozone only directly in the nadir, TOMS also provides ozone data for many points situated at oblique angles to the precise satellite path. The density of TOMS ozone measurements over Hawaii is illustrated in Section 4.4.2. An example of a series of TOMS–Dobson comparisons for the Arosa groundstation is shown in Figure 4.4. The center panel contains a plot of the ozone measured by the Dobson instrument at Arosa; the bottom panel shows the TOMS measurement of total ozone closest to Arosa each day, usually within 1 degree latitude and longitude; and the top panel plots the percentage difference between the two ozone measurements. Examination of the ozone values themselves (lower two panels) shows that both instruments track the large annual variation in ozone at 47°N latitude very well. The percentage-difference plot (upper panel) reveals differences that would not be clear in the individual ozone plots. The small annual modulation in the difference plot is usually interpreted as caused by a minor scattered light problem in the Dobson instrument that becomes apparent only when the

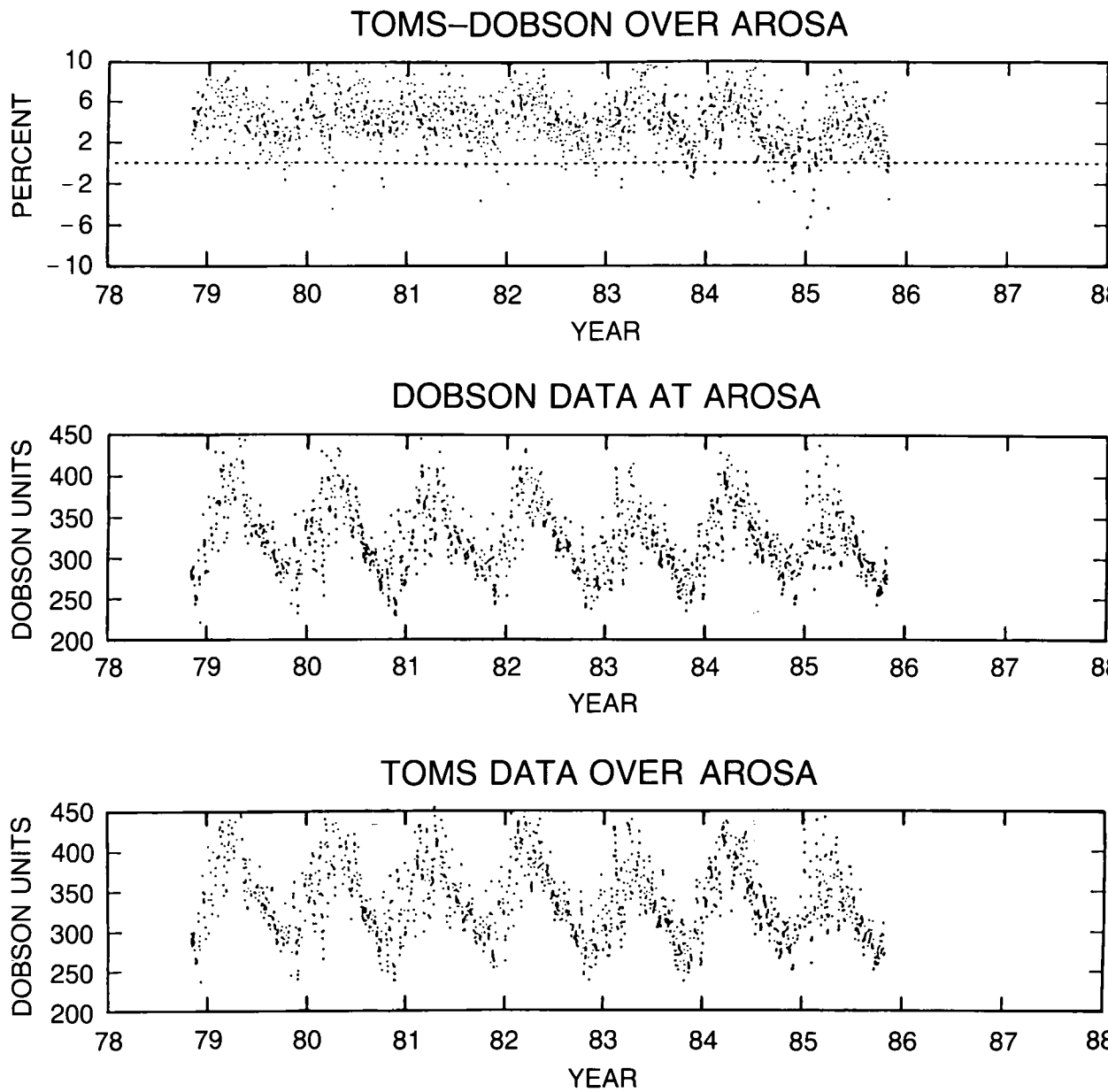

Figure 4.4 The top panel shows the percentage difference between measurements of the Dobson Spectrophotometer and the TOMS instrument at Arosa, Switzerland. The middle and bottom panels show the actual measurements of the Dobson and the TOMS instruments, respectively.

ozone is recorded with the large solar zenith angle observations necessary in midwinter at high-latitude stations. The major value of such comparison plots here is that abrupt changes in the record of an individual groundstation can be clearly detected.

Plots of the deviations at each groundstation from the first year of TOMS operation (Fleig et al., 1982) were published by the WMO–WODC, and other comparisons of the same data versus selected surface stations were made by Bhartia et al. (1984) and Fleig et al. (1986a). The TOMS data from 1979 to 1982 were further used in assessing the relative quality and performance of the Global Ozone Observing System total ozone measurements (Bojkov and Mateer, 1984b). Com-

pletely reevaluated TOMS data, applying the Bass and Paur (1985) ozone absorption coefficients, were recently provided by the Nimbus–7 processing team (Fleig et al., 1986a; Bhartia et al., 1988). With a sufficiently large number of comparisons, the effects of random errors should approach zero, leaving only the systematic bias. A systematic bias is always present because the ozone results from the groundstations, reported on the basis of the Vigroux ozone absorption coefficients, are always higher by 3–4 percent than the total ozone amounts calculated with the Bass–Paur coefficients.

In principle, either the ground-based or the satellite system could be assumed to be the standard, and the other system the one of uncertain quality to be tested against it. In practice, both systems have potentially serious errors that raise questions about the validity of the data reported from that system. Fortunately, the primary flaw for the ground-based system has a very different structure from the major flaw of the satellite system, so that useful intercomparisons can be made.

The chief uncertainty in ozone determinations with the satellite systems is the slow, relatively steady deterioration in the diffuser plate used as the calibrating agent for converting the various relative wavelength readings into absolute amounts of ozone (Chapter 2). The absolute amount of solar UV received from the diffuser plate has obviously diminished substantially at all wavelengths during the decade of operation of Nimbus–7 because of the diffuser plate degradation. However, the algorithm for converting UV radiances to total ozone is dependent primarily upon the ratio of radiances at two wavelengths rather than upon the absolute values, and was intended to compensate fully for the diffuser plate degradation. Moreover, this deterioration has occurred over a period of almost 10 years and has basically not shown erratic behavior on short time scales such as 1 week or 1 day.

Intercomparisons of satellite readings versus those of two groundstations on the same day can safely be assumed to have been made with an instrument having the same response characteristics for both overpasses. Five years later, the sensitivity of the satellite instrument is undoubtedly different, but effective intercomparisons can again be made for same-day overpasses. The satellite instruments can, therefore, provide accurate assessments of the ground-based measurement capabilities as long as this use as a transfer standard is restricted to short time periods of a few days, over which the degradation of the satellite diffuser plate is negligible.

In contrast, the most prominent flaw of the ground-based systems is the variability in the operating procedures used at each station. Although the individual Dobson instruments were very nearly identical when manufactured, their conditions of maintenance, repair, and general upkeep have diverged widely since installation. The training and supervision of operators can also be very different, so that stations with superficially identical equipment can provide ozone data of very widely different quality.

Given the distinctive characteristics of the possible flaws in the two systems, a "bootstrapping" operation becomes possible, with the result that the combined satellite–ground ozone data set is substantially better than either taken alone. The daily satellite–ground intercomparisons are used to provide tests of the quality of the data reported by individual groundstations, including the detection of suspect operating periods, and in principle allow correction and refinement of the ground data. A selected set of "good" groundstations can then be used to calibrate the slow deterioration of the satellite instrument and permit absolute comparisons of satellite data recorded a few years apart. These ground–satellite interactions are described now in greater detail.

4.3.1.1 Allowing for a Drift Between TOMS and the Groundstations

Comparisons have been made between the daily-mean total ozone concentrations measured at 92 surface-based stations (71 Dobson and 21 M–83 instruments) and the total ozone calculated from direct overpasses by the Nimbus–7 TOMS, from November 1978 to December 1985 (Bojkov et al., 1988). The satellite overpasses always occur at local noon, while the surface-based data are usually averaged from data collected symmetrically around local noon. The time difference between the satellite and ground observations is normally 3 hours or less.

The overpass analysis first established a basic Dobson–TOMS reference curve of monthly values of the network average bias, expressed as the Dobson ozone value minus the TOMS ozone divided by the Dobson ozone—(Dobson–TOMS)/Dobson. These values were calculated from the data provided by the 74 stations that reported most regularly over the period of satellite operation. Stations with short records, serious drifts (greater than 1 percent per year), or sudden steplike increases or decreases were excluded. The data for individual months from groundstations were included only if (a) at least 13 daily station vs. TOMS comparisons were available during the month, (b) the standard deviation of the daily differences contributing to the monthly mean difference was less than 5 percent, and (c) the absolute difference between the station monthly mean difference and the overall network mean difference was less than twice the standard deviation of the network mean. Application of these criteria each month reduced the number of participating stations in the monthly evaluations to a variable number between 50 and 65. These criteria for disregarding some overpasses were intended to eliminate the least satisfactory parts of the ground-based total ozone data set, including rejection of some parts of the data from stations that operated satisfactorily in other months.

The basic reference comparison curve, based on all types of ground measurements (direct Sun, zenith sky, etc.) is graphed in Figure 4.5, and the results are summarized as 6-month

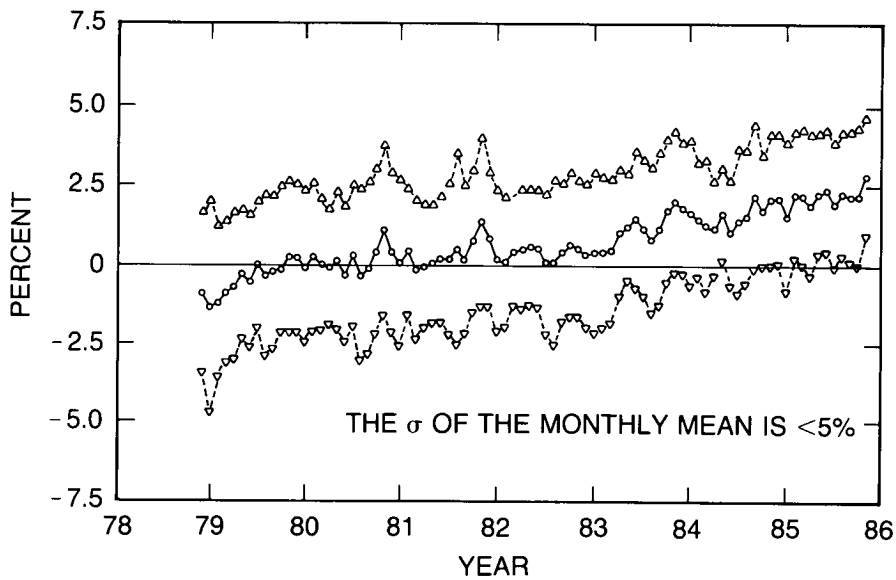

Figure 4.5 Monthly mean biases (Dobson–TOMS)/Dobson and their respective intrastation standard deviations ($\pm 1\sigma$). The solid curve is the basic reference curve based on all types of ground measurements. Positive values mean satellite underestimation of the total ozone amount relative to that measured at well-run groundstations (see text for inclusion of particular stations). The vertical markers indicate the position of the end (December) of the previous year.

averages in Table 4.8. Also included in Table 4.8 are the results found when only the direct-Sun ground-based measurements were used in the comparisons. It is clear that the set of comparisons made with only direct-Sun readings is quite similar to the results using all total ozone data. The upper and lower curves of Figure 4.5 indicate the one standard deviation limits for the mean reference curve. In most cases, these fall between 2 percent and 2.4 percent. The total drift is about 3.5 percent, varying from -1 percent in 1978 to +2.5 percent in 1985, indicating that the ozone reported by the satellite lessens with time relative to the ground-based observations. A linear regression to the data indicates that the satellite ozone needs to be increased by 0.42 ± 0.02 percent per year to compensate for the TOMS drift, essentially the same as that reported by Fleig et al. (1986a), based on comparison with 41 selected Dobson stations. However, the basic reference comparison curve does not appear to be smoothly linear in its change, but instead is characterized by initially increasing values, followed by a relatively flat plateau close to the zero line from mid-1979 through mid-1981. A further slow rise until early 1984 is followed by a final period of more rapid rise through the end of the record used in the analysis. After correction for the average bias for each individual month, the standard deviation of the mean of all monthly mean differences for the 7-year period is 0.38 percent when all observations were considered and 0.43 percent when only direct-Sun readings were taken into account. The standard error of 0.02 percent from the linear regression is probably an underestimate of the yearly error in the drift coefficient.

Table 4.8 Six-Month Average Bias (Dobson–TOMS)/Dobson Centered at February 1 and August 1 of Each Year as Deduced From All and From Only Direct-Sun Observations.

	All	Six-Month Difference	Direct-Sun	Six-Month Difference
1979				
Feb.	–0.90	0.72	–1.11	0.79
Aug.	–0.18	0.23	–0.32	0.18
1980				
Feb.	0.05	0.10	–0.14	0.45
Aug.	0.15	–0.06	0.31	–0.27
1981				
Feb.	0.09	0.41	0.04	0.38
Aug.	0.50	–0.11	0.42	–0.27
1982				
Feb.	0.39	–0.05	0.15	0.23
Aug.	0.34	0.26	0.38	– .01
1983				
Feb.	0.60	0.76	0.37	0.72
Aug.	1.36	0.11	1.09	0.15
1984				
Feb.	1.47	0.17	1.24	0.27
Aug.	1.64	0.38	1.51	0.20
1985				
Feb.	2.02	0.27	1.71	0.83
Aug.	2.29		2.54	

Bias is in percent. The 6-month differences between the average biases indicate a nonuniform drift.

Possible factors that might contribute to this drift between TOMS and Dobson ozone measurements were discussed by Fleig et al. (1986b). They include residual uncorrected drift in the SBUV/TOMS diffuser plate, an overall drift in the Dobson network, and differences in the response of the two systems to actual changes in the amounts of tropospheric ozone or ozone-simulating pollutants such as SO_2. Fleig et al. concluded that drift in the Dobson network was unlikely because their TOMS–Dobson drift appeared to be independent of any objective method of weighting the individual stations for data quality. Increases over time in the concentration of tropospheric ozone or SO_2 may contribute to the drift because the satellite systems respond only partially to changes near ground level either in ozone or in interfering absorbers, while the Dobson system responds fully (Komhyr and Evans, 1980). The influence of SO_2 on ground-based total ozone measurements has been shown to be very small except in heavily polluted urban areas (Basher, 1982).

Recent studies of ozonesonde observations (Angell and Korshover, 1983b; Bojkov and Reinsel, 1985; Logan, 1985; Tiao et al., 1986; and Bojkov, 1988a) do indeed indicate an increase in tropospheric ozone at slightly less than 1 percent per year, while surface ozone measurements suggest 1 percent to 1.5 percent yearly increases over the past two decades (Logan, 1985; Bojkov, 1987a). However, because tropospheric ozone contributes only about 10 percent of the total ozone column, an increase of 1 percent per year in tropospheric ozone would correspond to an increase of only 1 percent per decade in total ozone, substantially less than the 3.5 percent change found in less than 8 years. Because the satellite systems are not completely insensitive to tropospheric ozone, the changes in tropospheric ozone appear to be only a minor part of the observed drift between the Dobson and satellite systems, with the major contributor the residual uncorrected drift in the satellite diffuser plate.

Once determined, the average biases between TOMS and the groundstations were calculated as monthly averages and removed from the differences for each station. In the subsequent illustrations in Section 4.3, this overall bias has been removed from the individual station record. In this manner, the TOMS instrument is used as a transfer standard between individual groundstations, assists in evaluation of the quality of the data for each, and in particular allows comparison of data at that station relative to the other groundstations on a month-by-month basis. Furthermore, the 7-year period of continuous data permits identification of time-dependent changes in the record from any individual station. Figure 4.6 (note the expanded vertical scale relative to other similar figures) plots the monthly mean (Dobson–TOMS)/Dobson differences after the removal of the monthly biases identified in Table 4.8. (The total data set again includes some ozone measurements that were excluded from the average bias determination, as outlined earlier.) The course of the monthly mean differences lies within the ± 0.6 percent band.

A few details can be identified:

- In 7 years, only 3 individual months (each an October) showed means significantly exceeding the 0.6 percent difference range; the largest positive monthly differences (greater than 0.4 percent) occur from September–December.

- June and July show the largest negative differences (-0.15 percent and 0.29 percent), which is a possible reflection of the strong μ dependence (relative solar slant path) exhibited by the instruments at many stations.

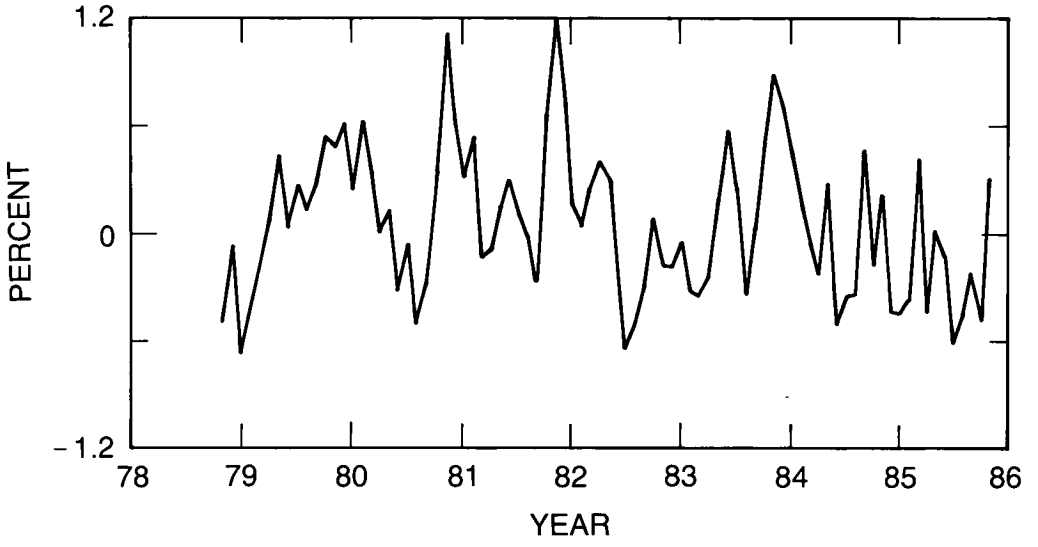

Figure 4.6 Monthly mean (Dobson–TOMS)/Dobson differences after the monthly biases have been removed. Stations where the σ of the monthly mean is less than 5 percent have not been included. The σ of the monthly averaged values is in most cases between 2 and 2.4 percent, and thus out of scale (note the expanded vertical scale relative to other similar figures).

- The standard deviations of the mean of the individual months show a small but well-pronounced annual dependence. The months with less than 0.30 percent are February–August; the smallest, 0.12 percent, occurs in February. September–January have δ greater than 0.38 percent, with the greatest value, 0.55 percent, occurring in October.

More than two-thirds of the 71 Dobson stations have less than 2 percent difference versus the network average estimated via TOMS for the entire 7-year period, as shown in the diagram in Figure 4.7. Only 20 percent of the stations have a difference greater than 3 percent. These statistics imply relatively good performance of two-thirds of the Dobson stations, while confirming stability in the short-term performance of the TOMS superimposed on the long-term drift. On the lower panel (Figure 4.7) the same plot for the 21 M–83 stations shows that only half fall within the good-performance category (less than 2 percent), and nearly 30 percent of them have differences larger than 3 percent.

Only 12 percent of the stations (seven Dobson and four M–83 filter) show absolute differences versus TOMS greater than 4 percent. These stations (with the percentage difference for TOMS versus their direct-Sun observations in parentheses) are (a) Dobson stations: Casablanca (-9.7), Cairns (-7.2), Hobart (-5.8), Brisbane (-5.7), Syowa (-5.7), Mauna Loa (-5.5), and Arosa (-4.8); and (b) M–83 stations: Heiss Island (9.6), Kuybishev (4.9), Dushanbe (4.6), and Alma Ata (4.0). In the case of Mauna Loa, for instance, an adjustment of about 2.9 percent is needed to allow for the tropospheric ozone sensed by TOMS, averaging its response over a wide oceanic area, but not by the mountaintop Dobson instrument (at 3400 meters). Similar terrain-height-induced adjustments of about 0.8 percent for Arosa and -0.6 percent for Alma Ata and Syowa (low-lying stations in mountainous regions) are also considered appropriate (Fleig et al., 1982). Such comparisons also make no allowance in judging the performance of an individual station between stations with differing natural variability. Tropical stations, for instance, show little day-to-day or seasonal variability.

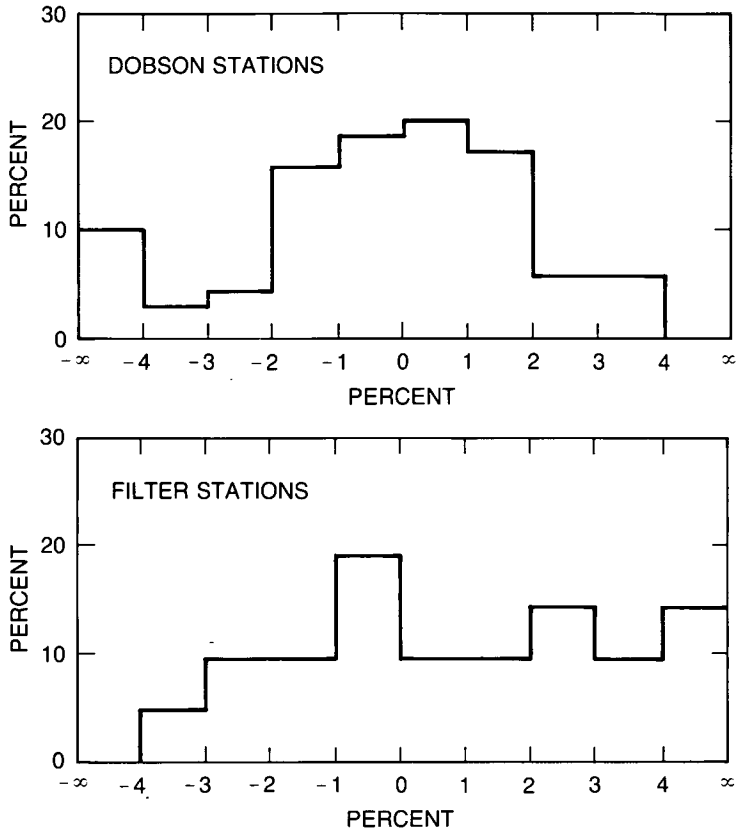

Figure 4.7 Fractional distribution of (top) 71 Dobson stations and (bottom) 21 M–83 filter stations according to the (station–TOMS)/station monthly mean differences in 1 percent intervals. More than two-thirds of the Dobsons, but only half of the M–83 stations, have less than 2 percent mean difference with the network average transferred via TOMS; 22 percent of all stations have differences $\geqslant$ 3 percent.

The analysis of the differences should consider information for the corresponding station variability. If the scattering of the daily differences is widely spread around the zero line, the annually averaged values could be misleadingly small. Another view of the (Dobson–TOMS)/Dobson differences, as a function of their relative variability (standard deviations expressed in percent of the total ozone at the given station), is presented in Figure 4.8. The upper panel shows the fractional distribution of 92 stations according to the relative variability of their monthly mean differences, in 1 percent intervals. The continuous line is for direct Sun and the dotted line for all observations, with no great differences between the averages of the two groups of observations. An important indicator of the stability of the monthly mean differences is that 60 percent of the stations reporting direct-Sun observations show less than 2 percent variability. Greater than 4 percent variability is shown at only 7.6 percent of the direct-Sun observing stations (10.9 percent of all). Here it should be noted that, although the number of stations with variability greater than 3 percent using Dobson or filter instruments is nearly the same, the fraction from all Dobson stations is only 12 percent for direct-Sun (16 percent for all) observations, while the filter stations' fraction is 63 percent (68 percent for all). This is a clear indication of the lesser variability of the Dobson vs. the filter stations (ratio better than 1:4). Table 4.9 lists all stations for which the variability of their monthly mean differences exceeded 3 percent. When the variability for the data reported by a particular station is too high, the implication is that the cause lies with some aspect of the ground-based system and marks the station as one that might be omitted from more detailed comparisons.

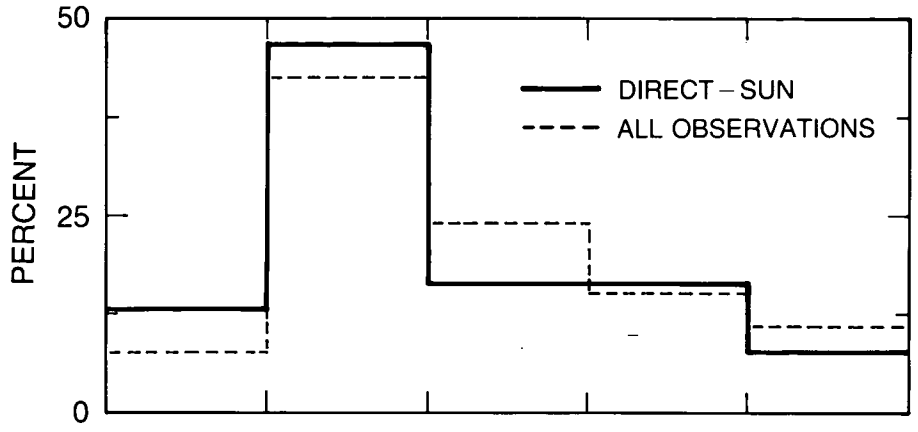

Figure 4.8 Fractional distribution of 92 stations according to the relative variability (σ in percent of the total ozone at a given station) of their monthly mean differences with TOMS. The solid curve indicates direct Sun and the dotted curve indicates all observations.

Table 4.9 Stations With Variability of Their Monthly Mean Differences With TOMS ≥3 Percent.

Station	Dobsons
Brindisi*	16.1
South Pole	8.0
Casablanca	6.6
Aarhus	5.1
Macquarie Island	4.7
Bangkok	3.7
Brisbane	3.6
Hobart	3.5
Churchill	3.5
Bracknell	3.3
Lerwick	3.2
Singapore	3.1
Resolute	3.0
Station	**Dobsons**
Dikson Island*	6.9
Heiss Island*	5.9
Nagaevo	5.2
Vladivostok	5.2
Riga	4.2
Murmansk	3.5
Odessa	3.4
Yakutsk	3.4
Kiev	3.3
Irkutsk	3.2
Maputo	3.1
Alma Ata	3.0
Sakhalin	3.0

*Limited data

4.3.1.2 Comparison of Individual Station Data With TOMS Overpass Data

A major advantage of the satellite–ground intercomparison is its identification of abrupt changes in the calibration of an individual groundstation, with the continued stable satellite–ground relationship for the rest of the network as evidence that the change should be attributed to some event at the groundstation. The intercomparison between the ODW data for Huancayo and the satellite shows an abrupt downward shift in late 1982 (Figure 4.9) that is directly traceable to recalibration of the Huancayo Dobson in October 1982. The satellite intercomparison serves as a warning to outside users that the data published in ODW are not suitable for trend analysis without reevaluation to adjust for the recalibration. Other examples of apparent calibration shifts are the changes in the satellite–ground responses for Bracknell (Figure 4.10), Singapore (Figure 4.11), and Brisbane (Figure 4.12).

By contrast, an example of great consistency in the overpasses between the ground-based readings and the corrected TOMS data set is shown in Figure 4.13 for the Shiangher station near Beijing. The data illustrate that a well-run Dobson station and an overhead satellite can provide a combined data set that creates confidence in the operation of both measurement systems. The smoothness and consistency of the observations at this station (σ of the 84 monthly differences is only 0.7 percent) will become more apparent after discussion of a few more of the less successful stations.

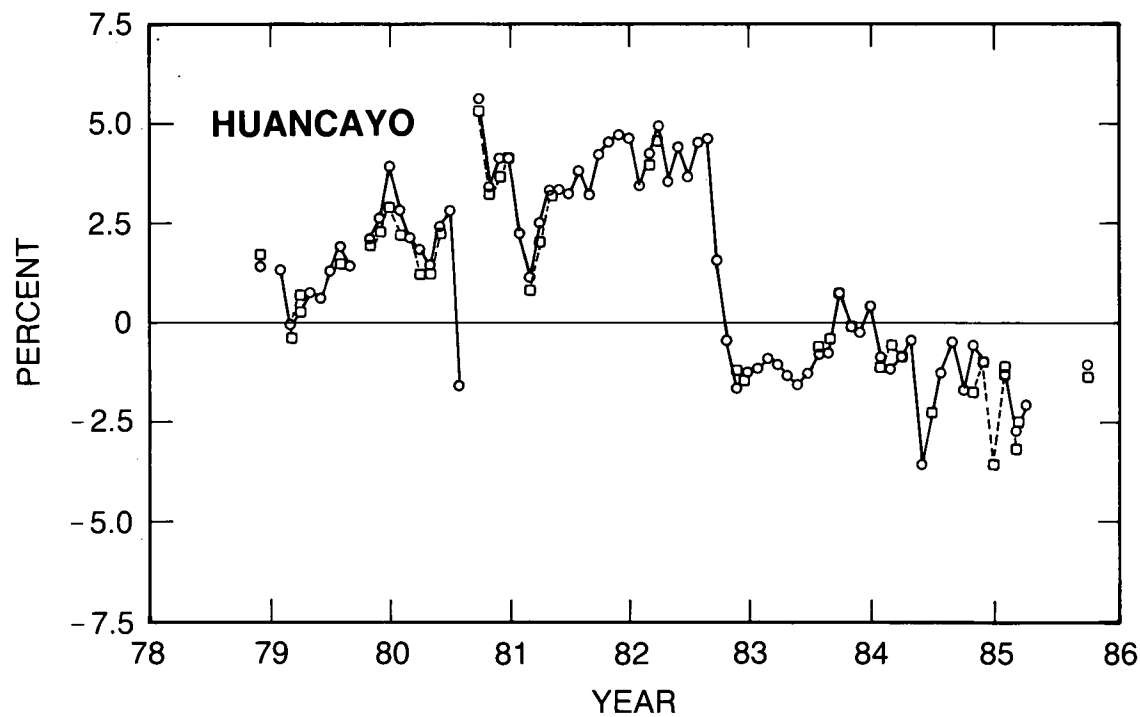

Figure 4.9 Monthly differences between ozone measured at Huancayo and by TOMS (BR is bias removed), showing a slow upward drift during the first 4 years and a sharp decline in October 1982 (result of calibration). The σ of the differences forming each monthly point is about 2.6 percent. The circles and the solid curves indicate direct-Sun observation, and the pluses and the dashed curves indicate all observations. A point is plotted only if there are at least 13 overpasses for the particular month. The record starts with November 1978.

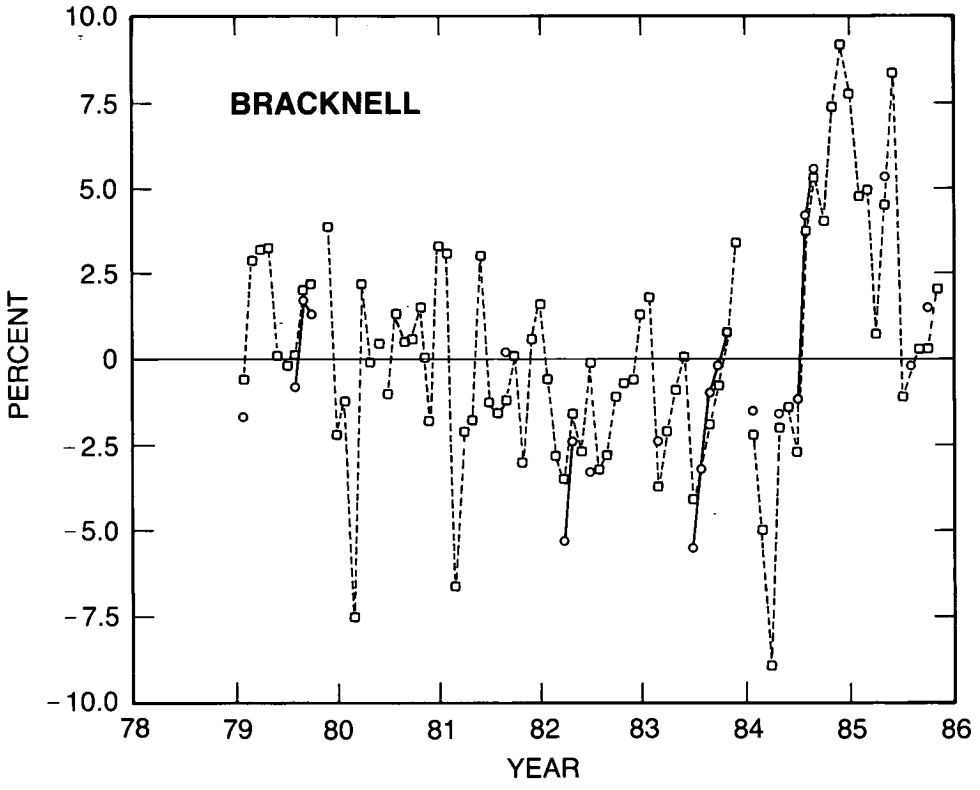

Figure 4.10 Monthly (Dobson–TOMS)/Dobson differences for Bracknell indicating a downward rift between 1981 and 1984, followed by a sudden upward shift. The σ of the differences forming each monthly point is about 5.6 percent and is among the largest in the network. The circles and the solid curves indicate direct-Sun observations, and the pluses and the dashed curves indicate all observations.

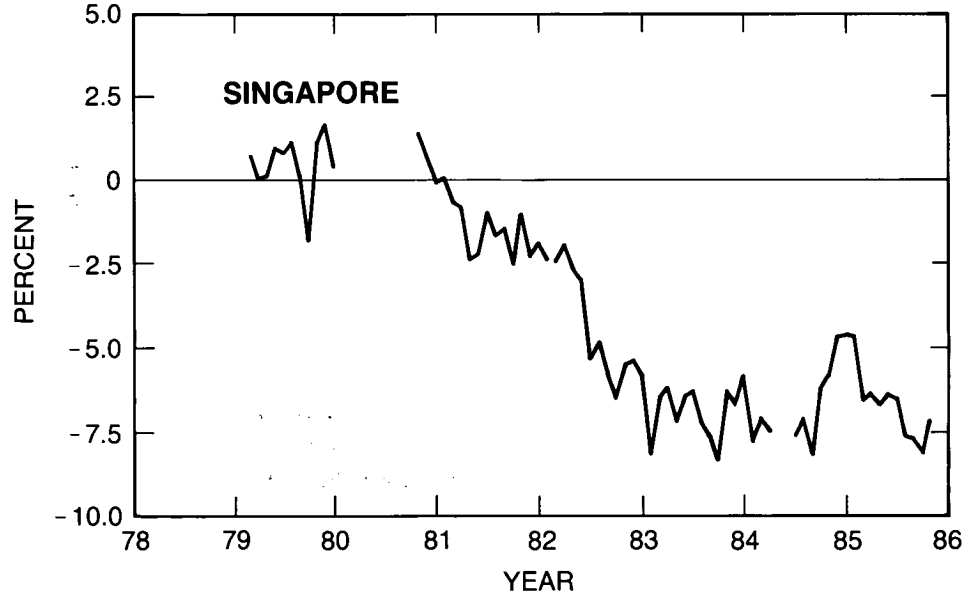

Figure 4.11 Monthly (Dobson–TOMS)/Dobson differences for Singapore showing a strong downward drift between 1980–1983, when, as a result of calibration, the instrument is stabilized but at a level about 7 percent too low. The σ of the differences forming each monthly point is about 2.4 percent. The circles and the solid curves indicate direct-Sun observations.

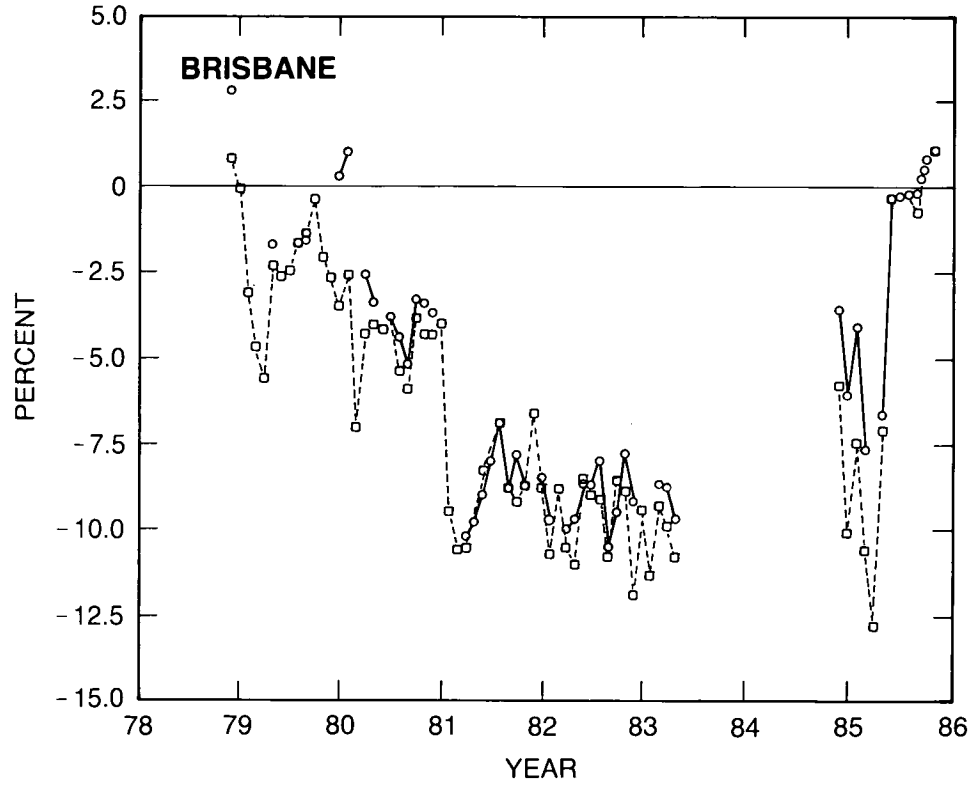

Figure 4.12 Monthly (Dobson–TOMS)/Dobson differences for Brisbane showing a downward drift until the end of 1980, followed by a sudden drop of about 5 percent. Only after calibration in early 1985 is the instrument restored to a state of agreement with the rest of the ozone network. The σ of the differences forming each monthly point is about 4.5 percent. The circles and the solid curves indicate direct-Sun observations, and the pluses and the dashed lines indicate all observations.

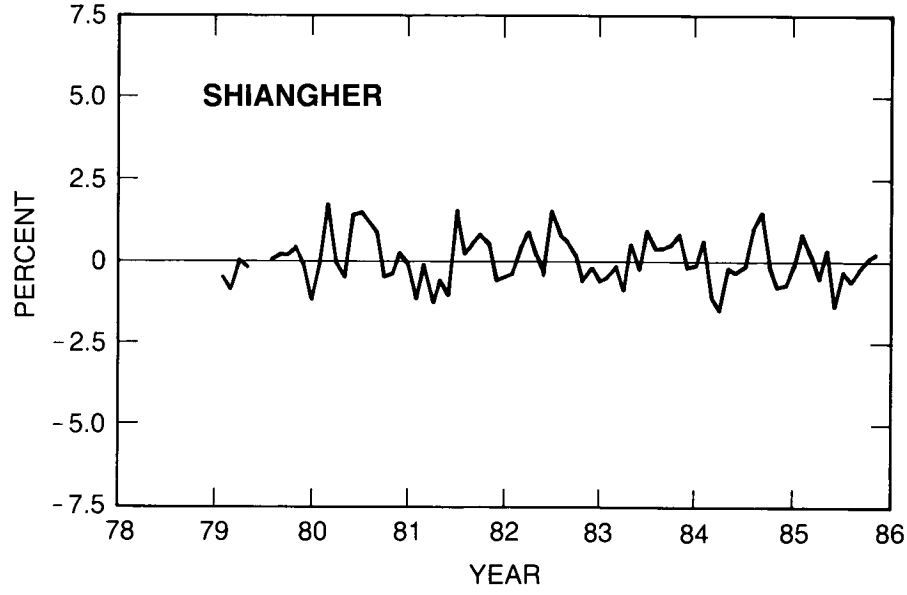

Figure 4.13 Monthly (Dobson–TOMS)/Dobson differences for Shiangher (near Beijing). The σ of the differences forming each monthly point is about 2.1 percent. The circles and the solid curves indicate direct-Sun observations.

One very common problem that appears in many stations is the strong μ-dependence of the instruments—i.e., an apparent ozone reading that is affected by the slant angle of the Sun at the time of measurement. This results in reported ozone values that are too low at high Sun during the summer months (June and July) and too high at low Sun (November–January) in the Northern Hemisphere. A good example of this problem is shown in the data from Potsdam (Figure 4.14), for which the December–January periods tend to show strong positive deviations. This data set also shows a shift in the overall comparison from mostly negative during 1979–1982 to mostly positive after 1983. Such a shift usually signifies a calibration problem, as could occur with a step-function recalibration in September 1982. The μ-dependence continues after the step function shift.

Another station whose data show a pronounced μ-dependence is Hobart, Tasmania (Figure 4.15). The deviations at Hobart are often strongly negative, corresponding to ozone readings lower by 30 or 40 DU than indicated from the satellite instrument. Identification of a strong μ-dependence from comparison with TOMS calls for a review of the extraterrestrial constant values used at the particular station. Appropriate corrections can be made to the station record given the existence and availability of an exact history of calibrations verifying the events, as is the case for Hohenpeissenberg. The top panel of Figure 4.16 shows the monthly differences for the originally published monthly ozone values: a seasonal variation is apparent. This μ-dependence is primarily an extraterrestrial-constant-related error, indicating incorrect calculation of the ΔN correction to the N-tables (see Dobson, 1957a, 1957b), and it was most probably introduced to the instrument through improper adjustments made during intercomparisons at Arosa in August 1977. This was not corrected until early 1985. When the μ-dependent variations were removed from the published record and calibration corrections for the period March 1985–August 1986 were introduced, the differences with TOMS overpasses

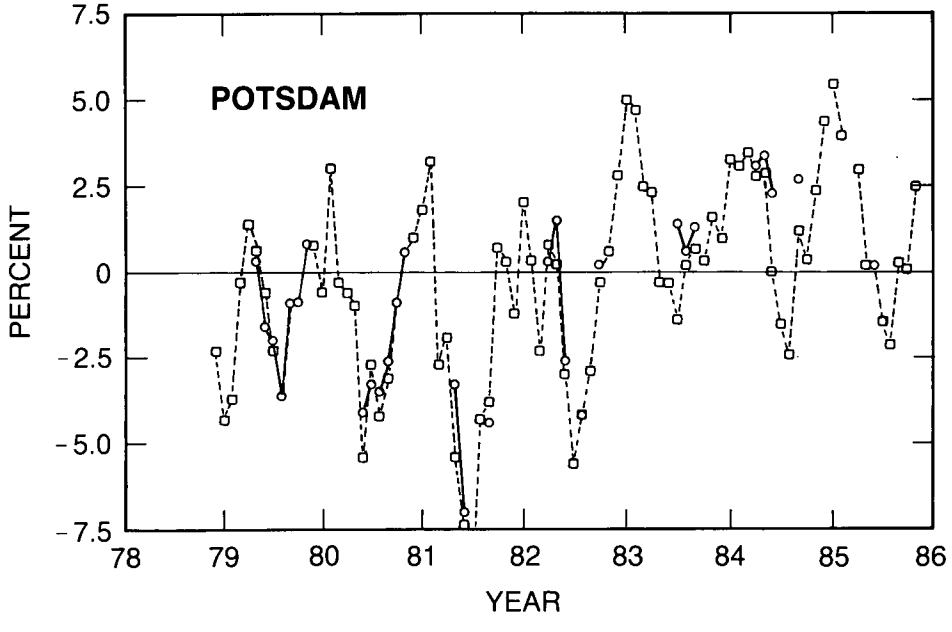

Figure 4.14 Monthly (Dobson–TOMS)/Dobson differences for Potsdam indicating a μ dependence as well as a shifting (in 1982–1983) of the level of ozone measured by the groundstation. The σ of the differences forming each monthly point is about 4.2 percent. The circles and the solid curves indicate direct-Sun observations, and the pluses and the dashed lines indicate all observations.

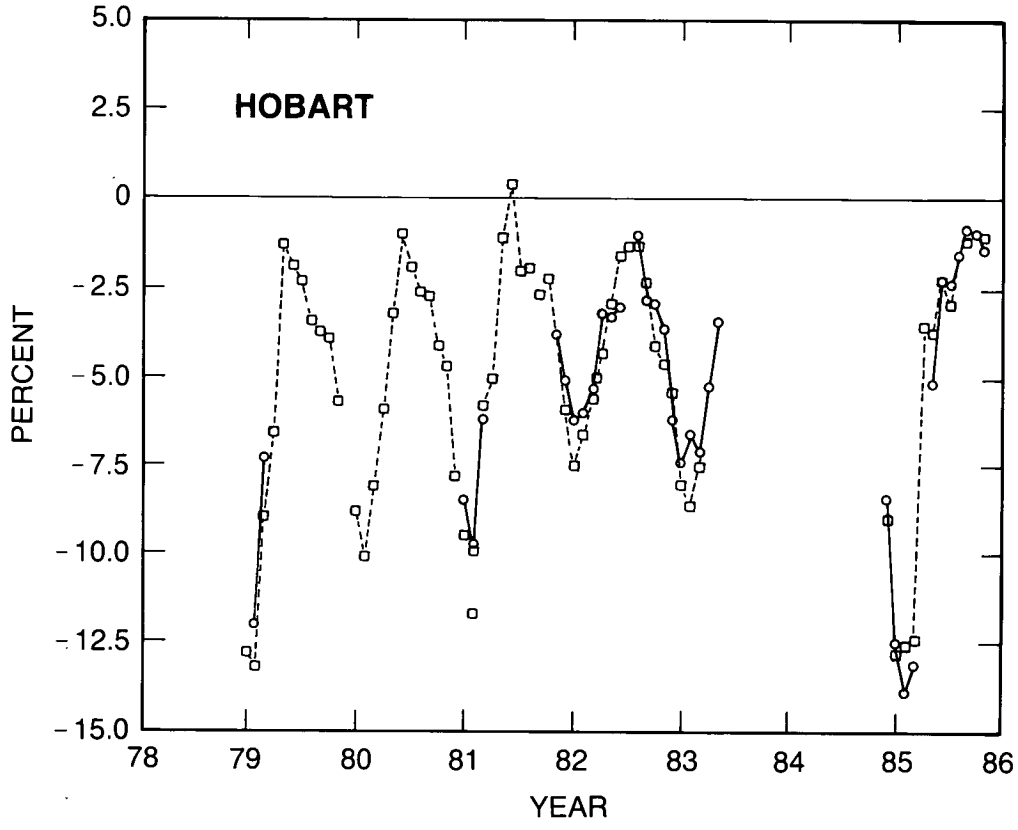

Figure 4.15 Monthly (Dobson–TOMS)/Dobson differences for Hobart showing an extremely large μ dependence and an erroneously low ozone level for the entire period of comparison. The σ of the differences forming each monthly point is about 4.7 percent. The circles and the solid curves indicate direct-Sun observations, and the pluses and the dashed lines indicate all observations.

(shown in the bottom panel of Figure 4.16) indicate a very stable record. There is a mean bias of about 2.5 percent, and this difference would probably be reduced to about 1.5 percent if a more accurate altitude correction were applied to the TOMS data to suit the elevated location of Hohenpeissenberg.

Discrepancies in a station record caused, for example, by difficulties with the transfer of zenith-sky observations (taken at very low Sun) to direct-Sun values, appear on Figure 4.17, which records the data from Churchill, Canada. For most of the year, this station shows a good ozone record having constant level differences (~2.3 percent with TOMS). However, December and January values are low by about 7 percent and 5 percent, respectively. The probable problem here is that direct-Sun observations are rarely possible in these months because of virtually constant cloudy conditions, while the zenith sky transfer charts used at Churchill were not calculated from observations made at that station.

Many more illustrative examples can be given by looking at the scatter diagrams of the daily differences with TOMS overpasses. Some of the greatest scattering is shown by Aarhus (Figure 4.18), Casablanca, and Bracknell. The σ of the differences forming each monthly point, based on the average from the annual samples for each of these stations, are 9.1 percent, 10.8 percent, and 5.6 percent, respectively. The readings from Aarhus are noteworthy not only for the very large

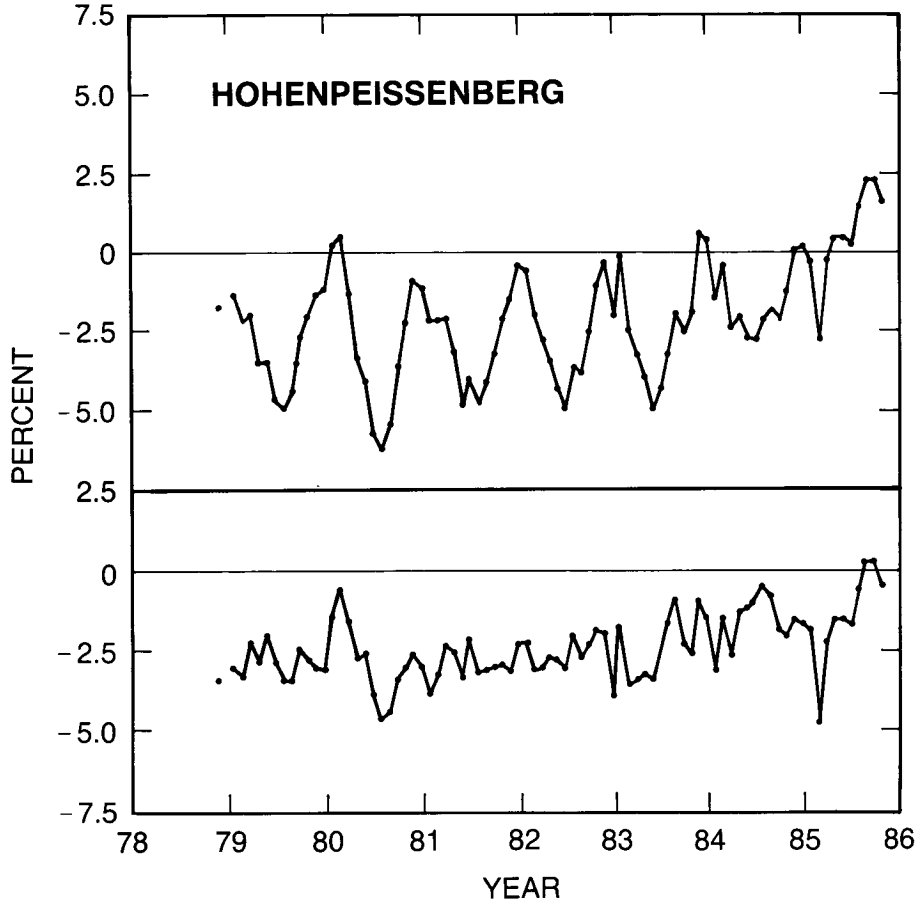

Figure 4.16 Monthly (Dobson–TOMS)/Dobson differences for Hohenpeissenberg. The top panel indicates a well-pronounced μ dependence until 1985. The bottom panel shows the same monthly differences after removal of the μ-dependent variations and application of the instrument calibration procedures, indicating a very stable course, except too low by about 2.5 percent. This difference would be reduced by about 1 percent if an altitude correction is applied to the TOMS data. The σ of the differences forming each monthly point is about 2.8 percent, and is among the smallest in the network. The circles and the solid curves indicate direct-Sun observations.

scatter versus the satellite data but also because not a single reading in the entire set represents a direct-Sun observation. Comparison of the ozone readings from Aarhus with those from nearby stations that might be expected to be in a similar meteorological regime also shows a very wide scatter. The data from Aarhus recorded in ODW have not been used either in the subsequent analysis of individual stations or in the compilation of latitudinal band averages.

At other stations, one can easily distinguish problems with zenith-sky observations. For example, the direct-Sun ozone observations from Toronto (Figure 4.19) agree well with the satellite observations, while its zenith-sky values are almost all high, with an average deviation from the direct-Sun values of +10 percent. The σ of the differences forming each monthly point is only ~2.2 percent for direct Sun but increases to a high of 4.6 percent when all observations are considered, as is usually done with the other stations. The likely explanation for such inconsistency between zenith-sky and direct-Sun observations is that the empirical zenith sky chart for Toronto is faulty.

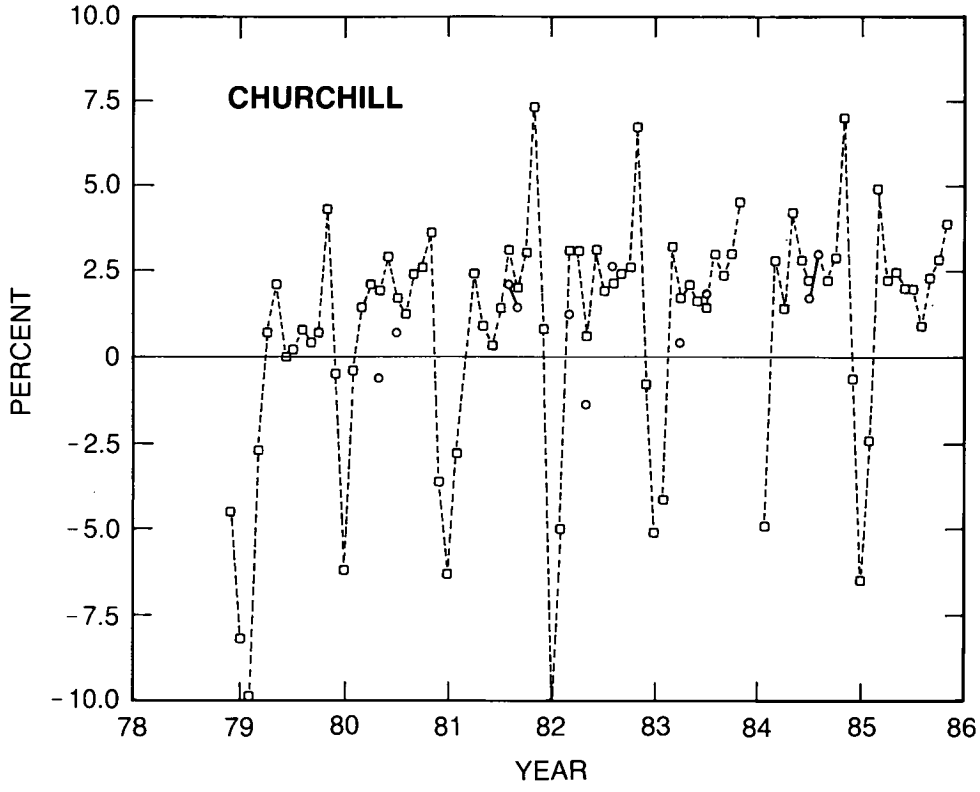

Figure 4.17 Monthly (Dobson–TOMS)/Dobson differences for Churchill indicating a constant difference of about 2.3 percent during most months, except for the winter (December and January are too low by about 7 and 5 percent, respectively). The σ of the differences forming each monthly point is about 5.1 percent. The circles and the solid curves indicate direct-Sun observations, and the pluses and the dashed lines indicate all observations.

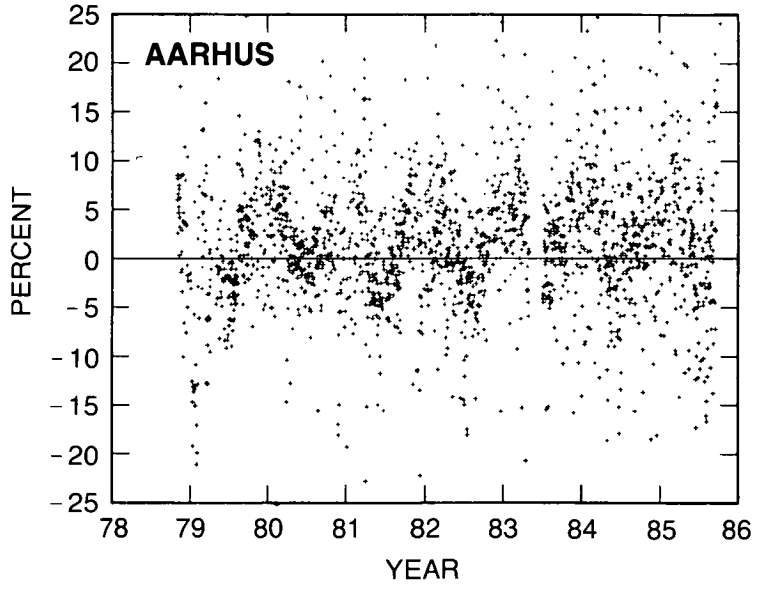

Figure 4.18 Daily differences for Aarhus indicating extremely great scattering. The σ of the difference forming the monthly points (not plotted) is about 9.1 percent, the second largest in the network.

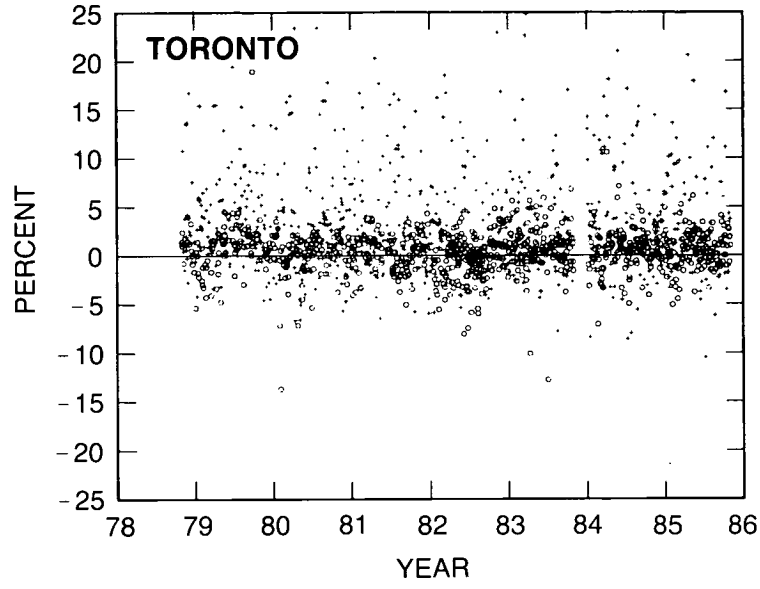

Figure 4.19 Daily differences for Toronto indicating stable direct-Sun readings (the σ of the differences of the monthly values is only about 2.2 percent) and very great scattering of the zenith-sky readings. The σ of the differences forming the monthly points from all observations (not plotted) is about 4.6 percent. The circles indicate direct-Sun observations, and the pluses show all other measurements.

4.3.2 The Station-Corrected Total Ozone Data From Belsk, Poland

The procedures for reporting data to ODW were described in Section 4.1.1.5. The pertinent points for this discussion are

- The authority and onus to report recalibrations and their effect on previous data are on the individual stations and not on ODW.
- Individual stations quite frequently are not staffed with enough trained manpower to carry out any retrospective data evaluation and correction.

The Dobson spectrophotometers are intended to be checked at least monthly with lamp tests, monitoring the instrumental spectral sensitivity response to a standardized exposure to UV radiation. The monthly lamp tests can indicate constancy, or a change in the wavelength selection by the instrumental slits. However, sometimes the monthly lamp tests provide information pointing either to an abrupt step change or to a steady ramp change in instrument response to the UV test. In addition, the individual Dobson instruments are occasionally recalibrated by direct comparison at a common location with either the world primary standard or with one of the secondary standards. The usual procedure after calibration is the immediate installation of the new calibration values. There should also be a retrospective reevaluation of any earlier data—including the measurements made according to the old calibration scale only a short time beforehand. In practice, such reevaluations are rarely performed, and unreported retrospective consideration of the data does not appear to be much more frequent.

In the ideal case, the complete station records are thoroughly investigated by the station itself following recalibration, and a revised data set is produced with the revisions made on a

reading-by-reading basis—i.e., each daily measurement is corrected, and the monthly average is then recalculated. Such a procedure was performed by the personnel of the Dobson station at Belsk, Poland, for the data up to the end of 1981 (Dziewulska–Losiowa et al., 1983), and the revised data set was published in ODW. However, in general, such revisions have not been published and, in most instances, not performed. Currently, detailed reviews are known to be in process in Potsdam, Hohenpeissenberg, Sapporo, Tateno, Kagoshima, some of the Australian stations (Atkinson, 1988), Invercargill (Farkas, 1988), some of the U.S. stations (Komhyr, 1988), and some Indian stations (Andreji, 1988). As stations complete such retrospective analyses, their revised data sets will be published in ODW and will be available for statistical trend analysis. Until such reevaluations have been made, we have constructed provisionally revised ozone data for a substantial number of stations using external techniques for determining the times during which calibration problems may have occurred. Before describing further the procedures used for these provisional revisions, we shall discuss the revaluation of ozone data as carried out at Belsk.

Figures 4.20 and 4.21 show, respectively, the "revised" Belsk ozone data as published in ODW (solid line) and the "old" ozone data set from Belsk, also published earlier in ODW. Substantial differences exist between them, and the statistically calculated trends changed from positive to negative with the revision. Finally, a procedure is described in the next section for making a "fast" correction to an ozone data set in need of retroactive adjustment because of recalibrations. The "fast" method can be contrasted with the preferred, but much more labor intensive, "slow" method of day-by-day, ozone-reading-by-reading recalculation of the data by the station personnel carried out at Belsk (Dziewulska–Losiowa et al., 1983). The ozone data for the fast and slow methods are compared in Figure 4.20. While the agreement between the two methods is not complete, the fast corrections provide a very much closer approximation to the best available revised Belsk data than does the uncorrected old data set from earlier editions of ODW.

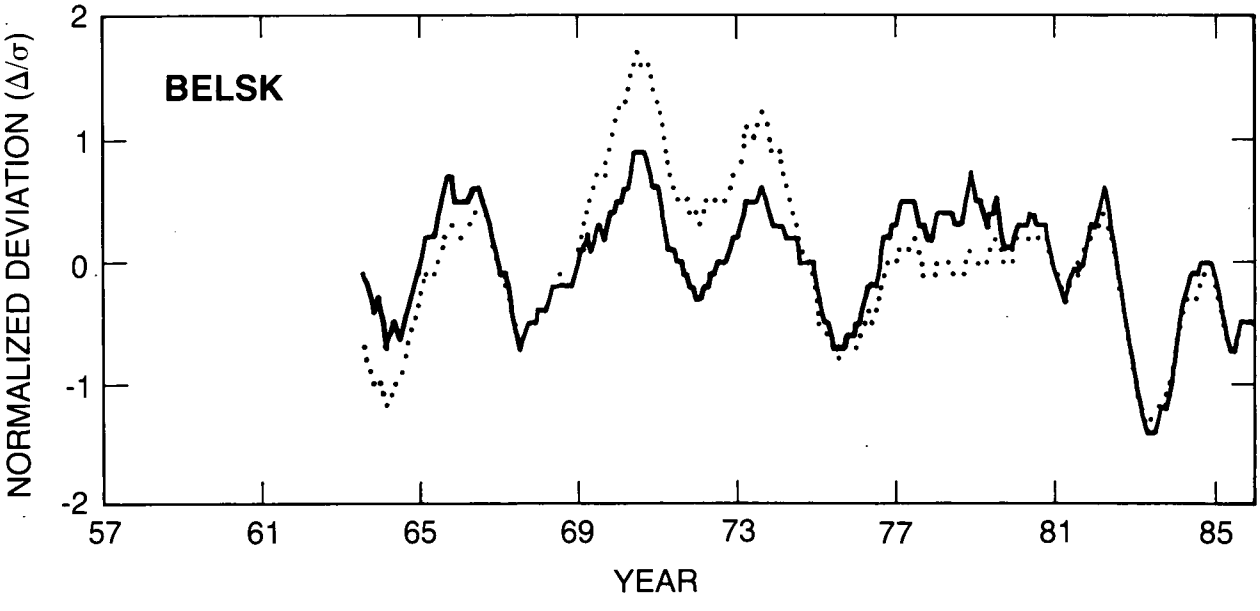

Figure 4.20 Comparison of the Belsk station-revised ozone data (—) and the "fast" revised record (. . .), including corrections found during the August 1986 intercomparisons. The data are plotted as monthly deviations that have been normalized and smoothed by taking the 12-month running mean.

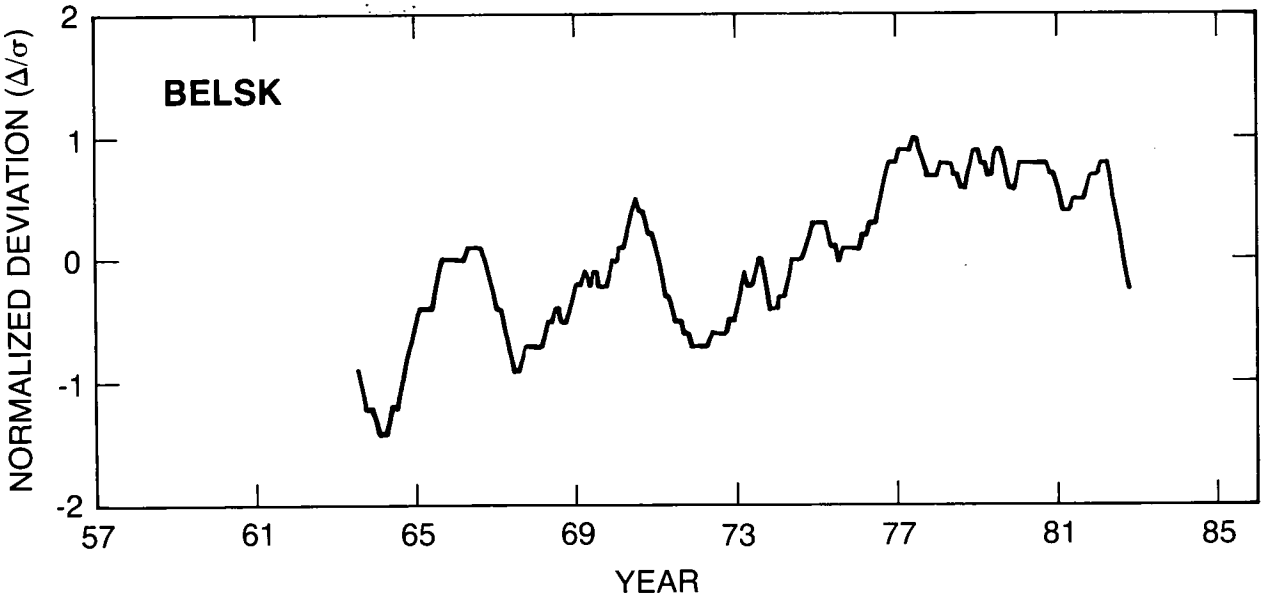

Figure 4.21 The Belsk total ozone record as it was originally published in *Ozone Data for the World.* The data are plotted as normalized monthly ozone deviations that have been smoothed.

The ozone data have been corrected in the fast method through calculation of the changes induced by recalibrations, using monthly average corrections applied to the monthly ozone averages. The times and magnitudes of the various recalibrations have all been identified by Belsk station personnel from their records, permitting ready revision of the old monthly ozone data. Application of the fast revision to data from other stations is likewise dependent upon the timing and magnitude of all recalibrations for changes in the sensitivity of the Dobson instrument; several techniques for identifying the approximate time intervals during which such calibrations probably occurred are also described below. It is worth restating that the best method of revision is the day-by-day, reading-by-reading reevaluation as carried out at Belsk. However, pending such revisions by the slow method at the individual stations, we have produced provisionally revised data sets for more than 20 Dobson stations by the fast technique. The provisionally revised data for Belsk using the fast technique were calculated for comparison purposes only and have not been used for statistical trend analysis.

4.3.3 DETECTION OF UNRECORDED DOBSON RECALIBRATIONS

4.3.3.1 Comparison of Data From Proximate Stations

The general technique for reevaluating data from a Dobson station begins with the identification of time periods during which calibration shifts have occurred. The satellite–ground intercomparison has been useful since November 1978, when Nimbus–7 data first became available. Two approaches that can be used for identifying possible calibration shifts prior to November 1978 are comparison of ozone readings from two or more nearby groundstations that are in similar synoptic scale meteorological regimes and comparisons for middle- and high-latitude stations with the local 100-millibar temperature readings.

When the 12-month running means of two nearby, well-run stations are compared, the curves should parallel each other closely, although often with a constant ozone differential. Conversely, a sudden change in the relative position of the curves is an indication that the measurements of one of the stations (or, very unlikely, of both at the same time) have gone awry, so that the detailed monthly calibrations for the two stations should be examined carefully. An excellent example of the information available from intercomparisons of two stations is given by the ozone data from two Indian stations, New Delhi and Varanasi (Figure 4.22). The patterns of the 12-month running means agree well with each other from 1977–1986 (including the entire period covered by Nimbus–7 TOMS), with the New Delhi instrument registering about 15 DU more than Varanasi. However, the earlier period, between 1969–1977, exhibited a very different pattern between the stations, with the New Delhi–Varanasi difference about -15 DU rather than +15 DU. This shift of 30 DU, or about 10 percent, appears to occur between 1973 and 1977, and is strongly suggestive of a large calibration change in one or both instruments.

The published data from Tateno and Kagoshima are compared in Figure 4.23, and two obvious features are present. First, there is a major disagreement between the two stations around 1961, with Kagoshima recording appreciably lower relative values than Tateno. No information was available concerning this discrepancy in the Kagoshima record, and so the early measurements have been excluded in the provisionally revised data. Second, there is an excellent correlation between the two since 1977. For the rest of the time, the short-term variations in the records are similar, although the relative levels may be changing by small amounts. For instance, from around 1970 to 1977, Kagoshima is slightly higher relative to Tateno than it is in the rest of the record, and around 1969 it is slightly lower. These last two observations do not lead to the conclusion that either instrument was incorrectly calibrated in these two periods, but they do suggest that it is worth checking the records for such a case.

In Figure 4.24, the Potsdam ozone data are compared with the revised Belsk data. Again, there is good agreement since 1977. Earlier in the record, Potsdam is first higher than Belsk (1966–1969), then lower (1969–1977). The Potsdam data have subsequently been corrected by the station staff, although the data were not available for this study.

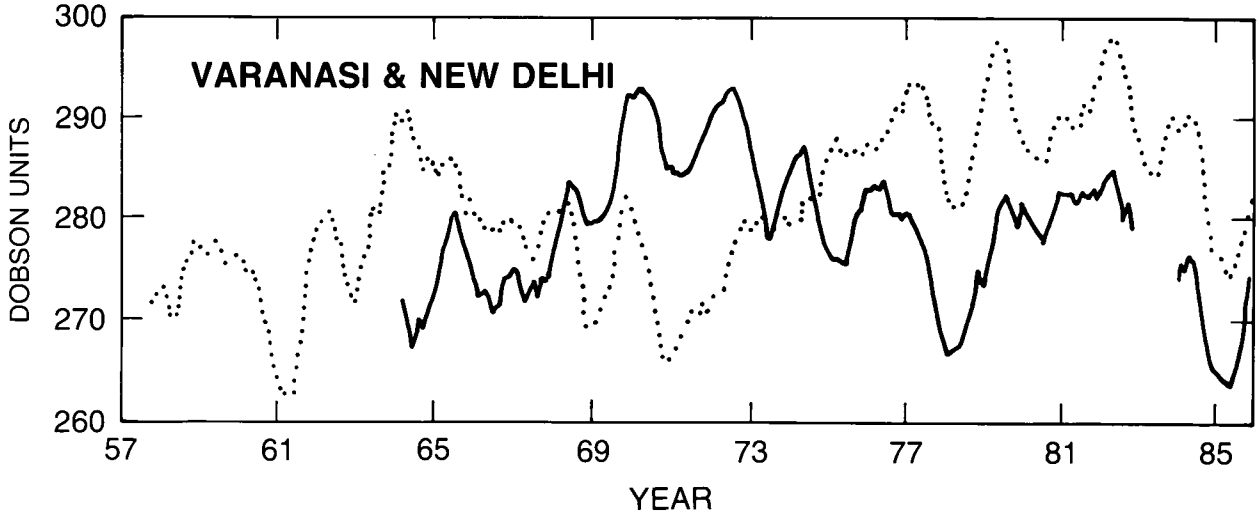

Figure 4.22 The 12-month running means of the total ozone measurements taken at Varanasi (—) and New Delhi (. . .) and that are recorded in *Ozone Data for the World.*

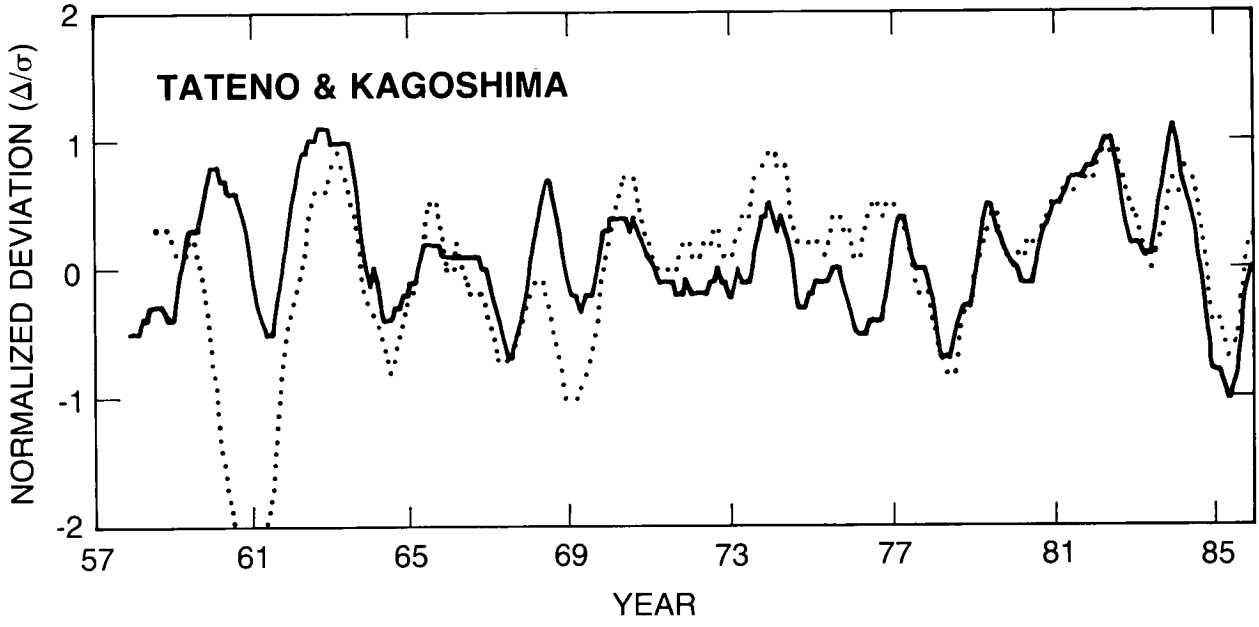

Figure 4.23 The monthly total ozone deviations (a smooth plot of the actual deviation divided by the particular month's interannual standard deviation) for Tateno (—) and Kagoshima (. . .) that are recorded in *ODW*.

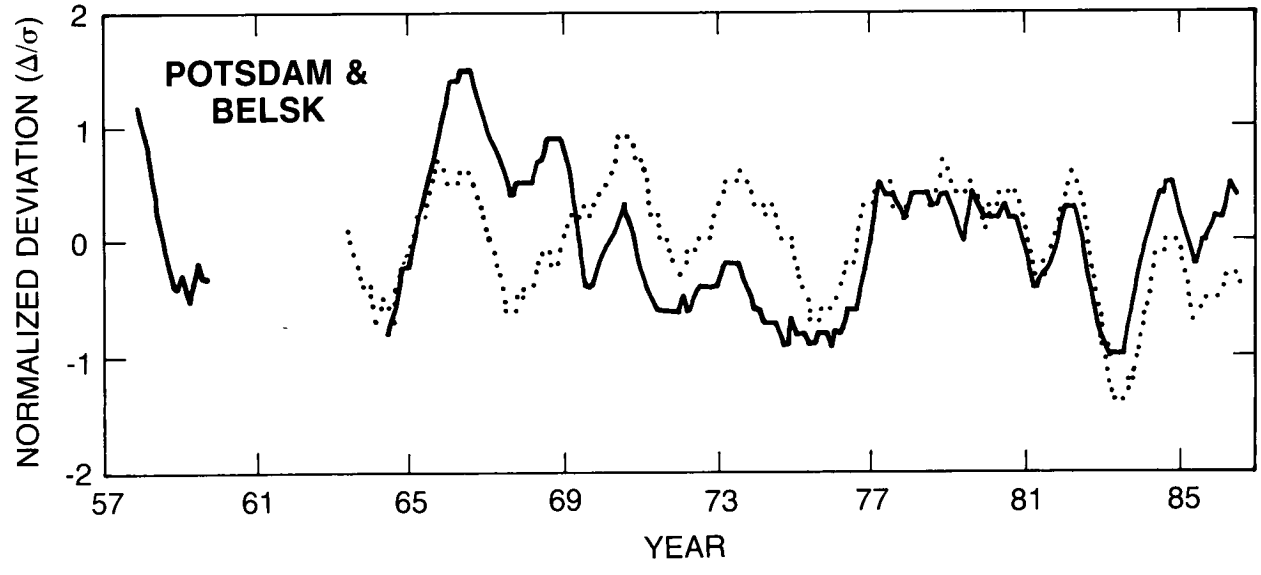

Figure 4.24 The monthly total ozone deviations (as in Figure 4.23) for Potsdam (—) and Belsk (. . .). The Potsdam data are taken from *ODW*, and the Belsk data are the station-corrected set that was also published in *ODW* and that replaced the original values reported to *ODW*.

4.3.3.2 Comparison of Total Ozone Data With 100 mbar Temperatures

The existence of a strong positive correlation between total ozone and stratospheric temperatures has been known for half a century (Meetham, 1936). Aspects of the complex physical relationships have been recently discussed by Rood and Douglass (1985) and by Douglass et al. (1985). The basic hypotheses are that warm air advection in the middle stratosphere should be associated with a positive ozone advection, and cold air advection should be accompanied by a negative ozone advection. Moreover, ascent of air causes a decrease in both ozone and temperature, while descent increases both. This picture is oversimplified: for example, the seasonal cycles of temperature and ozone are not in phase because of their different responses to the radiation balance. However, their responses to transport by the general circulation are similar. For example, at the time of Northern Hemisphere minimum stratospheric temperatures (in January), the general circulation supplies heat to the polar areas to balance the radiative cooling. This energy-balancing process is accompanied by an ozone transfer, resulting in an increase of total ozone. Sudden winter stratospheric warmings, whether caused by advection or subsidence, are accompanied by rapid increases in total ozone. The use of 100 mbar temperatures as an indicator of the course of total ozone is justified because the 100 mbar ozone and total ozone are so well correlated. When available, the 50 mbar temperatures were used as supplementary data. The effect of the differing seasonal cycles of temperature and total ozone is removed by deseasonalization of the two time series. (The correlations between total ozone and 100 mbar temperatures are never used for actual adjustment of ozone values; they serve merely as one of the diagnostic procedures used for discovery of possible unreported ozone recalibrations.)

The various versions of the Belsk ozone data are compared against the 100 mbar temperatures in Figures 4.25 to 4.27. In Figure 4.25, the 100 mbar temperatures are plotted against the old Belsk data prior to any revision, and without any corrections. Figure 4.26 contains the old data revised through 1981 plus the data recorded since 1981, all corrected by the fast method based on

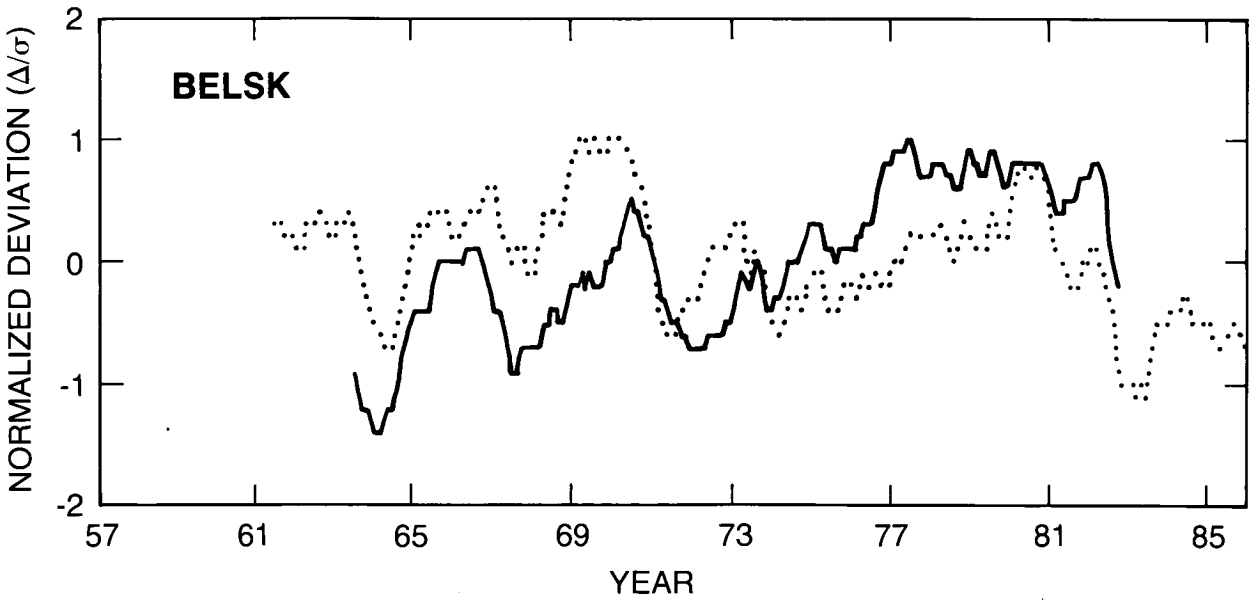

Figure 4.25 The monthly deviations (as in Figure 4.23) for the originally published Belsk total ozone record (—) and for the 100 mb temperature (. . .).

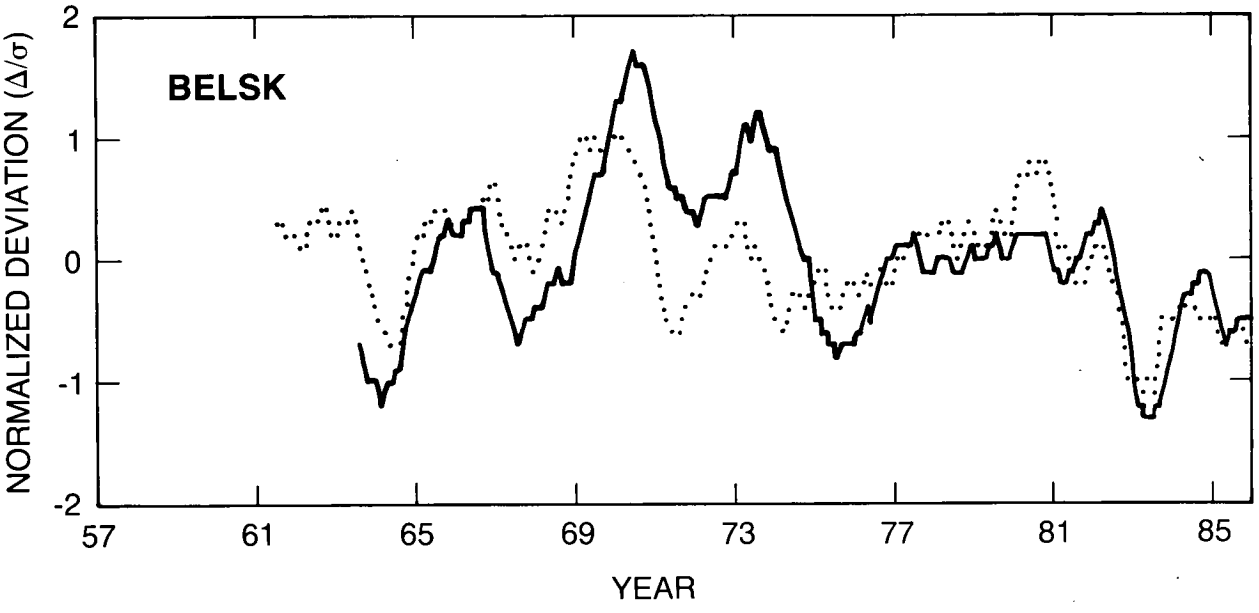

Figure 4.26 The monthly deviations (as in Figure 4.23) for the fast-revised Belsk total ozone record (—) and for the 100 mb temperature (. . .).

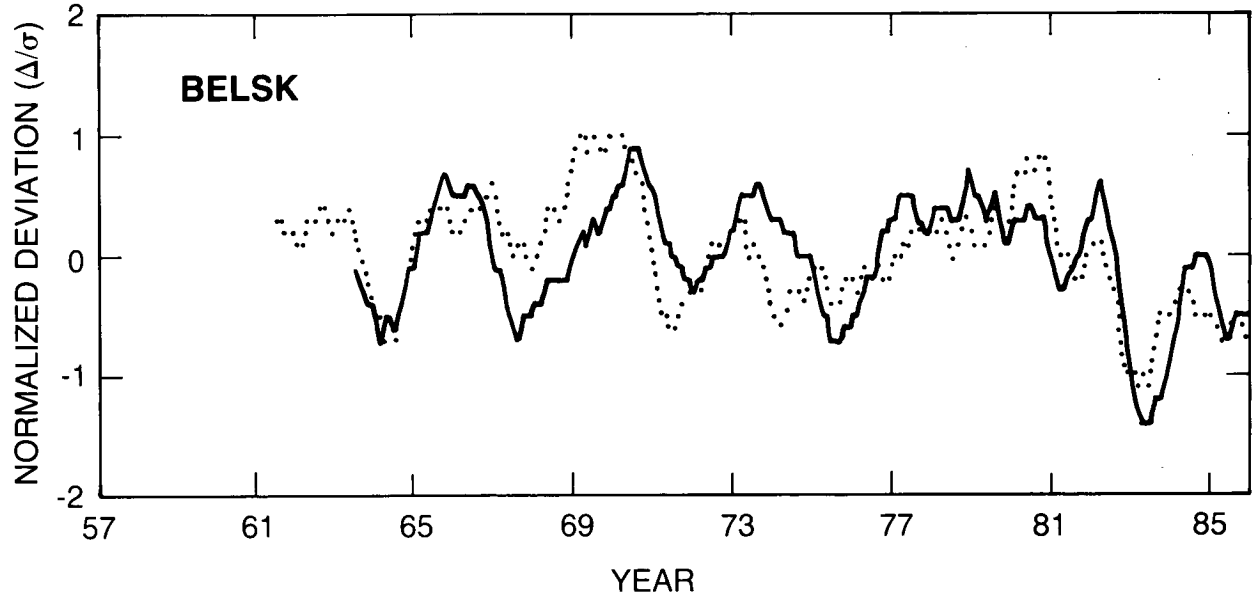

Figure 4.27 The monthly deviations (as in Figure 4.23) for the station-revised Belsk total ozone record (—) and for the 100 mb temperature (. . .). Since the station has, to date, revised the data only through December 1981, a provisional adjustment has been applied to the more recent data published in *ODW*.

monthly averages. Figure 4.27 shows the correlation between the current best revised set of Belsk data and the 100 mbar temperatures. The station-corrected data have been used to the end of 1981 in Figure 4.27 but, after 1981, a small fast correction has been made for a calibration error that was found at the international comparison at Arosa. This calibration change occurred after the major reevaluation of the Belsk data, and further post-1981 day-by-day revisions have not yet

been reported from Belsk. The agreement between total ozone and 100 mbar temperatures found in such comparisons furnishes the basis for raising questions about the ozone record at other stations for which the two data records diverge.

Figure 4.28 contains the ozone and 100 mbar temperatures for Churchill. The upper panel contains the published Churchill data and the lower one contains the provisionally revised Churchill data. It can be seen that only minor changes have been made. However, around 1981, when the published ozone deviations were high compared to the temperature deviations, a small adjustment can be seen to have been made, with the result that the two series lie closer together. However, there is still a period, roughly from 1969 to 1973, during which the ozone is running higher. This, again, is a period for which a further check of station records is desirable.

Figure 4.29 contains the provisionally revised Bismarck ozone data plotted against the 100 mbar temperature. Relatively low ozone values were observed in 1983 at Belsk, Churchill, and

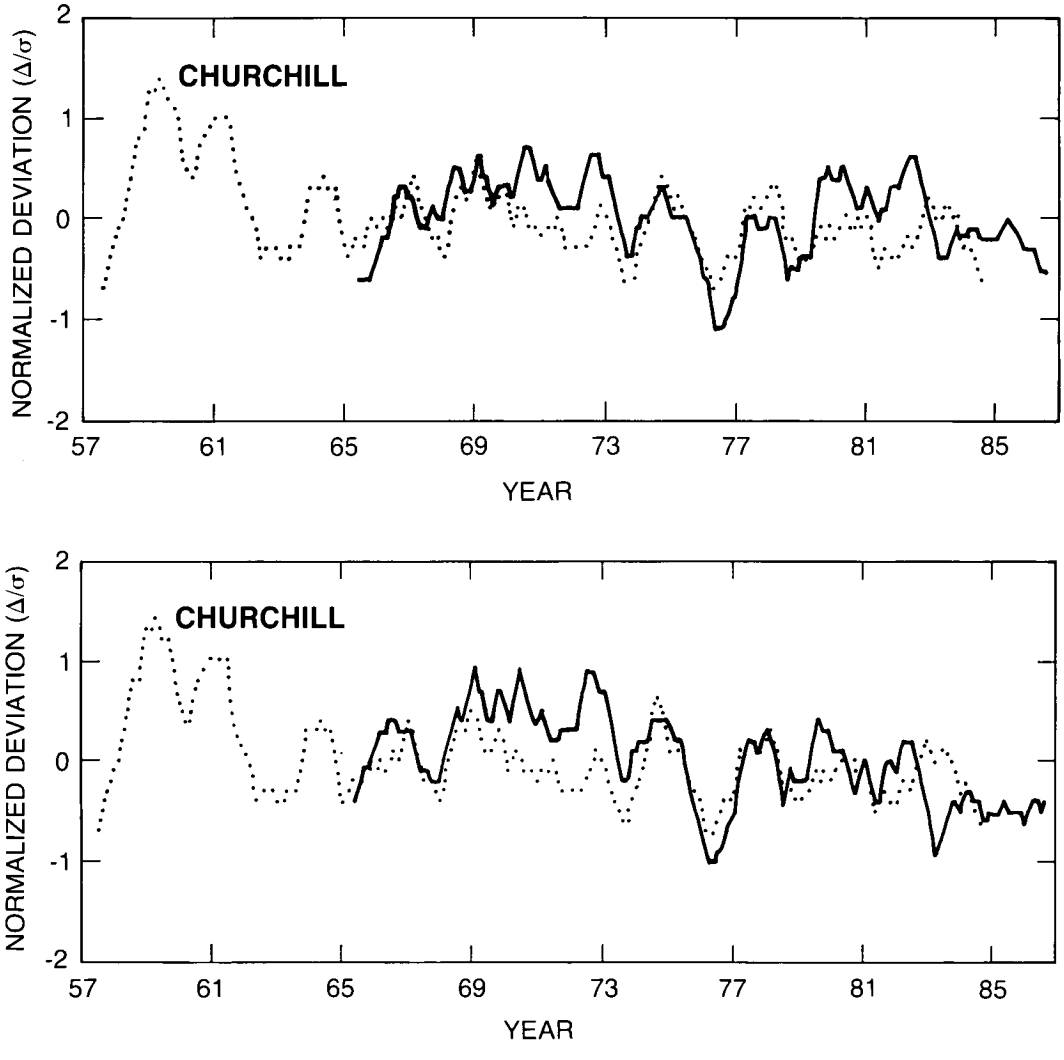

Figure 4.28 The monthly deviations (as in Figure 4.23) of the 100 mb temperature (. . .) are plotted against the total ozone data (—) from Churchill. In the upper panel, the ozone values published in *ODW* are shown, and in the lower panel the provisionally revised total ozone data set is plotted.

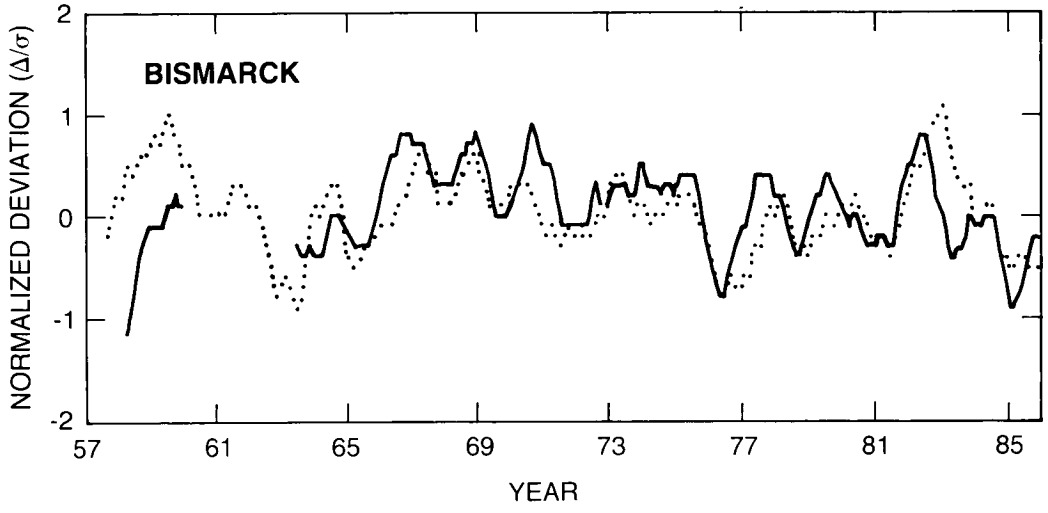

Figure 4.29 The provisionally revised total ozone data (—) and the 100 mb temperatures (. . .) for Bismarck are plotted.

Bismarck, reflecting the low northern midlatitude total ozone values of that year. The 100 mbar temperatures at Churchill and Bismarck do not exhibit the same abnormal decline as the ozone, as might be expected by analogy with the historical correlation.

4.3.4 Provisionally Revised Ozone Data Sets for Individual Stations

In the current study, the total ozone values published in ODW were examined for incongruities. The identification of problematic time periods in individual station records using the diagnostics described in the previous sections furnishes a basis for concern about the data published in ODW, but does not provide a basis for correction of such data. In many instances, however, the calibration records maintained by the individual stations but not always reported to ODW show clearly when a shift has occurred—e.g., the Huancayo data of Figure 4.9. With the additional information provided by these records of calibration changes, a revised set of total ozone data can be constructed for each station, eliminating the effects of sudden calibration shifts. The provisional revision in this report (Bojkov, private communication, 1987) applied each recalibration factor to the monthly data back to when the previous calibration took place, implicitly assuming that the changes took place abruptly. Sets of provisionally revised data for the 25 stations listed in Table 4.10 are given in Appendix 4.A(i) of this chapter. These tables are labeled "provisionally revised" (Bojkov, private communication, 1987).

Two procedures were used to handle a lack of daily measurements:

- If there was a day for which no value was recorded in ODW, but there were readings made on the days before and the days after, then an average value was inserted for the missing day.

- At least 13 daily values had to be available within the month for a legitimate monthly mean to be calculated.

Table 4.10 Provisionally Revised Station Data Used in the Time Series Analyses.

Arosa[1]	1/57–12/86
Aspendale	7/57–12/86
Belsk	1/63–12/86
Bismarck	1/63–12/86
Boulder	1/64–12/86
Bracknell	1/69–12/86
Cagliari–Elmas	1/57–12/86
Cairo	11/74–10/86
Caribou	6/62–12/86
Churchill	1/65–12/86
Edmonton	7/57–11/86
Goose Bay	1/62–11/86
Hohenpeissenberg	1/67–12/86
Hradec Kralove	1/62–12/86
Huancayo	2/64– 6/86
Kagoshima	4/61–12/86
Leningrad	8/68–12/85
Lerwick	1/57–11/86
MacQuarie Isle	1/63–12/86
Mauna Loa	1/63–12/86
Nashville	1/63–12/86
Quetta	8/69–12/86
Reykjavik	11/75–10/86
Rome (Vigna di Valle)	1/57–12/86
Samoa[2]	1/76–12/86
Sapporo	1/58–12/86
Srinigar	2/64– 5/86
Tateno	7/57–12/86
Toronto	1/60–12/86
Uccle	2/71–12/86
Wallops Island	1/70–12/86

[1]Data accepted in unrevised form from *Ozone Data for the World*.
[2]Data revised and supplied by W.D. Komhyr et al. (1987).
All other data are the monthly averages of total ozone published in *Ozone Data for the World* with the appropriate average monthly corrections applied. The amounts are given in Dobson Units.

After the first set of revised data had been prepared, the missing monthly values were treated as follows: if only 1 month was missing, the value substituted was the sum of the long-term monthly mean and the product of the interannual standard deviation of the missing month and the average of the two neighboring months' deviations (actual deviation divided by interannual standard deviation). These data sets were used for the comparison of the monthly means in two time periods. For the purpose of the full time series analyses, any other missing monthly values were replaced by the long-term monthly mean for that calendar month.

4.3.5 Sensitivity of the Method Used To Calculate the Provisionally Revised Data

If one ignores the details of the operation of the Dobson spectrophotometer, one can imagine two general cases that can be considered for the measurements prior to a hypothetical 3 percent

difference after recalibration of a Dobson instrument. The first situation is a step in which a 3 percent change in calibration is introduced at one instant, as could happen if the instrument were moved, accidentally jarred, etc. The other situation is a ramp that might occur through the slow deterioration of some part of the instrument. If a hypothetical situation is considered in which the actual column of ozone to be measured is absolutely constant over the period under consideration, then the recorded values would appear as a sudden step in the first case and as a uniformly varying ramp in the second. While no problem exists in such a hypothetical situation for distinguishing between the two situations, the real measurements are very much blurred by the natural variability of ozone over a particular measuring station.

The Belsk data can be used to test whether the assumptions made in correcting data prior to each recalibration introduce artificial trends into continuing data records. The arbitrary correction forms tested are a step change introduced immediately after the previous calibration (as used in the provisional revision), and a ramp between the two calibrations (i.e., a linear variation with time). In a real situation in which either a ramp or a step at a particular time is indicated by lamp tests or some other external information, the appropriate correction would be applied. Our concern here is directed toward whether an arbitrary choice of either a ramp or a step causes a serious error in the evaluation of secular trends. It should be remembered that the data as published in ODW represent *de facto* the arbitrary choice that the physical change represented by the recalibration was not present on the day before recalibration and took place suddenly as a single step.

The statistical model used for these analyses in Table 4.11 is similar to that used by Reinsel and Tiao (1987):

$$Y(t) = \mu + S(t) + W \cdot T(t) + N(t)$$

in which μ is the long-term mean; $S(t)$ is a term describing the seasonal variation, consisting of the sum of a sine wave with a period of 1 year, and its harmonics; $T(t)$ is a linear trend starting in 1970 with W as its coefficient (only a year-round model was used, not a model that allowed for different monthly trends); and $N(t)$ is an autocorrelated noise term. This model is *not* the same as that developed for the full trend analysis reported later in this chapter.

The ozone data from Belsk have been "corrected" for four different periods subject to retroactive calibration corrections, using either a ramp (R) or step (S) correction at each opportunity. The combination of the choice of R or S for each of four periods has provided 16 possible choices for how this correction should be applied—e.g., RRRR, RRRS, RRSR, etc. Comparisons with the revised data set can then be made of various versions of the fast correction—e.g., ramp or step at each recalibration, and with the old data set. The results of such trend analyses for all of these series are shown in Table 4.11. The data set used is that from March 1963 through July 1986, with just one missing monthly value.

Several points are worth noting:

- There is a large, significant difference between the trends calculated for the originally published data, $+0.68 \pm .37$ DU/yr, and the revised station data, $-0.40 \pm .29$ DU/yr.

- The trend calculated using the data set calculated by the method used in the provisional revision of other stations (designated SSSS) has a trend, $-0.47 \pm .31$ DU/yr, that is very close to that of the revised station data.

Table 4.11 Results of Trend Analyses of the Monthly Ozone Values at Belsk, Poland, for the Period 3/63–7/86. S = Step and R = Ramp Correction.

Data	W (DU/Year)
Old ODW	$+0.68 \pm 0.37$
Revised	-0.40 ± 0.29
SSSS	-0.47 ± 0.31
SSSR	-0.43 ± 0.31
SSRS	-0.46 ± 0.31
SSRR	-0.42 ± 0.31
SRSS	-0.22 ± 0.30
SRSR	-0.18 ± 0.30
SRRS	-0.20 ± 0.30
SRRR	-0.17 ± 0.30
RSSS	-0.18 ± 0.35
RSSR	-0.16 ± 0.35
RSRS	-0.18 ± 0.35
RSRR	-0.14 ± 0.35
RRSS	$+0.07 \pm 0.32$
RRSR	$+0.10 \pm 0.32$
RRRS	$+0.07 \pm 0.32$
RRRR	$+0.11 \pm 0.32$

- Although there is a substantial variation in the trends calculated among the 16 differently adjusted time series, all are closer to the trend of the station-revised data set than is the trend of the originally published data set.

Two conclusions can be drawn. First, the use of the correction factors found at the various recalibrations improves the quality of the data whether a ramp or step is assumed and, second, the use of step rather than ramp corrections is justified in the case of Belsk.

4.4 CALIBRATION OF TOMS DATA USING DOBSON DATA

In previous sections, the long-term TOMS record has been used to find abrupt changes in the records of individual Dobson stations. Relative changes that occur gradually over a period of several years could be caused either by the satellite instrument (SBUV/TOMS) or by an individual groundstation, but a drift relative to all of the Dobson stations is likely to have been caused by a calibration drift of the satellite instrument.

4.4.1 Comparison of TOMS Data With the Dobson Network

Fleig et al. (1986b) examined the drift of TOMS relative to an ensemble of 41 Dobson stations; this study was recently updated by Fleig et al. (1988). They found that TOMS total ozone values declined relative to the Dobson network at a rate of -0.25 percent per year between 1979 and

mid-1982, but declined at a rate of -0.51 percent per year until October 1985, the end of the period studied. The decline for SBUV was of similar magnitude. An alternative version of this comparison is described in detail in Section 4.2 of this chapter.

While the ozone concentrations indicated by the satellite instruments clearly declined relative to the values shown by the Dobson network, further tests are desirable of the assumption that this drift originates in the degradation of the satellite instruments. One such test involves internal calibration of the satellite instrument using radiances measured at wavelengths used in the primary ozone determination, as described in Chapter 2. A second such test can exist if circumstances exist during which nonroutine, intensive measurements are being made under favorable conditions for a ground-based Dobson instrument.

4.4.2 Comparison of TOMS Data With the International Primary Standard Dobson Instrument

A special opportunity for comparison exists for the International Standard Dobson Instrument No. 83 during its periodic recalibrations at Mauna Loa, Hawaii. As described in Section 4.1.1.4, Dobson instrument No. 83 was established in 1962 as the standard spectrophotometer for total ozone measurements in the U.S., and later as the International Primary Standard Dobson Instrument. The absolute calibration of this instrument over the period 1962–1987 has been maintained to within an uncertainty of ± 0.5 percent (Komhyr et al., 1988). Intercomparison of TOMS data with the data from these Mauna Loa recalibrations provides an opportunity for testing the possible drift of TOMS (and SBUV) within the accuracy of these calibrations. The 3.5 percent drift described in Section 4.3 is clearly much larger than the ± 0.5 percent stability of the International Primary Standard.

During a calibration using the Langley method, repetitive measurements of ozone are made on an individual day with different Sun angles and air masses to permit extrapolation to zero air mass and the determination of the extraterrestrial constant. These calibrations with Instrument No. 83 are repeated on a number of different days at Mauna Loa in a short period of time in order to determine the reproducibility of the calibration. Mauna Loa is an especially favorable site for such calibrations because its tropic, mountaintop location provides clean, generally aerosol-free air, stable ozone fields over time, and nearly overhead noontime Sun reducing the extrapolation to zero air mass. Such calibrations of Instrument No. 83 were performed at Mauna Loa in the summers of 1979, 1980, 1981, 1984, 1986, 1987, and 1988. For this report, TOMS observations have been compared with individual observations for each of these years except 1988. In 1979, for example, there were 31 days between June 11 and August 14 on which both instruments measured total ozone. The dashed circle in Figure 4.30 shows that Dobson Instrument No. 83 measured 278 DU of ozone on June 29 of that year. Of all the ozone measurements made by TOMS that day, the measurement of 278 DU was most nearly collocated with the Dobson station.

The Dobson total ozone values indicated for the calibrations were increased by 0.9 percent to account for the change in effective ozone absorption coefficients at Mauna Loa stratospheric temperatures. In most instances. the ozone values indicated by TOMS and by the Dobson correlated well except for two biases for which corrections can be made. One bias is the standard practice of evaluating the measurements with different assumed sets of ozone absorption coefficients (Bass–Paur for the satellite and Vigroux for Dobson). The second bias is an FOV problem: the Mauna Loa station is at 3.4 km altitude, and the Dobson cannot have as much tropospheric ozone in its column versus that seen nearby over the ocean by TOMS. The ozone measurements made by the two instruments should not agree exactly: in Figure 4.30, adjustments have been made for the stratospheric temperature and for the tropospheric ozone below the Dobson station, but not for the different absorption coefficients.

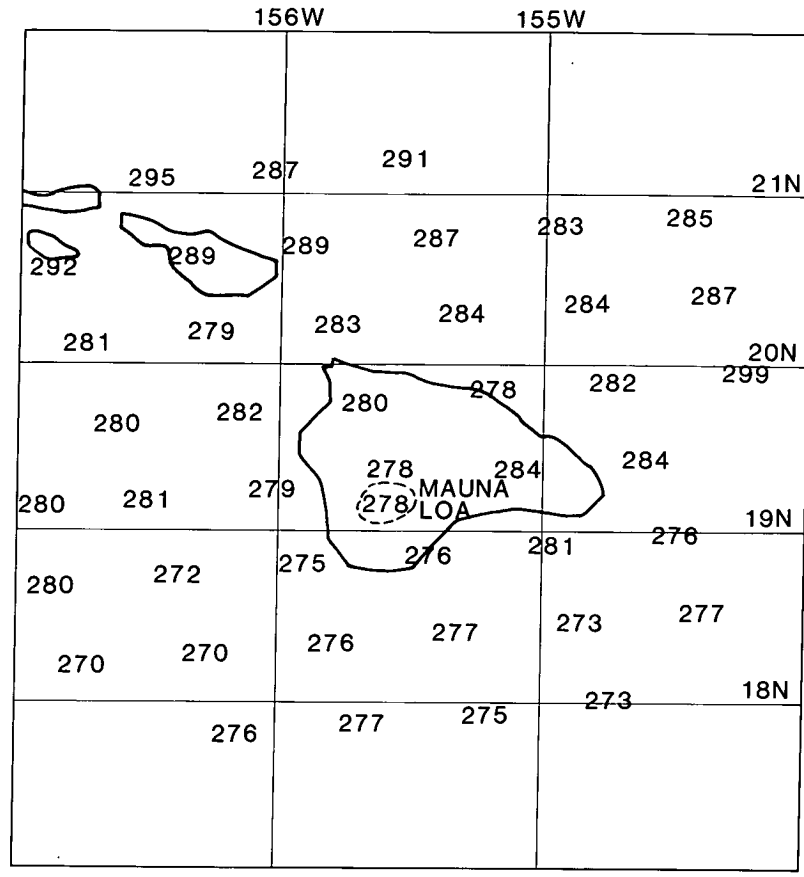

Figure 4.30 Intercomparison of TOMS overpass measurements of total ozone with World Primary Standard Dobson ozone measurements at Mauna Loa Observatory, Hawaii, June 29, 1979. The Mauna Loa measurement is enclosed in the broken circle.

The average ozone measured by TOMS in 1979 over Mauna Loa during the calibration period was 292.5 DU, while that measured by Instrument No. 83 was 279.2 DU, a difference of 4.8 percent. The comparisons can be made more comparable by the addition of a correction term to observations to account for the average amount of ozone present between the 3,400-meter altitude of the Mauna Loa Observatory and sea level, because the satellite senses an average value over a region of 1,600 km^2, almost all of which is ocean. This correction was determined from ozone vertical distribution measurements made with ECC ozonesondes released during 1983–1986 at Hilo, Hawaii (elevation 0.011 km). The added amounts of total ozone were slightly variable with the month of observation: 10 DU in May, 8 in June, 6 in July, and 7 in August. An average amount of 8 DU was uniformly subtracted from the actual TOMS values in Figure 4.30.

Corrections for the altitude mismatch in the observations reduces the average difference in 1979 from 4.8 percent to 1.9 percent, with a statistical uncertainty of ± 0.26 percent. Similarly calculated TOMS–Dobson percentage differences are plotted for each year in Figure 4.31. Two different results are given for the Dobson each year, labeled (1) and (2), that represent two slightly different calibrations for instrument No. 83. In case 1, the Dobson data are reduced using the 1976 wedge calibration for all years, while for case 2 the data are reduced using updated wedge calibrations. The results for both cases are shown to provide an estimate of the level of uncertainty in the Instrument No. 83 results.

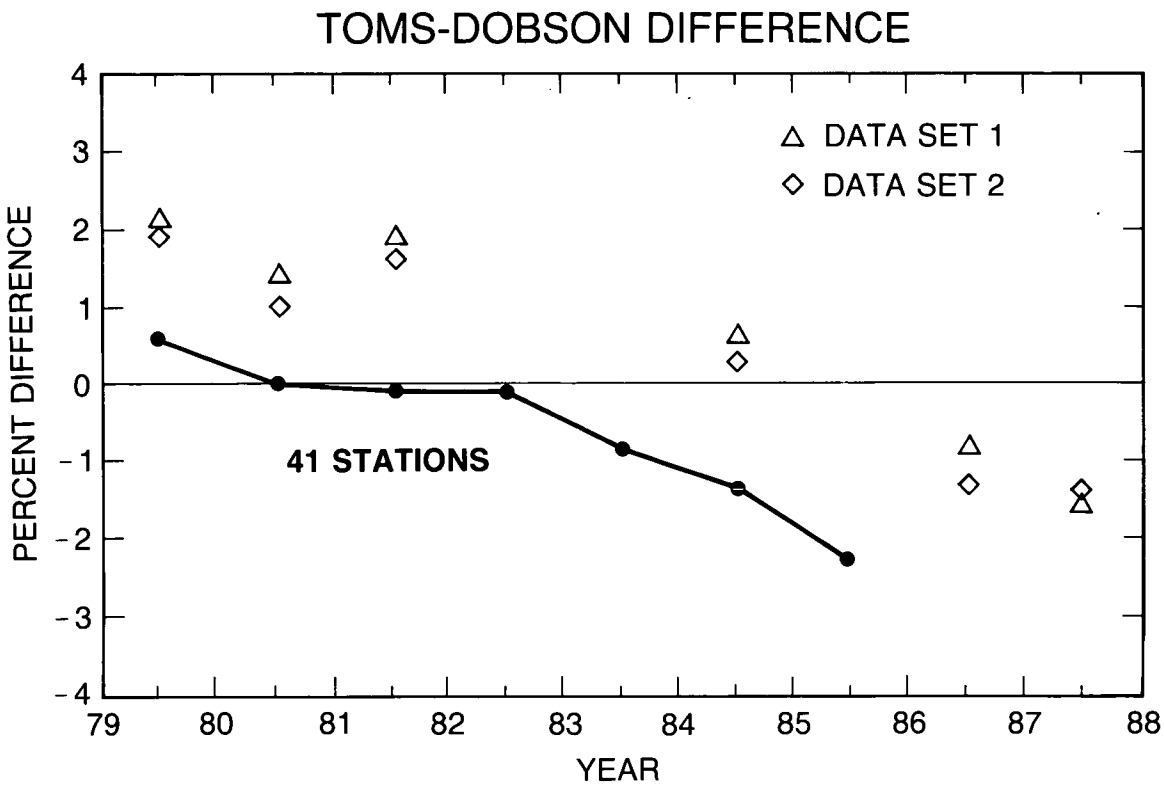

Figure 4.31 The variation of the (TOMS minus Dobson) percentage difference with time given for three different types of Dobson measurements. Data sets 1 and 2 (triangles and diamonds) are the result of comparisons of the TOMS data with slightly different calibrations of Dobson Instrument No. 83 (see text). while the circles represent the difference with an ensemble of 41 Dobson stations.

Ozone measurements with TOMS were relatively constant with respect to instrument No. 83 during the period 1979–1981. (Data for the ground-based instrument in 1980 are discounted because of known operator errors that year.) The average offset was +1.9 percent. By 1984, however, the difference was only +0.5 percent, a decline of 1.4 percent relative to the earlier period, and by 1987 the absolute difference was -1.5 percent, a relative decline of 3.4 percent. This decline relative to the International Primary Standard Dobson Instrument is consistent with the decline noted relative to the average of many individual stations, as described in Section 4.3.

Accepting the difference as real, could its origin be geophysical and not instrumental? One possibility that must be considered is that a secular increase in tropospheric ozone occurred at Mauna Loa during this period. The observed 3.4 percent TOMS–Dobson drift corresponds to about 10 DU of ozone, and a 20 DU change in tropospheric ozone (with 50 percent TOMS sensitivity) between 1981 and 1987 would be required to explain the difference. Such a change has not been observed. Measurements by ECC ozonesondes of the amount of ozone in the lowest 4 km at Mauna Loa (Komhyr, private communication) showed 8.3 DU in summer 1983 and 7.0 DU in summer 1986, a difference of only 1.3 DU. Based on these data, changes in tropospheric ozone must be discounted as a possible cause of the TOMS–Dobson difference in the experiments conducted at Mauna Loa.

Figure 4.31 shows both the TOMS/No.83 comparison and the yearly average TOMS–Dobson difference (dashed line) from the ensemble of 41 Dobson stations for 1979–1985 (Fleig et al.,

1986a). The important conclusion is that the same time dependence is observed for TOMS relative to either standard. If the calibration of Instrument No. 83 has been constant, the TOMS calibration must have drifted downward.

One final question to be resolved is whether the TOMS–Dobson drift could, in part, be an instrument artifact in TOMS other than the diffuser plate degradation discussed earlier. In 1982, TOMS began to experience a small number of cases of synchronization loss in the chopper that subtracts "dark current." These "sync-loss" effects are flagged automatically by the instrument, and indicate that only a few percent of the values were affected. Nevertheless, such effects need to be considered when drifts of only a few percent over almost a decade are involved. This possible source of error was discounted by examination of the SBUV–TOMS comparison data through 1986. The independent SBUV instrument shares only the diffuser plate with TOMS and had not then developed its own sync-loss problems. The SBUV–TOMS comparison showed that TOMS total ozone agreed with that from SBUV to within half a percent for the TOMS A pair. As indicated earlier, severe sync-loss problems developed for the SBUV instrument in February 1987, and this procedure for comparison is no longer valid.

4.4.3 Implications of TOMS–Dobson Drift

The conclusion that there was about 3.4 percent drift between TOMS and Dobson between 1979 and 1987, with much of the drift occurring after 1982, seems inescapable. The fact that the same pattern, relative stability before 1982 followed by a sharp decline between 1982 and 1986, occurred in the TOMS–Dobson comparisons for so many of the ensemble of 41 independent stations, and with the larger set of 92 Dobson and M–83 stations (Table 4.8), is strong evidence in itself. The complete confirmation by comparisons with the standard Dobson Instrument No. 83 for both TOMS and SBUV furnishes compelling additional evidence that this trend relative to Dobson is real.

4.5 PRELIMINARY EXAMINATION OF GROUND-BASED TOTAL OZONE MEASUREMENTS

Analyses of total ozone readings from any Dobson station in the Temperate Zone show ozone variations correlated with one dominant physical cycle, the seasonal variation, and three other potential contributors of lesser magnitude: the approximately 26-month cycle of the quasi-biennial oscillation (QBO) of the direction of the stratospheric winds in the Tropics, the 11-year solar sunspot cycle, and the formation of nitrogen oxides by the testing of nuclear bombs in the atmosphere 25–30 years ago (Reinsel, 1981; Reinsel et al., 1981; Reinsel and Tiao, 1987; Reinsel et al., 1987). A complete analysis of the total ozone data should take these effects into account before calculating any trends in recent years. The statistical model used in this study is presented in full in Section 4.6. This section contains a brief description of ozone climatology, followed by a simple analysis of both the ozone data published in ODW and the provisionally revised data discussed in Section 4.3 and given in Appendix 4.A.(i). Finally, a detailed description of the analysis of the Bismarck data is presented as a case study to show the effects of the various geophysical relationships.

4.5.1 Basic Total Ozone Distribution

Some early observations of total ozone were made as far back as 1913; routine Dobson spectrophotometer measurements were started at Arosa (Switzerland) and Oxford (England) in the late 1920's and at Tromso (Norway), Lerwick (Scotland), and some other stations in the

1930's. However, it was not until the International Geophysical Year (1957–1958) that observations at a sufficient number of stations became available to make possible global analysis of the total ozone distribution (e.g., London et al., 1976). The uneven geographical distribution of the stations, with a heavy concentration in the north Temperate Zone and only a few in the Southern Hemisphere, introduced a spatial sampling error into the global analysis that still persists.

The average distribution of ozone over the globe for 1957–1975 is shown in Figure 4.32. The main features are:

- A pronounced minimum over the equatorial belt, with increasing concentrations poleward to about 70 degrees, and with a secondary minimum at the poles;
- The belt of ozone minimum (240 DU) lies between 10°S and 15°N latitudes;
- The total ozone increases in a poleward direction in both hemispheres, but the north and south are not symmetrical to one another;

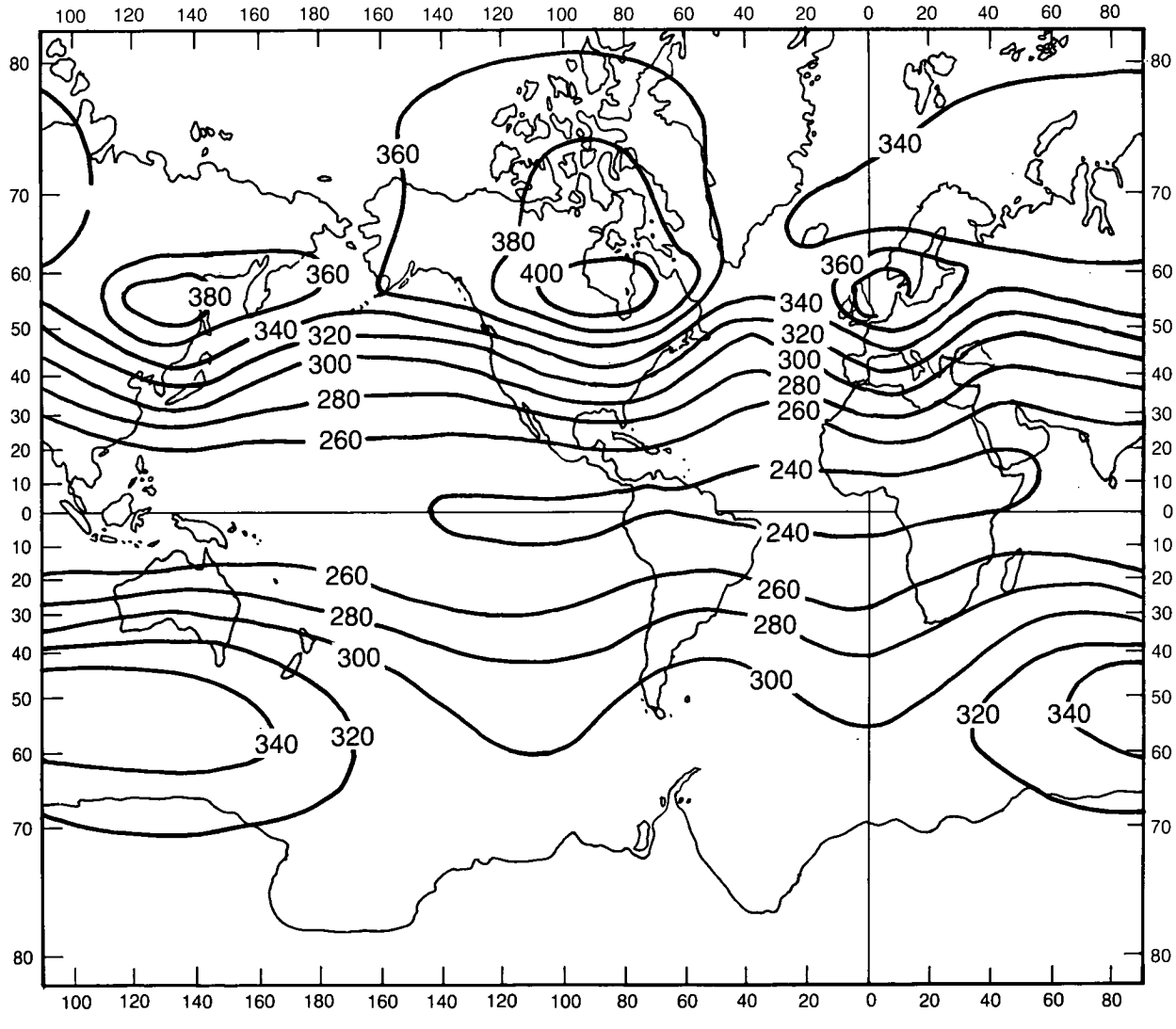

Figure 4.32 Average total ozone distribution for 1957–1975 derived from ground-based measurements.

- Pronounced longitudinal inhomogeneities exist, as indicated by ridges of higher ozone concentration over the eastern edges of the continents, a function of the climatological specifics of planetary circulation waves;

- The ozone concentration over the Antarctic is smaller than over the Arctic, reflecting differences in the patterns and behavior of the individual circumpolar vortices.

The average concentration of total ozone as a function of latitude and month is graphed in Figure 4.33 (London, 1980). In temperate and polar latitudes, substantial changes are observed with the seasons. Broad similarities exist between the two hemispheres: in each, the total ozone minimum is reached near the fall equinox and the maximum occurs near the spring equinox. There are also differences: the maximum is slightly later in the Southern Hemisphere, and the maximum rate of increase occurs in December/January (just after the winter solstice) in northern latitudes, while in the Southern Hemisphere the ozone increases fastest in September (close to the spring equinox). There are longitudinal inhomogeneities in each hemisphere that cannot be shown in Figure 4.33; these tend to be more pronounced in the Northern Hemisphere.

The rapid increase of total column ozone during the winter–spring season and its decrease during the summer toward an autumn minimum are shown in Figure 4.34 for 55 years of data from Arosa, Switzerland. The interannual standard deviations of each month are shown by the vertical bars in Figure 4.34. The long-term monthly means vary between 280 DU and 380 DU; the interannual standard deviation of the winter months is about 25 DU; and the interannual standard deviation of the summer months is about 10 DU. Data from other stations show that the variability increases at more northerly latitudes. These large natural variations make it hard to

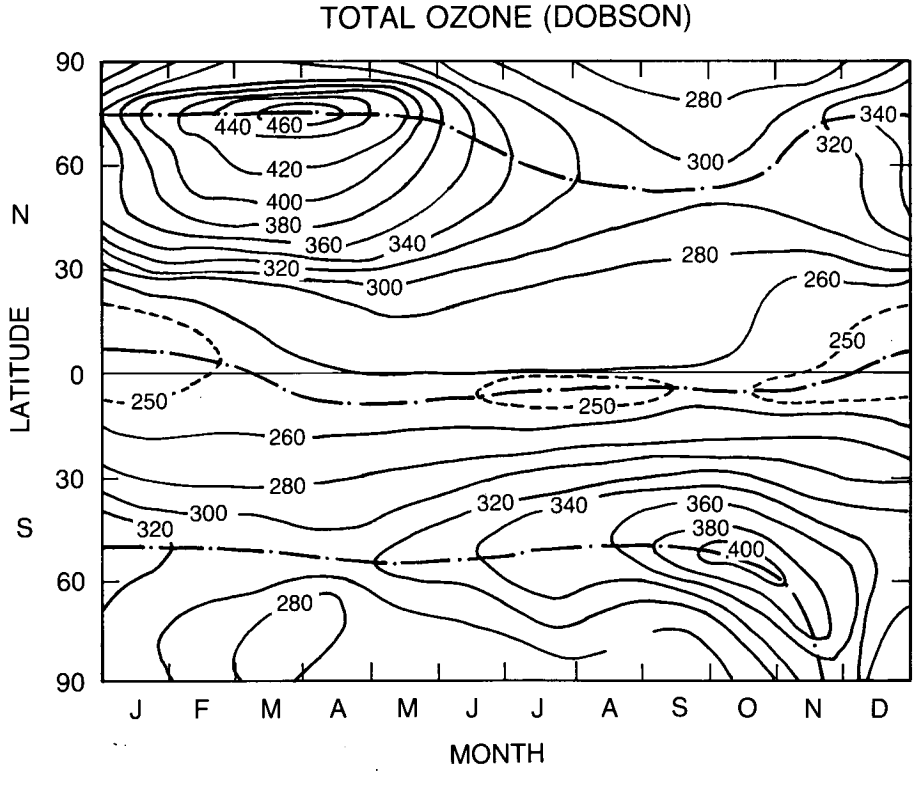

Figure 4.33 Variation of total ozone with latitude and season (from London, 1980).

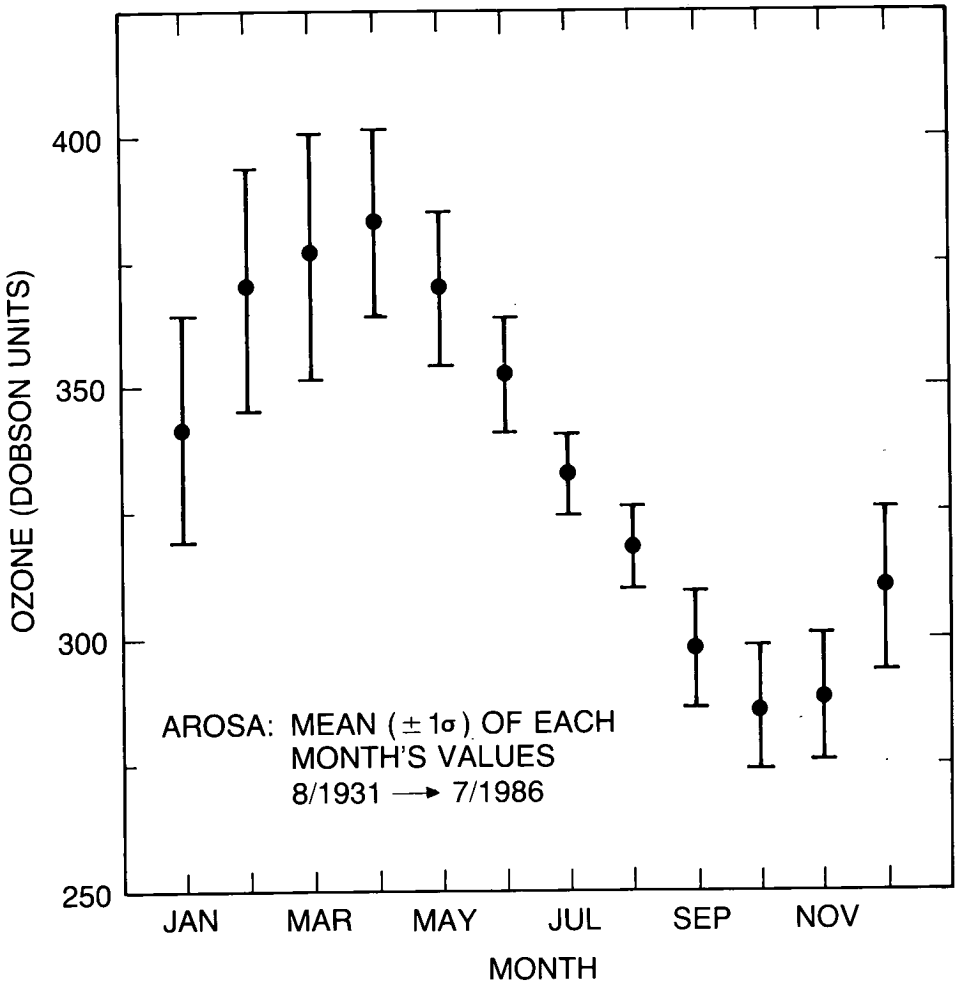

Figure 4.34 Long-term means of the monthly total ozone values at Arosa, Switzerland, for August 1931–July 1986. The associated interannual standard deviations for each month are shown as ± 1 sigma vertical bars.

detect a trend, particularly in the winter months. The annual cycle at Arosa is typical of the northern Temperate Zone, although there are longitudinal variations in the timing of the maximum and the amplitude of the annual cycle.

4.5.2 Changes at Selected Stations Deduced From the Data Published in *Ozone Data for the World* (ODW)

Harris and Rowland (1986) reported their observations that the ozone data from Arosa show strong evidence for a substantial wintertime loss in total column ozone at that location, combined with minimal losses in the summer months (Figure 4.35). They then demonstrated that a similar effect existed at other north Temperate Zone ozone stations. These patterns are illustrated in Figure 4.35 for the data as reported in ODW for five stations, four of which show a pattern similar to that found for Arosa. The Arosa data are based on the full 55-year data set, divided into two periods, August 1931–December 1969 and January 1970–July 1986. In the other five cases for which the data records are not so long, the average of the monthly total column ozone measurements over the 11-year period January 1976–December 1986 have been compared with the averages of the monthly data for a period of 11 or more years prior to 1976. The differences

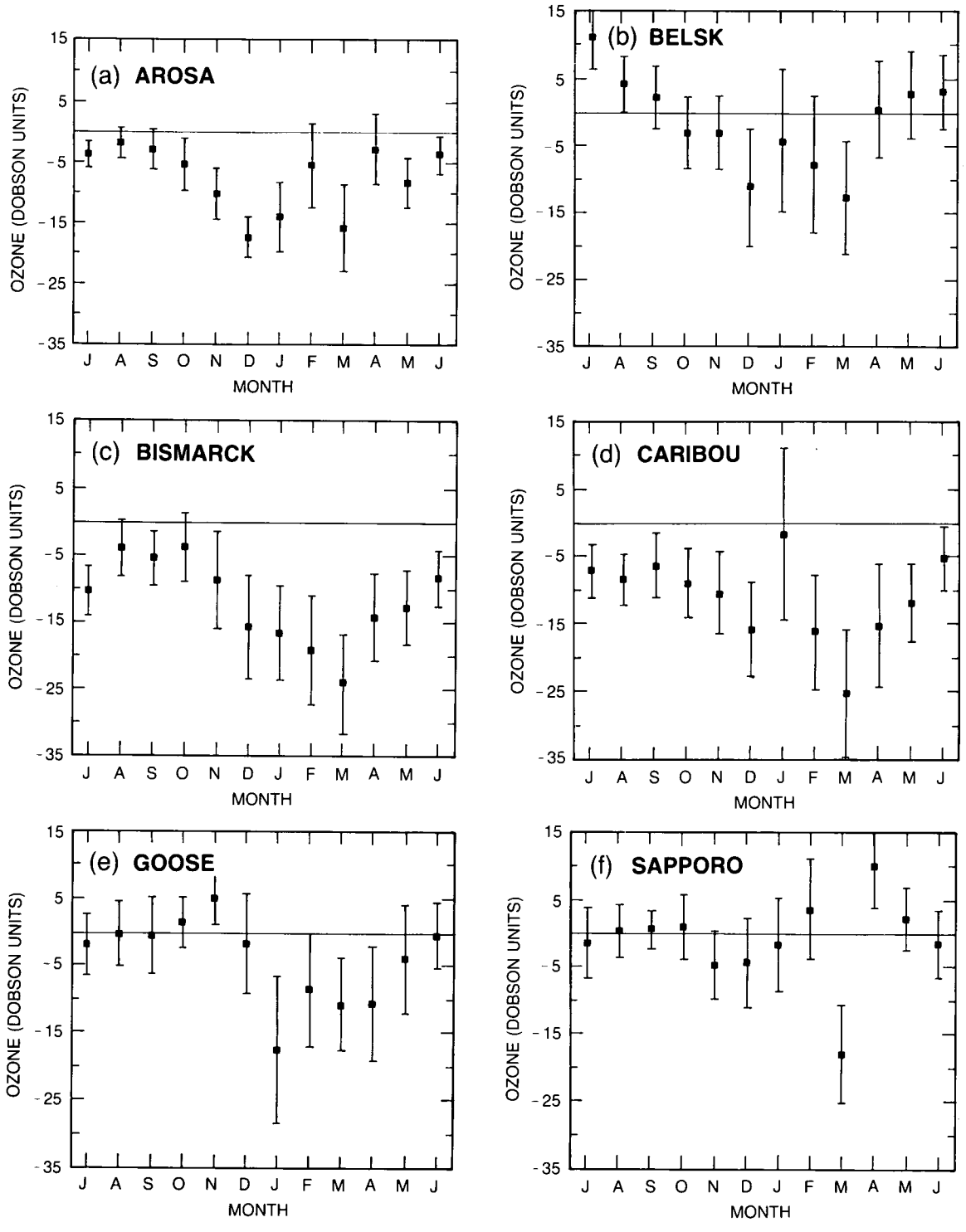

Figure 4.35 (a) Differences in the long-term monthly means at Arosa between August 1931–December 1969 and January 1970–July 1986. (b)–(f) Differences in the long-term monthly means at five other stations between the period prior to December 1975 and the period from January 1976 on. The first period has its starting date as the time when the station started making total ozone observations, and the second period ends in December 1986, except for Goose, where the data were available only through November 1986. Data are taken from *ODW*.

graphed illustrate the apparent gain or loss in ozone for each month, with negative values indicating a loss. The standard deviation of the mean is calculated for each period, and the vertical bar represents the uncertainty (±1 standard deviation) in the difference between the means for the earlier and later time periods. This procedure is satisfactory for determining whether the mean of the second time interval is significantly different from that of the first interval.

The same preliminary analyses have also been carried out for a selected set of 19 Northern Hemisphere ground-based Dobson stations between 31°–65°N latitude, using the ozone values as originally recorded in ODW. The criteria for station selection include at least 22 consecutive years of data and no special problems existing in the data sets (such as those discussed in Section 4.3). The individual station data for the 22-year period from 1965 to 1986 were used, and again the monthly averages of the earlier and later 11-year periods were compared. The choice of 11-year segments ensures that each period contains one solar cycle and about five QBO cycles, while the starting date avoids the nuclear bomb test effects almost completely.

The results are illustrated in Figures 4.36 and 4.37, in which we have averaged the differences for a 4-month "winter" season (December, January, February, March—DJFM) and a "summer" season (May, June, July, August—MJJA), rather than include all the monthly differences for all the stations. Negative values predominate especially strongly in the winter season (Figure 4.36), with 18 of the 19 stations showing ozone losses averaged over the winter period in this data set. The summer values (Figure 4.37) are more evenly distributed, with results from 11 stations showing ozone decreases, 6 showing increases, and 2 unchanged. In the annual averages, 17 of the 19 stations in Figures 4.36 and 4.37 show ozone losses. This analysis of the raw total ozone

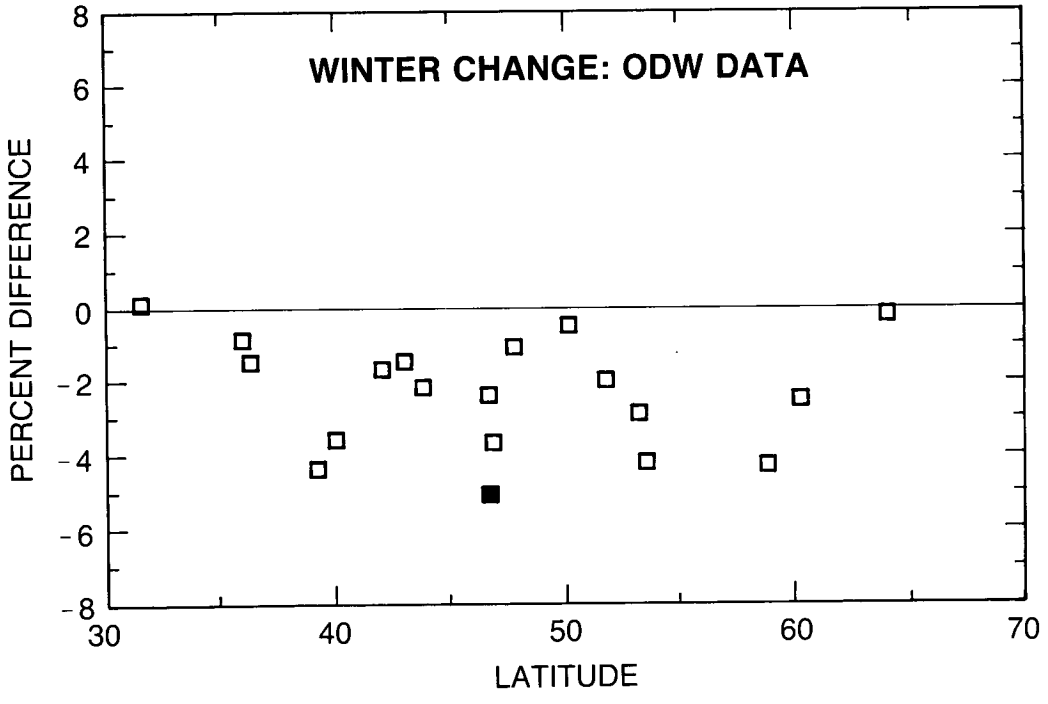

Figure 4.36 Differences in the means of the 4-month "winter" season (DJFM) for the 11-year periods from January 1965–December 1975 and January 1976–December 1986 are plotted for 19 Northern Hemisphere stations. Data are taken from *ODW*.

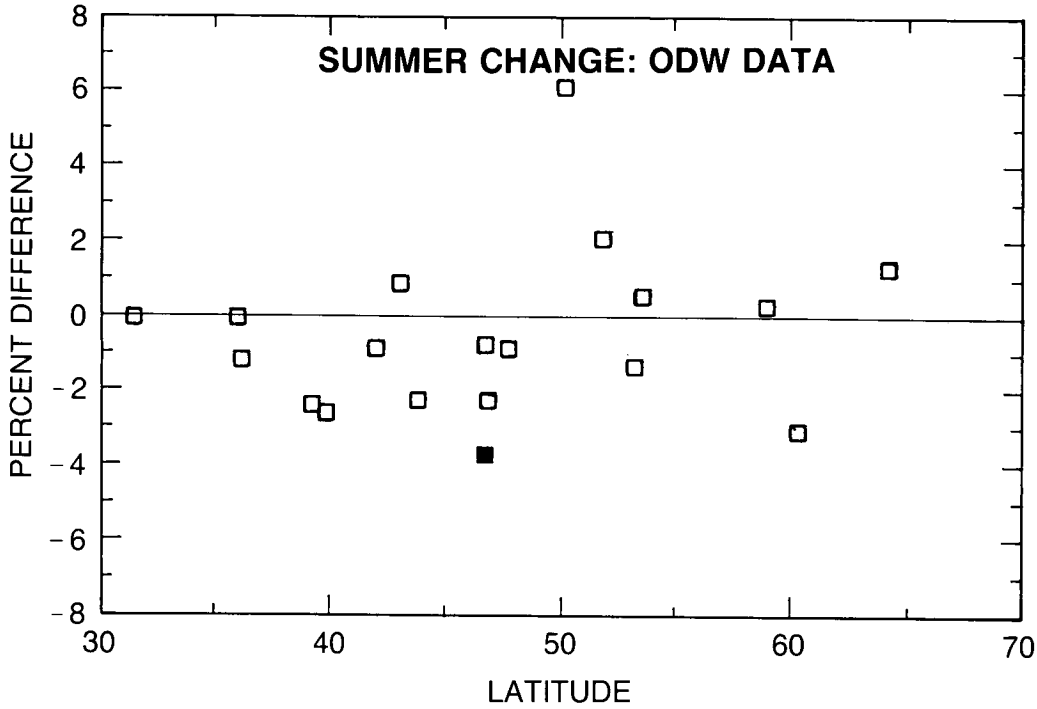

Figure 4.37 Differences in the means of the 4-month "summer" season (MJJA) for the 11-year periods from January 1965–December 1975 and January 1976–December 1986 are plotted for 19 Northern Hemisphere stations. Data are taken from *ODW*.

data published in ODW draws attention to the existence of a strong tendency for less ozone to be present during the most recent solar cycle than during the one preceding it, especially in wintertime. Because the solar cycle that peaked in 1979 was larger than that of 1969 (sunspot maximum of 165 versus 111 for the earlier maximum), any increase in ozone proportional to the cycle intensity would be greater in 1975–1986 and would therefore tend to result in positive values in Figures 4.36 and 4.37, a change opposite to the predominant observation.

The chief significance of Figures 4.36 and 4.37 is that they demonstrate an underlying change in ozone concentrations as recorded in ODW, with less ozone in the more recent years, especially in the winter months. This simple comparison of 11-year time segments provides no indications of a specific geophysical causal nature other than the apparent circumstance of larger average losses in the winter than in the summer. Subsequently, we expend most of our effort in statistical analyses of the provisionally revised set of ozone data (Section 4.3), which also shows preferential ozone losses, especially in the recent winter years (Table 4.12). However, as shown in Figures 4.36 and 4.37, this tendency is already present when the ozone data are used directly from ODW without any change. (No uncertainty analysis is presented here for these results using the data from ODW, but the statistical uncertainties given in Table 4.12 for the provisionally revised data set are approximately the same.)

4.5.3 Differences Between Published and Provisionally Revised Data

The same analysis was performed on the provisionally revised data for the same 19 stations, with the results shown in Figures 4.38 and 4.39. Comparison of these graphs with those calculated from the ODW data set discloses that, while there is more consistency within the

Table 4.12 Changes in Average Total Ozone Concentrations as Measured at Individual Dobson Stations Over the 22-Year Period 1965–1986, Inclusive. (Percentage Differences for 1976–1986 Compared to 1965–1975.)

North Latitude	Station	Winter[1]	Summer[2]	Annual
74.7	Resolute (Canada)	−1.4±1.8[3]	−0.8±0.9	−1.6±1.0
64.1	Reykjavik (Iceland)	−2.5±2.2	+1.7±1.3	+0.1±2.4
60.2	Lerwick (Scotland)	−3.8±2.0	−0.9±0.9	−1.6±1.0
58.8	Churchill (Canada)	−4.2±0.9	−1.4±0.8	−2.5±0.7
53.6	Edmonton (Canada)	−4.7±1.3	+0.8±0.9	−1.8±0.8
53.3	Goose Bay (Canada)	−2.4±1.3	−0.1±1.1	−0.8±0.9
51.8	Belsk (Poland)	−3.2±0.8	+1.2±1.0	−1.2±0.9
50.2	Hradec Kralove (Czech.)	−4.7±2.0	+1.1±0.9	−1.8±1.1
47.8	Hohenpeissenberg (FRG)	−1.8±1.7	+0.2±0.9	−1.0±0.9
46.9	Caribou (Maine, US)	−2.8±1.5	0.6±0.8	−1.8±0.9
46.8	Arosa (Switzerland)	−3.0±1.3	1.1±1.0	−2.0±0.9
46.8	Bismarck (N.D., US)	−3.0±1.2	−1.4±1.0	−2.0±0.7
43.8	Toronto (Canada)	−1.3±1.2	−1.3±0.8	−1.2±0.7
43.1	Sapporo (Japan)	−0.6±1.4	−0.1±0.9	−0.3±0.6
42.1	Vigna di Valle (Italy)	−2.9±1.2	+0.7±0.9	−0.9±0.9
40.0	Boulder (Colorado, US)	−3.9±1.3	−3.1±0.7	−3.3±0.8
39.3	Cagliari (Italy)	−2.5±1.7	−0.7±1.1	−1.1±1.2
36.3	Nashville (Tennessee, US)	−1.8±1.4	−3.3±0.7	−2.4±0.8
36.1	Tateno (Japan)	−0.7±1.6	−0.5±0.8	−0.4±0.7
31.6	Kagoshima (Japan)	+0.9±1.7	+0.5±1.0	+0.9±0.8
30.4	Tallahassee (Florida, US)	−1.7±1.9	−0.2±1.1	−1.3±1.4
30.2	Quetta (Pakistan)	−1.1±1.6	+0.1±0.8	−0.7±0.8
25.5	Varanasi (India)	−0.3±1.4	+0.4±0.9	−0.2±0.9
19.5	Mauna Loa (Hawaii, US)	−1.5±1.7	0.0±0.6	−0.9±0.6
	30°N to 60°N	−2.5±1.0	−0.5±0.6	−1.4±0.7
	40°N to 60°N	−3.0±0.9	−0.4±0.5	−1.6±0.6
	30°N to 39°N	−1.2±1.5	−0.7±1.0	−0.8±1.1

[1] Winter = Dec., Jan., Feb., March
[2] Summer = May, June, July, August
[3] Resolute is above the Arctic Circle, so that only less accurate moonlight measurements are available during actual winter. These "winter" data are the averages for the months of March and April.

corrected data set, there are no real differences in overall pattern; the wintertime losses are apparent in both Figures 4.36 and 4.38. The values given in Table 4.12 also refer to the provisionally revised data set. However, the calculations have been performed in two slightly different ways. In Table 4.12, the data period is from December 1964–November 1986. The choice of December 1964 instead of January 1965 as starting date was invoked for seasonal consistency when it became apparent that combination of months into "winter" (DJFM) and "summer" (MJJA) groupings became desirable. In this sense, the data set for Table 4.12 begins with the winter of 1964–1965. In the other, the calendar years 1965 through 1986 were used. Only minor

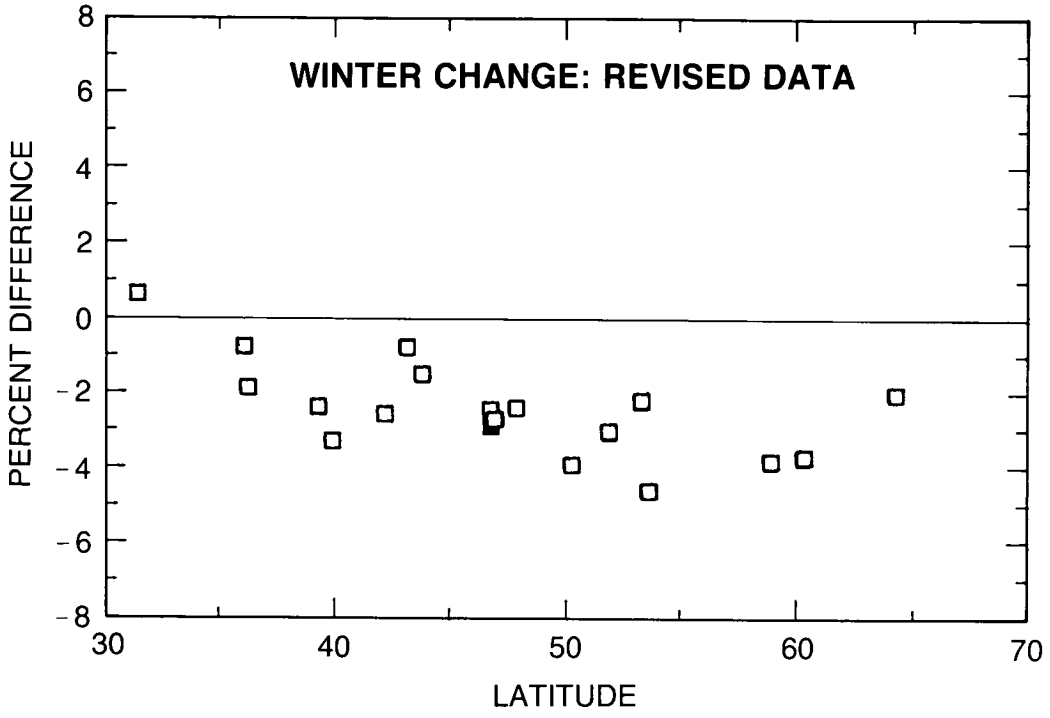

Figure 4.38 Differences in the means of the 4-month "winter" season (DJFM) for the 11-year periods from January 1965–December 1975 and January 1976–December 1986 are plotted for 19 Northern Hemisphere stations. Provisionally revised data are used.

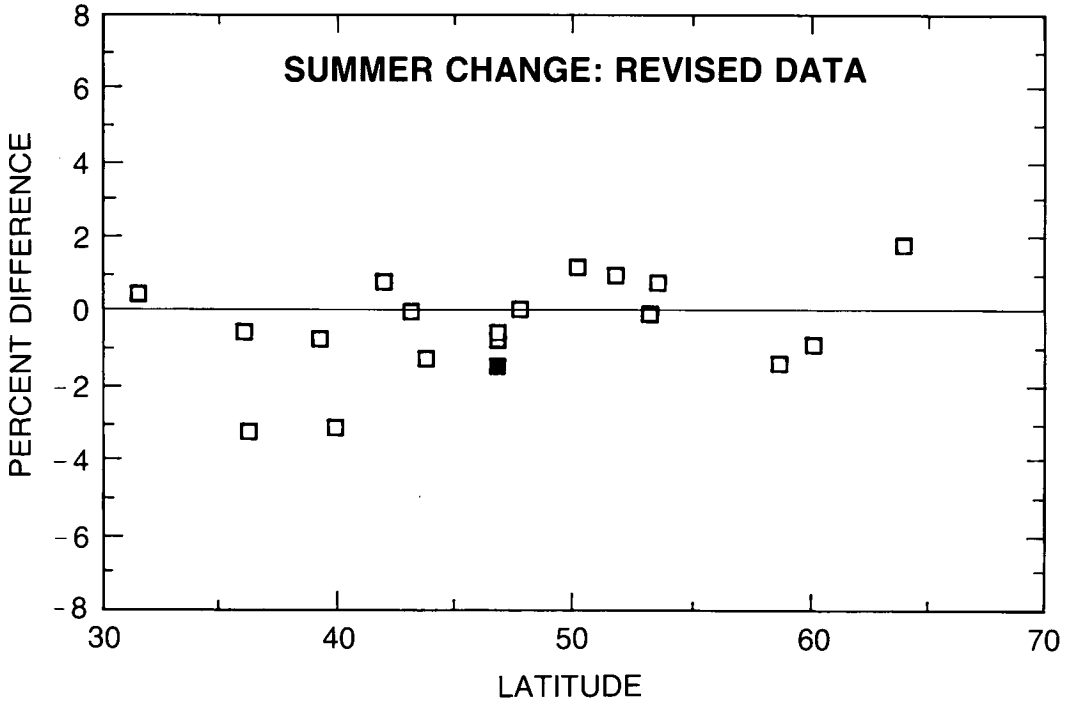

Figure 4.39 Differences in the means of the 4-month "summer" season (MJJA) for the 11-year periods from January 1965–December 1975 and January 1976–December 1986 are plotted for 19 Northern Hemisphere stations. Provisionally revised data are used.

numerical differences of no significance are found when December 1986 replaces December 1964 and the division point for the two 11-year periods is changed from December 1, 1975, to January 1, 1976.

Although there were no real differences in the pattern of a marked wintertime loss and mixed indications of summertime change found in each data set, there were major changes at particular stations. There is strong evidence of incongruities in many of the individual stations' published records, and there are sound physical reasons for all of the corrections to the data. Thus, only the provisionally revised data have been analyzed in greater detail; the results are presented and discussed in Section 4.6.

4.5.4 Bismarck: A Single Station Analysis

The complete time series statistical analyses of the provisionally revised data sets are discussed in Section 4.6. However before discussing the details, it is worth looking at the results of the analyses from a single station—Bismarck—to develop an understanding of the different phenomena that can affect total ozone. The statistical model used is described in full in Section 4.6 and will not be discussed here. The Bismarck data are marked with solid squares in Figures 4.36 to 4.39.

The daily total ozone data for Bismarck as reported to ODW covered the period from January 1963–December 1986, and are combined in ODW into 288 monthly averages. Some recalibration corrections were applied to these data to obtain the provisionally revised set of monthly average ozone values given in Appendix 4.A (i) of this chapter. When the complete 24-year data set is divided into two 12-year periods, January 1963–December 1974 and January 1975–December 1986, a decline in average ozone concentration is indicated in the second period relative to the first period, with the largest declines in the winter months, as shown in Figure 4.40. This simple observation stands out in both the ODW (Figure 4.40a) and provisionally revised (Figure 4.40b) data sets. The chief effect of the data recalibrations is (in this instance) to shift most monthly differences to less negative values without affecting the magnitude of the winter–summer spread.

The statistical assumption behind the calculations in Figure 4.40 effectively assumes that the ozone values for each calendar month are independent of one another so that the full time series can be divided into 12 separate series (i.e., all January values, etc.) without any loss of information. Phenomena such as the solar cycle, the QBO, and the atmospheric nuclear bomb tests around 1960, all of which are thought to affect total ozone, are ignored. This assumption of independence is not justified because the full time series is autocorrelated: i.e., the ozone concentrations in 1 month are influenced by the ozone concentrations in the preceding month. A more rigorous statistical analysis should consider the data set as a whole and allow for any effects on total ozone from known, or hypothesized, physical sources. Because its magnitude is clearly very large, further consideration of the complete data set normally begins with description of the seasonal cycle.

Time series statistical modeling of this data set can be most easily understood by considering the consequences from the successive inclusion of the various terms mentioned in the model description, although, in practice, many other model permutations were also calculated. The first step is to fit to the data a model containing only the seasonal term. After removal of the seasonal cycle, the residual series was then tested for autocorrelation and was found to exhibit significant autocorrelation (about 0.2) for lags of 1 month and 2 months. None of the correlations

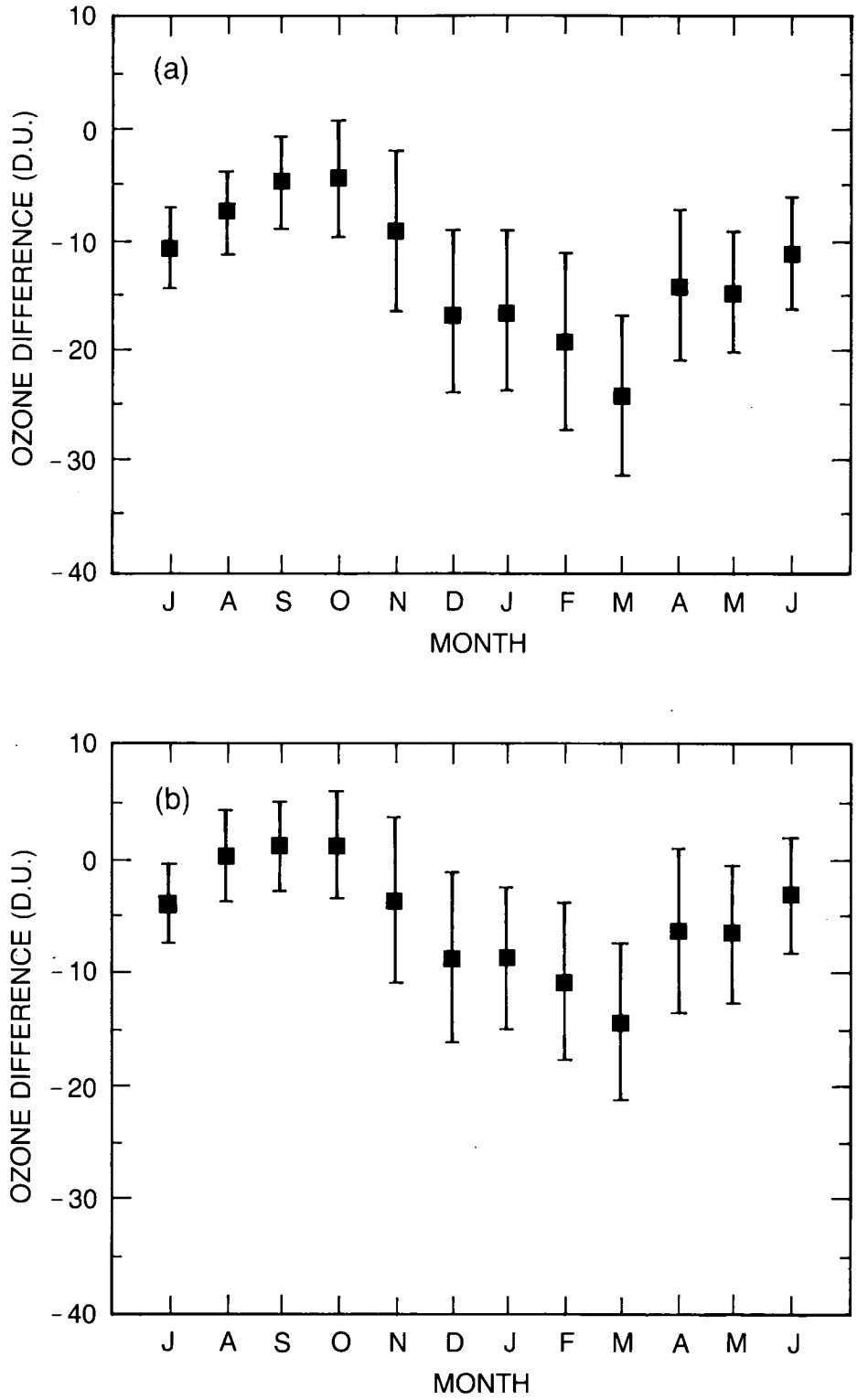

Figure 4.40 Changes in Monthly Average Ozone Total Amounts at Bismarck, North Dakota, Between January 1963–December 1974 and January 1975–December 1986. Using (a) the data as published in *Ozone Data for the World* and (b) the provisionally revised data, with monthly average corrections for instrument calibrations applied to the data recorded in *Ozone Data for the World*.

for 3 months or longer was statistically significant (all <0.1). When the terms for the autocorrelation were added to the noise model, the residual variance decreased substantially, and the autoregressive factors in the autocorrelation model were calculated to be 0.30 (1 month) and 0.16 (2 months). All subsequent calculations described below have included the autoregressive coefficients for 1 month and 2 months as part of the basic statistical model. The meteorological observations of the persistence of weather patterns are the underlying geophysical reason for the positive autocorrelations with lags of 1 month and 2 months in the monthly average ozone values.

The data were next tested for the importance of the QBO in its correlation with the ozone abundance over North Dakota. The 50 millibar Singapore wind velocity was used to describe the QBO, with westerly winds arbitrarily designated as positive. When the QBO was considered in coincidence with the total ozone over Bismarck, the multiple regression calculation showed a QBO coefficient of -8.0 ± 3.6, a decrease of 8 DU from minimum to maximum in the QBO, versus a yearly ozone average of about 350 DU. (The negative sign indicates that there is an anti-correlation between total ozone and the Singapore wind speed measured from the westerly direction; all quoted uncertainties in this section represent one standard deviation.) When tested for ozone concentrations lagging 6 months after the tropical wind speed variations, the regression coefficient was very much smaller, +1.0 ± 3.8 DU minimum-to-maximum. Further calculations with the Bismarck data set were carried out with the zero delay QBO correlation.

The next statistical test was the inclusion of the nuclear bomb test parameter. This parameter has been scaled linearly to the model results obtained with the Lawrence Livermore National Laboratory 2-D atmospheric model using the ozone changes calculated for the latitude appropriate to the station). The joint solution for Bismarck with QBO and the bomb tests maintained the QBO parameter as -8.0 ± 3.5 DU and indicated a nuclear effect with a coefficient of -0.44 ± 0.49. The magnitude of the ozone change associated with the aftermath of nuclear testing is given for each month by the product of the coefficient and the model predictions of loss for the latitude band containing the Bismarck station. The negative value of the coefficient indicates a loss of ozone 44 percent as large as calculated in the model, but with an uncertainty (±49%) large enough that a range of values from zero effect to the full magnitude of loss expected from the model is still plausible. Because the data set for Bismarck does not begin until 1963, past the time period for the maximum ozone depletion effect expected from nuclear testing, the nuclear test coefficient is never of more than marginal significance for this data set. Greater statistical significance could be obtained only if data were available for earlier periods, preferably encompassing the entire period of atmospheric nuclear bomb testing.

The multiple regression was then repeated with the further inclusion of a smoothed sunspot series representing the parameter for the 11-year solar cycle, with the results:

QBO	–7.8 ± 3.4 DU/cycle
Nuclear	–0.21 ± 0.49 times the model calculated depletions
Solar cycle	+6.3 ± 3.3 DU.

The solar cycle coefficient implies that ozone readings at Bismarck were about 6 ± 3 DU (about 2 ± 1%) higher in 1979–1980 than they were during the adjacent sunspot minima in 1975 and 1986. All of these coefficients represent the statistical fit on the assumption that no long-term trends exist in the total ozone data set.

The basic calculation was next extended with the inclusion of a linear yearly ramp function for which the long-term ozone concentrations were initially assumed to be constant, but then were allowed to vary after some fixed date, with the slope of this ramp determined by statistical best-fit techniques. Furthermore, the yearly ramp assumes that (a) any ozone variations that occurred after the onset of the ramp were year-round in nature, with no seasonal or monthly differences and (b) the variation is linear with time. These statistical results are the most comparable to previous calculations with the data from Bismarck, differing only in the date at which the ramp begins. Three different ramp starting dates were tested: January 1965, January 1970, and January 1976, with linear ramp coefficients k_{65}, k_{70}, and k_{76}, respectively; the coefficients determined for these three ramps are given in Table 4.13. Because the data set began only 2 years earlier, the value of the ramp coefficient k_{65} is almost the equivalent of a simple linear regression to the data.

Table 4.13 Parameter Values for Several Linear Ramp Statistical Calculations With Ozone Data from Bismarck.

Start of Ramp	1965	1970 (i)	1970 (ii)	1976
Parameter				
QBO	8.2 ± 3.2	8.6 ± 3.2	7.9 ± 3.0	8.1 ± 3.2
Solar	5.5 ± 3.5	5.3 ± 3.5	5.6 ± 3.1	5.5 ± 3.5
Nuclear	–0.92 ± 0.52	–0.70 ± 0.48	–0.67 ± 0.40	–0.50 ± 0.46
Trend (k)	–0.48 ± 0.18	–0.53 ± 0.20	–0.55 ± 0.18	–0.83 ± 0.33
Change in O_3 concentration, 1963–1986 (Dobson Units)	–10.6 ± 4.0	–9.0 ± 3.4	–9.4 ± 3.1	–9.1 ± 3.6

The units for these coefficients are: QBO—Dobson Units for a +40 meter/sec shift in wind direction from easterly to westerly (approximately the average shift at 50 mb from maximum easterly to maximum westerly direction; Solar—Dobson Units for a +150 change in sunspots, approximately the increase that occurred between solar minimum in 1975–1976 and solar maximum in 1979–1980; Nuclear—the numerical coefficient multiplied onto the calculated ozone depletion from the LLNL 2 D model; Trend—in Dobson Units per year (e.g., -0.48 ±0.18 DU/yr); for 22 years, from 1965–1986, this coefficient signifies a total ozone change of 22k, or -10.6 ±4.0 DU.

The column 1970 (i) contains the results using an autocorrelated noise term with 1- and 2-month lags, while column 1970 (ii) contains those for a noise term including just a 1-month autocorrelation coefficient.

An amplifying comment about the calculation of a "yearly ramp coefficient" is appropriate at this juncture. The natural variability of monthly average ozone values at Bismarck (and other north temperate and polar stations) is substantially larger in winter than in summer, as illustrated in Figure 4.34 for Arosa. Overreliance on fitting the highly variable winter data is normally suppressed by weighting each of the data points in the residual series according to the natural standard variation of the calendar month represented by the residual.

The coefficients for the QBO and the solar cycle are largely unaffected by the inclusion of ramps. This finding is typical of almost all of our calculations with the various stations. The apparent general conclusions from statistical modeling of the Bismarck data with the assumption of a constant ramp coefficient throughout the year are (a) a QBO effect of about 8 ± 3 DU in all calculations, (b) a year-round decrease of 9 ± 3 DU in total ozone at the beginning of 1987 relative to the concentrations observed prior to 1965, prior to 1970, or prior to 1976, (c) a solar cycle increase of about 5.5 DU for 1979–1980 versus the minima on either side, and (d) an appreciable

effect from nuclear bomb testing in the early 1960's, though the significance is not statistically robust because the Bismarck data start in January 1963, roughly coincident with the maximum predicted bomb test effect. Only minor numerical differences were found for the two 1970 ramp calculations with only 1-month autocorrelation, or with both 1- and 2-month autocorrelations included.

Exceptions to the general statement that QBO and solar cycle coefficients are generally not affected by the inclusion of ramps can be found with stations for which the record is short. The correlation between the ramp and the solar cycle is then larger, but the QBO coefficient usually remains stable in these cases. The correlation of the QBO and solar cycle parameters is low—less than 0.1 in all the analyses for Bismarck and similarly low for other stations. No attempt has been made in this study to investigate the possibility that the QBO effect on total ozone might be different at different stages of the solar cycle. An analogous finding has been reported for their joint effect on stratospheric temperatures (Labitzke and Van Loon, 1988). By contrast, the nuclear bomb test parameter is fairly strongly correlated with the ramp and solar cycle parameters. For the 1963–1986 record at Bismarck, the correlations for the model, in which all three geophysical phenomena were included, are:

	Bomb Test Parameter (a) Ramp	Correlation With (b) Solar Cycle
Yearly Ramp Starting in		
January 1965	0.53	0.29
January 1970	0.40	0.31
January 1976	0.26	0.31

Addition of the terms describing these geophysical phenomena which may affect total ozone does change the noise term in some cases, nearly always simplifying it. As more of the variability in the data is explained by the inclusion of such terms, the noise is reduced and its structure should become clearer. In the case of Bismarck for the model in which the QBO, the solar cycle, the nuclear bomb testing and a linear ramp starting in January 1970 are all included, the autocorrelation factors are calculated to be 0.25 ± 0.06 for the 1-month lag and 0.11 ± 0.06 for the 2-month lag. These factors are essentially the same as those (0.30, 0.16) found without any of the geophysical parameters included. When the noise term was changed so that it included only the 1-month autocorrelation factor, little change was found in the statistically calculated geophysical parameters. In the results quoted in this chapter, the better noise term (i.e., 1-month or 2-month autocorrelation) for that particular model is used.

However, the assumption of a year-round constant loss of ozone, either in DU or in percentage of total ozone, is not consistent with the general appearance of the Bismarck data as graphed in Figure 4.39, which indicates substantially larger losses in the winter months, or of the data from many other Northern Hemisphere stations graphed earlier in Figures 4.36 and 4.38. Alternative analyses for trends have been calculated with a model that provides each calendar month with a separate linear regression coefficient after a certain date—i.e., 12 separate ramp coefficients. These calculations have also been carried out in conjunction with most permutations of the three geophysical terms. In this model, each month is treated as independent with respect to the pattern of any changes in average amount of ozone (but still with autocorrelation for 1 month and 2 months); then the values of these 12 ramp coefficients can be determined, together with their standard statistical uncertainty. The results from models with ramps beginning in 1970 and 1976 are summarized in Table 4.14. The total data set includes 24

years, or slightly more than two solar cycles. We have calculated these ramp coefficients using the entire 24 years, and with the final 22 years (i.e., two solar cycles) beginning in January 1965. In the latter case, any effects on total ozone from nuclear bomb testing are sufficiently in the past that we have not included the nuclear parameter in the linear regressions.

Table 4.14 Statistical Analyses of Ozone Data From Bismarck.

Coefficients of various analyses that allow for differing monthly trends and including some or all of the variables for the QBO, the solar cycle, and the predicted nuclear depletion. Data for 24 years, from January 1963 to December 1986.

JA70	−1.10 ± .53			−1.10 ± .51	−1.25 ± .51
FE70	−1.08 ± .57			− .98 ± .54	−1.19 ± .54
MA70	−1.53 ± .55			−1.51 ± .53	−1.73 ± .53
AP70	− .73 ± .53			− .72 ± .51	− .92 ± .52
MY70	− .78 ± .48			− .79 ± .46	− .96 ± .46
JN70	− .56 ± .37			− .59 ± .36	− .73 ± .36
JL70	− .37 ± .30			− .41 ± .29	− .53 ± .29
AU70	− .09 ± .33			− .14 ± .32	− .25 ± .32
SE70	+ .30 ± .30			+ .23 ± .29	+ .12 ± .30
OC70	− .02 ± .43			− .09 ± .41	− .22 ± .41
NO70	− .26 ± .60			− .31 ± .58	− .46 ± .58
DE70	− .69 ± .57			− .71 ± .55	− .86 ± .55
QBO				−6.74 ±2.87	−7.20 ±2.82
SUNS				+7.42 ±2.90	+5.54 ± 2.97
NUC					− .80 ± .38
JA76	−1.84 ± .82	−1.81 ± .81	−1.85 ± .79		−1.95 ± .79
FE76	−1.09 ± .89	−1.05 ± .87	−1.01 ± .85		−1.16 ± .85
MA76	−2.28 ± .86	−2.22 ± .85	−2.27 ± .83		−2.42 ± .83
AP76	−1.39 ± .84	−1.35 ± .83	−1.40 ± .81		−1.54 ± .81
MY76	−1.43 ± .76	−1.40 ± .74	−1.45 ± .73		−1.58 ± .73
JN76	− .96 ± .59	− .96 ± .58	−1.01 ± .57		−1.11 ± .57
JL76	− .62 ± .47	− .65 ± .47	− .69 ± .46		− .78 ± .46
AU76	− .40 ± .53	− .45 ± .52	− .48 ± .51		− .57 ± .51
SE76	+ .42 ± .48	+ .34 ± .47	+ .32 ± .46		+ .23 ± .46
OC76	− .04 ± .68	− .14 ± .67	− .16 ± .65		− .25 ± .65
NO76	− .48 ± .95	− .56 ± .94	− .58 ± .92		− .68 ± .91
DE76	− .92 ± .90	− .98 ± .89	− .97 ± .87		−1.08 ± .87
QBO		−7.36 ±3.28	−6.86 ±2.84		−7.20 ±2.85
SUNS			+7.45 ±6.13		+6.14 ±3.00
NUC					− .55 ± .37

The top row contains the analyses where the ramps start in 1970, while the bottom row has those for 1976. JA70 is the trend coefficient for January, FE70 that for February, etc., where the ramp starts in 1970. Similarly, for 1976 there are JA76, FE76, etc. The units are DU yr^{-1}. The QBO coefficient has units of DU per (40m s^{-1}), and the solar cycle (SUNS) coefficient is in DU per 150 sunspots. The nuclear coefficient (NUC) should be used as a multiplying factor to the function shown in Fig. 4.44.

Several comments can be made about the various statistical treatments of the same data set:

- The coefficients for the solar cycle and QBO contributions to ozone change are not significantly altered by the introduction of either yearly or monthly trend coefficients, or by the choice of 1965, 1970, or 1976 for the beginning of the ramp.

- The yearly average ozone loss calculated with monthly trend coefficients is somewhat larger than calculated from a yearly trend coefficient. The chief cause for this difference is that each month is evenly weighted in the average of the monthly trends, while the summer months, with their smaller natural standard deviation and smaller ozone changes, are more heavily weighted in the determination of an overall trend fitted to all months simultaneously.

- The indicated change in ozone for individual months is approximately the same for trends fitted since 1970 and 1976, indicating that most of the change has occurred following 1976.

4.6 DETAILED ANALYSIS OF THE PROVISIONALLY REVISED GROUND-BASED DATA

In most Temperate Zone locations, the total ozone column concentrations are observed to vary regularly with the season, peaking about the beginning of spring and reaching a minimum in early autumn. Any statistical model used to treat total column ozone data must satisfactorily allow for this seasonal cycle before it can determine whether any other significant pattern is present in the data. Most statistical analyses (Angell and Korshover, 1983b; Angell, 1987b; Bloomfield et al., 1983; Hill et al., 1977; Oehlert, 1986; St. John et al., 1981, 1982) remove the seasonal cycle by converting the monthly averages into residuals representing the deviation of the monthly average in an individual year from the long-term average for that given month. This procedure assumes a constant seasonal cycle over the years and produces a series of 360 numbers for a 30-year period, or 264 for a 22-year period. These statistical treatments then deal with the data from each station as a sequence of consecutive "deseasonalized" deviations from long-term monthly averages. Reinsel et al. (1981, 1981, 1987, 1987) use a sine curve and its harmonics to describe the seasonal cycle rather than the monthly averages, but the underlying assumption is still that the seasonal cycle does not change.

In either case, the next step in the previous statistical modeling has been to assume that any secular change introduced into the ozone pattern would have a constant effect over the year, so that it can be described by a single trend coefficient. Because this approach has been applied to the monthly average ozone data in numerous earlier publications, it has also been applied here to all of the individual station data. Summaries of the yearly ramp coefficients calculated for these stations are given in the bottom lines of Appendices (a)–(f) under B(i). However, these yearly trend coefficients are now deemed inappropriate for description of the ozone variations actually occurring in the atmosphere.

4.6.1 Method of Analysis

Concern for the possibility that man's activities might be affecting the concentrations of stratospheric ozone has continually raised the question of whether any recent change has been detectable in measurements of total ozone. The customary approach has been to ask whether

changes have occurred during the past decade or two, rather than uniformly over the entire period of record. The most frequent test assumption has been the division of the data record into an earlier portion, assumed to have been constant, and a later portion to which a straight line has been fitted, joining smoothly to the constant from the early record and with the slope of the second part determined by least-squares fit to the data. This straight line, with its slope as a parameter to be fitted, has been designated as a "ramp," and the resultant combination of a constant value for the early time period and a later, usually sloped, section has been described colloquially as a "hockey stick" function (see Figure 4.41). Such a mathematical function makes no pretense of having direct geophysical significance, but is simply one approach to the question of whether or not the best statistical fit to the entire data set indicates changes from the long-term average over the most recent period. The sign of the change is not fixed, and calculations have been presented that have + signs for the ramp with certain stations, indicating more total column ozone in recent measurements than earlier, and - signs for other stations, indicating a loss of ozone in the more recent data.

A less frequently used alternative to the ramp formulation has been the application of a hypothetical trend of ozone versus time based on some approximation of the geophysical circumstances, usually from an atmospheric model. In this situation, the shape of the modeled ozone variation versus time has been assumed to be fixed, but its magnitude has been treated as a free parameter, allowed even to assume the opposite sign from that implied by the geophysical simulation. The geophysical utility of such a free parameter is obviously marginal when the fit to

DESCRIPTION OF TREND

a) MONOTONIC, YEAR-ROUND. ('HOCKEY STICK')

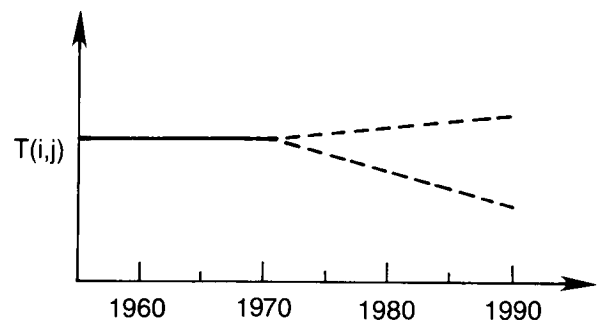

b) SEPARATE 'HOCKEY STICK' MODELS FOR EACH CALENDAR MONTH

$$T(i,j) = \sum_{L=1}^{12} k_j \cdot (i - i_0) \cdot \delta_{jL} \qquad \left.\begin{array}{l} \\ \\ \end{array}\right\} \; i > i_0$$

$$= k_j \, (i - i)$$

$$\text{AND } T(i,j) = 0 \qquad i \leq i_0$$

Figure 4.41 Description of trend (a) monotonic, year-round (hockey stick) and (b) separate hockey stick models for each calendar month.

the available data indicates that the sign of the change is incorrect—for example, if ozone were actually found to be increasing when ozone depletion has been calculated in an atmospheric model. In such a circumstance, the value of the parameter for the magnitude of the assumed functional form has no more significance than the value of a ramp coefficient—neither has any direct geophysical significance.

Another important difficulty that exists with this approach of using a geophysically based functional form taken from an atmospheric model calculation has been the lack of constancy in the predicted patterns of ozone change with improved measurements of pertinent parameters. The most frequent changes affecting the time pattern of ozone concentration in atmospheric modeling have originated with improvements in the chemical and photochemical bases used for the modeling, and in the expansion of the photochemical model itself from the 1-D models of the 1970's to the 2-D models of the 1980's: a new compound is proposed for inclusion, a new chemical reaction is proposed, a reaction rate constant is reevaluated, the time pattern is found to vary with latitude, etc. Over the past 10 or 15 years, in a typical atmospheric model the calculated ozone trend versus time of ozone concentrations has usually been nonlinear and often not even monotonic. Model improvements have often caused changes in the magnitude of predicted long-term ozone depletion and have usually been widely noted, but the patterns of ozone variation with time have also been altered in the process. These apparent changes in total ozone versus time have had many different functional forms over the past 14 years, including several that have called for slight minima or maxima in the ozone changes during the 1970's and 1980's. Without consistent agreement about the geophysically expected shape of ozone variation with time, each such statistical calculation would become obsolete with the next change in the evaluation of reaction rate constants. Fundamentally, the reliance on ramp coefficients fitted to the external data without any preconceived geophysical model simply tries to answer the question of whether variations in ozone concentrations are occurring in the environment, quite independent from the current state of atmospheric model calculations.

The procedure adopted in most statistical calculations until now has been the determination of a single linear ramp coefficient from the accumulated series of all of the monthly residuals. Implicit in this choice of modeling is the assumption that any ozone variation that may have taken place from the long-term averages has occurred consistently throughout the year. However, this approach will be misleading if the basic assumption is not correct: if the perturbation to the previous ozone pattern has a seasonal dependence of its own, then the assumption that the perturbation has equal effect over the entire year can produce substantial distortion in attempts to interpret the data. The distortion is more pronounced when the variability (and the statistical weighting) of the data is itself seasonally dependent, as is the case with total column ozone measurements at most Temperate Zone stations, for which the ozone distributions exhibit larger variances in the spring than in the autumn, as shown for Arosa in Figure 4.34. The situation can be further illustrated with a hypothetical two-component model.

Suppose (a) that the ozone concentrations in a particular location followed a steady pattern during the months from April through September for 20 years without change and (b) that the ozone concentrations from October through March followed a steady pattern for 10 years, and then declined linearly for the next 10 years with a ramp coefficient -k. If these two hypothetical components are equally weighted, then the resulting data fit of a single yearly ramp will produce constant values for the first 10 years, and then a declining ramp for the next 10 years, with a slope that is the direct average of the ramp for (a)—i.e., zero—and -k for (b)—and will have the value -k/2. If either of the hypothetical components has a smaller natural variance and is weighted accordingly, then minimization of the total variance will influence the composite ramp toward

the slope of the component with this smaller variance. In the hypothetical extreme that one of the components is known with infinite accuracy and the other is not, then the composite ramp will fit the accurately known component and force this shape upon the other data set. A few years ago, there were no geophysical reasons that led to the expectation that perturbations to total column ozone would have equivalent effects throughout the year or, conversely, that they would not. In this situation, the assumption of a single ramp coefficient equally applicable throughout the year is the simplest to apply, and is the procedure that has been widely used. Such statistical calculations also produce results most comparable to the predictions of 1-D photochemical models because their structure does not include information on possible seasonal or latitudinal variations. However, when the actual data disclose seasonally dependent changes in the magnitude of perturbations over time, as in Figures 4.36–39, the statistical model with a single ramp coefficient applicable throughout the year is no longer an appropriate model for treatment of the data.

A much more elaborate model, which allows for the possibility of different degrees of change on a monthly basis, replaces the single yearly ramp coefficient with 12 separate coefficients, 1 for each month. An approximation to the expected results can be obtained by separating the residuals into a series for each month and then calculating the appropriate ramp coefficient for each of the 12 separate data sets. Such separation into 12 series does not take into account the existence of short-term autocorrelation and can produce misleading error estimates. An alternative calculation can be performed on the complete data set with autocorrelation included and 12 separate ramp coefficients. The latter procedure has been used regularly in our calculations.

One interesting result from this monthly component evaluation is that strong differences are found to exist among the ramp coefficients, as expected from the observations of seasonally dependent differences in Figures 4.36–39. Many of the ramp coefficients are found to be strongly negative, others zero, and some positive. In addition, the yearly ramp coefficients are not approximately equal to the average of the 12 monthly coefficients, but are often quite different from the average.

Various possible influences on total column ozone exist that should be accounted for while determining a trend. Four important processes have been identified that can lead to changes in total column ozone, but that are not part of a long-term trend. The largest such effect is the seasonal variation caused by the atmospheric circulation. All data treatments begin with a method or function to account for this. Another known, cyclic process is the variation in the intensity for some wavelengths of solar ultraviolet radiation as part of the 11-year solar cycle. Because these wavelengths correspond to UV energies large enough to photodissociate O_2 and thereby create more O_3, a plausible connection exists by which total ozone is correlated with these solar cycles. Probably the best known manifestation of the solar cycle is the waxing and waning in the numbers of sunspots, for which accurate records are available for the past 250 years. The series of measurements at an individual station can be tested for the importance of a solar cycle effect through inclusion of a term attempting to mimic the response of the atmosphere to these solar variations. In our calculations, we have used the running 12-month average of sunspots to provide the functional form of any atmospheric response, as shown in Figure 4.42. (Sunspot data are provided by the National Geophysical Data Center, Boulder, Colorado.)

A set of related geophysical phenomena exists that includes the shifting geographical origin of the Asian monsoons; the differences in atmospheric pressure over tropical locations such as Darwin, Australia, and Tahiti; and the approximately biennial change of the direction of the zonal winds at altitudes of 15–30 km in the Tropics. The tropical zonal winds in the lower

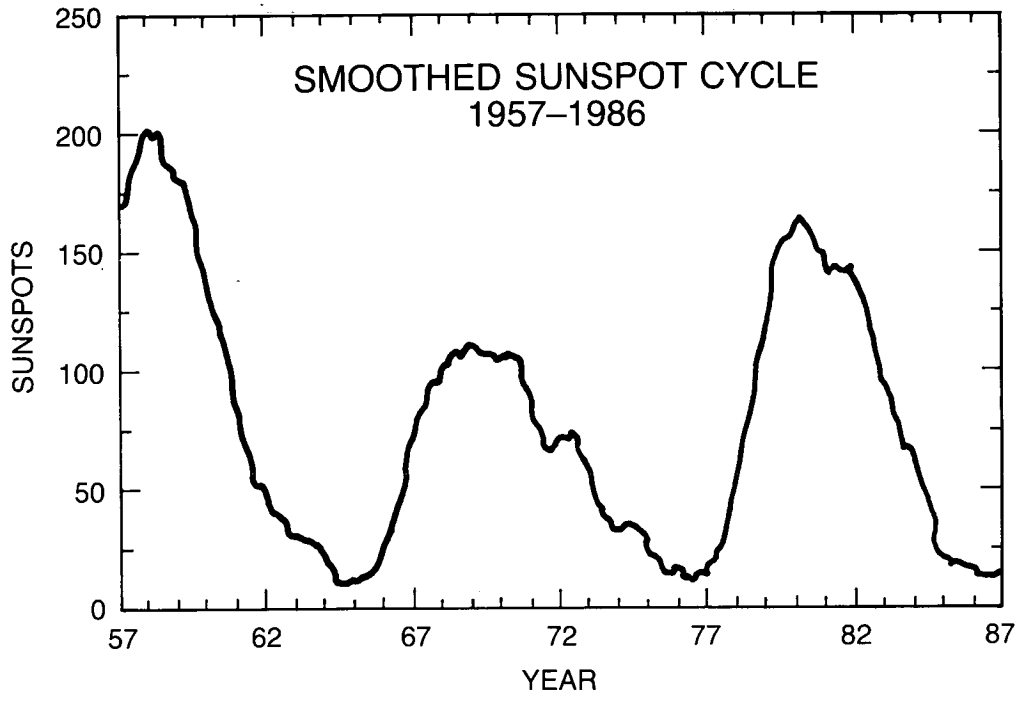

Figure 4.42 Smoothed sunspot cycle 1957–1986

stratosphere, for example, will tend to blow from a westerly direction for about a year, and then switch to an easterly direction for the following year, etc. The actual time period for a complete cycle in these tropical wind directions is somewhat irregular, averaging about 26–27 months, and is designated by the term quasi-biennial oscillation, or QBO (Reed et al., 1961). The amounts of total ozone (and the stratospheric temperatures) over particular measuring stations have long been known to have a cyclical variation in correlation with the QBO. In our statistical modeling, we have included the QBO through a term proportional to the zonal wind velocity at 50 millibars pressure (about 20 km altitude) over Singapore, as shown in Figure 4.43. The Singapore data are chosen simply because they provide an available, consistent, numerical set. Comparable changes take place at all longitudes within a few days as the winds reverse throughout the equatorial zone. However, the directional wind shift does not occur simultaneously at all altitudes, but works downward from above, so that the shift at the 30 mb level is followed in a month or two at 50 mb and then, after another delay, at 100 mb, etc. The QBO parameter could also be based on 30 mb or 100 mb wind velocities, with corresponding changes in the phase relationship between ozone and the QBO. The correlation of ozone changes with the QBO is known to be delayed at higher latitudes, and we have allowed for such delay by testing two ozone–QBO correlations for each station: no delay versus a lag of 6 months in the ozone response to a QBO shift.

Finally, nuclear bomb tests conducted in the atmosphere during the late 1950's and early 1960's are a known source of nitrogen oxides, which can change ozone concentrations in the stratosphere. The time variations of the proxy variable accounting for such changes has been shaped from the time behavior of the ozone changes at each latitude calculated with the LLNL 2-D atmospheric model, as shown in Figure 4.44. The magnitude of the coefficient for the nuclear bomb testing is then determined statistically.

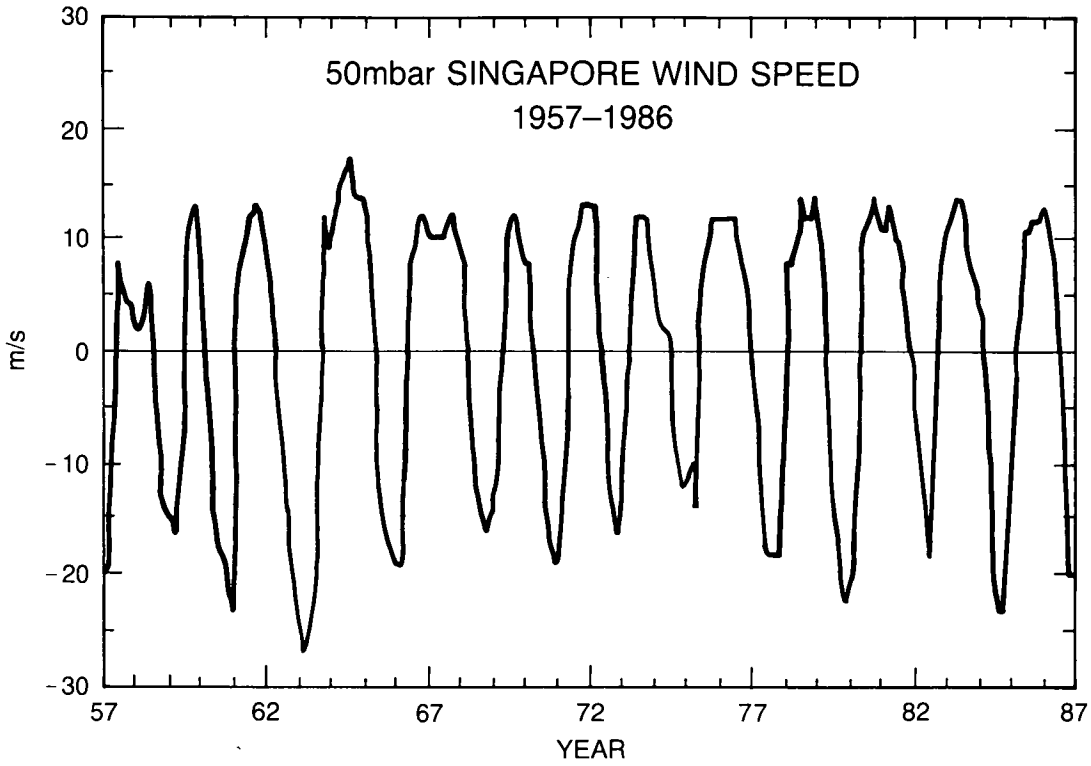

Figure 4.43 50 mbar Singapore wind speed, 1957–1986

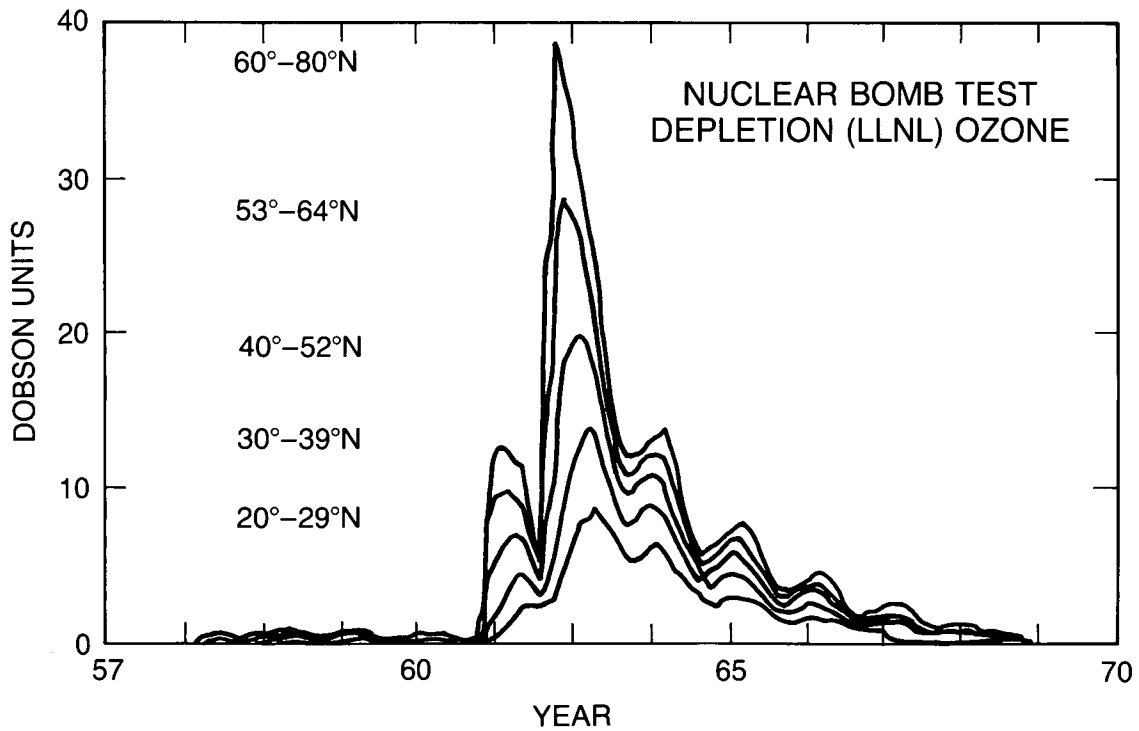

Figure 4.44 Ozone decreases caused by the atmospheric nuclear bomb tests as calculated by the 2-D LLNL photochemical model for five different latitude bands.

4.6.1.1 Description of the Statistical Model

The approach used in the analysis of the revised data has been to fit to the ozone data a model of the general form

$$oz(i,j) = S(i,j) + X(i,j) + T(i,j) + N(i,j).$$

The term $S(i,j)$ describes the seasonal behavior; $X(i,j)$ is a term that describes other phenomena (geophysical in origin) that can affect total ozone; $T(i,j)$ is a term that describes a possible long-term trend in total ozone; $N(i,j)$ is a term that describes the noise; i denotes the year; and j denotes the month. The overall approach is thus similar to that of Reinsel et al. No detailed comparisons are made here with the results from previous studies.

The seasonal variation is accounted for by allowing each month's long-term mean to be determined separately:

$$S(i,j) = \sum_{l=1}^{12} \mu_j \cdot \delta_{jl}$$

where δ_{jl} is a delta function that allows only 1 month's value to be nonzero for each reading. The chief advantage is that no predetermined functional form is forced on the data. (Note that deseasonalization of the data prior to analysis by subtracting the appropriate long-term monthly mean from each monthly value still eliminates the same number of degrees of freedom.)

The three phenomena that are thought to affect total ozone and that are included in this analysis of total ozone data are the QBO, the solar cycle, and the bomb tests in the late 1950's and early 1960's. The proxy variables used are, respectively:

- The 50-mbar east/west wind velocity at Singapore.
- A smoothed series of sunspot numbers made up of the averages of each pair of consecutive 12-month running means.
- The effect of the bomb tests on total ozone calculated by the 2-D LLNL photochemical model of Wuebbles et al. In these analyses, the bomb test effect is taken as the difference between a calculation that included the effects of the solar cycle, the nuclear bomb tests, and increases in trace gas concentrations, and one that included just the trace gases and the solar cycle. The ozone changes are calculated in this 2-D model for different latitudes but not different longitudes.

The term in the model that tests for trend has usually had the form of the hockey stick (shown in Figure 4.41). Many analyses have been performed for this report using this form with the ramp starting at three different times: January 1965, January 1970, and January 1976. The first and the last were chosen as corresponding closely to minima in the solar sunspot cycle (as is the end of the series), thus ensuring that any residual solar cycle effects not accounted for using the sunspots have as little influence on the trend coefficient as possible. This model postulates that any loss of ozone will occur as a steady year-round loss, and does not allow for the possibility that losses occur predominantly in one or two seasons. A more elaborate form of $T(i,j)$ has also been used in which a separate ramp is included for each month:

$$T(i,j) = \sum_{l=1}^{12} k_j \cdot \delta_{jl}$$

Again, δ_{jl} is a delta function and so has the effect of including only 1 month's trend coefficient for each month's data. The results from the year-round and monthly models are discussed later. Last, the autocorrelation within the time series is accounted for in the noise term $N(i,j)$.

4.6.1.2 Autocorrelation

The deseasonalized data series of monthly residuals has been tested to determine whether a correlation exists between successive monthly values. For example, if the September residual is positive in a given year, is the probability that the October residual will also be positive in that year greater than 50 percent? Such tests show that with ground-based stations, significant positive autocorrelation is always observed in the monthly values for a 1-month delay and frequently for a 2-month delay—both October and November are more likely to be positive after a positive residual in September. The autocorrelation coefficients are, in most cases, no longer statistically significant after 2 months. Such 1-month and 2-month correlations are geophysically plausible because of the tendency of weather patterns to persist. Because such conditions are often specific to geographical locations, no requirement exists that the same tendencies toward autocorrelation be exhibited at all groundstations worldwide. No tests have been made of more elaborate geophysically based hypotheses of autocorrelation—e.g., that the probability of a positive value in November following a positive October is different from that for June following a positive May.

The autocorrelation coefficients for ozone data within a latitude band, e.g., 40°N to 50°N, are larger than those for an individual station. For example, the autocorrelation coefficient for a 1-month delay is approximately 0.6 in satellite data for the average ozone concentration in a latitude band in comparison to the typical values of 0.2 found in groundstations in the same band. The difference in these coefficients presumably reflects the fact that motion eastward or westward can carry an air mass away from a groundstation, removing the autocorrelation at that station, but maintaining it in the latitude band. Thus, while a new air mass is detected at the station, the old air mass still contributes to the latitudinal average and continues to maintain some correlation between successive monthly values.

4.6.1.3 Weighting Procedures: Intra-Annual and Interannual Variations

Considerable differences exist in the year-to-year variations for the ozone values in different months. The standard deviations of the 12 monthly sets of 24 years of data from Bismarck are given in Table 4.15. These standard deviations are a measure of the year-to-year variation of the months and can be called the interannual standard deviations. Also shown in Table 4.15 are the averages of the standard deviations for the individual months calculated from the daily readings (mean intramonthly standard deviations). Both series show the same annual pattern with a maximum variability in the late winter and early spring and a minimum in the autumn.

In a least-squares analysis of the data, some kind of weighting should be used to ensure that each month contributes equally to the residual variance. If an unweighted analysis of the data is made, then the months with the largest interannual standard deviations will be the largest contributors to the residual variance, and these months will, in effect, be dominating the analysis at the expense of the months with smaller interannual standard deviations. In order to allow each month to be equally important in its contribution to the variance during the analysis, each monthly value should be weighted by the appropriate interannual standard deviation.

Table 4.15 Monthly Means and Standard Deviations at Bismarck (in DU).

	Interannual Standard Deviation	Mean Intramonthly Standard Deviation	Mean
January	16.4	34.9	367.5
February	17.7	40.6	391.8
March	17.2	35.4	400.0
April	16.9	30.8	387.2
May	15.2	26.8	370.7
June	11.9	23.8	345.9
July	9.5	16.5	324.1
August	10.6	14.9	310.5
September	9.6	20.0	301.0
October	13.6	23.3	296.5
November	19.1	26.3	317.0
December	18.2	32.5	339.0

A separate issue is whether to weight each month to allow for the variability within that month and the number of readings taken therein. To do this correctly requires using each individual standard deviation. It is a matter of debate whether the intramonthly variation need be considered in an analysis of monthly data, as the variability is on a very different time scale to that of the interannual variability and can effectively be considered unrelated. Two other factors complicate this type of analysis. First, the observed strong day-to-day autocorrelation within a month reduces the independence of the daily readings. This can be seen by looking at the ratio of the intramonthly standard deviations to the interannual ones. If all of the daily readings were independent, this ratio would be approximately the square root of the number of readings within that month, i.e., a factor of 4 to 5.5. Instead, it would appear that the number of "independent" readings in a month is, typically, about four, because the usual difference between the two columns is only a factor of two. This number is roughly the same as that for other midlatitude stations. Second, a trend versus time is found within most months so that the calculated standard deviation of a sample about a constant mean is not actually appropriate.

The statistical calculations were carried out using the SCA Statistical System (Version 3). The Gauss–Marquardt algorithm in this system implies a constant variance within the time series being analyzed, and the package does not include a weighting option. Accordingly, the monthly data of each variable were premultiplied by the inverse of the appropriate standard deviation (i.e., February values for all the variables included in the calculation were divided by February's standard deviation). Apart from the autocorrelated noise, this procedure is the same as a classical "sigma-squared weighting" routine, because the weighting by the standard deviation is squared before the calculation of the residual variance, the quantity that is minimized. Interannual standard deviations were used in all the analyses unless specific mention is made. For a few stations, the average of the intramonthly standard deviations was also tested, and no important differences were found in the estimates of the various parameters. Small differences were found in the uncertainty estimates for the parameters, but the two different weighting methods produced the same results within the uncertainties calculated. Only for the Bismarck data set was a calculation carried out in which each data point was weighted by its own intramonthly standard deviation. Again, no important differences were found in the results.

4.6.1.4 Missing Data

In most station records, months exist during which no readings were taken. These missing data might be caused by any one of a number of reasons—the instrument was undergoing calibration tests or an overhaul, the absence of the instrument technician, or some other similar reason. There are also many months in which only a few readings were taken, and, because of the large intramonthly standard deviations, the averages of these months might not be considered representative. As mentioned in Section 4.3.4, in the preparation of the provisionally revised data sets found in the Appendix to this chapter, every month with fewer than 13 daily readings was deemed to have had no usable monthly average. After the first set of revised data had been prepared, the missing monthly data were replaced as follows:

- With 2 or more consecutive months without a usable monthly average, the long-term monthly means for those months were used.
- If only 1 month was missing, the value substituted was that of the long-term monthly mean, adjusted by the product of the average of the 2 neighboring months' normalized deviations (actual deviation divided by standard deviation) and the standard deviation for the missing month.

4.6.2 Results From Individual Station Data

One major purpose of this report has been analysis of the existing record to find the magnitude, nature, and significance of any detectable changes in the amount and distribution of ozone in Earth's atmosphere. As described in Section 4.3, the published data on total ozone have been critically examined, and a set of provisionally revised data has been produced for many stations. A comparison of the results of an initial analysis of the original and revised data sets based on Dobson instruments shows that the provisional revision produces no substantive change in the behavior of the stations as a group, although in individual cases significant changes are seen (Figures 4.36–39). The data revision does result in greater consistency among the stations at similar latitudes, as might be expected if the cause(s) of any changes are global in nature rather than the consequence of some alteration in the close vicinity of the station. This greater consistency provides more confidence in the significance of latitude band averages; no attempt was made to construct latitude band averages from the original ODW data, so that no quantitative estimates are possible of reductions in the uncertainty estimates from the ODW to the provisionally revised data sets.

Various multiple regression analyses, then, have been made on the provisionally revised Dobson data, with the results described in the following sections. First, the analyses of the individual stations are considered. Next, there is a discussion of the analyses of the Dobson latitudinal band averages, together with some comments on the formation of these averages. Finally, the results from four regional averages of the total ozone data measured with the M–83 filter instruments are presented. In general, the conclusions to be drawn from the M–83 data parallel those from the Dobson data.

The statistical treatment of the total ozone data from the Bismarck station has been described in detail earlier in this chapter to illustrate the various influences acting on total ozone. Many possible statistical models have been tried with various combinations of the QBO, the solar cycle, and the effect from the atmospheric testing of nuclear weapons. The model results also depend upon whether a year-round trend is assumed or whether differing monthly trends are allowed. Still more analyses can be made by changing the time period being analyzed and the starting

dates of the proposed trends. The symbols used in the Appendix to this chapter list the effects included (Q for QBO, S for solar, and N if the bomb test parameter has been included) and the last two digits of the year in which the linear trend begins; e.g., QS70 describes an analysis including parameters for the QBO, the solar cycle, and a ramp beginning in 1970. Two possible QBO parameters were tested for each station; it was found that the one with zero lag (i.e., using concurrent monthly averages for the 50-mbar Singapore wind speed and the total ozone) was the more significant for nearly all stations except those between 19°N and 40°N. When the Singapore wind speed was lagged 6 months behind the ozone value, the stations in the 19°N–40°N band showed better correlation than for the concurrent values. Thus, the concurrent values are given for all stations outside this band, while the values found using the lagged QBO variable are given for the stations inside this band. The QBO effect will be discussed in more detail later in this chapter.

The results of 12 multiple regression models used to describe the data of the individual stations are given in Appendix 4.B.(i). Two selections of possible time periods for data to be analyzed have been made. In parts (a) and (b), monthly ozone averages measured between January 1965 and December 1986 are analyzed, while in parts (c) to (f) all data after January 1957 are treated. The quality and reliability of the band average data are much better after 1963, chiefly because many more stations are available (the U.S. station data effectively begin in 1963), and the pre-1965 data are complicated by the extensive atmospheric testing of nuclear weapons. For these reasons, the primary emphasis in our determination of statistical trends has been placed on band average and station data since January 1965. However, for completeness of record, station data prior to 1963 have also been included. Data prior to the International Geophysical Year (1957–1958) are so scarce that very little consideration has been given to any records before 1957.

Year-round and monthly linear trends starting in 1970 are calculated in parts (a), (c), and (e), whereas (b), (d), and (f) represent tests for trends starting in 1976. All models include terms for the QBO and the solar cycle, and parts (e) and (f) also include the term for the calculated atmospheric bomb test effect at the appropriate latitude. The parameters given in the tables for the geophysical effects are those calculated in the models that include individual monthly trends. The equivalent coefficients found from the year-round trend model are essentially the same, as illustrated earlier with the Bismarck data. It should be noted that not all stations provide data records suitable for testing by all six models, for various reasons: stations whose data record starts after 1965 are not tested for the nuclear effect, nor are those in the Southern Hemisphere where the bomb test effect is predicted by model calculations to be negligible; stations whose records start after 1976 are tested only for a trend starting in 1976.

4.6.2.1 Changes Between 1970 and 1986 Using Data From 1965 Onward

In the first part of this discussion, only data after 1965 are considered, the linear trends are taken as starting in 1970, and terms for the QBO and the solar cycle are included. All of these results are given in Appendix 4.B.(i).(a). Table 4.16 contains the summer and winter trends for the stations for which provisionally revised data are available. This table is similar to Table 4.12, where the differences in the monthly means between two 11-year periods, 1965–1975 and 1976–1986, are given. The figures in Table 4.16 represent trends in DU per year. The stations are divided according to the latitude bands in which they lie. It can be seen that the more northerly stations have larger wintertime (DJFM) losses than the more southerly stations: the simple arithmetic DJFM averages for the three sets of stations north of 30°N are -1.62, -1.09, and -0.28 DU per year for 53°–64°, 40°–53°, and 30°–39°N, respectively. These compare to average summertime (MJJA) trends of +0.02, -0.39, and -0.36 DU per year for the same three bands.

Table 4.16 Winter and Summer Trends for Individual Stations

Station	Summer Trend	Winter Trend
53°–64°		
Reykjavik*	+1.49 ± .79	−2.98 ± 1.51
Lerwick	−0.53 ± .27	−1.59 ± .47
Leningrad*	−0.18 ± .35	−1.58 ± .75
Churchill	−0.44 ± .32	−1.37 ± .48
Edmonton	+0.05 ± .31	−1.56 ± .55
Goose	−0.27 ± .31	−0.65 ± .53
40°–52°		
Belsk	+0.02 ± .29	−1.55 ± .57
Bracknell*	−0.62 ± .30	−1.43 ± .57
Uccle*	−1.31 ± .45	−0.87 ± .80
Hradec Kralove	+0.20 ± .32	−2.06 ± .60
Hohenpeissenberg*	−0.19 ± .26	−0.69 ± .52
Caribou	−0.35 ± .26	−1.48 ± .55
Bismarck	−0.54 ± .29	−1.15 ± .41
Arosa	−0.51 ± .23	−0.96 ± .50
Toronto	−0.56 ± .28	−0.82 ± .53
Sapporo	0.00 ± .29	−0.43 ± .46
Rome	+0.10 ± .26	−0.70 ± .44
Boulder	−0.96 ± .23	−0.96 ± .40
30°–39°		
Cagliari Elmas	−0.48 ± .28	−0.64 ± .45
Wallops Is.*	−0.39 ± .34	−0.30 ± .70
Nashville	−1.02 ± .25	−0.74 ± .42
Tateno	−0.19 ± .25	−0.10 ± .48
Srinigar	−0.25 ± .22	−0.30 ± .38
Kagoshima	−0.19 ± .24	+0.19 ± .30
Quetta*	+0.01 ± .26	−0.23 ± .47
Cairo*	−0.34 ± .42	−0.76 ± .95
Mauna Loa	−0.07 ± .16	−0.36 ± .33
Southern Hemisphere		
Huancayo	−0.16 ± .09	−0.20 ± .10
Samoa*	−1.24 ± .39	−1.13 ± .30
Aspendale	−0.69 ± .20	−0.61 ± .31
MacQuarie Isle	+0.15 ± .39	+0.36 ± .53

Trends are shown as Dobson Units per year. They are calculated using the data from 1965 onward with the ramp starting in 1970. An asterisk (*) denotes those stations whose records start after January 1965.

Notes: 1. Northern Hemisphere winter is December through March; Northern Hemisphere summer is May through August; Southern Hemisphere winter is June through July; and Southern Hemisphere summer is November through February. 2. Errors are estimates: the correct method is to include the covariance terms for each month. The approximation used here is to assume that the ratio of the covariance to the variance of each latitude band (as shown in Table 4.26) is the same as that for the individual stations.

A second point is that there is a larger difference between the winter–summer values for the more northerly stations. Some of the stations shown do not have 22 years of data from 1965 through 1986, and the results from those stations should be treated with more care. For instance, Reykjavik shows a very large winter loss of –2.98 DU per year compared to a mean for the six stations in that band of –1.62 DU per year. The summer value is also extreme, though this time in a positive sense, being +1.49 DU/yr compared to the band average of +0.02 DU/yr. The overall pattern of trends found by analyzing the individual station data is reassuringly similar to that found from the analyses of the band data. (Uncertainty estimates for the average trends from several stations are not given because the correlations between the data from nearby stations are not calculated. It is reasonable to suppose that the uncertainties are similar to those calculated for the latitude band averages discussed in Section 4.6.3, and slightly less than the individual station uncertainties given for the monthly trends in Appendix 4.A of this chapter. Reinsel et al. make allowance for the correlation involved when two stations measure ozone in the same parcel of air producing two sets of data not completely independent of one another.

The ozone changes for the 17 years after 1986 as calculated from the monthly trend coefficients are shown in Figure 4.45 for 17 different Dobson stations. Taking initially only the stations north of 40°N, the winter time loss and its contrast with summer are clearer at some stations (e.g., Bismarck, Edmonton, Belsk, Caribou, and Hradec Kralove) than at others (e.g., Bracknell, Uccle, Hohenpeissenberg, and Sapporo). Much of this apparent difference in behavior is the result of the natural variability of total ozone at any particular site, but there may be some systematic features at work as well. The rationale behind making latitude, and not longitude, the second dimension of a 2-D photochemical model is that latitudinal differences in ozone distribution and behavior are generally greater than longitudinal ones. This can be seen most clearly in the average global distribution of ozone shown in Figure 4.12. Longitudinal differences at comparable latitudes may be detectable through comparison of individual station results.

However, examination of the trends of seven stations in both Europe (Lerwick, Belsk, Bracknell, Hradec Kralove, Hohenpeissenberg, Arosa, and Rome) and North America (Churchill, Edmonton, Goose, Caribou, Bismarck, Toronto, and Boulder) reveals no difference in the seasonal trends over the two continents. These stations were chosen by the length of their record, and the same number was chosen for each continent. The unweighted numerical averages of the monthly trend coefficients for these stations are shown in Table 4.17. Also given in Table 4.17 are the ozone values for Sapporo, which is in a different meteorological region. There is very little difference between the European and North American blocks, and they can be contrasted with Sapporo, which does not exhibit a significant loss or gain of ozone at any season of the year. Losses appear in the Sapporo ozone record for December and March, but no shape is apparent in Figure 4.45. It is unfortunate that there is only one Dobson station in this region because of the possibility that any single station may be responding strongly to specific local effects. The other two Japanese stations, Tateno and Kagoshima, show a similar lack of significant wintertime change in ozone, but they are at lower latitudes, so that a fair comparison cannot be made between their observations and those from Western Europe and North America poleward of 40°N. The two Far Eastern M–83 stations also are not directly comparable because of their location, instrument, and time of record, but the indicated trends from the Far Eastern M–83's are generally similar to the Sapporo observations. In contrast, the Siberian and European M–83 ozone results do show the wintertime loss and winter–summer differences characteristic of North America and Western Europe.

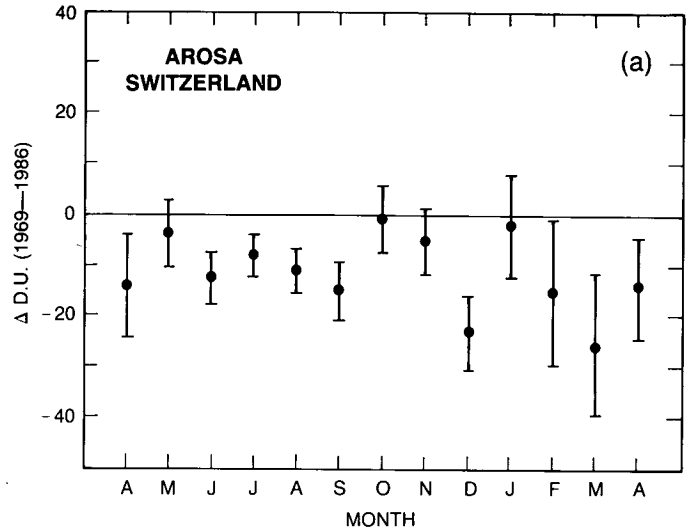
AROSA
SWITZERLAND
(a)
40
20
0
-20
-40
Δ D.U. (1969—1986)
A M J J A S O N D J F M A
MONTH

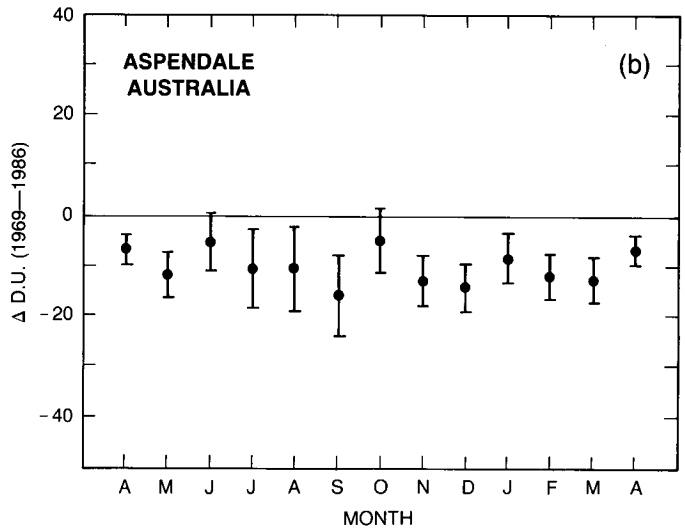
ASPENDALE
AUSTRALIA
(b)
40
20
0
-20
-40
Δ D.U. (1969—1986)
A M J J A S O N D J F M A
MONTH

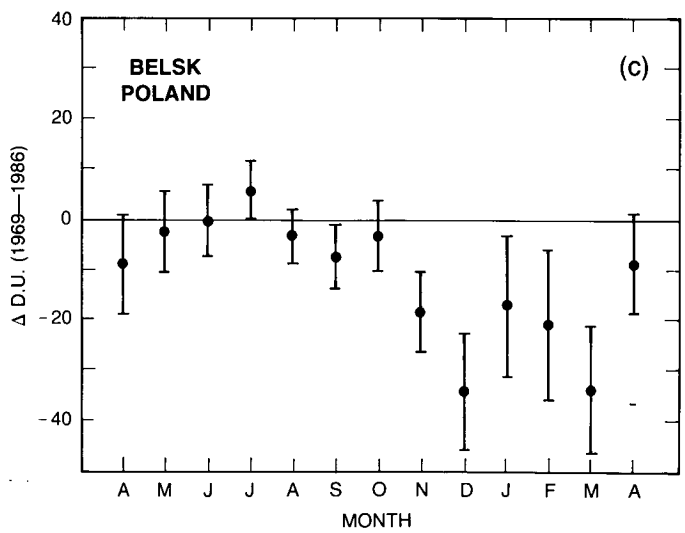
BELSK
POLAND
(c)
40
20
0
-20
-40
Δ D.U. (1969—1986)
A M J J A S O N D J F M A
MONTH

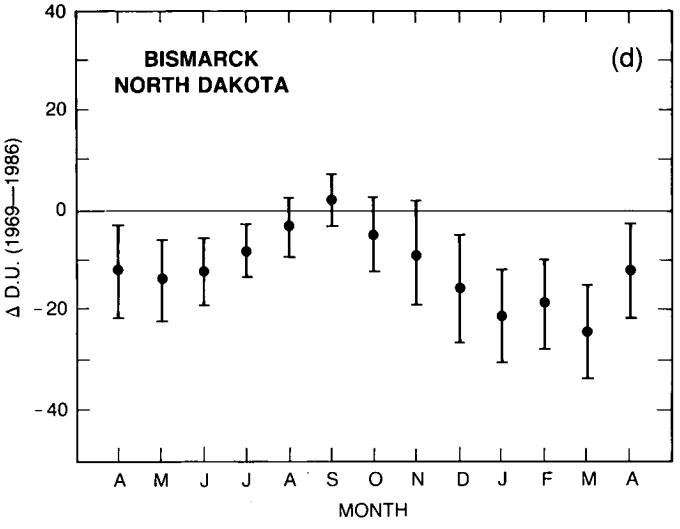
BISMARCK
NORTH DAKOTA
(d)
Δ D.U. (1969—1986)
40
20
0
-20
-40
A M J J A S O N D J F M A
MONTH

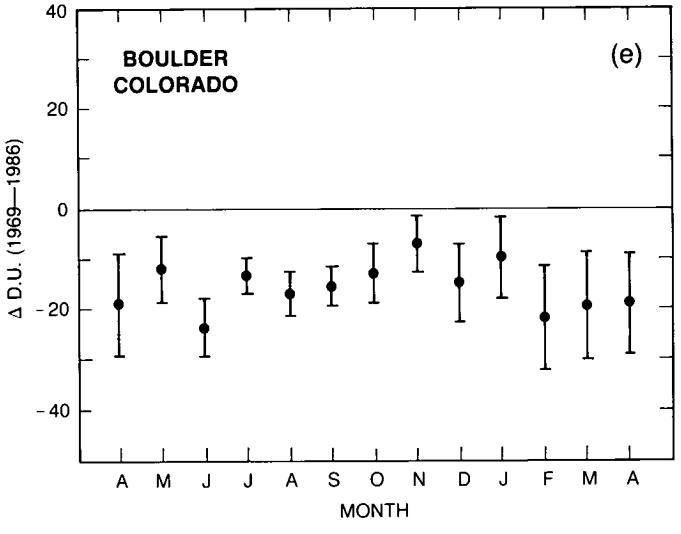
BOULDER
COLORADO
(e)
Δ D.U. (1969—1986)
40
20
0
-20
-40
A M J J A S O N D J F M A
MONTH

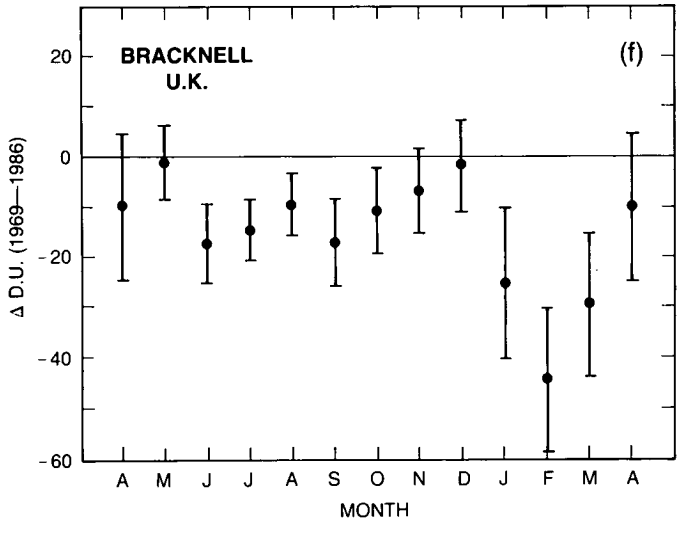
BRACKNELL
U.K.
(f)
Δ D.U. (1969—1986)
20
0
-20
-40
-60
A M J J A S O N D J F M A
MONTH

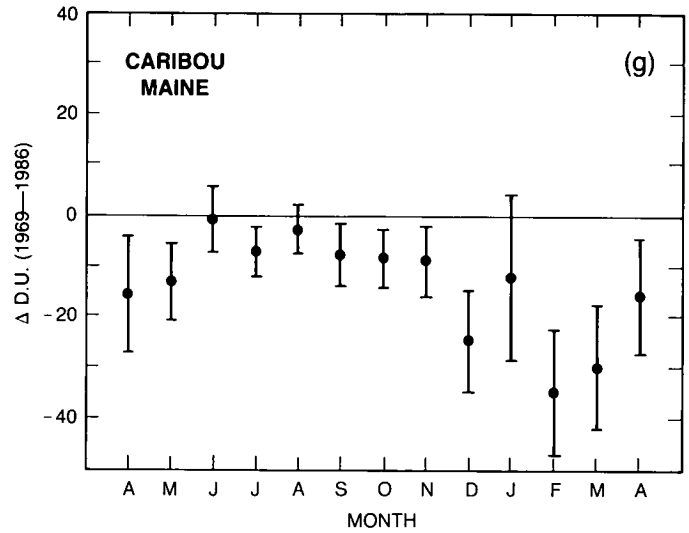
CARIBOU
MAINE
(g)
40
20
0
-20
-40
Δ D.U. (1969—1986)
A M J J A S O N D J F M A
MONTH

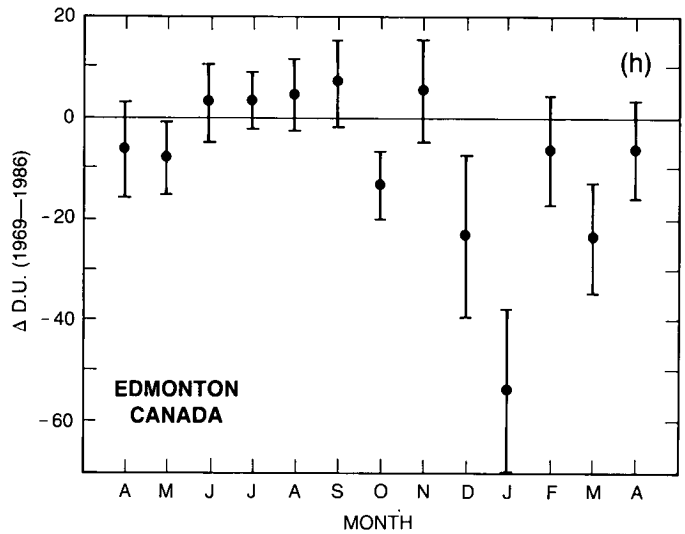
(h)
20
0
-20
-40
-60
Δ D.U. (1969—1986)
EDMONTON
CANADA
A M J J A S O N D J F M A
MONTH

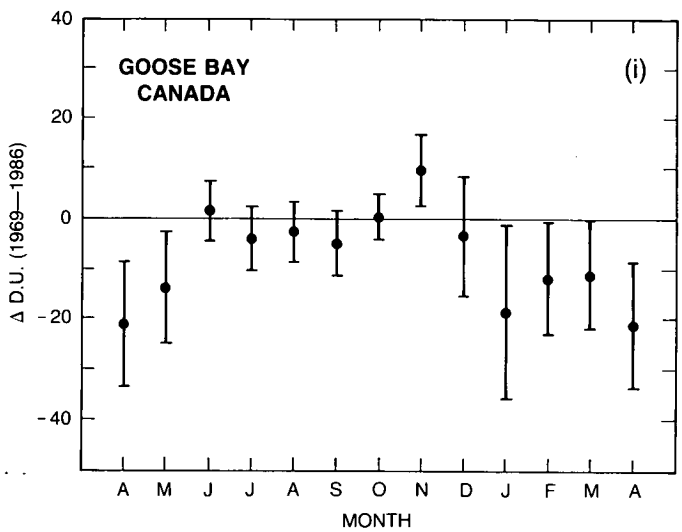
GOOSE BAY
CANADA
(i)
40
20
0
-20
-40
Δ D.U. (1969—1986)
A M J J A S O N D J F M A
MONTH

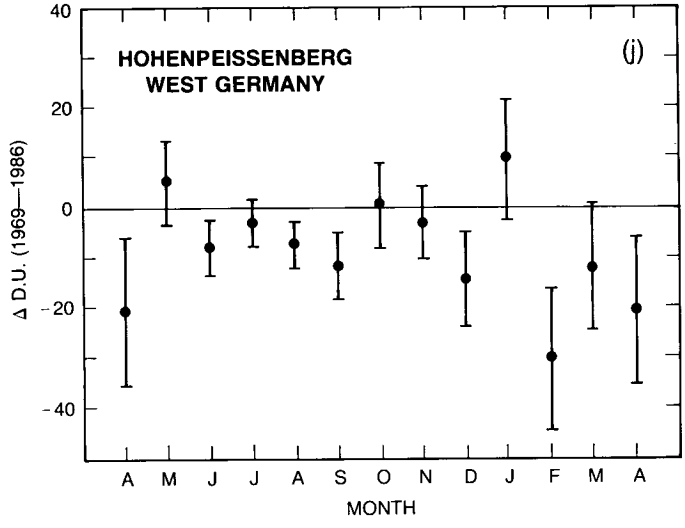
HOHENPEISSENBERG
WEST GERMANY
(j)
40
20
0
-20
-40
Δ D.U. (1969—1986)
A M J J A S O N D J F M A
MONTH

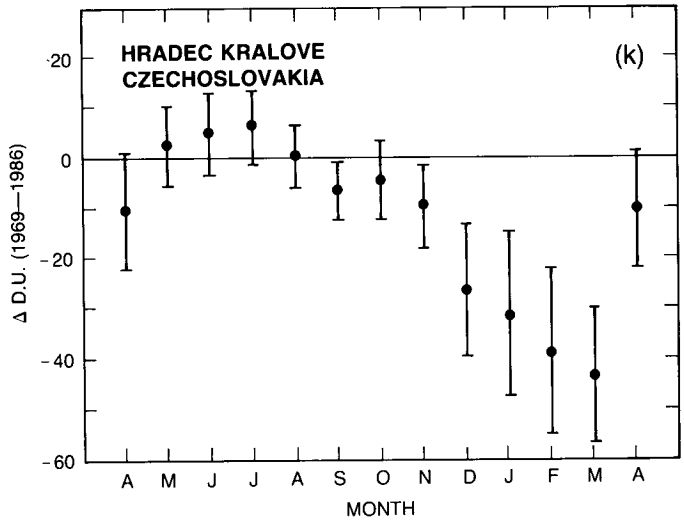
HRADEC KRALOVE
CZECHOSLOVAKIA
(k)
20
0
-20
-40
-60
Δ D.U. (1969—1986)
A M J J A S O N D J F M A
MONTH

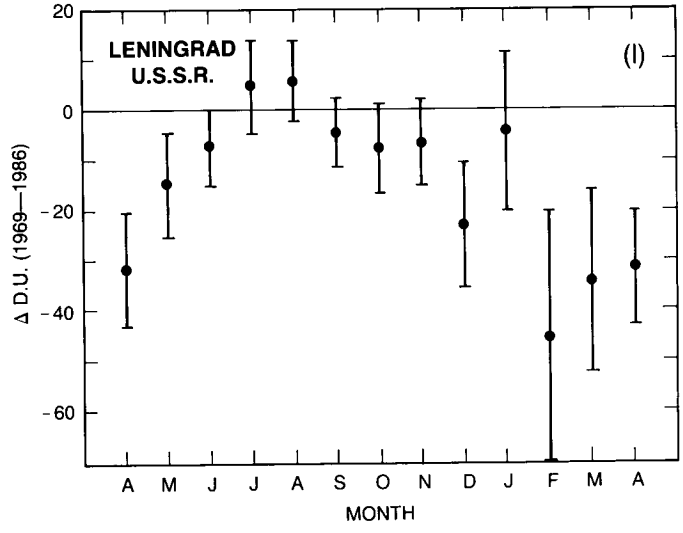
LENINGRAD
U.S.S.R.
(l)
20
0
-20
-40
-60
Δ D.U. (1969—1986)
A M J J A S O N D J F M A
MONTH

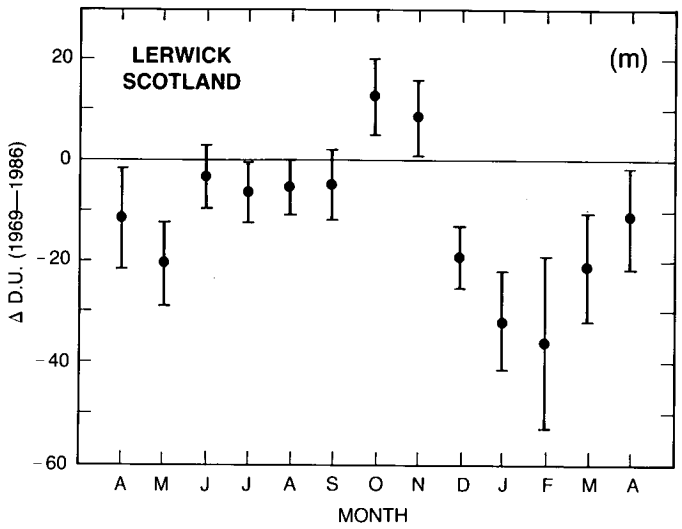
LERWICK
SCOTLAND
(m)
20
0
-20
-40
-60
Δ D.U. (1969—1986)
A M J J A S O N D J F M A
MONTH

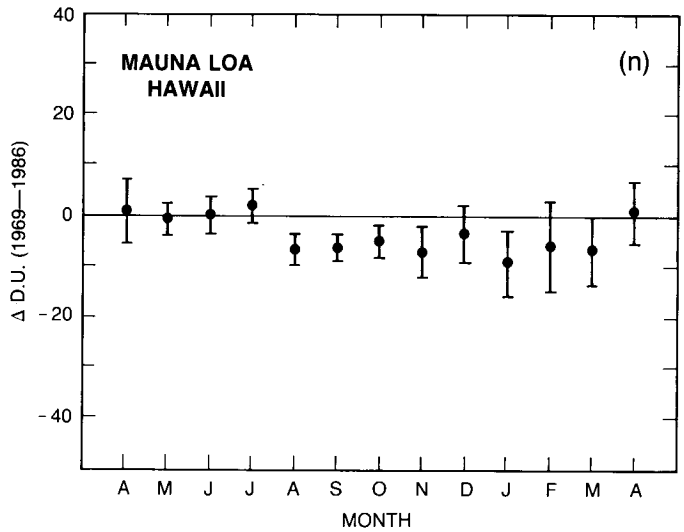
MAUNA LOA
HAWAII
(n)
40
20
0
-20
-40
Δ D.U. (1969—1986)
A M J J A S O N D J F M A
MONTH

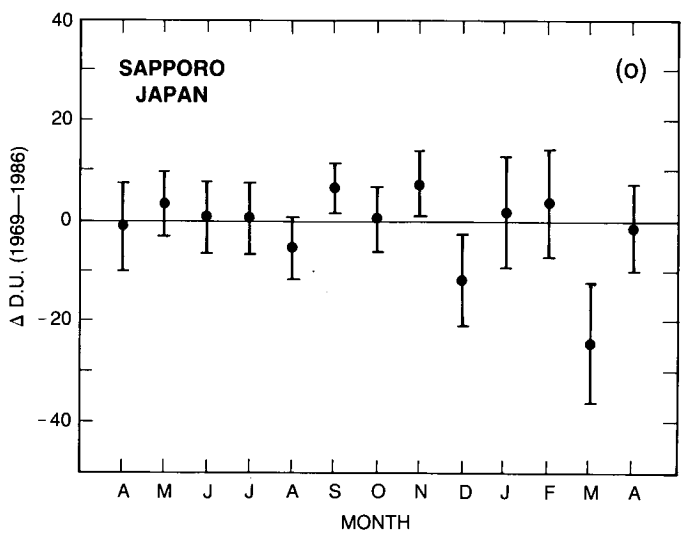
SAPPORO
JAPAN
(o)
40
20
0
-20
-40
Δ D.U. (1969—1986)
A M J J A S O N D J F M A
MONTH

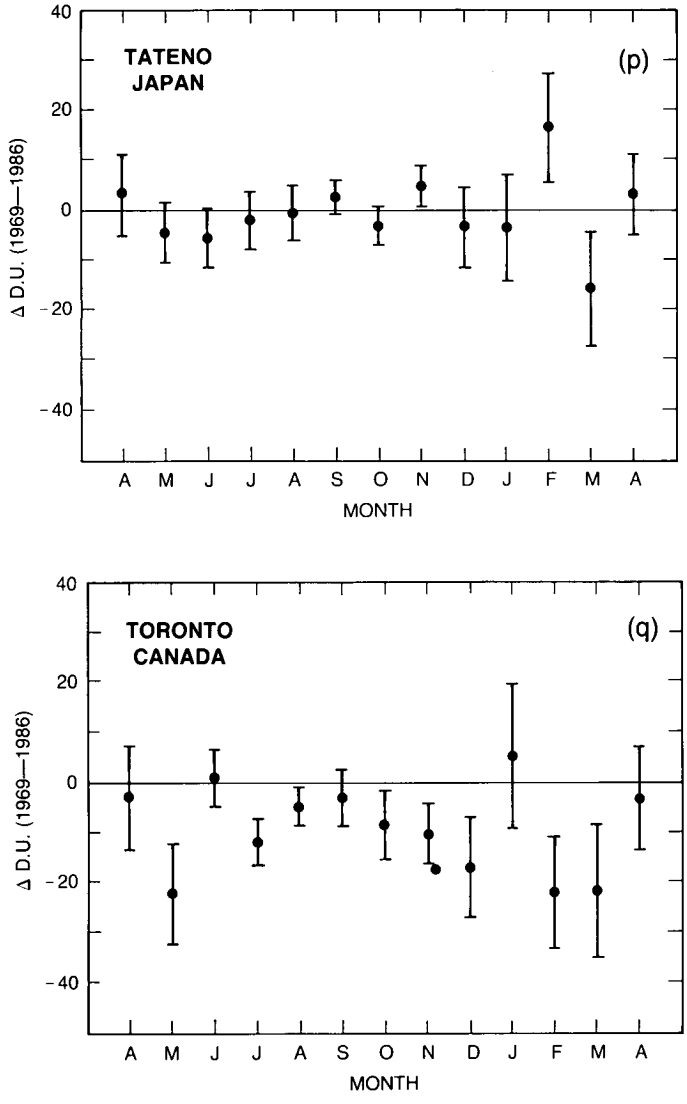

Figure 4.45 Ozone changes for various stations between 1970 and 1986. The statistical model used allowed for effects of the solar cycle and the quasi-biennial oscillation, and data from 1965 (or when the station started making total ozone measurements if it did so after 1965) to 1986 were used. The ozone change in each month was assumed to have occurred in a linear fashion after 1969. The monthly ozone changes plotted are not trends; they are found by multiplying the calculated trend by the 17-year period over which the loss was assumed to have occurred. The vertical bars represent ± one standard error in the estimate of the change. (a) Arosa, Switzerland, (b) Aspendale, Australia, (c) Belsk, Poland, (d) Bismarck, USA, (e) Boulder, USA, (f) Bracknell, UK, (g) Caribou, USA, (h) Edmonton, Canada, (i) Goose Bay, Canada, (j) Hohenpeissenberg, FRG, (k) Hradec Kralove, Czechoslovakia, (l) Leningrad, USSR, (m) Lerwick, UK, (n) Mauna Loa, USA, (o) Sapporo, Japan, (p) Tateno, Japan, (q) Toronto, Canada.

Two possibilities exist: either Japan is in a meteorological regime that does not allow the processes that are causing the winter loss to occur, or there is an instrumental problem that has not been identified. The latter is unlikely: the Japanese operate their own version of the Dobson, but satellite overpasses do not indicate any problems in recent years and there are no known reasons that would cause a seasonal change in total ozone to have been exactly cancelled by a

Table 4.17 Average Monthly Ozone Changes for Different Continents, 1970–1986 (Data for 1965–1986).

	Europe	North America	Japan (Sapporo)
January	−0.96	−1.15	+0.13
February	−1.56	−1.19	+0.22
March	−1.51	−1.14	−1.40
April	−0.69	−0.78	−0.06
May	−0.13	−0.82	+0.21
June	−0.28	−0.23	+0.05
July	−0.19	−0.41	+0.04
August	−0.27	−0.30	−0.31
September	−0.55	−0.18	+0.40
October	−0.02	−0.60	+0.04
November	−0.32	−0.14	+0.45
December	−1.10	−1.09	−0.67
Average	−0.63	−0.67	−0.08

The average trends of seven European and seven North American stations are given in the first two columns. In the third column are the trends for Sapporo, Japan. The trends cover the period 1970–1986 and are given in Dobson Units per year. They are taken from the model that contains terms for the QBO and the solar cycle with only the data after January 1965 used. The North American stations are Churchill, Edmonton, Goose, Caribou, Bismarck, Toronto, and Boulder. The European stations are Lerwick, Belsk, Bracknell, Hradec Kralove, Hohenpeissenberg, Arosa, and Rome. All are north of 40°N.

seasonal change in the instrument response. A scattered light or μ-dependence problem would be expected to show up most at the solstices in December and June. The most probable explanation is that Sapporo is sampling a meteorological regime less influenced by the processes causing wintertime loss over the major northern continental regions. Figure 4.46 does show that

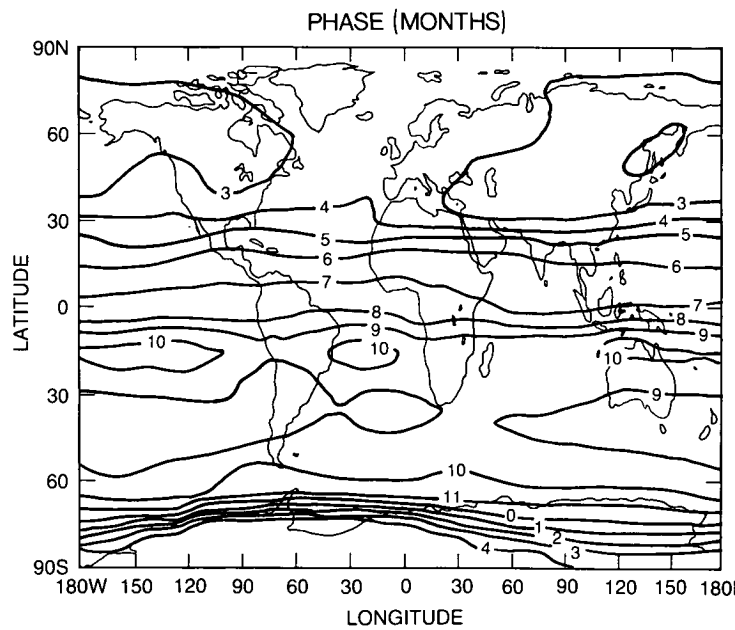

Figure 4.46 Phase of total ozone maximum (from Bowman and Krueger, 1985).

the total ozone maximum at Sapporo is reached at the beginning of March, one of the earliest ozone maxima in the Northern Hemisphere.

Between 30°N and 40°N, provisionally revised data have been prepared for eight stations. No strong seasonal variation is found in the trends at any of these stations, so that the yearly trend has as much meaning as any of the monthly trends. The average of the ramps using the year-round model is −0.16 DU/yr, while the average of the means of the monthly coefficients is −0.23 DU/yr, which indicates that there still is a greater loss in the months with the greater interannual variation. Propagation of the standard errors of the year-round trends gives an uncertainty of .06 for the former of these two annual loss estimates. There is a wide geographical distribution of these eight stations so that the interstation correlation is small and this uncertainty estimate is reasonable, although probably on the low side. Thus, between 30°N and 40°N, there is a year-round loss without any obvious seasonal character.

South of 30°N, the number of stations for which provisionally revised data sets have been produced is smaller, and we can have less confidence in the quality of the data as there is less detailed information available on the day-to-day running of the stations. The main exceptions are Mauna Loa, whose record is in the process of being totally reprocessed, and Samoa, whose record only starts in January 1976. The paucity of Dobson data for the three-quarters of the atmosphere that lies south of 30°N is very unfortunate. The records at Mauna Loa and Samoa (Appendix 4.B.(i).(b)) both show an ozone decrease in recent years. Neither shows much sign of any seasonal nature to the change. The 22-year record from 1965 at Mauna Loa exhibits a year-round trend of −0.24 ±0.13 DU per year since 1970, which corresponds to a drop of 1.5% ±0.8% between 1970 and 1986. Samoa, with its 11-year record from January 1976–December 1986, shows a year-round trend of −0.85 ±0.25 DU per year over the entire time period. This corresponds to a decrease of 3.7% ±1.1% over just 11 years. The 1976 annual average is the highest in the 11 years of Samoan measurements. The station closest to Samoa in latitude is Huancayo, Peru, which also shows a significant year-round loss of −0.33 ±0.10 DU per year (−1.4% ±0.43% over 11 years) from 1976 through to 1986, but only −0.18 ±0.06 DU per year (−1.2% ±0.43% over 17 years) when the ramp is started in 1970. The Huancayo data taken by themselves suggest that this ozone loss of about 1.3 percent occurred between 1976 and 1986. The yearly average of total ozone at Huancayo in 1976 is the highest in its 23 years of observations, with 4 months posting long-term highs and 3 others being the second highest on record. Some of the larger decrease seen at Samoa versus Huancayo (or Mauna Loa) could, thus, be the result of an unusually high year at the start of the Samoa record, and these calculated trends should be treated with appropriate caution.

Aspendale and MacQuarie Isle are the only two Southern Hemisphere stations outside the Tropics for which provisionally revised data have been produced. Of these, the Aspendale station is the more reliable, as MacQuarie Isle has traditionally had problems because of its unfavorable position both for the observer and for the actual observations, with most taken from cloudy skies with cloud transfer tables that need improvement (Atkinson and Easson, 1988). A decrease in total ozone is observed at Aspendale (−3.0% ±0.8% year-round from 1970 to 1986) but no season shows a greater change than any other. No significant change has been recorded at MacQuarie Isle.

4.6.2.2 Changes Between 1976 and 1986 Using Data From 1965 Onward

Faith in the robustness of the conclusions that have been drawn can be increased by examination of the observed differences when the start of the trend is set at 1976 rather than 1970.

Comparison of the results for the individual stations reveals that, in general, a more negative trend is found if the linear ramp is started in 1976. The error estimates of the trends at the individual stations also increase by about 50 percent, so that the significance of the coefficients of the shorter slopes is less. Table 4.18 contains the monthly trend averages for the same European and North American stations shown in Table 4.17, but using the results given in Appendix 4.B.(i).(b), and the results can again be taken as representative of more northerly latitudes. The differences between the two continents are again neither large nor significant, with the winter-time losses in each case being larger than the summertime loss.

Table 4.18 Average Monthly Ozone Changes for Different Continents, 1976–1986.

	Europe	North America	Japan (Sapporo)
January	−0.82	−1.38	+0.62
February	−1.62	−1.51	+0.55
March	−1.85	−1.77	−1.77
April	−1.29	−1.38	−0.47
May	−0.40	−1.29	+0.31
June	−0.58	−0.47	+0.44
July	−0.70	−0.67	+0.42
August	−0.36	−0.54	−0.65
September	−0.82	−0.36	+0.66
October	−0.38	−0.93	+0.33
November	−0.59	−0.21	+0.68
December	−1.11	−1.44	−0.72
Average	−0.88	−0.99	+0.03

The average trends of seven European and seven North American stations are given in the first two columns. In the third column are the trends for Sapporo, Japan. The trends cover the period 1976–1986 and are given in Dobson Units per year. They are taken from the model that contains terms for the QBO and the solar cycle with only the data after January 1965 used. The North American stations are Churchill, Edmonton, Goose, Caribou, Bismarck, Toronto, and Boulder. The European stations are Lerwick, Belsk, Bracknell, Hradec Kralove, Hohenpeissenberg, Arosa, and Rome. All are north of 40°N.

Comparing the trends given in Table 4.18 with those given in Table 4.17 reveals that the measured rates of loss at all times of year are generally greater when the hockey stick is pivoted at 1976 rather than 1970, although none of the results from particular months at individual stations shows linear trends from 1976 on that are significantly greater than the 1970 trends. In every month, the average trends over North America are larger when measured over the shorter time period, and the same is true over Europe, with the sole exception of January. The largest changes are seen for April–July. The lack of similarity to Sapporo is still marked. Not only is there no sign of any seasonal change there, but the trends of 8 of the months become more positive while the trends at the other 4 become more negative. The fitting of a linear trend to the data is, of course, simply a convenient, nonphysical treatment of the data. If the changes in ozone concentrations really were linear for the entire period from 1970 on, then the fitting of a ramp from 1976 on should result in a lesser apparent change in total ozone because the pretrend mean would have a lower value from the inclusion of 1970–1975 in the assumed stable mean before 1976. However, a first approximation check can be made by comparing the separately estimated ozone losses from 1970 and 1976 linear trends. For the European stations, the indicated average losses are 10.7 DU for the 1970 linear trend ($17 \times k_{70}$), and 9.7 DU for the 1976 trend ($11 \times k_{76}$). The comparable values for North America are −10.4 DU and −10.9 DU, respectively, and for Sapporo −1.4 DU

and +0.3 DU. These differences are all small, indicating that the major contributions to the calculated losses of ozone over Europe and North America occurred after 1976.

Moving south, less of an effect on the monthly or annual trends is observed. The year-round average trends for all the individual stations between 30°N and 40°N are all more negative when the linear ramp is started in 1976. The average of the station ramps using the year-round model is now −0.25 DU/yr, while the overall average of the station averages of the monthly coefficients is −0.30 DU/yr. The propagated standard error is +.08 DU/yr, without any allowance for interstation correlation.

As already mentioned, it is risky to apportion the same importance to the results of the remaining stations as would be warranted by the area that they cover. The calculated trend at Mauna Loa becomes slightly more negative without any sign of a seasonal pattern, and those at Huancayo and Samoa have been discussed. Aspendale shows more negative trend coefficients (k_{76} vs. k_{70}) for every month of the year. Two points are worth making here: (1) the increases in the absolute magnitude of the trend coefficients are spread very evenly throughout the year and (2) the most reliable data are those after 1978, and here a sizeable decrease is found (Atkinson and Easson, 1988). It is hard to see any pattern in the changes observed between the 1970 and 1976 linear trend regressions at MacQuarie Isle.

It is difficult, if not impossible, to say whether the observed more negative linear trends calculated for 1976–1986 over those calculated for 1970–1986 implies that there is a nonlinear decrease in total ozone. Superficial examination of the results would indicate this to be true, but the years 1983 and 1985 both were remarkable for the low level of total ozone, albeit in different parts of the globe. The plots of TOMS total ozone vs. year for various latitude bands (see Section 4.7) show the different latitudes that were affected in these years. Large negative deviations occurred at higher latitudes in the Northern Hemisphere in 1983, while 1985 was a relatively normal year there. (This can also be seen in the provisionally revised tables of data in Appendix 4.A.) At lower latitudes and in the Southern Hemisphere, larger negative deviations were seen in 1985. If these low levels were the result of a natural fluctuation that is not described by the statistical model, their position near the end of the record would cause a false impression that there has been a nonlinear decrease in total ozone. The large natural variability of total ozone makes it hard to pick up any weak signals.

4.6.2.3 Changes Between 1970 and 1986 Using All Available Data

The provisional revision of the data was carried back to the beginning of the station's record, or to January 1957 if observations were made before that date. As indicated earlier, the quantity and perhaps the quality of the data from 1957–1964 were not as high as later, when more stations were in operation and more regular intercomparisons were conducted. Further, the nuclear bomb testing in the atmosphere complicates the interpretation of pre-1965 data. For these reasons, less emphasis is placed in our conclusions upon the results of the statistical data analyses in this section.

Statistical Analyses Without Consideration of the Atmospheric Bomb Tests

These statistical analyses have an inherent lack of geophysical reality because they ignore an important known phenomenon affecting stratospheric ozone—namely, the testing of nuclear weapons in the atmosphere. This unreality is augmented by both the atmospheric modeling of the nuclear tests and the significant contributions from such testing indicated by statistical

calculations allowing for such effects. The results in this section are of interest primarily in numerical comparisons with the more complete geophysical description in the next section, and not for significant statements about the atmosphere itself.

Of the seven European stations that have been considered above as a group, only Lerwick, Arosa, and Rome have records that start in January 1957, while, for the North American stations, the station whose record starts earliest is Edmonton (July 1957). The time periods for which revised station data are available are given in Table 4.10. The wide variety of starting dates makes unwise the comparison of the two groups of stations as before, and it is better to examine them on an individual basis only. The record for Sapporo starts in January 1958, providing 1 year less than the 30-year record of the three European stations. The average of the monthly trends observed at Lerwick, Arosa, and Rome are shown in Table 4.19, together with those calculated at Edmonton and Sapporo. The results from Appendix 4.B.(i).(c) are used. There are clear signs of a wintertime loss in Europe and at Edmonton, although at Edmonton only the March trend is significant at the 2σ level of confidence. (The trend uncertainty estimates for the stations are given in the Appendix to this chapter.) The magnitude of the trends is more positive than those in Table 4.17 for every month except May. The year-round average is calculated as -0.22 DU/yr when the European data from 1957 is used as opposed to -0.66 DU/yr when the shorter time period is used. The reduction in the size of the decrease is not the consequence of using three European stations rather than seven. The average monthly trends for Lerwick, Arosa, and Rome using their data from 1965 to 1986 are shown in parentheses in the first column of Table 4.19, and the magnitudes of these trend coefficients are very similar to those shown in Table 4.17 for the group of seven European stations. Comparison of the annual averages of the two time periods for the 12 stations north of 40°N shows that 8 stations have more negative trends when the shorter time period is considered, 2 have more positive values, and 2 show little change. Little

Table 4.19 Average Monthly Ozone Changes, 1970–1986 (Data for 1957–1986).

	Arosa/Lerwick/Rome 1957–1986 (1965–1986)	Edmonton	Sapporo
January	−0.63 (−0.98)	−1.45	−0.22
February	−0.67 (−1.01)	−0.81	+0.18
March	−0.82 (−1.21)	−1.47	−1.14
April	−0.31 (−0.64)	−0.62	+0.40
May	−0.23 (−0.56)	−0.56	+0.36
June	+0.07 (−0.26)	+0.30	+0.24
July	−0.06 (−0.34)	+0.52	+0.19
August	+0.08 (−0.26)	+0.23	−0.10
September	0.00 (−0.46)	+0.34	+0.34
October	+0.49 (+0.30)	−0.31	+0.56
November	+0.14 (−0.02)	+0.72	+0.62
December	−0.76 (−1.14)	−0.19	−0.22
Average	−0.22 (−0.55)	−0.28	+0.10

The average trends of three European stations (Lerwick, Arosa, and Rome) are given in the first column. In the second and third columns are the trends for Edmonton, Canada, and Sapporo, Japan. The trends cover the period 1970–1986 and are given in Dobson Units per year. They are taken from the model that contains terms for the QBO and the solar cycle with all the available data used. The figures in parentheses in the first column are the average trend coefficients for the same three European stations using only the data from 1965. All these stations are north of 40°N.

noticeable change is found in the magnitude of the trends for the stations between 30°N and 40°N: using the shorter period, one annual average is lower, two show little change, and two show a slight increase. Similar comments apply to the more southerly stations.

Considering the Atmospheric Nuclear Bomb Test Effects

The observation that less negative trends in total ozone are observed only north of 40°N when measurements prior to 1965 are included in the calculations implies that lower ozone values were recorded at these more northerly stations only in the pre-1965 years. It is noteworthy in this respect that the major atmospheric bomb tests were conducted at high latitudes in the Northern Hemisphere and that the largest effects on total ozone from the subsequent injection of large quantities of nitrogen oxides into the stratosphere are calculated to be at these higher latitudes (see Figure 4.44).

Reinsel (1981) investigated the effect on ozone that the program of atmospheric testing of nuclear weapons might have had and concluded that the results of his analysis were "consistent with a maximum decrease in ozone of approximately 2 to 4.5% due to nuclear testing effects in the early 1960s." The function used was similar to that produced by the 1-D photochemical model of Chang et al. (1979) and consisted of a linear decrease from 1961 to 1963 followed by an exponential return with a halflife of about 2 years. Since it was based on a 1-D model, there was no allowance for a possible seasonal variation in response, an effect seen strongly in the current 2-D LLNL calculations. Aside from the seasonality, the two functions are very similar.

Only stations with records starting prior to January 1965 are statistically tested for a possible nuclear effect in the current calculations. Many of these station records start in the years after 1962, and the calculated nuclear coefficient for these stations should be treated carefully. Table 4.20 contains the nuclear coefficients and the standard error estimates for all these stations together with the latitudes and starting date for each station. The stations are split into two categories: those whose records start prior to 1960 and those whose records start between 1960 and 1965. In order to calculate the effect of the bomb tests on total ozone, one multiplies the coefficient shown in Table 4.20 by the value in Figure 4.44 corresponding to the time period of interest and the station's latitude.

For the purpose of this discussion, the maximum effects will be considered and Lerwick will be treated as lying in the 53°–64°N latitude band. The maximum predicted effect at Lerwick from the 2-D calculations is about 30 DU at the beginning of 1963, and, as Lerwick's bomb test coefficient is -0.71, the observed decrease is about 21 DU, or 6 percent. Approximately the same loss is seen at Edmonton, while at Arosa the maximum effect is found to be about -12 DU (20×-0.6), about a 4 percent drop. Similar calculations for the other stations show smaller, but similar, losses over Europe and North America in good agreement with Reinsel's analysis. The significance of the bomb test coefficients varies: those for Lerwick, Edmonton, and Arosa are all significantly different from zero at the 2 sigma level and that for Rome is 1.7 standard errors from zero. These four stations are the most likely to pick up a strong ozone signal from atmospheric testing, as their records start well before the major effect is calculated to have occurred and they are at latitudes where there should have been a large depletion.

There is some indication of a different response over Japan: Sapporo has a smaller coefficient than Arosa or Rome—the two most latitudinally similar of the stations with the long records—and Tateno has a coefficient of $+0.65 \pm 0.46$, which indicates that there was an increase of about 8 DU in early 1963. Cagliari, which is 3 degrees north of Tateno, has a coefficient of -0.38 ± 0.63.

Table 4.20 Statistical Evaluations of Ozone Depletion From Atmospheric Nuclear Testing Using Data From Individual Stations

Station	Bomb Test Coefficient	Observations Began	Latitude (°N)
Lerwick	−0.71 ± .27 (−0.70)	1/57	60
Edmonton	−0.62 ± .27 (−0.60)	7/57	54
Arosa	−0.60 ± .25 (−0.47)	1/57	47
Sapporo	−0.18 ± .31 (−0.22)	1/58	43
Rome	−0.55 ± .33 (−0.58)	1/57	42
Cagliari	−0.38 ± .63 (−0.33)	1/57	39
Tateno	+0.65 ± .46 (+0.58)	7/57	36
Goose	−0.04 ± .21 (−0.01)	1/62	53
Belsk	−0.37 ± .43 (−0.28)	1/63	52
Caribou	+0.09 ± .32 (+0.29)	6/62	47
Bismarck	−0.80 ± .38 (−0.54)	1/63	47
Toronto	+0.38 ± .29 (+0.42)	1/60	44
Boulder	−1.14 ± .67 (−0.27)	1/64	40
Nashville	−0.54 ± .49 (−0.10)	1/63	36
Srinigar	−0.72 ± .75 (−0.53)	2/64	34
Kagoshima	+0.46 ± .56 (+0.17)	4/61	32
Mauna Loa	−2.73 ±1.21 (−2.28)	1/63	20

The upper table contains the bomb test coefficients for stations whose records started before 1960, and the lower table contains the same information for stations whose records started between 1960 and 1965. The bomb test coefficients have no units and should be used as multipliers for the appropriate latitudinal function shown in Figure 4.13. The statistical model contained terms for the QBO and the solar cycle and assumed that there was a linear decrease in total ozone starting in 1970. The numbers in parentheses are the nuclear coefficients for the same model except that the linear decrease is started in 1976.

In all cases, however, the error bars are sufficiently large that the differences are only suggestive. Two interesting points are worth noting. First, the error estimates get larger as latitude decreases. Presumably, this inflation occurs because the signal being sought is smaller at lower latitudes. Second, when the bomb test coefficients for the model where the ramps are started in 1970 are compared with those for the model that starts the ramps in 1976, no change can be seen in the upper half of the table. However, in the case of the 10 stations whose data sets start after 1960, all of the bomb test coefficients are more positive for ramps beginning in 1976. Why this is so is not clear. Two main conclusions can be made from this discussion, each of which is in good agreement with those of Reinsel (1981):

- There was a decrease of several percent in total ozone in the early 1960's, which is consistent with the hypothesis of an effect from the atmospheric testing of nuclear weapons. Further, the more northerly stations with the longer records show the decrease more clearly, as would be expected if this hypothesis were true.

- The observed decrease is smaller than that calculated by the LLNL 2-D model. However, neither the significance of the disparity nor its possible causes is clear.

The effect of the inclusion of the bomb testing term on the trend coefficients is closely related to the size of the total ozone depletion from the bomb tests. The consequence of finding and

allowing for a depletion of ozone prior to the start of the linear ramp is that the unperturbed ozone levels are calculated to be higher than they would be if the depletion were not allowed for. If the unperturbed ozone levels are higher, then the trend coefficients that are calculated will be more negative. The average monthly trends for the three European stations (Lerwick, Arosa, and Rome) are shown in the first column of Table 4.21, and those for the Edmonton and Sapporo stations are given in the second and third columns. The equivalent trends calculated using the model that did not allow for the bomb test effect are shown in Table 4.19; comparison reveals that every single trend is more negative in the case where the bomb test term is included. This effect on recent trends is expected, as ozone depletions are calculated to have been caused by the atmospheric bomb tests for all of these stations.

Table 4.21 Monthly Trends in Ozone When Allowance Is Made for Depletion by Nuclear Testing.

	Arosa/Lerwick/Rome	Edmonton	Japan (Sapporo)
January	−0.81	−1.64	−0.26
February	−0.84	−1.00	+0.13
March	−0.98	−1.65	−1.19
April	−0.46	−0.79	+0.36
May	−0.36	−0.71	+0.32
June	−1.04	+0.17	+0.21
July	−0.16	+0.41	+0.16
August	−0.04	+0.09	−0.13
September	−0.13	+0.18	+0.30
October	+0.33	−0.50	+0.52
November	−0.04	+0.50	+0.58
December	−0.95	−0.39	−0.27
Average	−0.37	−0.44	−0.06

The average trends of three European stations (Lerwick, Arosa, and Rome) are given in the first column. In the second and third columns are the trends for Edmonton, Canada, and Sapporo, Japan. The trends cover the period 1970–1986 and are given in Dobson Units per year. They are taken from the model that contains terms for the atmospheric bomb testing effect as well as the QBO and the solar cycle with all the available data used. All these stations are north of 40°N.

Comparison with the results in Table 4.17 reveals that the negative trends calculated using only the data after 1965 are greater than is the case when all of the data are used and the bomb test term is included. Again, the significance of this difference is not clear, but examination of the raw data reveals that the measurements made in the years around 1960 were also low historically. This last fact is pertinent in the discussion of the effect of the solar cycle on total ozone. On the other hand, if the contributions to ozone loss were assumed to be correctly calculated by the atmospheric models (i.e., greater losses than indicated by the statistical calculations), then better agreement would be found between the negative trends for data starting in 1957 and 1965.

4.6.2.4 Effect of the Circulational Quasi-Biennial Oscillation

A quasi-biennial oscillation (QBO) in temperature, zonal winds, and column ozone at the Equator has been widely noted (Reed, 1960; Veryard and Ebdon, 1961; Wallace, 1973; Angell and Korshover, 1978; Coy, 1979; Tolson, 1981; Hasebe, 1983; Naujokat, 1986). A QBO in total ozone also exists at other latitudes, and Coy, for example, pointed out that the relationship between the QBO in the equatorial winds and total ozone at different latitudes varies according to latitude (see Figure 4.47). A similar variation has been found in our analysis both in terms of the phase

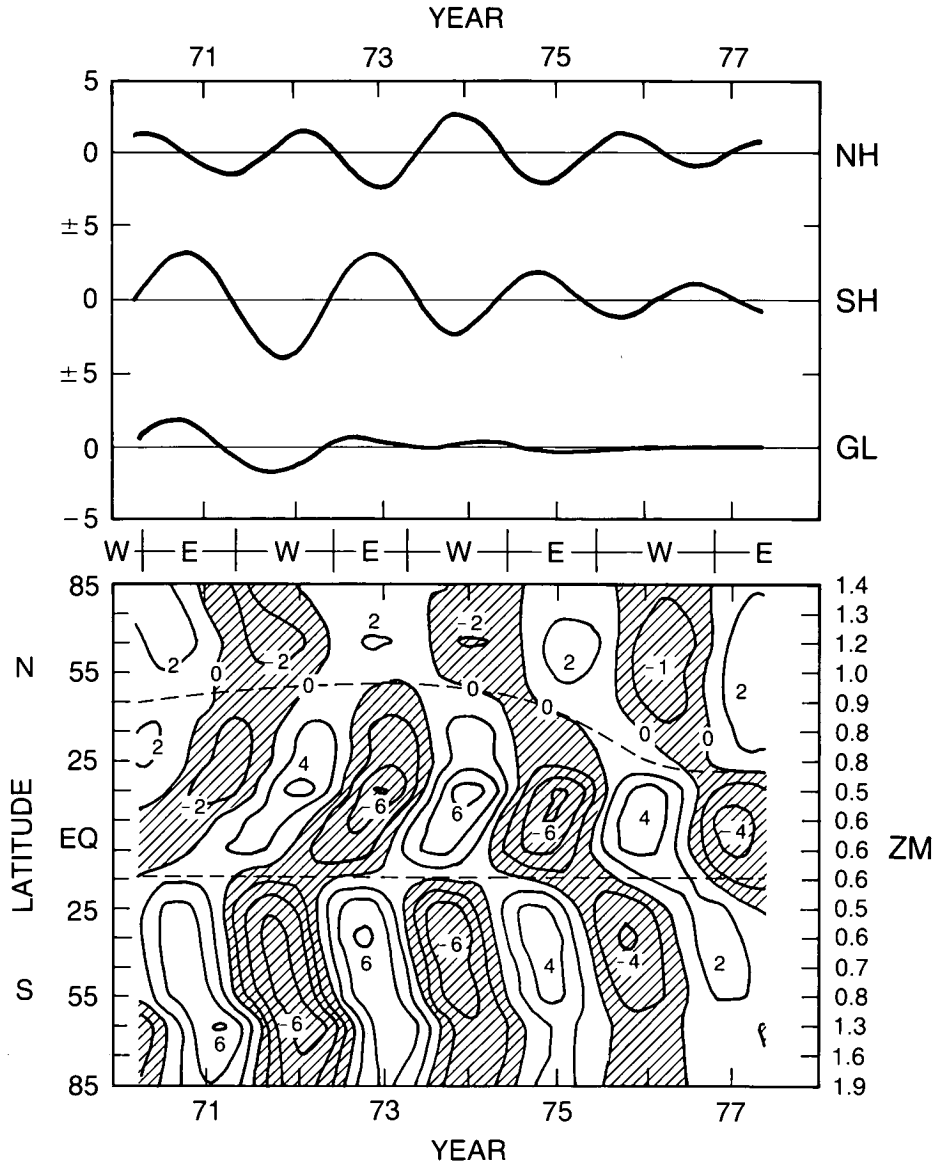

Figure 4.47 Quasi-biennial oscillation of total ozone (Dobson Units—DU) in the mean values of Northern Hemisphere (NH), Southern Hemisphere (SH), globe (GL), and zonal mean values (ZM). Vertical bars and the numerals on the right-end column of ZM indicate the estimates of errors as the confidence limits of about 70 percent. The isopleths in ZM are drawn with the interval of 2 DU, and the shaded areas correspond to those of negative deviations. Letters E and W situated between GL and ZM indicate the easterly and westerly phase, respectively, of the quasi-biennial zonal wind oscillation in the equatorial stratosphere at 50 mbar (taken from Coy, 1979).

and the magnitude. For simplicity, only two phases were tried in this analysis: no lag at all and a 6-month lag. There are four main points:

- Above 40°N, total ozone is found to be low when the Singapore 50-mbar winds are in the westerly phase.

- A minimum in the magnitude of the calculated QBO coefficients is found in the vicinity of 40°N latitude.

- Between 10°N and 40°N, a better correlation is found if the Singapore 50-mbar wind speeds lag the total ozone measurements by 6 months in the statistical model.

- The relatively high frequency of the QBO (there are about 10 cycles in the period 1965–1986) makes its inclusion or exclusion have a negligible effect on the trend estimates.

The first three points are in good agreement with previous analyses as well as with the results of a recent 2-D model (Gray and Pyle, 1988).

The statistical model postulates a simple linear relation between the 50-mbar wind speed at Singapore and total ozone, and such a correlation is observed. Figure 4.48 shows a plot of the magnitude of the QBO coefficients against latitude. All of the stations north of 40°N were tested with the concurrent wind speeds, while those south of 40°N were tested with the wind speed lagged by 6 months. The chances that the relationship is actually so simple are small. Labitzke and van Loon (1988) have proposed that the effect of the QBO and the solar cycle are interdependent. Larger ozone anomalies might then be observed when the solar cycle activity is high at the same time as the tropical 50-mbar winds are westerly. Schuster et al. (1988) examined the high-resolution TOMS data and concluded that, although there is a relationship between equatorial and extratropical QBO signal in the stratosphere, the interannual variability that can be seen in longitudinal time series at high latitudes implies that the equatorial QBO is not a good indicator of the high-latitude interannual variability. Further, they report that the QBO may be modified by a 4-year oscillation or by the eruption of El Chichón in April 1982. Thus, there are good reasons to suppose that the treatment of the QBO in this analysis is too simple. However the high significance of the calculated coefficients (especially at high and low latitudes) indicates that the simple model used does manage to extract much of the QBO's effect on total ozone.

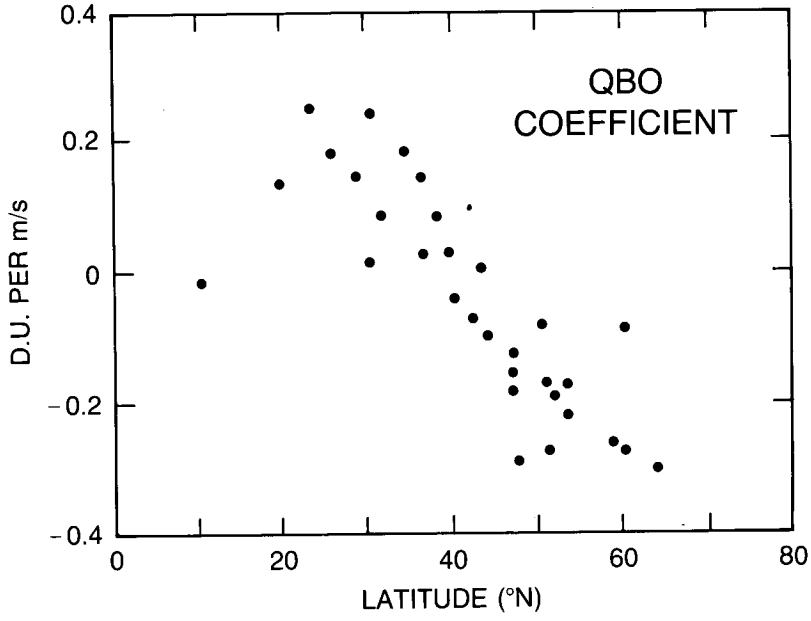

Figure 4.48 The calculated coefficients for the quasi-biennial term are plotted for 31 stations. At all latitudes except those between 30–39°N, the Singapore wind speed was kept concurrent with the total ozone (so that they are anticorrelated in northern latitudes). Between 30–39°N, a 6-month phase lag was imposed on the Singapore wind speed.

In view of the possible factors that are capable of perturbing the atmosphere's response to the QBO, it is worth reconsidering the possible nonlinearity of a decrease in ozone discussed earlier in this section. If there had been no exceptional natural events in the last few years, it would be reasonable to say that there is weak evidence to support the view that there has been a nonlinear decrease, with the rate of loss increasing in more recent years. However, both 1983 and 1985 were years in which low levels of ozone were observed, and they were also both years in which the QBO would be expected to cause negative deviations in total ozone. Two additional events occurred that might have affected total ozone in 1983: the El Chichón volcano erupted in April 1982, injecting large amounts of particulate matter, especially sulfate, into the stratosphere, and in 1983 there was an El Niño. Either the El Chichón eruption or the El Niño might modulate the QBO effect on total ozone as well as having an effect of their own, and because such a modulation is not included in the statistical model, the effects are not accounted for mathematically. In this context, it is worth recalling that in 1983, the 100-mbar temperatures diverged from their historical relationship with total ozone at Bismarck and Churchill, although not at Belsk.

The mechanism through which the QBO of the stratospheric winds at the Equator affects total ozone at other latitudes must be properly understood before it is realistically possible to judge how other events might modulate this effect. Further statistical analyses should be performed to elucidate the character of the relationship as much as possible.

4.6.2.5 Effect of the 11-Year Solar Cycle

The relationship of total ozone with the amount of solar radiation passing through the atmosphere is very complex. The amount of ozone at any place in the atmosphere is dependent on both photochemical and meteorological processes. Variations in the levels of solar radiation reaching the atmosphere will affect the rates of photochemical reactions and the amount of solar energy absorbed. Changes in the heating rates and the temperature distribution in the atmosphere will occur, leading to changes in the circulation patterns as well as affecting the rates of those chemical reactions that are temperature dependent. Further, it is possible that the responses of ozone concentrations to the natural variations in solar radiation are dependent on latitude, altitude, and season. Many studies have looked at the statistical relationship between the solar cycle and total ozone, some of which looked at the short time-scale of 27 days (e.g., Gille et al., 1984c; Hood, 1984; Chandra, 1985; and Keating et al., 1985). Others investigated the link with the 11- and 22-year cycles (e.g., Keating, 1981; Natarajan et al., 1980–1981; Brasseur and Simon, 1981; and Garcia et al., 1984). In a trend analysis where the changes might have occurred over a decade or so, it is important to allow for any total ozone variations that might have occurred on a similar time scale, i.e., the 11- and 22-year cycles. Because of the complexity of the relationship between the solar irradiance and total ozone, the proxy used in most trend analyses is a measured quantity that, it is hoped, is related to the total solar flux. A calculated response such as that for the atmospheric bomb tests has not been used. The 10.7 cm solar flux series was used by Reinsel et al. (1987) and Oehlert (1986). Reinsel et al. found that there was a positive change in global total ozone from solar minimum to maximum of about 1 percent, while Oehlert calculated the change to be +1.3 percent. These are compatible with the model estimates of Garcia et al. (1984). Similar trend studies using the SBUV data from Nimbus–7 are hampered by the fact that the total ozone measurements were started in 1979, near the maximum of the last solar cycle.

The current trend analyses use the smoothed sunspot series shown in Figure 4.42. Bishop (private communication) noted that the response of total ozone to the solar cycle is more

significant when the solar cycle indicator is smoothed and that it is more reasonable on physical grounds to use a smoothed series. (In this case the smoothing is performed by taking the mean of each pair of consecutive 12-month running means of the monthly values.) The calculated solar cycle coefficients for each station are given in Table 4.22 for the model whose results are shown in Appendix 4.B.(i).(a). It is hard to pick out any features within these values, except that there are occasional inconsistent results from geographically proximate stations. Any proportional relationship between the solar activity and total ozone appears to be marginally statistically significant. As mentioned, no attempt has been made to determine whether solar activity modulates the QBO or any other meteorological phenomena in this study.

Table 4.22 Statistical Evaluation of Ozone Variations in Response to the Solar Sunspot Cycle.

Station	Sunspot Coefficient
Reykjavik*	+14.6 ±4.4
Lerwick	+ 6.2 ±3.2
Leningrad	+ 1.4 ±3.9
Churchill	+ 6.0 ±3.2
Edmonton	+ 3.8 ±3.2
Goose	+ 7.6 ±3.0
Belsk	+ 4.4 ±3.3
Bracknell	+ 1.5 ±2.8
Uccle*	+ 4.2 ±3.5
Hradec Kralove	+ 2.6 ±3.8
Hohenpeissenberg	− 0.3 ±2.7
Caribou	+ 7.6 ±3.2
Bismarck	+ 6.2 ±3.0
Arosa	+ 2.7 ±2.2
Toronto	− 0.4 ±3.0
Sapporo	+ 7.0 ±3.2
Rome	+ 4.2 ±2.8
Boulder	+ 0.4 ±2.4
Cagliari	+ 7.6 ±3.6
Wallops Isle*	+ 0.3 ±2.4
Nashville	+ 5.4 ±2.7
Tateno	+ 3.0 ±2.7
Srinigar	+ 5.0 ±2.1
Kagoshima	− 0.3 ±3.6
Quetta	+ 3.0 ±2.8
Cairo	+ 2.0 ±1.6
Mauna Loa	+ 1.5 ±2.4
Huancayo	+ 1.2 ±1.2
Aspendale	+ 2.2 ±2.7
MacQuarie Isle	+ 9.9 ±4.6

The solar cycle coefficients for the individual stations from Appendix 4.B.(i).(a). The units are in Dobson Units per 150 sunspots. The (*) indicates stations whose record starts after January 1970 so that they cover 1.5 solar cycles or less.

4.6.3 Results of the Analysis of Latitudinal Averages of Dobson Data

The provisionally revised data were analyzed with the same sets of statistical parameters after the records from all the stations were combined to form latitudinal band averages. The use of these composite time series enables the inclusion of measurements from stations for which provisionally revised data have been prepared but that are not suitable for time series analysis on their own for reasons associated with length and completeness of records. For instance, measurements were taken at Uppsala, Sweden, from 1950 to 1966: obviously, they can not be tested for a decrease in recent years, but their inclusion increases the number of stations used in forming the early part of the latitudinal band averages.

The deviations of the yearly averages from their long-term means are plotted in Figure 4.49 for four latitude bands: 60–80°N, 53–64°N, 40–52°N, and 30–39°N. The deviations are shown as percentages of the respective belt average for 1957–1986, with the belt averages marked on the right-hand axis. The vertical bars above and below the curves show the approximate single

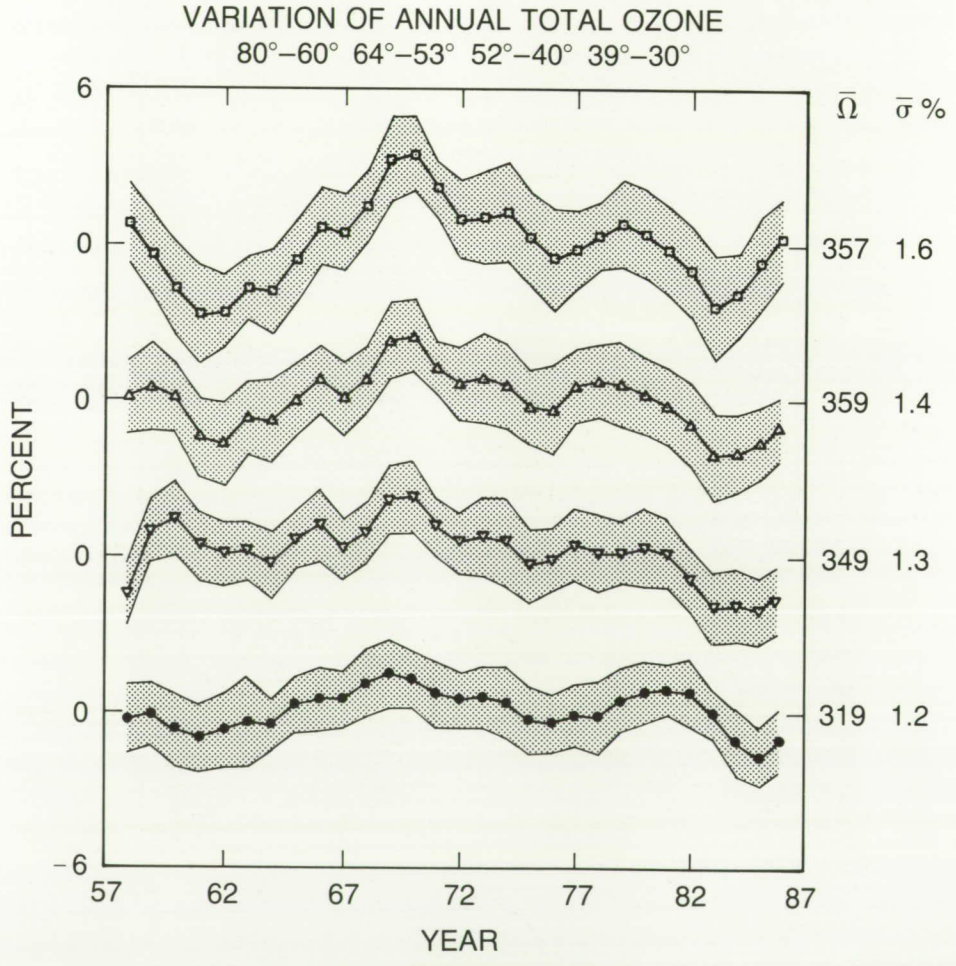

Figure 4.49 Variation of annual total ozone percentage deviations for the three latitude bands 53–64°N, 40–52°N, and 30–39°N. The curves are smoothed by a (1:2:1)/4 smoother. The vertical bars represent ± 1 standard deviation where the standard deviation is calculated from the combination of the individual stations' intramonthly standard deviations with no allowance made for any effects such as regional correlation between stations. The most northerly band has the highest ozone values.

standard deviation uncertainty associated with each point. (The possible uncertainty is found by combining the standard deviations for all the monthly values from the stations that are used to calculate that particular point in the latitudinal band average. No allowance for spatial correlation or autocorrelation is made.) Figure 4.50 shows the deviations and associated uncertainties for the winter values, and Figure 4.51 is the equivalent plot of the summer values for the same belts. The relative quality of the stations' data used to establish the combined files is considered to be moderate, better, best, and better, respectively. It should be noted that the stations located between 60°N and 65°N are included in two latitude belts. This was done to compensate for the scarcity of data at these latitudes and to try to reflect the extremely intensive meridional exchange existing there. However, the stations north of 65°N have varying periods of total polar darkness, and hence lack of data, throwing a heavy weighting onto the 60–65°N stations in the winter months. This 60–80°N latitudinal band average was formed to investigate the behavior of total ozone in the far north. The results should not be compared with the results of the more southerly bands, because there is less data and because some data are also used in the 53–64°N band average.

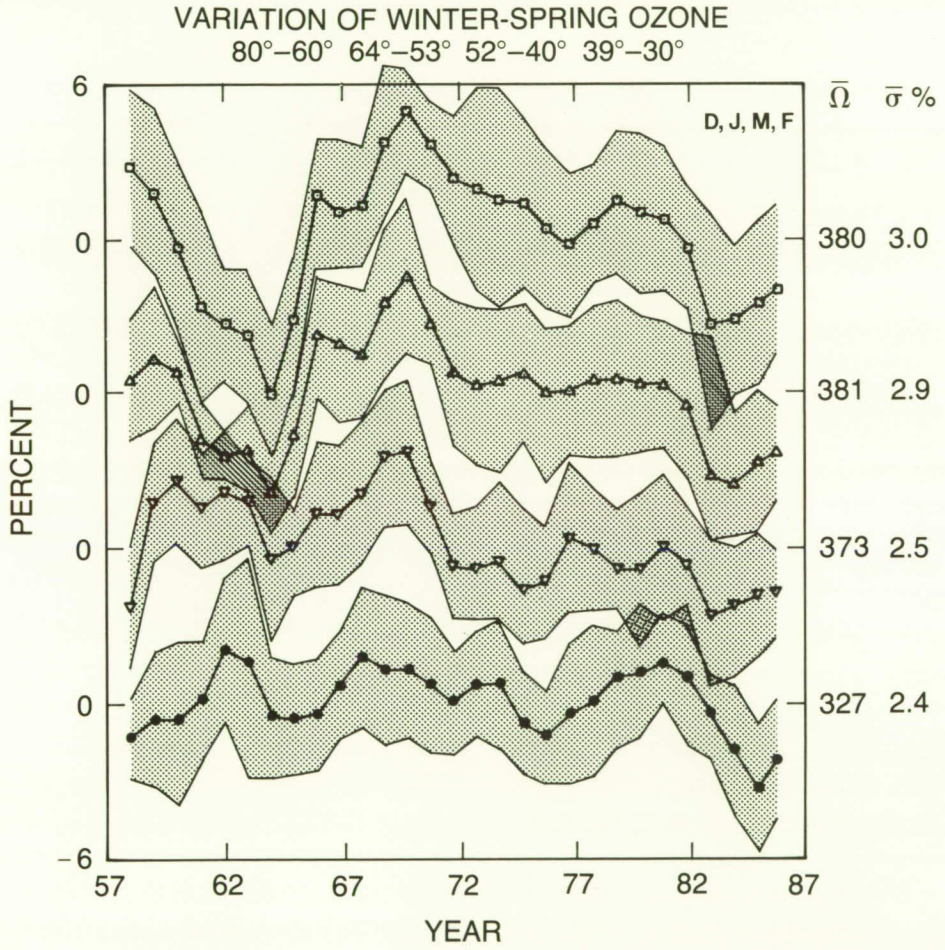

Figure 4.50 Variation of winter total ozone percentage deviations for the three latitude bands 53–64°N, 40–52°N, and 30–39°N. The curves are smoothed by a (1:2:1)/4 smoother. The vertical bars represent ± 1 standard deviation where the standard deviation is calculated from the combination of the individual stations' intramonthly standard deviations with no allowance made for any effects such as regional correlation between stations.

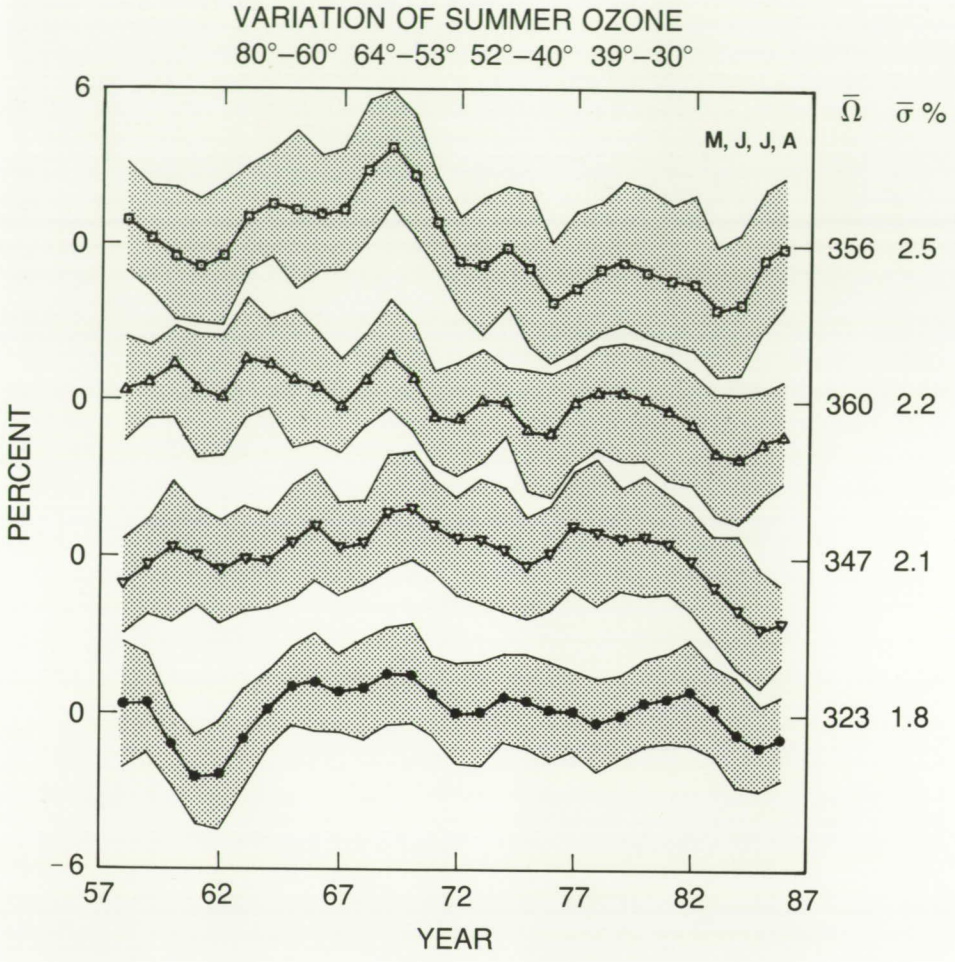

Figure 4.51 Variation of summer total ozone percentage deviations for the three latitude bands 53–64°N, 40–52°N, and 30–39°N. The curves are smoothed by a (1:2:1)/4 smoother. The vertical bars represent ± 1 standard deviation where the standard deviation is calculated from the combination of the individual stations' intramonthly standard deviations with no allowance made for any effects such as regional correlation between stations.

4.6.3.1 Results

The coefficients for the latitudinal band averages found from the six types of analyses described for the individual stations are given in Appendix 4.B.(ii). Table 4.23 contains the results of the model that uses the data from January 1965–1986, starts the ramps in 1970, and includes terms for the QBO and the solar cycle. The monthly losses corresponding to these trend coefficients over the period 1970–1986 are shown in Figure 4.52 for the three main bands. Table 4.24 contains the results of the model that used all the data and that included terms for the QBO, the solar cycle, and the atmospheric bomb tests. The main conclusions are in good agreement with the results of the station analyses:

- There is a high-latitude wintertime loss occurring in the Northern Hemisphere.

Table 4.23 Monthly Coefficients (in DU/Yr) for the Three Latitude Bands for 1965–1986 Data.*

Model Time Period	53–64°N 1/65–12/86	40–52°N 1/65–12/86	30–39°N 1/65–12/86
January	−1.84 ±0.50	−0.56 ±0.45	−0.42 ±0.30
February	−1.79 ±0.71	−1.18 ±0.51	−0.25 ±0.37
March	−1.07 ±0.36	−1.33 ±0.55	−0.72 ±0.38
April	−0.52 ±0.34	−0.58 ±0.41	−0.35 ±0.27
May	−0.52 ±0.27	−0.30 ±0.24	−0.35 ±0.18
June	+0.22 ±0.20	−0.39 ±0.21	−0.64 ±0.19
July	0.00 ±0.22	−0.43 ±0.20	−0.23 ±0.18
August	+0.03 ±0.24	−0.46 ±0.18	−0.18 ±0.18
September	+0.03 ±0.21	−0.53 ±0.19	−0.17 ±0.15
October	−0.19 ±0.21	−0.27 ±0.26	−0.15 ±0.14
November	+0.27 ±0.32	−0.44 ±0.25	−0.02 ±0.13
December	−1.17 ±0.46	−1.08 ±0.33	−0.38 ±0.20
Average	−0.55	−0.63	−0.32
QBO (DU/40ms^{-1})	−6.40 ±2.36	−4.40 ±2.28	+6.00 ±2.00
Solar (DU/150 sunspots)	+5.88 ±2.63	+2.64 ±2.48	+0.33 ±2.00
Yearly Coefficient	−0.14 ±0.13	−0.47 ±0.13	−0.16 ±0.11

*The data from 1965–1986 were analyzed, and trends from 1970, the QBO, and the solar cycle were allowed for in the model (QS70).

- The QBO coefficient is significant at all latitudes and is anticorrelated above 40°N and 6 months out of phase between 30° and 39°N.
- The solar cycle relationship is less clear: according to the band analyses, the effect on total ozone is minimal in the 30–39°N band. However, this is not clear from the results of the station analyses (see Table 4.23).
- The atmospheric nuclear bomb tests had a greater effect at higher latitudes.

The LLNL predictions of the nuclear bomb test effects on ozone appear to agree better at higher latitudes. However, the uncertainties associated with the bomb test parameters are sufficiently high that firm conclusions are difficult. During the early 1960's, ozone deficiency is most pronounced in the winter season plots. While it is possible to attribute these deficiencies to the nuclear bomb tests carried out in the atmosphere, one should not ignore that the QBO was in its westerly phase during 1961 and 1963–1964, and that there was an ENSO in 1964. Both these geophysical events are circulational conditions that could cause (or be coincident with) ozone deficiencies in the northern latitudes. The strongest known ENSO in this century occurred in 1982–1983, overlapping with the westerly phase of the 1983 QBO, and might have contributed substantially to the negative ozone deviations in the mid-1980's (Bojkov, 1987b).

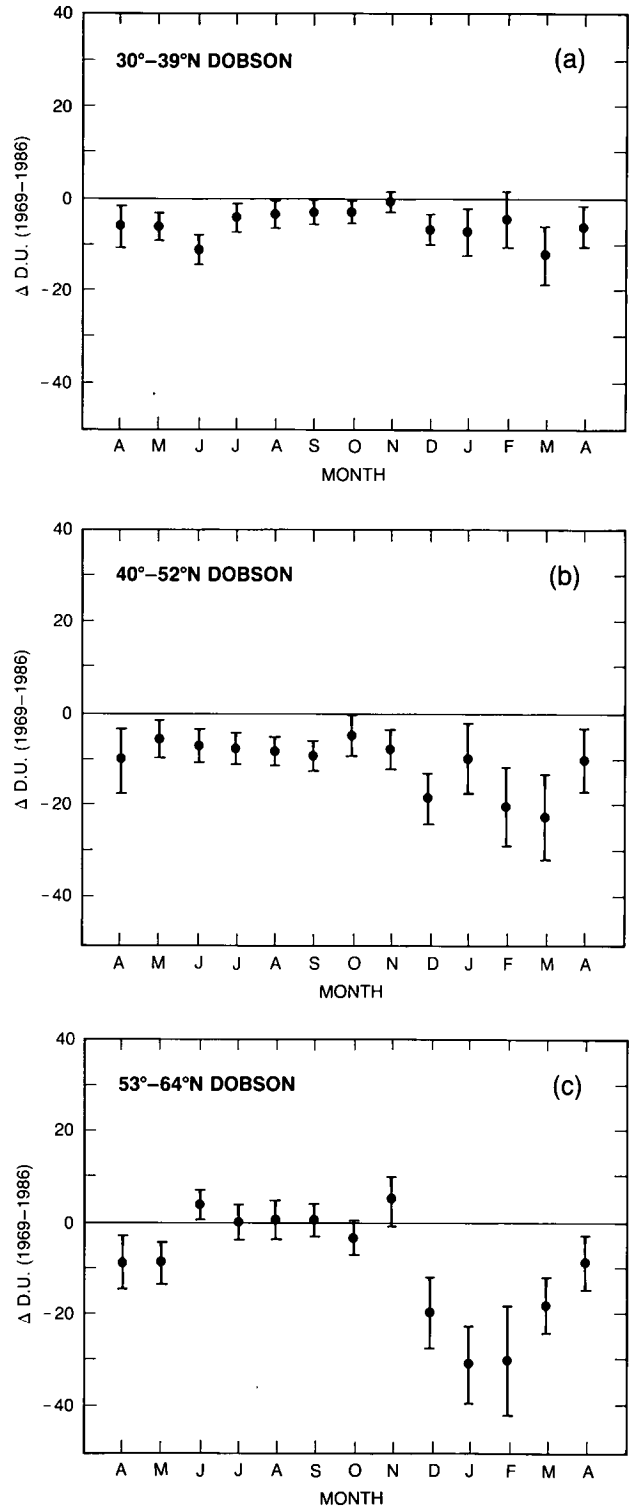

Figure 4.52 Ozone changes for the three latitude bands 53–64°N, 40–52°N, and 30–39°N between 1970 and 1986. The statistical model used allowed for effects of the solar cycle and the quasi-biennial oscillation, and data from 1965–1986 were used. The ozone change in each month was assumed to have occurred in a linear fashion after 1969. The monthly ozone changes plotted are not trends; they are found by multiplying the calculated trend by the 17-year period over which the loss was assumed to have occurred. The vertical bars represent ± 1 standard error in the estimate of the change. (a) 54–64°N, (b) 40–52°N, and (c) 30–39°N.

C-4

Table 4.24 Monthly Coefficients (in DU/Yr) for the Same Bands as in Table 4.23 for 1957–1986 Data.*

Model Time Period	53–64°N 1/57–12/86	40–52°N 1/57–12/86	30–39°N 1/57–12/86
January	− 1.10 ± .47	− 0.81 ± .43	− 0.31 ± .29
February	− 1.70 ± .66	− 1.15 ± .49	− 0.11 ± .36
March	− 0.83 ± .34	− 1.35 ± .53	− 0.43 ± .37
April	− 0.35 ± .33	− 0.48 ± .39	− 0.38 ± .27
May	− 0.51 ± .26	− 0.28 ± .24	− 0.28 ± .18
June	− 0.04 ± .19	− 0.17 ± .21	− 0.44 ± .19
July	− 0.06 ± .21	− 0.20 ± .20	+ 0.08 ± .18
August	− 0.22 ± .23	− 0.12 ± .18	+ 0.23 ± .18
September	+ 0.09 ± .20	− 0.21 ± .19	+ 0.13 ± .15
October	+ 0.10 ± .21	− 0.05 ± .26	+ 0.14 ± .14
November	+ 0.61 ± .32	− 0.44 ± .25	+ 0.12 ± .14
December	− 0.38 ± .44	− 1.14 ± .33	− 0.26 ± .20
Average	− 0.37	− 0.53	− 0.13
QBO (DU/ms^{-1})	− 6.80 ± 2.16	− 5.60 ± 2.28	+ 5.20 ± 1.88
Solar DU/150 sunspots)	+ 1.23 ± 2.02	− 2.52 ± 2.33	+ 0.96 ± 1.83
Nuclear	− 0.48 ± .19	− 0.50 ± .30	− 0.09 ± .32
Yearly coefficient	− 0.09 ± .14	− 0.24 ± .15	+ 0.05 ± .12

*The data from 1957–1986 were analyzed, and trends from 1970, the QBO the solar cycle, and the atmospheric bomb tests were allowed for in the model (QNS70).

4.6.3.2 Combination of Incomplete Station Data Into Band Averages

Although all of the groundstations in the north Temperate Zone exhibit very similar seasonal variations in total ozone, with maxima in March or April and minima in September, October, or November, difficulties can arise when these data sets are combined to form latitudinal band averages. A band average is supposed to be a set of data that are representative of the ozone levels within that band, and that can thus be directly compared to the results from 2-D model calculations for various latitudes. The 2-D model necessarily ignores any longitudinal variations in ozone concentrations. The process of combining the data from different stations is seemingly simple, and yet is actually the opposite.

From a statistical point of view, the ideal case would be one in which each station within a band is taking readings of total ozone drawn from the same parent population—i.e., the statistical behavior of the total ozone (seasonal means, standard deviations, etc.) is the same above each station; the measurements at one station are not correlated with those from any other station; and each station has been operating for the same length of time. In practice, none of these conditions is met. No two stations in a band measure from the same parent population because the meteorology at each station is different in at least some respects from that at any of

the others. The observed differences include different mean ozone levels, different timings for the ozone maxima, and different magnitudes of the yearly cycle (Bowman and Krueger, 1985). The first of these factors has been overcome in these calculations by normalizing the series from each station through division by its long-term mean, while the last of these factors was not accounted for in the analyses presented here.

The difference in the timing of the maxima does pose some problems when the data are analyzed for seasonal changes. There are two cases where special caution is needed. First, a large number of Soviet stations were improved by the introduction of the M–83 filter ozonometer in 1972; the measurements from these stations were not included in the latitudinal band averages because the ozone maximum over most of the USSR occurs later than over most Western stations (Figure 4.46). Second, for the cases where all the data from 1957 are analyzed in the two most northerly bands (53–64°N and 60–80°N), only a few stations were making measurements in the very early years. This problem has nothing to do with the quality of the data, and is caused only by the combination of incomplete sets of data that have different statistical characteristics. It is also well known that the readings from one station are correlated with those of nearby stations. Indeed, this fact was one of the criteria used in looking for possible errors in the ozone record from an individual station that might signify an unrecorded calibration of the basic instrument. Finally, Tables 4.3, 4.4, and 4.7 indicate that the station records are not fully coincident, but instead show wide variations in the period of time covered.

The problems involved in the combination of records of different length when the ozone maxima are displaced in time can be illustrated with the data from the Dobson stations at Belsk and Bismarck. These two stations experience approximately 1 month's difference in the timing of their ozone maxima and minima (see Figure 4.53) and so provide a good example. The available records for both stations cover the entire 24-year period from January 1963–December 1986, and show similar decreases in total ozone during the winter when the second 12-year period is compared with the first 12-year period (see Figure 4.35), or in an 11-year vs. 11-year period

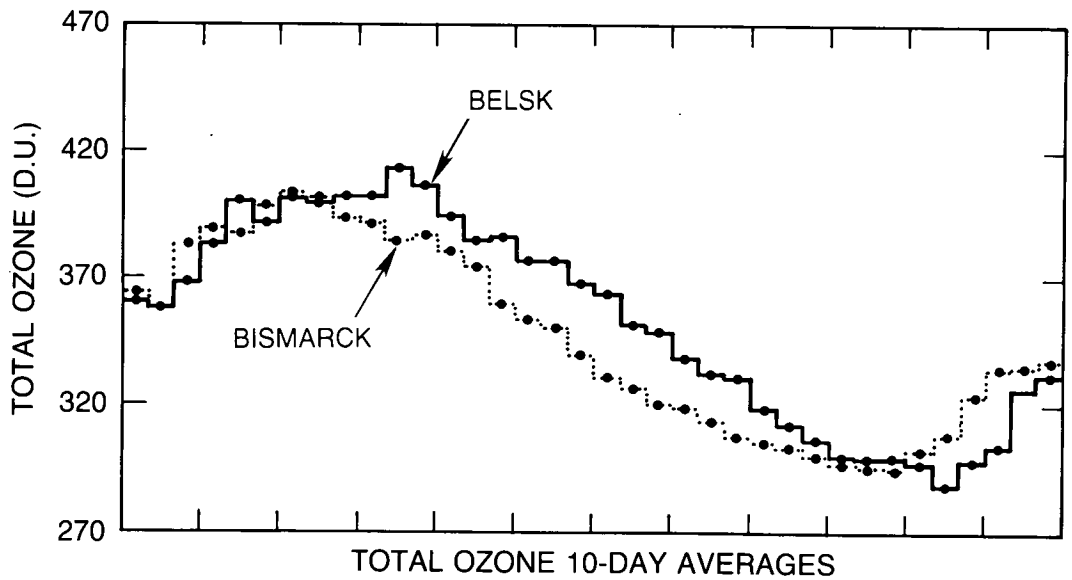

Figure 4.53 Annual total ozone cycles at Belsk and Bismark. The points represent the 10-day averages at each station calculated from 24 years of measure.

comparison for the final 22 years. The combination of these 24-year data sets has been carried out by first normalizing each by division of the long-term mean, and then averaging the normalized monthly concentrations to obtain a two-station value. The purpose of this combination is solely to illustrate the inherent problems in this process.

A hypothetical test of the combination of records of differing lengths can be obtained from these real data by assuming that the data from Bismarck are available only from January 1975 on, and not during the first 12-year period. Combination of the Belsk and Bismarck data for 1975–1986 can provide average values for this period. In this hypothetical instance, with only the Belsk data available for the first period, the 1963–1974 "average" will be just the Belsk data. An alternative illustration can be gained by using "Bismarck only" for the earlier period. Comparison of these average values presents a very different picture of the months in which ozone losses have appeared in the second period relative to the first (Figure 4.54). The full average is shown by the solid circles, with an average wintertime loss similar to that found for the individual stations. Both incomplete combinations displace the timing of ozone losses in Figure 4.54.

The addition of data from a large group of stations with different mean timing of their ozone maxima to a longer set of data could result in distortion of the seasonal observations. For this reason alone, the total ozone data collected with the M–83 instrument have not been blended into the overall band data, because their useful record begins only in 1972 and not in the early 1960's. Similarly, the monthly results for the 53–64°N and 60–80°N bands when all the data from 1957 are included should be treated carefully, as only a few stations were making measurements in the early years, with many joining in later on. These are the conditions that can tend to blur possible seasonal differences in ozone loss. However, in the basic analysis where the data from

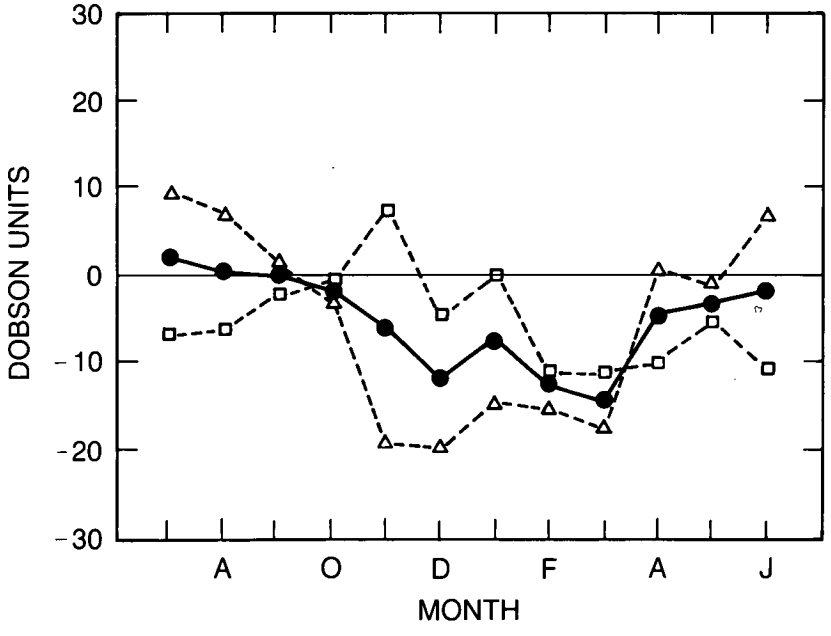

Figure 4.54 The points using the symbol • are the differences in the monthly averages for the periods January 1963–December 1974 and January 1975–December 1986 for a combined series of the data from Belsk and Bismarck. The equivalent results when only Belsk was taken as operating in the former period are shown with the symbol □, while those for the case where just Bismarck was taken for the first period have the symbol ▲. In all cases, both stations' data were used in the second period.

1965–1986 are considered, there is no significant disagreement between the seasonal trends calculated from the latitudinal band averages and the average seasonal trends of those stations within the latitude bands that have records that are long enough for time series analysis. The winter losses over the 17-year period from 1970–1986 for the three bands are (1) 53–64°N, -6.2 ±1.5%, and -7.2%, where the first value is for the analysis of the latitudinal band average (from Table 4.23) and the second value is the average of the individual station losses in Table 4.16 converted to a percentage; (2) 40–52°N, -4.7 ±1.5%, and -5.0%; and (3) 30–39°N, -2.3 ±1.3%, and -1.5%. Similarly, the summer (MJJA) losses are (1) 53–64°N, -0.2 ±0.8%, and +0.1%; (2) 40–52°N, -1.9 ±0.7%, and -1.9%; and (3) 30–39°N, -1.9 ±0.8%, and -1.9%. None of these pairs of estimates for the average loss in the different latitude bands shows any inconsistency in the results using the two methods for calculating the changes. Despite the potential problems in assembling latitudinal band averages, they do provide extra insight into the changes in total ozone because they include data from stations with short or incomplete records.

4.6.3.3 Year-Round Versus Monthly Loss Models

A comparison of the results from the year-round and monthly models illustrates how important the underlying assumptions for the two models are. Table 4.25 contains the yearly trend estimates calculated in three different ways for three latitude bands: (1) the coefficient from the year-round model, (2) the weighted mean of the monthly coefficients (using the square of the inverse of the standard error as the weighting factors), and (3) the unweighted mean of the monthly coefficients. For each band, the largest loss is that found by taking the unweighted average of the monthly trend estimates. The difference among the estimates is much greater in the more northerly belts, where there is a very pronounced seasonal difference between the monthly loss rates. Because the largest losses are occurring in the winter months, during which the uncertainty in the trend coefficient is greatest, the weighted average reduces the effect of these months on the year-round estimate. In each band, the winter months are the dominant contributors to the estimate of the unweighted mean because their absolute values are bigger, while the summer months are the more important in determining the weighted mean because their error estimates are smaller. Statistically, the assumption required to attach much meaning to an average is that each sample is drawn from the same parent population—i.e., the underlying losses for each month are the same. Because the current photochemical models predict different losses at different times of the year, and the data themselves show such behavior, this assumption is broken, and thus it is not clear exactly what a year-round average represents.

Table 4.25 Different Ways of Calculating an Annual Rate of Loss.

	Latitude band		
	53°–64°N	40°–52°N	30°–39°N
(a)	- 0.14 (.13)	- 0.47 (.13)	- 0.17 (.11)
(b)	- 0.19 (.13)	- 0.49 (.11)	- 0.25 (.09)
(c)	- 0.52 (.20)	- 0.63 (.17)	- 0.32 (.14)

In the top row (a) are shown the values calculated using a uniform year-round trend term, the classical "hockey stick," for the three latitudinal band averages. In row (b) are shown the weighted averages of the monthly loss rates calculated from the model that allows each calendar month to vary differently, while the bottom row contains the unweighted averages of the same monthly coefficients. One standard error bar is in parentheses. Allowance is made for the correlation between the different monthly coefficients.

The validity of the year-round hockey stick model is subject to the same criticisms as the averages from the monthly models. Unless supported by the data, the assumption of a constant

year-round loss should not be used, because the model is then misspecified. In the current analyses, this misspecification leads to rates of ozone loss that are smaller than either the weighted or unweighted means of the monthly values and it does not indicate the presence of the relatively large wintertime losses that are observed at higher latitudes.

4.6.3.4 Variation With Time of the Latitude Band Monthly Ramp Coefficients

The observation that the linear regression analysis with monthly ramp coefficients demonstrates losses of ozone for many of the months in each latitude band does not provide much information as to when the ozone loss occurred. The reasonable agreement between total ozone losses estimated for 17 years after 1969 (i.e., $17 \times k_{70}M$) and 11 years after 1975 (i.e., $11 \times k_{76}M$) indicates that much of the total loss occurred after 1976, but does not severely test the underlying assumption that ozone loss is spread over a 10–17-year period. With other geophysical events such as the large oceanic El Niño of 1982–1983 and the El Chichón volcanic eruption (April 1982) prominent during the period of indicated ozone loss, the possibility needs to be considered that such an event might have triggered a sudden large ozone loss, superimposed on a background of little or no loss for other reasons. Such hypotheses have been statistically tested by examining the linear regression coefficients as successive years of ozone data are included in the analysis. For these tests, the latitude band data from January 1965 on have been analyzed with the addition of 1-year increments of ozone data from 1980–1986. For each of the three latitude bands, the regression analysis was carried out successively for 16 years of data (1965–1980), 17 years (1965–1981), 18 years (1965–1982), and so on through 22 years (1965–1986), with monthly linear ramps from 1969–198x (i.e., $k_{70}M$).

The monthly linear coefficients for the seven calculations are graphed for latitude bands 53–64°N, 40–52°N, and 30–39°N in Figures 4.55–57. The standard errors become steadily smaller as the number of years of data is increased. For 31 of the 36 monthly coefficients, the one-sigma standard errors of all seven (1980–1986) of the yearly coefficients overlap one another. For 4 consecutive months (AMJJ) in the 40–52°N band, the regression coefficients become steadily more negative and the one-sigma errors do not overlap. For the month of December in the 40–52°N band, the linear regression coefficients become steadily less negative and the one-sigma errors also fail to overlap. The relatively small changes in the trend coefficients over this period suggest that the geophysical events of 1982–1983 did not dominate the sign or magnitude of the monthly trend coefficients. In particular, the strong trend toward negative coefficients is already apparent in 1980 and 1981 for the winter months (DJFM) in both the 53–64°N and 40–52°N latitude bands.

A simple evaluation of the general suitability of the linear relationships for fitting the ozone data can be made by calculating the numerical change in the linear regression coefficients as the endpoint of the data goes from 1980 to 1986, scaled by the standard errors of the analyses. Figure 4.58 shows the distribution of these numerical changes divided by the standard errors for the 36 monthly coefficients in the three bands. For example, the linear coefficients for March in the 53–64°N band were -0.40 ± 0.62 for an endpoint of 1980 and -1.07 ± 0.35 for 1986. The scaled change in the coefficient, -0.67 divided by the combined error of 0.71, is graphed as -0.94. As indicated, 31 of the 36 monthly coefficients have values within $\pm 1\sigma$, indicating that the linear model is generally satisfactory. The median value of the change in regression coefficients from 1980 to 1986 is negative, suggesting a tendency toward more ozone loss in the 1980's than during the 1970's.

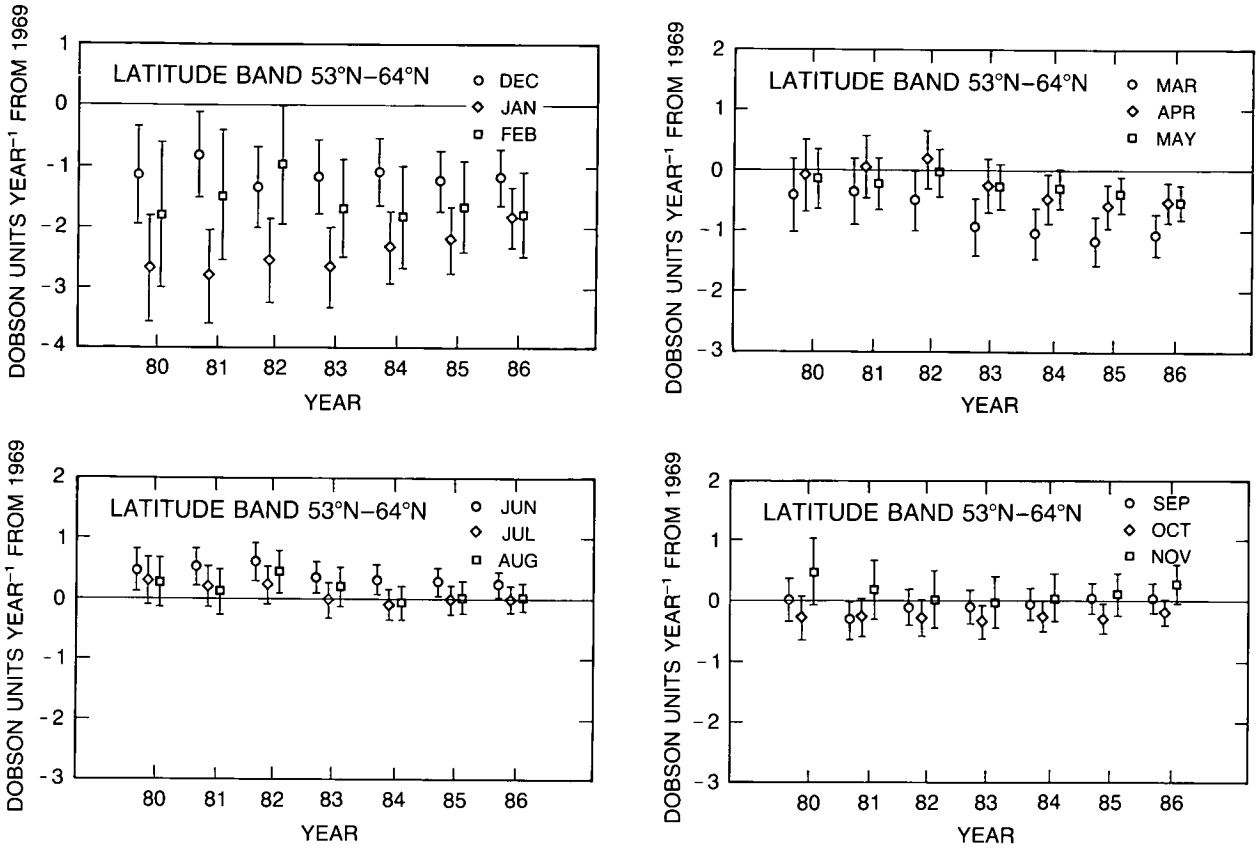

Figure 4.55 The total ozone trends for the individual months are shown for the latitude band between 53°N and 64°N illustrating the effect of the addition of successive years of data. The ozone change in each month was assumed to have occurred in a linear fashion from 1969 until the year shown, and the data used were from 1965 until the year shown. The statistical model used allowed for effects of the solar cycle and the quasi-biennial oscillation. The monthly ozone trends are given in DU/yr.

The regression coefficients have also been calculated for an alternate model in which the ozone changes are not evaluated with linear ramps, but with changes proportional to the organochlorine (CL) burden of the troposphere—i.e., about twice as much as yearly change in 1986 as in 1970. These coefficients for the successive models from 1980–1986 are shown in Figures 4.59–61, and the changes in the values of the coefficient are graphed in Figure 4.62. The conclusions from these calculations are very similar to those from the linear model, with a small drift toward more negative regression coefficients in 1986 than in 1980. In this statistical model, the magnitude of the indicated ozone losses are marginally higher for 1965–1986 than from the linear regression model. Such a result is expected if an overall ozone loss has occurred because the CL model also fits a loss from 1965–1969, while the linear model fits a constant value for the same period. The data fits are comparable with either the linear or CL statistical models, and neither is enough superior to warrant its choice as the clearly better model.

4.6.3.5 Calculation of the Seasonal Error Estimates

The standard error, $\sigma_{\bar{k}}$, for the 4-month winter and summer season trend coefficients given in Table 4.23 are calculated according to Equation 1.

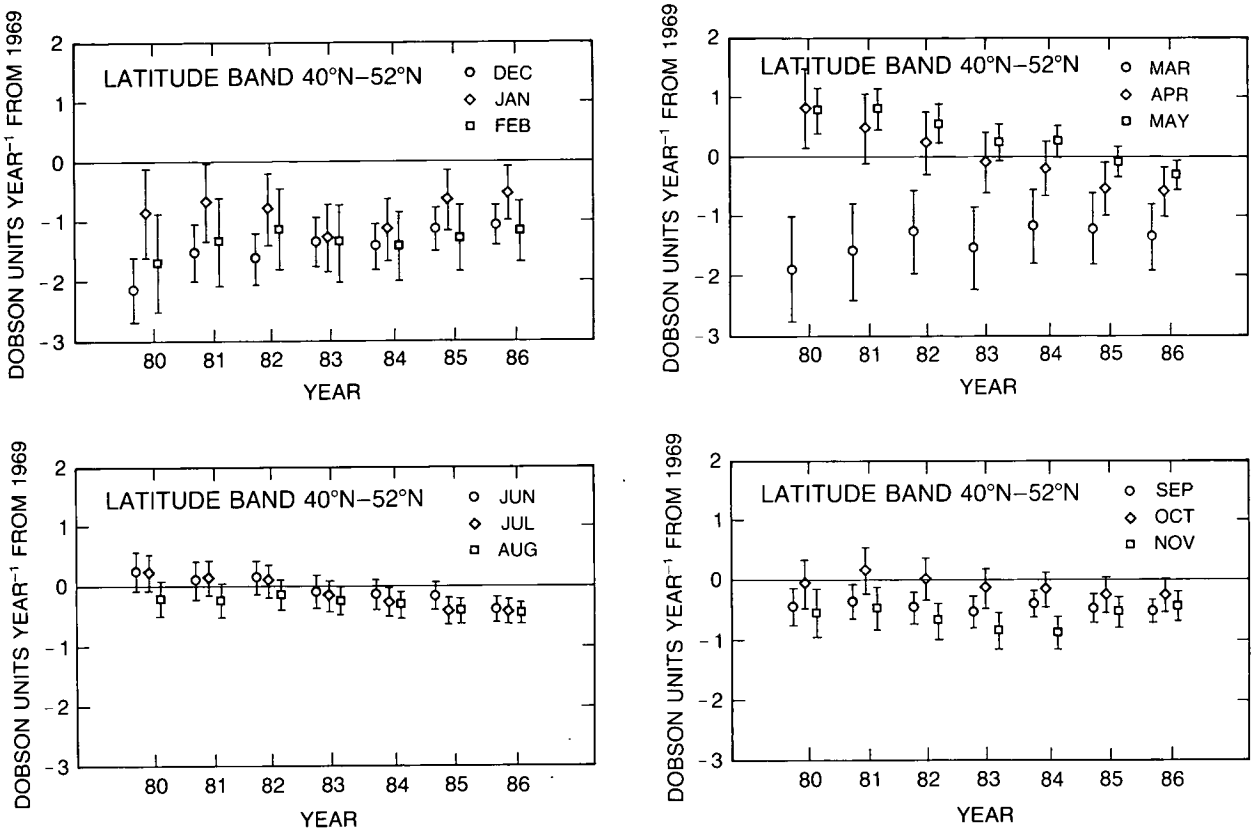

Figure 4.56 The total ozone trends for the individual months are shown for the latitude band between 40°N and 52°N illustrating the effect of the addition of successive years of data. The ozone change in each month was assumed to have occurred in a linear fashion from 1969 until the year shown, and the data used were from 1965 until the year shown. The statistical model used allowed for effects of the solar cycle and the quasi-biennial oscillation. The monthly zone trends are given in DU/yr.

$$\sigma_{\bar{k}}^2 = \frac{1}{4^2} \cdot \left(\sum_{i=1}^{4} \sigma_i^2 + 2 \sum_{i=1}^{3} \sum_{j=i+1}^{4} \sigma_{ij} \right) \tag{1}$$

where σ_i is the standard error for each monthly trend coefficient (so that σ_i^2 is the variance estimate); σ_{ij} is the covariance between months i and j and is the product of the standard error for the 2 months with the correlation coefficient of the two monthly trend parameters as shown in Equation 2.

$$\sigma_{ij} = \rho_{ij} \cdot \sigma_i \cdot \sigma_j \tag{2}$$

Because an unweighted seasonal loss rate is calculated, it is appropriate to use these expressions to find the standard error. The same method is used in calculating the standard error of the unweighted annual mean trend in the discussion compares the year-round coefficient with the unweighted and weighted means of the monthly trends. Equation 3 is used to calculate the standard error of the weighted mean, $\sigma_{\bar{k}_w}$.

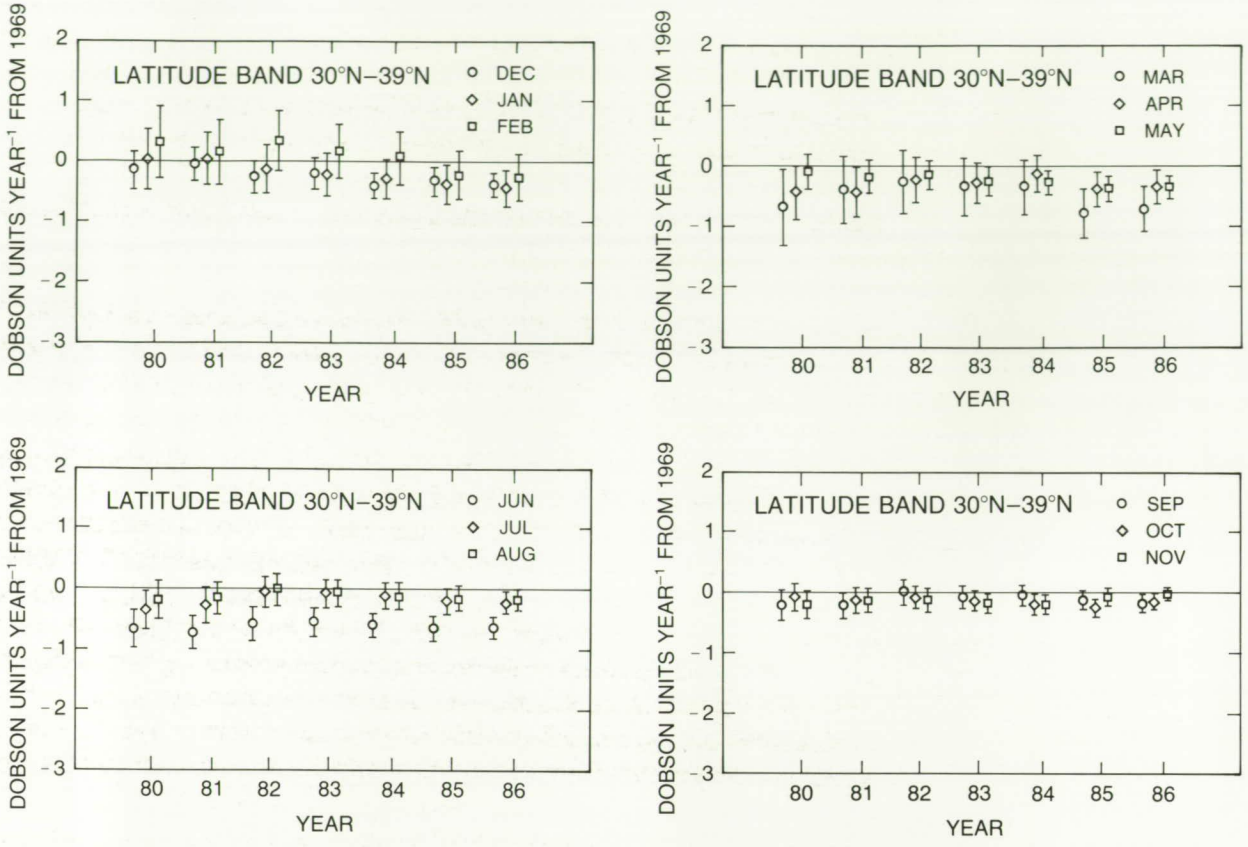

Figure 4.57 The total ozone trends for the individual months are shown for the latitude band between 30°N and 39°N illustrating the effect of the addition of successive years of data. The ozone change in each month was assumed to have occurred in a linear fashion from 1969 until the year shown and the data used was from 1965 until the year shown. The statistical model used allowed for effects of the solar cycle and the quasi-biennial oscillation. The monthly ozone trends are given in DU/yr.

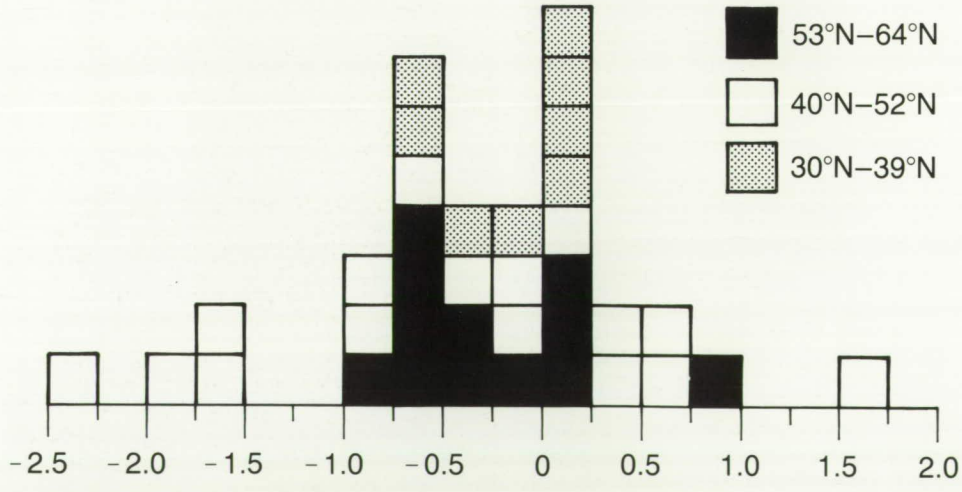

Figure 4.58 Distribution of the changes between 1980 and 1986 in the 36 monthly trend coefficients for the three latitude bands shown in Figures 4.55, 4.56, and 4.57. The difference between the trends calculated for any particular month when the data through 1980 are used and when the data through 1986 are used is divided by the combined standard error of the two trend coefficients.

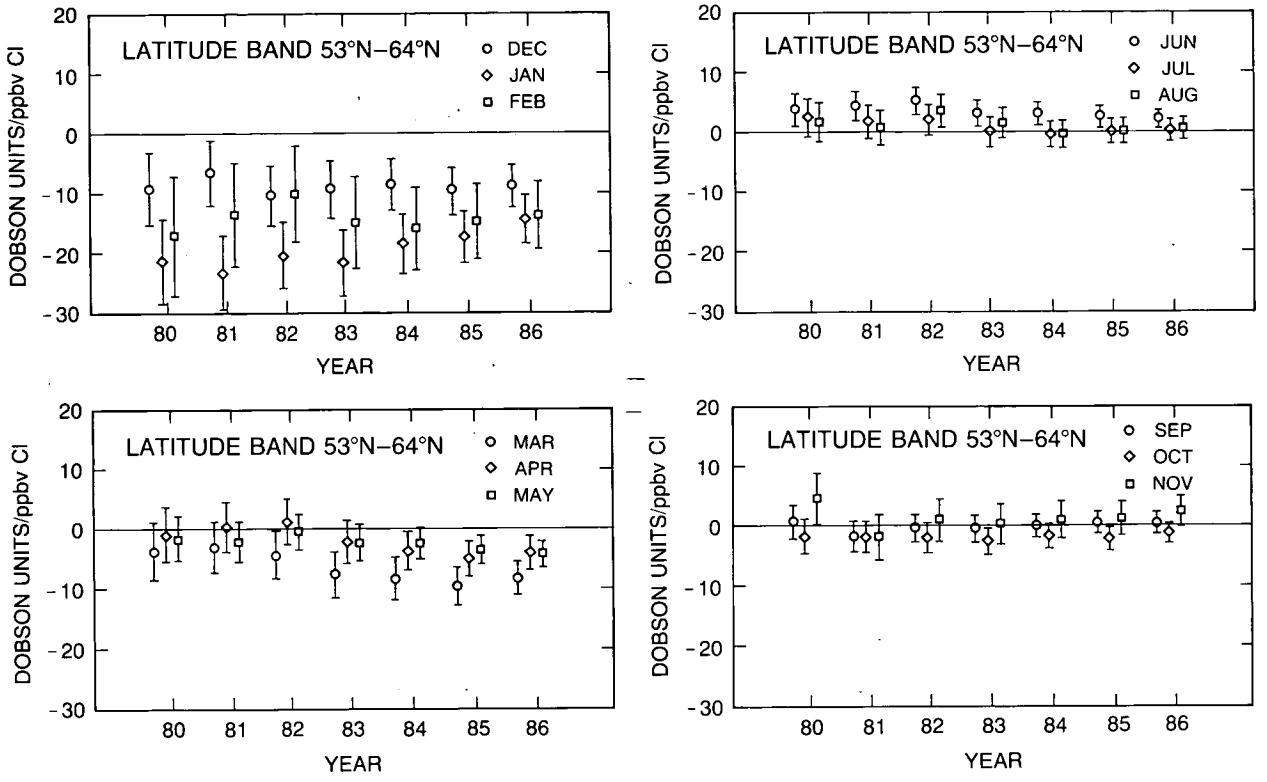

Figure 4.59 The total ozone trends for the individual months are shown for the latitude band between 53°N and 64°N illustrating the effect of the addition of successive years of data. The ozone change in each month was assumed to have occurred in proportion to the organochlorine burden of the troposphere, i.e., in a nonlinear fashion until the year shown, and the data used were from 1965 until the year shown. The statistical model used allowed for effects of the solar cycle and the quasi-biennial oscillation. The monthly ozone *trends* are given in DU/yr.

$$\sigma_{\bar{k}_w}^2 = \left(\sum_{i=1}^{n} \frac{1}{\sigma_i^2} \right)^{-2} \cdot \left(\sum_{i=1}^{n} \frac{1}{\sigma_i^2} + 2 \sum_{i=1}^{n-1} \sum_{j=i+1}^{n} \sigma_{ij} \cdot \frac{1}{\sigma_i^2} \cdot \frac{1}{\sigma_j^2} \right) \tag{3}$$

The relative sizes of the first and second terms in Equation 1 are shown in Table 4.26 for the winter and summer seasons of three latitude bands. The greater importance of the cross term in the southern band is due to the higher autocorrelation present, which causes the monthly trend parameters to be more dependent on one another.

4.6.4 Results From M–83 Regional Averages

As described in Section 4.1.3, the instrument used in the USSR, the M–83, uses a filter rather than a grating to separate the incoming UV light. Since the filter has a larger bandwidth than a grating, the measurements taken show greater scatter, which shows up in the statistical analysis in the form of larger uncertainties. There is also the potential for greater μ-dependent errors when measurements are taken in winter or away from local noon. The upgraded M–83 instruments have been operated since 1972, so that the length of record is shorter than for most Dobson stations. However, the M–83 monitoring system covers a large area and provides valuable

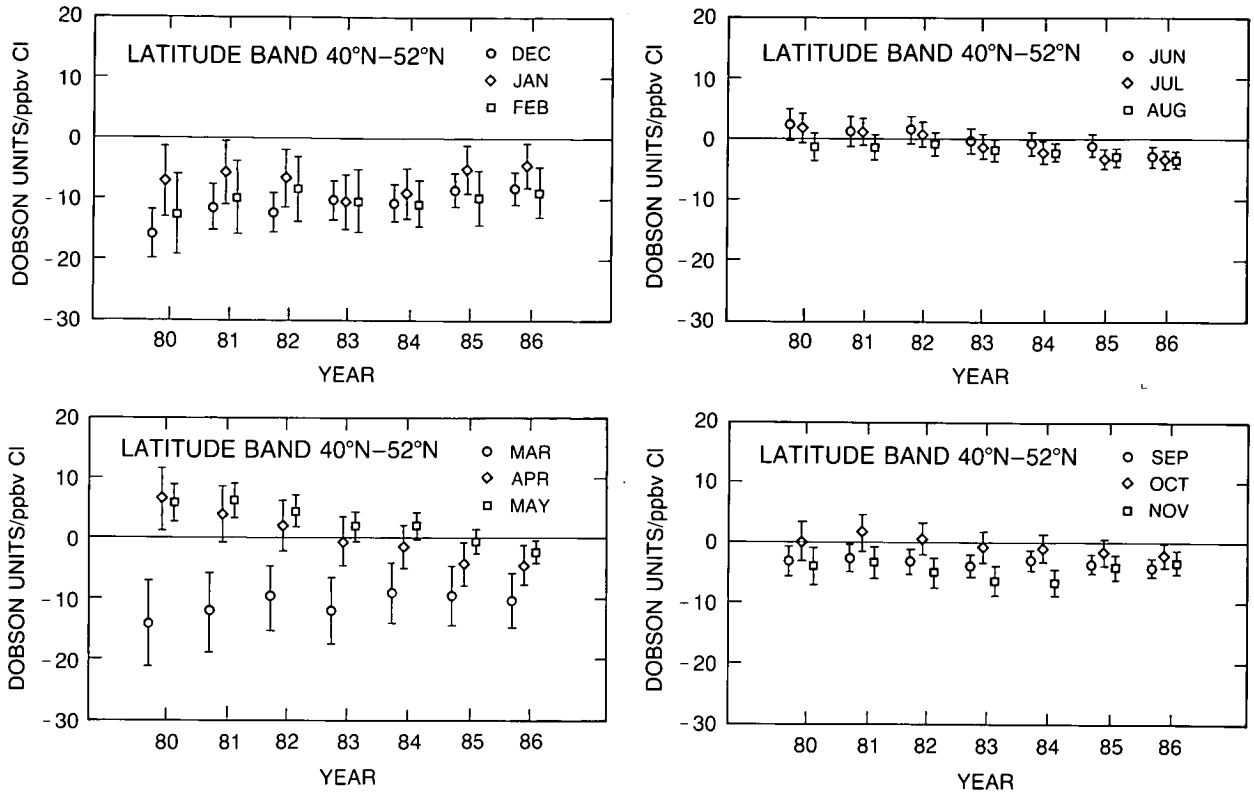

Figure 4.60 The total ozone trends for the individual months are shown for the latitude band between 40°N and 52°N illustrating the effect of the addition of successive years of data. The ozone change in each month was assumed to have occurred in proportion to the organochlorine burden of the troposphere, i.e., in a nonlinear fashion until the year shown, and the data used were from 1965 until the year shown. The statistical model used allowed for effects of the solar cycle and the quasi-biennial oscillation. The monthly ozone *trends* are given in DU/yr.

Table 4.26 Variance and Covariance of the Monthly Trend Estimates Used in Calculating Seasonal Averages.

	Variance	Covariance	Error Estimate
Winter (DJFM)			
53–64°N	1.06	0.95	0.35
40–52°N	0.87	0.94	0.34
30–39°N	0.41	0.60	0.25
Summer (MJJA)			
53–64°N	0.22	0.19	0.16
40–52°N	0.17	0.20	0.15
30–39°N	0.14	0.21	0.15

The relative magnitudes of the variance and covariance of the monthly trend estimates used in calculating seasonal averages. The units are Dobson Units per year.

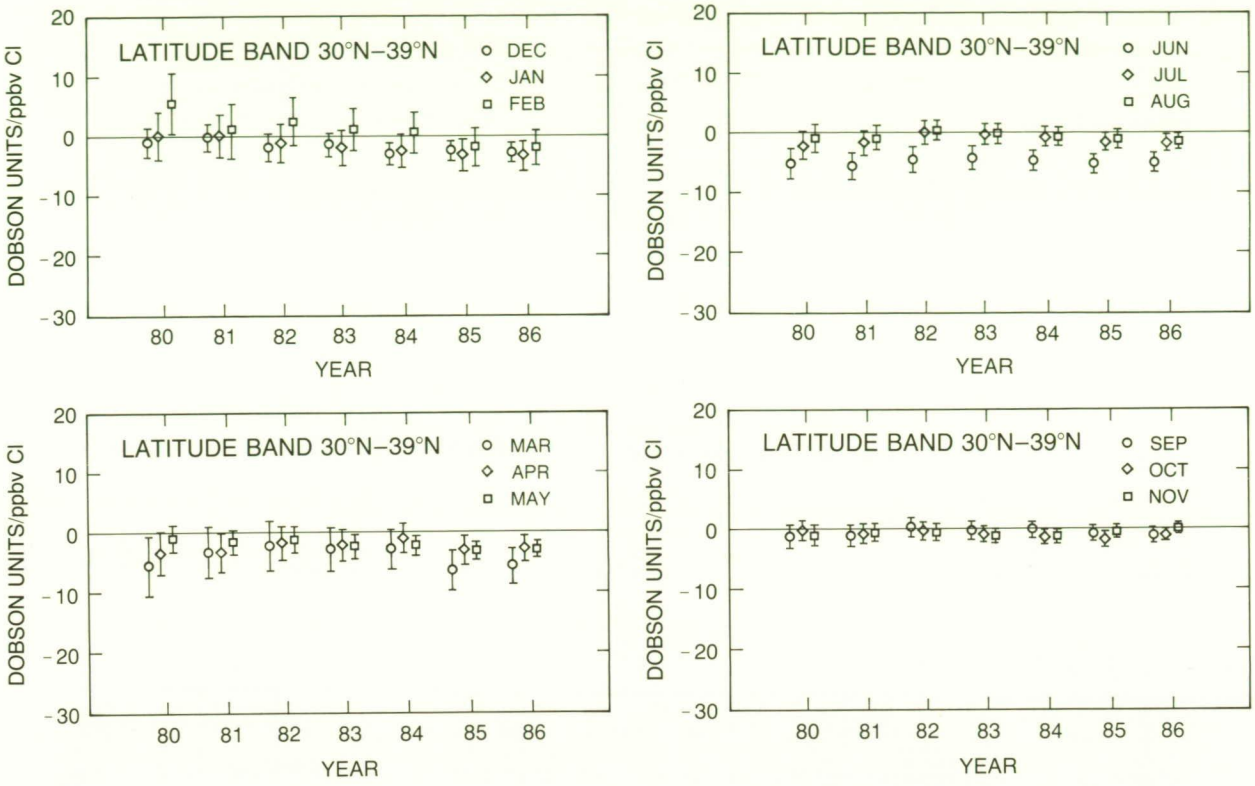

Figure 4.61 The total ozone trends for the individual months are shown for the latitude band between 30°N and 39°N illustrating the effect of the addition of successive years of data. The ozone change in each month was assumed to have occurred in proportion to the organochlorine burden of the troposphere, i.e., in a nonlinear fashion until the year shown, and the data used were from 1965 until the year shown. The statistical model used allowed for effects of the solar cycle and the quasi-biennial oscillation. The monthly ozone *trends* are given in DU/yr.

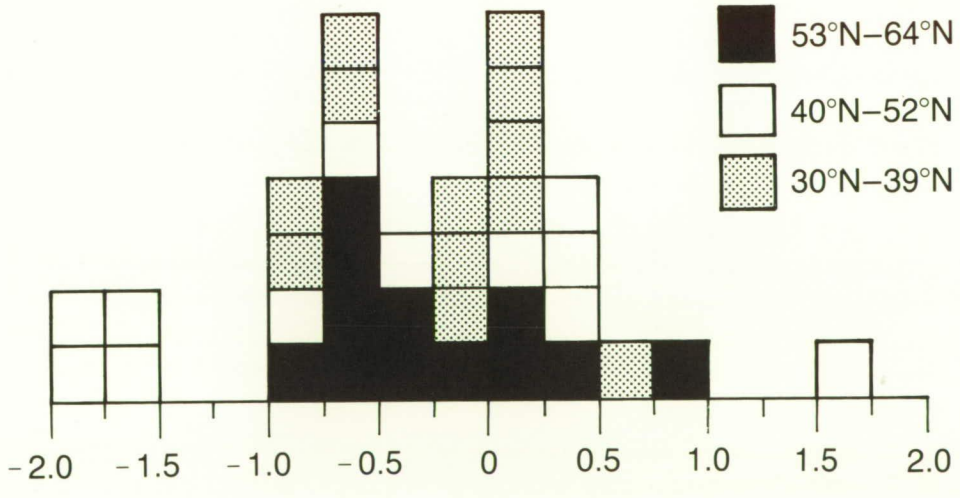

Figure 4.62 Distribution of the changes between 1980 and 1986 in the 36 monthly trend coefficients for the three latitude bands shown in Figures 4.59, 4.60, and 4.61. The difference between the trends calculated for any particular month when the data through 1980 are used and when the data through 1986 are used is divided by the combined standard error of the two trend coefficients.

information where no other ground-based measurements are taken. For the purposes of this report, the data from the M–83 stations were combined to form regional averages, which were analyzed with the same time series technique. The results of these analyses are presented in Appendix 4.B.(ii).

Plots of the monthly losses over 1972–1985 are shown in Figure 4.63 for the four chosen M–83 regions—the European, Siberian, South Central Asian, and Far Eastern parts of the USSR. In both the European and Siberian areas, losses appear to occur in both the fall (September, October, and November) and in the late spring (March, April, and May). The former tendency is

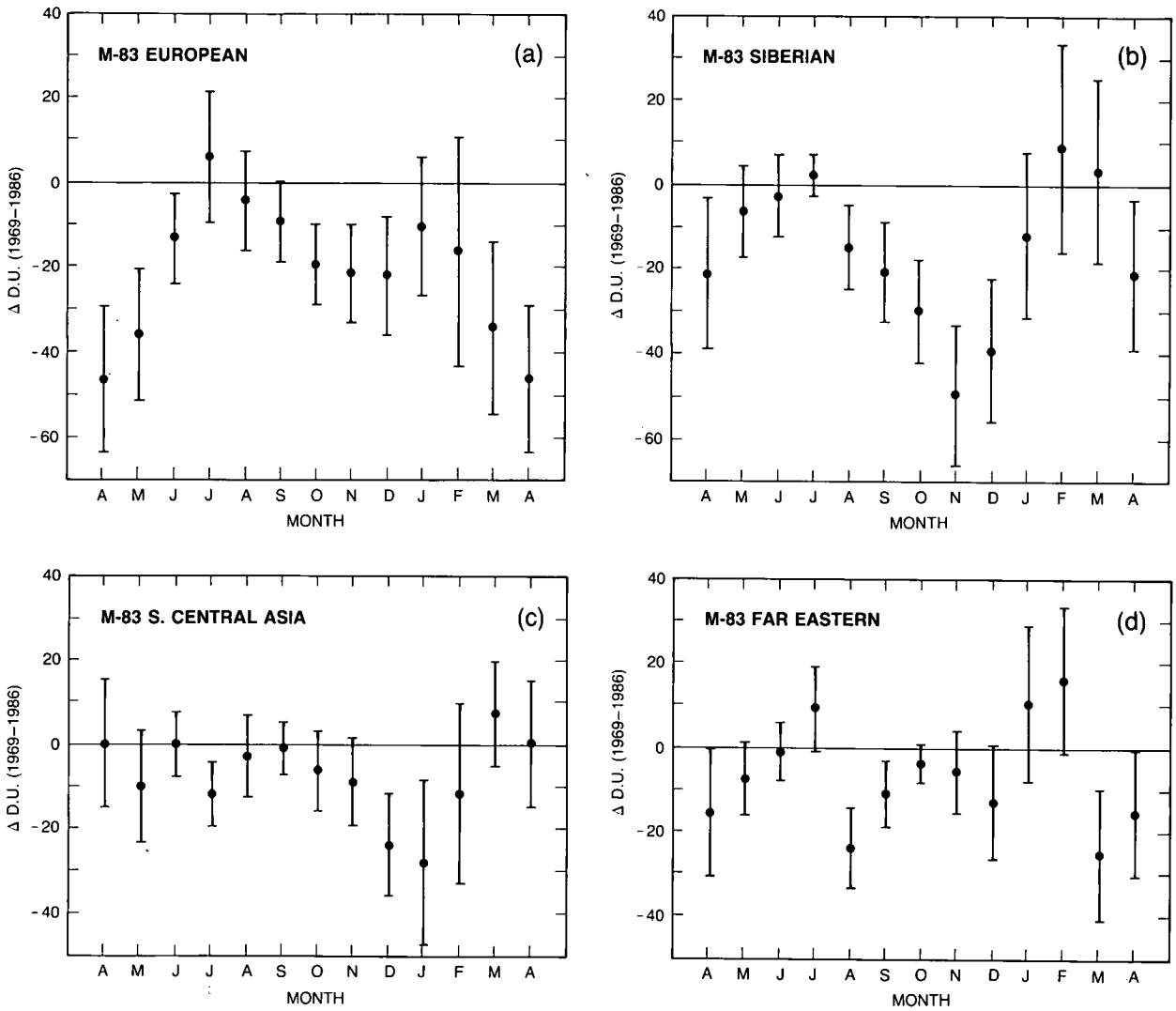

Figure 4.63 Ozone changes for four regional averages composed from the USSR M–83 data taken between 1972 and 1986. The statistical model used allowed for effects of the solar cycle and the quasi-biennial oscillation, and all the available data were used from 1972. The ozone change in each month was assumed to have occurred in a linear fashion. The monthly ozone changes plotted are not *trends*; they are found by multiplying the calculated trend by the period over which the loss was assumed to have occurred. The vertical bars represent ± 1 standard error in the estimate of the change. (a) European region, (b) Siberian region, (c) South Central Asian region, (d) Far Eastern region.

stronger in Siberia while the latter is stronger in the European part. The losses in January and February are small. In the data from the South Central Asian region, there is not much evidence for a loss; the 2 months with the largest negative trends are December and January. The Far Eastern results (from only two stations) show no pattern at all toward a loss or a gain. It is worth recalling that the Japanese stations have observed ozone losses different from the European and North American stations. Sapporo (43.1°N) does not show a wintertime loss; decreases in total ozone are observed in both December and March, but not in January or February. Thus, there is some sign of the bimodal losses measured in the European and Siberian parts of the USSR at equivalent latitudes. However, the statistical significance of these patterns is not strong enough to reach any firm conclusions at the current time.

4.7 ANALYSIS OF TOMS DATA NORMALIZED TO THE DOBSON NETWORK

The primary advantage of a satellite instrument is its ability to make truly global measurements (all but the regions in polar darkness). The TOMS instrument has been described in Section 4.2 of this chapter, and the slight adjustment to its data to use the long-term calibration of the Dobson network has been described in Section 4.4. All of the data reported in this section use this adjusted data set. The adjustment corresponds to about 3 percent added to the data in 1987.

4.7.1 Global and Hemispheric Trends

Figure 4.64 shows the latitudinal–seasonal variation of the TOMS total ozone measurements averaged over 9 years from 1979–1987. The distribution is very similar to that constructed from the ground-based measurements shown in Figure 4.32 earlier in this chapter. Figure 4.65 shows

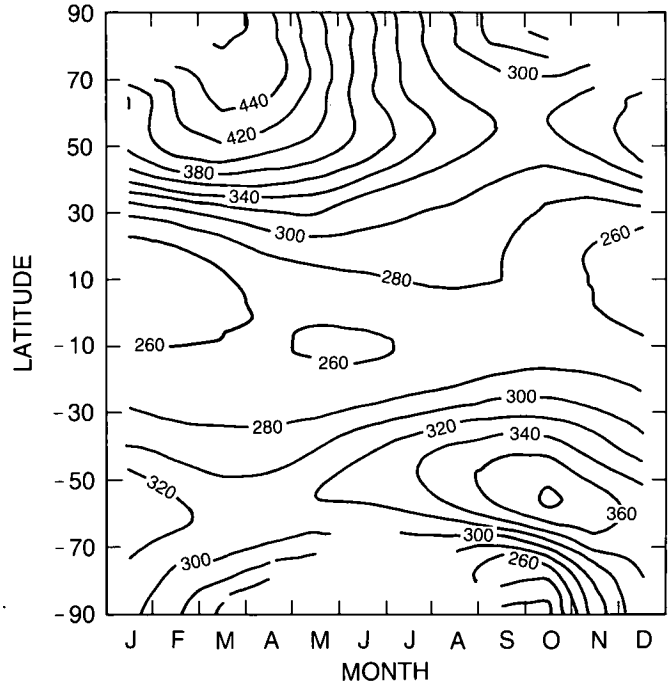

Figure 4.64 Variation of total ozone with latitude and season derived from TOMS measurements between 1979 and 1987.

the same latitudinal–seasonal total ozone distribution for each of the 9 years of TOMS data. Evident in the figure is that the distribution is similar for each year, with some important differences. The Northern Hemisphere springtime maximum shows interannual variability with the maximum already appearing to have occurred during the polar night in some years. Similarly, significant interannual variability exists in the magnitude of the Southern Hemisphere springtime maximum. Finally, the growth of the springtime Antarctic minimum is evident.

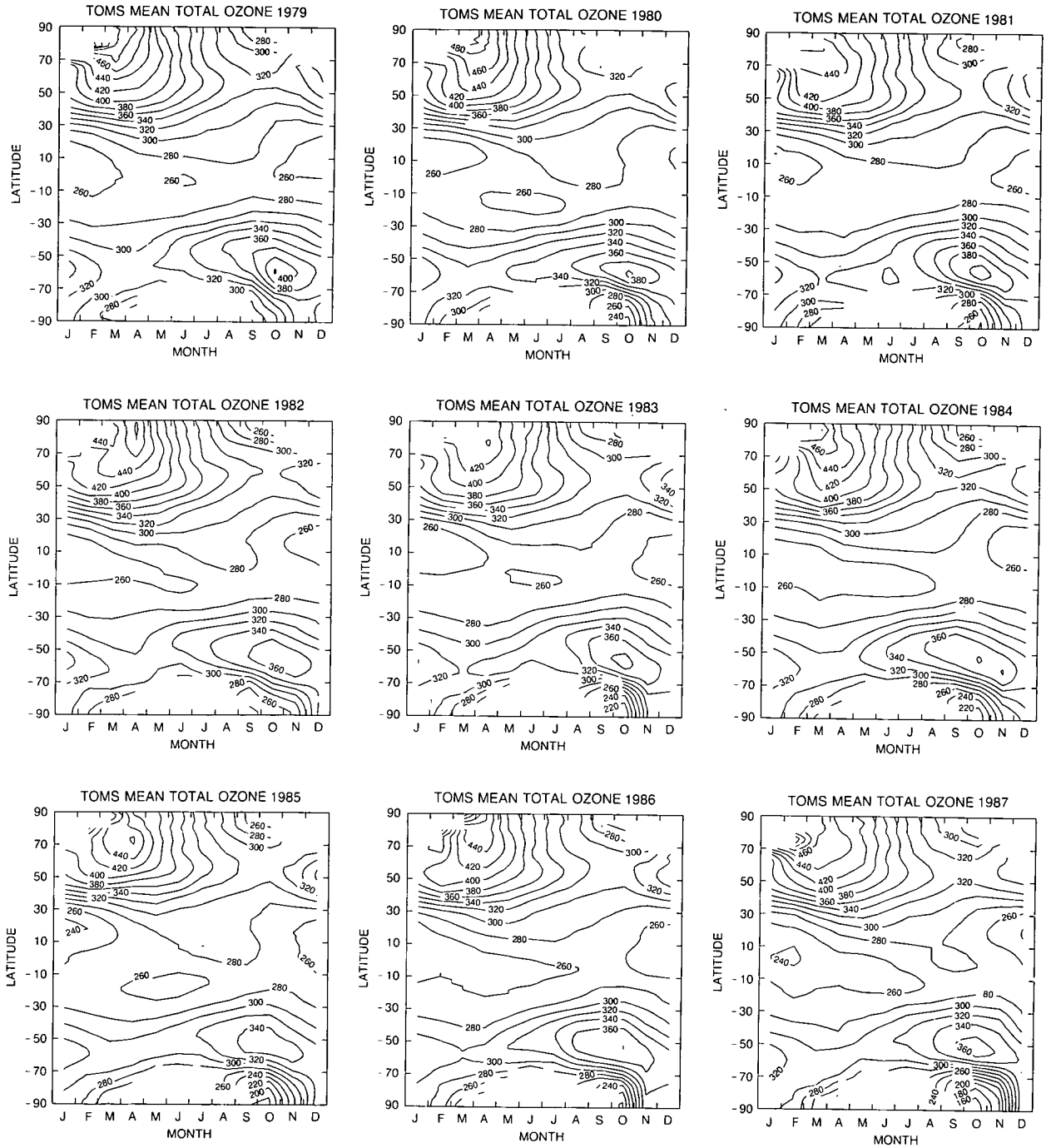

Figure 4.65 Variation of total ozone with latitude and season derived from TOMS for each year from 1979 to 1987.

A useful evaluation of global ozone change can be obtained from these data by integrating over the globe. Figure 4.66 is a plot of the daily global ozone column as measured by TOMS from November 1978–December 1987. Each year has two maxima, one in the Northern Hemisphere and one in the southern spring when midlatitude ozone is peaking in the Southern Hemisphere. The solid line is a simple linear least-squares regression line through the data, giving a linear trend of -0.4 percent per year. Figure 4.67 shows the same data with the characteristic seasonal cycle removed. The result is plotted as deviation from the seasonal mean. It is clear that the data during the first few years of the record are some 2–3 percent higher than the data near the end of the record. It is difficult to say from this short data record whether the observed decrease is the result of a negative linear trend or of a significant 11-year solar cycle variation. Figure 4.67(b) shows a similar integration of the TOMS data in which the integral is extended only to 53 degrees latitude to eliminate the effects resulting from any direct changes in polar ozone. Again, the record shows higher ozone in the period around 1980 than in the mid- to late 1980's. A linear trend has been calculated from these data with an autoregressive model. The results are given in the first row of Table 4.27. The trend was fit first from the beginning of the data in November 1978–October 1985, a period of 7 years, most of which was during the declining phase of the solar cycle. The result was a cumulative change of -2.6 $\pm$0.5%. A similar linear trend analysis extending from November 1978–November 1987, or 9 years of data, showed a cumulative change of -2.5 $\pm$0.6%. This confirms the conclusion that there appears to be a flattening of the ozone change over the last 2 years of the record, and is not inconsistent with the notion that there is some solar cycle component to the global total ozone change.

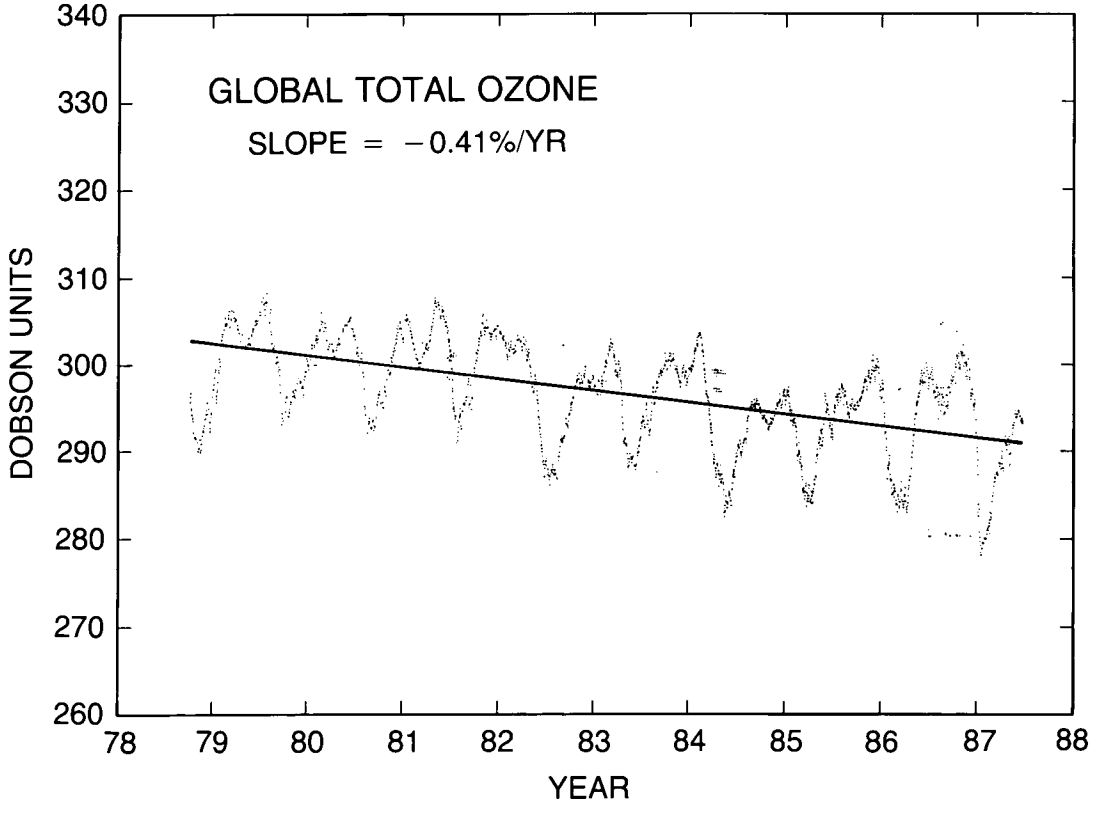

Figure 4.66 Globally averaged total ozone from November 1978–December 1987 derived from TOMS measurements. The solid line is a simple linear least squares fit of the data with a slope of -0.4% yr^{-1}.

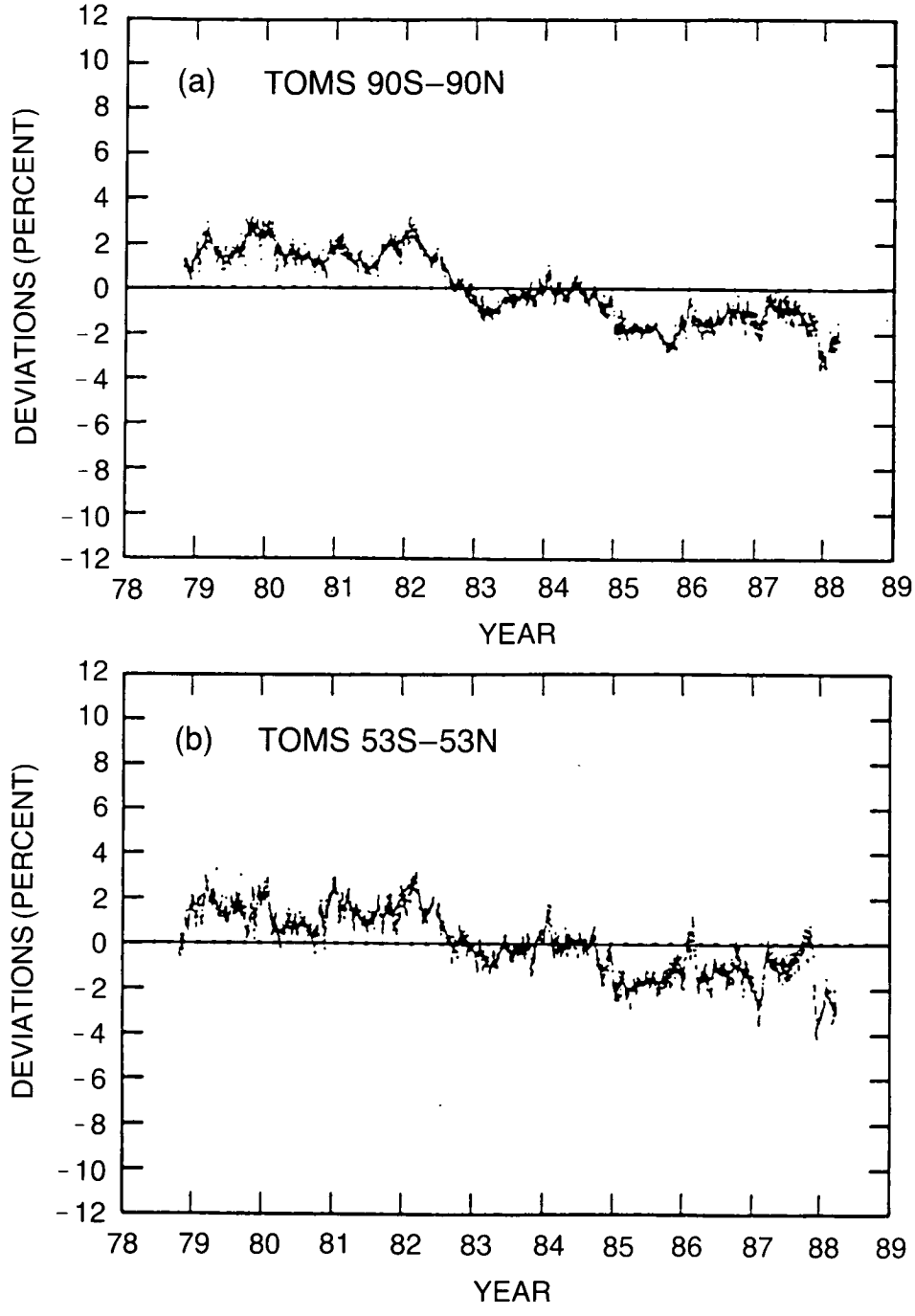

Figure 4.67 (a) Deseasonalized global total ozone derived from TOMS. (b) Deseasonalized total ozone between 53°N and 53°S derived from TOMS. Percentage deviations from the seasonal means are plotted.

Figure 4.68a,b shows the same area means, again plotted as deviations from the seasonal mean, broken down into Northern and Southern Hemispheres. Both the Northern and Southern Hemisphere means show more deviation than the global mean. The Northern Hemisphere has significant negative deviations in the winters of 1982–1983 and 1984–1985, as has been previously demonstrated from ground-based data (e.g., Bojkov, 1988). The Southern Hemisphere shows a

Table 4.27 Percentage Changes in Total Column Ozone (Measured by TOMS on Nimbus–7, Calibrated by Comparison With Ground-Based Measurements)

Latitude Band	Total Change From 11/1978–10/1985	From Table C-12 (1969–1986)	Total Change From 11/1978–11/1987
Global, except high latitudes			
53°S–53°N	−2.6±0.5		−2.5±0.6
Hemisphere			
0–53°S	−2.6±0.9		−2.9±0.9
0–53°N	−2.1±1.5		−1.8±1.4
Bands			
53°S–65°S	−9.0±1.8		−10.6±1.6
39°S–53°S	−5.0±1.8		−4.9±1.8
29°S–39°S	−3.2±2.4		−2.7±2.1
19°S–29°S	−2.5±1.9		−2.6±1.5
0–19°S	−1.1±0.8		−2.1±0.8
0–19°N	−1.1±1.5		−1.6±1.3
19°N–29°N	−3.5±2.2		−3.1±1.9
29°N–39°N	−3.7±2.0	−1.7±0.7	−2.5±1.7
39°N–53°N	−2.7±1.7	−3.0±0.8	−1.2±1.5
53°N–65°N	−2.4±1.6	−2.3±0.7	−1.4±1.4

(Linear trends with an autoregressive model through TOMS data, with uncertainties at the one sigma level of significance.)

significant apparent quasi-biennial oscillation with a particularly large negative deviation in the summer of 1985–1986. The fitted linear trends using an autoregressive model are again given in Table 4.27. As with the global change, the 9-year trends are approximately equal cumulatively to the 7-year trends. The Southern Hemisphere has a slight increase in the downward change with the added 2 years, while the Northern Hemisphere actually shows somewhat less total change. (Note added: Inclusion of data through October 1988 indicates a tendency toward reversal of the downward trend in the Southern Hemisphere, but not in the Northern Hemisphere.) Any conclusions about whether there is any reversal or flattening of the trend are made on variations that are within the one-sigma limits of the data and should, therefore, be viewed with caution. Likewise, it should be remembered that this analysis did not include any evaluation of a contribution from the 11-year solar cycle.

4.7.2 Trends in Latitude Bands

The TOMS data can be further broken down by latitude bands. Figure 4.69a–j shows the daily deviations of TOMS total ozone data from weekly means. Deviations are given in percent, and, as above, all data have been normalized to the observed mean drift of TOMS with respect to the Dobson stations during the overpasses of Nimbus–7 over 41 stations. The latitude regions shown were chosen to correspond to an analysis of the Dobson network by Bojkov (1988). They are a) 53–65°S, b) 39–53°S, c) 29–39°S, d) 19–29°S, e) 0–19°S, f) 0–19°N, g) 19–29°N, h) 29–39°N, i) 39–53°N, and j) 53–65°N. Note that the scale of the deviations has been doubled compared to the global and hemispheric plots.

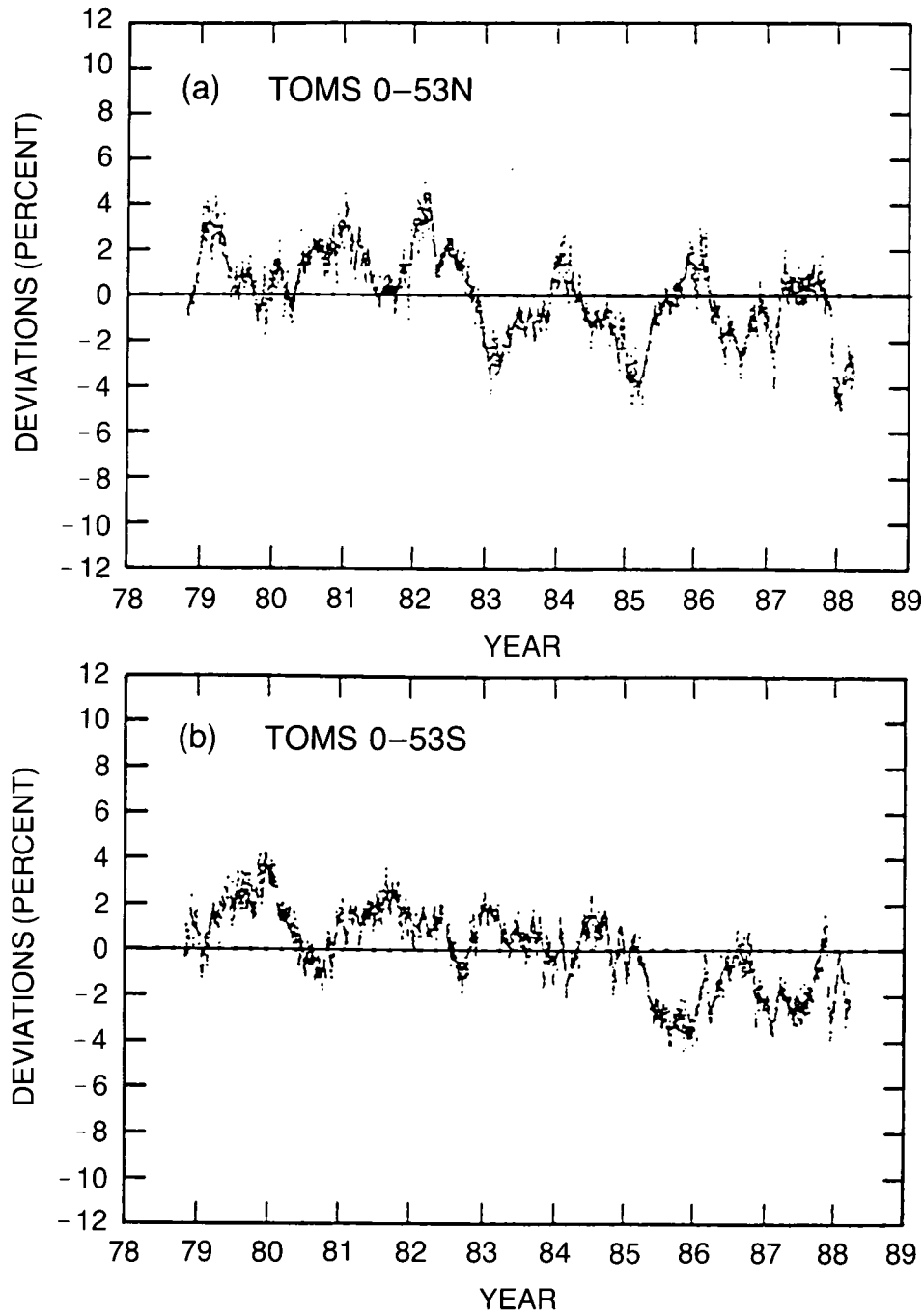

Figure 4.68 Zonal means of total ozone derived from TOMS for the areas between (a) 0–53°N and (b) 0–53°S. Percentage deviations from the seasonal means are plotted.

The Northern Hemisphere minimum of the winter of 1982–1983 does not appear in the tropical data from the Equator to 19°N but does appear in the rest of the latitude bands up to 65°N. The minimum of the winter of 1984–1985 also is not in the tropical data, nor is it in the 53–65°N data. However, it is more pronounced in the data from 19–39°N than is the minimum of the winter of 1982–1983. It is suggestive that this northern hemispheric minimum is coincident with the spread of aerosol from the El Chichón eruption throughout the Northern Hemisphere,

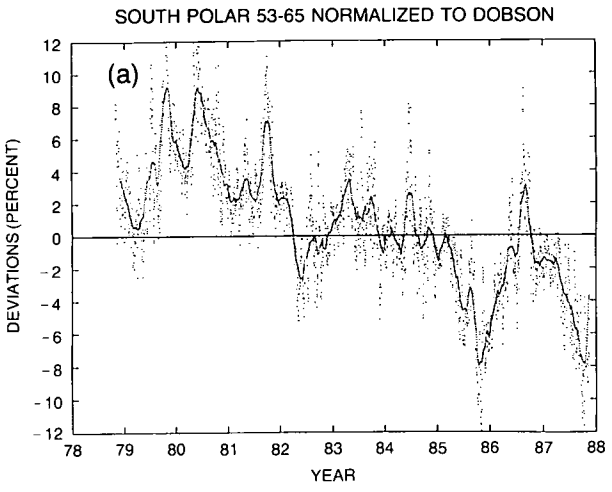
SOUTH POLAR 53-65 NORMALIZED TO DOBSON
(a)
DEVIATIONS (PERCENT)
YEAR

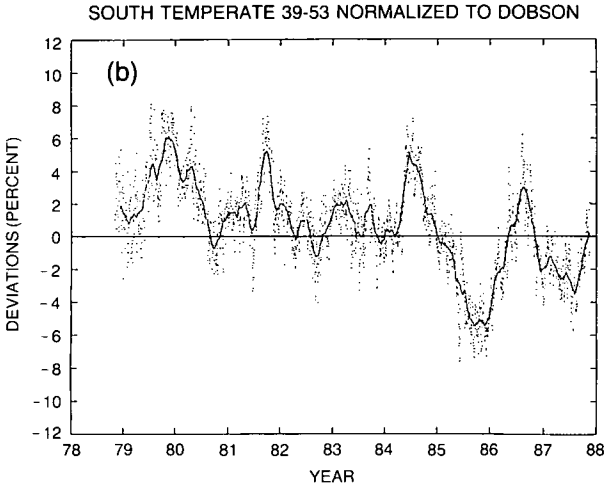
SOUTH TEMPERATE 39-53 NORMALIZED TO DOBSON
(b)
DEVIATIONS (PERCENT)
YEAR

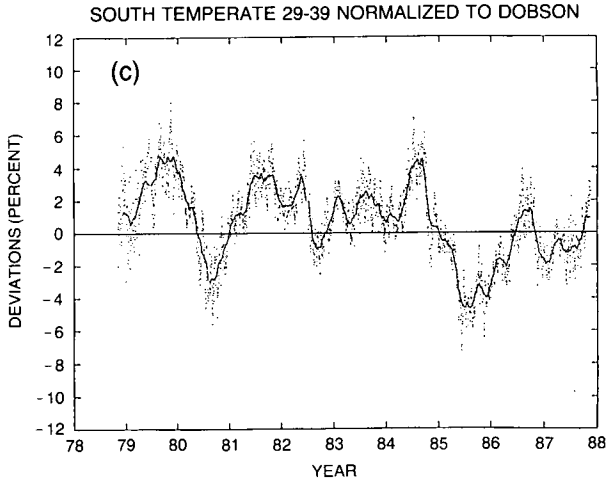
SOUTH TEMPERATE 29-39 NORMALIZED TO DOBSON
(c)
DEVIATIONS (PERCENT)
YEAR

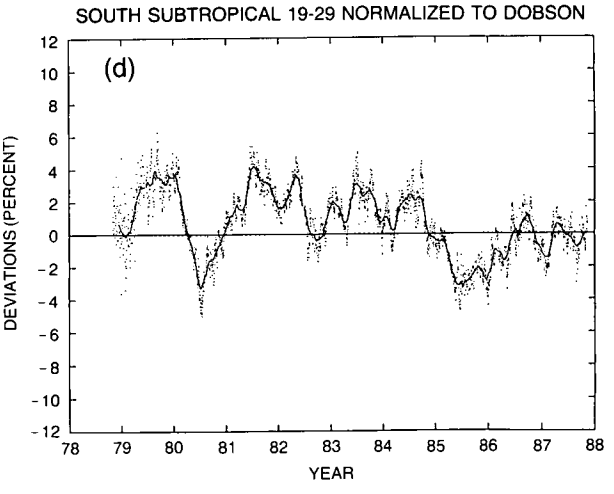
SOUTH SUBTROPICAL 19-29 NORMALIZED TO DOBSON
(d)
DEVIATIONS (PERCENT)
YEAR

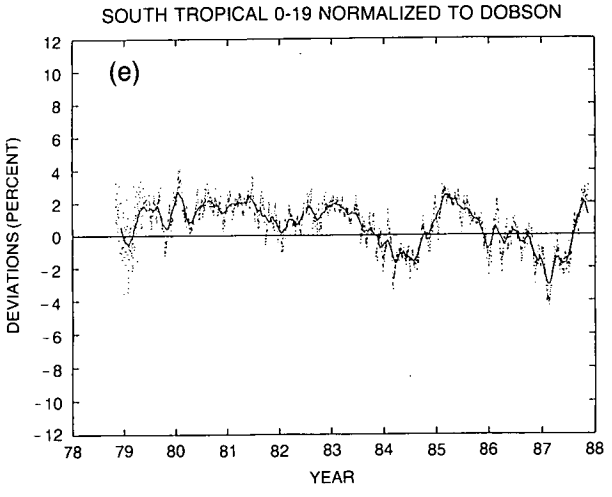
SOUTH TROPICAL 0-19 NORMALIZED TO DOBSON
(e)
DEVIATIONS (PERCENT)
YEAR

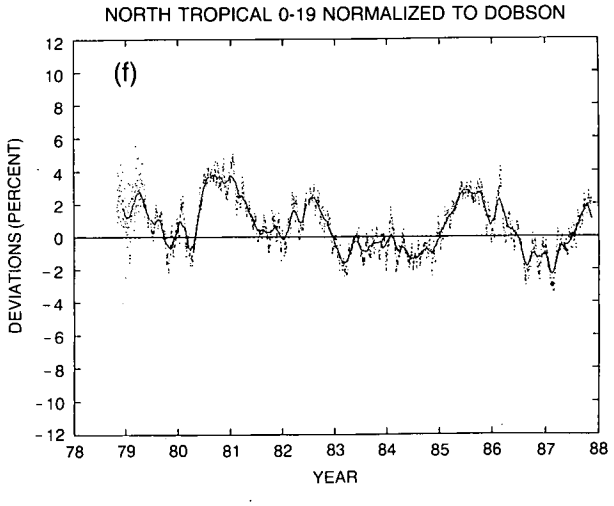
NORTH TROPICAL 0-19 NORMALIZED TO DOBSON
(f)
DEVIATIONS (PERCENT)
YEAR

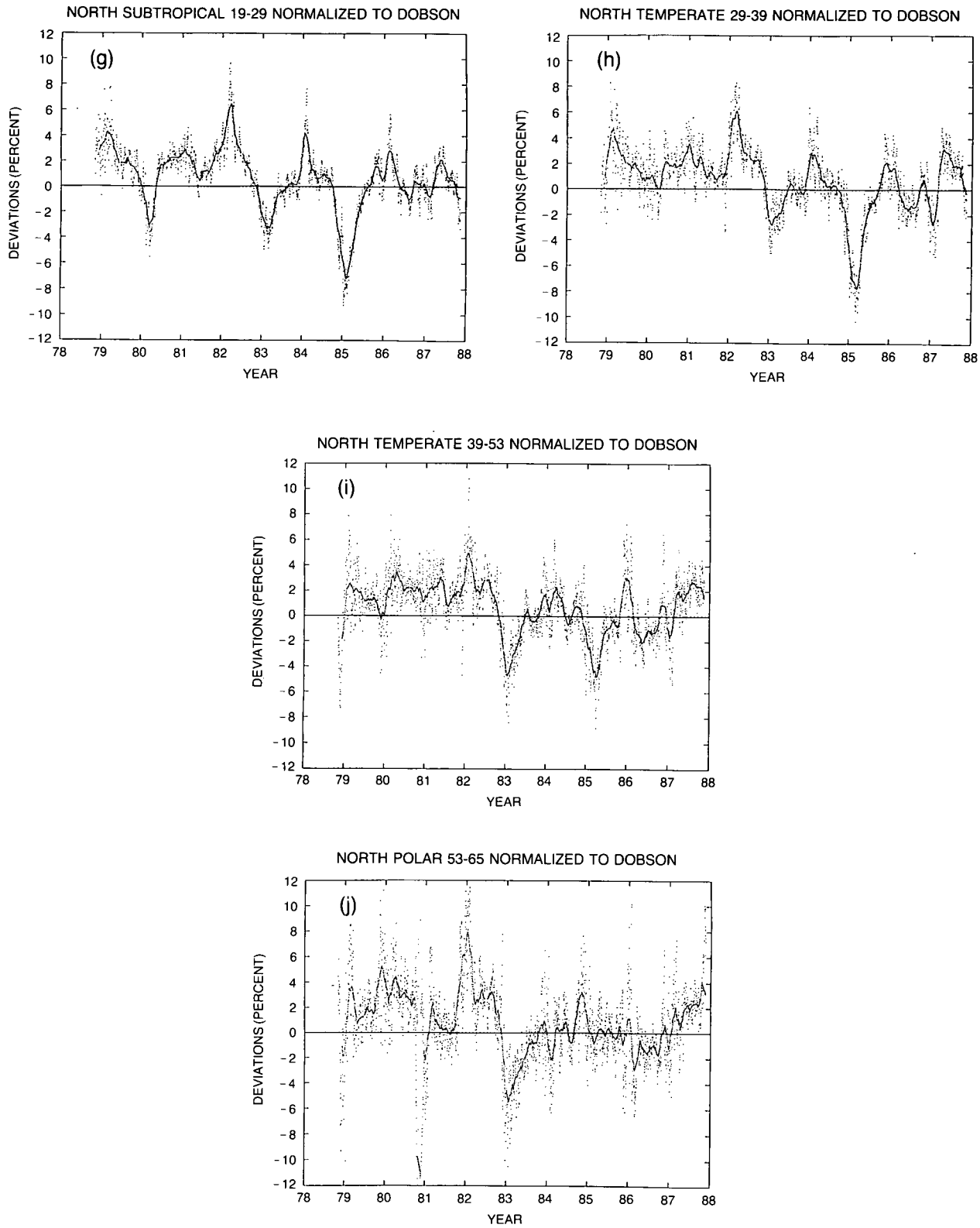

Figure 4.69 Zonal means of total ozone derived from TOMS for various latitude bands are plotted as percentage deviations from the weekly means. (a) 53–65°S, (b) 39–53°S, (c) 29–39°S, (d) 19–29°S, (e) 0–19°S, (f) 0–19°N, (g) 19–29°N, (h) 29–39°N, (i) 39–53°N, (j) 53–65°N.

although no cause and effect relationship has been established, and Schuster et al. (1988) have proposed that the observed perturbation to total ozone levels could be due to a modification of the QBO signal by the El Chichón aerosol. Another possible cause was the strong El Niño in 1982–1983. The Southern Hemisphere minimum that spans mid- to late 1985 extends over all latitudes from 19–65°N, and another strong minimum appears between 19–39°N in late 1980.

The linear trends for the first 7 years and the entire 9-year data set deduced with an autoregressive model are shown in Table 4.27. The trends are all negative, but generally not significant at the two-sigma level. The main exceptions are the two most southerly latitude bands. The decreases in these bands occur primarily in the southern circumpolar ring of high ozone and have been noted in previous studies of the Antarctic ozone hole (e.g., Stolarski et al., 1986; Stolarski and Schoeberl, 1986).

4.7.3 Global Maps of the Difference Between 1986–1987 and 1979–1980 Total Ozone

The behavior of many of the time series shown in the previous section is that the total ozone amount is relatively constant for the first few years of the record and then again relatively constant at a lower value near the end of the record. This suggests that some understanding of the change may be gained by comparing these two portions of the record as a function of season, latitude, and longitude. Figure 4.70 is a contour plot of the difference in total ozone between the

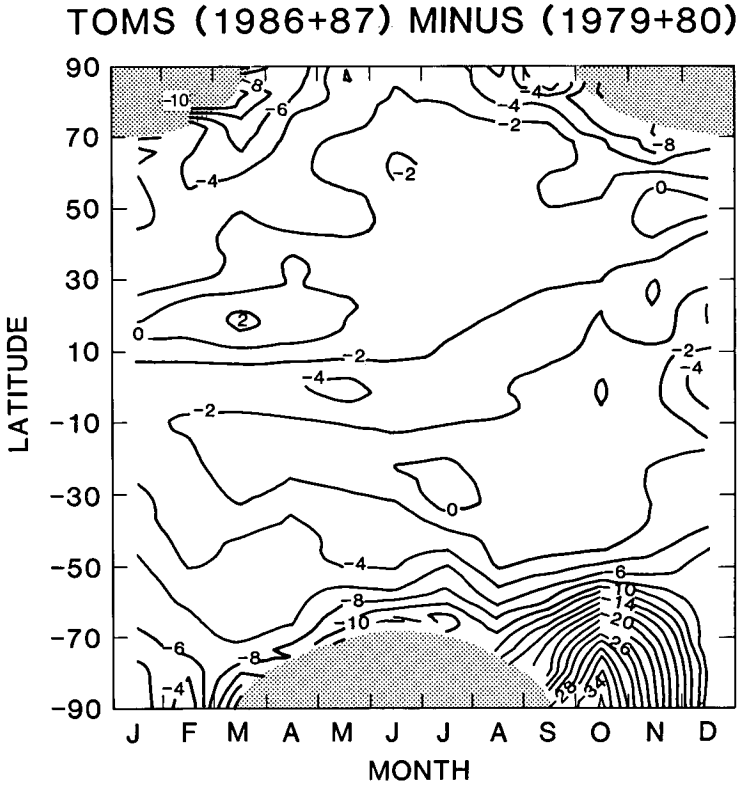

Figure 4.70 Changes by month and latitude in total ozone between 1979–1980 and 1986–1987 as measured with TOMS on the Nimbus–7 satellite (2-year averages are used to minimize differences originating with the QBO). Contour plots are given for intervals of 2 percent change. The TOMS instrument operates with sunlight scattered from the atmosphere and, therefore, provides no data from the areas in the polar night.

last 2 full years of the record (1986 and 1987) and the first 2 full years (1979 and 1980) as a function of latitude and season. The most obvious feature of this figure is the springtime Antarctic ozone hole. A general decrease of greater than 5 percent also appears at all latitudes south of 50°S for all seasons. The rest of the globe shows smaller changes, which are more negative than positive. The northern high-latitude spring has a small region of greater than 5 percent decrease, which raises the possibility that this is related to processes occurring in the northern winter (see section above on ground-based data).

Further details of the ozone change from 1979–1980 to 1986–1987 can be obtained by examining global maps versus latitude and longitude for specific months; these are shown in Figure 4.71a–l. The Antarctic springtime ozone hole is again obvious. Changes over most of the globe are negative, but significant positive change regions also exist. It is not clear from these data whether there is any physical significance to these positive regions. More likely, if other years are taken, the regions of positive and negative will move around but will still be predominantly negative. The north polar region shows interesting behavior in a number of months. For example, in March a large negative change is observed over the northern USSR, while a large positive region is observed over northeastern Canada and Greenland. This pattern results primarily from a shift in the pattern of the pole-centered high between the two sets of years that have been compared.

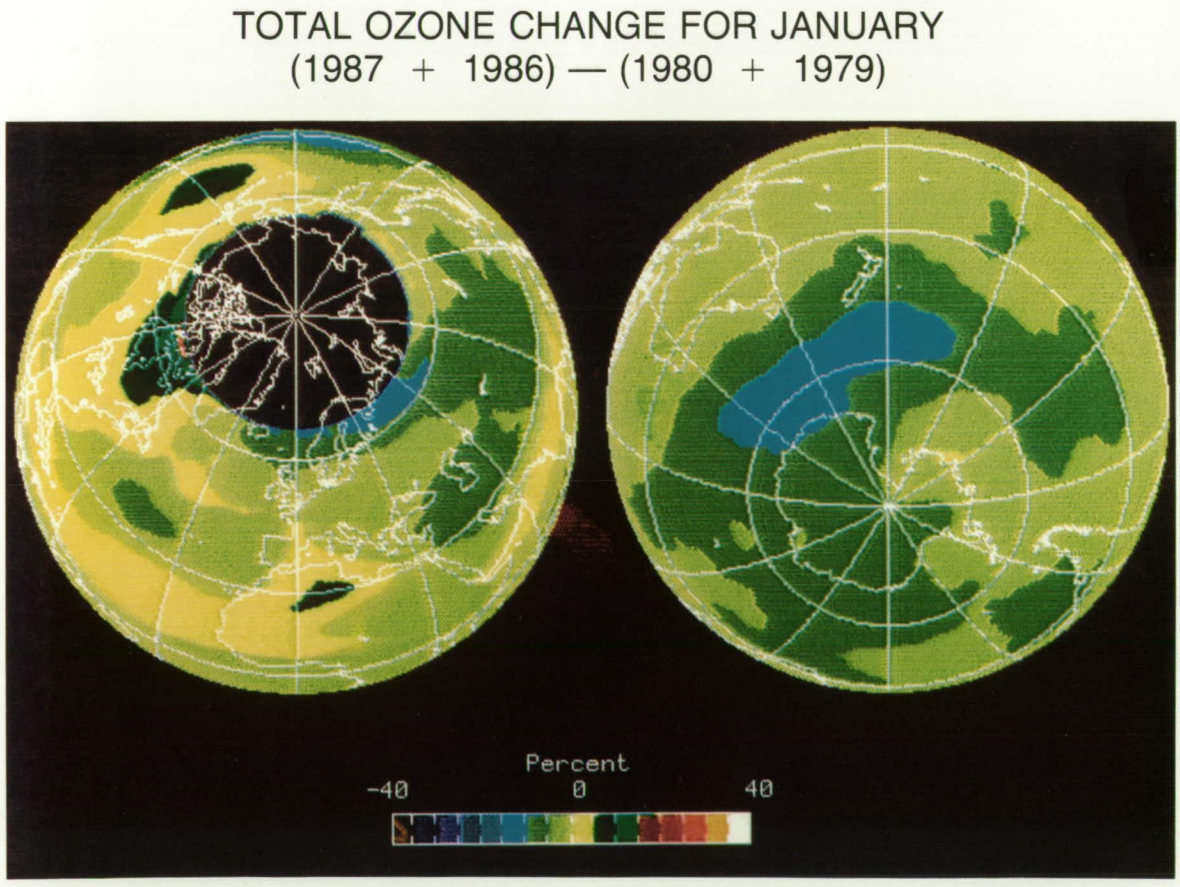

Figure 4.71 (a–1) TOMS maps of monthly (January through December) total ozone change averaged from 1979 through 1987. Left side of each panel shows Northern Hemisphere; right side of panel shows Southern Hemisphere. Total ozone is given in Dobson Units (milli-atmosphere-cm) as indicated in color bar.

TOTAL OZONE CHANGE FOR FEBRUARY
(1987 + 1986) — (1980 + 1979)

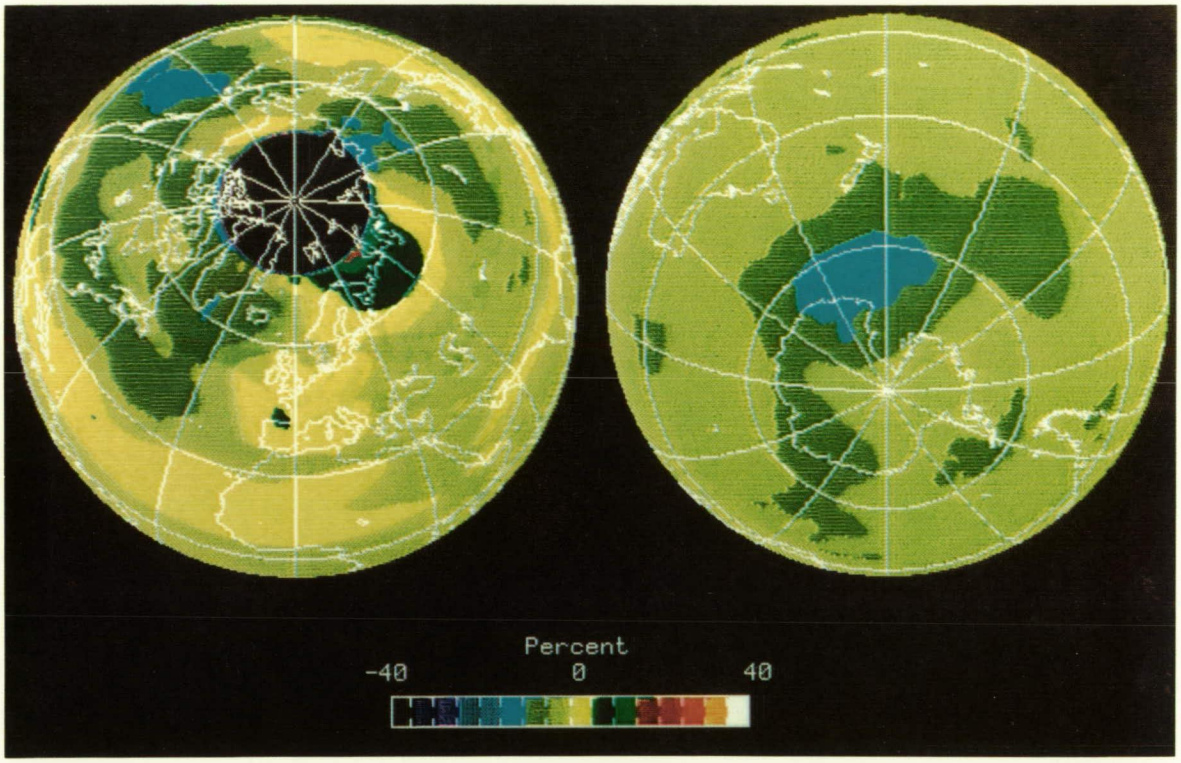

TOTAL OZONE CHANGE FOR MARCH
(1987 + 1986) — (1980 + 1979)

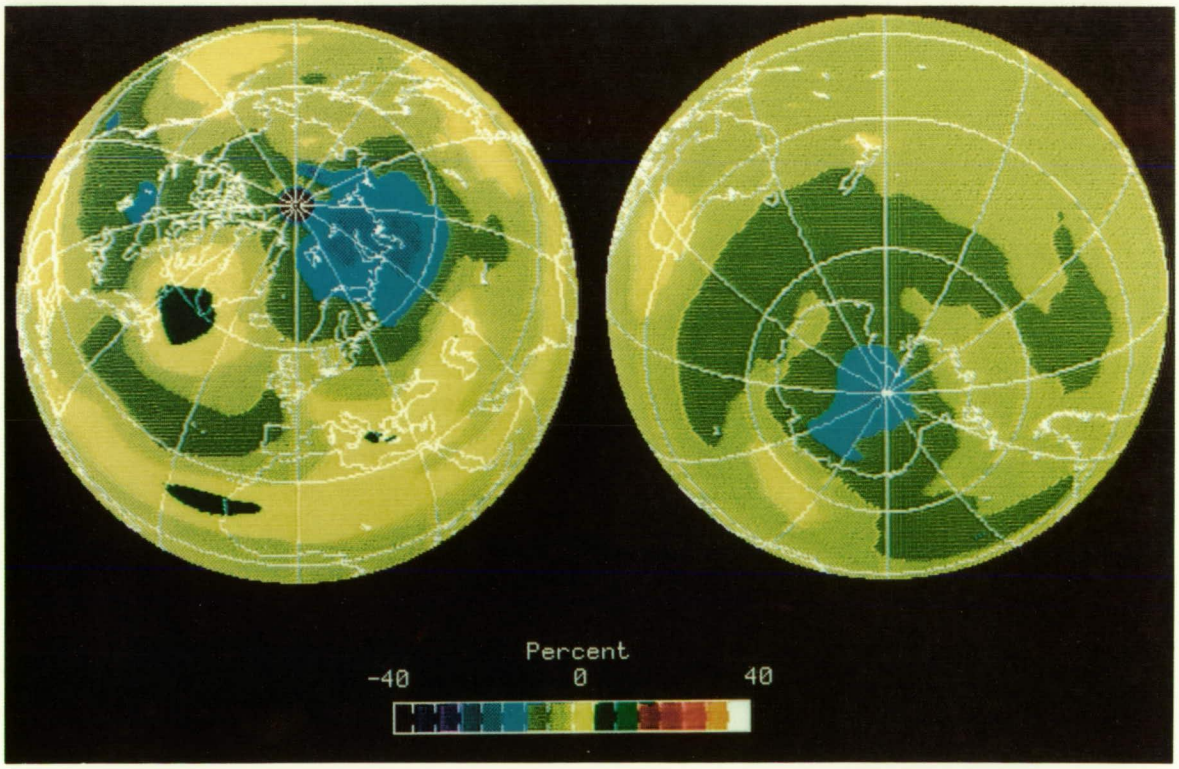

TOTAL OZONE CHANGE FOR APRIL
(1987 + 1986) — (1980 + 1979)

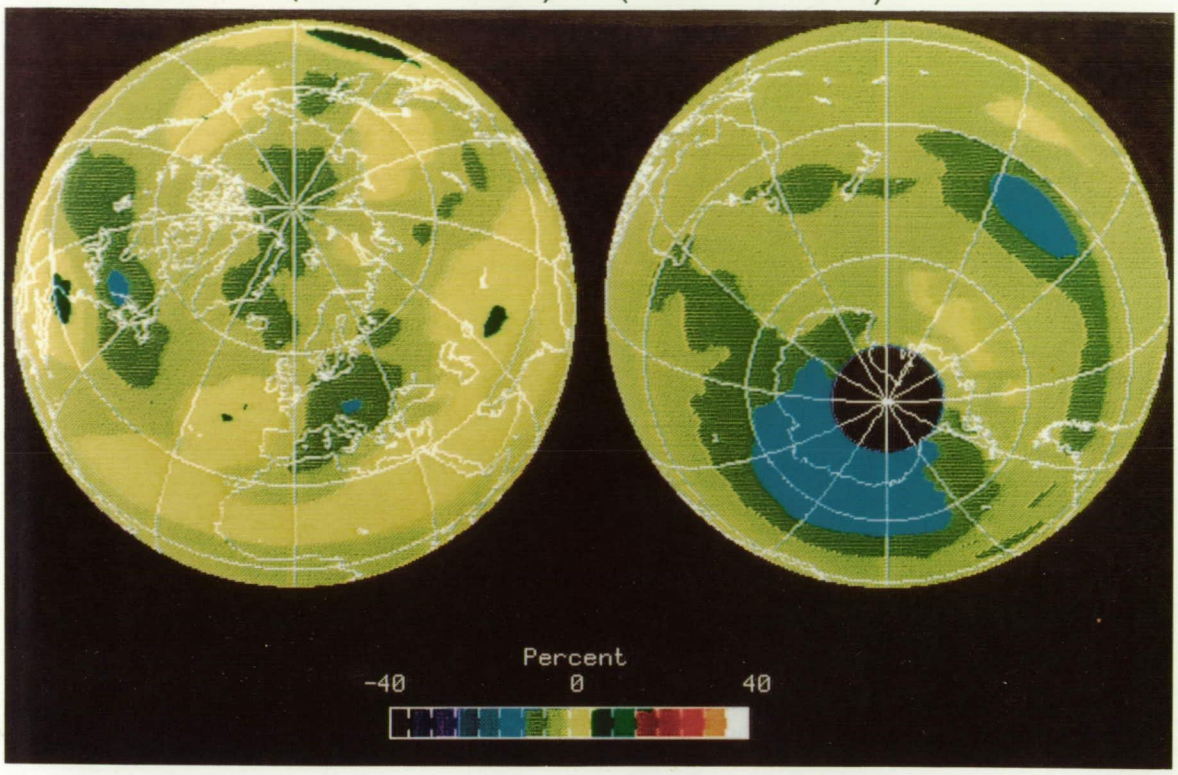

TOTAL OZONE CHANGE FOR MAY
(1987 + 1986) — (1980 + 1979)

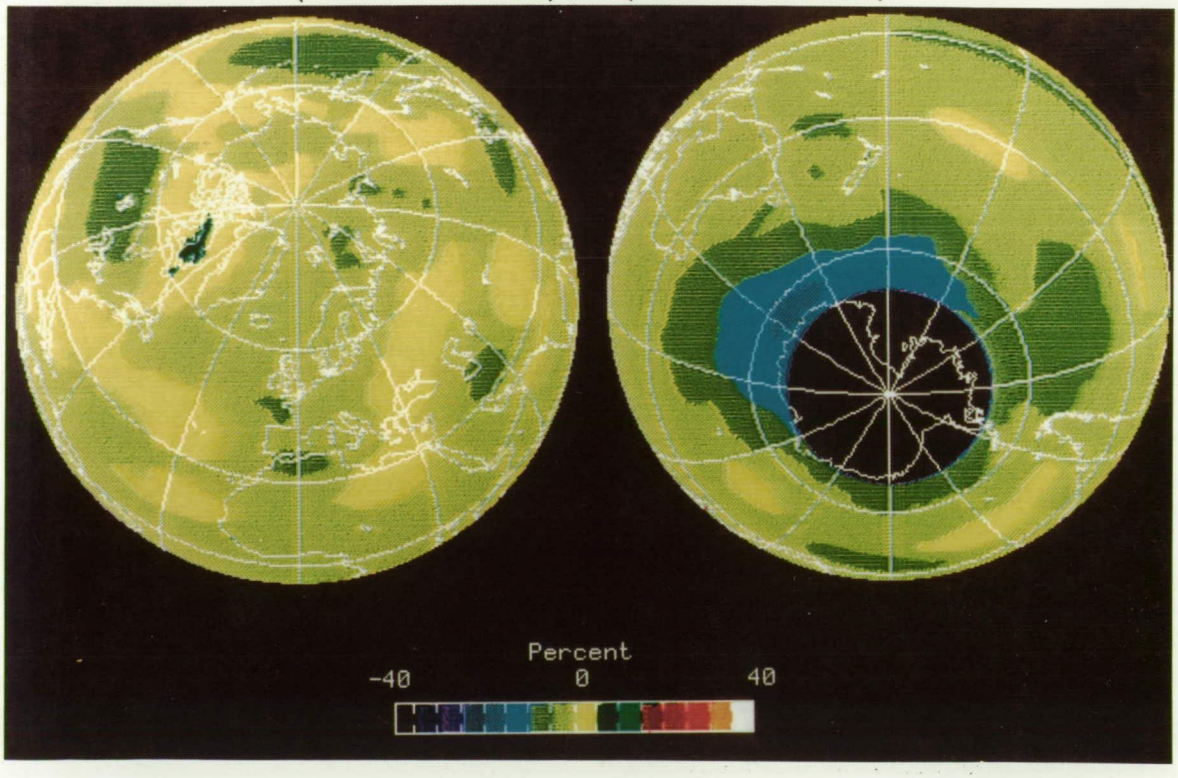

TOTAL OZONE CHANGE FOR JUNE
(1987 + 1986) — (1980 + 1979)

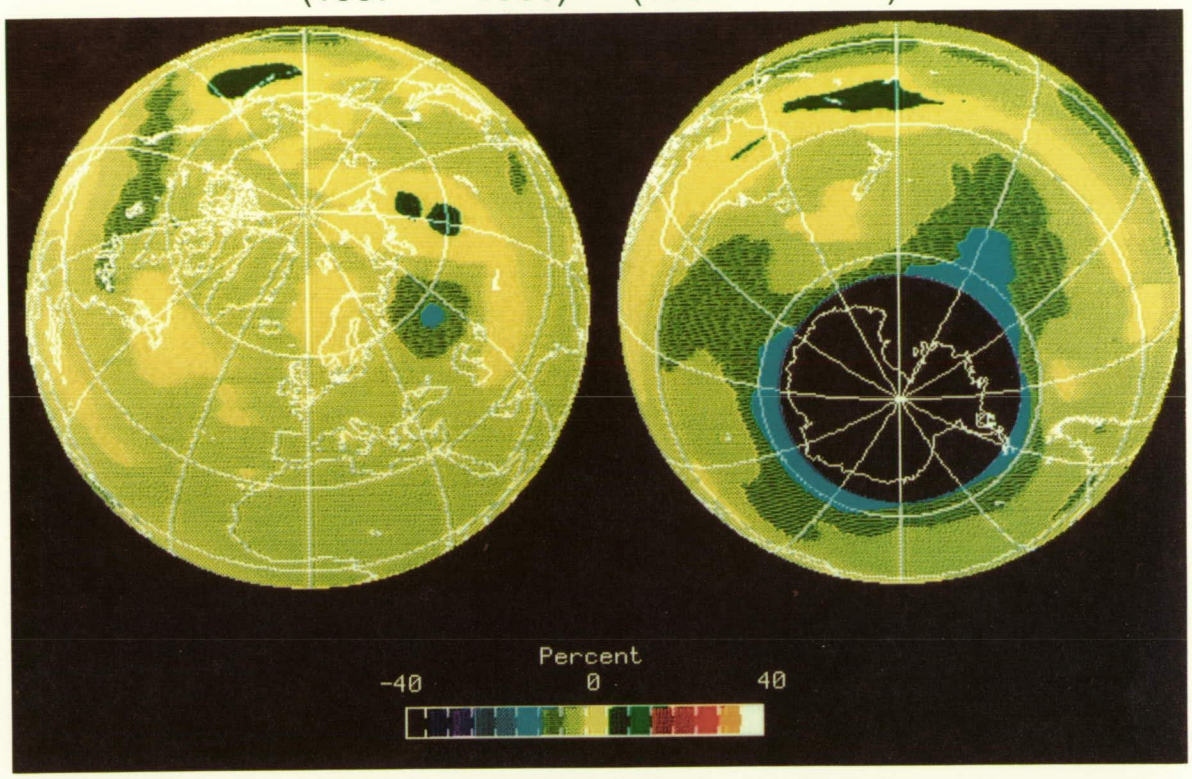

TOTAL OZONE CHANGE FOR JULY
(1987 + 1986) — (1980 + 1979)

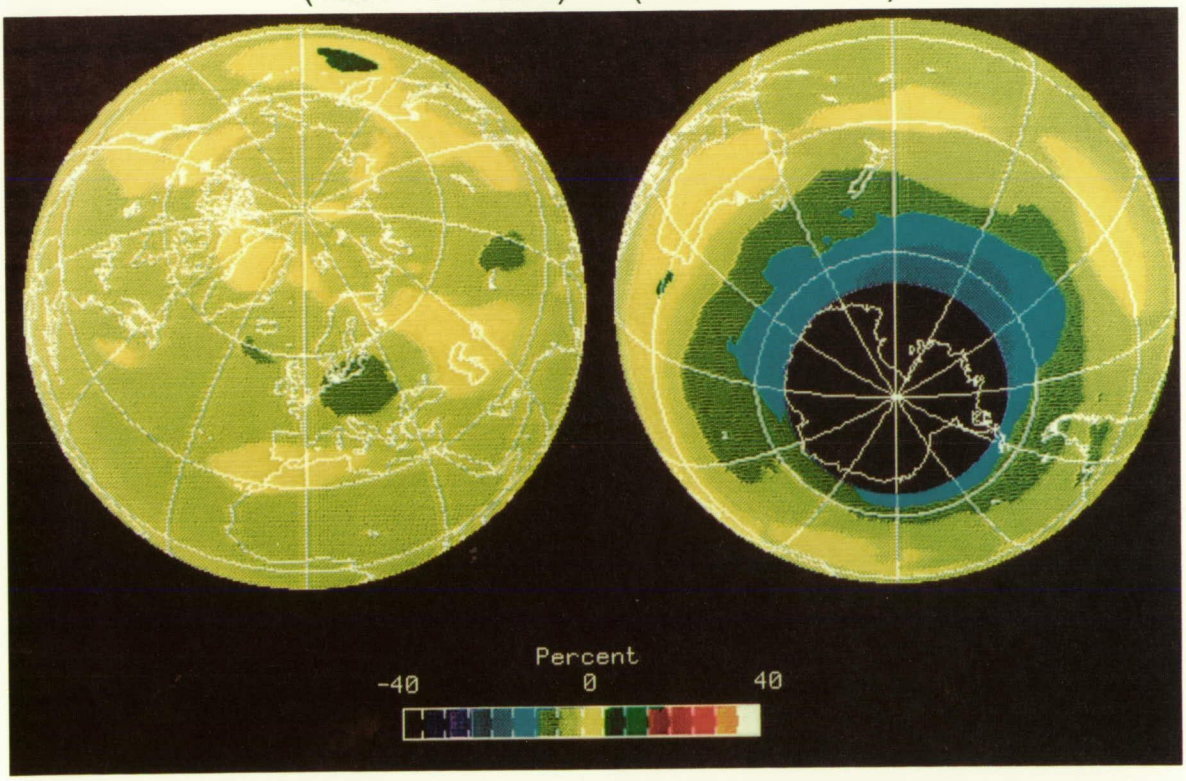

TOTAL OZONE CHANGE FOR AUGUST
(1987 + 1986) — (1980 + 1979)

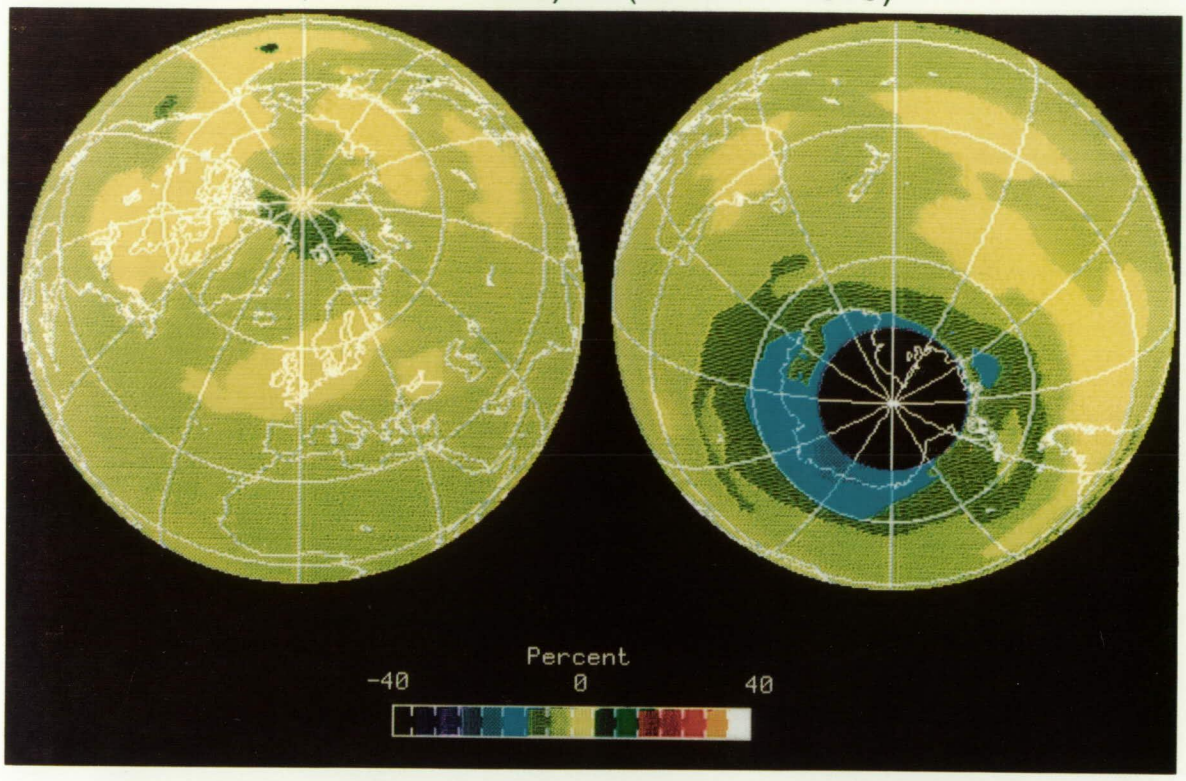

TOTAL OZONE CHANGE FOR SEPTEMBER
(1987 + 1986) — (1980 + 1979)

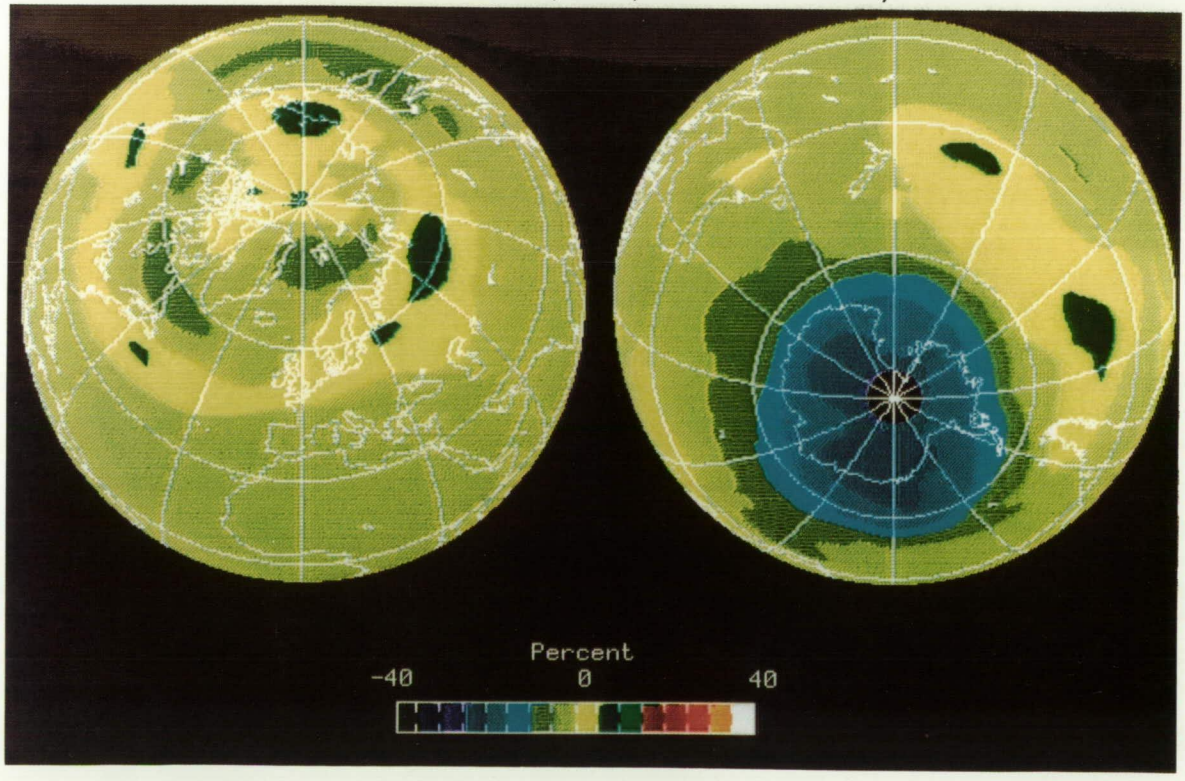

TOTAL OZONE CHANGE FOR OCTOBER
(1987 + 1986) — (1980 + 1979)

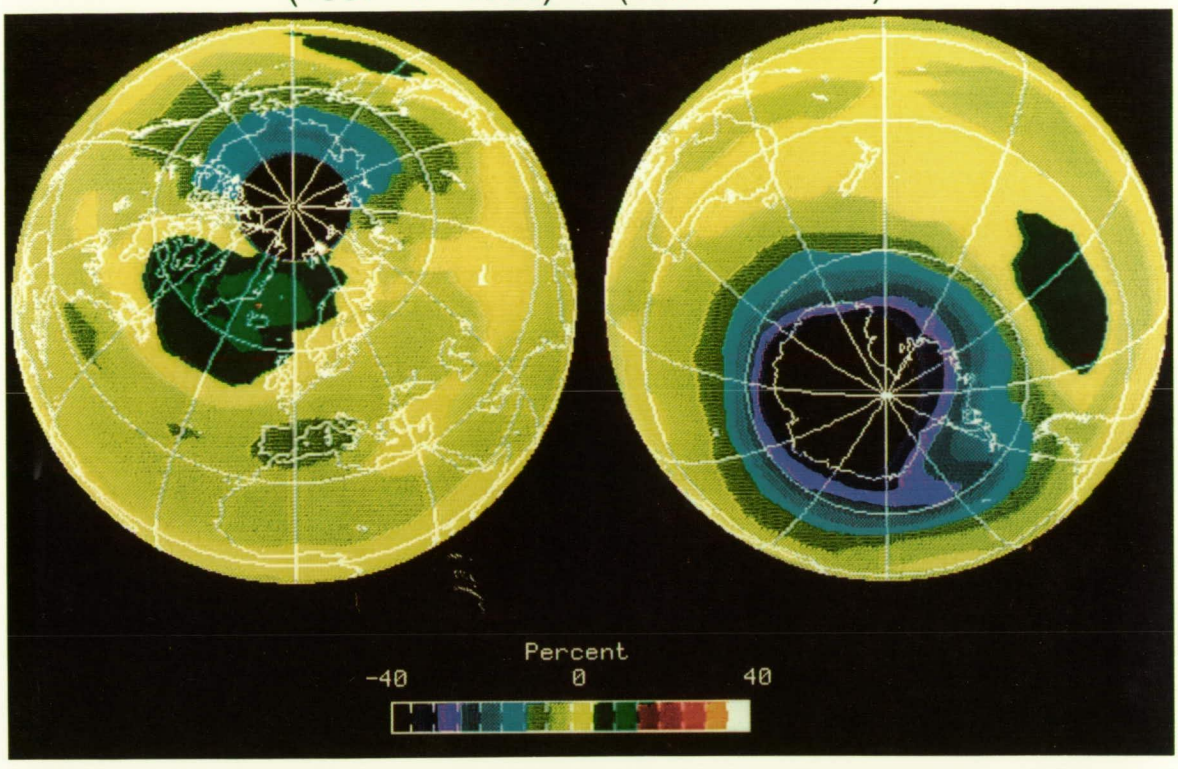

TOTAL OZONE CHANGE FOR NOVEMBER
(1987 + 1986) — (1980 + 1979)

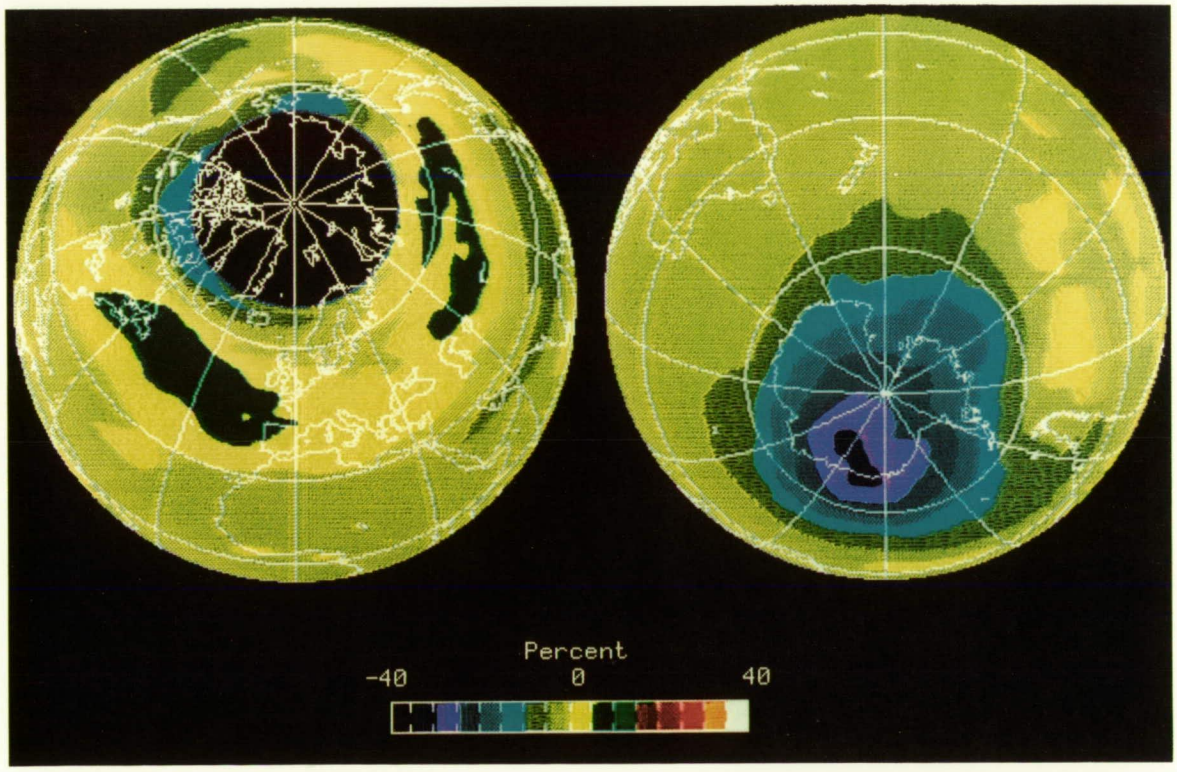

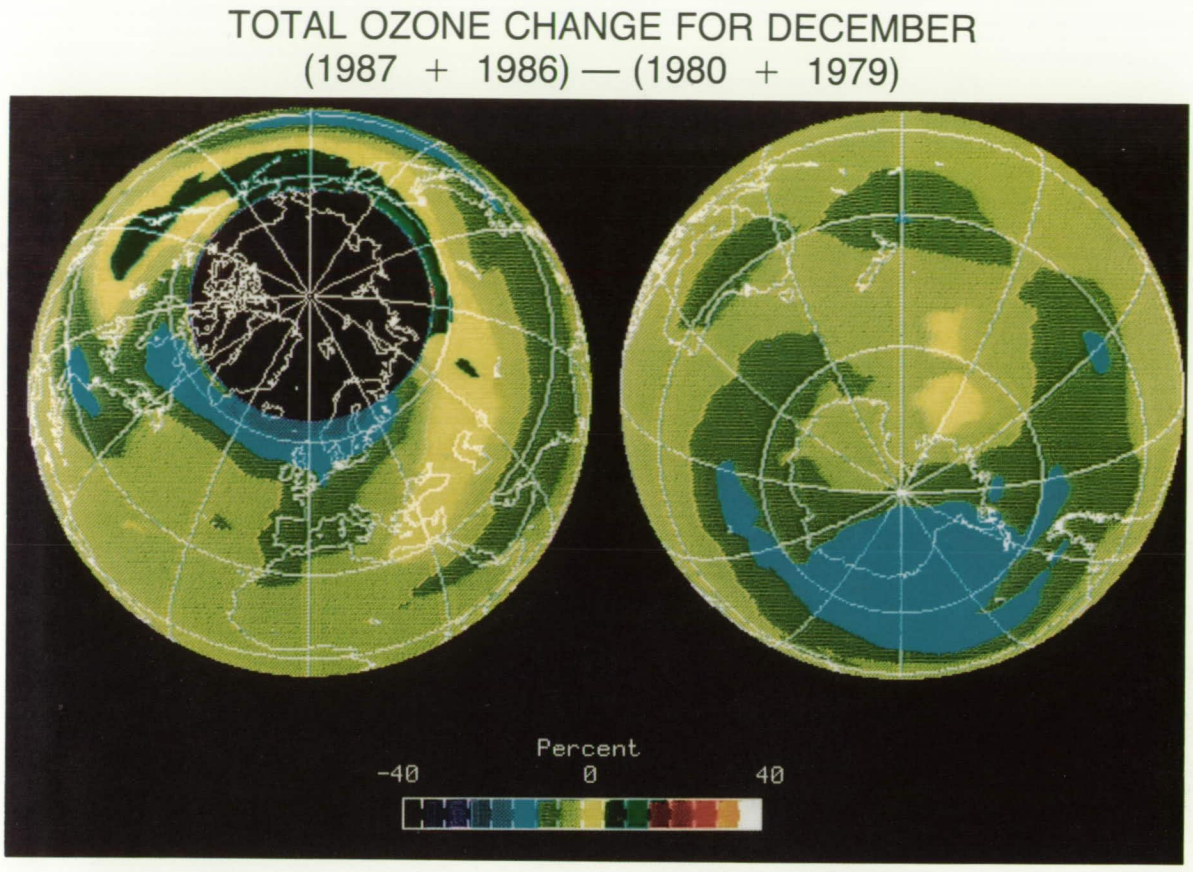

4.8 SUMMARY

It is important to ensure that the best available data are used in any determination of possible trends in total ozone in order to have the most accurate estimates of any trends and the associated uncertainties. Accordingly, the existing total ozone records have been examined in considerable detail. Once the best data set has been produced, the statistical analysis must examine the data for any effects that might indicate changes in the behavior of global total ozone. The changes at any individual measuring station could be local in nature, and in this study particular attention has been paid to the seasonal and latitudinal variations of total ozone, because 2-D photochemical models indicate that any changes in total ozone would be most pronounced at high latitudes during the winter months. The conclusions derived from this detailed examination of available total ozone can be split into two categories, one concerning the quality and the other the statistical analysis of the total ozone record.

Data Quality

The published data of both ground-based and satelliteborne instruments have been shown to contain incongruities that have been traced back to instrument calibration problems. In the case of the ground-based record, the corrections for these calibrations have not been applied to the data before publication in ODW. Correcting the data for known calibrations is essential if one is to believe the results of statistical analyses of the data set. Fortunately, complete revisions of the total ozone data set can be performed at many ground-based stations because good day-to-day records have been kept. At stations whose daily records have been lost, the correct adjustments

to the total ozone data are irrecoverable. For the purposes of this report, a provisionally revised data set was prepared, with the corrections caused by recalibrations being applied to the monthly averages and not to the individual daily measurements. The provisionally revised data are taken as being the best currently available set for two reasons: the effects of the known, periodic recalibrations of the Dobson instruments are accounted for and the consistency of external data such as measurements from proximate stations, stratospheric temperatures, and satellite overpasses is found to be greater with the provisionally revised data sets than with the data published in ODW.

The TOMS satellite data have been compared with measurements taken by the International Primary Standard Dobson Instrument (No. 83) while it was being calibrated at Mauna Loa; it was found that the two instruments had drifted relative to each other. A similar result was found in a TOMS–Dobson data comparison during overpasses of the TOMS instrument at 92 ground-based stations. The SBUV data have been drifting in a similar manner, and the conclusion was reached that the cause of this effect was the degradation of the diffuser plate on Nimbus–7, the only common component of the TOMS and SBUV systems. The TOMS data were then normalized to agree with the 92 ground-based stations. Because Instrument No. 83 is used as the main calibrating instrument for the Dobson network and because the TOMS satellite data revision is also based partially on the results of a comparison with Instrument No. 83, a detailed review of the absolute calibrations used with this instrument was made and no problems were discovered.

Analysis

Initial examination of both the published (ODW) and provisionally revised data sets indicates that, in recent years, a decrease in total ozone has occurred at latitudes poleward of 40°N, particularly in the winter months (see Figures 4.45–48). This result showed the need for a statistical analysis of the revised data that investigated the effects of season and latitude on any changes. Unfortunately, the spatial distribution of the Dobson stations is poor, with most of the instruments placed in Europe or North America, so that the portion of the globe for which there is reasonable coverage is limited to the latitudes from 30–80°N. Even in this area, the longitudinal coverage is poor, although it was greatly extended in 1972 when the upgraded M–83 filter ozonometers were introduced in the USSR. A time series model for the ground based total ozone record was used that included terms for the natural seasonal cycle, the natural autocorrelation, the effects of such geophysical phenomena as the quasi biennial oscillation, the solar cycle, and the atmospheric nuclear bomb testing that took place between 1957 and 1963. Statistical tests for possible trends in recent years were conducted using both the older assumption of no seasonality in any ozone trends, and with allowance for different trends for each calendar month.

The analysis of the provisionally revised data from 1965–1986 again showed that there had been a significant wintertime loss at higher latitudes since 1969, and that between 30°N and 39°N there had been a year-round decrease. The data period from 1965–1986 is advantageous for three reasons: it contains two complete solar cycles, minimizing any residual effects from an inadequate modeling of the effects of the solar cycle on total ozone; any effects of the atmospheric nuclear bomb tests ending in the early 1960's will be small; and before 1965, fewer stations were taking measurements. When the data from 1957–1986 was considered, the wintertime loss was still apparent. The trends were slightly smaller than those calculated using the shorter time period, but they easily lay within the combined uncertainties. The modeled effect of the atmospheric bomb tests was found to be slightly larger than that derived from the statistical analysis of the measurements, although within the calculated uncertainty. The effect of the QBO on total ozone was statistically significant at most latitudes, while the effect of the solar cycle was

marginally significant. When the earlier data were included in the analysis, the calculated effect of the solar cycle was reduced, making it hard to reach any firm conclusions about the relationship between the solar cycle and total ozone. The period of low total ozone values over the Northern Hemisphere in 1982–1983 was not the dominant cause of the measured ozone decreases since 1969. In particular, the seasonal nature of the losses is evident in the data record through 1981.

Conclusions

The main conclusions of this chapter can be listed as follows:

- Examination of the published total ozone record reveals a need for a revision of the data.
- Provisionally revised sets of measurements have been prepared for both the ground-based stations and the TOMS satellite instrument.
- Statistically significant losses have occurred in the late winter and early spring in the Northern Hemisphere. For example, in the latitude band from 53–64°N, a loss of 6.2 percent is measured for December, January, February, and March from 1969–1986 when the data from 1965–1986 are considered.
- The seasonal and the latitudinal variations of these losses agree with the results of current 2-D photochemical models in nature, if not in magnitude.
- There is some evidence for longitudinal variations in the measured trends.

Chapter 4 Appendix

Contents

*If the enclosed ozone data are used in future work, consideration should be given to the method of revision utilizing calibration, intercomparison data, stratospheric temperatures, and TOMS data for flagging major discrepancies.

A. (i) Provisionally revised station data used in the time series analyses.

Arosa[1]	1/57–12/86	Leningrad	8/68–12/85
Aspendale	7/57–12/86	Lerwick	1/57–11/86
Belsk	1/63–12/86	MacQuarie Isle	1/63–12/86
Bismarck	1/63–12/86	Mauna Loa	1/63–12/86
Boulder	1/64–12/86	Nashville	1/63–12/86
Bracknell	1/69–12/86	Quetta	8/69–12/86
CagliarivElmas	1/57–12/86	Reykjavik	11/75–10/86
Cairo	11/74–10/86	Rome (Vigna di Valle)	1/57–12/86
Caribou	6/62–12/86	Samoa[2]	1/76–12/86
Churchill	1/65–12/86	Sapporo	1/58–12/86
Edmonton	7/57–11/86	Srinigar	2/64– 5/86
Goose Bay	1/62–11/86	Tateno	7/57–12/86
Hohenpeissenberg	1/67–12/86	Toronto	1/60–12/86
Hradec Kralove	1/62–12/86	Uccle	2/71–12/86
Huancayo	2/64– 6/86	Wallops Island	1/70–12/86
Kagoshima	4/61–12/86		

[1]Data accepted in unrevised form from *Ozone Data for the World.*
[2]Data revised and supplied by W.D. Komhyr et al. (1987).
[3]All other data are the monthly averages of total ozone published in *Ozone Data for the World* with the appropriate average monthly corrections applied. The amounts are given in Dobson Units.

Average Ozone Values at AROSA

Year	Jan	Feb	Mar	Apr	May	Jun	Jul	Aug	Sep	Oct	Nov	Dec
1957	327	326	336	359	372	338	320	312	292	271	287	321
1958	346	336	393	398	358	349	336	311	286	291	287	308
1959	356	362	366	382	375	355	324	319	304	289	297	321
1960	342	381	405	388	365	341	335	314	307	304	285	318
1961	356	324	334	357	364	339	328	304	279	277	294	299
1962	341	360	425	383	358	342	323	300	293	267	295	299
1963	359	410	379	377	372	348	318	310	284	275	278	295
1964	304	337	348	374	362	324	315	311	293	288	272	307
1965	331	384	379	372	374	332	329	317	304	276	280	314
1966	347	339	395	375	366	344	324	317	297	279	314	315
1967	354	358	351	366	343	346	316	312	292	273	269	301
1968	338	386	381	372	346	344	324	328	306	276	274	332
1969	335	418	362	377	347	356	327	327	290	278	305	334
1970	325	408	408	416	382	355	329	321	296	286	274	312
1971	344	351	409	366	361	352	324	305	314	276	292	303
1972	345	363	382	369	363	350	327	309	315	291	291	308
1973	320	384	363	428	348	343	342	311	290	286	270	299
1974	329	369	343	378	361	350	316	308	289	327	297	282
1975	308	340	368	365	353	344	317	310	283	283	295	289
1976	340	352	360	375	351	346	325	326	309	277	286	311
1977	358	391	347	373	369	352	335	322	302	271	291	301
1978	328	363	346	386	373	355	330	315	289	287	277	294
1979	345	378	373	402	365	337	328	314	289	287	281	306
1980	327	334	358	390	378	354	328	305	286	278	285	300
1981	324	378	357	365	370	329	323	310	295	290	281	309
1982	334	375	389	367	359	345	318	318	284	282	273	288
1983	291	354	331	359	344	333	313	314	287	273	270	296
1984	339	371	378	364	369	339	318	316	299	284	279	291
1985	355	336	353	344	342	332	312	295	279	276	301	288
1986	356	386	356	380	342	331	320	303	286	279	286	298

Provisionally Revised Average Ozone Values at Aspendale

Year	Jan	Feb	Mar	Apr	May	Jun	Jul	Aug	Sep	Oct	Nov	Dec
1957	0	0	0	0	0	0	348	354	358	345	328	311
1958	309	294	294	280	295	345	376	366	399	382	341	322
1959	291	300	292	279	308	323	318	332	350	346	318	316
1960	293	285	288	287	318	341	353	383	388	367	341	315
1961	302	303	283	283	292	300	313	337	329	335	315	303
1962	293	288	288	282	308	316	344	378	374	386	339	319
1963	306	292	294	286	304	338	356	359	369	346	340	317
1964	311	317	284	283	302	337	357	365	364	359	327	326
1965	304	292	286	295	301	328	357	361	358	352	338	305
1966	301	287	289	286	302	309	333	334	356	341	323	307
1967	296	286	288	278	296	306	347	361	367	355	340	330
1968	287	293	283	287	314	321	342	368	370	364	333	324
1969	297	291	286	282	300	320	317	328	355	340	340	325
1970	310	297	297	289	308	333	349	373	389	368	341	327
1971	312	300	285	287	315	329	337	356	359	362	336	319
1972	300	301	286	277	297	322	362	364	376	361	345	312
1973	300	297	301	289	296	323	332	351	358	357	325	310
1974	288	298	285	289	308	329	359	378	380	367	342	319
1975	317	294	292	289	296	322	330	357	348	354	328	298
1976	288	287	295	292	299	319	333	353	365	374	342	317
1977	303	291	287	284	307	331	346	356	356	350	323	298
1978	290	288	300	286	308	329	351	375	384	360	333	327
1979	290	287	288	295	306	317	335	366	374	366	349	313
1980	309	293	286	284	298	316	325	326	339	338	323	303
1981	291	284	293	272	296	333	348	367	344	361	342	310
1982	294	289	290	292	312	324	334	322	357	356	317	310
1983	280	270	261	281	286	314	329	353	346	361	334	302
1984	291	283	274	278	301	321	354	358	370	348	330	309
1985	292	284	272	279	284	299	311	334	337	335	309	297
1986	295	280	271	272	284	315	333	350	356	356	323	310

Provisionally Revised Average Ozone Values at Belsk

Year	Jan	Feb	Mar	Apr	May	Jun	Jul	Aug	Sep	Oct	Nov	Dec
1963	370	430	410	386	395	391	347	327	295	293	288	314
1964	318	371	386	414	395	344	339	334	307	295	275	328
1965	358	407	423	413	405	367	352	335	304	289	319	354
1966	402	393	445	397	388	363	354	330	316	296	311	353
1967	380	371	401	383	356	362	338	323	296	282	280	347
1968	406	400	401	385	368	355	347	333	310	291	273	361
1969	366	415	408	417	375	375	344	345	298	291	303	353
1970	360	452	428	427	381	383	356	334	327	313	312	328
1971	352	406	415	406	379	384	333	304	334	296	298	317
1972	365	365	404	395	381	370	340	327	315	315	307	321
1973	345	399	399	438	385	374	367	333	304	311	321	335
1974	351	383	355	405	403	380	355	326	300	331	296	302
1975	340	358	387	402	367	359	346	324	294	295	303	302
1976	354	363	397	392	384	368	348	338	316	288	297	349
1977	380	427	388	408	383	376	367	337	316	287	307	316
1978	364	400	379	410	400	390	364	340	315	288	290	306
1979	386	401	427	438	395	359	366	333	300	298	294	339
1980	343	360	402	428	406	376	370	332	310	297	300	323
1981	347	376	378	392	396	356	347	329	308	316	298	340
1982	352	404	421	410	392	385	352	342	301	298	273	291
1983	309	355	371	372	355	355	337	326	293	290	281	301
1984	356	354	391	400	384	382	358	328	324	301	277	305
1985	375	399	383	382	372	371	343	307	303	283	295	323
1986	388	404	363	396	374	361	354	330	295	294	285	321

Provisionally Revised Average Ozone Values at Bismarck

Year	Jan	Feb	Mar	Apr	May	Jun	Jul	Aug	Sep	Oct	Nov	Dec
1963	387	394	406	398	382	337	321	302	282	276	311	322
1964	371	398	420	383	365	345	323	313	302	295	304	343
1965	358	383	415	379	355	334	319	302	311	288	296	352
1966	390	418	398	411	383	363	323	326	296	314	326	357
1967	373	446	385	383	387	353	338	322	287	294	323	329
1968	375	402	406	389	383	356	334	324	310	304	334	365
1969	366	397	430	365	366	361	319	299	293	303	304	353
1970	388	392	429	408	367	348	330	309	312	330	370	333
1971	373	381	407	376	373	342	328	304	308	286	304	343
1972	368	392	390	387	366	343	332	301	315	299	339	350
1973	365	369	376	404	390	352	331	314	302	306	316	339
1974	369	399	423	391	373	340	321	332	304	283	321	348
1975	377	390	402	412	378	359	319	318	312	299	312	331
1976	349	371	384	360	354	334	315	308	294	302	335	334
1977	400	380	418	376	359	348	331	324	304	309	319	372
1978	374	386	374	373	370	340	322	313	292	288	307	334
1979	376	399	403	404	391	347	334	313	299	303	333	312
1980	356	391	406	382	371	346	326	320	307	298	307	294
1981	355	392	385	390	378	353	320	317	292	304	311	360
1982	388	414	403	412	380	366	343	312	297	295	313	339
1983	338	361	393	400	385	342	311	300	310	300	302	358
1984	363	389	405	379	370	346	320	302	314	301	308	318
1985	336	371	370	354	332	345	315	322	308	306	349	355
1986	366	396	368	356	341	308	316	302	306	287	308	322

Provisionally Revised Average Ozone Values at Boulder

Year	Jan	Feb	Mar	Apr	May	Jun	Jul	Aug	Sep	Oct	Nov	Dec
1964	345	370	399	380	352	338	299	312	294	281	279	335
1965	328	346	382	350	347	325	312	302	295	278	285	313
1966	354	385	366	378	367	340	318	319	297	301	296	321
1967	324	354	335	342	353	343	311	315	295	272	283	319
1968	324	347	377	376	355	333	314	313	304	288	291	308
1969	304	352	392	362	336	346	306	310	305	296	289	312
1970	328	342	398	387	368	345	315	314	305	313	298	302
1971	329	366	359	372	365	335	322	315	310	292	295	317
1972	345	347	339	359	348	329	311	296	290	285	316	313
1973	342	318	379	390	348	332	318	305	303	286	302	308
1974	344	357	364	380	340	334	315	313	299	281	284	332
1975	328	344	365	384	364	338	310	317	305	290	288	308
1976	310	326	364	349	344	325	304	303	299	300	294	295
1977	342	361	387	364	347	324	318	305	284	278	274	298
1978	312	315	337	328	339	319	309	304	291	278	282	286
1979	347	361	369	372	358	319	314	301	289	280	305	294
1980	314	340	372	361	360	312	303	299	290	286	279	281
1981	316	341	357	335	361	315	307	301	293	287	283	298
1982	336	361	370	379	361	339	308	304	290	270	284	314
1983	302	316	370	376	364	324	306	289	285	273	277	336
1984	336	353	374	368	333	321	304	300	289	299	289	289
1985	319	335	322	336	322	313	295	293	289	272	308	295
1986	319	314	340	328	334	311	300	300	288	278	280	305

Provisionally Revised Average Ozone Values at Bracknell

Year	Jan	Feb	Mar	Apr	May	Jun	Jul	Aug	Sep	Oct	Nov	Dec
1969	365	415	413	404	409	384	360	352	313	291	306	313
1970	375	412	436	434	389	382	368	358	329	302	300	327
1971	394	391	412	397	393	384	352	341	316	296	295	318
1972	369	418	419	401	403	395	359	331	313	315	290	324
1973	338	374	379	445	399	369	364	336	308	302	282	294
1974	378	400	396	401	394	392	350	343	332	332	327	298
1975	330	374	419	401	406	375	357	338	318	304	297	299
1976	339	369	374	384	393	355	348	344	321	301	303	333
1977	365	390	396	422	414	386	363	335	295	286	306	320
1978	353	379	382	420	386	369	345	326	283	283	292	310
1979	353	381	418	435	408	372	353	346	302	304	295	332
1980	336	360	398	403	406	387	365	333	303	303	306	312
1981	310	371	393	399	405	368	361	326	317	316	287	337
1982	366	402	411	386	388	371	352	347	304	294	287	289
1983	332	340	346	417	401	358	334	331	298	287	267	309
1984	363	360	410	384	426	374	348	335	320	311	299	312
1985	360	363	384	370	381	384	341	335	292	284	308	317
1986	347	376	386	445	391	361	356	352	316	292	304	327

Provisionally Revised Average Ozone Values at Cagliari

Year	Jan	Feb	Mar	Apr	May	Jun	Jul	Aug	Sep	Oct	Nov	Dec
1957	330	326	345	360	366	333	310	301	292	284	303	309
1958	342	349	384	394	348	349	319	307	312	293	319	308
1959	340	355	363	378	371	351	321	312	304	299	298	338
1960	340	346	371	381	344	340	322	313	324	297	279	334
1961	341	328	343	345	351	347	312	303	301	286	299	306
1962	347	363	383	367	351	337	311	292	296	280	297	316
1963	348	393	380	385	386	355	327	314	303	297	292	312
1964	319	329	339	356	359	334	325	317	304	301	280	327
1965	343	385	371	394	364	346	312	315	314	299	306	312
1966	338	327	382	382	381	350	340	320	327	300	309	328
1967	354	360	347	361	347	353	314	316	306	292	297	334
1968	379	371	385	360	349	338	322	316	316	309	307	344
1969	334	356	360	374	342	358	333	332	334	315	312	351
1970	361	363	374	387	381	353	334	327	323	301	310	332
1971	348	380	401	376	364	343	314	324	309	313	323	334
1972	366	379	385	394	380	350	347	328	325	317	300	327
1973	343	382	381	368	341	340	318	320	306	295	295	323
1974	346	372	386	395	360	333	319	311	297	306	297	301
1975	307	348	370	354	362	347	318	321	287	280	294	308
1976	320	351	362	365	346	346	322	310	301	286	302	321
1977	360	371	357	373	370	345	323	325	322	299	297	303
1978	357	334	362	391	376	349	330	324	320	302	311	300
1979	350	383	380	412	378	349	323	327	323	300	306	322
1980	331	336	376	391	388	351	338	317	310	298	303	320
1981	342	359	369	374	360	337	330	320	310	298	303	331
1982	376	406	385	378	348	322	326	313	311	300	311	312
1983	309	344	351	355	340	330	321	320	309	299	298	326
1984	344	370	395	378	360	335	325	323	319	306	303	311
1985	316	322	343	340	336	317	312	315	303	292	312	322
1986	342	359	369	374	360	343	330	310	302	295	325	315

Provisionally Revised Average Ozone Values at Cairo

Year	Jan	Feb	Mar	Apr	May	Jun	Jul	Aug	Sep	Oct	Nov	Dec
1974	0	0	0	0	0	0	0	0	0	0	266	291
1975	291	294	310	314	324	316	308	297	291	276	275	294
1976	307	314	329	318	320	309	302	297	288	282	276	290
1977	318	311	320	327	329	322	302	298	290	286	271	293
1978	267	286	302	301	300	302	294	293	284	286	301	289
1979	306	298	323	321	328	316	305	302	295	280	275	296
1980	297	310	306	312	318	308	303	300	291	281	282	282
1981	318	317	339	329	335	311	304	298	289	286	292	293
1982	300	359	351	325	339	315	310	302	293	281	291	280
1983	302	300	322	319	324	305	300	298	290	282	281	289
1984	301	294	311	333	319	305	300	295	293	281	279	277
1985	250	279	291	309	316	298	298	294	288	279	284	293
1986	294	303	322	318	338	296	293	298	287	284	0	0

Provisionally Revised Average Ozone Values at Caribou

Year	Jan	Feb	Mar	Apr	May	Jun	Jul	Aug	Sep	Oct	Nov	Dec
1962	0	0	0	0	0	360	344	324	310	306	315	366
1963	413	439	428	419	411	368	345	348	316	308	326	373
1964	382	418	434	425	390	377	346	337	312	313	319	358
1965	380	399	431	420	384	361	350	335	304	318	331	378
1966	388	432	432	441	417	369	367	344	342	324	319	363
1967	388	430	435	401	409	361	347	330	314	303	334	348
1968	426	440	412	396	398	364	351	339	306	311	332	365
1969	364	415	447	430	405	360	367	334	324	321	314	361
1970	427	444	447	432	379	379	348	340	323	322	328	362
1971	395	420	421	416	371	382	348	330	309	286	311	354
1972	364	404	414	412	378	369	342	331	299	336	339	342
1973	364	415	378	395	395	357	344	326	329	307	339	340
1974	368	419	459	423	391	361	355	334	313	324	319	356
1975	369	406	410	418	387	362	339	327	316	310	321	337
1976	376	395	384	360	389	347	346	318	315	316	326	353
1977	475	396	423	441	405	392	349	324	318	315	302	362
1978	373	425	422	410	371	355	346	319	315	315	291	340
1979	376	422	409	437	378	365	353	336	313	312	323	361
1980	380	449	424	415	408	382	360	326	327	309	316	366
1981	386	374	419	427	397	382	359	331	318	318	333	337
1982	394	414	417	420	386	376	359	357	313	308	304	318
1983	344	369	383	383	381	355	345	332	304	302	312	341
1984	366	390	427	409	382	362	343	331	322	304	322	316
1985	402	405	384	402	385	370	341	333	310	312	326	373
1986	382	397	401	388	374	352	338	327	294	304	325	321

Provisionally Revised Average Ozone Values at Churchill

Year	Jan	Feb	Mar	Apr	May	Jun	Jul	Aug	Sep	Oct	Nov	Dec
1965	400	445	451	431	411	351	356	339	332	334	331	398
1966	422	464	460	449	417	380	362	341	318	347	366	388
1967	397	464	463	442	416	374	351	334	301	334	343	369
1968	433	440	438	456	412	382	379	355	315	336	370	398
1969	417	425	482	443	455	420	366	331	309	325	329	389
1970	430	503	469	470	443	367	362	350	334	346	356	365
1971	410	456	465	447	419	389	373	331	317	333	351	374
1972	406	469	473	452	419	376	378	341	366	339	371	398
1973	401	484	436	448	405	383	364	334	329	333	328	354
1974	379	443	518	459	420	388	365	343	331	329	363	391
1975	411	438	479	454	407	378	353	372	317	330	337	362
1976	351	432	459	412	404	359	345	314	320	320	349	368
1977	390	428	486	453	382	389	375	370	322	326	366	370
1978	380	403	493	452	411	394	365	346	303	318	322	349
1979	404	466	464	444	420	396	357	355	319	330	378	370
1980	403	436	494	412	397	392	367	336	338	316	358	345
1981	360	442	457	475	426	392	351	318	310	303	360	400
1982	416	444	460	472	408	402	367	339	311	310	355	356
1983	379	420	438	422	437	359	340	322	327	319	356	390
1984	396	451	454	410	420	371	358	314	330	306	370	361
1985	380	434	448	436	407	373	359	334	316	332	342	327
1986	404	428	454	430	391	393	360	345	327	318	331	344

Provisionally Revised Average Ozone Values at Edmonton

Year	Jan	Feb	Mar	Apr	May	Jun	Jul	Aug	Sep	Oct	Nov	Dec
1957	0	0	0	0	0	0	326	305	278	283	294	317
1958	319	407	431	425	365	350	334	296	315	296	354	357
1959	384	419	436	422	399	360	334	335	312	309	306	376
1960	377	442	422	400	399	379	322	328	301	296	341	329
1961	366	413	407	430	386	332	325	297	310	309	322	338
1962	325	452	432	400	371	355	331	308	292	282	301	305
1963	346	383	418	387	402	365	343	312	277	301	323	306
1964	387	409	448	404	388	360	330	321	320	294	310	359
1965	374	415	415	388	388	362	328	302	313	300	302	392
1966	403	426	430	417	381	386	350	329	293	320	344	366
1967	405	403	433	394	374	352	327	301	280	309	323	316
1968	376	377	405	410	382	368	342	333	309	318	336	376
1969	414	412	417	379	382	344	344	310	297	295	312	375
1970	423	406	442	422	387	334	333	316	316	312	331	351
1971	397	389	423	398	368	366	336	290	303	305	322	360
1972	397	412	402	405	371	345	357	301	335	297	359	384
1973	391	415	402	406	376	364	344	318	292	311	330	340
1974	386	423	460	401	396	354	340	311	277	289	361	379
1975	392	396	419	417	400	374	324	315	290	319	319	358
1976	337	408	415	372	374	367	336	304	277	289	319	354
1977	363	380	451	404	393	362	361	333	318	309	350	359
1978	366	375	388	388	381	352	337	323	299	285	299	335
1979	374	433	394	415	402	376	342	317	295	306	336	336
1980	375	397	443	377	373	369	349	339	306	297	328	309
1981	339	397	393	418	382	390	347	304	294	294	327	378
1982	398	428	410	437	391	360	352	324	291	294	323	364
1983	347	380	407	380	376	354	336	306	313	290	335	376
1984	364	409	393	393	387	361	334	309	319	305	351	361
1985	319	390	399	381	358	361	330	322	310	320	342	303
1986	373	405	400	394	353	344	348	309	314	280	321	0

Provisionally Revised Average Ozone Values at Goose Bay

Year	Jan	Feb	Mar	Apr	May	Jun	Jul	Aug	Sep	Oct	Nov	Dec
1962	326	305	278	283	294	317	319	407	431	425	365	350
1963	334	296	315	296	354	357	384	419	436	422	399	360
1964	334	335	312	309	306	376	377	442	422	400	399	379
1965	322	328	301	296	341	329	366	413	407	430	386	332
1966	325	297	310	309	322	338	325	452	432	400	371	355
1967	331	308	292	282	301	305	346	383	418	387	402	365
1968	343	312	277	301	323	306	387	409	448	404	388	360
1969	330	321	320	294	310	359	374	415	415	388	388	362
1970	328	302	313	300	302	392	403	426	430	417	381	386
1971	350	329	293	320	344	366	405	403	433	394	374	352
1972	327	301	280	309	323	316	376	377	405	410	382	368
1973	342	333	309	318	336	376	414	412	417	379	382	344
1974	344	310	297	295	312	375	423	406	442	422	387	334
1975	333	316	316	312	331	351	397	389	423	398	368	366
1976	336	290	303	305	322	360	397	412	402	405	371	345
1977	357	301	335	297	359	384	391	415	402	406	376	364
1978	344	318	292	311	330	340	386	423	460	401	396	354
1979	340	311	277	289	361	379	392	396	419	417	400	374
1980	324	315	290	319	319	358	337	408	415	372	374	367
1981	336	304	277	289	319	354	363	380	451	404	393	362
1982	361	333	318	309	350	359	366	375	388	388	381	352
1983	337	323	299	285	299	335	374	433	394	415	402	376
1984	342	317	295	306	336	336	375	397	443	377	373	369
1985	349	339	306	297	328	309	339	397	393	418	382	390
1986	347	304	294	294	327	378	398	428	410	437	391	0

Provisionally Revised Average Ozone Values at Hohenpeissenberg

Year	Jan	Feb	Mar	Apr	May	Jun	Jul	Aug	Sep	Oct	Nov	Dec
1967	360	364	360	372	345	347	326	320	296	274	269	310
1968	350	390	392	380	362	358	342	334	312	277	275	337
1969	337	412	373	400	356	365	331	332	293	282	306	341
1970	330	426	415	426	385	359	339	327	297	287	291	323
1971	356	373	407	374	359	359	329	308	309	263	288	294
1972	343	369	384	374	371	354	334	311	320	297	298	311
1973	329	389	378	459	355	344	343	317	292	292	276	308
1974	341	383	335	382	371	361	324	311	295	330	295	288
1975	310	342	376	371	360	353	324	319	287	279	302	292
1976	363	360	358	381	357	341	326	328	308	279	292	317
1977	374	403	364	383	378	361	343	329	310	278	294	308
1978	356	395	363	405	388	370	341	318	283	269	272	283
1979	363	376	378	406	373	345	339	317	289	283	286	316
1980	346	340	379	391	389	362	341	309	289	278	281	311
1981	337	374	362	372	368	337	330	313	297	297	281	329
1982	348	385	404	373	369	356	328	321	284	284	273	293
1983	298	339	340	355	343	339	319	319	291	273	271	310
1984	349	370	396	395	387	361	337	325	311	290	279	304
1985	361	359	369	360	354	350	325	309	286	281	300	295
1986	360	361	369	380	357	347	337	320	296	289	299	314

Provisionally Revised Average Ozone Values at Hradec Kralove

Year	Jan	Feb	Mar	Apr	May	Jun	Jul	Aug	Sep	Oct	Nov	Dec
1962	389	399	446	377	369	342	326	308	294	266	316	342
1963	384	431	404	395	386	377	330	311	293	295	299	318
1964	333	374	374	399	377	331	318	310	289	282	288	315
1965	373	413	414	399	375	347	336	324	303	283	311	330
1966	392	383	420	398	382	360	347	315	313	296	324	338
1967	404	401	411	364	348	349	327	316	293	282	289	347
1968	441	414	411	390	351	350	330	330	305	296	283	395
1969	410	464	411	428	375	373	338	338	297	291	319	358
1970	345	436	438	427	396	372	345	327	310	296	299	322
1971	356	392	413	389	374	363	336	314	320	287	292	295
1972	368	374	395	380	382	362	334	314	318	309	302	315
1973	352	441	391	448	382	364	354	328	293	301	314	329
1974	359	386	359	400	396	382	345	327	299	337	309	313
1975	330	351	397	395	365	360	344	326	298	300	317	309
1976	362	369	392	386	378	355	345	337	323	292	303	331
1977	390	411	383	406	378	369	356	336	312	287	307	317
1978	373	393	379	409	396	377	356	331	310	288	295	309
1979	385	389	412	423	384	386	330	299	294	290	331	289
1980	347	350	392	422	397	375	370	330	299	292	296	334
1981	366	391	370	388	395	349	353	332	306	304	306	344
1982	362	396	412	398	379	370	343	333	296	295	279	298
1983	312	359	357	375	359	352	330	328	301	279	285	319
1984	365	371	388	401	380	373	350	328	316	297	283	306
1985	373	391	376	373	365	366	330	308	296	280	307	318
1986	371	400	362	386	364	350	341	323	290	293	303	333

Provisionally Revised Average Ozone Values at Huancayo

Year	Jan	Feb	Mar	Apr	May	Jun	Jul	Aug	Sep	Oct	Nov	Dec
1964	0	261	257	253	252	248	248	253	264	261	259	259
1965	259	260	254	253	257	254	256	262	264	269	263	257
1966	253	249	256	252	249	253	259	267	268	264	260	261
1967	256	260	264	259	252	255	253	264	265	261	260	257
1968	252	256	259	253	251	253	254	258	267	263	256	260
1969	258	258	257	246	249	250	257	260	264	267	266	264
1970	255	255	255	252	252	254	259	264	266	270	263	267
1971	261	265	262	261	250	255	261	264	264	258	262	263
1972	260	259	259	254	259	255	255	258	259	258	257	255
1973	258	253	261	253	250	250	256	262	259	272	261	259
1974	259	260	246	246	258	259	260	262	267	268	263	261
1975	260	260	259	253	249	254	261	256	264	261	263	262
1976	261	266	262	257	258	262	260	265	270	267	265	259
1977	247	251	249	246	248	248	247	255	258	260	257	259
1978	258	257	257	251	256	259	259	262	262	263	264	255
1979	253	252	252	254	256	258	261	262	259	258	263	259
1980	259	255	252	246	247	252	252	259	265	261	260	258
1981	258	258	256	258	253	259	256	263	266	269	267	261
1982	253	257	259	251	253	251	257	261	260	271	262	254
1983	256	258	254	253	251	251	259	261	265	265	260	260
1984	259	258	250	252	249	242	248	255	259	259	258	254
1985	252	252	250	249	252	253	256	258	262	264	260	256
1986	255	252	252	244	246	250	0	0	0	0	0	0

Provisionally Revised Average Ozone Values at Kagoshima

Year	Jan	Feb	Mar	Apr	May	Jun	Jul	Aug	Sep	Oct	Nov	Dec
1961	0	0	0	307	299	283	274	267	260	260	267	278
1962	321	325	330	315	317	305	281	288	274	295	275	283
1963	320	318	336	338	320	314	296	275	264	289	252	268
1964	278	288	305	309	316	320	283	268	260	255	260	270
1965	301	300	331	324	333	317	283	290	286	284	264	273
1966	283	286	302	312	328	328	290	283	277	272	247	274
1967	272	283	308	306	315	304	276	273	278	264	256	294
1968	275	299	331	324	313	318	288	273	271	256	249	244
1969	265	268	307	308	315	315	288	281	267	269	262	260
1970	326	305	320	343	336	321	306	295	275	274	261	269
1971	283	276	315	314	331	305	295	287	282	275	259	275
1972	279	302	319	328	320	310	292	285	290	273	272	269
1973	296	283	306	315	324	329	305	291	288	281	282	307
1974	291	297	318	320	329	323	297	296	285	263	258	250
1975	284	302	314	326	328	331	296	287	281	264	274	276
1976	285	299	304	319	320	315	301	283	298	286	277	279
1977	281	294	304	324	321	321	293	287	274	271	261	254
1978	263	292	303	308	315	298	286	276	269	263	260	322
1979	292	322	323	332	341	328	297	290	291	273	268	275
1980	289	289	304	322	328	320	299	297	288	272	263	288
1981	295	302	327	339	329	311	301	295	285	273	267	281
1982	300	306	318	344	329	336	309	301	291	279	271	264
1983	274	301	318	305	332	323	300	290	278	271	276	292
1984	298	297	335	351	330	310	297	291	288	282	260	252
1985	269	272	274	310	316	310	293	283	274	272	272	276
1986	294	318	319	318	315	311	280	284	277	281	257	260

Provisionally Revised Average Ozone Values at Leningrad

Year	Jan	Feb	Mar	Apr	May	Jun	Jul	Aug	Sep	Oct	Nov	Dec
1968	0	0	0	0	0	0	0	322	298	293	288	323
1969	363	471	433	440	397	386	345	319	316	304	301	343
1970	343	426	447	427	394	378	361	320	331	314	315	333
1971	366	428	434	432	389	372	346	327	319	309	319	330
1972	349	378	425	421	399	367	321	311	303	316	305	343
1973	339	463	431	440	382	366	352	337	317	322	314	364
1974	356	384	350	416	405	368	333	332	312	320	324	369
1975	406	402	409	425	375	360	344	320	302	285	293	309
1976	393	351	429	449	401	384	344	326	306	299	289	338
1977	396	434	430	433	396	375	365	337	320	302	316	341
1978	362	394	393	427	388	368	355	334	321	305	316	340
1979	374	396	441	443	388	363	362	320	305	292	292	328
1980	358	366	408	419	421	375	356	340	313	310	314	339
1981	336	404	404	421	380	354	335	330	300	320	303	333
1982	347	416	414	405	401	390	347	351	321	302	286	300
1983	337	377	397	398	367	364	334	323	310	306	312	318
1984	360	372	400	404	374	376	355	322	315	318	296	315
1985	369	426	393	407	379	363	352	312	317	280	305	328

Provisionally Revised Average Ozone Values at Lerwick

Year	Jan	Feb	Mar	Apr	May	Jun	Jul	Aug	Sep	Oct	Nov	Dec
1957	330	430	395	375	400	363	344	322	308	278	280	300
1958	320	405	417	396	405	346	338	323	291	291	265	315
1959	330	341	411	418	368	352	326	303	283	281	300	305
1960	340	413	420	394	384	369	362	339	291	274	290	315
1961	350	390	376	414	388	369	355	328	294	300	274	280
1962	343	331	426	408	385	366	354	339	298	267	274	305
1963	328	407	416	428	414	377	358	348	318	287	290	284
1964	297	341	387	434	398	377	364	344	308	292	270	301
1965	327	326	392	416	405	372	357	338	314	285	300	335
1966	360	402	442	429	428	360	355	332	312	308	287	305
1967	345	365	410	405	395	365	350	337	322	292	280	330
1968	375	380	422	415	424	378	358	343	315	290	280	330
1969	355	413	402	438	416	388	364	329	319	288	304	320
1970	340	430	459	445	403	371	365	335	337	302	300	315
1971	365	409	408	407	402	381	349	335	308	295	280	320
1972	350	415	436	412	405	390	338	331	297	308	287	315
1973	325	381	379	447	401	380	351	332	306	298	280	310
1974	345	350	379	391	391	368	362	340	334	320	297	315
1975	345	360	409	439	400	379	359	326	323	309	300	305
1976	320	365	402	385	406	361	341	317	305	309	279	310
1977	350	394	434	451	411	396	369	340	331	299	295	305
1978	335	382	410	429	405	373	365	332	298	306	301	315
1979	330	385	445	442	440	364	371	341	315	296	317	325
1980	325	345	396	403	395	385	365	331	317	327	285	305
1981	320	380	410	422	396	371	357	325	310	303	277	315
1982	360	412	415	411	410	383	345	354	330	305	285	275
1983	290	303	381	415	380	352	335	313	311	300	290	310
1984	346	351	402	397	396	377	348	314	312	320	300	310
1985	320	366	380	400	380	384	357	341	310	284	282	300
1986	325	351	397	420	381	360	341	333	308	318	325	0

Provisionally Revised Average Ozone Values at MacQuarie Isle

Year	Jan	Feb	Mar	Apr	May	Jun	Jul	Aug	Sep	Oct	Nov	Dec
1963	320	300	294	326	326	340	334	354	380	370	384	358
1964	328	299	323	321	330	330	337	384	413	415	391	322
1965	295	297	302	296	316	347	360	350	402	423	360	325
1966	331	295	279	324	329	344	329	326	322	344	359	327
1967	310	304	295	302	318	319	334	345	408	414	385	334
1968	315	308	298	316	322	325	330	344	422	443	394	332
1969	314	283	305	331	338	354	358	366	381	381	339	325
1970	286	309	290	319	318	322	370	374	445	428	352	329
1971	285	275	296	300	318	340	339	325	393	397	346	318
1972	309	271	287	314	327	343	363	382	421	410	364	356
1973	324	303	315	309	357	343	330	332	379	388	370	324
1974	294	277	277	276	313	313	338	391	360	393	356	329
1975	305	310	282	307	358	354	358	385	399	370	339	331
1976	304	289	282	294	347	348	350	325	337	402	360	326
1977	308	297	281	314	333	369	380	358	372	410	368	324
1978	312	280	282	279	327	336	368	383	379	412	394	336
1979	350	326	308	312	316	326	359	379	405	425	389	367
1980	336	320	326	304	337	339	353	366	405	406	389	339
1981	335	318	299	328	318	319	335	374	432	435	370	325
1982	320	303	293	303	327	316	329	371	378	406	359	327
1983	311	284	309	319	332	332	340	345	366	401	352	315
1984	281	285	270	307	317	368	364	361	390	403	389	336
1985	316	311	304	308	306	328	314	327	366	377	366	315
1986	294	287	292	316	324	369	357	383	411	403	390	331

Provisionally Revised Average Ozone Values at Mauna Loa

Year	Jan	Feb	Mar	Apr	May	Jun	Jul	Aug	Sep	Oct	Nov	Dec
1964	241	258	261	276	283	273	271	263	261	252	253	250
1965	259	278	278	286	284	280	269	267	265	262	246	243
1966	242	241	254	277	276	275	272	274	267	259	257	248
1967	260	270	274	300	289	278	267	274	268	262	267	263
1968	259	252	277	294	285	285	280	271	269	257	239	239
1969	240	252	263	278	287	285	277	278	273	267	263	257
1970	244	248	284	295	296	289	280	280	273	260	256	247
1971	243	255	263	284	288	284	281	281	274	266	265	272
1972	263	267	271	297	302	281	275	266	272	264	255	241
1973	240	241	275	278	289	283	280	274	269	266	268	264
1974	262	287	292	296	306	296	285	275	270	269	260	240
1975	240	259	267	279	289	286	286	278	274	270	262	266
1976	265	267	292	290	296	284	274	275	271	266	260	251
1977	245	251	276	296	298	298	279	272	259	251	238	233
1978	238	235	256	283	286	270	275	269	265	256	259	259
1979	260	260	282	300	298	287	279	274	269	257	257	241
1980	239	236	259	267	287	275	277	276	267	267	257	253
1981	244	256	274	296	289	281	277	277	278	271	259	258
1982	263	257	295	297	292	280	271	268	261	249	244	237
1983	225	236	248	280	279	282	271	269	263	261	255	254
1984	249	272	263	299	290	278	278	274	270	258	243	246
1985	230	234	252	276	284	280	267	266	266	256	260	250
1986	242	261	270	292	282	278	267	258	259	260	247	249

Provisionally Revised Average Ozone Values at Nashville

Year	Jan	Feb	Mar	Apr	May	Jun	Jul	Aug	Sep	Oct	Nov	Dec
1963	342	348	360	351	353	344	331	323	306	285	294	317
1964	324	360	343	332	335	331	333	312	300	309	293	309
1965	322	330	366	330	337	333	327	319	291	295	297	303
1966	337	356	365	370	363	352	331	327	314	297	301	312
1967	320	363	326	323	358	332	338	322	313	288	297	297
1968	336	380	366	342	363	339	342	334	314	300	292	309
1969	320	348	372	361	364	339	335	335	316	291	317	319
1970	342	357	393	361	361	343	359	349	309	311	316	292
1971	328	311	354	405	365	345	332	315	306	289	279	277
1972	305	339	355	344	365	345	330	331	304	302	298	293
1973	324	347	326	361	358	331	330	326	302	302	299	312
1974	316	348	345	353	344	356	339	326	304	310	291	308
1975	306	325	341	339	344	336	336	318	297	285	291	299
1976	324	309	328	319	339	337	325	312	303	302	306	302
1977	355	359	319	357	352	334	334	313	302	302	277	294
1978	314	329	322	331	351	331	316	312	293	286	274	286
1979	335	338	371	374	368	331	325	314	305	302	287	301
1980	316	360	343	372	355	335	320	313	303	306	286	313
1981	323	344	346	329	356	322	324	321	303	287	288	318
1982	318	339	357	365	347	338	325	321	315	289	273	293
1983	315	324	343	366	343	336	315	312	302	294	280	309
1984	325	352	371	374	349	328	328	314	296	280	296	268
1985	321	317	300	327	340	326	325	311	295	280	285	315
1986	332	331	337	340	339	320	314	310	287	295	304	302

Provisionally Revised Average Ozone Values at Quetta

Year	Jan	Feb	Mar	Apr	May	Jun	Jul	Aug	Sep	Oct	Nov	Dec
1969	0	0	0	0	0	0	0	288	286	289	281	285
1970	300	295	293	305	289	297	296	293	291	273	271	279
1971	285	287	290	295	298	283	270	279	289	280	281	282
1972	280	317	311	313	310	295	276	287	293	289	277	286
1973	291	308	314	289	287	283	281	284	278	282	280	289
1974	314	319	310	299	300	297	290	292	285	281	281	285
1975	296	299	316	313	286	292	286	280	267	264	271	260
1976	286	298	318	318	292	294	278	276	272	265	266	285
1977	304	297	308	320	312	297	283	279	276	267	277	283
1978	287	298	322	305	294	283	276	273	278	271	274	276
1979	308	309	318	300	310	294	291	290	288	273	270	278
1980	280	292	314	295	303	292	288	289	279	275	269	275
1981	290	289	303	304	292	295	289	284	278	276	280	289
1982	299	333	324	309	308	299	301	294	291	280	269	279
1983	280	289	283	304	297	288	289	285	274	265	264	276
1984	303	325	303	300	296	290	289	285	285	268	257	273
1985	267	258	263	273	289	282	281	280	276	276	281	279
1986	294	299	319	305	300	286	285	282	287	289	289	299

Provisionally Revised Average Ozone Values at Reykjavik

Year	Jan	Feb	Mar	Apr	May	Jun	Jul	Aug	Sep	Oct	Nov	Dec
1975	0	0	0	0	0	0	0	0	0	0	0	290
1976	309	343	384	400	380	345	310	300	290	286	250	270
1977	348	375	390	385	375	356	340	330	311	301	324	336
1978	316	361	435	392	406	368	335	307	293	293	295	320
1979	340	408	457	432	423	360	350	341	330	293	313	350
1980	330	373	411	430	413	376	363	336	320	292	294	300
1981	320	409	462	392	394	375	352	333	297	288	278	320
1982	330	450	417	424	410	382	359	347	343	307	299	260
1983	285	301	406	397	375	364	342	328	298	292	286	298
1984	326	346	404	423	390	372	348	322	306	298	298	315
1985	333	367	380	384	382	368	360	334	317	279	286	270
1986	290	314	414	396	392	357	341	325	295	305	0	0

Provisionally Revised Average Ozone Values at Rome

Year	Jan	Feb	Mar	Apr	May	Jun	Jul	Aug	Sep	Oct	Nov	Dec
1957	333	322	350	362	366	332	318	304	296	286	297	325
1958	358	365	405	410	352	351	325	307	302	293	310	327
1959	365	368	365	376	377	356	313	317	314	305	308	345
1960	352	390	401	414	373	345	333	314	320	307	296	346
1961	359	345	345	370	373	358	329	315	303	291	309	319
1962	354	379	409	384	357	347	320	296	297	279	303	329
1963	371	423	392	401	391	355	323	309	295	291	291	305
1964	323	344	354	378	364	327	319	309	301	305	287	332
1965	345	409	389	406	387	347	324	318	309	291	309	322
1966	369	338	413	383	369	349	343	315	311	291	320	326
1967	361	352	358	365	342	350	319	307	299	281	282	330
1968	387	381	400	374	350	348	327	331	318	299	298	346
1969	350	386	384	385	345	343	338	329	310	289	312	365
1970	361	385	408	417	392	350	332	318	307	299	297	320
1971	348	375	413	382	375	358	339	312	323	294	313	318
1972	358	368	384	381	375	353	346	327	323	311	304	331
1973	350	406	384	401	349	357	335	330	308	302	295	339
1974	354	388	368	409	376	350	325	315	303	320	309	311
1975	321	353	384	374	365	361	325	326	296	299	305	308
1976	334	361	372	383	356	361	334	327	314	289	301	324
1977	362	380	361	382	370	358	338	330	322	298	297	302
1978	355	349	365	400	382	354	337	328	305	290	298	288
1979	366	382	385	413	370	362	335	329	317	299	304	319
1980	347	336	377	399	390	359	341	317	309	317	299	316
1981	363	383	373	392	378	356	343	325	310	297	309	337
1982	347	389	394	381	370	354	326	325	306	306	294	321
1983	310	362	359	361	342	352	321	325	306	293	292	321
1984	359	398	407	396	379	359	327	333	319	294	292	317
1985	342	345	369	352	360	334	322	321	303	292	309	324
1986	353	373	379	386	366	350	333	309	300	294	304	319

Average ozone values at Samoa

Year	Jan	Feb	Mar	Apr	May	Jun	Jul	Aug	Sep	Oct	Nov	Dec
1976	264	262	261	255	261	267	263	268	264	276	269	263
1977	255	253	251	252	252	252	253	252	245	252	261	262
1978	256	260	260	257	259	265	267	263	269	266	261	264
1979	255	255	253	257	259	262	260	260	267	269	260	263
1980	259	254	244	243	247	245	241	255	258	261	258	256
1981	250	250	255	250	258	259	259	253	261	260	264	260
1982	252	252	253	250	245	245	244	246	253	253	257	264
1983	256	250	251	255	252	257	256	256	258	264	264	253
1984	246	246	243	245	250	254	252	252	256	258	262	264
1985	255	254	249	251	253	235	245	251	260	266	264	259
1986	246	247	249	246	250	253	253	254	261	269	250	246

Provisionally Revised Average Ozone Values at Sapporo

Year	Jan	Feb	Mar	Apr	May	Jun	Jul	Aug	Sep	Oct	Nov	Dec
1958	410	427	467	420	408	376	324	309	292	319	326	390
1959	446	427	422	413	391	382	345	312	314	316	350	384
1960	441	460	441	414	397	376	331	288	299	288	325	367
1961	415	435	441	410	379	369	331	320	311	289	325	391
1962	429	449	454	390	388	342	311	287	290	296	323	371
1963	453	445	441	398	391	350	333	315	330	297	324	365
1964	398	442	436	383	390	366	325	291	312	315	339	366
1965	407	440	456	425	397	368	339	299	303	307	328	391
1966	448	433	447	429	401	386	347	297	309	325	336	410
1967	431	432	427	406	371	370	325	306	297	312	333	404
1968	435	471	463	401	406	374	344	315	312	318	325	354
1969	410	427	440	403	412	365	332	316	310	325	335	402
1970	431	449	496	426	390	374	330	310	301	317	338	392
1971	404	459	438	410	396	381	333	310	307	329	336	372
1972	381	416	415	406	386	370	327	305	306	312	351	378
1973	400	438	472	407	399	378	320	301	315	326	361	403
1974	437	414	437	405	408	356	338	302	295	313	347	371
1975	410	449	428	431	396	370	327	300	303	321	337	383
1976	408	411	406	420	376	349	317	315	301	306	335	382
1977	429	469	436	421	398	373	318	311	303	301	316	368
1978	413	444	438	434	390	344	305	298	309	313	327	386
1979	422	418	455	429	426	367	347	315	314	298	328	365
1980	423	464	437	430	401	370	349	330	310	313	338	403
1981	433	445	442	418	392	389	332	318	321	320	354	387
1982	442	466	439	419	403	380	357	304	312	317	335	355
1983	387	428	408	382	391	386	344	298	305	330	337	400
1984	438	463	470	428	408	364	323	297	312	317	332	380
1985	415	410	408	387	392	381	323	291	315	317	349	393
1986	437	456	419	421	397	364	335	296	304	325	355	362

Provisionally Revised Average Ozone Values at Srinigar

Year	Jan	Feb	Mar	Apr	May	Jun	Jul	Aug	Sep	Oct	Nov	Dec
1964	0	342	313	297	320	304	298	281	279	260	271	281
1965	301	322	325	304	306	299	287	283	280	270	272	276
1966	303	290	293	304	302	298	281	270	269	292	291	298
1967	307	299	317	321	313	294	284	286	275	281	290	303
1968	334	335	331	316	315	303	298	296	285	276	275	299
1969	306	296	288	309	297	290	280	274	284	288	287	291
1970	306	323	321	304	311	302	297	284	281	266	275	286
1971	301	307	297	292	302	290	292	285	283	272	276	280
1972	296	322	315	323	314	297	296	277	284	288	268	286
1973	310	302	305	291	301	290	284	278	276	276	285	295
1974	318	318	308	296	308	299	291	283	280	276	278	291
1975	306	317	319	326	320	308	296	283	276	272	285	285
1976	276	302	305	298	297	286	283	281	276	273	270	293
1977	314	319	300	313	322	310	286	281	283	277	269	298
1978	309	322	333	306	287	284	278	277	282	276	278	292
1979	325	363	345	296	315	297	287	280	289	277	269	305
1980	308	318	338	298	302	295	284	285	279	276	278	300
1981	309	313	337	316	299	301	286	279	278	275	281	311
1982	291	344	318	315	323	302	293	278	288	281	275	288
1983	292	303	311	316	309	306	295	280	276	277	282	296
1984	329	333	308	316	302	286	278	272	278	276	278	291
1985	288	287	285	291	302	286	275	269	271	269	284	277
1986	311	326	340	312	312	0	0	0	0	0	0	0

Provisionally Revised Average Ozone Values at Tateno

Year	Jan	Feb	Mar	Apr	May	Jun	Jul	Aug	Sep	Oct	Nov	Dec
1957	0	0	0	0	0	0	300	281	285	271	273	309
1958	320	335	385	357	351	339	308	294	279	281	274	309
1959	324	338	356	353	372	364	316	305	293	282	281	307
1960	343	376	389	378	371	347	321	297	290	275	292	290
1961	313	369	355	359	330	330	302	294	280	274	294	330
1962	378	379	399	386	362	341	322	295	287	285	288	339
1963	387	401	408	367	360	330	319	298	295	267	287	301
1964	325	350	373	344	359	347	307	282	279	274	287	300
1965	334	352	382	372	357	340	315	300	285	284	276	311
1966	345	346	358	348	356	350	316	298	287	290	276	318
1967	340	338	348	339	341	333	306	290	276	272	273	323
1968	337	378	397	360	367	353	330	302	291	285	276	291
1969	311	313	368	353	351	339	323	299	289	292	285	300
1970	352	349	376	370	355	341	323	301	289	283	282	310
1971	342	348	359	342	353	334	313	293	288	289	280	304
1972	315	349	369	358	340	338	306	294	297	278	293	306
1973	332	331	364	329	355	358	310	290	291	286	299	335
1974	355	353	375	345	344	338	317	291	292	275	279	281
1975	326	365	365	363	353	345	312	295	288	286	286	306
1976	309	331	327	337	337	322	309	295	288	280	279	303
1977	321	363	352	359	366	343	318	297	283	280	268	296
1978	317	350	371	358	340	313	301	290	286	280	283	328
1979	344	359	372	358	366	333	323	304	295	269	282	300
1980	326	346	349	347	350	327	318	304	285	270	287	332
1981	350	351	361	372	347	347	320	306	296	282	291	317
1982	354	368	365	379	346	350	333	307	298	281	280	289
1983	315	348	349	322	350	345	327	299	294	284	292	324
1984	350	368	397	373	362	335	306	295	292	279	277	292
1985	309	330	302	339	338	333	306	287	283	279	289	305
1986	341	387	374	363	349	341	310	291	286	295	280	297

Provisionally Revised Average Ozone Values at Toronto

Year	Jan	Feb	Mar	Apr	May	Jun	Jul	Aug	Sep	Oct	Nov	Dec
1960	393	428	477	401	390	369	351	328	313	310	320	371
1961	402	386	386	445	404	353	344	329	296	311	310	340
1962	372	429	453	437	369	360	354	334	328	315	315	365
1963	418	404	411	413	400	375	367	357	320	307	325	369
1964	372	399	429	392	365	354	343	333	309	317	308	341
1965	378	383	415	409	369	357	351	336	306	311	322	351
1966	386	417	424	422	421	368	353	340	340	330	319	358
1967	362	415	395	373	399	345	346	340	322	295	323	319
1968	381	430	397	371	403	359	346	328	309	305	323	364
1969	350	402	439	402	394	364	337	330	319	316	326	365
1970	416	417	418	394	365	353	350	331	312	308	327	333
1971	417	392	430	420	382	353	351	333	307	279	312	325
1972	356	406	426	392	430	372	348	333	303	322	339	333
1973	356	394	381	411	400	353	353	336	313	307	318	338
1974	358	417	414	402	388	376	347	340	321	316	331	363
1975	368	403	411	409	390	366	347	337	329	306	320	351
1976	382	368	386	384	402	358	353	335	330	324	350	350
1977	452	420	410	402	387	381	359	328	321	311	314	360
1978	366	394	403	383	375	360	335	322	308	310	295	325
1979	380	413	402	423	389	367	352	337	317	322	312	334
1980	361	432	406	412	373	377	340	327	323	317	319	346
1981	378	399	429	395	402	370	342	340	324	323	324	336
1982	379	391	408	412	374	378	344	336	326	291	305	325
1983	361	367	386	382	376	354	327	325	313	300	315	345
1984	378	385	429	416	402	350	338	329	316	293	321	300
1985	399	399	362	377	361	359	342	329	304	288	311	360

Provisionally Revised Average Ozone Values at Uccle

Year	Jan	Feb	Mar	Apr	May	Jun	Jul	Aug	Sep	Oct	Nov	Dec
1971	0	412	431	424	416	406	375	352	333	302	324	320
1972	376	397	418	414	411	385	355	344	338	315	306	321
1973	361	410	388	442	407	373	376	345	315	319	319	311
1974	374	386	378	404	395	384	354	335	314	348	335	301
1975	325	350	405	406	387	372	344	328	314	300	310	291
1976	357	354	376	392	372	354	341	340	327	291	289	335
1977	368	415	399	411	403	381	356	346	312	285	313	336
1978	373	387	378	419	395	380	369	349	291	291	290	310
1979	359	392	327	450	403	377	356	328	301	297	300	334
1980	340	353	393	415	416	386	363	324	320	307	297	327
1981	350	380	391	405	392	365	359	326	314	320	280	344
1982	370	402	433	393	389	376	351	348	302	301	275	288
1983	300	351	355	396	396	352	336	332	301	286	268	304
1984	362	350	403	391	421	380	350	336	319	308	289	312
1985	364	355	386	371	375	383	338	328	293	284	316	331
1986	378	396	388	427	371	349	343	337	286	292	307	316

Provisionally Revised Average Ozone Values at Wallops Is.

Year	Jan	Feb	Mar	Apr	May	Jun	Jul	Aug	Sep	Oct	Nov	Dec
1970	338	365	406	366	354	353	333	320	300	293	301	300
1971	328	325	360	383	358	341	319	315	302	277	293	293
1972	322	358	369	357	383	358	331	315	309	307	304	293
1973	321	360	341	363	366	329	332	324	302	298	296	308
1974	309	359	366	361	351	343	336	312	295	306	282	307
1975	306	323	349	368	353	343	328	319	301	289	293	307
1976	338	313	329	344	352	338	332	323	311	309	311	313
1977	395	386	345	371	387	363	336	319	309	304	287	308
1978	330	338	341	338	354	331	323	308	300	294	277	295
1979	350	355	370	374	347	341	323	314	290	295	284	305
1980	317	373	353	370	363	358	330	322	303	304	286	321
1981	341	350	375	351	370	324	328	321	307	296	305	322
1982	346	332	361	378	377	341	337	328	310	287	272	283
1983	324	329	353	370	350	340	327	315	303	299	286	290
1984	337	350	367	369	361	343	327	318	302	281	291	277
1985	328	323	316	333	336	335	325	315	304	282	288	321
1986	347	349	348	386	356	331	325	316	295	295	308	295

A. (ii) Latitudinal band averages prepared from provisionally revised data (Bojkov, private communication, 1987)

60°–80° North
53°–64° North
40°–52° North
30°–39° North

and M–83 regional averages (USSR), prepared by Bojkov (1988a)

European part
South Central Asia
Siberia
Far Eastern Asia

N.B. The latitudinal band averages are made up from the provisionally revised Dobson instrument records only, with the exception of the band between 30° and 39°N, which contains one M–83 filter instrument record.

Average Monthly Ozone Values for 60°N–80°N, Derived From the Provisionally Revised Data Sets; Dobson Only

Year	Jan	Feb	Mar	Apr	May	Jun	Jul	Aug	Sep	Oct	Nov	Dec
1957	346	456	411	397	403	377	333	318	309	297	289	310
1958	356	454	464	438	411	366	346	324	305	303	292	345
1959	376	383	441	448	400	371	332	318	299	292	300	289
1960	373	445	420	416	391	367	343	319	293	273	276	303
1961	351	392	443	425	390	361	338	318	287	288	292	296
1962	349	357	420	407	390	362	338	319	299	277	274	309
1963	350	430	444	434	406	371	347	324	314	294	295	295
1964	305	344	415	448	402	367	349	332	303	277	286	314
1965	351	372	415	425	408	361	343	323	305	292	292	355
1966	385	417	459	451	409	364	353	328	305	307	305	323
1967	358	394	417	409	392	360	346	320	302	299	295	322
1968	384	403	431	433	423	373	353	333	307	300	307	341
1969	368	422	443	444	414	388	354	322	311	301	313	336
1970	369	452	454	452	416	368	355	330	325	309	315	332
1971	377	424	442	431	396	367	345	323	310	311	312	333
1972	361	407	444	427	401	372	337	320	310	313	315	346
1973	349	435	438	449	391	362	339	318	311	315	303	338
1974	355	385	431	429	399	368	340	318	315	320	323	352
1975	381	393	438	435	390	362	334	317	303	295	305	316
1976	343	372	418	414	395	358	328	304	302	296	290	320
1977	371	407	444	432	394	370	347	326	308	308	325	338
1978	348	385	433	427	397	371	343	321	300	303	306	325
1979	358	410	457	443	409	368	349	327	313	302	318	346
1980	356	378	431	428	403	373	353	327	313	310	314	323
1981	333	405	434	427	392	367	342	321	303	302	301	340
1982	361	427	431	439	410	379	346	335	313	303	302	296
1983	322	344	409	413	392	357	334	315	305	297	301	322
1984	361	370	421	415	396	372	348	315	309	305	308	318
1985	355	401	430	426	393	371	350	329	312	290	303	304
1986	337	355	417	444	396	367	347	330	306	313	324	337

Average Monthly Ozone Values for 53°N–64°N, Derived From the Provisionally Revised Data Sets; Dobson Only

Year	Jan	Feb	Mar	Apr	May	Jun	Jul	Aug	Sep	Oct	Nov	Dec
1957	346	456	411	397	403	377	342	326	310	297	291	309
1958	345	426	442	420	403	365	350	330	309	305	299	350
1959	375	389	432	433	395	373	341	325	302	299	315	320
1960	371	448	424	404	394	378	360	350	307	295	309	326
1961	357	391	403	417	390	368	353	328	307	305	297	300
1962	358	389	423	409	381	366	345	326	305	281	281	323
1963	361	419	431	420	415	381	354	338	310	303	302	307
1964	331	370	417	426	400	371	349	335	319	295	297	326
1965	360	382	414	416	400	363	347	331	316	300	297	365
1966	392	418	438	427	410	369	356	332	313	317	313	339
1967	365	400	427	401	387	359	340	324	298	306	305	321
1968	397	403	422	416	400	369	353	335	307	305	314	351
1969	376	413	433	428	407	382	360	328	317	305	311	342
1970	385	444	449	438	406	361	353	331	329	313	316	337
1971	386	416	426	417	388	371	346	321	313	305	311	337
1972	368	410	430	414	395	363	343	321	320	314	324	355
1973	362	426	406	424	384	369	347	327	312	310	310	330
1974	363	401	427	413	396	364	346	329	313	311	328	351
1975	384	399	423	425	393	367	337	325	306	307	308	324
1976	344	382	414	399	389	363	334	314	301	301	298	327
1977	373	402	432	427	397	376	363	342	323	309	328	342
1978	353	389	428	420	398	371	351	330	309	304	305	326
1979	357	416	436	435	408	370	357	335	315	302	320	347
1980	362	388	423	412	402	379	362	335	319	310	317	325
1981	338	401	426	425	394	376	349	326	302	307	307	345
1982	374	428	423	431	409	382	356	347	320	304	306	308
1983	329	354	398	398	384	360	337	319	311	301	308	332
1984	361	379	410	405	394	373	348	318	316	310	317	330
1985	357	398	404	404	384	366	349	330	315	297	311	312
1986	356	379	415	414	381	365	348	328	312	312	327	329

Average Monthly Ozone Values for 40°N–52°N Derived From the Provisionally Revised Data Sets; Dobson Only

Year	Jan	Feb	Mar	Apr	May	Jun	Jul	Aug	Sep	Oct	Nov	Dec
1957	344	348	350	358	374	345	320	309	295	277	290	323
1958	356	380	406	407	375	361	337	315	294	296	313	345
1959	382	392	403	396	378	353	333	311	306	300	318	341
1960	372	414	429	402	379	360	345	320	309	304	312	353
1961	386	370	374	399	383	358	338	323	301	298	311	330
1962	377	395	430	393	371	350	330	309	300	283	306	333
1963	388	423	406	397	388	365	336	324	301	290	306	324
1964	345	378	393	395	375	347	329	320	303	299	295	335
1965	361	395	408	398	380	353	340	323	311	294	310	342
1966	380	390	411	404	391	364	347	328	315	310	321	343
1967	373	390	385	379	366	356	331	321	302	288	299	337
1968	385	406	405	386	374	357	339	331	312	299	302	354
1969	359	412	408	399	377	368	341	332	309	301	314	353
1970	372	416	430	420	386	366	343	330	313	309	313	335
1971	371	392	411	393	378	365	341	320	318	292	306	323
1972	362	385	398	390	384	364	339	321	316	310	316	330
1973	353	396	389	422	380	361	347	326	308	306	309	330
1974	364	393	387	401	384	365	339	326	308	322	315	321
1975	342	372	398	398	379	362	335	325	307	300	310	318
1976	355	367	381	383	372	352	335	329	316	300	310	335
1977	390	403	392	399	385	369	346	329	310	294	304	329
1978	363	382	380	399	382	362	340	323	301	292	293	314
1979	371	393	397	419	389	360	342	323	305	301	310	326
1980	355	379	395	405	393	367	346	322	308	302	305	322
1981	358	385	390	390	387	357	338	323	309	309	307	340
1982	370	401	408	397	380	367	341	328	303	297	294	314
1983	326	362	368	381	369	350	327	318	301	292	293	331
1984	366	381	408	395	386	360	334	322	314	301	299	316
1985	367	372	374	368	360	356	327	314	299	291	318	333
1986	372	389	378	390	363	343	333	317	300	298	309	323

Average Monthly Ozone Values for 30°N–39°N, Derived From the Provisionally Revised Data Sets

Year	Jan	Feb	Mar	Apr	May	Jun	Jul	Aug	Sep	Oct	Nov	Dec
1957	317	309	320	335	342	319	298	291	291	286	289	299
1958	318	329	360	357	347	342	319	309	301	289	291	312
1959	316	328	338	343	348	335	310	303	295	289	286	306
1960	322	332	351	365	342	326	310	296	300	286	285	306
1961	319	333	334	337	330	324	305	297	291	284	296	309
1962	338	349	358	351	341	321	300	287	283	283	286	307
1963	338	355	350	354	349	327	312	298	291	286	282	293
1964	311	333	334	335	345	330	315	301	293	287	284	300
1965	323	341	356	351	348	334	312	308	299	297	290	301
1966	326	323	348	349	352	343	319	307	303	293	291	311
1967	325	333	335	337	339	329	311	305	297	288	289	313
1968	335	356	367	345	345	334	322	313	302	293	289	304
1969	315	325	343	346	340	334	317	310	305	299	299	316
1970	338	344	361	357	350	337	327	315	302	292	292	301
1971	322	329	349	349	344	326	311	304	301	292	291	298
1972	317	343	352	349	349	329	315	306	303	297	291	305
1973	328	337	344	339	338	325	313	305	300	297	299	318
1974	323	345	350	352	343	333	321	309	298	297	286	299
1975	312	334	347	340	343	337	317	307	295	287	290	301
1976	317	322	332	335	334	325	313	304	299	296	297	310
1977	341	347	333	351	354	335	317	308	300	295	285	301
1978	314	327	340	334	334	318	309	303	296	289	290	305
1979	336	349	358	348	352	328	312	308	303	291	287	307
1980	323	339	346	343	344	329	315	310	300	297	293	309
1981	326	335	356	344	342	325	317	309	300	292	294	310
1982	330	356	357	354	346	332	324	313	308	294	288	294
1983	308	324	337	340	337	328	316	306	297	291	289	308
1984	332	345	352	355	343	324	314	305	301	288	287	290
1985	300	306	306	322	331	318	307	303	295	288	296	307
1986	326	340	349	347	343	326	314	306	297	298	296	298

M–83 Average Monthly Ozone Measurements for the European Part of the USSR

Year	Jan	Feb	Mar	Apr	May	Jun	Jul	Aug	Sep	Oct	Nov	Dec
1972	339	368	414	414	397	367	317	315	318	323	310	336
1973	339	435	440	434	388	379	362	337	320	314	317	338
1974	359	384	364	411	402	367	344	335	315	313	311	342
1975	367	404	406	402	373	356	335	320	299	289	296	301
1976	370	371	428	423	396	378	345	332	315	302	297	343
1977	386	442	432	432	401	388	380	350	331	308	331	325
1978	367	399	399	430	401	377	363	343	331	306	302	334
1979	378	395	417	433	375	364	366	322	305	304	295	340
1980	370	378	416	423	408	377	356	343	316	305	306	334
1981	364	402	398	420	395	356	336	331	302	310	309	332
1982	357	417	411	396	388	384	353	342	308	299	284	299
1983	333	377	383	383	357	364	342	331	306	294	301	319
1984	361	368	399	393	372	368	349	333	315	312	293	319
1985	351	426	391	391	369	355	346	307	316	290	300	324

M–83 Average Monthly Ozone Measurements for the South Central Asian Part of the USSR

Year	Jan	Feb	Mar	Apr	May	Jun	Jul	Aug	Sep	Oct	Nov	Dec
1972	360	358	365	345	350	324	307	304	298	295	290	329
1973	349	346	352	327	345	313	313	301	305	305	321	344
1974	362	392	353	353	354	339	325	301	299	283	309	348
1975	359	387	378	362	352	321	303	283	293	296	315	323
1976	343	375	359	332	319	318	299	291	302	315	315	347
1977	388	384	361	357	358	325	313	307	304	312	306	333
1978	351	371	385	336	330	315	300	298	294	294	300	315
1979	368	379	383	333	355	323	303	301	302	292	288	325
1980	369	372	372	336	340	334	307	306	302	299	306	316
1981	349	366	378	355	328	318	309	302	295	294	296	318
1982	354	388	379	349	338	320	310	301	315	302	305	319
1983	324	338	367	352	328	319	302	287	294	288	299	322
1984	361	397	365	366	357	332	306	281	297	287	298	334
1985	325	335	350	317	344	320	298	311	297	302	312	323

M–83 Average Monthly Ozone Measurements for the Siberian Part of the USSR

Year	Jan	Feb	Mar	Apr	May	Jun	Jul	Aug	Sep	Oct	Nov	Dec
1972	359	377	422	423	406	376	338	327	322	332	341	349
1973	384	378	430	390	372	347	340	330	352	338	348	352
1974	373	392	369	421	391	368	333	329	325	308	322	341
1975	398	446	432	432	402	359	347	342	316	320	320	332
1976	365	394	396	413	387	364	349	317	325	329	304	321
1977	390	429	437	412	399	360	343	346	320	328	315	336
1978	382	400	389	414	401	353	344	333	321	312	319	327
1979	389	387	429	422	383	377	340	322	311	311	291	347
1980	394	378	435	406	382	379	349	339	321	311	303	337
1981	366	431	420	413	397	359	341	324	309	299	314	304
1982	415	436	435	382	388	361	348	334	309	299	291	295
1983	350	397	414	379	396	350	336	331	326	309	309	312
1984	381	374	428	438	401	369	340	311	332	326	299	322
1985	365	406	388	397	375	360	343	316	307	308	306	339

M–83 Average Monthly Ozone Measurements for the Far Eastern Part of the USSR

Year	Jan	Feb	Mar	Apr	May	Jun	Jul	Aug	Sep	Oct	Nov	Dec
1972	407	440	449	427	398	385	336	321	322	333	359	386
1973	403	445	478	421	411	383	317	314	339	345	371	412
1974	460	450	483	434	416	365	347	311	314	331	363	398
1975	423	457	441	451	413	382	344	318	322	336	366	405
1976	420	430	440	452	394	373	332	336	315	336	371	403
1977	445	484	477	454	414	390	340	331	325	338	343	371
1978	430	456	455	452	414	375	333	323	329	335	343	404
1979	433	444	466	433	424	384	352	322	327	326	362	371
1980	444	484	470	460	414	372	346	324	325	341	351	389
1981	437	471	463	439	402	388	335	322	336	339	371	399
1982	456	479	464	439	413	388	356	307	326	335	343	371
1983	407	455	436	403	393	388	352	303	306	337	351	411
1984	439	464	469	435	402	372	327	303	317	334	354	386
1985	419	424	433	410	396	375	330	301	318	328	366	404
1986	454	473	435	437	412	378	348	307	316	337	369	376

B. (i) Coefficients from individual station analyses

Part	Data Used	Trend Starts	Effects Allowed For		
			QBO	Solar Cycle	Nuclear Effect
(a)	1965–1986	1970	yes	yes	n/a
(b)	1965–1986	1976	yes	yes	n/a
(c)	1957–1986	1970	yes	yes	no
(d)	1957–1986	1976	yes	yes	no
(e)	1957–1986	1970	yes	yes	yes
(f)	1957–1986	1976	yes	yes	yes

For example, part (a) contains the results of analyses that used data from January 1965 to December 1986 and a model that allows for the quasi-biennial oscillation and the solar cycle, and that posits a trend that starts in January 1970.

Notes:

(1) If a station does not have a complete record for the whole time period, as much as possible is used—e.g., for Bismarck, whose record starts in January 1963, the last four analyses are performed on the complete Bismarck data set (1/63–12/86). The estimate of the nuclear bomb test parameter should be treated very carefully because the maximum predicted effect occurred as the ozone observations started.

(2) No data prior to January 1957 were analysed.

(3) The units of the QBO and solar cycle parameters are Dobson Unit per $m.s^{-1}$, and Dobson Units per 100 sunspots, respectively. To find the magnitude of these effects, see Figures 4.10 and 4.11.

(4) The nuclear bomb test parameter shows that the photochemical model prediction and the analysis agree when it has a value of -1. If it has a value of -0.5, the magnitude of the effect calculated from the data is one half that predicted by the LLNL model.

(5) The trend coefficients are all given in Dobson Units per year.

(6) The provisionally revised data (Bojkov, private communication, 1987) are used.

(a) Not using data prior to 1/65
Coefficients for individual stations
Dobson Units per year change for 1976 through 1986. Model: QS76

Station:	Reykjavik	Lerwick	Leningrad
Monthly calculation:			
January	−2.26 ± 1.66	−2.37 ± 0.86	−1.14 ± 1.30
February	−3.24 ± 3.04	−3.06 ± 1.53	−2.21 ± 2.10
March	−0.54 ± 1.72	−1.79 ± 0.98	−2.19 ± 1.51
April	+0.19 ± 1.51	−1.19 ± 0.91	−2.91 ± 0.93
May	−0.22 ± 1.57	−1.91 ± 0.75	−1.37 ± 0.85
June	+1.59 ± 0.91	−0.49 ± 0.59	−0.38 ± 0.62
July	+2.64 ± 1.11	−0.79 ± 0.54	+0.35 ± 0.74
August	+1.88 ± 0.94	−0.43 ± 0.51	+0.10 ± 0.65
September	+0.77 ± 1.31	−0.53 ± 0.63	−0.07 ± 0.56
October	+0.68 ± 0.69	+0.68 ± 0.68	−0.60 ± 0.76
November	+1.18 ± 1.69	+0.75 ± 0.69	−0.62 ± 0.74
December	−2.28 ± 2.04	−1.52 ± 0.58	−2.33 ± 1.07
Average	+0.03	−1.05	−1.11
QBO	−0.30 ± 0.11	−0.28 ± 0.080	−0.086 ± 0.096
Solar	+9.69 ± 2.88	+4.42 ± 2.12	+1.30 ± 2.61
Yearly calculation:			
Ramp	+0.86 ± 0.53	−0.80 ± 0.30	−0.66 ± 0.38

Not using data prior to 1/65
Coefficients for individual stations
Dobson Units per year change for 1976 through 1986. Model: QS76

Station:	Churchill	Edmonton	Goose
Monthly calculation:			
January	−1.54 ± 1.07	−4.11 ± 1.42	−0.71 ± 1.51
February	−2.12 ± 1.14	−0.47 ± 0.98	−1.14 ± 1.01
March	−1.42 ± 1.02	−2.35 ± 0.97	−0.80 ± 0.96
April	−1.55 ± 0.94	−0.66 ± 0.86	−1.87 ± 1.13
May	−0.82 ± 0.82	−1.18 ± 0.65	−1.22 ± 0.99
June	+0.20 ± 0.80	−0.03 ± 0.69	+0.13 ± 0.54
July	−0.81 ± 0.51	+0.17 ± 0.51	−0.22 ± 0.56
August	−1.30 ± 0.78	+0.26 ± 0.64	−0.29 ± 0.53
September	−0.25 ± 0.71	+1.01 ± 0.76	−0.82 ± 0.58
October	−2.06 ± 0.60	−1.01 ± 0.59	+0.03 ± 0.41
November	+0.08 ± 0.83	+0.30 ± 0.91	+0.99 ± 0.67
December	−2.70 ± 1.05	−2.13 ± 1.49	+0.57 ± 1.11
Average	−1.19	−0.85	−0.45
QBO	−0.27 ± 0.080	−0.22 ± 0.080	−0.18 ± 0.073
Solar	+4.33 ± 2.10	+2.70 ± 2.06	+5.12 ± 2.01
Yearly calculation:			
Ramp	−1.13 ± 0.27	−0.46 ± 0.28	−0.17 ± 0.27

Not using data prior to 1/65
Coefficients for individual stations
Dobson Units per year change for 1976 through 1986. Model: QS76

Station:	Belsk	Bracknell	Uccle
Monthly calculation:			
January	−0.62 ± 1.23	−1.24 ± 1.14	−0.45 ± 1.27
February	−1.24 ± 1.35	−2.97 ± 1.16	−1.63 ± 1.47
March	−2.36 ± 1.14	−1.91 ± 1.16	−0.81 ± 1.52
April	−1.22 ± 0.91	−0.75 ± 1.19	−1.86 ± 1.15
May	−0.24 ± 0.74	−0.10 ± 0.62	−1.19 ± 0.90
June	−0.21 ± 0.65	−1.21 ± 0.63	−1.52 ± 0.84
July	+0.18 ± 0.55	−1.11 ± 0.49	−1.67 ± 0.71
August	−0.42 ± 0.49	−0.44 ± 0.50	−0.94 ± 0.55
September	−0.71 ± 0.58	−1.20 ± 0.70	−2.51 ± 0.85
October	−0.61 ± 0.63	−1.09 ± 0.70	−1.80 ± 0.97
November	−1.90 ± 0.73	−0.61 ± 0.70	−2.32 ± 1.07
December	−2.28 ± 1.06	+0.25 ± 0.75	+0.13 ± 0.95
Average	−0.97	−1.03	−1.38
QBO	−0.20 ± 0.082	−0.28 ± 0.081	−0.17 ± 0.106
Solar	+3.02 ± 2.21	+1.36 ± 2.03	+2.53 ± 2.58
Yearly calculation:			
Ramp	−0.73 ± 0.29	−0.82 ± 0.27	−1.35 ± 0.35

Not using data prior to 1/65
Coefficients for individual stations
Dobson Units per year change for 1976 through 1986. Model: QS76

Station:	Hradec Kralove	Hohenpeissenberg	Caribou
Monthly calculation:			
January	1.59 ± 1.42	+0.75 ± 1.01	−0.84 ± 1.45
February	2.16 ± 1.46	−2.20 ± 1.23	−2.70 ± 1.09
March	3.22 ± 1.21	−0.38 ± 1.10	−2.28 ± 1.12
April	1.30 ± 1.02	−1.96 ± 1.28	−1.34 ± 1.04
May	0.34 ± 0.70	+0.09 ± 0.74	−1.03 ± 0.68
June	+0.03 ± 0.71	−0.63 ± 0.49	−0.12 ± 0.59
July	+0.07 ± 0.63	−0.26 ± 0.41	−0.52 ± 0.43
August	+0.17 ± 0.56	−0.48 ± 0.42	+0.08 ± 0.43
September	0.74 ± 0.51	−0.89 ± 0.57	−0.79 ± 0.55
October	0.85 ± 0.69	−0.22 ± 0.74	−0.88 ± 0.53
November	1.11 ± 0.73	−0.40 ± 0.63	−0.54 ± 0.63
December	1.38 ± 1.17	−0.59 ± 0.83	−2.01 ± 0.89
Average	1.06 − 0.60	−1.08	
QBO	0.09 ± 0.09	−0.29 ± 0.069	−0.13 ± 0.076
Solar	+1.85 ± 2.52	+0.15 ± 1.80	+5.34 ± 2.14
Yearly calculation:			
Ramp	0.69 ± 0.34	−0.51 ± 0.23	−0.63 ± 0.29

Not using data prior to 1/65
Coefficients for individual stations
Dobson Units per year change for 1976 through 1986. Model: QS76

Station:	Bismarck	Arosa	Toronto
Monthly calculation:			
January	−1.94 ± 0.83	+0.25 ± 0.88	+0.47 ± 1.26
February	−1.02 ± 0.88	−0.86 ± 1.30	−1.45 ± 0.96
March	−2.11 ± 0.86	−1.70 ± 1.25	−1.67 ± 1.19
April	−1.37 ± 0.84	−1.62 ± 0.90	−0.46 ± 0.92
May	−1.45 ± 0.76	−0.55 ± 0.60	−2.17 ± 0.90
June	−1.13 ± 0.59	−1.34 ± 0.46	−0.38 ± 0.51
July	−0.73 ± 0.48	−0.89 ± 0.38	−1.28 ± 0.42
August	−0.55 ± 0.53	−0.96 ± 0.40	−0.47 ± 0.34
September	+0.20 ± 0.48	−1.31 ± 0.51	−0.54 ± 0.49
October	−0.34 ± 0.68	−0.49 ± 0.60	−1.09 ± 0.60
November	−0.75 ± 0.95	−0.47 ± 0.58	−0.99 ± 0.54
December	−1.10 ± 0.90	−1.55 ± 0.65	−1.69 ± 0.89
Average	−1.02	−0.96	−0.98
QBO	−0.19 ± 0.076	−0.13 ± 0.056	−0.11 ± 0.063
Solar	+4.39 ± 2.02	+2.10 ± 1.49	+0.36 ± 1.72
Yearly calculation:			
Ramp	−0.81 ± 0.27	−1.02 ± 0.19	−0.87 ± 0.24

Not using data prior to 1/65
Coefficients for individual stations
Dobson Units per year change for 1976 through 1986. Model: QS76

Station:	Sapporo	Rome	Boulder
Monthly calculation:			
January	+0.62 ± 0.97	−0.89 ± 0.85	−0.99 ± 0.74
February	+0.55 ± 0.94	−0.07 ± 1.09	−1.65 ± 0.92
March	−1.77 ± 1.08	−0.81 ± 0.97	−1.77 ± 0.98
April	−0.47 ± 0.78	−1.02 ± 0.81	−2.01 ± 0.92
May	+0.31 ± 0.58	+0.15 ± 0.72	−1.16 ± 0.60
June	+0.44 ± 0.64	−0.20 ± 0.51	−1.97 ± 0.52
July	+0.42 ± 0.63	−0.43 ± 0.43	−1.27 ± 0.32
August	−0.65 ± 0.55	+0.03 ± 0.47	−1.49 ± 0.38
September	+0.66 ± 0.45	−0.39 ± 0.47	−1.35 ± 0.35
October	+0.33 ± 0.59	−0.11 ± 0.44	−1.13 ± 0.54
November	+0.68 ± 0.58	−0.38 ± 0.48	−0.59 ± 0.52
December	−0.72 ± 0.82	−0.72 ± 0.78	−1.05 ± 0.71
Average	+0.03	−0.40	−1.37
QBO	+0.069 ± 0.078	−0.079 ± 0.070	−0.053 ± 0.058
Solar	+4.63 ± 2.10	+2.84 ± 1.94	+0.64 ± 1.58
Yearly calculation:			
Ramp	+0.26 ± 0.27	−0.34 ± 0.25	−1.35 ± 0.21

Not using data prior to 1/65
Coefficients for individual stations
Dobson Units per year change for 1976 through 1986. Model: QS76

Station:	Cagliari	Wallops Is.	Nashville
Monthly calculation:			
January	−0.97 ± 0.87	+1.07 ± 1.23	−0.09 ± 0.60
February	−0.65 ± 1.11	−0.79 ± 1.20	−1.20 ± 0.91
March	−0.69 ± 0.83	−1.22 ± 1.20	−1.43 ± 1.08
April	−0.88 ± 0.84	+0.20 ± 0.89	−0.08 ± 1.06
May	−0.81 ± 0.75	−0.74 ± 0.79	−1.20 ± 0.52
June	−1.61 ± 0.48	−0.93 ± 0.65	−1.49 ± 0.44
July	−0.03 ± 0.44	−0.38 ± 0.31	−1.69 ± 0.49
August	−0.45 ± 0.43	−0.04 ± 0.29	−1.49 ± 0.50
September	−0.44 ± 0.57	−0.13 ± 0.35	−0.95 ± 0.39
October	−0.38 ± 0.45	−0.83 ± 0.56	−1.01 ± 0.47
November	+0.72 ± 0.52	−0.32 ± 0.65	−0.96 ± 0.59
December	−0.74 ± 0.66	−0.45 ± 0.78	−0.07 ± 0.68
Average	−0.58	−0.38	−0.97
QBO	+0.030 ± 0.092	+0.084 ± 0.075	+0.045 ± 0.079
Solar	+5.38 ± 2.43	+0.21 ± 1.62	+3.90 ± 1.98
Yearly calculation:			
Ramp	−0.48 ± 0.31	−0.27 ± 0.22	−1.12 ± 0.26

Not using data prior to 1/65
Coefficients for individual stations
Dobson Units per year change for 1976 through 1986. Model: QS76

Station:	Tateno	Srinigar	Kagoshima
Monthly calculation:			
January	−0.10 ± 0.94	−0.29 ± 0.66	−0.11 ± 0.79
February	+1.35 ± 0.96	+0.69 ± 0.87	+0.72 ± 0.72
March	−1.18 ± 1.04	+0.79 ± 0.80	−0.34 ± 0.72
April	+0.39 ± 0.74	+0.09 ± 0.55	+0.54 ± 0.67
May	−0.33 ± 0.54	−0.08 ± 0.48	−0.07 ± 0.45
June	−0.30 ± 0.52	−0.35 ± 0.45	−0.32 ± 0.58
July	−0.08 ± 0.52	−0.74 ± 0.40	+0.15 ± 0.45
August	−0.02 ± 0.34	−0.86 ± 0.36	+0.41 ± 0.44
September	+0.14 ± 0.29	−0.24 ± 0.28	+0.04 ± 0.49
October	−0.07 ± 0.35	−0.36 ± 0.42	+0.55 ± 0.48
November	+0.29 ± 0.37	+0.00 ± 0.40	+0.33 ± 0.43
December	−0.35 ± 0.73	+0.16 ± 0.57	−0.21 ± 0.85
Average	−0.02	−0.10	+0.14
QBO	+0.14 ± 0.074	+0.18 ± 0.058	+0.090 ± 0.088
Solar	+1.93 ± 1.82	+3.52 ± 1.40	−0.54 ± 2.45
Yearly calculation:			
Ramp	+0.09 ± 0.23	−0.26 ± 0.19	+0.33 ± 0.31

Not using data prior to 1/65
Coefficients for individual stations
Dobson Units per year change for 1976 through 1986. Model: QS76

Station:	Quetta	Cairo
Monthly calculation:		
January	0.25 ± 0.59	−1.64 ± 1.38
February	0.43 ± 0.82	−0.30 ± 1.48
March	0.86 ± 1.03	−0.24 ± 1.18
April	0.92 ± 0.54	+0.41 ± 0.66
May	+0.08 ± 0.43	+0.75 ± 0.79
June	0.46 ± 0.34	−1.49 ± 0.57
July	+0.49 ± 0.42	−0.59 ± 0.38
August	0.08 ± 0.46	−0.04 ± 0.23
September	0.13 ± 0.44	−0.01 ± 0.25
October	0.14 ± 0.50	−0.07 ± 0.24
November	0.21 ± 0.46	+0.81 ± 0.81
December	+0.28 ± 0.48	−0.73 ± 0.51
Average	−0.22	−0.26
QBO	0.24 ± 0.08	+0.011 ± 0.054
Solar	+2.15 ± 1.92	+1.34 ± 1.11
Yearly calculation:		
Ramp	−0.21 ± 0.25	−0.06 ± 0.19

Not using data prior to 1/65
Coefficients for individual stations
Dobson Units per year change for 1976 through 1986. Model: QS76

Station:	Mauna Loa
Monthly calculation:	
January	−0.85 ± 0.56
February	−0.56 ± 0.79
March	−0.81 ± 0.61
April	+0.23 ± 0.56
May	−0.25 ± 0.31
June	−0.05 ± 0.34
July	+0.16 ± 0.31
August	−0.52 ± 0.27
September	−0.39 ± 0.23
October	−0.41 ± 0.29
November	−0.67 ± 0.45
December	−0.22 ± 0.52
Average	−0.36
QBO	+0.147 ± 0.059
Solar	+1.13 ± 1.56
Yearly calculation:	
Ramp	−0.36 ± 0.20

Not using data prior to 1/65
Coefficients for individual stations
Dobson Units per year change for 1976 through 1986. Model: QS76

Station:	Huancayo	Samoa
Monthly calculation:		
January	−0.24 ± 0.19	1.23 ± 0.44
February	−0.37 ± 0.22	1.21 ± 0.38
March	−0.59 ± 0.24	1.10 ± 0.43
April	−0.38 ± 0.22	0.80 ± 0.36
May	−0.30 ± 0.19	0.91 ± 0.39
June	−0.41 ± 0.23	1.71 ± 0.71
July	−0.31 ± 0.24	1.22 ± 0.61
August	−0.32 ± 0.20	1.13 ± 0.46
September	−0.32 ± 0.19	0.14 ± 0.50
October	−0.10 ± 0.26	0.17 ± 0.54
November	−0.11 ± 0.17	0.65 ± 0.38
December	−0.51 ± 0.19	0.98 ± 0.43
Average	−0.33	0.94
QBO	+0.066 ± 0.028	+0.12 ± 0.06
Solar	+0.90 ± 0.75	0.85 ± 1.40
Yearly calculation:		
Ramp	0.33 ± 0.10	−0.85 ± 0.25

Not using data prior to 1/65
Coefficients for individual stations
Dobson Units per year change for 1976 through 1986. Model: QS76

Station:	Aspendale	MacQuarie Isle
Monthly calculation:		
January	−0.80 ± 0.42	+0.25 ± 0.91
February	−1.20 ± 0.38	+0.55 ± 0.79
March	−1.48 ± 0.38	+0.47 ± 0.76
April	−0.80 ± 0.26	+0.50 ± 0.73
May	−1.17 ± 0.38	−1.05 ± 0.69
June	−0.79 ± 0.48	+0.50 ± 0.87
July	−1.10 ± 0.68	−0.63 ± 0.88
August	−1.34 ± 0.71	+0.58 ± 1.15
September	−1.57 ± 0.70	−0.05 ± 1.52
October	−0.80 ± 0.55	+0.17 ± 1.19
November	−1.33 ± 0.44	+1.66 ± 0.94
December	−1.15 ± 0.41	−0.25 ± 0.68
Average	−1.13	+0.22
QBO	−0.26 ± 0.066	−0.25 ± 0.12
Solar	+1.96 ± 1.59	+6.51 ± 3.13
Yearly calculation:		
Ramp	−1.01 ± 0.20	−0.01 ± 0.40

(b) Not using data prior to 1/65
Coefficients for individual stations
Dobson Units per year change for 1970 through 1986. Model: QS70

Station:	Reykjavik	Lerwick	Leningrad
Monthly calculation:			
January	−2.26 ± 1.66	−1.86 ± 0.57	−0.27 ± 0.93
February	−3.24 ± 3.04	−2.12 ± 0.99	−2.69 ± 1.50
March	−0.54 ± 1.72	−1.25 ± 0.63	−2.02 ± 1.07
April	+0.19 ± 1.51	−0.68 ± 0.59	−1.87 ± 0.66
May	−0.22 ± 1.57	−1.21 ± 0.48	−0.88 ± 0.61
June	+1.59 ± 0.91	−0.20 ± 0.38	−0.44 ± 0.44
July	+2.64 ± 1.11	−0.38 ± 0.35	+0.27 ± 0.53
August	+1.88 ± 0.94	−0.32 ± 0.33	+0.32 ± 0.46
September	+0.77 ± 1.31	−0.29 ± 0.41	−0.28 ± 0.40
October	+0.68 ± 0.69	+0.75 ± 0.44	−0.45 ± 0.52
November	+1.18 ± 1.69	+0.50 ± 0.44	−0.38 ± 0.51
December	−2.28 ± 2.04	−1.13 ± 0.36	−1.36 ± 0.73
Average	+0.03	−0.68	−0.84
QBO	−0.30 ± 0.11	−0.28 ± 0.08	−0.09 ± 0.10
Solar	+9.69 ± 2.88	+4.14 ± 2.11	+0.87 ± 2.60
Yearly calculation:			
Ramp	+0.86 ± 0.53	−0.49 ± 0.19	−0.43 ± 0.26

Not using data prior to 1/65
Coefficients for individual stations
Dobson Units per year change for 1970 through 1986. Model: QS70

Station:	Churchill	Edmonton	Goose
Monthly calculation:			
January	−1.63 ± 0.71	−3.15 ± 0.94	−1.08 ± 1.01
February	−1.60 ± 0.74	−0.36 ± 0.64	−0.69 ± 0.66
March	−0.36 ± 0.66	−1.38 ± 0.64	−0.64 ± 0.63
April	−0.92 ± 0.61	−0.36 ± 0.56	−1.24 ± 0.74
May	−0.85 ± 0.53	−0.46 ± 0.42	−0.80 ± 0.65
June	+0.22 ± 0.51	+0.18 ± 0.45	+0.09 ± 0.35
July	−0.53 ± 0.33	+0.20 ± 0.33	−0.23 ± 0.37
August	−0.59 ± 0.50	+0.27 ± 0.42	−0.14 ± 0.35
September	−0.05 ± 0.46	+0.41 ± 0.50	−0.27 ± 0.38
October	−1.46 ± 0.39	−0.76 ± 0.38	+0.03 ± 0.27
November	+0.15 ± 0.54	+0.33 ± 0.59	+0.58 ± 0.42
December	−1.89 ± 0.68	−1.35 ± 0.94	−0.20 ± 0.70
Average	−0.79	−0.54	−0.38
QBO	−0.26 ± 0.08	−0.22 ± 0.08	−0.17 ± 0.07
Solar	+4.00 ± 2.10	+2.52 ± 2.06	+5.10 ± 2.01
Yearly calculation:			
Ramp	−0.73 ± 0.17	−0.24 ± 0.18	−0.11 ± 0.17

Not using data prior to 1/65
Coefficients for individual stations
Dobson Units per year change for 1970 through 1986.Model: QS70

Station:	Belsk	Bracknell	Uccle
Monthly calculation:			
January	0.99 ± 0.82	−1.48 ± 0.88	−0.63 ± 1.09
February	1.22 ± 0.88	−2.61 ± 0.84	−1.72 ± 1.26
March	1.98 ± 0.74	−1.73 ± 0.84	−1.21 ± 1.23
April	0.51 ± 0.59	−0.59 ± 0.86	−1.65 ± 0.93
May	0.12 ± 0.48	−0.06 ± 0.45	−1.23 ± 0.73
June	0.00 ± 0.42	−1.02 ± 0.46	−1.53 ± 0.68
July	+0.36 ± 0.35	−0.87 ± 0.36	−1.55 ± 0.57
August	−0.18 ± 0.32	−0.55 ± 0.36	−0.94 ± 0.44
September	0.42 ± 0.38	−1.00 ± 0.51	−2.27 ± 0.69
October	0.17 ± 0.41	−0.63 ± 0.51	−1.59 ± 0.78
November	1.06 ± 0.48	−0.40 ± 0.50	−2.13 ± 0.86
December	2.00 ± 0.68	+0.10 ± 0.55	+0.10 ± 0.77
Average	0.69	−0.90	−1.36
QBO	0.19 ± 0.08	−0.28 ± 0.08	−0.18 ± 0.10
Solar	+2.88 ± 2.19	+0.95 ± 1.94	+2.84 ± 2.41
Yearly calculation:			
Ramp	−0.35 ± 0.19	−0.68 ± 0.19	−1.28 ± 0.26

Not using data prior to 1/65
Coefficients for individual stations
Dobson Units per year change for 1970 through 1986. Model: QS70

Station:	Hradec Kralove	Hohenpeissenberg	Caribou
Monthly calculation:			
January	−1.84 ± 0.97	+0.57 ± 0.71	−0.71 ± 0.96
February	−2.28 ± 0.97	−1.79 ± 0.84	−2.04 ± 0.72
March	−2.56 ± 0.80	−0.69 ± 0.75	−1.75 ± 0.72
April	−0.61 ± 0.68	−1.22 ± 0.87	−0.92 ± 0.67
May	+0.14 ± 0.47	+0.30 ± 0.50	−0.77 ± 0.44
June	+0.29 ± 0.47	−0.46 ± 0.33	−0.04 ± 0.38
July	+0.35 ± 0.42	−0.17 ± 0.28	−0.41 ± 0.28
August	+0.02 ± 0.37	−0.43 ± 0.28	−0.16 ± 0.28
September	−0.38 ± 0.34	−0.69 ± 0.39	−0.44 ± 0.36
October	−0.26 ± 0.46	+0.03 ± 0.50	−0.49 ± 0.34
November	−0.56 ± 0.48	−0.18 ± 0.43	−0.52 ± 0.41
December	−1.56 ± 0.78	−0.85 ± 0.56	−1.44 ± 0.58
Average	−0.77	−0.46	−0.81
QBO	−0.08 ± 0.09	−0.29 ± 0.07	−0.12 ± 0.07
Solar	+1.67 ± 2.48	−0.19 ± 1.80	+5.12 ± 2.07
Yearly calculation:			
Ramp	−0.29 ± 0.22	−0.36 ± 0.15	−0.48 ± 0.18

Not using data prior to 1/65
Coefficients for individual stations
Dobson Units per year change for 1970 through 1986. Model: QS70

Station:	Bismarck	Arosa	Toronto
Monthly calculation:			
January	−1.24 ± 0.55	−0.12 ± 0.59	+0.31 ± 0.85
February	−1.06 ± 0.58	−0.88 ± 0.85	−1.30 ± 0.66
March	−1.43 ± 0.56	−1.49 ± 0.82	−1.28 ± 0.79
April	−0.71 ± 0.55	−0.83 ± 0.59	−0.18 ± 0.61
May	−0.81 ± 0.49	−0.21 ± 0.39	−1.32 ± 0.59
June	−0.72 ± 0.39	−0.73 ± 0.30	+0.05 ± 0.34
July	−0.46 ± 0.31	−0.46 ± 0.25	−0.70 ± 0.28
August	−0.19 ± 0.35	−0.64 ± 0.26	−0.28 ± 0.22
September	+0.13 ± 0.31	−0.87 ± 0.34	−0.18 ± 0.33
October	−0.28 ± 0.44	−0.04 ± 0.39	−0.50 ± 0.40
November	−0.49 ± 0.62	−0.29 ± 0.38	−0.60 ± 0.35
December	−0.87 ± 0.59	−1.35 ± 0.43	−1.00 ± 0.59
Average	−0.68	−0.66	−0.58
QBO	−0.18 ± 0.076	−0.11 ± 0.06	−0.10 ± 0.07
Solar	+4.14 ± 2.02	+1.85 ± 1.51	−0.26 ± 1.99
Yearly calculation:			
Ramp	−0.51 ± 0.17	−0.60 ± 0.12	−0.45 ± 0.17

Not using data prior to 1/65
Coefficients for individual stations
Dobson Units per year change for 1970 through 1986. Model: QS70

Station:	Sapporo	Rome	Boulder
Monthly calculation:			
January	+0.13 ± 0.65	−0.97 ± 0.56	−0.57 ± 0.49
February	+0.22 ± 0.62	−0.02 ± 0.72	−1.28 ± 0.60
March	−1.40 ± 0.71	−0.89 ± 0.63	−1.14 ± 0.64
April	−0.06 ± 0.51	−0.42 ± 0.52	−1.12 ± 0.60
May	+0.21 ± 0.38	+0.25 ± 0.47	−0.70 ± 0.39
June	+0.05 ± 0.42	+0.14 ± 0.33	−1.39 ± 0.34
July	+0.04 ± 0.41	−0.18 ± 0.28	−0.77 ± 0.21
August	−0.31 ± 0.36	+0.19 ± 0.30	−0.98 ± 0.25
September	+0.40 ± 0.29	−0.23 ± 0.31	−0.90 ± 0.23
October	+0.04 ± 0.38	+0.18 ± 0.29	−0.76 ± 0.35
November	+0.45 ± 0.38	−0.27 ± 0.31	−0.41 ± 0.34
December	−0.67 ± 0.54	−0.93 ± 0.51	−0.86 ± 0.46
Average	−0.075	−0.26	−0.91
QBO	+0.00 ± 0.08	−0.07 ± 0.07	−0.04 ± 0.06
Solar	+4.66 ± 2.12	+2.76 ± 1.94	+0.27 ± 1.59
Yearly calculation:			
Ramp	+0.10 ± 0.17	−0.12 ± 0.16	−0.87 ± 0.13

Not using data prior to 1/65
Coefficients for individual stations
Dobson Units per year change for 1970 through 1986. Model: QS70

Station:	Cagliari	Wallops Is.	Nashville
Monthly calculation:			
January	−0.92 ± 0.52	+1.03 ± 1.03	−0.19 ± 0.39
February	−0.31 ± 0.74	−0.63 ± 0.94	−1.19 ± 0.59
March	−0.38 ± 0.54	−1.43 ± 0.94	−1.44 ± 0.69
April	−0.41 ± 0.55	−0.03 ± 0.70	−0.13 ± 0.68
May	−0.34 ± 0.49	−0.54 ± 0.62	−0.86 ± 0.33
June	−1.03 ± 0.31	−0.76 ± 0.51	−0.92 ± 0.28
July	−0.26 ± 0.29	−0.23 ± 0.24	−1.16 ± 0.31
August	−0.28 ± 0.28	−0.02 ± 0.23	−1.14 ± 0.32
September	−0.53 ± 0.37	−0.07 ± 0.27	−0.71 ± 0.25
October	−0.41 ± 0.29	−0.44 ± 0.44	−0.53 ± 0.30
November	+0.22 ± 0.34	−0.41 ± 0.51	−0.89 ± 0.38
December	−0.95 ± 0.43	−0.16 ± 0.61	−0.13 ± 0.43
Average	−0.47	−0.31	−0.77
QBO	+0.027 ± 0.091	+0.082 ± 0.075	+0.044 ± 0.075
Solar	+5.11 ± 2.42	+0.16 ± 1.62	+3.65 ± 1.85
Yearly calculation:			
Ramp	−0.38 ± 0.20	−0.18 ± 0.17	−0.78 ± 0.16

Not using data prior to 1/65
Coefficients for individual stations
Dobson Units per year change for 1970 through 1986. Model: QS70

Station:	Tateno	Srinigar	Kagoshima
Monthly calculation:			
January	−0.21 ± 0.63	−0.26 ± 0.44	+0.05 ± 0.53
February	+0.96 ± 0.64	+0.64 ± 0.58	+0.74 ± 0.48
March	−0.93 ± 0.68	+0.64 ± 0.52	−0.25 ± 0.47
April	+0.18 ± 0.48	+0.01 ± 0.36	+0.48 ± 0.43
May	−0.27 ± 0.35	−0.01 ± 0.32	+0.06 ± 0.29
June	−0.33 ± 0.34	−0.15 ± 0.29	−0.05 ± 0.37
July	−0.12 ± 0.34	−0.38 ± 0.25	+0.34 ± 0.29
August	−0.03 ± 0.22	−0.47 ± 0.23	+0.41 ± 0.28
September	+0.17 ± 0.19	−0.08 ± 0.18	+0.25 ± 0.32
October	−0.18 ± 0.23	−0.29 ± 0.27	+0.37 ± 0.31
November	+0.28 ± 0.24	−0.15 ± 0.25	+0.50 ± 0.28
December	−0.20 ± 0.47	+0.18 ± 0.36	+0.17 ± 0.53
Average	−0.057	−0.027	+0.26
QBO	+0.142 ± 0.074	+0.182 ± 0.058	+0.086 ± 0.086
Solar	+1.99 ± 1.82	+3.32 ± 1.41	−0.21 ± 2.39
Yearly calculation:			
Ramp	+0.72 ± 0.14	−0.15 ± 0.12	+0.35 ± 0.19

Not using data prior to 1/65
Coefficients for individual stations
Dobson Units per year change for 1970 through 1986. Model: QS70

Station:	Quetta	Cairo
Monthly calculation:		
January	−0.13 ± 0.46	−1.68 ± 1.39
February	−0.25 ± 0.65	−0.35 ± 1.49
March	−0.27 ± 0.81	−0.27 ± 1.19
April	−0.51 ± 0.43	+0.40 ± 0.66
May	+0.11 ± 0.33	+0.74 ± 0.79
June	−0.29 ± 0.27	−1.49 ± 0.57
July	+0.39 ± 0.33	−0.59 ± 0.38
August	−0.16 ± 0.36	−0.04 ± 0.23
September	−0.34 ± 0.33	+0.01 ± 0.25
October	−0.37 ± 0.37	+0.07 ± 0.24
November	−0.27 ± 0.34	+0.79 ± 0.81
December	−0.27 ± 0.34	−0.75 ± 0.51
Average	−0.20	−0.26
QBO	+0.242 ± 0.078	+0.011 ± 0.054
Solar	+2.04 ± 1.92	+1.34 ± 1.11
Yearly calculation:		
Ramp	−0.18 ± 0.19	−0.06 ± 0.18

Not using data prior to 1/65
Coefficients for individual stations
Dobson Units per year change for 1970 through 1986. Model: QS70

Station:	Mauna Loa
Monthly calculation:	
January	−0.53 ± 0.38
February	−0.34 ± 0.53
March	−0.39 ± 0.40
April	+0.06 ± 0.37
May	−0.03 ± 0.20
June	+0.02 ± 0.22
July	+0.12 ± 0.20
August	−0.38 ± 0.18
September	−0.34 ± 0.15
October	−0.28 ± 0.19
November	−0.40 ± 0.29
December	−0.19 ± 0.34
Average	−0.22
QBO	+0.147 ± 0.059
Solar	+1.01 ± 1.57
Yearly calculation:	
Ramp	−0.24 ± 0.13

Not using data prior to 1/65
Coefficients for individual stations
Dobson Units per year change for 1970 through 1986. Model: QS70

Station:	Huancayo
Monthly calculation:	
January	−0.10 ± 0.13
February	−0.19 ± 0.15
March	−0.39 ± 0.16
April	−0.24 ± 0.15
May	−0.13 ± 0.13
June	−0.17 ± 0.15
July	−0.15 ± 0.15
August	−0.24 ± 0.13
September	−0.22 ± 0.12
October	−0.08 ± 0.17
November	−0.02 ± 0.11
December	−0.31 ± 0.12
Average	−0.19
QBO	+0.066 ± 0.029
Solar	+0.80 ± 0.77
Yearly calculation:	
Ramp	−0.18 ± 0.065

Not using data prior to 1/65
Coefficients for individual stations
Dobson Units per year change for 1970 through 1986. Model: QS70

Station:	Aspendale	MacQuarie Isle
Monthly calculation:		
January	−0.48 ± 0.29	+0.27 ± 0.62
February	−0.70 ± 0.27	+0.37 ± 0.52
March	−0.74 ± 0.26	+0.15 ± 0.50
April	−0.39 ± 0.18	−0.02 ± 0.48
May	−0.69 ± 0.26	−0.27 ± 0.45
June	−0.30 ± 0.33	+0.40 ± 0.57
July	−0.61 ± 0.46	−0.10 ± 0.58
August	−0.60 ± 0.49	+0.81 ± 0.76
September	−0.92 ± 0.48	−0.35 ± 1.00
October	−0.26 ± 0.38	+0.07 ± 0.78
November	−0.75 ± 0.30	+0.99 ± 0.62
December	−0.83 ± 0.28	−0.20 ± 0.45
Average	−0.61	+0.18
QBO	−0.24 ± 0.072	−0.26 ± 0.12
Solar	+1.51 ± 1.80	+6.65 ± 3.11
Yearly calculation:		
Ramp	−0.57 ± 0.15	−0.12 ± 0.25

(c) Using all data
Coefficients for individual stations.
Dobson Units per year change for 1970 through 1986. Model: QS70

Station:	Reykjavik	Lerwick	Leningrad
Monthly calculation:			
January		−0.85 ± 0.54	
February		−1.71 ± 0.97	
March		−0.71 ± 0.61	
April		−0.02 ± 0.57	
May		−0.43 ± 0.47	
June		+0.24 ± 0.37	
July		−0.11 ± 0.34	
August		−0.18 ± 0.32	
September	No Data	+0.41 ± 0.40	No Data
October		+1.26 ± 0.43	
November		+0.81 ± 0.43	
December		−0.24 ± 0.35	
Average		−0.13	
QBO		−0.24 ± 0.08	
Solar		−1.66 ± 1.94	
Yearly calculation:			
Ramp		+0.02 ± 0.20	

Using all data
Coefficients for individual stations.
Dobson Units per year change for 1970 through 1986. Model: QS70

Station:	Churchill	Edmonton	Goose
Monthly calculation:			
January		−1.45 ± 0.83	−1.07 ± 0.93
February		−0.81 ± 0.59	−0.93 ± 0.61
March		−1.47 ± 0.58	−0.98 ± 0.58
April		−0.62 ± 0.51	−1.36 ± 0.69
May		−0.56 ± 0.39	−0.74 ± 0.60
June		+0.30 ± 0.41	−0.11 ± 0.33
July		+0.52 ± 0.34	−0.01 ± 0.34
August		+0.23 ± 0.38	−0.02 ± 0.32
September	No Data	+0.34 ± 0.45	−0.27 ± 0.36
October		−0.31 ± 0.35	+0.01 ± 0.25
November		+0.72 ± 0.54	+0.62 ± 0.39
December		−0.19 ± 0.84	−0.37 ± 0.65
Average		−0.28	0.44
QBO		−0.12 ± 0.08	−0.15 ± 0.07
Solar		+1.42 ± 1.93	+4.65 ± 1.91
Yearly calculation:			
Ramp		−0.06 ± 0.19	−0.13 ± 0.16

Using all data
Coefficients for individual stations.
Dobson Units per year change for 1970 through 1986. Model: QS70

Station:	Belsk	Bracknell	Uccle
Monthly calculation:			
January	−0.51 ± 0.77		
February	−1.22 ± 0.83		
March	−1.75 ± 0.70		
April	−0.39 ± 0.56		
May	−0.09 ± 0.46		
June	+0.03 ± 0.40		
July	+0.43 ± 0.34		
August	−0.22 ± 0.30		
September	−0.33 ± 0.36	No Data	No Data
October	−0.17 ± 0.39		
November	−0.78 ± 0.45		
December	−1.76 ± 0.65		
Average	−0.56		
QBO	−0.22 ± 0.08		
Solar	+3.59 ± 2.09		
Yearly calculation:			
Ramp	−0.30 ± .18		

Using all data
Coefficients for individual stations.
Dobson Units per year change for 1970 through 1986. Model: QS70

Station:	Hradec Kralove	Hohenpeissenberg	Caribou
Monthly calculation:			
January			−0.78 ± 0.86
February			−1.90 ± 0.64
March			−1.76 ± 0.67
April			−0.96 ± 0.62
May			−0.88 ± 0.41
June			−0.16 ± 0.36
July			−0.34 ± 0.26
August			−0.28 ± 0.25
September	No Data	No Data	−0.39 ± 0.32
October			−0.40 ± 0.31
November			−0.48 ± 0.37
December			−1.63 ± 0.52
Average			−0.83
QBO			−0.11 ± 0.07
Solar			+4.48 ± 1.90
Yearly calculation:			
Ramp	−0.07 ± 0.21		−0.50 ± 0.16

Using all data
Coefficients for individual stations.
Dobson Units per year change for 1970 through 1986. Model: QS70

Station:	Bismarck	Arosa	Toronto
Monthly calculation:			
January	−1.10 ± 0.51	−0.33 ± 0.49	−0.05 ± 0.77
February	−0.98 ± 0.54	+0.01 ± 0.73	−0.98 ± 0.58
March	−1.51 ± 0.53	−1.24 ± 0.70	−1.65 ± 0.72
April	−0.72 ± 0.51	−0.56 ± 0.51	−0.65 ± 0.56
May	−0.79 ± 0.46	−0.36 ± 0.34	−0.92 ± 0.54
June	−0.59 ± 0.36	−0.40 ± 0.26	+0.06 ± 0.31
July	−0.41 ± 0.29	−0.34 ± 0.22	−0.74 ± 0.25
August	−0.14 ± 0.32	−0.28 ± 0.23	−0.32 ± 0.20
September	+0.23 ± 0.29	−0.51 ± 0.29	−0.04 ± 0.30
October	−0.09 ± 0.41	−0.03 ± 0.34	−0.51 ± 0.37
November	−0.31 ± 0.58	−0.26 ± 0.33	−0.32 ± 0.32
December	−0.71 ± 0.55	−1.16 ± 0.37	−1.27 ± 0.54
Average	−0.59	−0.46	−0.62
QBO	−0.17 ± 0.07	−0.13 ± 0.05	−0.15 ± 0.06
Solar	+4.93 ± 1.93	+2.42 ± 1.18	−0.19 ± 1.72
Yearly calculation:			
Ramp	−0.42 ± 0.16	−0.42 ± .11	−0.43 ± .13

Using all data
Coefficients for individual stations.
Dobson Units per year change for 1970 through 1986. Model: QS70

Station:	Sapporo	Rome	Boulder
Monthly calculation:			
January	−0.22 ± 0.56	−0.70 ± 0.50	−0.53 ± 0.48
February	+0.18 ± 0.54	−0.30 ± 0.63	−1.37 ± 0.59
March	−1.14 ± 0.62	−0.50 ± 0.57	−1.36 ± 0.62
April	+0.40 ± 0.45	−0.34 ± 0.47	−1.21 ± 0.59
May	+0.36 ± 0.34	+0.11 ± 0.43	−0.68 ± 0.38
June	+0.24 ± 0.37	+0.37 ± 0.30	−1.41 ± 0.33
July	+0.19 ± 0.37	+0.28 ± 0.25	−0.64 ± 0.21
August	−0.10 ± 0.32	+0.70 ± 0.27	−1.00 ± 0.24
September	+0.34 ± 0.26	+0.10 ± 0.28	−0.84 ± 0.22
October	+0.56 ± 0.34	+0.24 ± 0.26	−0.68 ± 0.34
November	+0.62 ± 0.33	−0.12 ± 0.28	−0.30 ± 0.33
December	−0.22 ± 0.47	−0.89 ± 0.46	−1.06 ± 0.45
Average	+0.10	−0.09	−0.92
QBO	+0.08 ± 0.07	−0.08 ± 0.07	−0.06 ± 0.06
Solar	+4.54 ± 1.70	+1.26 ± 1.68	+0.88 ± 1.53
Yearly calculation:			
Ramp	+0.26 ± 0.15	+0.16 ± 0.17	−0.83 ± 0.13

Using all data
Coefficients for individual stations.
Dobson Units per year change for 1970 through 1986. Model: QS70

Station:	Cagliari	Wallops Is.	Nashville
Monthly calculation:			
January	−0.46 ± 0.53		−0.17 ± 0.36
February	−0.02 ± 0.66		−1.12 ± 0.55
March	−0.00 ± 0.50		−1.30 ± 0.65
April	−1.14 ± 0.50		+0.06 ± 0.63
May	−0.23 ± 0.45		−0.65 ± 0.31
June	−0.77 ± 0.29		−0.87 ± 0.26
July	+0.26 ± 0.27		−1.10 ± 0.29
August	+0.31 ± 0.26		−1.00 ± 0.30
September	−0.05 ± 0.34	No Data	−0.66 ± 0.24
October	+0.03 ± 0.27		−0.53 ± 0.28
November	+0.55 ± 0.31		−0.84 ± 0.35
December	−0.56 ± 0.40		−0.34 ± 0.41
Average	−0.17		−0.71
QBO	−0.01 ± 0.08		−0.02 ± 0.07
Solar	+1.98 ± 2.07		+4.31 ± 1.74
Yearly calculation:			
Ramp	+0.04 ± 0.20		−0.75 ± 0.13

Using all data
Coefficients for individual stations.
Dobson Units per year change for 1970 through 1986.Model: QS70

Station:	Tateno	Srinigar	Kagoshima
Monthly calculation:			
January	−0.50 ± 0.56	−0.19 ± 0.43	−0.56 ± 0.51
February	+0.14 ± 0.57	+0.68 ± 0.59	+0.20 ± 0.46
March	−1.40 ± 0.63	+0.71 ± 0.51	−0.51 ± 0.46
April	−0.24 ± 0.45	+0.12 ± 0.35	+0.40 ± 0.43
May	−0.45 ± 0.32	−0.12 ± 0.31	+0.19 ± 0.29
June	−0.37 ± 0.32	−0.21 ± 0.28	+0.16 ± 0.37
July	−0.01 ± 0.32	−0.46 ± 0.24	0.48 ± 0.29
August	+0.05 ± 0.20	−0.46 ± 0.22	+0.63 ± 0.28
September	+0.22 ± 0.17	−0.07 ± 0.17	+0.62 ± 0.31
October	+0.07 ± 0.21	−0.11 ± 0.26	+0.21 ± 0.30
November	+0.10 ± 0.22	−0.07 ± 0.25	+0.41 ± 0.27
December	−0.30 ± 0.43	+0.28 ± 0.35	+0.08 ± 0.53
Average	−0.22	+0.01	+0.19
QBO	+0.06 ± 0.07	−0.17 ± 0.06	−0.05 ± 0.08
Solar	+1.27 ± 1.57	+3.58 ± 1.38	+0.24 ± 2.47
Yearly calculation:			
Ramp	+0.10 ± 0.15	−0.13 ± 0.12	+0.42 ± 0.20

Using all data
Coefficients for individual stations.
Dobson Units per year change for 1970 through 1986. Model: QS70

Station:	Mauna Loa
Monthly calculation:	
January	−0.62 ± 0.37
February	−0.56 ± 0.52
March	−0.39 ± 0.39
April	+0.07 ± 0.36
May	−0.02 ± 0.20
June	+0.05 ± 0.22
July	+0.12 ± 0.20
August	−0.31 ± 0.18
September	−0.29 ± 0.15
October	−0.20 ± 0.18
November	−0.37 ± 0.29
December	−0.20 ± 0.33
Average	−0.23
QBO	+0.13 ± 0.06
Solar	+1.69 ± 1.55
Yearly calculation:	
Ramp	−0.19 ± 0.13

Using all data
Coefficients for individual stations.
Dobson Units per year change for 1970 through 1986. Model: QS70

Station:	Huancayo
Monthly calculation:	
January	−0.12 ± 0.12
February	−0.19 ± 0.15
March	−0.37 ± 0.15
April	−0.23 ± 0.14
May	−0.12 ± 0.13
June	−0.13 ± 0.16
July	−0.07 ± 0.15
August	−0.15 ± 0.13
September	−0.22 ± 0.12
October	−0.04 ± 0.17
November	−0.00 ± 0.11
December	−0.29 ± 0.12
Average	−0.16
QBO	+0.05 ± 0.03
Solar	+1.12 ± 0.78
Yearly calculation:	
Ramp	−0.16 ± 0.07

(d) Using all data
Coefficients for individual stations.
Dobson Units per year change for 1970 through 1986. Model: QS70

Station:	Aspendale	MacQuarie Isle
Monthly calculation:		
January	−0.53 ± 0.26	0.15 ± 0.59
February	−0.77 ± 0.24	0.32 ± 0.50
March	−0.64 ± 0.24	−0.09 ± 0.48
April	−0.20 ± 0.16	−0.28 ± 0.46
May	−0.60 ± 0.24	−0.28 ± 0.44
June	−0.49 ± 0.31	0.38 ± 0.55
July	−0.67 ± 0.43	0.06 ± 0.56
August	−0.67 ± 0.45	0.50 ± 0.73
September	−0.90 ± 0.44	−0.49 ± 0.96
October	−0.32 ± 0.35	0.15 ± 0.75
November	−0.50 ± 0.28	0.48 ± 0.59
December	−0.75 ± 0.26	−0.26 ± 0.43
Average	−0.59	+0.05
QBO	−0.22 ± 0.06	−0.19 ± 0.12
Solar	−0.30 ± 1.50	−4.97 ± 3.05
Yearly calculation:		
Ramp	−0.45 ± 0.14	−0.02 ± 0.25

Using all data
Coefficients for individual stations.
Dobson Units per year change for 1976 through 1986. Model: QS76

Station:	Reykjavik	Lerwick	Leningrad
Monthly calculation:			
January	No Data	−1.44 ± 0.90	No Data
February		−2.83 ± 1.62	
March		−1.28 ± 1.03	
April		−0.43 ± 0.96	
May		−1.08 ± 0.79	
June		+0.63 ± 0.63	
July		−0.46 ± 0.57	
August		−0.29 ± 0.54	
September		+0.31 ± 0.67	
October		+1.46 ± 0.72	
November		+1.18 ± 0.72	
December		−0.57 ± 0.61	
Average		−0.45	
QBO		−0.24 ± 0.08	
Solar		−1.74 ± 1.94	
Yearly calculation:			
Ramp		−0.19 ± 0.33	

Using all data
Coefficients for individual stations.
Dobson Units per year change for 1976 through 1986. Model: QS76

Station:	Churchill	Edmonton	Goose
Monthly calculation:			
January	No Data	−2.64 ± 1.38	−0.82 ± 1.47
February		−1.07 ± 0.97	−1.43 ± 0.98
March		−2.58 ± 0.96	−1.23 ± 0.93
April		−1.00 ± 0.85	−2.08 ± 1.10
May		−1.28 ± 0.64	−1.20 ± 0.97
June		+0.18 ± 0.68	−0.08 ± 0.53
July		+0.59 ± 0.50	+0.01 ± 0.55
August		+0.27 ± 0.63	−0.16 ± 0.52
September		+0.93 ± 0.75	−0.80 ± 0.57
October		−0.57 ± 0.58	+0.01 ± 0.40
November		+0.84 ± 0.89	+1.07 ± 0.66
December		−0.94 ± 1.47	+0.30 ± 1.09
Average		−0.61	−0.53
QBO		−0.12 ± 0.08	−0.15 ± 0.07
Solar		+1.46 ± 1.91	+4.59 ± 1.92
Yearly calculation:			
Ramp		−0.24 ± 0.32	−0.19 ± 0.26

Using all data
Coefficients for individual stations.
Dobson Units per year change for 1976 through 1986. Model: QS76

Station:	Belsk	Bracknell	Uccle
Monthly calculation:			
January	−0.22 ± 1.20	No Data	No Data
February	−1.32 ± 1.32		
March	−2.23 ± 1.11		
April	−1.09 ± 0.89		
May	−0.44 ± 0.72		
June	−0.16 ± 0.63		
July	+0.28 ± 0.53		
August	−0.46 ± 0.48		
September	−0.62 ± 0.57		
October	−0.60 ± 0.61		
November	−1.64 ± 0.72		
December	−2.14 ± 1.03		
Average	−0.89		
QBO	−0.22 ± 0.08		
Solar	+3.65 ± 2.08		
Yearly calculation:	−0.67 ± 0.28		
Ramp	+		

Using all data
Coefficients for individual stations.
Dobson Units per year change for 1976 through 1986. Model: QS76

Station:	Hradec Kralove	Hohenpeissenberg	Caribou
Monthly calculation:			
January			−0.97 ± 1.37
February			−2.70 ± 1.03
March			−2.39 ± 1.07
April			−1.42 ± 0.99
May			−1.19 ± 0.65
June			−0.24 ± 0.57
July			−0.46 ± 0.41
August			−0.09 ± 0.41
September	No Data	No Data	−0.75 ± 0.52
October			−0.80 ± 0.50
November			−0.54 ± 0.60
December			−2.30 ± 0.84
Average			−1.15
QBO			−0.12 ± 0.07
Solar			+4.76 ± 1.98
Yearly calculation:			
Ramp	0.46 ± 0.35		−0.68 ± 0.27

Using all data
Coefficients for individual stations.
Dobson Units per year change for 1976 through 1986. Model: QS76

Station:	Bismarck	Arosa	Toronto
Monthly calculation:			
January	−1.85 ± 0.79	−0.07 ± 0.81	+0.13 ± 1.23
February	−1.01 ± 0.85	+0.04 ± 1.21	−1.51 ± 0.94
March	−2.27 ± 0.83	−1.65 ± 1.17	−2.30 ± 1.17
April	−1.40 ± 0.81	−1.34 ± 0.84	−1.04 ± 0.90
May	−1.46 ± 0.73	−0.72 ± 0.56	−1.81 ± 0.88
June	−1.01 ± 0.57	−1.00 ± 0.43	−0.33 ± 0.50
July	−0.70 ± 0.46	−0.77 ± 0.36	−1.36 ± 0.41
August	−0.48 ± 0.51	−0.62 ± 0.37	−0.53 ± 0.33
September	+0.32 ± 0.46	−0.99 ± 0.48	−0.36 ± 0.48
October	−0.16 ± 0.65	−0.42 ± 0.56	−1.12 ± 0.59
November	−0.58 ± 0.92	−0.47 ± 0.54	−0.72 ± 0.52
December	−0.97 ± 0.87	−1.55 ± 0.61	−2.08 ± 0.87
Average	−0.96	−0.80	−1.09
QBO	−0.17 ± 0.07	−0.14 ± 0.05	−0.15 ± 0.06
Solar	+4.97 ± 1.93	+2.56 ± 1.14	−0.11 ± 1.67
Yearly calculation:			
Ramp	−0.73 ± 0.27	−0.85 ± 0.19	−0.89 ± 0.22

Using all data
Coefficients for individual stations.
Dobson Units per year change for 1976 through 1986. Model: QS76

Station:	Sapporo	Rome	Boulder
Monthly calculation:			
January	+0.15±0.92	−0.77±0.83	−0.97±0.73
February	+0.48±0.90	−0.37±1.06	−1.80±0.91
March	−1.68±1.03	−0.51±0.96	−2.02±0.97
April	+0.11±0.75	−0.91±0.80	−2.12±0.92
May	+0.51±0.56	+0.05±0.72	−1.15±0.60
June	+0.62±0.61	+0.16±0.51	−2.02±0.51
July	+0.56±0.60	+0.12±0.43	−1.15±0.32
August	−0.40±0.52	+0.70±0.46	−1.52±0.38
September	+0.64±0.43	−0.02±0.47	−1.31±0.35
October	+0.93±0.56	+0.04±0.44	−1.07±0.53
November	+0.95±0.55	−0.23±0.47	−0.49±0.52
December	−0.29±0.79	−0.88±0.78	−1.29±0.71
Average	+0.22	−0.22	−1.41
QBO	+0.09±0.07	−0.08±0.07	−0.06±0.06
Solar	+4.45±1.69	+1.03±1.70	+0.98±1.52
Yearly calculation:			
Ramp	+0.46±0.26	−0.01±0.28	−1.34±0.20

Using all data
Coefficients for individual stations.
Dobson Units per year change for 1976 through 1986. Model: QS76

Station:	Cagliari	Wallops Is.	Nashville
Monthly calculation:			
January	−0.59±0.86		−0.22±0.57
February	−0.29±1.09		−1.23±0.87
March	−0.24±0.83		−1.37±1.04
April	−0.54±0.84		+0.12±1.02
May	−0.65±0.75		−1.01±0.50
June	−1.40±0.48		−1.47±0.42
July	+0.32±0.45		−1.67±0.47
August	+0.24±0.43		−1.39±0.48
September	+0.02±0.57	No Data	−0.92±0.38
October	+0.07±0.46		−1.02±0.45
November	+1.09±0.52		−0.97±0.57
December	−0.49±0.66		−0.30±0.65
Average	−0.20		−0.94
QBO	+0.02±0.08		+0.02±0.07
Solar	+2.02±2.04		+4.21±1.82
Yearly calculation:			
Ramp	0.00±0.34		−1.10±0.24

Using all data
Coefficients for individual stations.
Dobson Units per year change for 1976 through 1986. Model: QS76

Station:	Tateno	Srinigar	Kagoshima
Monthly calculation:			
January	−0.50 ± 0.93	−0.23 ± 0.65	−0.77 ± 0.82
February	+0.51 ± 0.95	+0.71 ± 0.89	+0.21 ± 0.75
March	−1.87 ± 1.05	+0.87 ± 0.80	−0.64 ± 0.75
April	−0.09 ± 0.75	+0.20 ± 0.54	+0.50 ± 0.70
May	−0.58 ± 0.54	−0.19 ± 0.48	+0.08 ± 0.47
June	−0.40 ± 0.53	−0.42 ± 0.45	−0.07 ± 0.60
July	+0.04 ± 0.53	−0.84 ± 0.40	+0.37 ± 0.47
August	+0.08 ± 0.34	−0.86 ± 0.36	+0.71 ± 0.46
September	+0.25 ± 0.29	−0.23 ± 0.28	+0.50 ± 0.51
October	+0.18 ± 0.35	−0.19 ± 0.42	+0.40 ± 0.50
November	+0.12 ± 0.37	+0.07 ± 0.40	+0.29 ± 0.45
December	−0.49 ± 0.73	+0.27 ± 0.57	−0.27 ± 0.88
Average	−0.23	−0.07	+0.11
QBO	+0.06 ± 0.07	+0.17 ± 0.06	+0.05 ± 0.08
Solar	+1.27 ± 1.57	+3.73 ± 1.36	+0.41 ± 2.53
Yearly calculation:			
Ramp	+0.15 ± 0.25	−0.25 ± 0.20	+0.44 ± 0.33

Using all data
Coefficients for individual stations.
Dobson Units per year change for 1976 through 1986. Model: QNS76

Station:	Mauna Loa
Monthly calculation:	
January	−1.01 ± 0.55
February	−0.83 ± 0.77
March	−0.88 ± 0.59
April	+0.17 ± 0.55
May	−0.34 ± 0.31
June	−0.13 ± 0.33
July	+0.06 ± 0.30
August	−0.56 ± 0.27
September	−0.45 ± 0.23
October	−0.43 ± 0.28
November	−0.73 ± 0.43
December	−0.31 ± 0.50
Average	−0.43
QBO	+0.16 ± 0.06
Nuclear	−2.28 ± 1.16
Solar	+0.60 ± 1.57
Yearly calculation:	−0.42 ± 0.20

Using all data
Coefficients for individual stations.
Dobson Units per year change for 1976 through 1986. Model: QS76

Station:	Huancayo
Monthly calculation:	
January	−0.26 + 0.19
February	−0.38 + 0.22
March	−0.58 + 0.24
April	−0.37 + 0.22
May	−0.29 + 0.20
June	−0.42 + 0.26
July	−0.25 + 0.25
August	−0.25 + 0.21
September	−0.32 + 0.19
October	−0.07 + 0.27
November	−0.08 + 0.17
December	−0.50 + 0.19
Average	−0.31
QBO	+0.05 + 0.03
Solar	+1.22 ± 0.76
Yearly calculation:	−0.31 ± 0.10

Using all data
Coefficients for individual stations.
Dobson Units per year change for 1976 through 1986. Model: QS76

Station:	Aspendale	MacQuarie Isle
Monthly calculation:		
January	−0.88 + 0.42	+0.15 + 0.90
February	−1.35 + 0.38	+0.52 + 0.78
March	−1.39 + 0.39	+0.20 + 0.76
April	−0.57 + 0.26	+0.20 + 0.73
May	−1.12 + 0.39	−1.03 + 0.68
June	−0.99 + 0.50	+0.52 + 0.86
July	−1.21 + 0.69	−0.43 + 0.87
August	−1.41 + 0.73	+0.33 + 1.15
September	−1.62 + 0.72	−0.22 + 1.51
October	−0.83 + 0.56	+0.27 + 1.18
November	−1.08 + 0.45	+1.15 + 0.93
December	−1.17 + 0.41	−0.49 + 0.68
Average	−1.14	+0.10
QBO	−0.23 + 0.06	−0.19 + 0.12
Solar	+0.01 + 1.39	+4.96 ± 3.07
Yearly calculation:	−0.98 ± 0.22	−0.16 ± 0.40

(e) Using all data
Coefficients for individual stations.
Dobson Units per year change for 1970 through 1986. Model: QNS70

Station:	Reykjavik	Lerwick	Leningrad
Monthly calculation:			
January		−1.09 + 0.54	
February		−1.94 + 0.95	
March		−0.92 + 0.61	
April		−0.22 + 0.57	
May		−0.60 + 0.47	
June		+0.10 + 0.37	
July		−0.24 + 0.34	
August		−0.35 + 0.32	
September	No Data	+0.23 + 0.40	No Data
October		+1.04 + 0.43	
November		+0.55 + 0.43	
December		−0.50 + 0.36	
Average		−0.33	
QBO		−0.28 + 0.08	
Solar		−3.57 ± 2.00	
Nuclear		−0.71 + 0.27	
Yearly calculation:		−0.18 ± 0.20	

Using all data
Coefficients for individual stations.
Dobson Units per year change for 1970 through 1986. Model: QNS70

Station:	Churchill	Edmonton	Goose
Monthly calculation:			
January		−1.64 + 0.83	−1.08 + 0.93
February		−1.00 + 0.59	−0.94 + 0.62
March		−1.65 + 0.58	−1.00 + 0.59
April		−0.79 + 0.51	−1.38 + 0.69
May		−0.71 + 0.39	−0.75 + 0.61
June		+0.17 + 0.41	−0.12 + 0.33
July		+0.41 + 0.30	−0.02 + 0.34
August		+0.09 + 0.38	−0.04 + 0.33
September	No Data	+0.18 + 0.45	−0.29 + 0.36
October		−0.50 + 0.35	−0.01 + 0.26
November		+0.50 + 0.54	+0.61 + 0.40
December		−0.39 + 0.84	−0.39 + 0.65
Average		−0.44	−0.46
QBO		−0.16 + 0.08	−0.15 + 0.07
Nuclear		−0.62 + 0.27	−0.04 + 0.21
Solar		−0.20 ± 1.95	+4.54 ± 1.98
Yearly calculation:		−0.20 ± 0.19	−0.14 ± 0.17

Using all data
Coefficients for individual stations.
Dobson Units per year change for 1970 through 1986. Model: QNS70

Station:	Belsk	Bracknell	Uccle
Monthly calculation:			
January	−0.58 + 0.77		
February	−1.32 + 0.84		
March	−1.85 + 0.71		
April	−0.48 + 0.57		
May	−0.17 + 0.47		
June	−0.04 + 0.41		
July	+0.37 + 0.34		
August	−0.27 + 0.31		
September	−0.39 + 0.36	No Data	No Data
October	−0.23 + 0.39		
November	−0.85 + 0.46		
December	−1.83 + 0.65		
Average	−0.64		
QBO	−0.22 + 0.08		
Nuclear	−0.37 + 0.43		
Solar	+3.02 ± 2.18		
Yearly calculation:	−0.35 ± 0.19		

Using all data
Coefficients for individual stations.
Dobson Units per year change for 1970 through 1986. Model: QNS70

Station:	Hradec Kralove	Hohenpeissenberg	Caribou
Monthly calculation:			
January			−0.76 + 0.86
February			−1.87 + 0.65
March			−1.74 + 0.67
April			−0.93 + 0.62
May			−0.86 + 0.41
June			−0.15 + 0.36
July			−0.33 + 0.26
August			−0.27 + 0.26
September	No Data	No Data	−0.37 + 0.33
October			−0.37 + 0.32
November			−0.45 + 0.38
December			−1.60 + 0.53
Average			−0.81
QBO			−0.11 + 0.07
Nuclear			+0.09 + 0.32
Solar			+5.05 ± 1.98
Yearly calculation:	−0.20 + .023		−0.47 ± 0.18

Using all data
Coefficients for individual stations.
Dobson Units per year change for 1970 through 1986. Model: QNS70

Station:	Bismarck	Arosa	Toronto
Monthly calculation:			
January	−1.25 ± 0.51	−0.49 ± 0.49	+0.06 ± 0.77
February	−1.20 ± 0.54	−0.14 ± 0.73	−0.88 ± 0.59
March	−1.73 ± 0.53	−1.38 ± 0.70	−1.55 ± 0.72
April	−0.92 ± 0.52	−0.69 ± 0.50	−0.56 ± 0.56
May	−0.96 ± 0.46	−0.48 ± 0.34	−0.84 ± 0.54
June	−0.73 ± 0.36	−0.51 ± 0.26	+0.12 ± 0.31
July	−0.53 ± 0.29	−0.44 ± 0.22	−0.69 ± 0.26
August	−0.25 ± 0.32	−0.39 ± 0.23	−0.25 ± 0.21
September	+0.12 ± 0.30	−0.62 ± 0.29	+0.03 ± 0.30
October	−0.22 ± 0.41	−0.16 ± 0.34	−0.43 ± 0.37
November	−0.46 ± 0.58	−0.42 ± 0.33	−0.22 ± 0.33
December	−0.86 ± 0.55	−1.32 ± 0.37	−1.16 ± 0.54
Average	−0.75	−0.59	−0.53
QBO	−0.18 ± 0.07	−0.15 ± 0.05	−0.13 ± 0.06
Nuclear	−0.80 ± 0.38	−0.60 ± 0.25	+0.38 ± 0.29
Solar	+3.69 ± 1.98	+1.25 ± 1.24	+0.59 ± 1.79
Yearly calculation:	−0.54 ± 0.18	−0.53 ± 0.12	−0.35 ± 0.14

Using all data
Coefficients for individual stations.
Dobson Units per year change for 1970 through 1986. Model: QNS70

Station:	Sapporo	Rome	Boulder
Monthly calculation:			
January	−0.26 ± 0.57	−0.85 ± 0.50	−0.66 ± 0.48
February	+0.13 ± 0.55	−0.44 ± 0.63	−1.55 ± 0.59
March	−1.19 ± 0.63	−0.64 ± 0.57	−1.54 ± 0.63
April	+0.36 ± 0.43	−0.47 ± 0.47	−1.38 ± 0.59
May	+0.32 ± 0.34	+0.00 ± 0.43	−0.82 ± 0.39
June	+0.21 ± 0.37	+0.28 ± 0.30	−1.52 ± 0.33
July	+0.16 ± 0.37	+0.19 ± 0.26	−0.74 ± 0.21
August	−0.13 ± 0.32	+0.61 ± 0.28	−1.09 ± 0.25
September	+0.30 ± 0.26	−0.01 ± 0.28	−0.93 ± 0.23
October	+0.52 ± 0.35	+0.12 ± 0.27	−0.78 ± 0.35
November	+0.58 ± 0.34	−0.26 ± 0.29	−0.41 ± 0.34
December	−0.27 ± 0.48	−1.04 ± 0.46	−1.18 ± 0.46
Average	−0.06	−0.21	−1.05
QBO	+0.08 ± 0.07	−0.10 ± 0.07	−0.05 ± 0.06
Nuclear	−0.18 ± 0.31	−0.55 ± 0.33	−1.14 ± 0.67
Solar	+4.16 ± 1.82	+0.17 ± 1.75	−0.06 ± 1.61
Yearly calculation:	+0.22 ± 0.16	+0.06 ± 0.17	−0.92 ± 0.14

Using all data
Coefficients for individual stations.
Dobson Units per year change for 1970 through 1986. Model: QNS70

Station:	Cagliari	Wallops Is.	Nashville
Monthly calculation:			
January	−0.53 ± 0.54		−0.25 ± 0.37
February	−0.10 ± 0.67		−1.20 ± 0.56
March	−0.07 ± 0.51		−1.40 ± 0.65
April	−0.21 ± 0.52		−0.03 ± 0.64
May	−0.29 ± 0.46		−0.74 ± 0.32
June	−0.82 ± 0.30		−0.95 ± 0.27
July	+0.21 ± 0.28		−1.16 ± 0.30
August	+0.27 ± 0.27		−1.06 ± 0.30
September	−0.10 ± 0.35	No Data	−0.71 ± 0.24
October	−0.02 ± 0.29		−0.60 ± 0.29
November	+0.49 ± 0.33		−0.91 ± 0.36
December	−0.63 ± 0.41		−0.42 ± 0.41
Average	−0.15		−0.78
QBO	−0.00 ± 0.08		+0.01 ± 0.07
Nuclear	−0.38 ± 0.63		−0.54 ± 0.49
Solar	+1.46 ± 2.24		+3.68 ± 1.82
Yearly calculation:	0.00 ± 0.21		−0.81 ± 0.14

Using all data
Coefficients for individual stations.
Dobson Units per year change for 1970 through 1986. Model: QNS70

Station:	Mauna Loa
Monthly calculation:	
January	−0.69 ± 0.36
February	−0.62 ± 0.50
March	−0.48 ± 0.38
April	−0.02 ± 0.35
May	−0.14 ± 0.20
June	−0.09 ± 0.22
July	−0.00 ± 0.20
August	−0.44 ± 0.18
September	−0.41 ± 0.15
October	−0.30 ± 0.18
November	−0.47 ± 0.28
December	−0.29 ± 0.32
Average	−0.33
QBO	+0.16 ± 0.06
Nuclear	−2.73 ± 1.21
Solar	+0.33 ± 1.57
Yearly calculation:	−0.31 ± 0.13

Using all data
Coefficients for individual stations.
Dobson Units per year change for 1970 through 1986. Model: QNS70

Station:	Tateno	Srinigar	Kagoshima
Monthly calculation:			
January	−0.37 ± 0.56	−0.25 ± 0.43	−0.46 ± 0.52
February	+0.27 ± 0.57	+0.62 ± 0.59	+0.30 ± 0.47
March	−1.27 ± 0.63	+0.63 ± 0.52	−0.40 ± 0.48
April	−0.12 ± 0.45	+0.04 ± 0.36	+0.50 ± 0.44
May	−0.35 ± 0.33	−0.19 ± 0.32	+0.27 ± 0.30
June	−0.29 ± 0.32	−0.27 ± 0.29	+0.23 ± 0.37
July	+0.06 ± 0.32	−0.51 ± 0.25	+0.54 ± 0.29
August	+0.12 ± 0.21	−0.51 ± 0.23	+0.68 ± 0.28
September	+0.30 ± 0.18	−0.11 ± 0.18	+0.67 ± 0.31
October	+0.16 ± 0.21	−0.16 ± 0.27	+0.28 ± 0.31
November	+0.20 ± 0.23	−0.12 ± 0.25	+0.49 ± 0.29
December	−0.17 ± 0.44	+0.22 ± 0.36	+0.18 ± 0.54
Average	−0.12	−0.05	+0.27
QBO	+0.07 ± 0.07	+0.18 ± 0.06	+0.06 ± 0.08
Nuclear	+0.65 ± 0.46	−0.72 ± 0.75	+0.46 ± 0.56
Solar	+2.23 ± 1.64	+3.13 ± 1.45	+0.96 ± 2.55
Yearly calculation:	+0.18 ± 0.15	−0.19 ± 0.13	+0.50 ± 0.21

(f) Using all data
Coefficients for individual stations.
Dobson Units per year change for 1976 through 1986. Model: QNS76

Station:	Reykjavik	Lerwick	Leningrad
Monthly calculation:			
January		−1.71 ± 0.89	
February		−3.08 ± 1.59	
March		−1.15 ± 1.01	
April		−0.65 ± 0.94	
May		−1.27 ± 0.77	
June		−0.11 ± 0.62	
July		−0.61 ± 0.57	
August		−0.49 ± 0.53	
September	No Data	+0.09 ± 0.66	No Data
October		+1.19 ± 0.71	
November		+0.88 ± 0.72	
December		−0.87 ± 0.61	
Average		−0.68	
QBO		−0.28 ± 0.08	
Solar		−3.49 ± 1.97	
Nuclear		−0.70 ± 0.25	
Yearly calculation:			
Ramp		−0.43 ± 0.33	

Using all data
Coefficients for individual stations.
Dobson Units per year change for 1976 through 1986. Model: QNS76

Station:	Churchill	Edmonton	Goose
Monthly calculation:			
January	No Data	−2.75 ± 1.36	−0.82 ± 1.47
February		−1.24 ± 0.96	−1.43 ± 0.99
March		−2.76 ± 0.95	−1.23 ± 0.94
April		−1.17 ± 0.84	−2.08 ± 1.10
May		−1.44 ± 0.64	−1.20 ± 0.97
June		+0.05 ± 0.67	−0.09 ± 0.53
July		+0.47 ± 0.50	+0.01 ± 0.55
August		+0.15 ± 0.62	−0.16 ± 0.52
September		+0.76 ± 0.74	−0.80 ± 0.57
October		−0.79 ± 0.58	+0.01 ± 0.41
November		+0.59 ± 0.89	+1.06 ± 0.66
December		−1.01 ± 1.45	+0.30 ± 1.09
Average		−0.76	−0.54
QBO		−0.17 ± 0.07	−0.15 ± 0.07
Solar		−0.21 ± 1.73	+4.57 ± 2.00
Nuclear		−0.60	−0.01 ± 0.21
Yearly calculation:			
Ramp		−0.41 ± 0.31	−0.20 ± 0.27

Using all data
Coefficients for individual stations.
Dobson Units per year change for 1976 through 1986. Model: QNS76

Station:	Belsk	Bracknell	Uccle
Monthly calculation:			
January	−0.27 ± 1.20	No Data	No Data
February	−1.40 ± 1.32		
March	−2.31 ± 1.11		
April	−1.16 ± 0.89		
May	−0.50 ± 0.73		
June	−0.22 ± 0.64		
July	+0.23 ± 0.54		
August	−0.51 ± 0.48		
September	−0.66 ± 0.57		
October	−0.65 ± 0.62		
November	−1.69 ± 0.72		
December	−2.19 ± 1.03		
Average	−0.94		
QBO	−0.23 ± 0.08		
Solar	+3.20 ± 2.18		
Nuclear	−0.28 ± 0.41		
Yearly calculation:			
Ramp	−0.72 ± 0.29		

Using all data
Coefficients for individual stations.
Dobson Units per year change for 1976 through 1986. Model: QNS76

Station:	Hradec Kralove	Hohenpeissenberg	Caribou
Monthly calculation:			
January	No Data	No Data	−0.88 ± 1.37
February			−2.62 ± 1.03
March			−2.31 ± 1.07
April			−1.35 ± 0.99
May			−1.13 ± 0.65
June			−0.19 ± 0.57
July			−0.42 ± 0.41
August			−0.03 ± 0.41
September			−0.68 ± 0.52
October			−0.71 ± 0.51
November			−0.44 ± 0.60
December			−2.21 ± 0.85
Average			−1.08
QBO			−0.10 ± 0.07
Solar			+5.30 ± 2.04
Nuclear			+0.29 ± 0.31
Yearly calculation:			
Ramp	−0.61 ± 0.35		−0.61 ± 0.28

Using all data
Coefficients for individual stations.
Dobson Units per year change for 1976 through 1986. Model: QNS76

Station:	Bismarck	Arosa	Toronto
Monthly calculation:			
January	−1.95 ± 0.79	−0.21 ± 0.81	+0.26 ± 1.22
February	−1.16 ± 0.85	−0.09 ± 1.21	−1.38 ± 0.94
March	−2.42 ± 0.83	−1.78 ± 1.16	−2.18 ± 1.16
April	−1.54 ± 0.81	−1.46 ± 0.83	−0.93 ± 0.90
May	−1.58 ± 0.73	−0.83 ± 0.56	−1.72 ± 0.87
June	−1.11 ± 0.57	−1.09 ± 0.43	−0.25 ± 0.50
July	−0.78 ± 0.46	−0.86 ± 0.36	−1.30 ± 0.41
August	−0.57 ± 0.51	−0.71 ± 0.37	−0.46 ± 0.33
September	+0.23 ± 0.46	−1.09 ± 0.48	−0.27 ± 0.48
October	−0.25 ± 0.65	−0.54 ± 0.56	−1.01 ± 0.59
November	−0.68 ± 0.91	−0.61 ± 0.54	−0.59 ± 0.53
December	−1.08 ± 0.87	−1.70 ± 0.61	−1.94 ± 0.87
Average	−1.07	−0.91	−0.98
QBO	−0.18 ± 0.07	−0.16 ± 0.05	−0.14 ± 0.06
Solar	+4.09 ± 2.00	+1.71 ± 1.20	+0.77 ± 1.73
Nuclear	−0.54 ± 0.37	−0.47 ± 0.23	+0.42 ± 0.27
Yearly calculation:			
Ramp	−0.82 ± 0.27	−0.96 ± 0.19	−0.79 ± 0.22

Using all data
Coefficients for individual stations.
Dobson Units per year change for 1976 through 1986. Model: QNS76

Station:	Sapporo	Rome	Boulder
Monthly calculation:			
January	+0.09 ± 0.92	−0.95 ± 0.83	−1.00 ± 0.74
February	+0.41 ± 0.90	−0.55 ± 1.06	−1.84 ± 0.92
March	−1.74 ± 1.03	−0.68 ± 0.96	−2.07 ± 0.98
April	+0.05 ± 0.75	−1.06 ± 0.79	−2.16 ± 0.92
May	+0.46 ± 0.56	−0.09 ± 0.71	−1.19 ± 0.60
June	+0.58 ± 0.61	+0.04 ± 0.51	−2.05 ± 0.52
July	+0.52 ± 0.60	+0.01 ± 0.43	−1.18 ± 0.33
August	−0.44 ± 0.53	+0.58 ± 0.46	−1.55 ± 0.38
September	+0.59 ± 0.43	−0.16 ± 0.47	−1.34 ± 0.35
October	+0.87 ± 0.57	−0.11 ± 0.44	−1.10 ± 0.54
November	+0.87 ± 0.56	−0.42 ± 0.48	−0.52 ± 0.53
December	−0.37 ± 0.79	−1.07 ± 0.78	−1.32 ± 0.71
Average	+0.16	−0.37	−1.44
QBO	+0.08 ± 0.07	−0.10 ± 0.07	−0.06 ± 0.06
Solar	+4.00 ± 1.78	−0.03 ± 1.75	+0.76 ± 1.61
Nuclear	−0.22 ± 0.30	−0.58 ± 0.32	−0.27 ± 0.62
Yearly calculation:			
Ramp	+0.40 ± 0.27	−0.15 ± 0.28	−1.35 ± 0.21

Using all data
Coefficients for individual stations.
Dobson Units per year change for 1976 through 1986. Model: QNS76

Station:	Cagliari	Wallops Is.	Nashville
Monthly calculation:			
January	−0.66 ± 0.87		−0.04 ± 0.58
February	−0.36 ± 1.10		−1.24 ± 0.88
March	−0.31 ± 0.84		−1.39 ± 1.04
April	−0.61 ± 0.84		+0.10 ± 1.02
May	−0.70 ± 0.76		−1.02 ± 0.51
June	−1.45 ± 0.49		−1.49 ± 0.43
July	+0.28 ± 0.45		−1.68 ± 0.48
August	+0.20 ± 0.44		−1.40 ± 0.48
September	−0.02 ± 0.58	No Data	−0.93 ± 0.38
October	+0.02 ± 0.47		−1.03 ± 0.46
November	+1.03 ± 0.53		−0.98 ± 0.57
December	−0.56 ± 0.67		−0.32 ± 0.66
Average	−0.26		−0.95
QBO	+0.01 ± 0.08		+0.02 ± 0.07
Solar	+1.59 ± 2.18		+4.08 ± 1.92
Nuclear	−0.33 ± 0.60		−0.10 ± 0.49
Yearly calculation:			
Ramp	−0.05 ± 0.35		−1.11 ± 0.25

Using all data
Coefficients for individual stations.
Dobson Units per year change for 1976 through 1986. Model: QNS76

Station:	Tateno	Srinigar	Kagoshima
Monthly calculation:			
January	−0.37 ± 0.92	−0.27 ± 0.65	−0.73 ± 0.82
February	+0.65 ± 0.94	+0.67 ± 0.89	+0.25 ± 0.76
March	−1.74 ± 1.04	+0.81 ± 0.80	−0.59 ± 0.76
April	+0.03 ± 0.74	+0.14 ± 0.55	+0.53 ± 0.71
May	−0.48 ± 0.54	−0.24 ± 0.49	+0.12 ± 0.48
June	−0.32 ± 0.52	−0.47 ± 0.46	−0.05 ± 0.61
July	+0.11 ± 0.52	−0.87 ± 0.40	+0.39 ± 0.48
August	+0.15 ± 0.34	−0.89 ± 0.37	+0.73 ± 0.46
September	+0.32 ± 0.29	−0.26 ± 0.29	+0.52 ± 0.51
October	+0.27 ± 0.35	−0.22 ± 0.43	+0.43 ± 0.51
November	+0.23 ± 0.37	+0.04 ± 0.40	+0.33 ± 0.46
December	−0.36 ± 0.73	+0.22 ± 0.58	+0.23 ± 0.89
Average	−0.13	−0.11	+0.14
QBO	+0.08 ± 0.066	+0.18 ± 0.06	+0.06 ± 0.08
Solar	+2.02 ± 1.62	+3.39 ± 1.44	+0.68 ± 2.66
Nuclear	+0.58 ± 0.44	−0.53 ± 0.69	+0.17 ± 0.55
Yearly calculation:			
Ramp	+0.23 ± 0.25	−0.29 ± 0.20	+0.48 ± 0.34

Using all data
Coefficients for individual stations.
Dobson Units per year change for 1976 through 1986. Model: QNS76

Station:	Mauna Loa
Monthly calculation:	
January	−1.01 ± 0.55
February	−0.83 ± 0.77
March	−0.88 ± 0.59
April	+0.17 ± 0.55
May	−0.34 ± 0.31
June	−0.13 ± 0.33
July	+0.06 ± 0.30
August	−0.56 ± 0.27
September	−0.45 ± 0.23
October	−0.43 ± 0.28
November	−0.73 ± 0.43
December	−0.31 ± 0.50
Average	−0.43
QBO	+0.16 ± 0.06
Nuclear	−2.28 ± 1.16
Solar	+0.60 ± 1.57
Yearly calculation:	−0.42 ± 0.20

B. (ii) Coefficients from latitudinal band averages prepared from the provisionally revised data (Bojkov, private communication, 1987)

60°–80°North
53°–64°North
40°–52°North
30°–39°North

and M–83 USSR regional averages (Bojkov, 1988a)

European part
South Central Asia
Siberia
Far Eastern Asia.

Dobson Only: Latitudes 60–80 Degrees North

Model **Time Period**	**QS70** **1/65–12/86**	**QS76** **1/65–12/86**
January	−1.60 ± 0.51	−2.09 ± 0.77
February	−2.16 ± 0.90	−3.03 ± 1.38
March	−0.83 ± 0.42	−1.41 ± 0.65
April	−0.45 ± 0.40	−0.59 ± 0.62
May	−0.69 ± 0.25	−0.69 ± 0.39
June	+0.05 ± 0.18	+0.17 ± 0.28
July	−0.15 ± 0.20	+0.13 ± 0.32
August	+0.02 ± 0.18	+0.29 ± 0.28
September	−0.06 ± 0.20	−0.08 ± 0.31
October	−0.11 ± 0.32	−0.36 ± 0.49
November	+0.23 ± 0.37	+0.18 ± 0.57
December	−1.06 ± 0.56	−1.72 ± 0.87
Average	−0.56	−0.77
QBO	−0.20 ± 0.057	−0.20 ± 0.57
Solar	+4.78 ± 1.55	+4.84 ± 1.56
Yearly coefficient	−0.12 ± 0.14	−0.05 ± 0.22

Dobson Only: Latitudes 60–80 Degrees North

Model Time Period	QS70 1/57–12/86	QS76 1/57–12/86
January	−0.82 ± 0.51	−1.42 ± .84
February	−1.92 ± 0.91	−3.06 ± 1.53
March	−0.51 ± 0.43	−1.10 ± 0.72
April	−0.08 ± 0.41	−0.21 ± 0.69
May	−0.39 ± 0.26	−0.46 ± 0.44
June	+0.09 ± 0.19	+0.22 ± 0.32
July	+0.09 ± 0.21	+0.36 ± 0.35
August	+0.10 ± 0.19	+0.36 ± 0.31
September	+0.28 ± 0.21	+0.33 ± 0.35
October	+0.60 ± 0.33	+0.53 ± 0.55
November	+1.00 ± 0.38	+1.16 ± 0.63
December	+0.17 ± 0.57	−0.35 ± 0.96
Average	−0.12	−0.30
QBO	−0.12 ± 0.060	−0.11 ± 0.060
Solar	+2.73 ± 1.43	+2.69 ± 1.43
Yearly coefficient	+0.12 ± 0.14	+0.22 ± 0.25

Dobson Only: Latitudes 60–80 Degrees North

Model Time Period	QS70 1/57–12/86	QS76 1/57–12/86
January	−0.91 ± 0.51	−1.53 ± 0.84
February	−2.01 ± 0.91	−3.16 ± 1.51
March	−0.58 ± 0.43	−1.19 ± 0.71
April	−0.15 ± 0.41	−0.29 ± 0.68
May	−0.45 ± 0.26	−0.53 ± 0.43
June	+0.04 ± 0.19	+0.16 ± 0.32
July	+0.04 ± 0.21	+0.31 ± 0.35
August	+0.03 ± 0.19	+0.28 ± 0.32
September	+0.21 ± 0.21	+0.24 ± 0.35
October	+0.52 ± 0.33	+0.42 ± 0.55
November	+0.91 ± 0.38	+1.04 ± 0.63
December	+0.08 ± 0.57	−0.46 ± 0.96
Average	−0.19	−0.39
QBO	−0.13 ± .060	−0.13 ± .060
Solar	+2.12 ± 1.47	+2.11 ± 1.45
Nuclear	−0.22 ± 0.17	−0.22 ± .16
Yearly coefficient	+0.05 ± 0.15	+0.15 ± 0.25

Dobson Only: Latitudes 53–64 Degrees North

Model Time Period	QS70 1/65–12/86	QS76 1/65–12/86
January	−1.84 ± 0.50	−2.31 ± 0.75
February	−1.79 ± 0.71	−2.33 ± 1.05
March	−1.07 ± 0.36	−1.57 ± 0.54
April	−0.52 ± 0.34	−0.84 ± 0.51
May	−0.52 ± 0.27	−0.72 ± 0.42
June	+0.22 ± 0.20	+0.28 ± 0.30
July	0.00 ± 0.22	+0.10 ± 0.34
August	+0.03 ± 0.24	+0.05 ± 0.36
September	+0.03 ± 0.21	+0.07 ± 0.32
October	−0.19 ± 0.21	−0.34 ± 0.32
November	+0.27 ± 0.32	+0.29 ± 0.50
December	−1.17 ± 0.46	−1.77 ± 0.70
Average	−0.55	−0.73
QBO	−0.16 ± 0.059	−0.19 ± 0.056
Solar	+3.92 ± 1.75	+4.4 ± 1.5
Yearly coefficient	−0.14 ± 0.13	−0.24 ± 0.21

Dobson Only: Latitudes 53–64 Degrees North

Model Time Period	QS70 1/57–12/86	QS76 1/57–12/86
January	−0.95 ± 0.48	−1.56 ± 0.79
February	−1.55 ± 0.67	−2.49 ± 1.11
March	−0.69 ± 0.34	−1.29 ± 0.57
April	−0.23 ± 0.33	−0.57 ± 0.55
May	−0.40 ± 0.26	−0.66 ± 0.44
June	+0.06 ± 0.19	+0.12 ± 0.32
July	+0.02 ± 0.21	+0.11 ± 0.36
August	−0.11 ± 0.23	−0.11 ± 0.38
September	+0.21 ± 0.20	+0.30 ± 0.34
October	+0.25 ± 0.21	+0.18 ± 0.34
November	+0.77 ± 0.32	+0.94 ± 0.53
December	−0.21 ± 0.45	−0.76 ± 0.75
Average	−0.24	−0.48
QBO	−0.14 ± 0.054	−0.14 ± 0.054
Solar	+1.99 ± 1.30	+1.96 ± 1.29
Yearly coefficient	+0.03 ± 0.13	−0.03 ± 0.22

Dobson Only: Latitudes 53–64 Degrees North

Model Time Period	QS70 1/57–12/86	QS76 1/57–12/86
January	−1.10 ± 0.47	−1.73 ± 0.78
February	−1.70 ± 0.66	−2.65 ± 1.10
March	−0.83 ± 0.34	−1.44 ± 0.57
April	−0.35 ± 0.33	−0.71 ± 0.54
May	−0.51 ± 0.26	−0.78 ± 0.44
June	−0.04 ± 0.19	+0.07 ± 0.32
July	−0.06 ± 0.21	+0.01 ± 0.35
August	−0.22 ± 0.23	−0.24 ± 0.38
September	+0.09 ± 0.20	+0.15 ± 0.34
October	+0.10 ± 0.21	+0.01 ± 0.34
November	+0.61 ± 0.32	+0.74 ± 0.52
December	−0.38 ± 0.44	−0.96 ± 0.74
Average	−0.37	−0.63
QBO	−0.17 ± 0.054	−0.17 ± 0.054
Solar	+0.82 ± 1.35	+0.90 ± 1.32
Nuclear	−0.48 ± 0.19	−0.47 ± 0.18
Yearly coefficient	−0.09 ± 0.14	−0.18 ± 0.22

Dobson Only: Latitudes 40–52 Degrees North

Model Time Period	QS70 1/65–12/86	QS76 1/65–12/86
January	−0.56 ± 0.45	−0.40 ± 0.67
February	−1.18 ± 0.51	−1.33 ± 0.77
March	−1.33 ± 0.55	−1.61 ± 0.83
April	−0.58 ± 0.41	−1.18 ± 0.62
May	−0.30 ± 0.24	−0.72 ± 0.37
June	−0.39 ± 0.21	−0.77 ± 0.32
July	−0.43 ± 0.20	−0.78 ± 0.30
August	−0.46 ± 0.18	−0.78 ± 0.28
September	−0.53 ± 0.19	−0.86 ± 0.29
October	−0.27 ± 0.26	−0.61 ± 0.40
November	−0.44 ± 0.25	−0.64 ± 0.37
December	−1.08 ± 0.33	−1.10 ± 0.51
Average	−0.63	−0.90
QBO	−0.11 ± 0.057	−0.12 ± 0.056
Solar	+1.76 ± 1.65	+2.04 ± 1.61
Yearly coefficient	−0.47 ± 0.13	−0.83 ± 0.21

Dobson Only: Latitudes 40–52 Degrees North

Model Time Period	QS70 1/57–12/86	QS76 1/57–12/86
January	−0.68 ± 0.43	−0.65 ± 0.70
February	−1.02 ± 0.49	−1.33 ± 0.80
March	−1.23 ± 0.54	−1.69 ± 0.89
April	−0.37 ± 0.40	−0.93 ± 0.66
May	−0.18 ± 0.24	−0.55 ± 0.39
June	−0.09 ± 0.21	−0.41 ± 0.34
July	−0.12 ± 0.19	−0.43 ± 0.32
August	−0.04 ± 0.18	−0.30 ± 0.30
September	−0.11 ± 0.19	−0.40 ± 0.31
October	+0.06 ± 0.26	−0.21 ± 0.43
November	−0.31 ± 0.24	−0.53 ± 0.40
December	−1.01 ± 0.32	−1.20 ± 0.54
Average	−0.42	−0.72
QBO	−0.12 ± 0.057	−0.13 ± 0.057
Solar	−0.75 ± 1.50	−0.79 ± 1.48
Yearly coefficient	−0.15 ± 0.15	−0.47 ± 0.25

Dobson Only: Latitudes 40–52 Degrees North

Model Time Period	QS70 1/57–12/86	QS76 1/57–12/86
January	−0.81 ± 0.43	−0.79 ± 0.69
February	−1.15 ± 0.49	−1.47 ± 0.80
March	−1.35 ± 0.53	−1.82 ± 0.88
April	−0.48 ± 0.39	−1.05 ± 0.65
May	−0.28 ± 0.24	−0.66 ± 0.39
June	−0.17 ± 0.21	−0.51 ± 0.34
July	−0.20 ± 0.20	−0.52 ± 0.32
August	−0.12 ± 0.18	−0.40 ± 0.30
September	−0.21 ± 0.19	−0.51 ± 0.31
October	−0.05 ± 0.26	−0.33 ± 0.43
November	−0.44 ± 0.25	−0.67 ± 0.40
December	−1.14 ± 0.33	−1.35 ± 0.54
Average	−0.53	−0.84
QBO	−0.14 ± 0.057	−0.14 ± 0.057
Solar	−1.68 ± 1.55	−1.57 ± 1.51
Nuclear	−0.50 ± 0.30	−0.46 ± 0.29
Yearly coefficient	−0.24 ± 0.15	−0.58 ± 0.25

Dobson Only: Latitudes 30–39 Degrees North

Model Time Period	QS70 1/65–12/86	QS76 1/65–12/86
January	−0.42 ± 0.30	−0.55 ± 0.44
February	−0.25 ± 0.37	−0.43 ± 0.56
March	−0.72 ± 0.38	−0.95 ± 0.58
April	−0.35 ± 0.27	−0.44 ± 0.41
May	−0.35 ± 0.18	−0.50 ± 0.28
June	−0.64 ± 0.19	−0.91 ± 0.30
July	−0.23 ± 0.18	−0.34 ± 0.29
August	−0.18 ± 0.18	−0.22 ± 0.28
September	−0.17 ± 0.15	−0.20 ± 0.24
October	−0.15 ± 0.14	−0.23 ± 0.21
November	−0.02 ± 0.13	+0.04 ± 0.21
December	−0.38 ± 0.20	−0.54 ± 0.31
Average	−0.32	−0.44
QBO	+0.15 ± 0.050	+0.15 ± 0.051
Solar	+0.22 ± 1.33	+0.27 ± 1.34
Yearly coefficient	−0.16 ± 0.11	−0.21 ± 0.17

Dobson Only: Latitudes 30–39 Degrees North

Model Time Period	QS70 1/57–12/86	QS76 1/57–12/86
January	−0.29 ± 0.28	−0.46 ± 0.46
February	−0.10 ± 0.36	−0.27 ± 0.59
March	−0.42 ± 0.37	−0.69 ± 0.62
April	−0.36 ± 0.26	−0.51 ± 0.43
May	−0.26 ± 0.18	−0.45 ± 0.29
June	−0.43 ± 0.19	−0.74 ± 0.31
July	+0.09 ± 0.18	+0.02 ± 0.30
August	+0.24 ± 0.18	+0.26 ± 0.30
September	+0.14 ± 0.15	+0.14 ± 0.25
October	+0.16 ± 0.13	+0.12 ± 0.22
November	+0.14 ± 0.13	+0.22 ± 0.22
December	−0.24 ± 0.19	−0.43 ± 0.32
Average	−0.11	−0.23
QBO	+0.13 ± 0.046	+0.14 ± 0.046
Solar	+0.76 ± 1.13	+0.73 ± 1.13
Yearly coefficient	+0.05 ± 0.11	+0.03 ± 0.19

Dobson Only: Latitudes 30–39 Degrees North

Model Time Period	QS70 1/57–12/86	QS76 1/57–12/86
January	−0.31 ± 0.29	−0.48 ± 0.46
February	−0.11 ± 0.36	−0.29 ± 0.59
March	−0.43 ± 0.37	−0.71 ± 0.62
April	−0.38 ± 0.27	−0.53 ± 0.44
May	−0.28 ± 0.18	−0.46 ± 0.30
June	−0.44 ± 0.19	−0.75 ± 0.32
July	+0.08 ± 0.18	+0.01 ± 0.30
August	+0.23 ± 0.18	+0.25 ± 0.30
September	+0.13 ± 0.15	+0.13 ± 0.25
October	+0.14 ± 0.14	+0.11 ± 0.23
November	+0.12 ± 0.14	+0.20 ± 0.23
December	−0.26 ± 0.20	−0.45 ± 0.33
Average	−0.13	−0.25
QBO	+0.13 ± 0.047	+0.13 ± 0.047
Solar	+0.64 ± 1.22	+0.61 ± 1.20
Nuclear	−0.09 ± 0.32	−0.09 ± 0.31
Yearly coefficient	+0.05 ± 0.12	+0.02 ± 0.19

European M–83 Regional Average.

Model	QS70	QS76
January	−0.60 ± 0.97	−0.95 ± 1.06
February	−0.95 ± 1.60	−0.67 ± 1.74
March	−2.01 ± 1.21	−2.15 ± 1.38
April	−2.73 ± 1.02	−3.19 ± 1.18
May	−2.12 ± 0.90	−2.45 ± 1.04
June	−0.77 ± 0.63	−0.93 ± 0.72
July	+0.36 ± 0.91	+0.08 ± 1.05
August	−0.25 ± 0.70	−0.52 ± 0.81
September	−0.54 ± 0.56	−0.57 ± 0.65
October	−1.13 ± 0.56	−1.03 ± 0.65
November	−1.26 ± 0.68	−1.33 ± 0.78
December	−1.29 ± 0.82	−1.30 ± 0.95
Average	−1.11	−1.25
QBO	−0.22 ± 0.11	−0.22 ± 0.11
Solar	+2.09 ± 3.17	+2.03 ± 3.11
Yearly coefficient	−0.99 ± 0.40	−1.19 ± 0.46

Far Eastern M–83 Regional Average.

Model	QS70	QS76
January	+0.62 ± 1.09	+0.59 ± 1.17
February	+0.95 ± 1.02	+0.92 ± 1.15
March	−1.49 ± 0.92	−1.73 ± 1.04
April	−0.91 ± 0.89	−1.47 ± 1.01
May	−0.43 ± 0.51	−0.63 ± 0.58
June	−0.05 ± 0.41	−0.03 ± 0.47
July	+0.56 ± 0.59	+0.49 ± 0.66
August	−1.40 ± 0.57	−1.80 ± 0.65
September	−0.64 ± 0.46	−0.72 ± 0.52
October	−0.21 ± 0.26	−0.23 ± 0.29
November	−0.33 ± 0.57	−0.28 ± 0.65
December	−0.76 ± 0.80	−0.84 ± 0.91
Average	−0.34	−0.48
QBO	+0.13 ± 0.079	+0.13 ± 0.078
Solar	+2.36 ± 1.58	+2.35 ± 1.56
Yearly coefficient	−0.30 ± 0.19	−0.40 ± 0.22

Siberian M–83 Regional Average.

Model	QS70	QS76
January	−0.70 ± 1.16	−0.80 ± 1.28
February	−0.70 ± 1.16	+0.04 ± 1.68
March	+0.20 ± 1.28	+0.28 ± 1.51
April	−1.24 ± 1.05	−1.61 ± 1.23
May	−0.37 ± 0.64	−0.46 ± 0.75
June	−0.15 ± 0.58	−0.13 ± 0.68
July	+0.14 ± 0.29	+0.04 ± 0.34
August	−0.87 ± 0.59	−1.17 ± 0.70
September	−1.21 ± 0.69	−1.21 ± 0.81
October	−1.75 ± 0.73	−1.86 ± 0.86
November	−2.94 ± 0.98	−2.99 ± 1.15
December	−2.31 ± 1.01	−2.43 ± 1.19
Average	−0.89	−1.02
QBO	−0.046 ± 0.083	−0.046 ± 0.084
Solar	+0.40 ± 1.78	+0.41 ± 1.82
Yearly coefficient	−0.39 ± 0.25	−0.55 ± 0.29

South Central Asian M–83 Regional Average.

Model	QS70	QS76
January	−1.66 ± 1.15	−1.89 ± 1.25
February	−0.69 ± 1.26	−1.19 ± 1.44
March	+0.43 ± 0.74	+0.29 ± 0.86
April	+0.01 ± 0.89	−0.11 ± 1.04
May	−0.59 ± 0.78	−0.56 ± 0.90
June	+0.00 ± 0.46	+0.00 ± 0.54
July	−0.71 ± 0.45	−0.76 ± 0.52
August	−0.17 ± 0.57	−0.07 ± 0.66
September	−0.06 ± 0.37	−0.06 ± 0.43
October	−0.38 ± 0.56	−0.54 ± 0.65
November	−0.53 ± 0.61	−0.71 ± 0.71
December	−1.41 ± 0.71	−1.53 ± 0.82
Average	−0.48	−0.59
QBO	−0.01 ± 0.09	−0.01 ± 0.09
Solar	+0.29 ± 2.04	+0.26 ± 2.02
Yearly coefficient	−0.28 ± 0.26	−0.36 ± 0.31

CHAPTER 5

Trends in Ozone Profile Measurements

Panel Members

H. Johnston, Chair

A. Aikin
R. Barnes
S. Chandra
D. Cunnold
J. DeLuisi
J. Gille
R. Hudson
M. P. McCormick
L. McMaster
A. J. Miller
R. Nagatani
W. Planet
E. Remsberg
D. Rusch
C. Trepte
R. Veiga
P. Wang
C. Wellemeyer
J. Zawodny

Chapter 5

Trends in Ozone Profile Measurements

Contents

5.1 SUMMARY AND INDEX

After a general introduction to the nature of this chapter, a brief summary of each section is given as an extended index.

5.1.1 Introduction

Atmospheric modelers predicted (in 1984, for example) that, within about a century, release of chlorofluorocarbons at the 1980 rate (along with a doubling of carbon dioxide and methane and a 20 percent increase of nitrous oxide) would change the global average ozone column between +0.2 and −5.2 percent, and that the change in local ozone at 40 km would be −35 to −55 percent (*WMO*, 1986, Chapter 13). Because local ozone in the upper stratosphere has great sensitivity to chlorine, there is an emphasis on studying this region as a possible early indicator of global ozone change. The Solar Backscatter Ultraviolet (SBUV) satellite instrument has four channels that are used to measure total ozone, and other channels that are used to measure the vertical profile of ozone in the upper stratosphere. The ground-based Dobson stations measure the total ozone vertical column; some Dobson instruments are used in the Umkehr mode to measure the vertical profile of ozone. Chapter 4 is concerned with trends that have occurred in the ozone vertical column, and Chapter 5 addresses trends in the vertical profiles of ozone in the upper stratosphere, where ozone is especially sensitive to chlorine. This region is variously given as 30 km to 50 km, 16 mb to 1 mb, or Umkehr layers 6 through 9.

The SBUV instrument was launched on the Nimbus–7 satellite in October 1978. For the period 1979–1985, the newly (1986) interpreted data showed, among many other things, 1) that the maximum local ozone reduction occurred at an altitude of 50 km, instead of at the theoretically predicted 40 km (*WMO*, 1986, Chapter 13) and 2) that, between ±30 degrees latitude, the maximum local ozone reduction was 20 to 25 percent instead of the theoretically predicted 10 to 15 percent (*WMO*, 1986, page 761). The relatively narrow purpose of this chapter is to confirm, disprove, or modify the SBUV-reported ozone changes in the middle and upper stratosphere. Eight other satellite and ground-based systems were identified that give information about the ozone vertical profile between 1979 and 1987 and that are judged applicable to this study (Table 5.1). To the extent that the SBUV trends are not supported, the question becomes: What trends in ozone are indicated by the other observations?

Table 5.1 Ozone Measuring Systems and Periods of Available Data

Type	Description	Time Period
Satellite	SBUV	October 1978 to February 1987
Satellite	SAGE	February 1979 to November 1981
Satellite	SAGE–II	November 1984 to present
Satellite	SBUV–II	December 1984 to present
Ground-based	Umkehr stations using Dobson spectrophotometer	1950's to present
Satellite	SME	January 1982 to December 1986
Satellite	SMM	(SMM or UVSP) 1985 to present
Satellite	LIMS	October 1978 to May 1979
Rocket	ROCOZ–A	1985

5.1.2 Solar Backscatter Ultraviolet (SBUV) Instrument

According to the archived SBUV data for 1979–1986, the ozone changes are not subtle effects buried in noisy data, requiring a detailed analysis to see whether they are statistically significant. They are large effects, clearly visible to the naked eye (Figures 5.1–4). The approach of this chapter is first to compare the SBUV results against other satellite and ground-based systems in terms of conspicuous aspects of the primary data, and only later to examine derived statistical quantities.

5.1.3 Ozone Trends From Comparison of Stratospheric Aerosol and Gas Experiment (SAGE) –I and –II

5.1.3.1 Conspicuously Visible Results

A comparison of SAGE–I and SBUV ozone measurements is presented for February 1979 through November 1981, and of SAGE–II and SBUV ozone measurements for October 1984 through December 1986. The SBUV data were searched for those events nearly coincident in time and space to the SAGE–I and –II events (Figure 5.5). The working data for such coincidences were analyzed as time series in several latitude bands; e.g., see Figures 5.6–11 for Umkehr layers 6 to 9 at 40°N and 40°S. With some exceptions at layer 6, SAGE–I ozone layer amounts are consistently lower, by 4 or 5 percent, than SBUV amounts in 1979–1981, but SAGE–II ozone layer amounts are consistently higher, by 10 ± 3 percent, than SBUV amounts in 1984–1986—a change of up to 15 percent. For Umkehr layers 6 through 9, the 1980–1985 offset between SAGE and SBUV data increases monotonically with altitude by between 4 percent and 15 percent (Figure 5.16). The magnitude and sign of this conspicuous offset are a large fraction of the entire change in ozone given by SBUV data between 1979 and 1986 (Figure 5.4). The large decrease in ozone that SBUV reports in layers 7 to 9 over this same period, 8 to 17 percent, is not supported by SAGE–I and SAGE–II data comparisons. On the basis of conclusions reached in Chapters 2 and 3, this difference is ascribed to an insufficiently corrected degradation of the SBUV diffuser plate.

5.1.3.2 Small Ozone Changes Requiring Careful Statistical Analysis

SAGE–I and SAGE–II satellite data were used to estimate the change in the upper stratospheric ozone profile between 1980–1981 and 1985–1986. The fundamental SAGE measurements are concentration profiles as a function of geometric altitude from 25 km to 50 km. On the basis of spatial intersections between SAGE–I and SAGE–II over corresponding 2-year periods that are 5 years apart, comparisons are performed between SAGE–I and SAGE–II ozone concentration measurements. (Because of the differences in the sampling pattern, the number of intersections between SAGE–I and SAGE–II is much smaller than the number of coincidences between SAGE and SBUV, causing the SAGE–I and –II comparisons to be noisy. Compare Figure 5.5) The percentage differences are averaged in time within 10-degree latitude bands and plotted versus altitude in Figure 5.17. The magnitude of the differences is only on the order of 5 percent. The altitudes of maximum percentage ozone reduction are between 40 km and 45 km, and the magnitudes of these reductions vary between 2 and 8 percent. With some exceptions, the pattern is an ozone decrease in the upper stratosphere and another decrease, near 25 km, between 1980 and 1986.

These ozone profiles were averaged over the region of maximum density of SAGE–I and –II coincidences, 20–50°N and 20–50°S (Figure 5.18). The average ozone profiles show an ozone

decrease between 35 km and 45 km, with the maximum ozone reduction of 3 percent occurring at 40 km; another region of similar percentage ozone decrease occurring at about 25 km; and essentially zero ozone change at 30 km and at 50 km. The 95 percent confidence level for the average ozone reduction in the upper stratosphere indicated by SAGE over the 5-year period is ± 3 percent. The estimated relative systematic error is ± 2 percent between the SAGE–I and SAGE–II instruments. The unexpected 3 percent ozone reduction indicated at 25 km, near the ozone concentration maximum, should be given careful consideration in the future to see if it is a weak manifestation of the low-temperature ozone destruction process shown in the Antarctic spring.

5.1.4 Solar Backscatter Ultraviolet II (SBUV–2)

The national plan for ozone monitoring is to launch other SBUV instruments, about every 2 years, to obtain overlapping periods of ozone satellite data, and to use this matching procedure, along with the Dobson instruments, to correct for instrumental degradation. The first example of this plan was the SBUV–2 system, launched in December 1984, which has been returning data suitable for deriving total ozone and ozone profiles since early 1985. The most powerful method of verifying, modifying, or disproving the SBUV-reported trends would be to compare at least two aspects of SBUV and validated SBUV–2 data: 1) the ozone magnitudes reported by the twin instruments immediately after launch, and 2) any change using the first 2 years of SBUV and the corresponding 2 years of SBUV–2 5 years later (as was done with SAGE–I and –II). Members of the team responsible for SBUV–2 data told the Ozone Trends Panel in January 1988 that the reinterpreted data were so preliminary and so incompletely examined (even 3 years after launch) that they should not be used in this report.

5.1.5 Umkehr Measurements of Upper Stratospheric Ozone

Direct examination of the Umkehr data for layers 6, 7, and 8 shows that ozone decreased noticeably between 1979 and 1986, but this simple method of inspection is complicated by the large effect of aerosols from the El Chichón eruption in the middle of this period (Figures 5.24–26). In terms of the injected quantity of stratospheric sulfate aerosols, El Chichón was one of the most powerful volcanoes of the century. An objective method for correcting the effect of aerosols on Umkehr observations uses stratospheric aerosol profiles observed by light detection and ranging (lidar), a particle-size distribution based on stratospheric (but not site-coincident) measurements, ozonesonde profiles, and radiative transfer theory similar to that for the Umkehr inversion algorithm. This method was applied to five northern midlatitude Umkehr stations (between 36°N and 52°N) to estimate changes in the ozone profile from 1978 through 1987. Combining statistical errors and estimated errors caused by aerosols, Umkehr data for five stations show ozone changes: −3 ± 3 percent in layer 6; −8 percent ± 4 percent in layer 7; and −9 percent ± 5 percent in layer 8, between 1979 and 1986. At layer 8, for example, the ozone change given by SBUV is about −15 percent (Figure 5.4) and that given by SAGE–I and –II is −3 ± 3 percent (Figure 5.18). The SAGE and Umkehr error estimates are for a 95 percent confidence level but do not include possible systematic errors.

5.1.6 SBUV, SAGE–I, Limb Infrared Monitor of the Stratosphere (LIMS) Ozone Intercomparison (Spring 1979)

These data show that three totally different, newly launched satellite systems agree with each within a range of about 4 percent in measuring zonal mean ozone amounts in Umkehr layers 6 to 9.

5.1.7 Trends at Upper Boundary of the Stratosphere (SBUV, Solar and Mesosphere Explorer [SME], and Solar Maximum Mission [SMM])

At 1 mb, the upper altitude limit of SBUV measurements and the lower altitude limit of SME measurements, 5 years of SME data (1982–1986) and 3 years of SMM data (1985–1987) at 55 km show no conspicuous ozone decrease. This absence of trend at 55 km is evidence against a 20 percent decrease at 50 km, which is given by SBUV.

5.1.8 Rocket Ozonesonde (ROCOZ–A)

In March to April 1979 and 1985, two series of rocket ozone soundings were conducted at Natal, Brazil. Above 22 km, stratospheric ozone variability was 2 percent or less during the 3 weeks of each measurement campaign, with stratospheric temperature and pressure variabilities half that amount. ROCOZ–A was used as a transfer instrument to compare various satellites during one of these periods of quiet atmosphere. For Umkehr layers 6, 7, 8, and 9, five instruments (in 1979, SBUV, LIMS, and SAGE–I; in 1985, SBUV, SAGE–II, and ROCOZ–A) gave instrument-to-instrument variability of 4 or 5 percent.

In Section 5.1.2 it is stated that this chapter looks first for conspicuous trends in the data, readily seen by the eye. In this section, this approach is extended to obtain an overall judgment about the ability of satellites to measure trends in upper stratospheric ozone.

5.2 SOLAR BACKSCATTER ULTRAVIOLET INSTRUMENT (SBUV)

The SBUV instrument, launched on the Nimbus–7 satellite in October 1978, was in operation until February 1987. It measured backscattered ultraviolet solar radiation at a time close to local noon; algorithms translated these measurements into vertical profiles of ozone from the middle to the top of the stratosphere. Additional channels of the instrument simultaneously measured the total vertical ozone column. In its circumpolar orbit, SBUV obtained enough data in a day to yield the total ozone column and the vertical ozone profile between about 30 km to 50 km over the entire globe, except the region of polar night (Bhartia et al., 1985). This accumulation of ozone measurements has gone on continually from late 1978 to mid-1987 to yield a magnificent body of data.

These ozone data are the product of remote measurements, and the final product is the result of an inversion of the physical measurements using a mathematical algorithm and requiring input of other atmospheric quantities. The NASA Ozone Processing Team translated the raw physical measurements from SBUV and deposited the results in a publicly available archive. For the period 1979–1985, the newly interpreted data showed, among other things, that the maximum local ozone reduction occurred at an altitude of 50 km and that there was more than a 20 percent local ozone reduction from pole to pole at 50 km. For 1985 relative to 1979, atmospheric modelers calculate that chlorofluorocarbons and variations in the solar cycle would have reduced local ozone by a maximum of about 5 to 12 percent and the altitude of maximum reduction would be about 40 km (see Chapter 7 of this report).

In the summer of 1986, a member of the NASA Ozone Processing Team presented the SBUV results to the Subcommittee on Health and the Environment of the House Committee on Energy and Commerce. Members of Congress expressed their concern that if ozone is really decreasing two or three times faster than the atmospheric modelers predict, and in a different region of the

stratosphere, it is very important to understand why it is happening. In direct response to the Congressional request, the Ozone Trends Panel was established. The following samples of SBUV data illustrate the features that stimulated the formation of the Ozone Trends Panel.

The global series (70°S to 70°N) of monthly average ozone data for November 1978 through September 1984 is shown for Umkehr layers 6 to 9 in Figure 5.1. The plots in the left column show the original data in Dobson units, and those in the right column show data that have been deseasonalized by removing the annual and semiannual seasonal components (Reinsel et al., 1988). The plots show a definite downward trend in the SBUV ozone data, and annual variations that are larger than the decreasing trend. The graphs of ozone in Umkehr layer 6 show a sharp dip beginning in mid-1982, ascribed to the volcanic eruption of El Chichón in April 1982.

The ozone data at the 1-mb level from the SBUV files are plotted for 40°N and 10°N latitudes and as a function of time from fall 1978 to spring 1987 in Figure 5.2 (Aikin, private communication, 1987). Like Figure 5.1, this figure shows conspicuous ozone decreases between 1979 and 1987, and seasonal oscillations of ozone even larger than the decreasing trend. Figure 5.2 illustrates an important sampling requirement for any attempt to check the SBUV data against limited data sets. If one used n + ½ years of data, for example, one would produce strongly different linear trends depending on whether the first point was at the minimum or maximum of the seasonal cycle. One should use an exactly integral number of years of data or a proper statistical method to remove seasonal oscillations.

Another presentation of SBUV data is given in Figure 5.3, which for 50°S shows vertical profiles of ozone mixing ratios from 25 km to 57 km and for the intervals 1979–1982, 1979–1984, and 1979–1986 (Chandra, 1987). For 1979–1986, the maximum ozone reduction, 25 percent, occurs at 50 km. Figure 5.4 shows a more extensive set of similar data given as contour plots of local ozone reduction as a function of altitude and latitude. This figure shows local ozone reductions at 50 km to be 20 percent or more at all latitudes (Chandra, 1987).

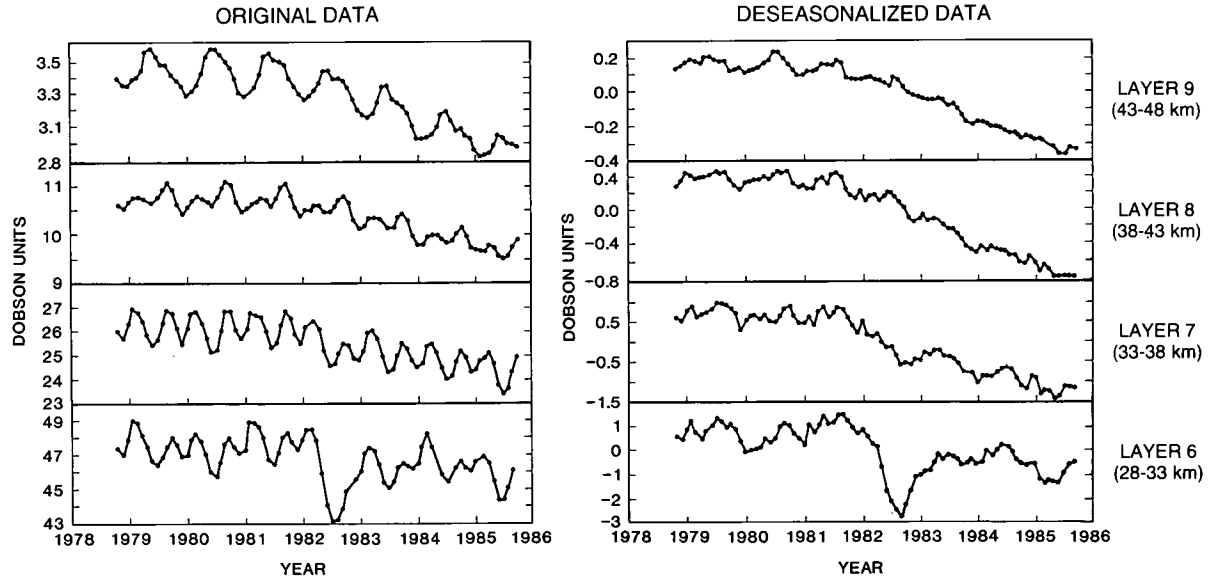

Figure 5.1 Global averages of SBUV ozone data for November 1978 to September 1984 using data between 70°S and 70°N with equal surface weighting, including Umkehr layers 6 to 9.

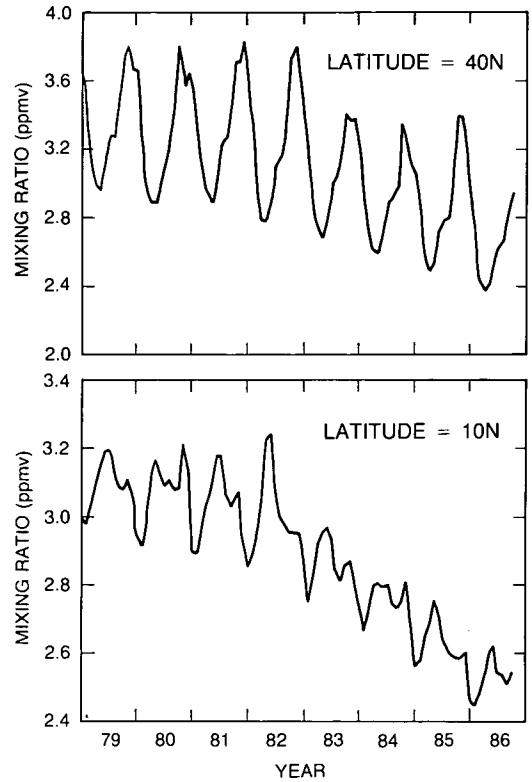

Figure 5.2 The SBUV weekly mean mixing ratios at 1.0 mb (about 50 km) for latitudes 10°N and 40°N.

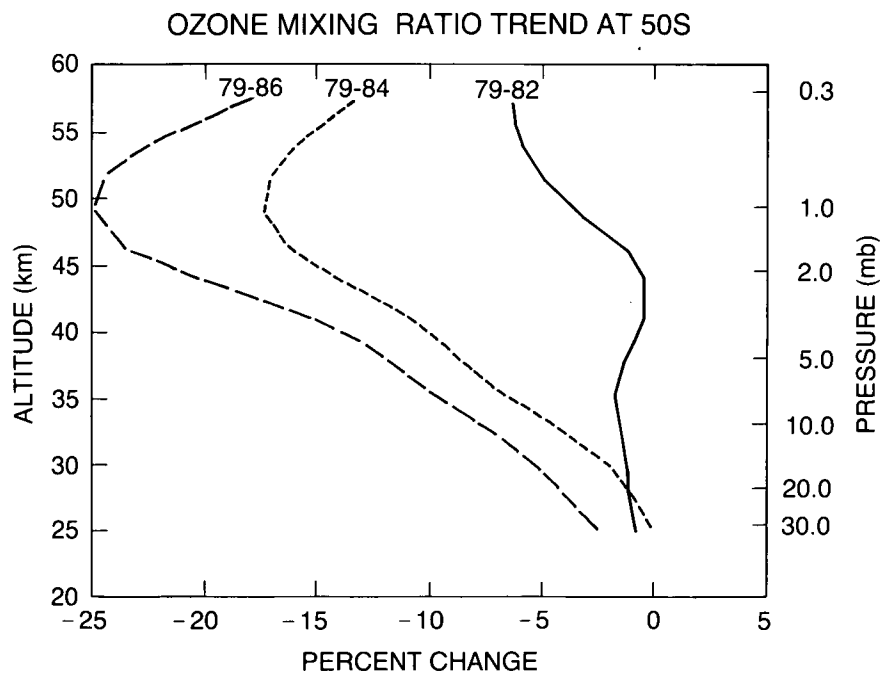

Figure 5.3 The trend in SBUV ozone mixing ratio as a function of height for three periods, January 1979 to March 1982 (pre-El Chichón period), January 1979 to December 1984, and January 1979 to October 1986. For each period, the percentage change is computed using a least square fit of a time series containing the annual, semiannual, and linear trend terms (Chandra, 1987).

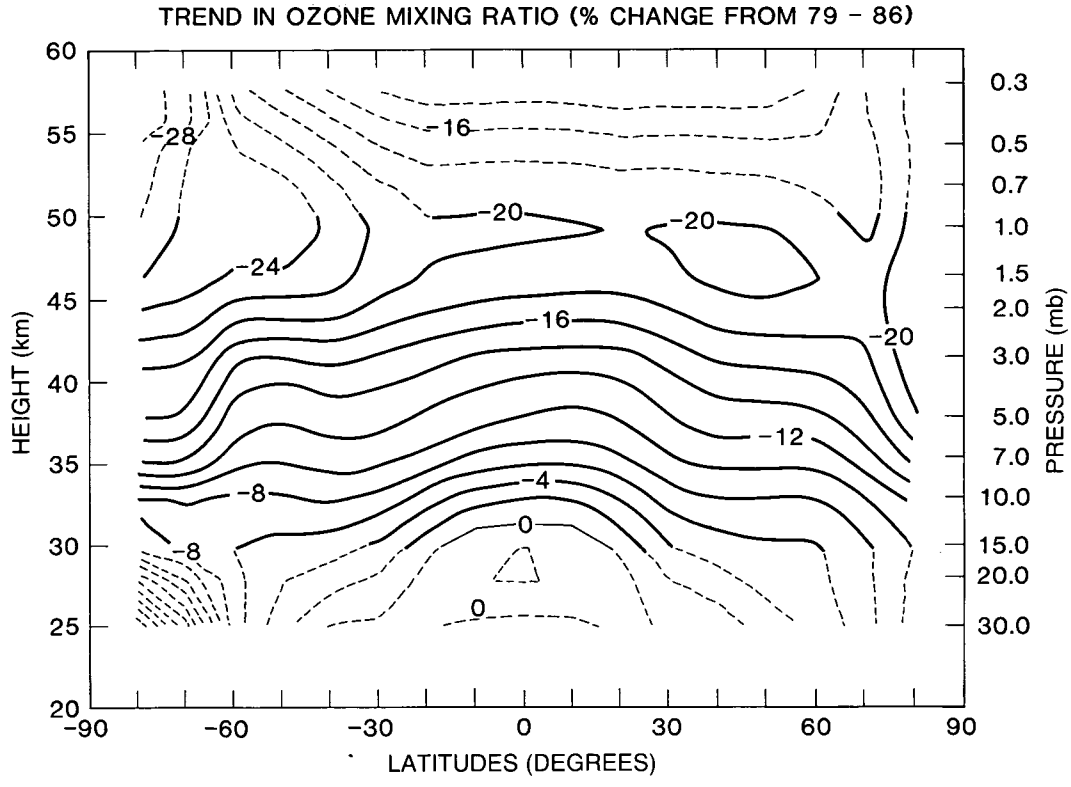

Figure 5.4 The percentage change in ozone mixing ratio as a function of altitude and latitude from 1979–1986. The percentage change is computed for each pressure and latitude, as in Figure 5.3.

Eight other systems (listed in Table 5.1) give information about the ozone vertical profile between 1979 and 1987 and are judged to be applicable to this study. In checking the SBUV trends, it must be appreciated that the SBUV data represent the only complete global set collected on a daily basis over an 8-year period. Other ozone data sets have one or more restrictions: limited time coverage, limited spatial coverage, or limited altitude range. In most comparisons reported here, the data of these restricted systems are matched in space and time with a portion of the data of the complete SBUV set. For any single comparison, differences between SBUV and the other system could be due to systematic errors in SBUV, to systematic errors in the other system, to the mutual errors of the two systems, or to sampling errors.

As discussed in Chapter 2, the different instruments measure different properties of ozone; it is sometimes not a straightforward matter to compare one system with another. For example, the primary data product from SBUV is the column of ozone over the Umkehr ozone layers, defined in terms of atmospheric pressure, and the primary data product from SAGE is the ozone concentration as a function of altitude. For these two systems to be compared, it is necessary to translate the SAGE concentrations into SBUV pressure layers using local atmospheric temperatures and pressures from roughly coincident auxiliary meteorological observations. Between the beginning of this study in December 1986 and its conclusion in April 1988, most of the satellite data sets were reevaluated from the beginning to maximize their value in testing for ozone trends.

Since the archived SBUV data challenge the results of current theoretical models, theoretical models are not used as a screen for what to believe or not as far as the data are concerned. The

first examination of the data is strictly empirical; evaluations are based on considerations such as calibration, algorithms, statistics, and searching examinations for systematic errors. The stratosphere is extremely complex, and not all data studied here point in the same direction. The approach used is one of considering all the data, considering the results from this report's chapters on calibrations and algorithms, and formulating general conclusions, including estimates of errors. These general conclusions, derived from the observational data, are then compared with theoretical predictions of the atmospheric models.

5.3 OZONE TRENDS FROM COMPARISON OF SAGE–I and SAGE–II

5.3.1 Introduction

The two satellite experiments, SAGE–I and SAGE–II, infer atmospheric constituents by measuring the solar-spectral transmission profiles attenuated by the Earth's limb during a local satellite sunrise or sunset (solar occultation technique). This method is suited to measuring long-term changes in atmospheric species because it is self-calibrating—that is, the measured solar irradiances are normalized with respect to the observed unattenuated solar irradiance for each profile. The presence of ozone is inferred from the transmission measurements in the 600 nm region at the center of the Chappius band, using an iterative onion peel inversion scheme (discussed in detail in Chapter 3). The constructed ozone profiles extend from cloud tops upward to a height where the signal-to-noise ratio limits the usefulness of the information; for SAGE–I, the upper limit is about 55 km, and for SAGE–II it is approximately 65 km. The vertical resolution of the retrieved ozone profile is 1 km, but because of increased random noise at higher altitudes, each profile of ozone concentration is smoothed over a 5 km layer at heights greater than about 45 km.

SAGE–I and SAGE–II use essentially the same instrument design; both instruments have almost identical optical pathway assemblies. Minor differences between the two sensors lie in the addition of three more channels to the SAGE–II instrument to the four on SAGE–I, the use of a rectangular field of view on SAGE–II versus a circular one on SAGE–I, and the use of narrower band passes on SAGE–II.

The principal sources of error in the measurement of an individual ozone profile are radiometric imprecision, digitizer truncation, and scan-mirror pointing errors. These random errors are approximately uncorrelated vertically; their combined effect on an individual retrieved ozone profile is estimated at each point on the profile from the variance of the measurements from approximately four to five scans of the SAGE mirror across the viewing altitude. This uncertainty is provided to the data user in the form of error bars for each ozone profile. Each SAGE profile, however, also possesses an uncertainty in reference altitude of approximately 0.25 km, which contributes to uncertainties in profile repeatability.

Table 5.2 lists the expected systematic errors of SAGE–I and SAGE–II ozone measurements. The principal uncertainties arise from instrument scan-mirror calibration and our knowledge of the absorption cross-section of ozone at 0.6 fm convolved with instrument bandpass and solar spectrum. Aerosols can also produce biases in the ozone retrievals, but only at altitudes where aerosol concentrations are large (i.e., mostly below 25 km). Table 5.3 lists the random-error estimates of the SAGE–I and –II instruments. As can be seen, the random error components for both SAGE instruments are about 10 percent, for a vertical resolution of 1 km. As indicated in Table 5.2, the imprecision is much less for SAGE estimates of the ozone content of Umkehr

Table 5.2 SAGE Systematic Errors

	SAGE–I	SAGE–II
Ozone absorption cross-section	6 %	6 %
Scan mirror calibration	2.0%	1.0%
Rayleigh cross-section	0.5%	0.5%
Aerosol optical properties		
Altitudes <25 km	4.0%	4.0%
Altitudes >25 km	<1.0%	<1.0%

Table 5.3 SAGE Errors Affecting the Precision and Repeatability of Ozone Measurements for a Vertical Resolution of 1 km

	Random errors	
Altitude (km)	SAGE–I and –II (%)	Ozone errors due to 0.25 km uncertainty in reference height (%)
45	12	6
35	9	6
25	8	3

layers. Thus, the absolute uncertainty in the SAGE measurements is approximately 6 percent between 25 km and 50 km altitude, provided a sufficient number of measurements is made. The relative systematic error between the SAGE instruments is expected to be 2 percent or less (Cunnold et al., 1984 and 1989; McCormick et al., 1984a). For the sake of this report, all SAGE–I and SAGE–II ozone data were recalculated on a common basis using the most recent physical and spectroscopic data. This major reworking of raw data and indepth interpretation of the results were completed by the SAGE team in 6 months.

5.3.2 Calculation of SAGE–I and –II Umkehr Layer Amounts

The primary ozone data product of SAGE–II is concentration as a function of geometric altitude with a vertical resolution of 1 km. In order to generate a data product from SAGE–I and –II, comparable to that of SBUV, SAGE–I and –II profiles must be vertically integrated over pressure levels corresponding to the Umkehr layers used with the SBUV data. Thus, there must be a conversion from SAGE–I and –II altitudes to pressure levels. Meteorological information used to make this conversion was obtained from the National Meteorological Center (NMC) global data set.

Given an Umkehr layer bounded by pressure levels p_b and p_t, the objective is to obtain an estimate of the layer amount as given by the integral

$$N = \int_{h_b}^{h_t} n(h)\, dh$$

where $n(h)$ is the SAGE–I and –II ozone number density and h is altitude, with h_b and h_t the altitudes corresponding to the pressure levels p_b and p_t, respectively. The trapezoidal rule was

used to obtain the approximation to N. The only assumption was that the logarithm of pressure varies linearly with altitude over the range of 1 km or less. Linear interpolation was used to obtain estimates of the SAGE–I and –II ozone concentration corresponding to the pressure levels pb and pt. Only layer amounts corresponding to Umkehr layers 6 to 9 were computed and compared in this study.

5.3.3 Generation of Matching Pairs Between SAGE and SBUV Data

Interannual atmospheric variability of ozone, combined with the differences between SAGE–I and –II and SBUV geographical coverage, preclude any simple comparison between the ozone layer amounts reported by both instruments. To minimize these inherent differences, the SBUV Nimbus–7 Compressed Profile Ozone (CPOZ) Version 5 data were searched for those events nearest in space and time to individual SAGE–I and –II events. The "pairing" of the satellite observations is expected to eliminate biases in the comparison due to seasonality and spatial sampling differences. SAGE–I and –II pairs were generated in the following manner: for each SAGE–I or SAGE–II event, all SBUV events within 12 hours of the SAGE event were isolated; from these SBUV events, the one that was spatially closest in longitude and latitude to the SAGE event was chosen.

The SBUV data search produced approximately 6,500 SAGE–I/SBUV pairs that, on average, were separated by 0.3 ± 0.1 day in time, 7 ± 6 degrees in longitude, and 1 ± 1 degrees in latitude. Approximately 19,000 SAGE–II/SBUV pairs were generated that, on average, had a separation of 0.3 ± 0.1 day in time, 6 ± 4 degrees in longitude, and 1 ± 1 degrees in latitude. The working set of SAGE–I and –II/SBUV pairs encompassed the periods February 22, 1979, to September 28, 1981, and October 25, 1984, to December 31, 1986; the first period corresponds to almost all of the measurement period for SAGE–I, and the second to the first 2 years of SAGE–II measurements.

SAGE–I and –II scan the atmosphere at Earth's limb near the terminator twice on each of its 15 daily orbits. The orbital inclination causes the observation latitude to range periodically from approximately 75°S to 75°N. The latitudes of the SAGE–I measurement locations are displayed in Figure 5.5. Due to the SAGE–I orbital elements, the exact date of repeat coverage changes from year to year. The latitudes of SAGE–II measurement locations also are displayed in Figure 5.5. Unlike SAGE–I, almost perfect overlap occurs in latitude from one year to the next. Any gaps in the curves are periods during which no satellite occultations occurred. Because of power problems on the satellite, only sunset data were taken by SAGE–I after July 1979.

For analysis purposes, the SAGE–I and –II and SBUV pairs were spatially grouped into 13 latitude bands of a 10-degree width each. These are marked in Figure 5.5, with bands centered at 0, ±10, ±20, ±30, ±40, ±50, and ±60 degrees. The pairs were also temporally grouped into clusters. A cluster is a collection of events sampled between the time SAGE–I and –II enter, and subsequently exit, a given latitude band. The duration defining a cluster is limited to a maximum of 1 week. A given latitude band might contain more than one cluster if SAGE sampled the latitude for a period greater than 1 week.

5.3.4 Characteristics of the SAGE–I and –II and SBUV Layer Amounts

When arranged in a time series, the sequence of cluster means displays the expected features of seasonal ozone variability. The cluster means of SAGE–I and SBUV are shown in Figures 5.6,

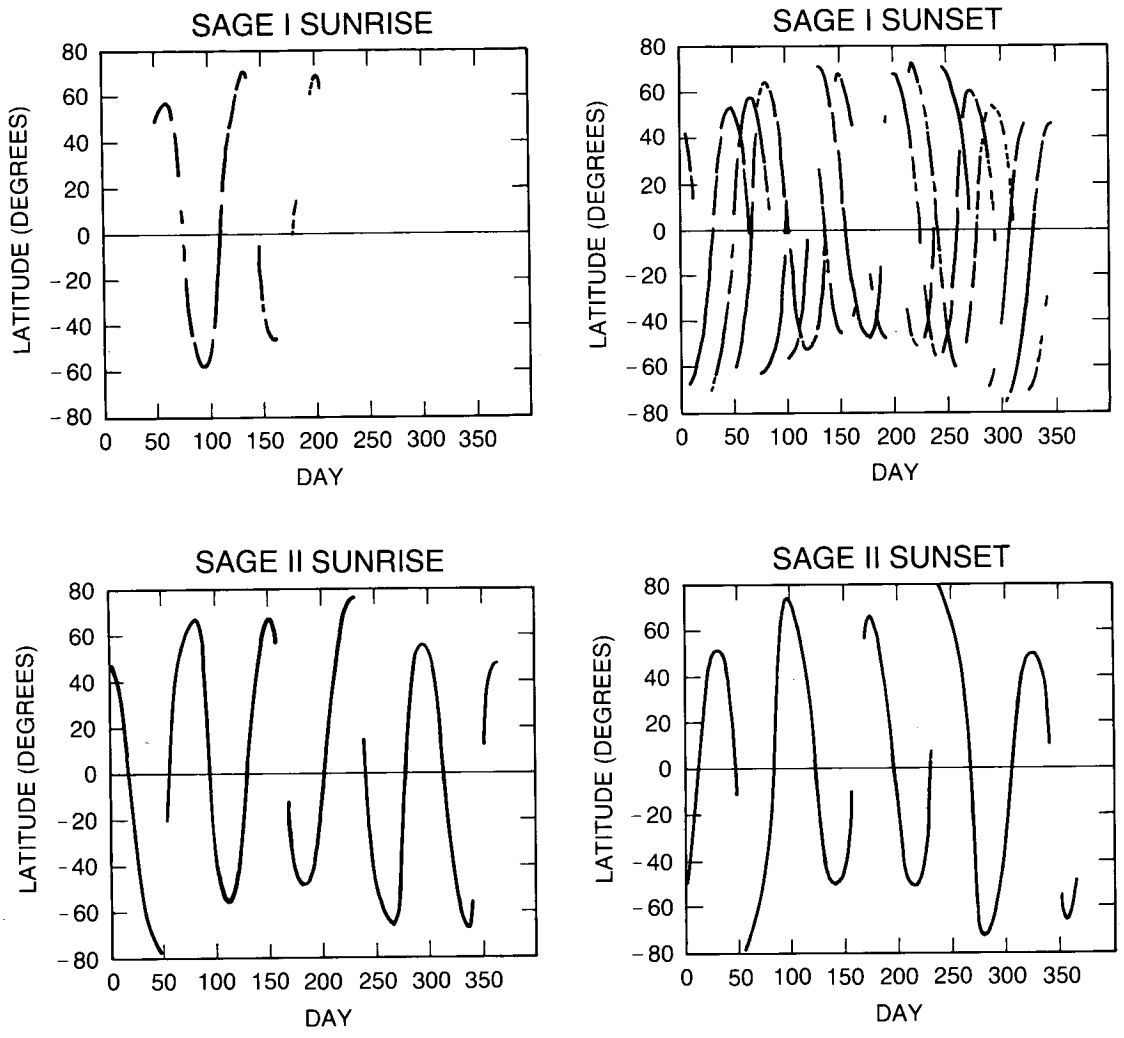

Figure 5.5 SAGE–I and SAGE–II yearly latitudinal coverage. In order to differentiate between the years in SAGE–I sunset, the peak at julian day 80 occurred in 1979; the peak at julian day 67 occurred in 1980; the peak at julian day 49 occurred in 1981. Note that because of almost perfect overlap, the SAGE–II latitudinal coverage appears as a single curve even though several years are plotted.

5.7, and 5.8 for 40°S, Equator, and 40°N, respectively. Those for SAGE–II and SBUV are shown in Figures 5.9, 5.10, and 5.11 for 40°S, Equator, and 40°N, respectively.

Both the SAGE–I/SBUV and the SAGE–II/SBUV comparisons clearly display the annual variation of ozone at midlatitudes and the semiannual oscillation at the Equator. Furthermore, both instruments appear to respond in a manner similar to shorter term variations. It is clear from Figures 5.7, 5.8, and 5.9 that SAGE–I and SBUV track each other reasonably well, with a slight tendency for the SAGE–I layer amounts to be lower than the corresponding SBUV layer amounts. The results indicate the positive finding that both SAGE–I and –II and SBUV showed similar seasonal and shorter term fluctuations in the ozone in Umkehr layers 6 to 9. This detailed agreement as a function of time is significant when one considers that the techniques are totally different, incorporating extinction in the green wavelength region at spacecraft sunrise or sunset, as compared to backscattered ultraviolet measurements taken from a different spacecraft at the nadir.

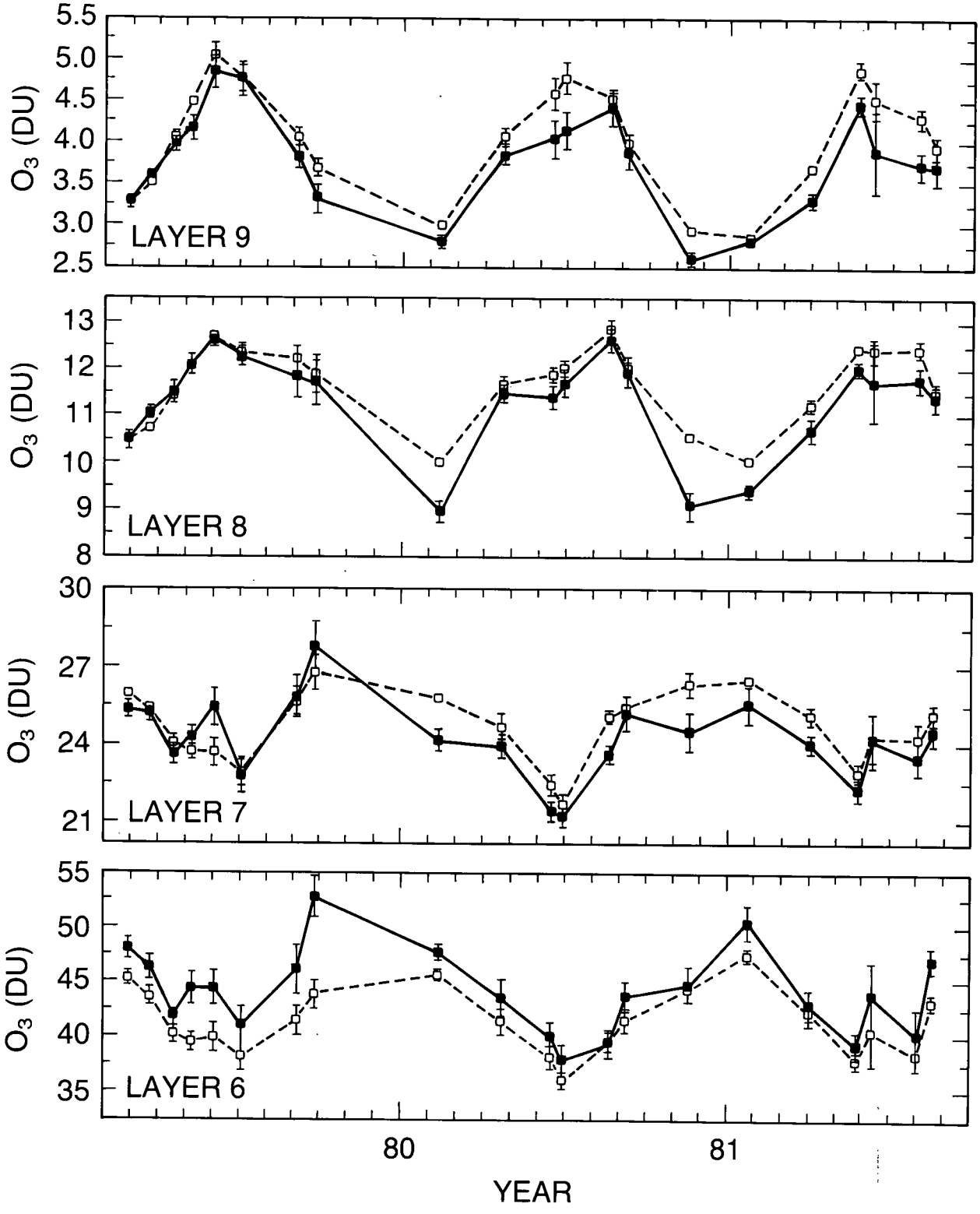

Figure 5.6 Cluster means of SAGE–I and SBUV at 40°S. The vertical bar is the 95 percent confidence interval on the cluster mean. Lines connecting means are intended only as a visual aid. SAGE-I, solid squares; SBUV, open squares.

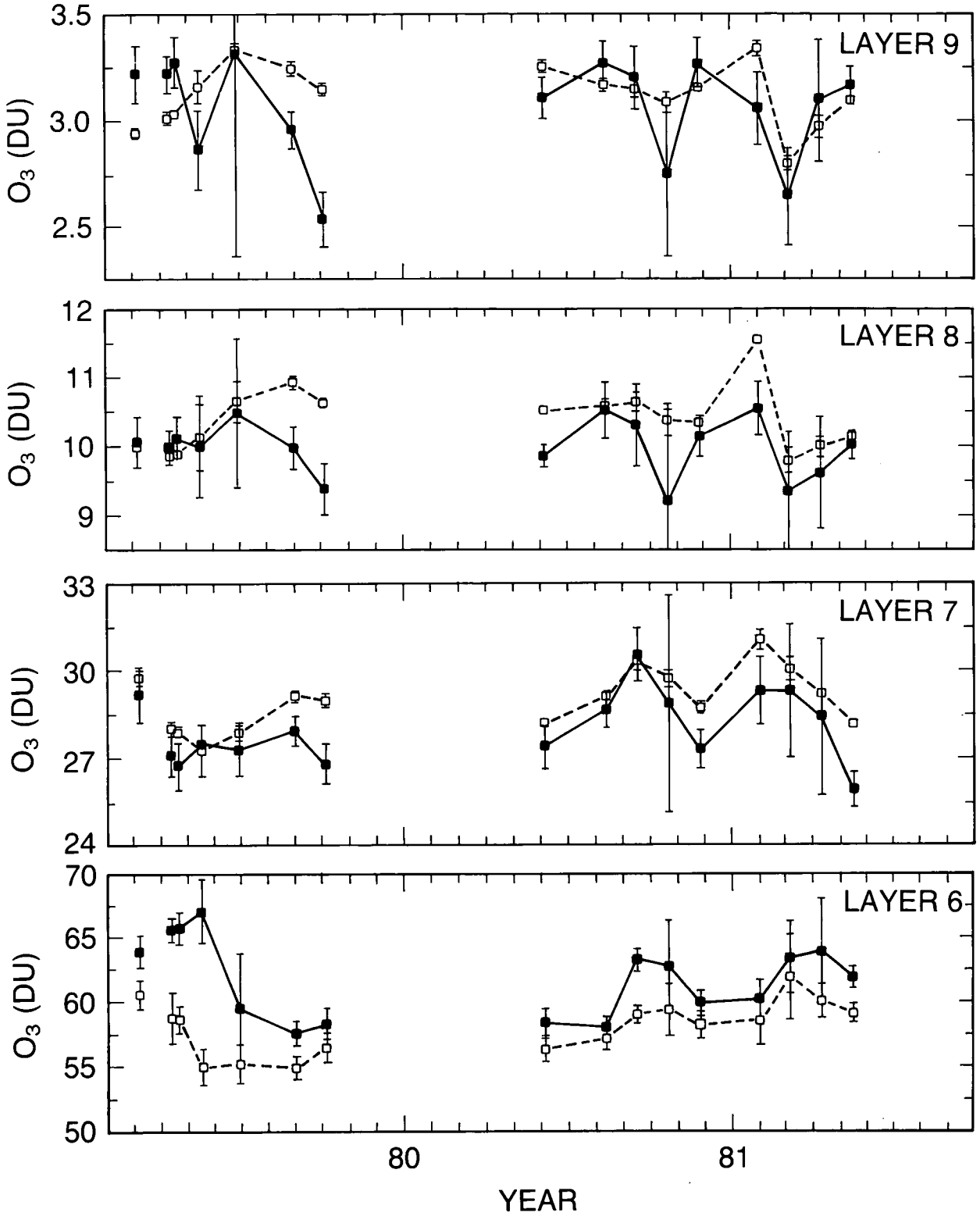

Figure 5.7 Cluster means of SAGE–I and SBUV at the Equator. The vertical bar is the 95 percent confidence interval on the cluster mean. Lines connecting means are intended only as a visual aid.

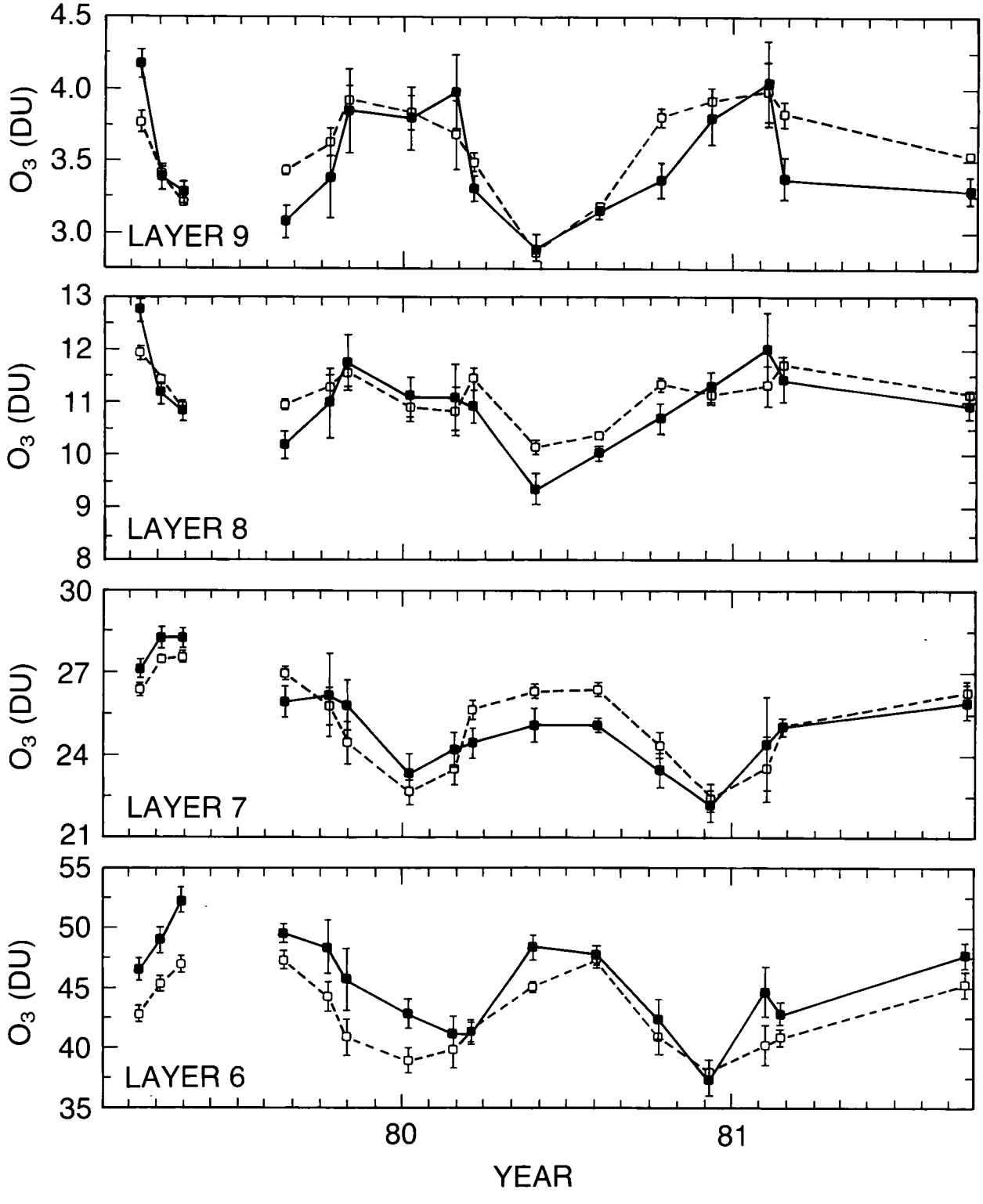

Figure 5.8 Cluster means of SAGE–I and SBUV at 40°N. The vertical bar is the 95 percent confidence interval on the cluster mean. Lines connecting means are intended only as a visual aid.

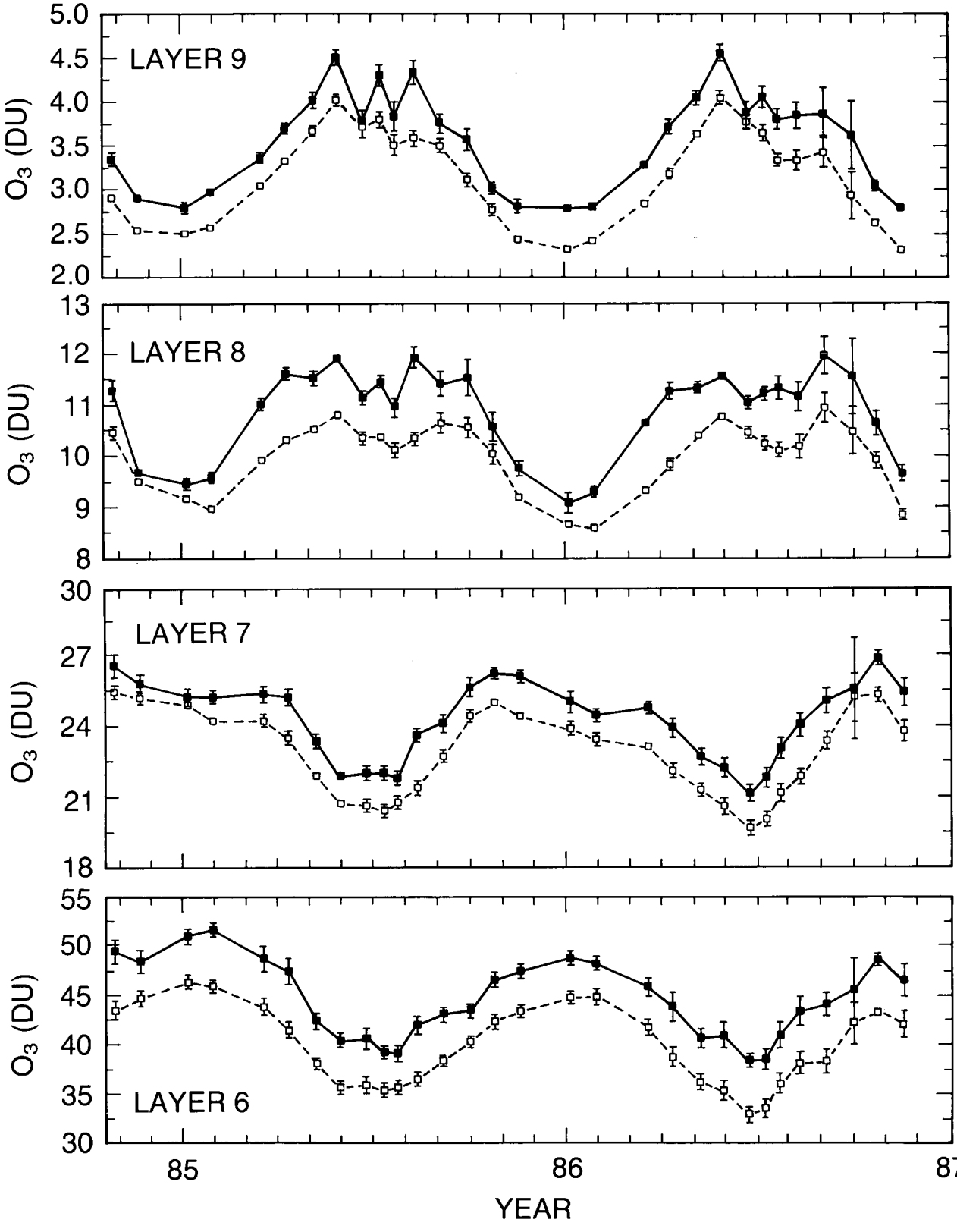

Figure 5.9 Cluster means of SAGE–II and SBUV at 40°S. The vertical bar is the 95 percent confidence interval on the cluster mean. Lines connecting means are intended only as a visual aid. SAGE-II, solid squares; SBUV, open squares.

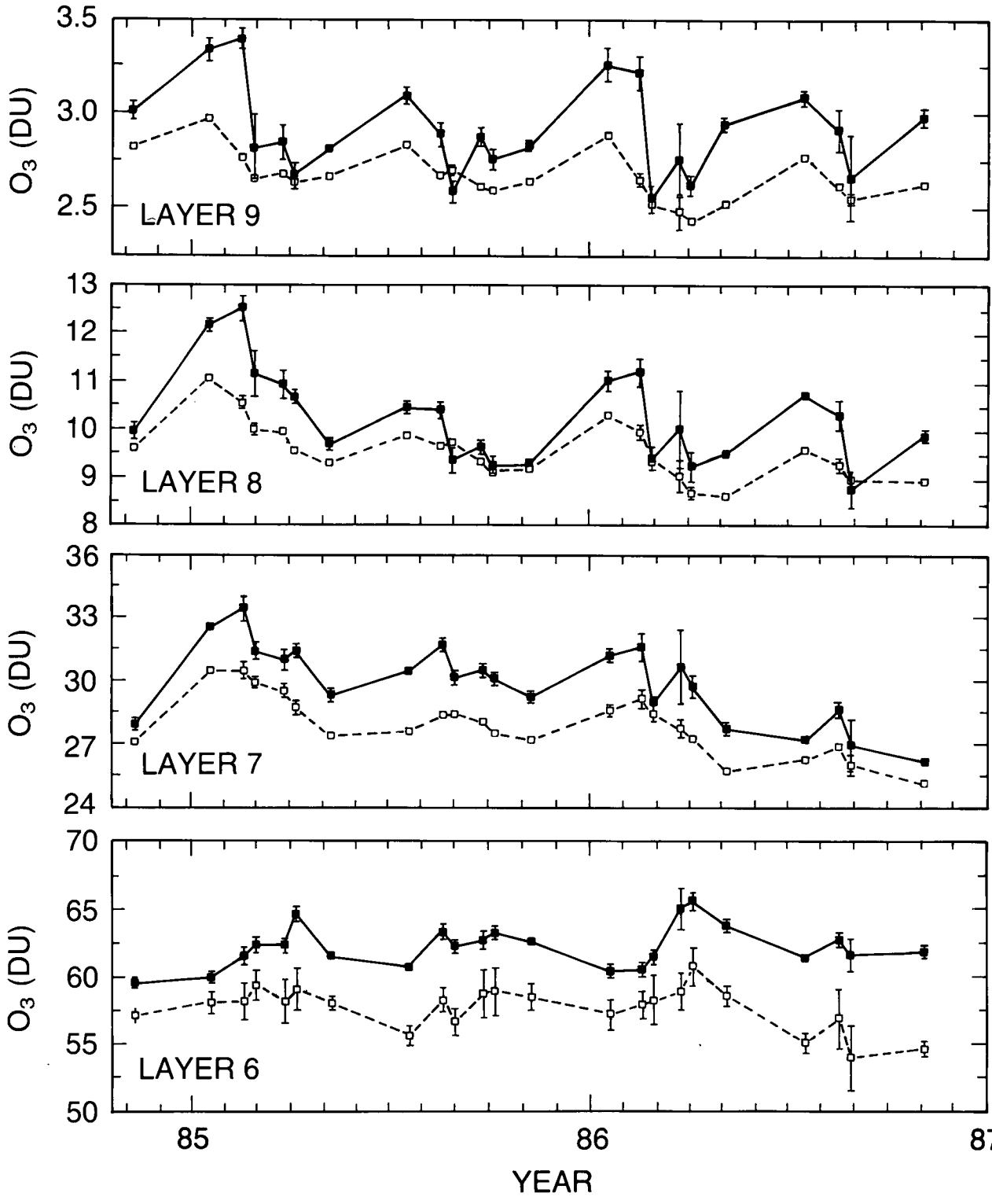

Figure 5.10 Cluster means of SAGE–II and SBUV at the Equator. The vertical bar is the 95 percent confidence interval on the cluster mean. Lines connecting means are intended only as a visual aid.

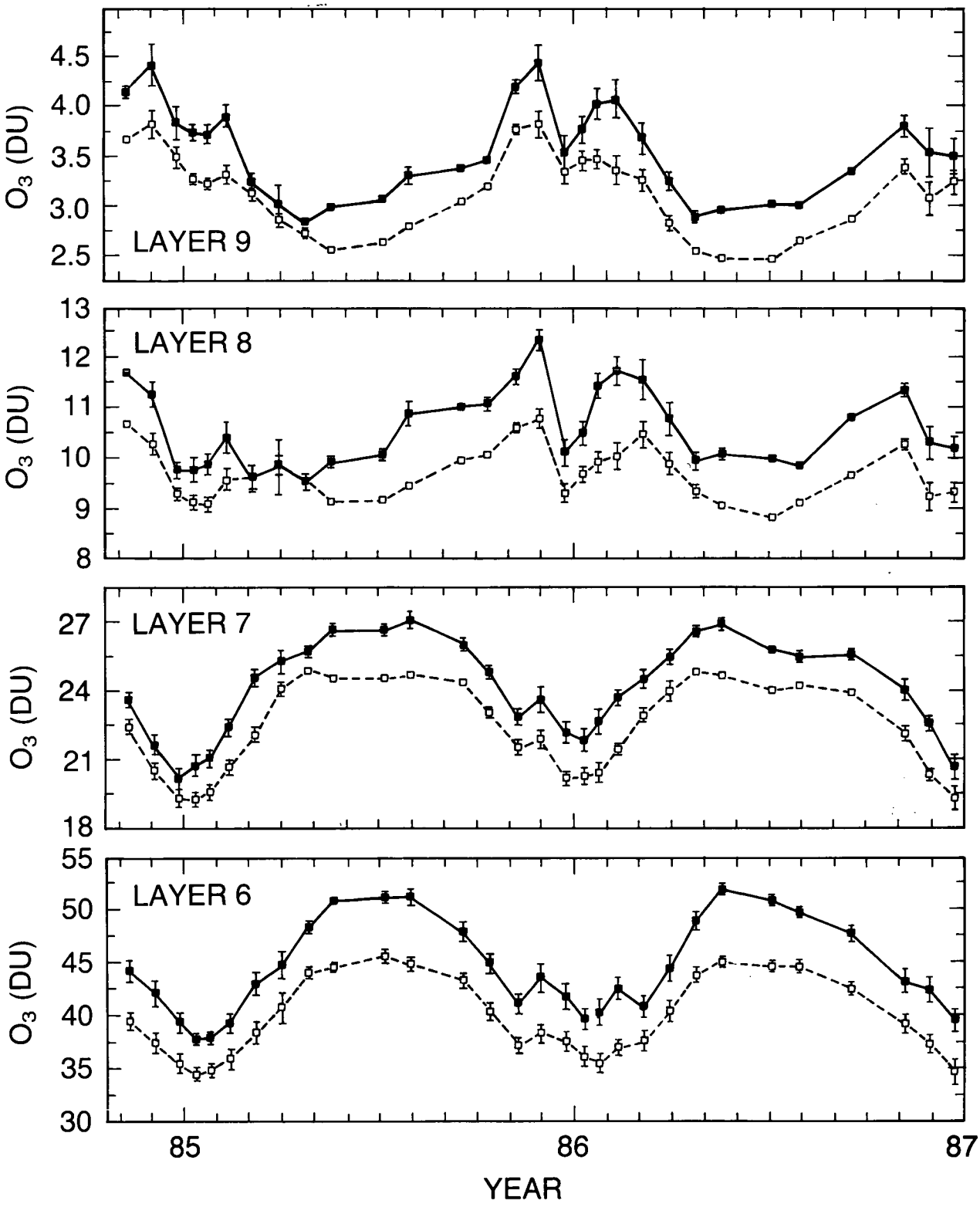

Figure 5.11 Cluster means of SAGE–II and SBUV at 40°N. The vertical bar is the 95 percent confidence interval on the cluster mean. Lines connecting means are intended only as a visual aid.

When contrasting SAGE–II with SBUV (Figures 5.9 through 5.11), it is apparent that the two instruments track each other well—i.e., the shapes are similar; however, SBUV layer amounts are systematically lower than the corresponding SAGE–II layer amounts.

To reduce the large seasonal variability seen in Figures 5.6 through 5.11, the cluster means are averaged over an integral number of years. The 24-month averages are presented in Figure 5.12 as a function of latitude for the four Umkehr layers for the SAGE–I period, October 24, 1979, to October 23, 1981, and for the SAGE–II period, October 24, 1984, to October 23, 1986. Figure 5.12 shows that the latitudinal variation is similar for both the SAGE–I and SBUV instruments, with SBUV zonal ozone greater than SAGE–I at all levels other than 6. These same latitudinal variations are also evident in the SAGE–II/SBUV comparisons; however, a larger consistent bias exists at all latitudes with SBUV averages lower than SAGE–II zonal averages.

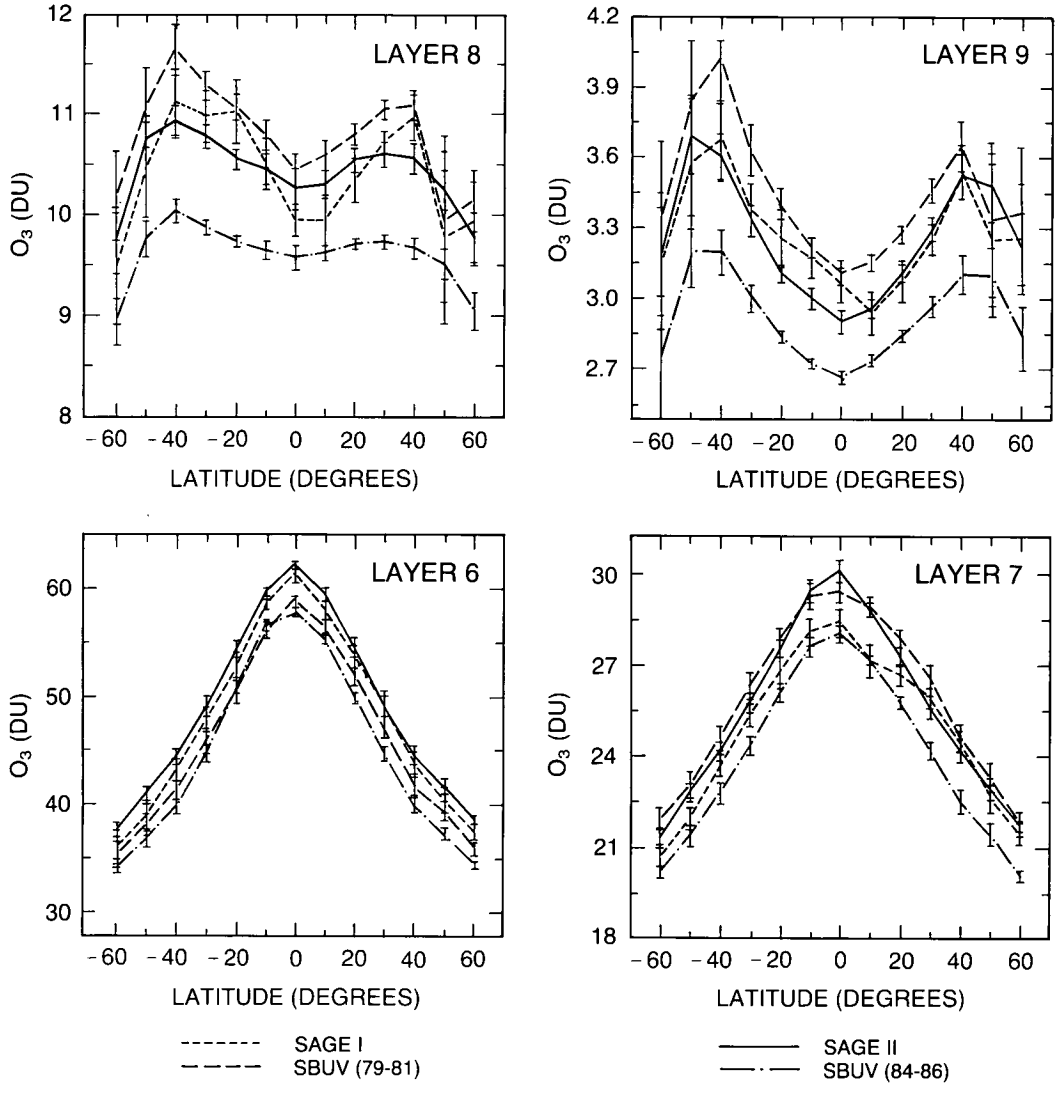

Figure 5.12 Time average of the cluster means. The averaging period for SAGE–I was October 24, 1979, to October 23, 1981. The averaging period for SAGE–II was October 24, 1984, to October 23, 1986. The corresponding SBUV data were similarly averaged. The vertical bars are the standard error of the mean of the cluster means. The sizes of the error bars reflect the seasonal ozone variability.

The latitudinal cluster-mean averages of the SBUV data show a decrease at all levels except 6 between the two periods at all latitudes. Any apparent differences between SAGE–I and SAGE–II are accentuated by the fact that their corresponding cluster means were not "paired"; hence, seasonality may affect the differences. The same holds for the SBUV (1979–1981) and SBUV (1984–1986) cluster-mean averages.

5.3.5 Difference Between SAGE–I and –II and SBUV Pairs

To quantify the information contained in the time series of the previous section, averages of the cluster-mean percentage differences are computed. Figure 5.13 displays the differences between SAGE–I/SBUV and SAGE–II/SBUV, with SBUV as the reference. The percentage differences are essentially constant across the latitudes, and the means are almost always significantly different.

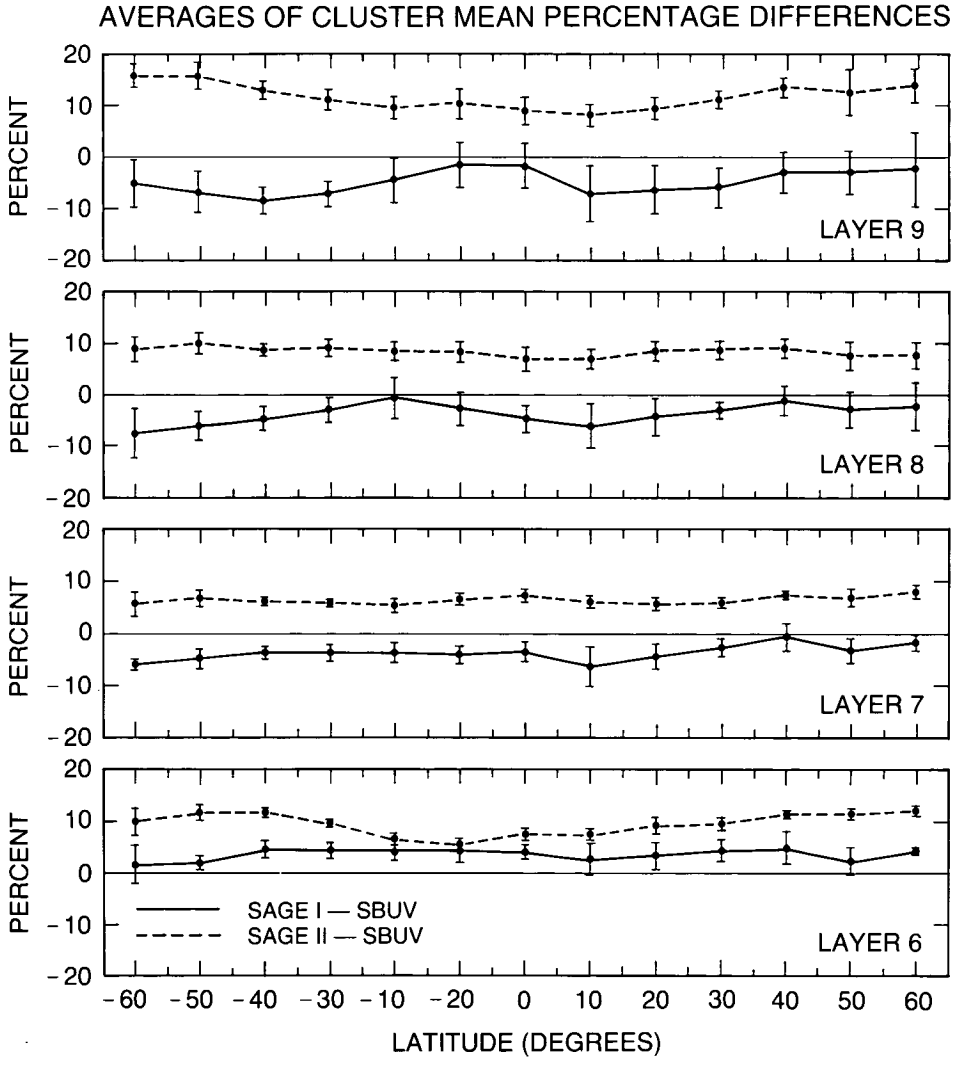

Figure 5.13 The average of the percentage difference between SAGE–I and –II and SBUV cluster means with SBUV the reference. The vertical bars are the 95 percent confidence interval of the time average. Only variation between the cluster mean percentage differences contributed to the size of each confidence interval. The averaging period was identical to that used for Figure 5.12.

The cluster-mean differences presented in Figure 5.14 were averaged in latitude and are shown in Figure 5.15. In this figure, the SBUV ozone layer amounts are greater on average than the SAGE–I amounts in layers 7 to 9 by about 4 to 5 percent and are smaller than the SAGE–I amounts in layer 6 by 4 percent. Much larger differences are found between SAGE–II and the SBUV layer amounts in these four layers, with SBUV lower by between 6 to 11 percent.

Because of seasonal sampling differences, the averaging process used to produce Figures 5.13 and 5.14 should not be used to compare SAGE–I with SAGE–II, nor SBUV (1979–1981) with SBUV (1984–1986). A method that reduces seasonal and spatial biases selects sets of profiles in which SAGE–I and SAGE–II sample the same month of the year within the same latitude band. Such a period of time is called an "intersection" and is defined to be a period of time in the year, of approximately 1 month's duration, during which both SAGE–I and SAGE–II sampled the same latitude band. It should be noted that an intersection is independent of the actual year during which measurements were made; it is defined strictly in terms of the month within the year. Within the 13 latitude bands being considered, 102 intersections were isolated such that both halves of the year were equally represented. The SAGE–I and SAGE–II profiles were averaged

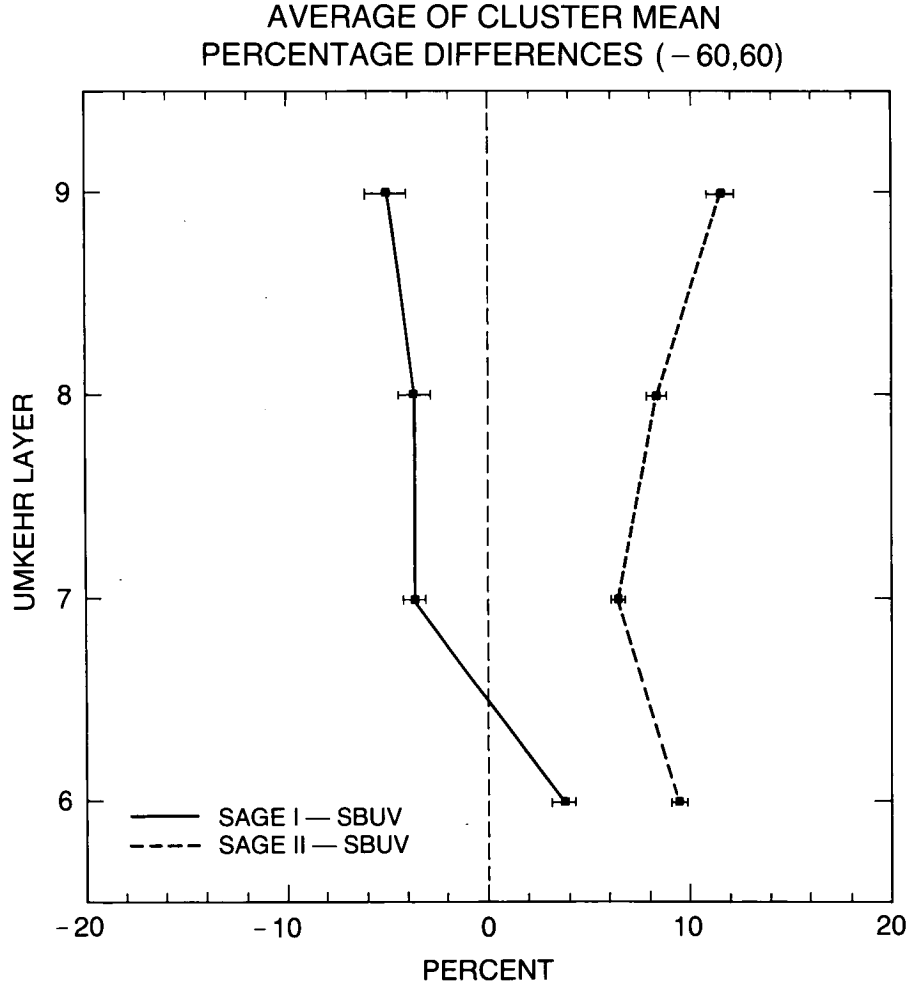

Figure 5.14 Time averages of the percentage difference between SAGE–I and –II and SBUV cluster means with SBUV the reference. Averaging was done over all latitude bands for the time period used in Figure 5.12. The horizontal bars are the 95 percent confidence interval of the time average.

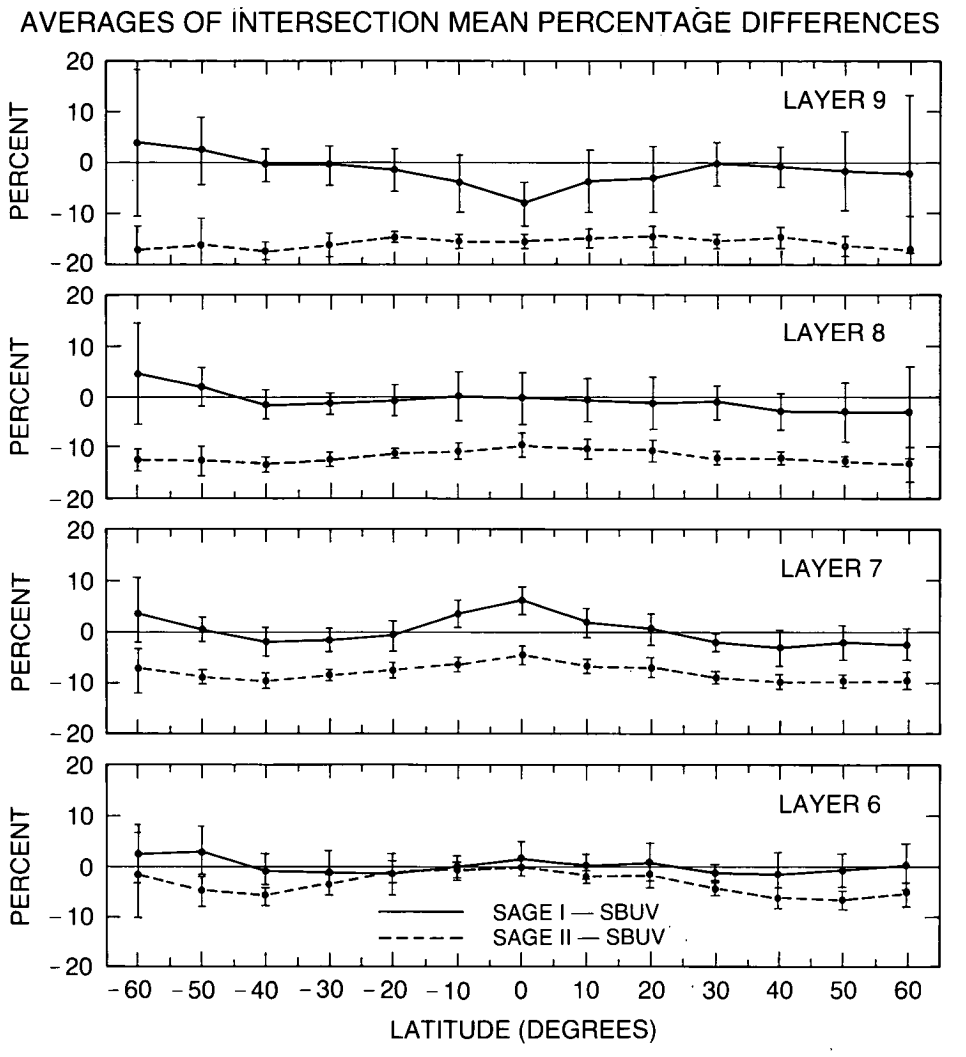

Figure 5.15 Averages of the percentage difference between the cluster means of SAGE–II and SAGE–I (SAGE–I the reference) or SBUV (1984–1986) and SBUV (1979–1981) (SBUV 1979–1981 the reference). Percentage differences were computed at SAGE–I and SAGE–II intersections. For each latitude band there were approximately eight intersections and thus eight percentage differences that were averaged to produce one point on the graph. The vertical bar represents twice the standard error of the mean percentage difference and reflects only the variation between the eight percentage differences in the latitude band.

for each intersection. The percentage difference between the SAGE–II mean and the SAGE–I mean was computed within each intersection. The SAGE–I mean was taken as reference. The SBUV (1979–1981) and SBUV (1984–1986) profiles were processed in a fashion analogous to the SAGE–I and SAGE–II profiles. SBUV (1979–1981) was used as reference for the percentage calculations. As in Figure 5.13, percentage differences are displayed as a function of latitude in Figure 5.15. Again, there is only slight variation in the differences with latitude. The percentage differences are averaged in latitude and are presented as a function of Umkehr layer in Figure 5.16. It should be noted, in Figure 5.16, that the magnitude of the difference between SBUV (1984–1986) and SBUV (1979–1981) steadily increases from approximately 3 percent at layer 6 to 16 percent at layer 9. However, the differences between SAGE–II and SAGE–I remain relatively constant and are less than 2 percent.

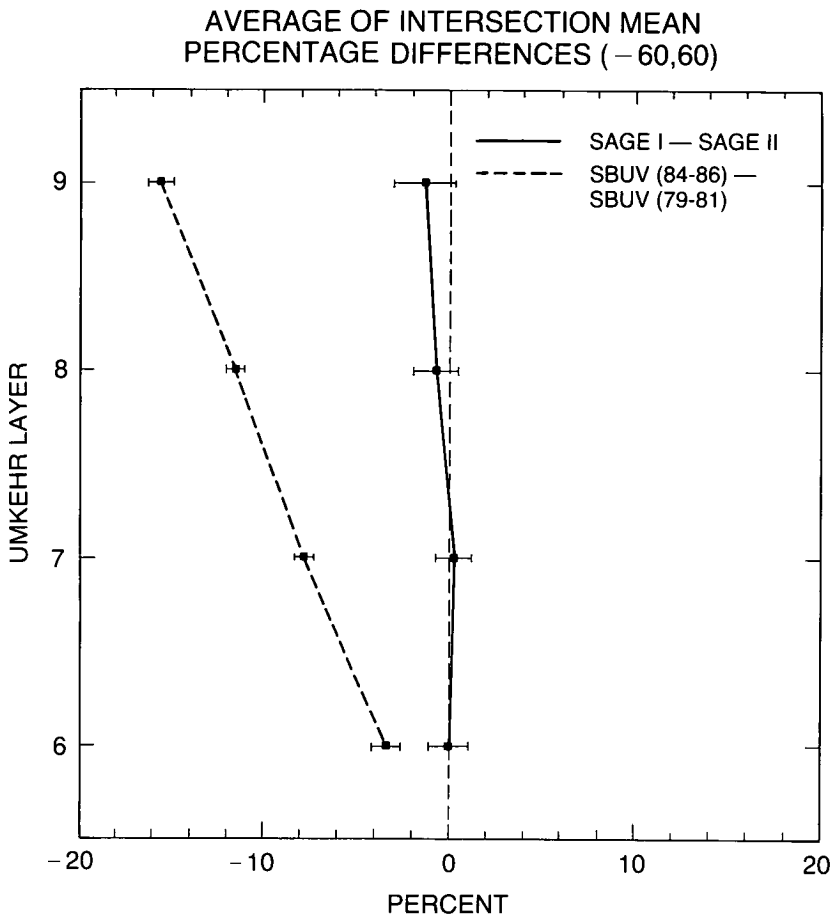

Figure 5.16 Latitudinally averaged mean percentage difference between SAGE–II and SAGE–I (SAGE–I the reference) or between SBUV (1984–1986) and SBUV (1979–1981) (SBUV 1979–1981 the reference). The horizontal bars represent twice the standard error of the mean percentage difference.

The differences between Figures 5.13 and 5.15 and between Figures 5.14 and 5.16 are a result of different sampling criteria. Figures 5.13 and 5.14 include all two-way coincidences between SAGE–I or SAGE–II and SBUV. Figures 5.15 and 5.16 include three-way coincidences: SAGE–II with seasons and latitude corresponding to SAGE–I but 5 years apart, and with SBUV.

5.3.6 Changes in SAGE–I to SAGE–II at Geometric Altitudes

The previous comparisons between SAGE–I and SAGE–II involved the Umkehr-layer amounts and were designed to compare SAGE–I and –II with SBUV observations. The conversion to Umkehr-layer amounts is not necessary when comparing SAGE–I and SAGE–II alone. In the following development, the fundamental SAGE measurements are used; that is, the SAGE–I and –II concentration profiles are defined in terms of geometric altitude, ranging from 25 km to 50 km. Again, only profiles corresponding to the SAGE–II and SAGE–I intersections are used. The cluster percentage differences are averaged in time within 10-degree-latitude bands and plotted against altitude in Figure 5.17. The magnitude of the differences is only on the order of 5 percent. Because of small sample sizes, these comparisons are noisy. With some notable exceptions at high altitudes and also near the Equator, the prevailing pattern is an ozone decrease in the upper stratosphere and another decrease near 25 km between 1980 and 1986.

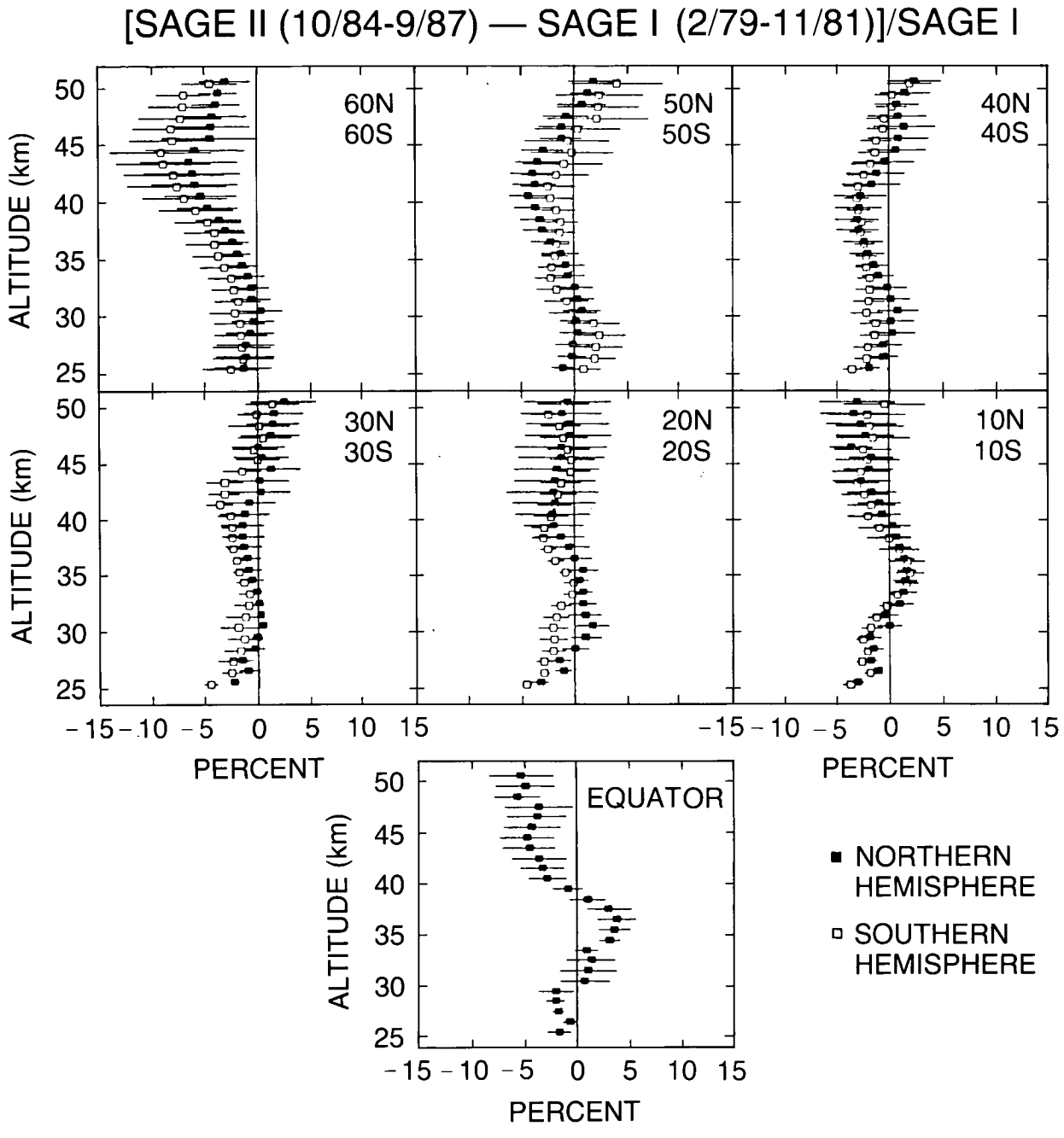

Figure 5.17 Mean percentage difference between SAGE–II and SAGE–I at the geometric altitudes of SAGE (SAGE–I is the reference). For each latitude band approximately eight intersections were available from which to compute percentage differences. The average percentage difference along with its standard error are plotted. The standard error reflects only the variation between the eight percentage differences in a given latitude band.

The identical analysis is performed using two wider latitude bands: 20°N to 50°N and 20°S to 50°S, an area over which there is relatively dense sampling. The mean percentage differences appear in Figure 5.18. The agreement between the two hemispheres is apparent, with the magnitude of the ozone change from SAGE–I to SAGE–II being less than 5 percent at any altitude. Between 35 km and 45 km there is an ozone-reduction profile with a maximum ozone reduction of about 3 percent centered at 40 km, at about 30 km there is zero change, at about 50 km there is zero ozone change (unlike SBUV), and, near 25 km, there is another region of ozone reduction. As in the previous analyses using Umkehr layer amounts and considering potential systematic errors, the SAGE–I and –II measurements do not support a large decrease in global stratospheric ozone above 25 km.

5.4 SOLAR BACKSCATTER ULTRAVIOLET II (SBUV–2)

The National Oceanic and Atmospheric Administration (NOAA)–9 satellite with the SBUV–2 instrument package onboard was launched on December 12, 1984 (Oslik, 1984). While some instruments on NOAA–9 are no longer operating, the SBUV–2 is still sending data back on a daily basis. The SBUV–2, while similar to the SBUV, is different, as shown in Table 5.4.

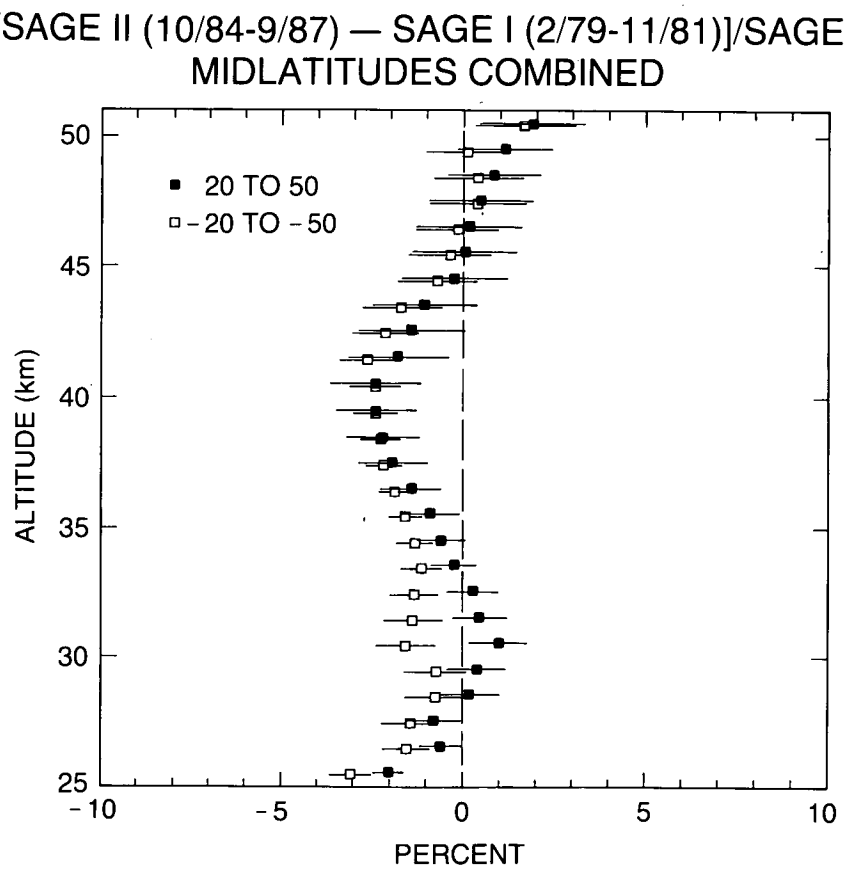

Figure 5.18 Mean percentage difference between SAGE–II and SAGE–I at the geometric altitudes of SAGE (SAGE–I is the reference). All intersections occurring between 20°N to 50°N (or 20°S to 50°S) were combined into one sample. The percentage difference at each intersection was computed. These percentage differences were averaged and plotted for each altitude. The sample standard error was also computed and plotted as the horizontal bar at each point. Within each hemisphere, approximately 2,500 SAGE–I profiles and 6,000 SAGE–II profiles were used in computing the statistics.

Table 5.4 Comparison of Important Features Between SBUV–2 and SBUV

Features	SBUV–2	SBUV
Monochromator mode	4 (discrete, sweep, wavelength, and position)	4 (step, continuous, wavelength and cage [cam])
Control of monochromator	FIX System; FLEX system mode (wavelengths can be changed by command)	One fixed system
Scene mode	4 (Earth, Sun, wavelength calibrate, diffuser check)	2 (Earth and Sun)
Diffuser position	4 (stow, Sun, wavelength calibration, or diffuser check & decontamination)	2 (stow and Sun)
Mercury Lamp position	2 (stowed and deployed)	1
CCR wavelength	379 nm	343 nm
Shortest wavelength of discrete mode (other 11 wavelengths match)	252 nm (in FIX system)	255.5 nm
Wavelength calibration steps	12	5
Electronic calibration	Every scan in retrace	By command
Scanning		
discrete mode	32 sec	32 sec
sweep mode	192 sec	112 sec
Sampling time		
discrete	1.25 sec	1 sec
sweep	0.1 sec	0.08 sec
Diffuser check	Yes	No
Diffuser Decontamination	Yes	No
Gain Range	Two from PMT anode 1 from PMT cathode	Three from PMT One from ref. diode
IFOV	11.3 × 11.3 degrees	11.3 × 11.3 degrees
Discrete (step scan) scanning direction	From short to long wavelengths	From long to short wavelengths

SBUV data show a surprisingly large decrease of stratospheric ozone, especially in the upper stratosphere, from 1978 to the present (Heath, 1986), but the Algorithm and Calibration subgroups of the Trends Panel suggest that the apparent decrease could be due in whole or in part to degradation of the reflector plate in the SBUV system. SBUV–2 takes the same great volume and the same kind of data as SBUV, and has the same flight pattern. The most powerful method of verifying, modifying, or disproving the SBUV-reported trends would be to compare at least two aspects of SBUV and validated SBUV–2 data: 1) the ozone magnitudes reported by the twin instruments immediately after launch (if SBUV–2 is consistently higher than SBUV, then the ozone decrease shown by SBUV is probably correspondingly in error) and 2) a systematic difference between the first 2 years of SBUV and the corresponding 2 years of SBUV–2 to get a good estimate of how much ozone has changed over the intervening period. The other

sections of the report of this subcommittee of the Trends Panel have intercompared upper stratospheric SBUV data with those of other satellites or ground-based instruments, which measure different ozone properties, make far fewer ozone measurements, and cover different spatial trajectories than the SBUV instrument. This procedure is more indirect and less revealing than the direct comparison between the two twin, overlapping, SBUV instruments would be.

Using a convenient but inappropriate algorithm, SBUV–2 data have been analyzed and saved since April 1985. These data show seasonal variations similar to those of SBUV, but, in view of known deficiencies of the algorithm used to process the data, no quantitative use is made of these data (Nagatani and Miller, 1987). This subcommittee of the Trends Panel issued requests between April 1987 and July 1987 for the SBUV–2 reinterpreted data. NOAA scientists began to reinterpret the SBUV–2 data in September 1987, using an appropriate algorithm. The newly processed data for August 1985 were issued in preliminary form in late 1987. The differences between SBUV–2 and SBUV data are positive throughout. The aging SBUV instrument reports less ozone than the newly launched twin instrument, indicating that the older instrument had degraded more than it was believed to have in 1986 (Heath 1986). However, the SBUV–2 data were so preliminary at the time of this report that they were not used. These have since been discussed in a recent report (Ohring et al., 1989).

The national plan for monitoring stratospheric ozone is to use Dobson stations and SBUV satellites as mutually interactive systems, to send up another SBUV instrument about every 2 years, and to establish calibration continuity between successive instruments by studying overlapping measurements.

SBUV–2 was launched 2 months after SAGE–II in 1984. The differences between SAGE–I and SAGE–II are at least as great as those between SBUV and SBUV–2. Although it is not SAGE's job to monitor stratospheric ozone, the SAGE team made a great effort to reinterpret all the SAGE–I and SAGE–II ozone data in about 6 months; they produced the meaningful account given in Section 5.3. It is the job of the National Environmental Satellite, Data, and Information Service (NESDIS) of NOAA to monitor stratospheric ozone using SBUV satellites and Dobson ground-based stations. Although January 1988 is more than 3 years since SBUV–2 was launched, the NOAA team said in January 1988 that the SBUV–2 data were not interpreted well enough to go into this report.

5.5 UMKEHR MEASUREMENTS OF UPPER STRATOSPHERIC OZONE

5.5.1 Comparison of Upper Stratospheric Umkehr Ozone Patterns With SBUV Observations at the Same Time and Place

Eight years' worth of archived data from the SBUV were collocated in time and space with all of the Umkehr station reports available as of July 1987 from the World Ozone Center. The criteria for matching were that SBUV and groundstation data be from the same day, and that the center of the SBUV field of view be within 1 degree of latitude and 10 degrees longitude of the station. For this study, 11 stations were selected to provide the greatest temporal coverage over the 7-year period: Kagoshima (31.6°N), New Delhi (28.6°N), Sapporo (43.1°N), Tateno (36.1°N), Arosa (46.8°N), Boulder (40.0°N), Belsk (51.8°N), Lisbon (38.8°N), Perth (31.9°S), Poona (18.5°N), and Naha/Kagamizu (26.2°N).

As discussed in the algorithm chapter of this report, the Umkehr gives its best ozone results in layers 4 to 8 to a vertical resolution of about 2.5 layers (12 km); the SBUV provides information for layers 6 to 9 with a vertical resolution of 10 km. Layers 6 to 8 are presented in this comparison.

Sample data for the Tateno station are shown for Umkehr layers 6, 7, and 8 in Figures 5.19 to 5.21. In each case, the upper panel gives the collocated SBUV ozone measurements in Dobson units, and the lower panel gives the corresponding Umkehr data. Both methods show the large seasonal variations of ozone. The SBUV data are less noisy than those obtained by the Umkehr method. From 1982 to 1983, Umkehr layer 8 shows a strong downward perturbation by the El Chichón volcano, and levels 6 and 7 show a smaller volcanic effect. These SBUV data show no conspicuous effect of El Chichón, but, in Figure 5.1, SBUV showed a 9 percent decrease in layer 6

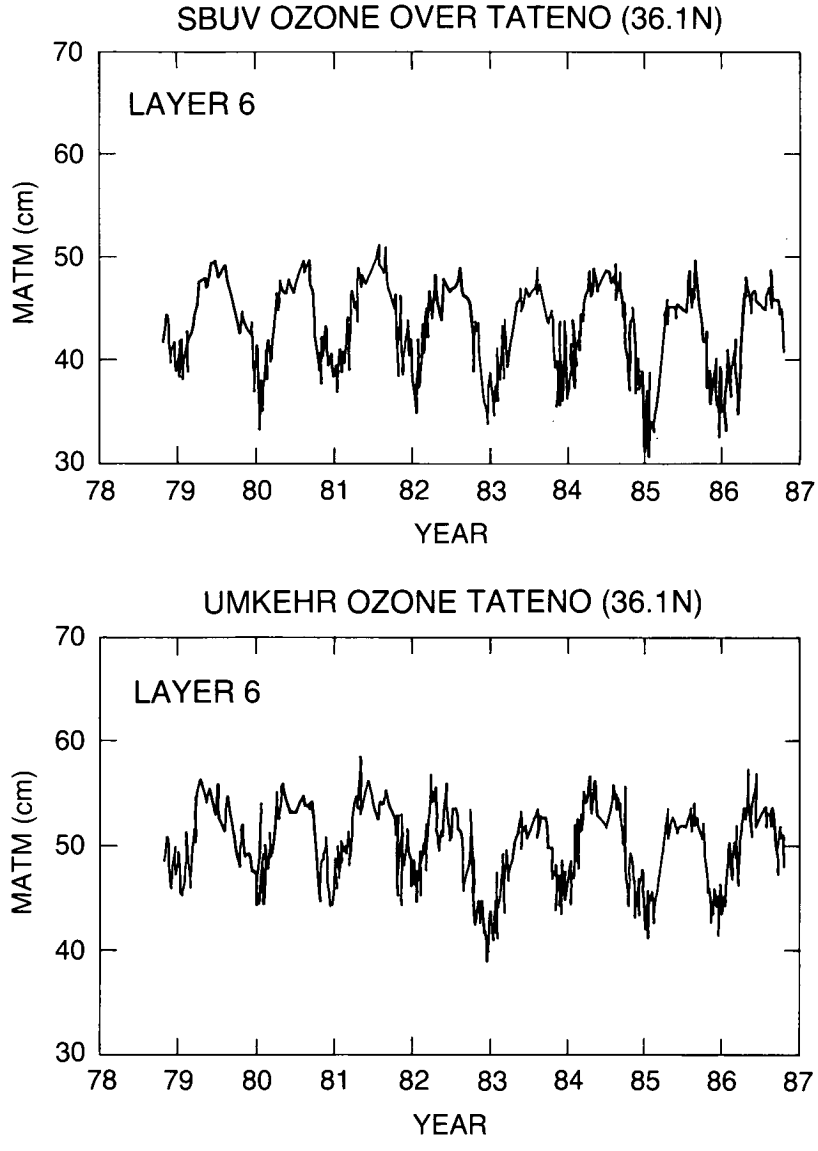

Figure 5.19 Direct presentation of ozone observations (Dobson units) from the Umkehr station at Tateno (36°N) in the lower panel and collocated SBUV ozone observations in the upper panel from 1979 through 1986 for Umkehr layer 6.

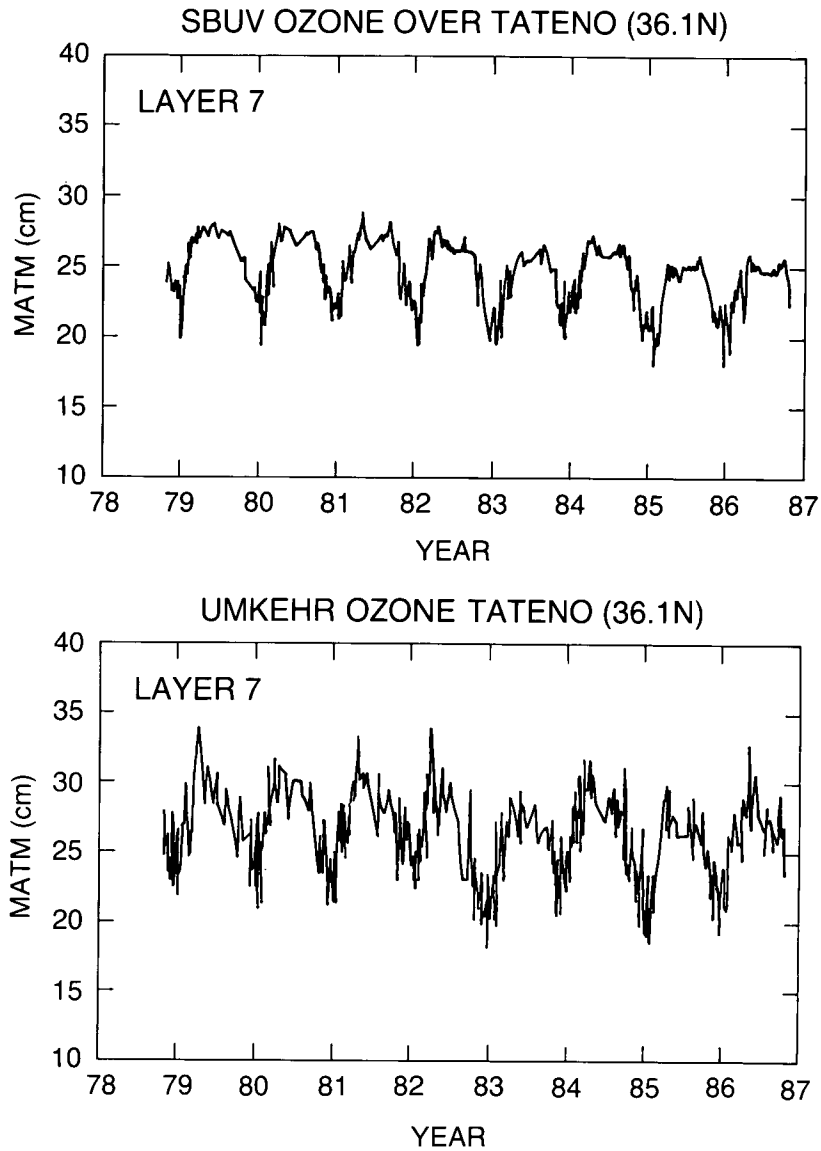

Figure 5.20 Same as 5.19, except for Umkehr layer 7.

late in 1982, presumably caused by El Chichón. The Umkehr method must look up through the volcanic cloud to observe layers 6 to 8, but the SBUV system looks down; these layers lie largely (but not entirely) above the volcanic cloud. In the upper panels of Figures 5.19 to 5.21, the SBUV data show a clear-cut decrease over the 8 years in levels 7 and 8, and perhaps a slight decrease in level 6. A comparison of the early years with the last years of the Umkehr data shows a distinct ozone decrease, but the trend is confused by the effects of El Chichón during the middle years.

Another way to compare the collocated SBUV and Umkehr data visually is to plot the ratio, Umkehr–SBUV, against time at layer 8 for all 11 Umkehr stations (Figure 5.22). El Chichón erupted in month 40 on this plot. By taking ratios, the seasonal variations are largely removed. If this ratio is parallel to the time axis throughout the period, the Umkehr station is in agreement with the SBUV overflights in trend. Flaws in the data include noise in the ratio, sparsity of data and gaps of data at some stations, and the effect of El Chichón. For those stations with a large

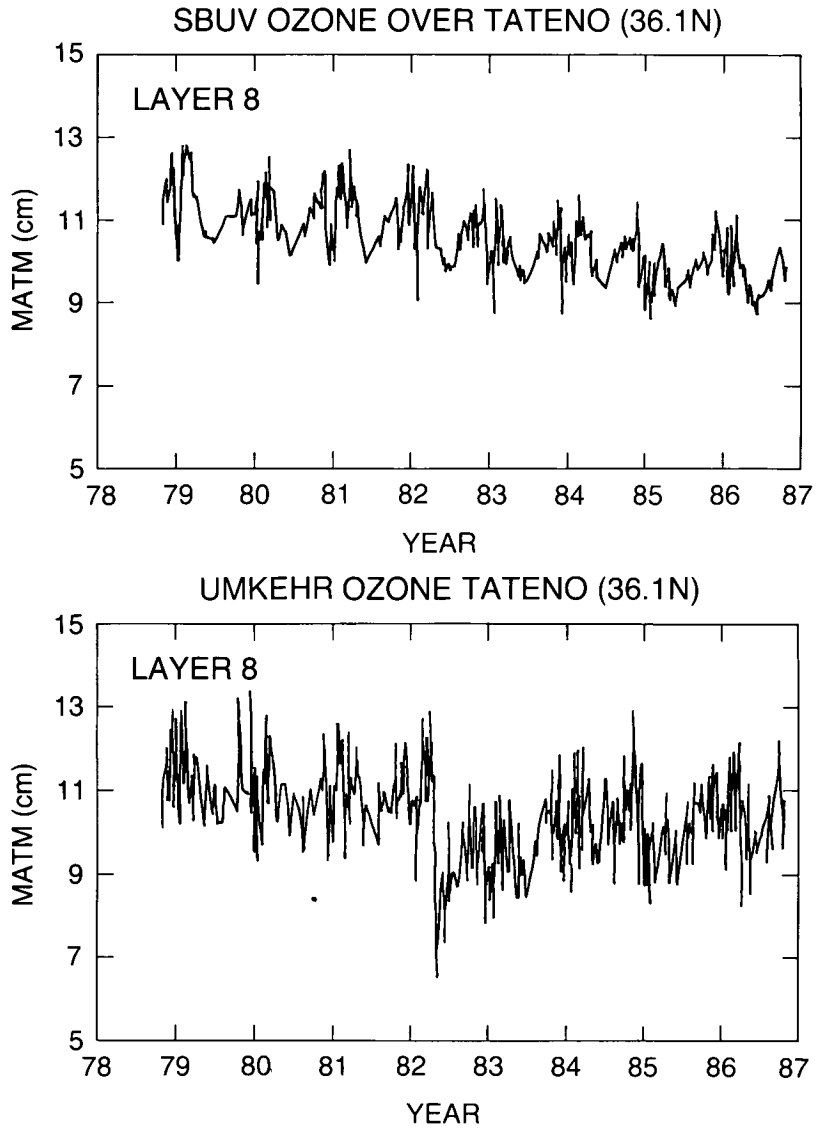

Figure 5.21 Same as 5.19, except for Umkehr layer 8.

density of points, visual comparison of the Umkehr–SBUV ratio during the first and the last year appears to show Umkehr ozone to be larger than that for SBUV by 5 to 10 percent. The decrease of ozone at this Umkehr layer, indicated by the collocated SBUV, is 15 percent; thus, this visual comparison indicates that the ozone decrease seen by Umkehr is less than that seen by SBUV over this period.

A time series statistical analysis was carried out for the SBUV trend shown for observations coincident with each Umkehr station (omitting Boulder) and for the bias, SBUV–Umkehr. To minimize the effect of El Chichón in the comparison, all Umkehr measurements for 36 months after the eruption of El Chichón were eliminated from the regression. This means that Umkehr comparisons are based on only 5 years of data: 3.5 years of data before the eruption, and only 1.5 years of data after the 3-year gap.

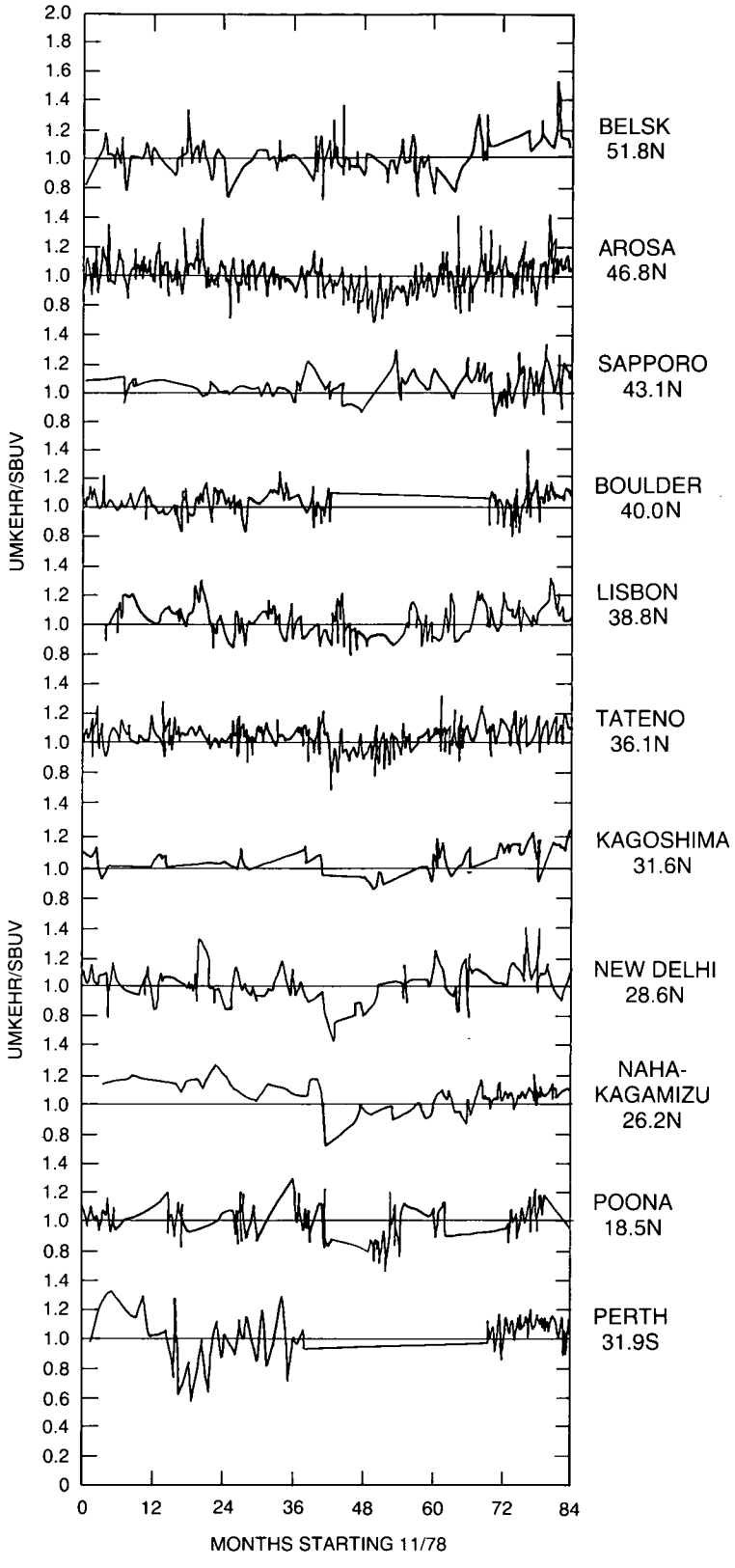

Figure 5.22 Ratio of Umkehr ozone measurements in layer 8 to collocated SBUV measurements for 7 years after launching of SBUV in November 1978. Eleven Umkehr stations are included.

In order to remove residual seasonal variation remaining in the bias and to derive the drift between the long-term trend of the two time series, a linear regression model was fit to the percent difference, Δ = SBUV–Umkehr, such that:

$\Delta = b + dt + a_1\cos 2\pi t + a_2\sin 2\pi t + a_3\cos 4\pi t + a_4\sin 4\pi t.$
$\Delta = 100 \times$ (SBUV–Umkehr)/SBUV.
$t =$ time in year measured from November 1, 1978, the starting day of SBUV measurements.
$b =$ intercept of the regression line at $t = 0$, representing the bias (systematic difference) between SBUV and Umkehr.
$d =$ drift between SBUV and Umkehr (percent per year).

The annual and semiannual terms were included to model second-order seasonal effects in the SBUV–Umkehr difference. The regression model was fit individually to the data in each layer from each station, and an estimate of the drift (d) for the network was computed along with its 95 percent confidence interval. The results of the individual stations were combined using a weighting function proportional to the number of observations and inversely proportional to the square of the standard deviation. The change in SBUV ozone was estimated using the same regression model (described above) applied to the coincident SBUV data. Table 5.5 shows the 8-year drift of SBUV relative to the Umkehr network, the total change in SBUV over the Umkehr network, and the change in Umkehr computed using the SBUV as a transfer standard. The 95 percent confidence intervals (not including possible systematic errors) are included in the table.

Table 5.5 SBUV Trend Collocated With 11 Umkehr Stations, the Trend of the Difference (SBUV–Umkehr), and the Derived Umkehr Trend for 1979 to 1986

Trends are expressed as percent change in 8 years (95 percent confidence level). No corrections are made for aerosols except to omit 3 years of data after eruption of El Chichón. Compare with line (B) in Table 5.7

	% ozone change in 8 years		
Quantity	Layer 6	Layer 7	Layer 8
SBUV	−7 ± 1	−12 ± 1	−15 ± 2
(SBUV–Umkehr)	−5 ± 3	−3 ± 3	−5 ± 4
Umkehr	−2.4 ± 2.6	−9.6 ± 3.3	−10.4 ± 4.3

This method of reducing the effect of El Chichón aerosols on the Umkehr network is regarded as insufficient, and the problem of correcting for aerosols is considered in the next section.

5.5.2 An Analysis of Northern Midlatitude Umkehr Measurements Corrected for Stratospheric Aerosols for 1979 to 1986

5.5.2.1 Introduction

This section is based on a report by DeLuisi et al. (1983), some of which is directly quoted here. This report is also discussed in Chapter 10, and that discussion is not repeated here.

Umkehr observations of ozone profiles have been used in a variety of ways to assess characteristics, variations, and trends in ozone concentration in the upper stratosphere (e.g., Bojkov, 1969a; Angell and Korshover, 1983b; Reinsel et al., 1984; and others). They have also been used for comparison with ozone profile data from other observational methods such as ozone-

sondes, satellite, and lidar (Craig et al., 1967; DeLuisi and Mateer, 1971; DeLuisi and Nimira, 1977; DeLuisi et al., 1979; DeLuisi et al., 1985; Megie et al., 1985, and many others). Moreover, they are the observations that revealed a serious drift in the sensing of upper stratospheric ozone by the SBUV (Fleig et al., 1981).

It is well known that the Umkehr is affected by the presence of stratospheric aerosols (DeLuisi, 1969 and 1979; Dave et al., 1979) that act as additional scatterers and attenuators not included in the present inversion algorithm for ozone profiles (Mateer and Dütsch, 1964). The empirically derived errors are well matched by the theoretical calculations of Dave et al. (1979), who accounted for multiple scattering and atmospheric sphericity. In principle, an observed aerosol profile using lidar can be used to calculate the error to a concurrent Umkehr observation (see Chapter 10).

5.5.2.2 Procedure

Monthly averages of lidar aerosol profile data from Langley, VA; Boulder, CO; Aberystwyth, Wales; Haute Provence, France; and Garmisch–Partenkirchen, F.R.G., were used in a radiative transfer computer code developed for the previous work of Dave et al. (1979). The aerosol size distribution was selected from a collection of samples made by NASA/Ames U2 flights to the interior of the El Chichón cloud (Oberbeck et al., 1983). The radiative transfer code requires realistic midlatitude ozone profiles that vary with season. The ozone profile data used in these calculations were supplied from the work of Tiao et al. (1986).

The radiative transfer code by Dave et al. (1979) was used to compute an Umkehr with stratospheric aerosols and an Umkehr without stratospheric aerosols. The difference between the Umkehr with stratospheric aerosols and the corresponding one without is called the "Umkehr error."

5.5.2.3 Results and Discussion

Figure 10.22 is a plot of monthly average stratospheric aerosol optical thickness vs. time derived from the lidar observations. The results of the aerosol observations and calculated ozone profile errors (Figure 10.21) are used to correct Umkehr measurements from five stations in the northern midlatitudes. These stations are Belsk, Poland; Arosa, Switzerland; Lisbon, Portugal; Boulder, CO; and Tateno, Japan (compare Figure 5.22). These stations were chosen solely on the basis of their higher frequency of measurements compared to other stations. Data are analyzed in terms of monthly averages, from 1979 to 1986, of the five Umkehr stations.

The monthly average Umkehr errors (the corrections to be applied to the data) and the lidar optical depths are given over the 8-year period in Table 5.6. The maximum optical thickness of 0.113 occurred in January 1983, and the maximum corrections for aerosols were -4.6 percent for layer 6, -14.7 percent for layer 7, and -26.0 percent for layer 8. For layer 7, for example, the corrections were about -0.5 percent in 1979 and -2 percent in 1986, showing less than total recovery from El Chichón even in 1986.

One check on the corrected Umkehr data is to take Figure 5.11, which gives the time series of the SAGE–II and SBUV cluster mean at 40°N, and to insert the corrected Umkehr data on the plot, as in Figure 5.23. The SAGE–II and SBUV data are the zonal average of the matched clusters; the Umkehr data are from the Tatena, Arosa, Belsk, and Lisbon stations. The Umkehr data show the same seasonal trends at all layers as those shown by SAGE–II and SBUV, including the opposite

Table 5.6 Corrections for Aerosols Applied to Umkehr Data on the Basis of Lidar Measurements and DeLuisi's Model

The values are the calculated percentage error due to aerosols in the monthly average ozone reported for the stations Tateno, Arosa, Boulder, Belsk, and Lisbon at Umkehr layers 6, 7, and 8. "Tau" is the aerosol optical thickness as determined by lidar.

Month	Year	Layer 6	Layer 7	Layer 8	Tau
JAN	1979	-0.4	-0.8	-0.4	0.001
APR		-0.2	-0.3	-0.5	0.001
JUL		-0.2	-0.6	-0.9	0.002
OCT		-0.3	-0.8	-0.3	0.001
JAN	1980	-0.1	-0.5	-0.8	0.002
APR		-0.3	-0.6	-0.8	0.002
JUL		-0.1	-0.7	-1.9	0.008
OCT		-0.1	-1.0	-1.3	0.006
JAN	1981	0.0	-0.2	-0.8	0.003
APR		-0.2	-0.6	-0.9	0.002
JUL		0.0	-1.0	-2.4	0.006
OCT		-0.5	-1.8	-1.5	0.004
JAN	1982	-0.1	-0.2	-0.9	0.005
APR		-0.8	-1.9	-2.2	0.010
JUL		-0.4	-2.7	-7.2	0.022
OCT		-0.8	-5.1	-15.1	0.044
JAN	1983	-4.6	-14.7	-26.0	0.111
APR		-1.9	-7.0	-14.8	0.081
JUL		-0.9	-6.0	-12.5	0.050
OCT		-0.3	-5.3	-8.7	0.036
JAN	1984	-0.7	-2.6	-6.7	0.029
APR		-0.6	-2.2	-6.3	0.022
JUL		-0.3	-2.2	-4.5	0.013
OCT		-0.4	-2.3	-3.6	0.013
JAN	1985	-0.5	-1.2	-3.8	0.013
APR		-0.3	-0.7	-3.5	0.011
JUL		-0.1	-1.1	-2.9	0.008
OCT		-0.2	-1.7	-2.7	0.009
JAN	1986	-0.4	-0.7	-2.4	0.007
APR		-0.1	-0.3	-2.4	0.007
JUL		-0.7	-1.9	-3.1	0.011
OCT		-0.5	-2.3	-3.4	0.009

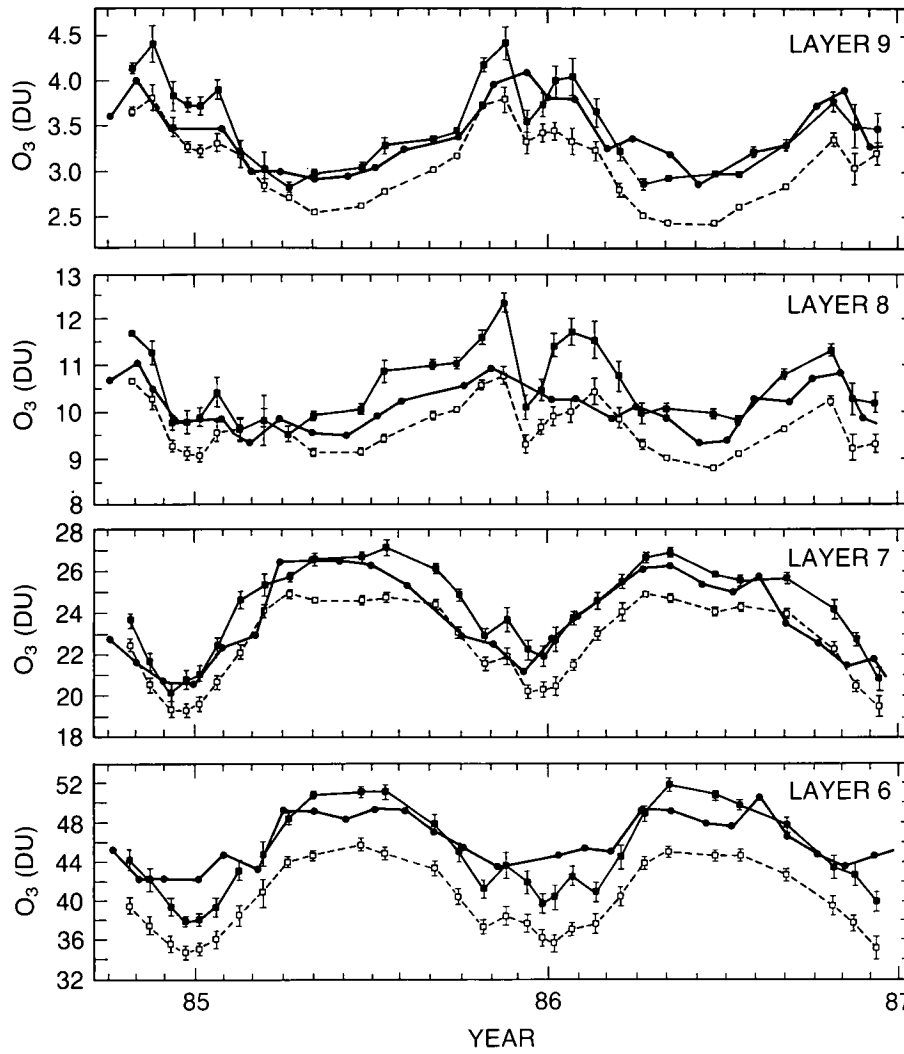

Figure 5.23 Aerosol-corrected Umkehr observations (Arosa, Belsk, Lisbon, and Tateno) plotted as a function of time in comparison with zonal average SAGE–II and SBUV data at 40°N latitude. This figure is a copy of Figure 5.11 with the Umkehr data added.

phases at layers 6 and 7 relative to layer 9. In absolute value, Umkehr agrees very well with SAGE–II in layers 6 and 9, the agreement is good in layer 7, and, in layer 8, Umkehr parallels SBUV better than SAGE–II parallels SBUV (layer 8 is in the transition region between the out-of-phase layers 7 and 9, and comparisons here are strongly dependent on details of sampling). This good agreement between the time series data of Umkehr and the satellites is not necessarily evidence for the validity of the aerosol correction factors for Umkehr, since these corrections are already small for the data in this figure (compare Table 5.6).

For 1979–1986, the uncorrected Umkehr data and the corresponding corrected Umkehr data are plotted for layers 6, 7, and 8 in Figures 5.24 to 5.26. The uncorrected data show a notable decrease between mid-1982 and mid-1983. The correction removes most of the anomaly, but the final values remain lower at the end of the record compared to the beginning. If one examines the long-term features in these figures, it is obvious that the ozone in layers 7 and 8 tends toward lower values.

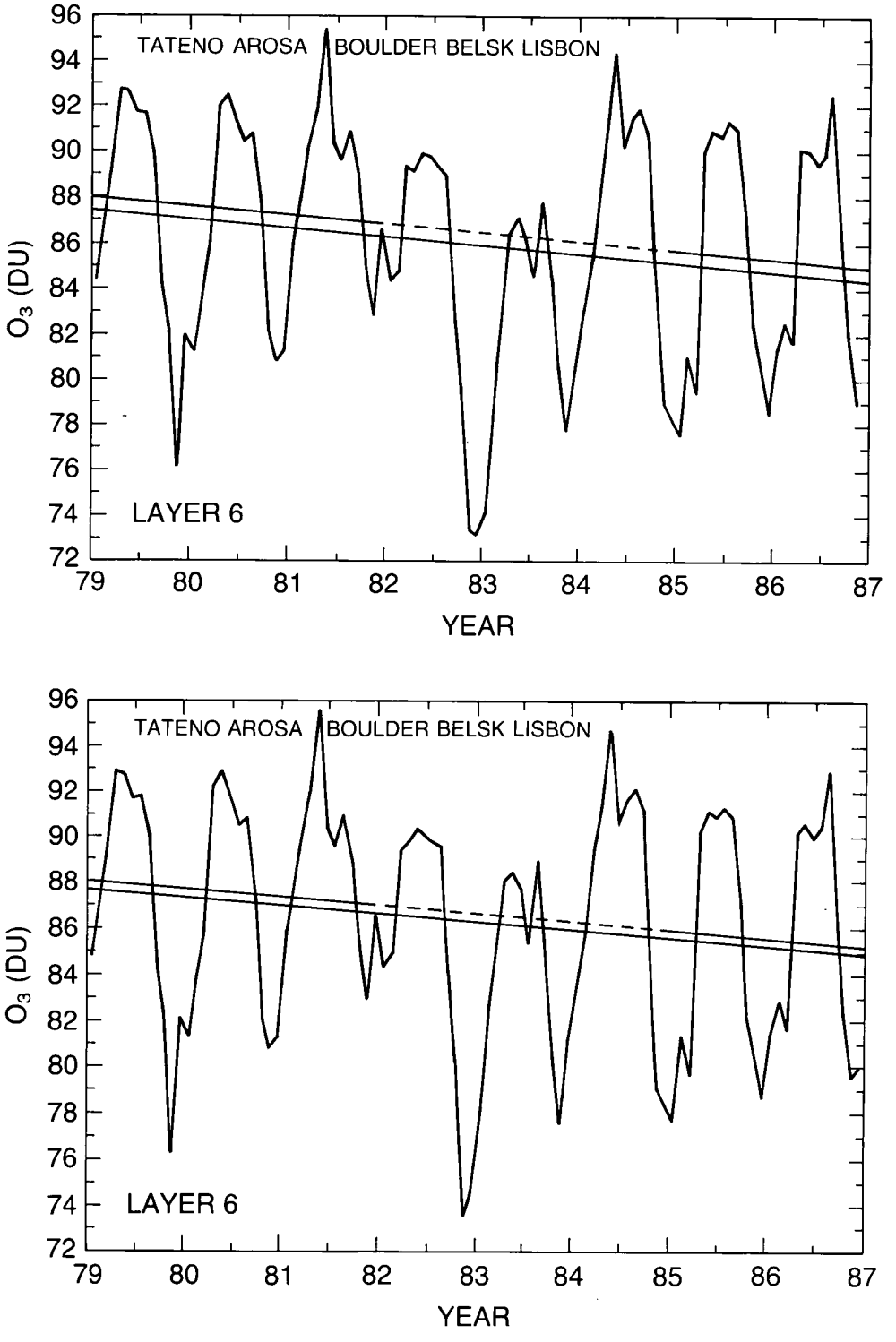

Figure 5.24 Plots of monthly average ozone concentration vs. time in Umkehr layer 6 for five Umkehr stations for precisely 7 years, including 1979 through 1986. Data were supplied courtesy of the World Ozone Data Center in Toronto. The data in the upper panel data have not been corrected for stratospheric aerosol error. Note the error effects of El Chichón during the winter of 1982–1983. The data in the lower panel have been corrected for aerosols by DeLuisi et al. (private communication, 1988). The least-squares lines are: Solid line includes all 7 years of data; Solid-dashed-solid line omits precisely the 3 years 1982, 1983, and 1984.

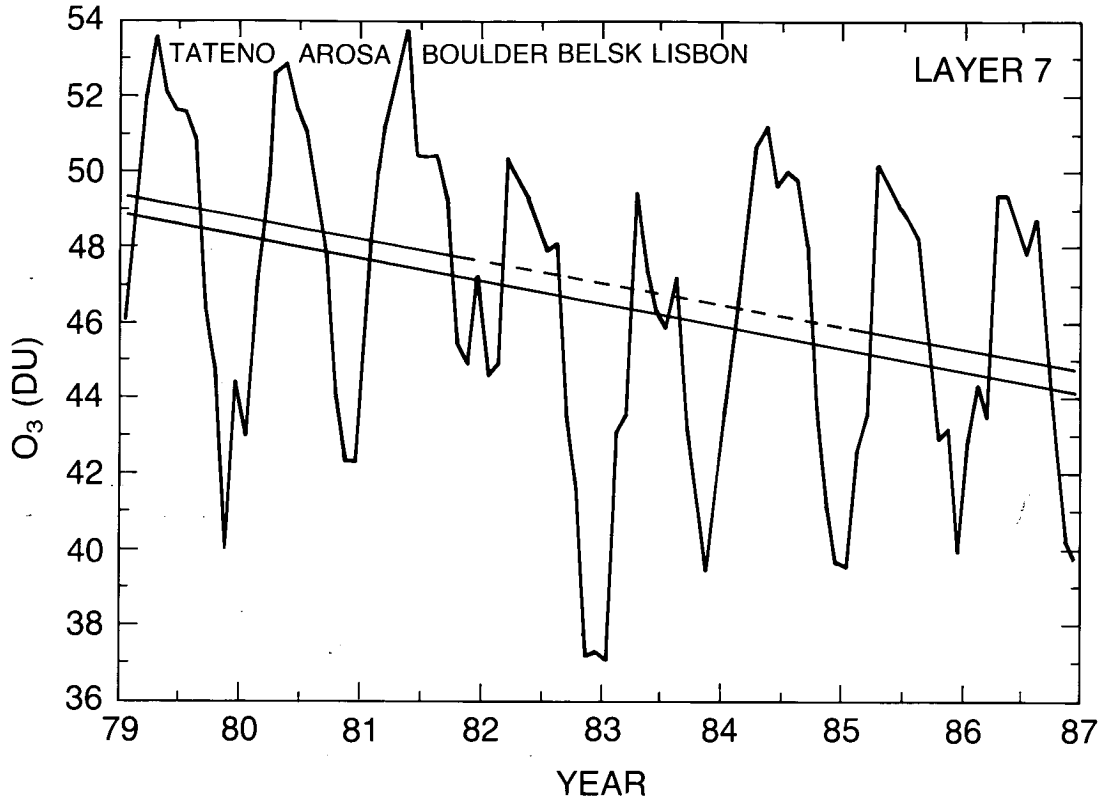

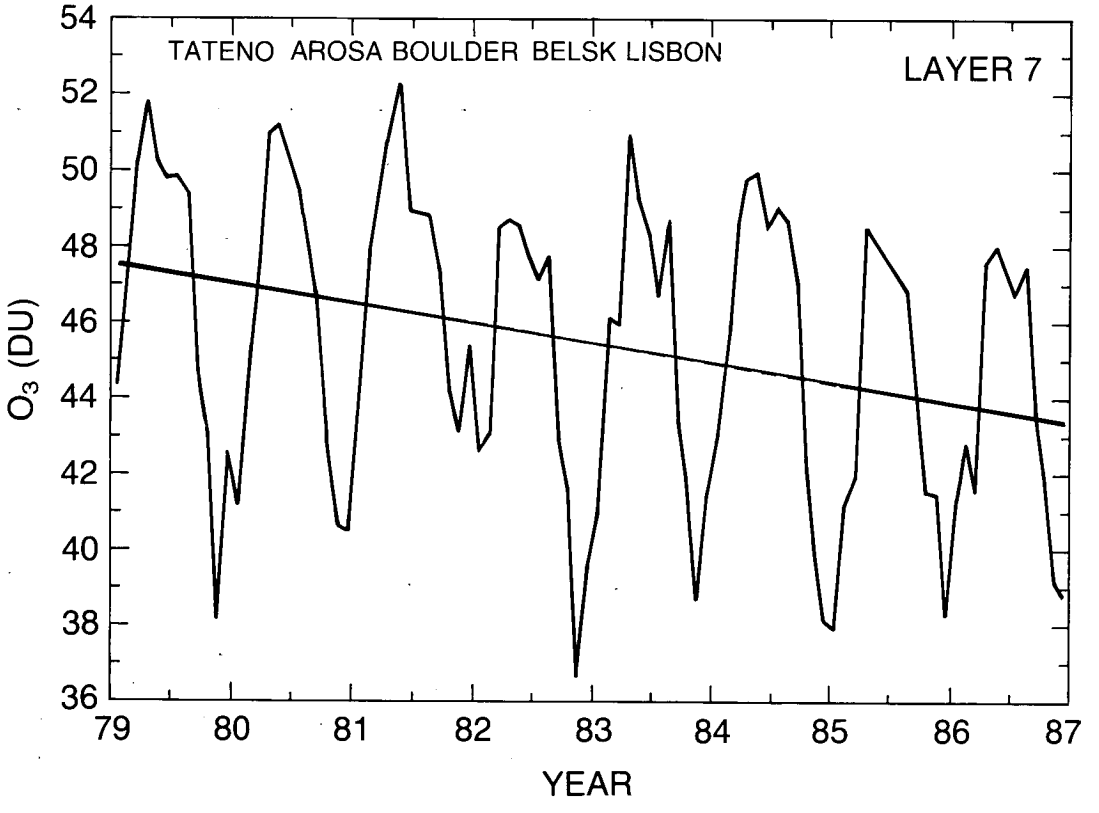

Figure 5.25 Same as 5.24, except it is for layer 7.

For each of the six panels of these figures, there are two lines. The solid line is simply a linear least-squares fit of all the data (including seasonal cycles) from January 1, 1979, through December 31, 1986. The other line is similar, including the data from January 1, 1979, through December 31, 1981, omitting data from January 1, 1982, through December 31, 1984 (the El Chichón eruption occurred in the spring of 1982), and including data from January 1, 1985, through December 31, 1986. All 12 lines show an ozone decrease between 1979 and 1986. In any one figure, the slope of the line including 8 years of data and the slope of the line omitting 3 years of data (mostly after El Chichón) appear to be about the same. These slopes are given in Table 5.7. In all cases, the decreasing slope is less steep when aerosol corrections are made; the greatest difference, occurring in layer 8, is -12.6 percent without correction and -8.7 percent with correction. In each case, the slope for the full 8 years is close to that with 3 years of data removed (1982, 1983, and 1984). For Umkehr layers 6, 7, and 8, the ozone change over the 8-year period (including aerosol correction) is -3.1, -8.5, and -8.7 percent, respectively. SBUV reports ozone changes of about -5, -10, and -15 percent at these altitudes. The maximum ozone change shown by SAGE–I and SAGE–II is about -3 ± 3 percent at Umkehr layer 8 with an estimated systematic error of ± 2 percent.

Table 5.7 Linear Least-Squares Ozone Trends in Umkehr Layers 6, 7, and 8 From January 1, 1979, to December 31, 1986

Trends were derived from four different ways of treating the data: (A) All data, uncorrected for aerosols, (B) Excluding data from January 1, 1982, to December 31, 1984, uncorrected for aerosols, (C) All data, corrected for aerosols, (D) Excluding data from January 1, 1982, to December 31, 1984, corrected for aerosols. Percent change over the 8-year period. Compare Figures 5.23 to 5.25.

Aerosol correction	Years excluded	% ozone change in 8 years		
		Layer 6	Layer 7	Layer 8
(A) Uncorrected		-3.5	-10.0	-12.6
(B) Uncorrected	1982, 1983, 1984	-3.5	-9.7	-11.4
(C) Corrected		-3.1	-8.5	-8.7
(D) Corrected	1982, 1983, 1984	-3.2	-8.8	-8.9

Simple visual inspection of the Umkehr figures or examination of the least-squares slopes presented in the figures shows that the five north midlatitude Umkehr stations give an ozone reduction in the upper stratosphere smaller than that indicated by SBUV and greater than that given by SAGE–I and –II. The next section examines the problem of error estimates of the Umkehr data.

5.5.3 Error Estimates for the Umkehr Trends

5.5.3.1 Sensitivity to Assumed Particle Size Distribution

One uncertainty in calculating the aerosol corrections is the size distribution of the particles. A sensitivity study was made using three different size distributions (including two extreme cases) for each of three different periods (Table 5.8). Where the corrections are large, the two-sigma spread of the correction due to extreme variations in assumed size distributions is about 20 percent of the correction itself—4.6 percentage units out of 21.5—and the average of the three extreme distributions is not largely different from the preferred distribution based on

observed aerosols. The correction for aerosols is not highly dependent on the aerosol size distribution used.

Table 5.8 Sensitivity Study of the Effect of Three Different Assumed Size Distributions for Aerosols: The Distribution Function Based on Observed Aerosols and Two Widely Different Arbitrary Distributions

The mean Umkehr error or the calculated aerosol correction factor is given in percentage units, and twice the standard deviation of the three correction factors is given in the same percentage units. The second set of three values gives the Umkehr error based on the preferred distribution function that was used. The optical thickness is γ.

		Mean Umkehr error $\pm 2\sigma$ (%)		
Date	γ	Layer 6	Layer 7	Layer 8
December 1982	0.087	-1.5 ± 1.0	-9.4 ± 3.8	-21.5 ± 4.6
August 1983	0.041	-1.1 ± 0.4	-6.4 ± 2.0	-10.4 ± 2.4
December 1985	0.008	-0.3 ± 0.2	-0.9 ± 0.2	-2.3 ± 0.8
		Corresponding values for the preferred distribution function		
		Layer 6	Layer 7	Layer 8
December 1982	0.087	-2.1	-10.3	-23.3
August 1983	0.041	-1.4	-7.4	-11.6
December 1985	0.008	-0.3	-1.1	-2.6

5.5.3.2 Sensitivity to Choice of Umkehr Stations

There is one common condition under which a comparison can be made between a 5-station Umkehr network and an 11-station Umkehr network. The last line of Table 5.5 is to be compared with line (B) of Table 5.7. These results are for uncorrected Umkehr data with 3 years omitted to minimize the effect of El Chichón for the 11-station study (Wellemeyer, private communication, 1987) and the 5-station study (DeLuisi et al., private communication, 1988), respectively. For the three Umkehr layers, 6, 7, and 8, these two analyses give, respectively, the 8-year ozone changes (-2.4, -3.5), (-9.6, -9.7), and (-10.4, -11.4). The maximum difference is 1.1 percentage point. The weighting factors used to combine the stations give low weight to the sparse, noisy cases shown in Figure 5.22, and the entire network gives very nearly the same trends as the five stations with the largest density of observations.

Another sensitivity test was to compare results using the five stations with the results found by eliminating either Lisbon or Boulder. Essentially the same results were reached, with or without Lisbon or Boulder.

5.5.3.3 Estimated Trend Error Due to Uncertainty in the Aerosol Correction Algorithm

There is a line of argument that gives insight into the magnitude of the aerosol error. A comparison of the corrected and uncorrected Umkehr time series in Figures 5.24 to 5.26 at the time of maximum aerosol correction (January 1983) suggests that the correction at layer 8 may be too large. One may take as the uncertainty due to aerosols one-half the spread between applying and not applying the correction used here. In percentage points, the full spread between the 8-year ozone decrease, with and without any aerosol correction, is

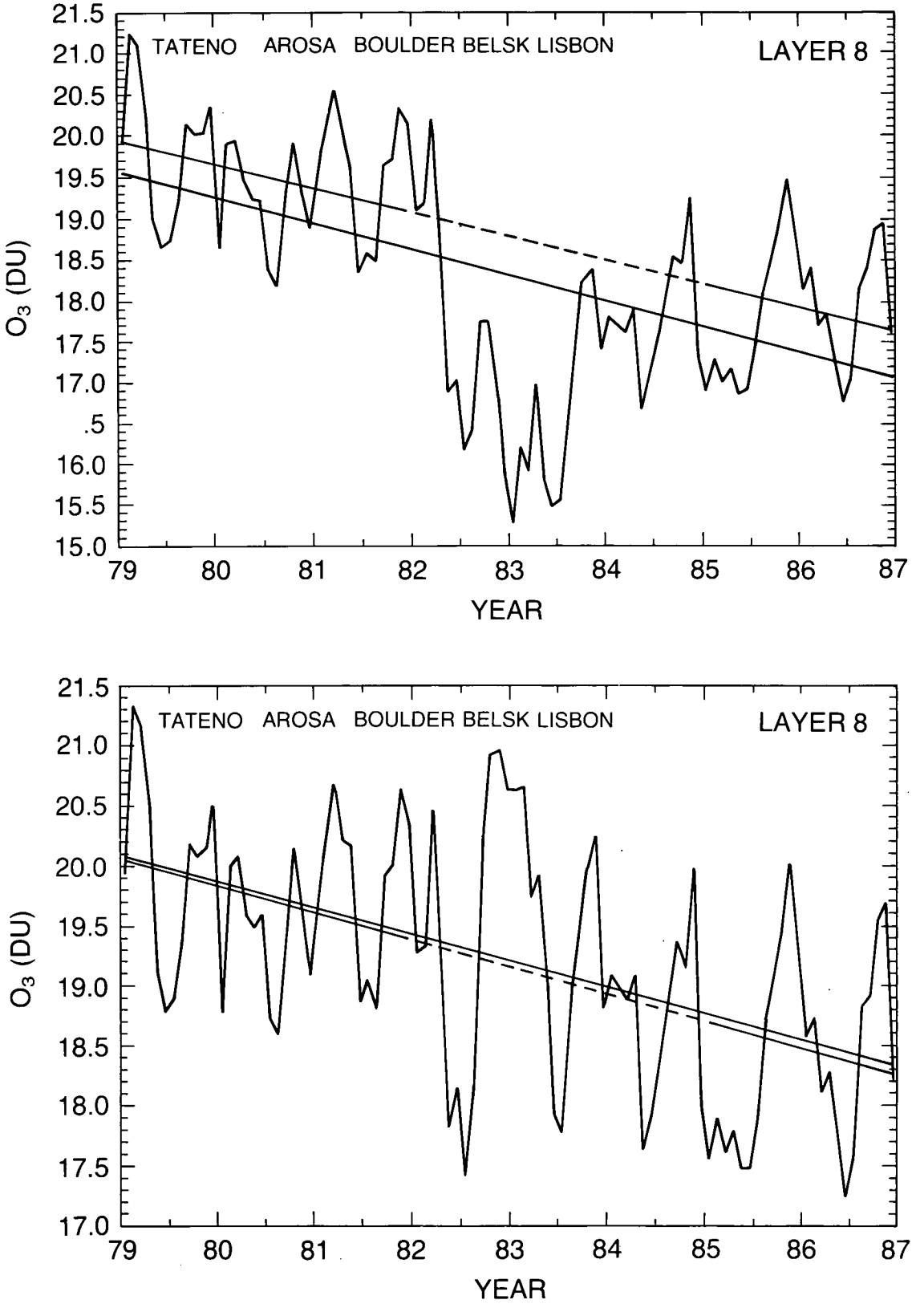

Figure 5.26 Same as 5.24, except it is for layer 8.

-3.1 to -3.5 at layer 6
-8.5 to -10.0 at layer 7
-8.7 to -12.6 at layer 8 (Table 5.7).

With these assignments, the ozone decreases over the 8-year period, including errors just for uncertainty in the aerosol corrections, are

-3.1 ± 0.2 at layer 6
-8.5 ± 0.8 at layer 7
-8.7 ± 2.0 at layer 8.

5.5.3.4 Statistical Errors

Pending an analysis of the statistical errors of the aerosol-corrected Umkehr trends (Table 5.7), the statistical error estimates from the uncorrected 11-station study (Table 5.5) are adopted for the aerosol-corrected trends. This approach may overestimate the error for the five stations selected for their high density of observations, since it includes the stations with sparse and noisy data (Figure 5.22). However, the sparse, noisy data are given low weight by the N/σ^2 weighting function. The estimated random errors are then:

± 2.6 percent at layer 6
± 3.3 percent at layer 7
± 4.3 percent at layer 8.

5.5.3.5 Sampling or Systematic Error

For the five midlatitude stations used in this section, the average reduction of total ozone (as found by local Dobson measurements) across the 8-year period is 6.6 percent, whereas the average value for the renormalized Total Ozone Mapping Spectrometer (TOMS) data at comparable latitudes is 3 or 4 percent (Chapter 4). In the Umkehr method, ozone values reported at layers 6 to 8 are based on features of the observations that are not strongly dependent on total ozone, and a sampling difference in total ozone may make no difference in the upper stratospheric profile. If the large change in total ozone is caused by drift in calibration, then the reduction of ozone reported in the upper stratosphere is probably overestimated. At present, this possible error is not quantified.

5.5.3.6 Central Values and Combined Aerosol and Statistical Error Estimates

The central values of the Umkehr trends are taken to be those corrected for aerosols, including the full 8 years of data (line (C) of Table 5.7). The (95 percent confidence level) statistical error estimates (Section 5.5.3.4) are combined (root sum of squares) with the estimate of the maximum aerosol errors (Section 5.5.3.3). The 8-year ozone changes derived from Umkehr, rounded to the nearest percentage point, are regarded as:

-3 ± 3 percent at layer 6
-8 ± 4 percent at layer 7
-9 ± 5 percent at layer 8.

These error estimates do not include the effect of possible systematic errors besides aerosols.

5.6 SBUV, SAGE–I, AND LIMS OZONE INTERCOMPARISON (SPRING 1979)

The purpose of this study is to examine quantitatively the degree of consistency in stratospheric ozone measurements from three satellite instruments, SBUV, SAGE–I, and LIMS, which were operating at the same time during spring 1979 (Gille and Russell, 1984; Remsberg et al., 1984). The analysis is an intercomparison of the ozone data from these instruments in terms of ozone column abundance in four Umkehr layers (6 to 9). In the case of SAGE–I and LIMS, it is necessary to convert their primary measured ozone quantities to ozone Umkehr layer amount for comparison purposes. Since the sampling locations of the SAGE–I instrument are distributed in a narrow latitudinal belt for a 24-hour period, as opposed to the nearly global observations of the SBUV and LIMS for the same period, the comparison analysis is carried out by following the SAGE–I latitudinal sampling progression. Because the three satellite instruments never sampled at the same locations and times, the comparison is made in terms of the zonally averaged ozone layer amount in these Umkehr layers. The ozone data from SBUV are from the version 5 retrieval, the SAGE–I ozone data are a recently revised product (Chapters 2 and 3), and the LIMS data are the combined mode zonal mean coefficients from the LIMS Map Archival Tapes (LAMAT).

The SAGE–I instrument takes 15 sunrise and 15 sunset measurements per day, which are distributed almost evenly in the longitudinal direction along a nearly constant latitude circle. The mean value derived from these 15 sunrise/sunset SAGE–I daily measurements represents the zonal mean for that day. The corresponding daily zonal means of SBUV and LIMS were obtained by interpolation with latitude. Table 5.9 gives the latitudinal progression of the daily SAGE–I data for both sunrise and sunset measurements during spring 1979.

Table 5.9 The Beginning and Ending Dates (in 1979) and Latitudes of Four Cases of Longitudinal Progression of the SAGE–I Observations

	Begin		End	
SAGE–I	Date	Latitude	Date	Latitude
1 Sunrise	March 2	57.1°N	March 31	55.4°S
2 Sunset	March 2	37.3°S	March 21	64.0°N
3 Sunrise	April 6	57.7°S	April 29	41.8°N
4 Sunset	April 1	50.7°N	April 28	51.8°S

For the cases of March 1979 sunrise and of April 1979 and SAGE–I sunset, the zonal mean ozone layer amounts are given in Figures 5.27 and 5.28. The standard deviation of the SAGE–I instrument about its zonal means, shown by the vertical bar, is less than 10 percent except at high latitudes. The standard deviation for LIMS about its zonal mean is about 4 percent, and that for SBUV is about 2 percent. The three satellite systems show the same pattern with latitude. The same data are presented in Figures 5.29 and 5.30 as the deviation of each instrument against the mean of the three. The results displayed in these two figures show that SBUV data are about 3 percent systematically lower than the other instruments in layer 6, but not systematically different from the other satellite instruments in layers 7, 8, and 9.

For each of the three satellite instruments, the four Umkehr layers, and the four times, the root-mean-square deviation from the average of the three instruments is given in Table 5.10. For 15 of 48 entries in the table, the deviations are less than 3 percent; for 23 of 48 entries the deviations are between 3 percent and 5 percent; and for 10 of 48 entries the deviations are greater than 5 percent but less than 10 percent. These data give an example of how closely three totally

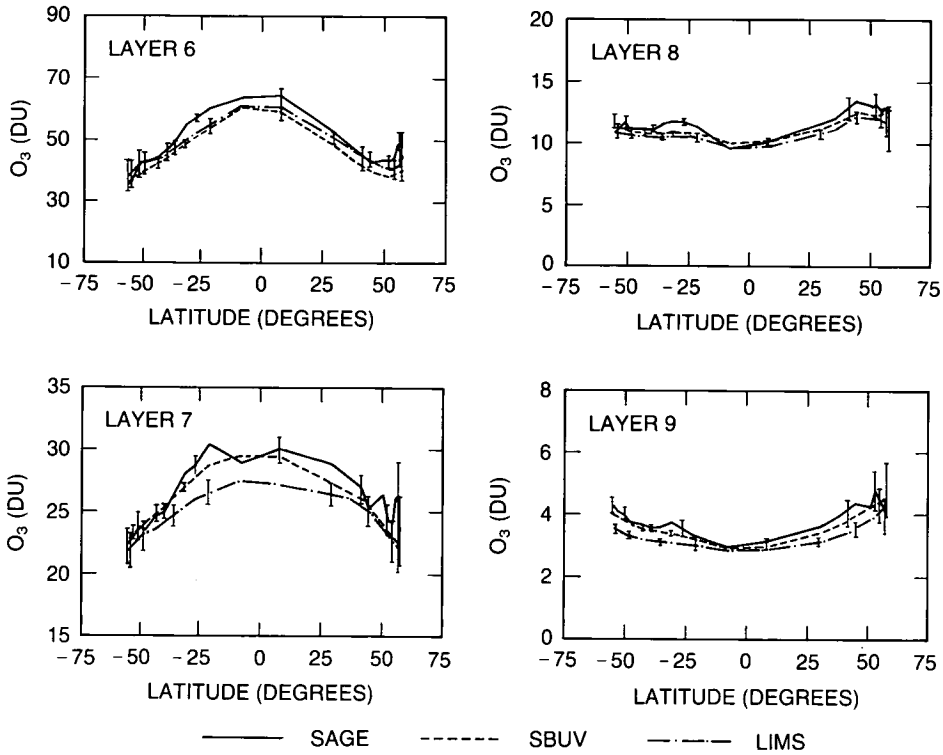

Figure 5.27 Comparison of zonal mean ozone layer amount calculated from the SBUV, SAGE–I, and LIMS observations for the case of March 1979 SAGE–I sunrise (Table 5.9).

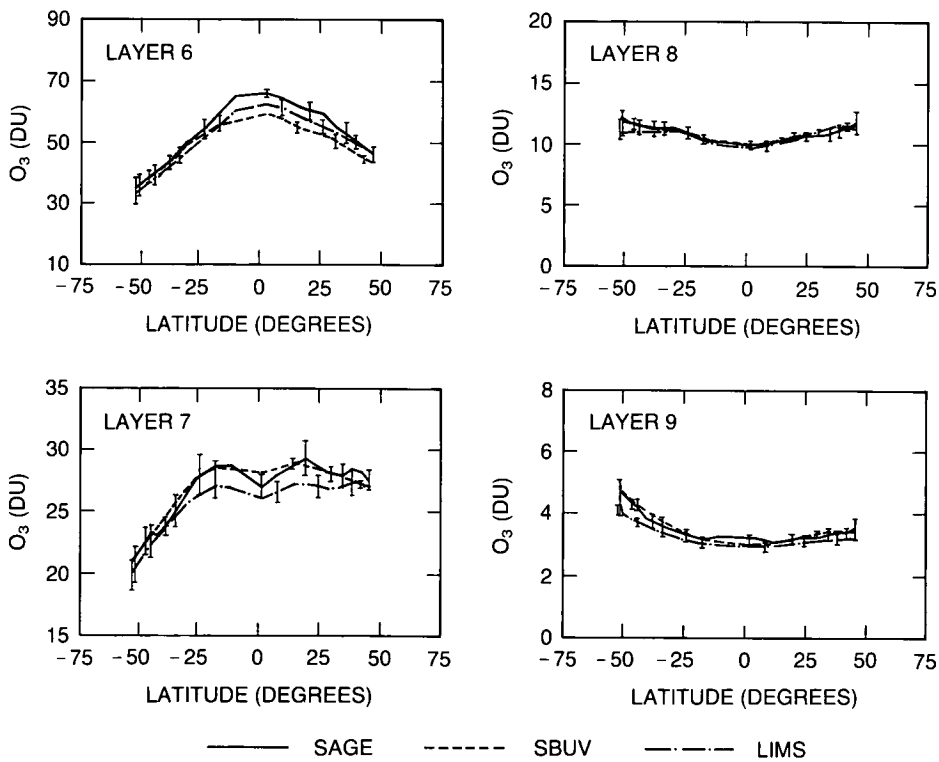

Figure 5.28 Same as Figure 5.27 except for April 1979 SAGE–I sunset.

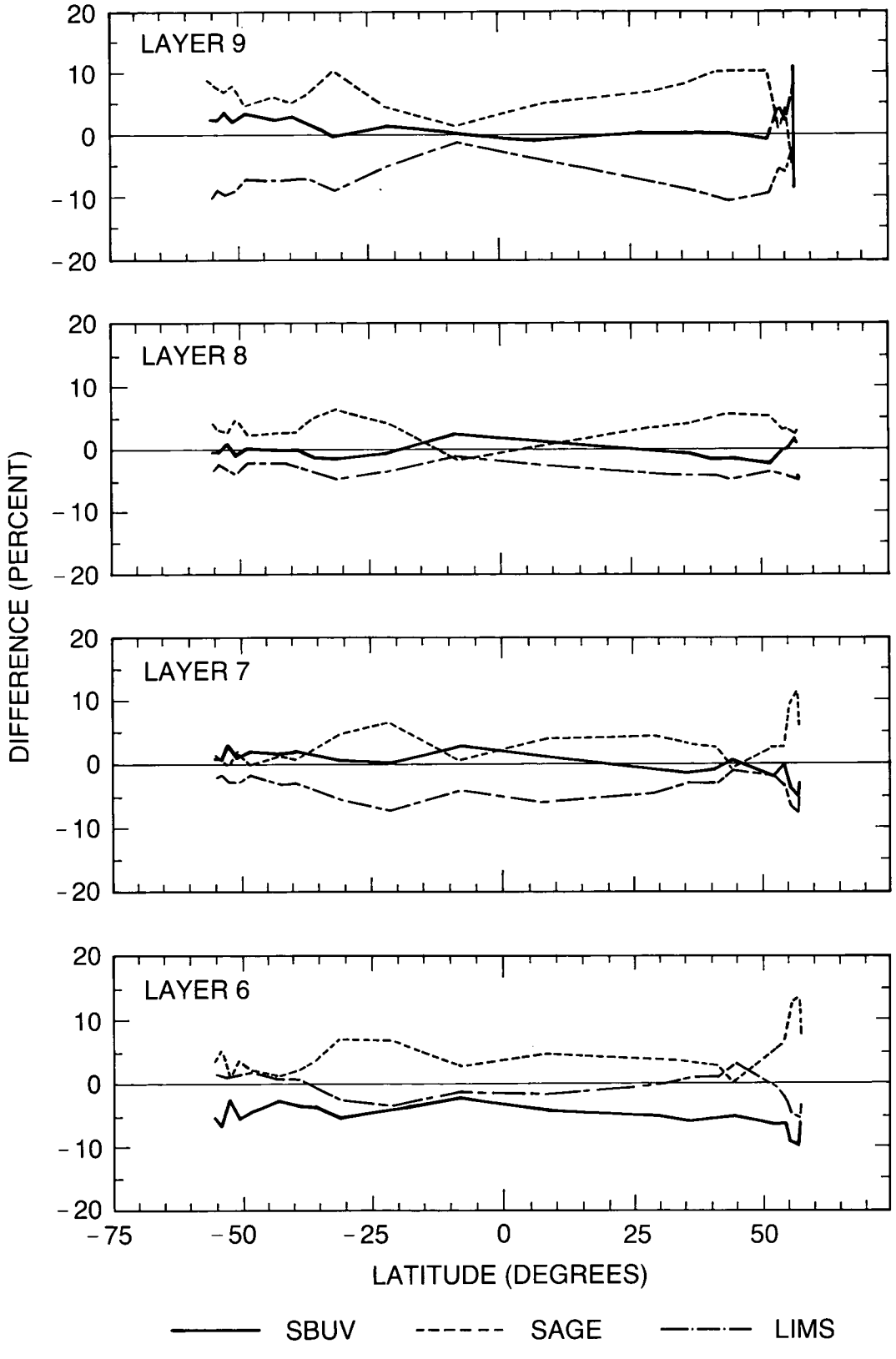

Figure 5.29 Percentage difference of zonal mean ozone layer amount of SBUV, SAGE–I, and LIMS from the average for the case of March 1979 SAGE–I sunrise (Table 5.9).

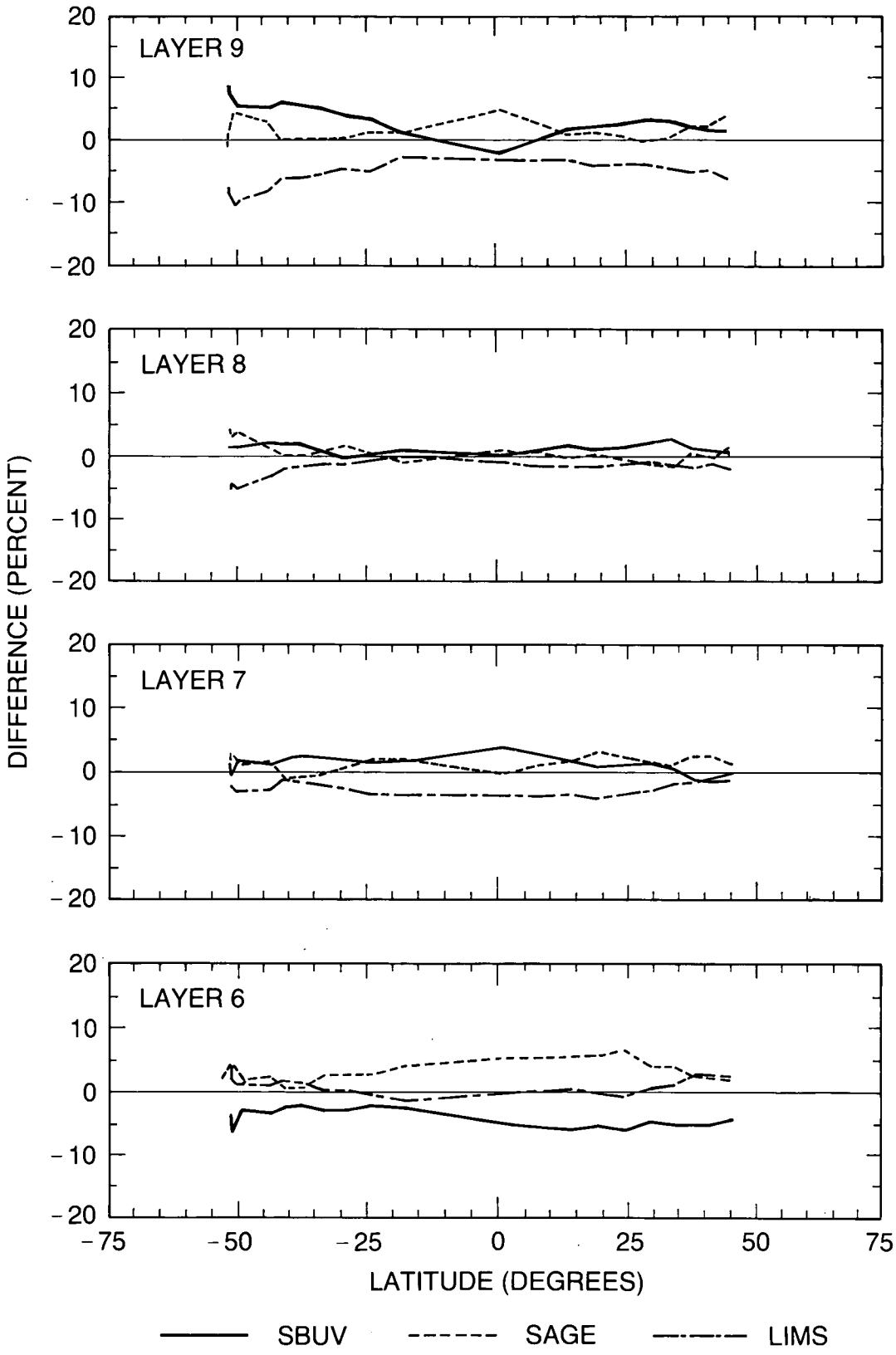

Figure 5.30 Same as Figure 5.29 except for April 1979 SAGE–I sunset.

different, newly launched satellite systems agree with each other in measuring zonal mean ozone amounts in the four Umkehr layers in the middle to upper stratosphere (about 4 percent).

Table 5.10 Estimated Overall Percentage Differences of the Calculated Zonal Mean Ozone Layer Amount of SBUV, SAGE–I, and LIMS With Respect to the Average of These Instruments

	Umkehr Layer					
	Layer 6			Layer 7		
SAGE–I	SBUV	SAGE	LIMS	SBUV	SAGE	LIMS
1 Sunrise (March 1979)	4.5	6.3	2.6	2.4	4.2	4.6
2 Sunset (March 1979)	2.8	3.1	1.6	3.8	2.8	4.0
3 Sunrise (April 1979)	5.1	3.7	1.3	2.9	1.5	3.7
4 Sunset (April 1979)	3.8	3.6	1.2	2.8	1.4	3.4
	Layer 8			Layer 9		
	SBUV	SAGE	LIMS	SBUV	SAGE	LIMS
1 Sunrise (March 1979)	1.6	3.6	4.4	4.2	6.1	8.9
2 Sunset (March 1979)	3.0	4.1	4.2	3.3	7.7	8.6
3 Sunrise (April 1979)	1.6	3.2	3.9	3.0	7.3	9.5
4 Sunset (April 1979)	2.6	1.7	3.3	6.2	1.8	6.9

5.7 TRENDS AT UPPER BOUNDARY OF THE STRATOSPHERE (SBUV, SME, SMM)

5.7.1 SBUV Results

The SBUV instrument reports the largest percentage local ozone reduction at 50 km, the upper boundary of the stratosphere (Figure 5.4), and the upper limit of direct information content from SBUV (Chapter 3). Two satellite instruments have measured ozone in the mesosphere down to an altitude just above the upper limit of SBUV (Rusch et al., 1984; Aikin et al., 1984; Aikin, private communication, 1987). Although these instruments do not cleanly overlap SBUV, they provide evidence about ozone trends at the upper boundary of the SBUV region. The time series data of these two instruments are examined here.

5.7.2 Solar Mesospheric Explorer

The Solar Mesospheric Explorer (SME) is described by Rusch et al. (1984) and in the calibration and algorithm chapters of this report. The SME spacecraft measures ozone by means of two instruments. The ultraviolet spectrometer (UVS) operates as an ultraviolet backscatter instrument, as is the case with SBUV, but the SME UVS is used in a limb-viewing mode rather than the nadir, as with the SBUV. The near-infrared spectrometer (NIRS) operates by limb viewing the 1.27 μ airglow emission that arises from excited molecular oxygen produced during ozone photodissociation. Ozone concentrations can be derived from the 1.27 μm emission.

Certain instruments on the SME are known to drift with time, and SME has onboard methods for the indirect calibration of the drifting instruments (Chapter 3). In 1987, the SME team reinterpreted and updated the SME data, including an analysis of the drift of the ultraviolet spectrometer (Rusch and Clancy, 1988). The sensitivity of the upper channel of the ultraviolet

spectrometer was judged to have decreased 4.8 ± 1.37 percent per year. This correction and its uncertainty affect the ozone trends, as indicated by both the UVS and the NIRS methods.

The ozone-mixing ratios as measured by the SME UVS (+) and the SBUV (*) at 1.0 mb in 1982 are shown as a function of latitude in Figure 5.31. The data are monthly averaged values for the two instruments. The absolute values of the ozone-mixing ratio and the latitude dependence are in agreement for most times and locations. The results agree generally within 10 percent.

Trends in ozone at 0.75 mb are evaluated from the SME data by both the airglow and infrared methods. The trends are derived using average (0° to 60°N) ozone-mixing ratios from each instrument for the first 2 weeks in June for the 5 years 1982–1986. The SME data are limited to the June period, as processing for other times is not yet complete and the satellite attitude was optimum in June. The trends, derived from the June data by use of a linear least-squares fit, are 1.57 percent per year for the UVS and 2.4 percent per year for the NIRS. The airglow results can be evaluated by a method that is independent of the UVS and that relies only on the spacecraft attitudes determined by the horizon sensors; this method gives an ozone increase of 1.8 percent per year. By using the extremes (2σ) of the uncertainties in the UVS sensitivities in inverting the data (4.8 ± 1.37 percent per year), the range in the trends is shown in Figure 5.32. The values of the ozone trends at the extremes of the sensitivity changes are -0.7 and +4.1 percent per year. These values from SME are inconsistent with the large ozone decreases displayed by SBUV in Figures 5.3 and 5.4.

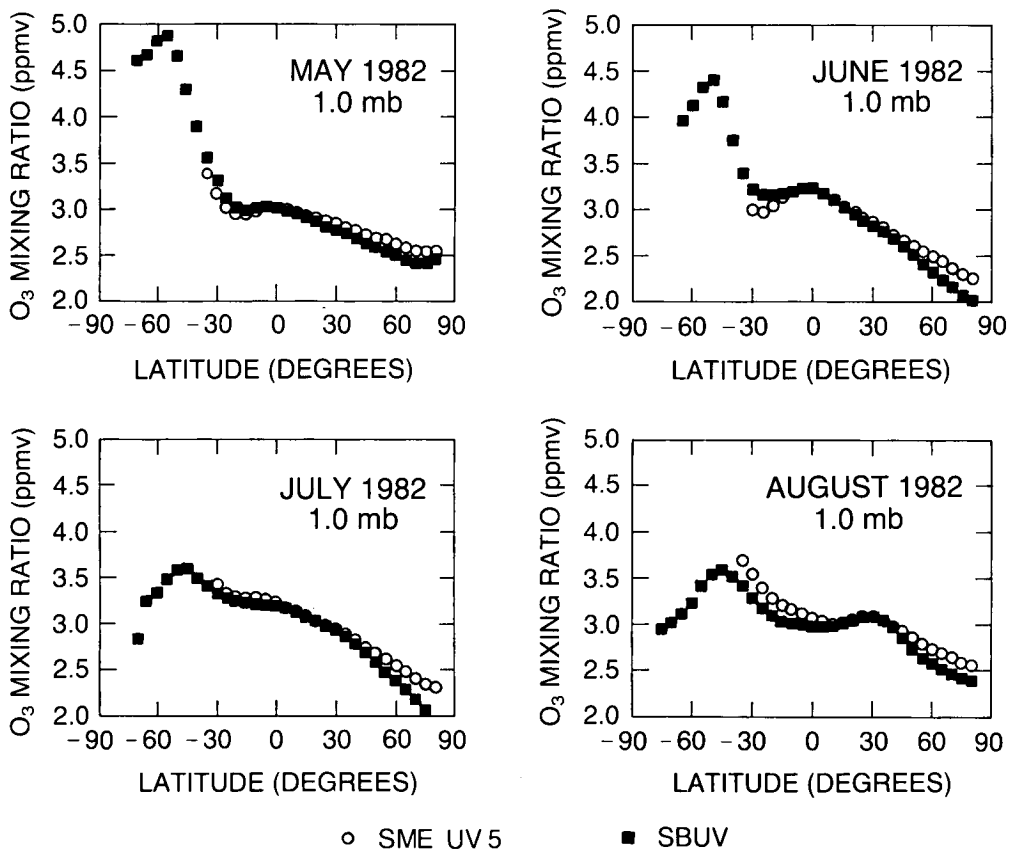

Figure 5.31 SME UVS (+) and SBUV (*) average (0° to 60°N) mixing ratios at 1.0 mb for May, June, July, and August.

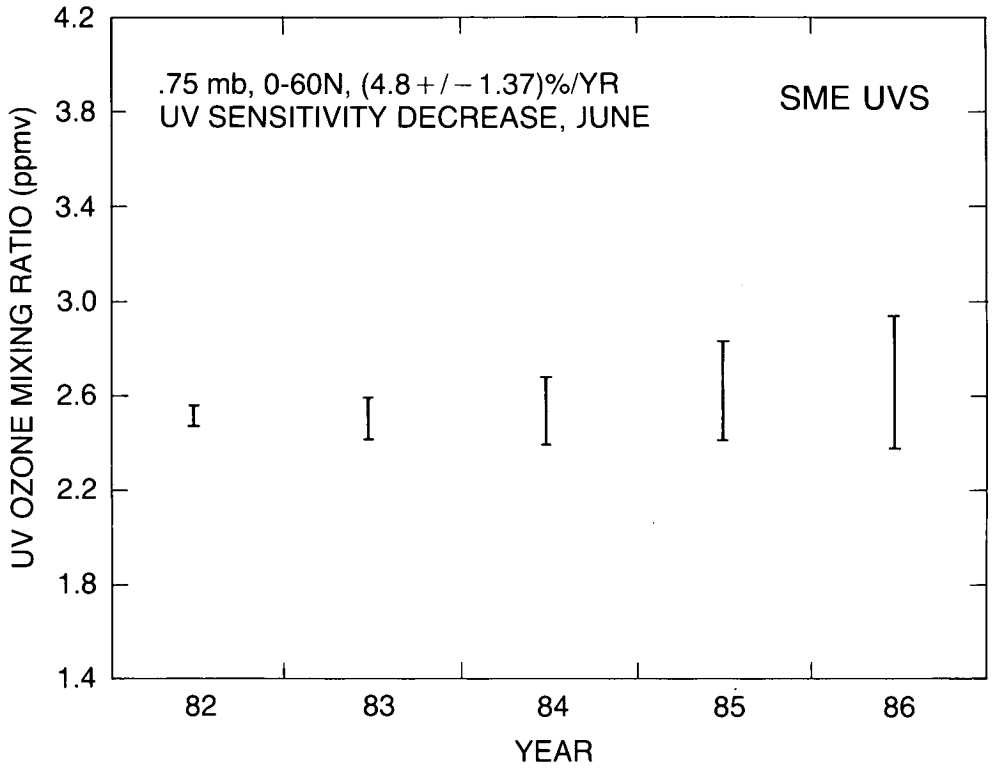

Figure 5.32 Envelope of maximum (2σ) trend of ozone mixing ratios from the UVS instrument of SME for June 1982 to 1986 at 0.75 mb. The error bars denote the range of the data (2σ) resulting from uncertainty in the determination of UVS sensitivity change with time.

5.7.3 Solar Maximum Mission

Ozone altitude profile data from 1984–1988 have been obtained by observing solar occultation with the Ultraviolet Spectrometer Polarimeter (UVSP) on the Solar Maximum Mission (SMM) spacecraft. Launch occurred in early 1980, and solar pointing was lost in late 1980. In-orbit spacecraft repairs were effected in 1984; operations have continued since that time. Details of the instrument and its performance are described by Woodgate et al. (1980). The method of obtaining ozone concentrations as a function of altitude is given by Aikin et al. (1984) and by Aikin (private communication, 1987).

The SAGE instrumentation operates on the same solar occultation principle as the SMM experiment, except that longer wavelengths are employed by SAGE. The altitude range of SAGE is about 25 km to 60 km. Several SMM and SAGE profiles were compared; for example, see Figure 5.33. The concentration of ozone reported by SAGE–II is systematically neither higher or lower than that of SMM (UVSP on the figure).

Figures 5.34 and 5.35 present the weekly mean ozone concentration at an altitude of 55 km plotted as a function of time for the latitude of 20° north and south. Also shown as a histogram is the total number of occultations included in each weekly mean. Since occultation observations were interrupted for a variety of reasons, the data record is not continuous, and there is not a uniform number of points in each sample. The SMM data show seasonal variations, but no obvious trend.

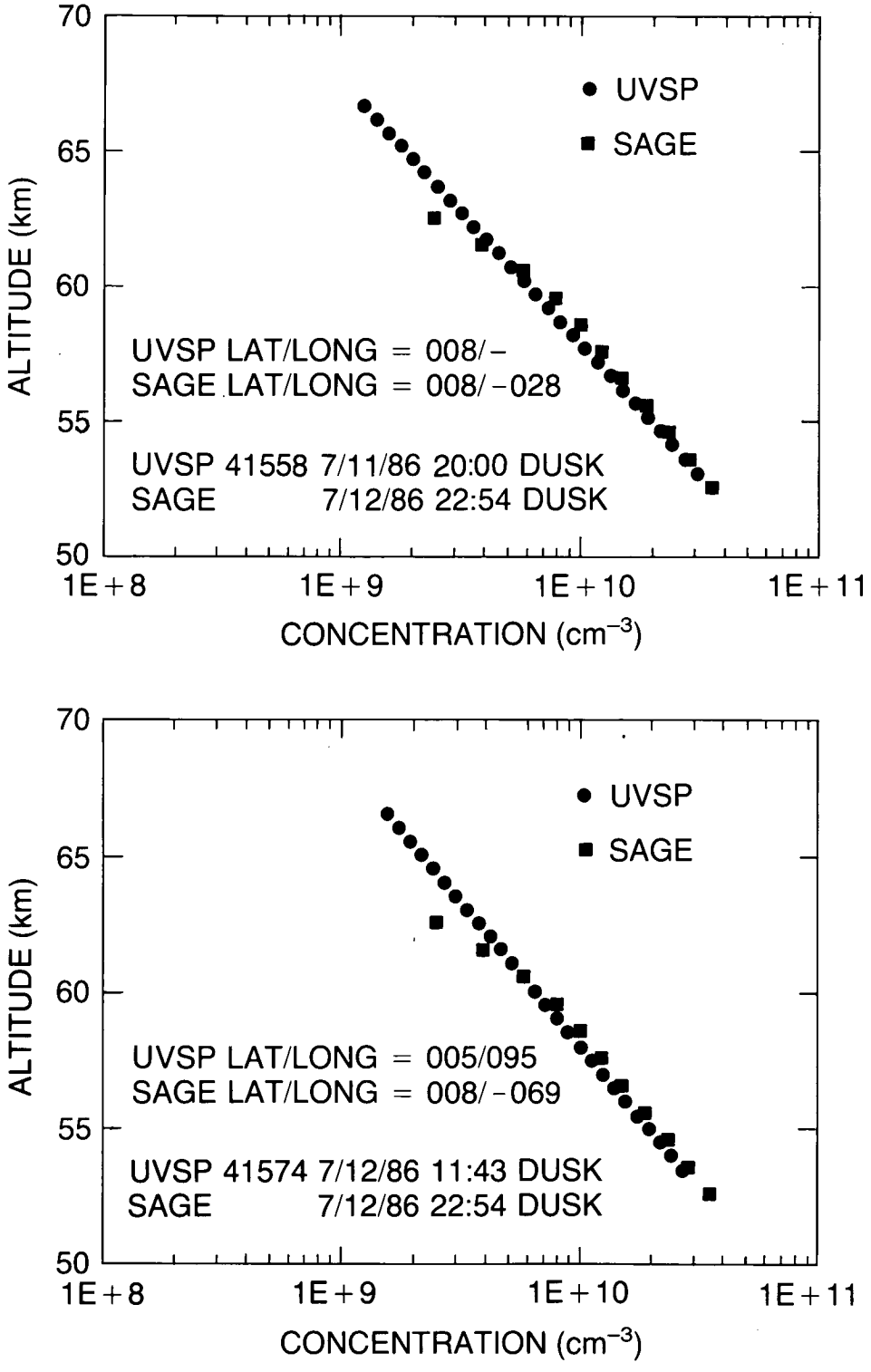

Figure 5.33 Ozone concentration versus altitude for SMM (UVSP) and for SAGE–II.

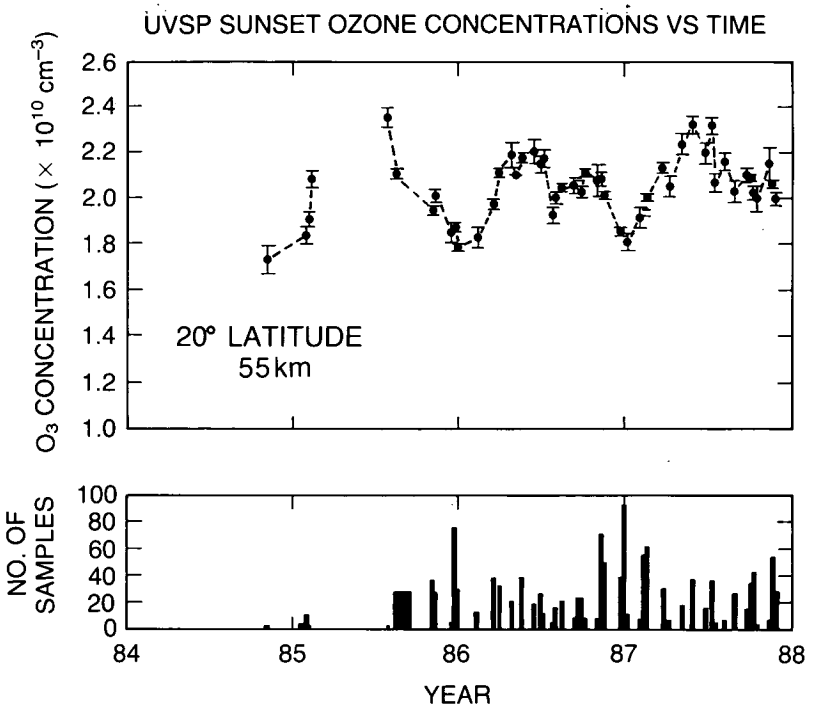

Figure 5.34 Sunset ozone concentrations from the SMM instrument in the 53–57 km region plotted as a function of time for 20°N. Each point represents a weekly mean. The histogram gives the number of profiles, contributing to each weekly mean point. The solid curve is the SBUV 0.4 mb weekly mean ozone concentration. The SBUV and SMM data were taken at different local times; at these altitudes, ozone changes during the diurnal cycle.

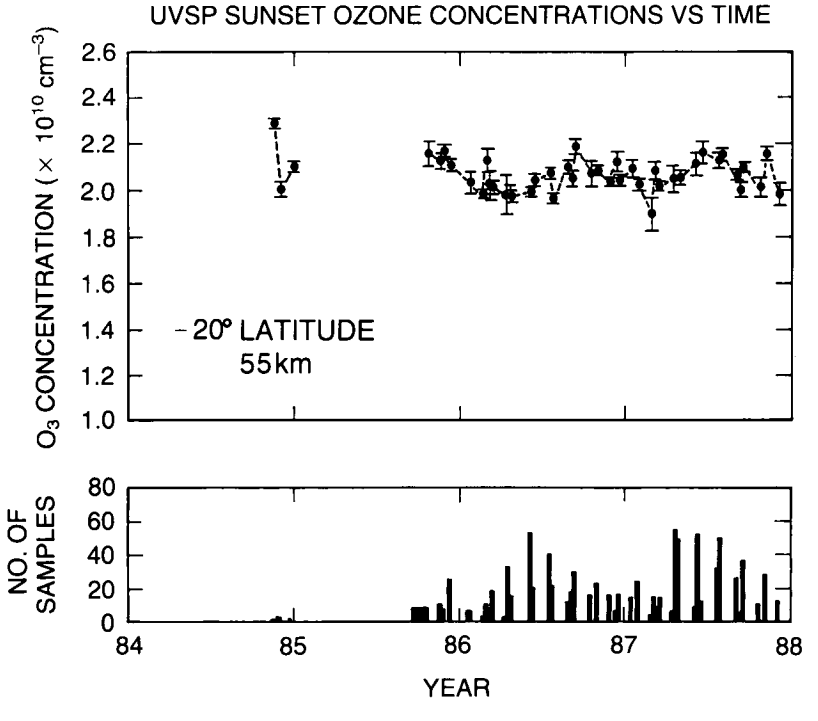

Figure 5.35 Same as Figure 5.34, except at 20°S.

5.7.4 Conclusions

The body of ozone data taken by SME and SMM between 53 and 57 km supports the conclusion by SAGE–I and –II that no large ozone decreases occurred at 50 km between 1979 and 1987.

5.8 ROCKET OZONESONDE (ROCOZ–A)

5.8.1 Introduction

The ROCOZ–A ozonesonde measures the solar ultraviolet irradiance over its four filter wavelengths as the instrument descends on a parachute. The amount of ozone between the ROCOZ–A radiometer and the Sun is calculated from the attenuation of solar flux as the instrument falls, using the Beer–Lambert law. The fundamental measurement from ROCOZ–A is ozone overburden (column amount) versus radar altitude from 20 km to 52 km. Aspects of ROCOZ–A included in this section are discussed by Barnes and Simeth (1986) and Barnes et al. (1986 and 1987), and in Chapter 2.

5.8.2 Estimates of the Accuracy of ROCOZ–A Ozone Profiles

The accuracy estimates for ROCOZ–A come from an internal, unpublished error analysis. A laboratory flight simulator based on long-path-length photometry (DeMore and Patapoff, 1976) has been constructed to calibrate ROCOZ–A ozone readings. The accuracy of the ozone column amounts and ozone number densities from ROCOZ–A, including auxiliary pressure and temperature measurements, has been estimated at 6 to 8 percent.

5.8.3 Comparison With In Situ Instruments

ROCOZ–A ozone measurements have been compared with those from an in situ UV absorption photometer during the Balloon Ozone Intercomparison Campaign (BOIC) (Hilsenrath et al., 1986). In one comparison, ROCOZ–A measured 5 to 10 percent higher than the in situ photometer for atmospheric pressures between 50 mb and 4 mb. In a subsequent balloon flight spanning 6 mb to 2 mb, a ROCOZ–A ozonesonde was compared with the same photometer and with a mass spectrometer from the University of Michigan (Anderson and Mauersberger, 1981); ROCOZ–A read higher than the in situ photometer by 8 percent and lower than the mass spectrometer by 4 percent. There is cause for concern in this intercomparison, since the in situ photometer and the mass spectrometer are both considered to be absolute instruments.

Hilsenrath et al. (1986) report laboratory comparisons of in situ photometers during BOIC. There is good agreement between the photometers flown on BOIC and similar agreement between the photometers and the ozone standard instrument from NBS. There is strong evidence to support the quality of the ozone measurements from the in situ photometers in BOIC.

On the other hand, there is a series of high-quality laboratory results with the Minnesota mass spectrometer. Hanson and Mauersberger (1985 and 1986) have used the mass spectrometer to study the vapor pressure of ozone at liquid argon temperatures. Mauersberger et al. (1987)

used long-path photometry to show 0.5 percent agreement between the thermodynamic vapor pressure standard and the ozone cross-section at 253.65 nm.

5.8.4 Ozone Measurements at Natal, Brazil

In the late 1970's and early 1980's, satellite measurements of the equa-torial stratosphere and mesosphere showed low variability in ozone during the Southern Hemisphere autumn (Frederick et al., 1984; McPeters et al., 1984; Rusch et al., 1984). In March and April 1985, NASA and the Brazilian space agency (INPE) conducted a series of ozone soundings at Natal, Brazil. The measurements were made in conjunction with over-passes of the SME, the SAGE–II instrument on the Earth Radiation Budget Satellite, and the SBUV spectrometers on Nimbus–7 and NOAA–9. Seven series of flights were conducted from March 25 to April 15, 1985, producing atmospheric profiles of ozone, pressure, and temperature from the ground to 52 km (Barnes, 1988). Above 22 km, stratospheric ozone variability was 2 percent or less during the 3 weeks of the measurement campaign, with stratospheric tempera-ture and pressure variabilities half that amount.

5.8.5 Estimates of Instrument Repeatabilities, an Upper Limit on Their Imprecision

The 2 percent variability in upper stratospheric ozone at Natal, Brazil, for 3 weeks in March and April 1985 implies a comparable uniformity for ozone profiles over a large area around the measurement site. This condition removes the requirement of exact concurrence between satellite and in situ ozone measurements, allowing comparisons of larger data sets. For ROCOZ–A, the sample at Natal includes seven profiles from March 25 to April 15, 1985. For SBUV, the samples were taken from March 20 to April 19, with 32 profiles in 1979 and 38 profiles in 1985. All of the SBUV measurements were within 2 degrees in latitude and 24 degrees in longitude from Natal. For SAGE–II, the sample set includes 14 measurements from March 22 to April 17, 1985. Each SAGE–II profile is within 12 degrees in latitude and 15 degrees in longitude from Natal. The sampling area for SAGE–II reflects its more sparse spatial coverage, when compared with SBUV. The SAGE–I samples from 1979 are similar to those from SAGE–II in number and coverage, both in time and space. The LIMS measurements were taken from March 17 to April 20, 1979, and cover the latitude range from the Equator to 8°S latitude. The selection of LIMS, SBUV, SAGE–I, and SAGE–II data from the archives for this comparison with ROCOZ–A is described by Barnes et al. (1987).

The instrument comparisons are presented in terms of ozone amounts within Umkehr layers, the nominal primary product from the standard SBUV algorithm. For ROCOZ–A, both SAGE instruments, and LIMS, conversion to this form requires a significant change in units as well as independent knowledge of the temperature and pressure fields. Table 5.11 presents the ozone columns in Umkehr layers 6 to 9 as found by SBUV, SAGE–I, and LIMS in 1979 and as found by SBUV, SAGE–II, and ROCOZ–A in 1985. The reproducibility of each instrument is given by the standard deviations reported in Table 5.11, except that this figure includes any atmospheric variability, which for SAGE observations includes latitudinal variations over about a 12-degree range. The single layer reproducibilities vary from 1.4 to 7.3 percent, and the average of the 24 cases is 3.3 percent. These measures of reproducibility may be interpreted as an upper limit of the imprecision of the various instruments. The standard deviations of the means, involving from 6 to 38 profiles among the various instruments, are mostly less than 1 percent, and all are less than 2 percent. This high reproducibility of the individual systems suggests that most discrepancies reported between different instruments are due to systematic errors of the systems.

Table 5.11 Reproducibility of Satellite and Rocket Systems in Measuring Upper Stratospheric Ozone Near Natal, Brazil, During Periods of Atmospheric Stability in 1979 and 1985

Umkehr Layer	Ozone Layer Amount (a)	σ% (b)	Sample Size	σ of Mean %
	SBUV (1979)			
9	7.96(16) (c)	1.8	32	0.32
8	2.62(17)	1.4		0.24
7	7.60(17)	1.4		0.25
6	1.56(18)	2.5		0.44
	SAGE–I (1979)			
9	8.62(16)	6.1	13	1.54
8	2.76(17)	6.2		0.88
7	7.66(17)	7.1		1.26
6	1.74(18)	4.1		1.25
	LIMS (1979)			
9	7.89(16)	1.9	30	0.34
8	2.64(17)	2.2		0.41
7	7.22(17)	3.0		0.54
6	1.70(18)	1.7		0.29
	SBUV (1985)			
9	7.12(18)	1.7	38	0.27
8	2.58(17)	2.6		0.42
7	7.74(17)	2.2		0.36
6	1.58(18)	3.6		0.58
	SAGE–II (1985)			
9	7.84(16)	7.3	14	1.96
8	2.89(17)	4.3		1.16
7	8.10(17)	3.4		0.92
6	1.68(18)	2.0		0.53
	ROCOZ–A (1985)			
9	8.59(16)	1.9	6	0.78
8	2.92(17)	4.4		1.79
7	8.19(17)	3.9		1.49
6	1.67(18)	2.5		0.93

(a) Molecules cm^{-2} over Umkehr layer. (b) Relative standard deviation. (c) Read 7.96(16) as 7.96×10^{16}, etc.

Using the same data as in Table 5.11, an estimate of how much the individual instruments differ from each other is obtained; the average deviations of three instruments from their own average value are given in Table 5.12 for 1979 and 1985. These instruments, with the uniform atmosphere near Natal and the good reproducibility shown in Table 5.11, give an instrument-to-instrument variability of 4 or 5 percent.

Table 5.12 Replication of Upper Stratospheric Ozone by Sets of Three Instruments*

The average of the three instruments and the standard deviation of the three instruments from the average.

Umkehr Layer	1979 Average Layer Amount (a)	σ %	1985 Average Layer Amount (a)	σ %
9	8.16(16)	5.0	7.85(16)	9.4
8	2.67(17)	2.8	2.80(17)	6.6
7	7.49(17)	3.2	8.01(17)	3.0
6	1.67(18)	5.8	1.64(18)	3.1
	Average	4.2	Average	5.5

*Compare Table 5.11.
(a) Molecules cm^{-2} over Umkehr layer.

5.8.6 Comparison of SAGE–II and SBUV With ROCOZ–A Ozone Vertical Profiles

The composite ozone vertical profile obtained by ROCOZ–A and by chemical ozonesondes at Natal in spring 1985 (Barnes et al., 1987) is presented in terms of ozone concentration as a function of geometric altitude in Figure 5.36. The profiles of the percentage difference between ROCOZ–A and the ozone vertical profiles given by SBUV and by SAGE–II overflights are included in the figure. The comparisons are made in terms of the primary data from the respective satellite instruments. SAGE–II provides ozone concentrations versus altitude. Between 25 and 50 km, the differences, SAGE minus ROCOZ–A, are sometimes positive and sometimes negative, with an average of about -1 percent, and never exceeding 5 percent. The ROCOZ–A ozone data are translated into columns over Umkehr layers, and the difference, SBUV minus ROCOZ–A, is included on the figure. For Umkehr layers 6, 7, 8, and 9, the differences are all negative; that is, SBUV values are less than those of ROCOZ–A. The differences are 18 percent at layer 9 and 5 percent at layer 6.

5.8.7 Discussion of Instrument Comparisons Given in Sections 5.6, 5.7, and 5.8

The 12 percent difference between stratospheric ozone measurements from the Minnesota mass spectrometer and the ultraviolet spectrometers flown in the BOIC (Section 5.8.3) gives rise to the following speculation: there may be some unrecognized atmospheric optical effects that perturb ozone measurements by some of the remote sensing instruments. For example, nitric oxide fluorescence near 255 nm is known to overlap one of the SBUV lines, but such fluorescence lines, which are observed in the laboratory with decreasing intensity at intervals up to about 390 nm, might also cause variations in apparent ozone in some instruments. Other unrecognized atmospheric fluorescence or absorptions may be occurring.

The data in Section 5.6 give an example of how closely three totally different, newly launched satellite systems agree with each other over a 6-month period in measuring zonal mean ozone

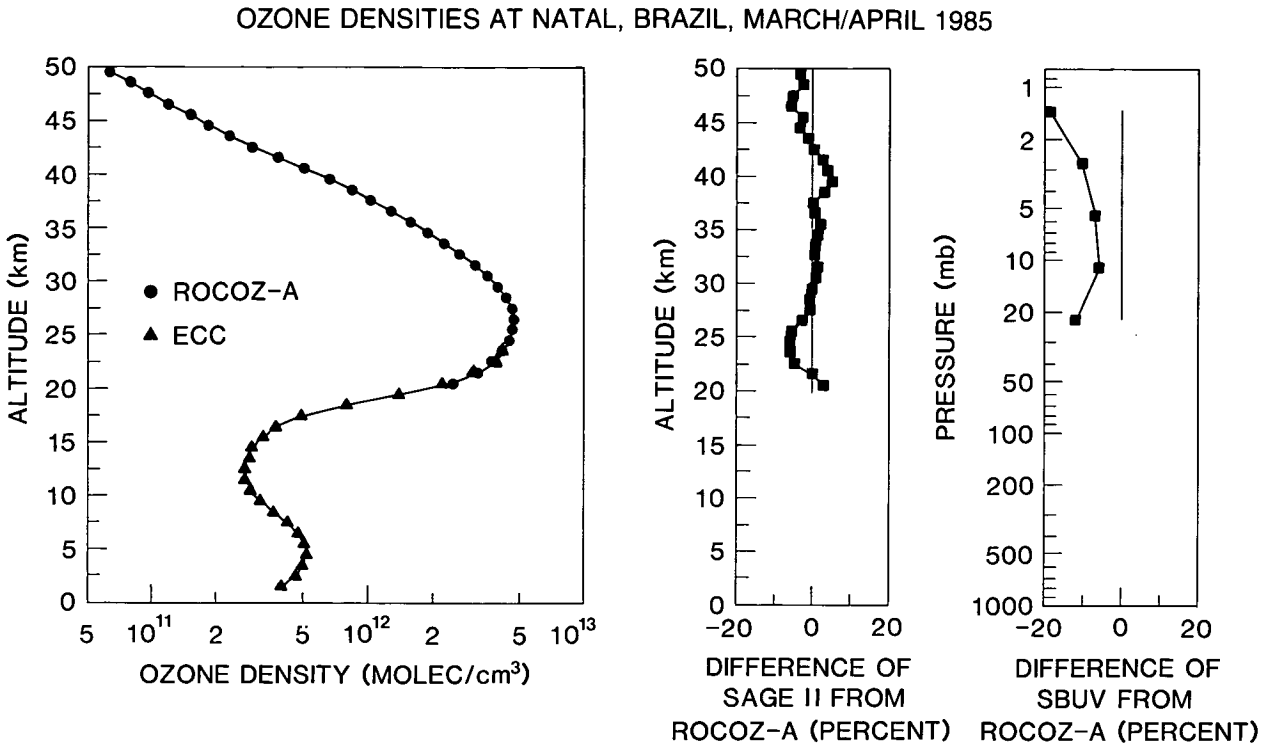

Figure 5.36 Average ozone vertical profile based on ROCOZ–A and chemical ozonesondes at Natal, Brazil, in March and April 1985. Middle panel: SAGE–II minus ROCOZ–A, vertical profile of ozone percentage difference at Natal in 1985 as a function of geometrical altitude. Right panel: SBUV minus ROCOZ–A, vertical profile of ozone percentage difference at Natal in 1985 at Umkehr layers and as a function of pressure.

amounts in the four Umkehr layers in the middle to upper stratosphere (about 4 percent). For a 2-year period, the zonal average ozone values over four Umkehr layers for the newly launched SBUV and SAGE–I instruments agreed within about 4 percent from 60°N to 60°S (Figure 5.13). In the relatively uniform and slowly changing tropical stratosphere, two sets of three-way instrument comparisons (Section 5.8.5) showed the average deviations of each instrument from the average of the three to be about 5 percent. By extension, one is led to believe that the ability of current satellite systems to measure the absolute value of ozone in the upper stratosphere is not much better than about 4 percent. By further extension, it is difficult to believe that presently available remote sensing satellites can reliably detect changes in upper stratospheric ozone of much less than 4 percent.

5.9 CONCLUSIONS

From an examination of the agreements and differences between different satellite instruments (Sections 5.3. 5.6, 5.7, and 5.8), it is difficult to believe that existing satellite instruments determine upper stratospheric ozone much better than 4 percent; by extension, it probably would require at least a 4 percent change to be reliably detected as a change.

The best estimates of the vertical profiles of ozone change in the upper stratosphere between 1979 and 1986 are judged to be those given by the two SAGE satellite instruments.

- SAGE–II minus SAGE–I gives a much lower ozone reduction than that given by the archived SBUV data; for example, at temperate latitudes and at 40 km, SBUV gives 15 percent and SAGE gives 3 percent. With added considerations from Chapters 2 and 3, the difference is largely ascribed to systematic error in the treatment of the SBUV diffuser plate.

- The average SAGE profiles of ozone changes between 20 and 50 degrees north and between 20 and 50 degrees south are given by Figure 5.18. The altitude of maximum ozone reduction is 40 km, in agreement with atmospheric models. The magnitude of maximum ozone reduction is 3 ± 3 percent (95 percent confidence level) at 40 km. The central value of this ozone reduction is less than the consensus of current theoretical models; a set of different models gives ozone reductions that range from 5 to 12 percent at an altitude near 40 km (Chapter 7). The relative systematic error between SAGE–I and –II is estimated to be 2 percent (see Chapter 2); an error estimate for the models is not available.

- The SAGE–I and –II comparison gives an ozone reduction of about 4 percent at 25 km over temperate latitudes. This altitude is near the ozone concentration maximum, and this ozone change represents a much larger reduction of the ozone column than that given at 40 km. This observed ozone change at 25 km is larger than that given by theoretical models, and future studies should concentrate on the reality and explanation of this ozone reduction (for example, is it a weak manifestation of the features that give the large Antarctic ozone reduction?).

Five ground-based Umkehr stations between 36 and 52 degrees north, corrected for the effects of volcanic aerosols, report an ozone reduction between 1979 and 1987 at Umkehr layer 8 of 9 ± 5 percent (95 percent confidence level, including a term for uncertainty in the aerosol correction, but not including possible systematic errors). The central estimate of upper stratospheric ozone reduction given by SAGE at 40 km is less than the central value estimated by the Umkehr method at layer 8.

In the future, the best way to improve knowledge of ozone profile changes between 1979 and 1987 will be to compare the first 2 years of validated SBUV–2 data against seasonally matched 2 years of the early SBUV data, similar to the procedure used by SAGE–I and –II.

To measure upper stratospheric ozone changes as small as 5 percent in 10 years, the instrument operators and data interpreters must have an extremely high level of ability, sophistication, dedication, and financial support. Such a measurement is a formidable scientific and engineering challenge. It requires continual attention to instrument performance, calibration, and verification; there needs to be a large number of duplicate, overlapping measurements. This task will not be achieved if it is regarded as a routine monitoring operation.

omit to end

R

References

Appendix: References

Adriani, A., F. Congeduti, G. Fiocco, and G.P. Gobbi, One year lidar observations of the stratospheric aerosol at Frascati, March 1982–March 1983, *Geophys. Res. Lett., 10,* 1005–1008, 1983.

Aikin, A.C., and R.D. McPeters, Meteoric material and the behavior of upper stratospheric polar ozone, *Geophys. Res. Lett., 13,* 1300–1303, 1986.

Aikin, A.C., B. Woodgate, and H.J.P. Smith, Atmospheric ozone determination by solar occultation using the UV spectrometer on the Solar Maximum Mission, *Appl. Optics, 21,* 2412–2424, 1982.

Aikin, A.C., B. Woodgate, and H.J.P. Smith, Equatorial ozone profiles from the Solar Maximum Mission—A comparison with theory, *Planet. Space Sci., 32,* 503–513, 1984.

Anderson, S., and K. Mauersberger, Calibration of a mass spectrometer experiment for ozone, *Rev. Sci. Instrum., 52,* 1025–1028, 1981.

Andreji, P.D., Evaluation of various factors affecting homogeneity of the total ozone time-series, in *Proc. Quadr. Ozone Symposium—1988,* Göttingen, edited by R.D. Bojkov and P. Fabian, Deepak Publ., USA, in press.

Andrews, D.G., Some comparisons between the middle atmosphere dynamics of the Southern and Northern Hemispheres, *Pure Appl. Geophys., 130,* 213–232, 1989.

Andrews, D.G., and M.E. McIntyre, Planetary waves in horizontal and vertical shear: The generalized Eliassen–Palm relation and the mean zonal acceleration, *J. Atmos. Sci., 33,* 2031–2048, 1976.

Andrews, D.G., J.R. Holton, and C.B. Leovy, Extratropical zonal-mean circulation, in *Middle Atmospheric Dynamics,* pp. 295–312, Academic Press, Orlando, Florida, 1987.

Angell, J.K., The close relation between Antarctic total-ozone depletion and cooling of the Antarctic low stratosphere, *Geophys. Res. Lett., 13,* 1240–1243, 1986.

Angell, J.K., Rocketsonde evidence for a stratospheric temperature decrease in the Western Hemisphere during 1973–85, *Mon. Weather Rev., 115,* 2569–2577, 1987a.

Angell, J.K., Seasonal differences in the trend of total ozone and contributions from tropospheric and stratospheric layers, *Mon. Weather Rev., 115,* 753, 1987b.

Angell, J.K., and J. Korshover, Global analysis of recent total ozone fluctuations, *Mon. Weather Rev., 104,* 63–75, 1976.

Angell, J.K., and J. Korshover, Global ozone variations: An update into 1976, *Mon. Weather Rev., 106,* 725–737, 1978.

Angell, J.K., and J. Korshover, Global temperature variations in the troposphere and stratosphere, *Mon. Weather Rev., 11,* 901–921, 1983a.

Angell, J.K., and J. Korshover, Global variation in total ozone and layer-mean ozone: An update through 1981, *J. Clim. and Appl. Meteor., 22,* 1611–1627, 1983b.

Angell, J.K., J. Korshover, and W.G. Planet, Ground-based and satellite evidence for a pronounced total-ozone minimum in early 1983 and responsible atmospheric layers, *Mon. Weather Rev., 113,* 641–646, 1985.

Atkinson, R.J., and J.R. Easson, Re-evaluation of the Australian total ozone record, in *Proc. Quadr. Ozone Symposium—1988,* Göttingen, edited by R.D. Bojkov and P. Fabian, Deepak Publ., USA, in press.

Avaste, O.A., A.V. Fedynsky, G.M. Grechko, V.I. Sevastyanov, and Ch.I. Willmann, Advances in noctilucent cloud research in the space era, *PAGEOPH, 118,* 528–580, 1980.

Bailey, P.L., and J.C. Gille, Inversion of limb radiance measurements: An operational algorithm, *J. Geophys. Res., 91,* 2757–2774, 1986.

REFERENCES

Baldwin, A.C., and D.M. Golden, Heterogeneous atmospheric reactions—Sulphuric acid aerosols as tropospheric sinks, *Science, 206*, 562–563, 1979.

Ball Aerospace Systems Division, *SBUV/2 Technical Description, Document Number B6802–10, Revision B*, Boulder, Colorado, 40 pp., November 16, 1981.

Bandeen, W.R., and R.S. Fraser, Radiative effects of the El Chichón volcanic eruption: Preliminary results concerning remote sensing, *NASA Tech. Memorandum 84959*, 1982.

Barnes, R.A., Changes in SBUV ozone profiles near Natal, Brazil, from 1979 to 1985, *J. Geophys. Res., 93*, 1704–1707, 1988.

Barnes, R.A., and P.G. Simeth, Design of a rocket-borne radiometer for stratospheric ozone measurements, *Rev. Sci. Instrum., 57*, 544–550, 1986.

Barnes, R.A., A.R. Bandy, and A.L. Torres, Electrochemical concentration cell ozonesonde accuracy and precision, *J. Geophys. Res., 90*, 7881–7887, 1985.

Barnes, R.A., A.C. Holland, and H.S. Lee, An improved rocket ozonesonde (ROCOZ-A) 2. Preparation of stratospheric ozone profiles, *J. Geophys. Res., 91*, 14521–14531, 1986.

Barnes, R.A., A.C. Holland, and V.W.J.H. Kirchhoff, Equatorial ozone profiles from the ground to 52 km during the Southern Hemisphere autumn, *J. Geophys. Res., 92*, 5573–5583, 1987.

Barnett, J.J., and M.E. Corney, Middle atmosphere reference model derived from satellite data, edited by K. Labitzke, J.J. Barnett, and B. Edwards, *Handbook for MAP, Vol. 16*, pp. 47–85, SCOSTEP, Urbana, Illinois, 1985.

Barnett, J.J., and M.E. Corney, Temperature comparisons between the Nimbus–7 SAMS, rocket/radiosondes and the NOAA–6 SSU, *J. Geophys. Res., 89*, 5294–5302, 1984.

Barnett, J.J., R.S. Harwood, J.T. Houghton, C.G. Morgan, C.D. Rodgers, and E.J. Williamson, *Atmospheric Physics Memorandum*, Clarendon Laboratory, University of Oxford, England, 1974.

Barth, C.A., The ultraviolet spectroscopy of planets, in *The Middle Ultraviolet: Its Science and Technology*, edited by A.E.S. Green, pp. 177–218, John Wiley and Sons, New York, 1966.

Barth, C.A., R.W. Sanders, R.J. Thomas, B.M. Jakosky, and R.A. West, Formation of the El Chichón aerosol cloud, *Geophys. Res. Lett., 10*, 993–996, 1983.

Basher, R.E., Review of the Dobson spectrophotometer and its accuracy, *WMO Ozone Report #13*, 1982.

Bass, A.M., and R.J. Paur, The ultraviolet cross-sections of ozone: I. The measurements, in *Atmospheric Ozone, Proceedings of the Quadrennial Ozone Symposium*, Halkidiki, Greece, September 3–7, 1984, edited by C.S. Zerefos and A. Ghazi, pp. 606–610, D. Reidel, Dordrecht, The Netherlands, 1985.

Bass, A.M., A.E. Ledford, Jr., and A.H. Laufer, Extinction coefficients of NO_2 and N_2O_4, *J. of Res. of the N.B.S–A. Phys. and Chem., 80A*, 143–166, 1976.

Bates, D.R., Rayleigh scattering by air, *Planet. Space Sci., 32*, 785–790, 1984.

Bauer, E., A catalog of perturbing influences on stratospheric ozone, 1955–1975, *J. Geophys. Res., 84*, 6929–6940, 1979.

Benjamini, Y., Is the "t test" really conservative when the parent distribution is long-tailed? *J. Amer. Statist. Assoc., 78*, 645–654, 1983.

Bhartia, P.K., K.F. Klenk, V.G. Kaveeshwar, S. Ahmad, A.J. Fleig, R.D. McPeters, and C.L. Mateer, Algorithm for Vertical Ozone Profile Determination for the Nimbus–4 BUV Data Set, in *Proceedings of the 4th Conference on Atmospheric Radiation*, pp. 27–32, American Meteorological Society, Boston, MA, 1981.

Bhartia, P.K., K.F. Klenk, C.K. Wong, D. Gordon, and A.J. Fleig, Intercomparison of the Nimbus 7 SBUV/TOMS total ozone data sets with Dobson and M83 results, *J. Geophys. Res., 89*, 5239–5248, 1984.

Bhartia, P.K., C.K. Wong, and A.J. Fleig, An evaluation of the performance of Umkehr stations by SBUV experiment, in *Atmospheric Ozone, Proceedings of the Quadrennial Ozone Symposium*, Halkidiki, Greece, September 3–7, 1984, edited by C.S. Zerefos and A. Ghazi, pp. 229–233, D. Reidel, Dordrecht, The Netherlands, 1985.

Bhartia, P.K., S. Taylor, and A.J. Fleig, Estimation of errors in the long-term change in ozone reported by the SBUV/TOMS instruments—A new way of looking at the old data, *Proc. Quadr. Ozone Symposium—1988*, Göttingen, edited by R.D. Bojkov and P. Fabian, Deepak Publ., USA, in press.

Birrer, W., *Homogenisierung und Diskussien der Totalozon–Missreihe von Arosa 1926–1971*, Laboratorium für Atmosphärenphysik, 1975.

Bishop, L., and W.J. Hill, Analyzing total ozone for natural and man-made trend variability, *Geophys. Res. Lett., 9*, 485–488, 1982.

Blackmon, M.L., J.E. Geosler, and E.J. Pitcher, A general circulation model study of January climate anomaly patterns associated with interannual variation of equatorial Pacific sea surface temperatures, *J. Atmos. Sci., 40*, 1410–1425, 1983.

Blake, D.R., and F.S. Rowland, Continuing worldwide increase in tropospheric methane, 1978 to 1987, *Science, 239*, 1129–1131, 1988.

Blake, D.R., and F.S. Rowland, World-wide increase in tropospheric methane, *J. Atmos. Chem., 4*, 43–62, 1986.

Bloomfield, P., M.L. Thompson, and S. Zeger, A statistical analysis of Umkehr measurements of 32–46 km. ozone, *J. Appl. Meteorol., 21*, 1828–1837, 1982.

Bloomfield, P., G. Oehlert, M.L. Thompson, and S. Zeger, A frequency domain analysis of trends in Dobson total ozone records, *J. Geophys. Res., 88*, 8512–8522, 1983.

Bojkov, R.D., Computing the vertical ozone distribution from its relationship with total ozone amount, *J. Appl. Meteor., 8*, 284–292, 1969a.

Bojkov, R.D., Differences in Dobson spectrophotometer and filter ozonometer measurements of total ozone, *J. Appl. Meteor., 8*, 362–368, 1969b.

Bojkov, R.D., Global total ozone distribution (1957–1965), NCAR manuscript presented at the Ozone Symposium, Monaco, 1968.

Bojkov, R.D., The 1979–1985 ozone decline in Antarctica as reflected in ground based observations, *Geophys. Res. Lett., 13*, 1236–1239, 1986a.

Bojkov, R.D., The 1983 and 1985 anomalies in ozone distribution in perspective, *Mon. Weather Rev., 115*, 2187–2201, 1987b.

Bojkov, R.D., On the long-term changes of tropospheric ozone, in *Proc. Quadr. Ozone Symposium—1988*, Göttingen, edited by R.D. Bojkov and P. Fabian, Deepak Publ., USA, in press.

Bojkov, R.D., Ozone changes at the surface and in the free troposphere, in *Tropospheric Ozone—Regional and Global Scale Interactions*, edited by I.S.A. Isaksen, pp. 83–96, D. Reidel, Norwell, Massachusetts, 1988b.

Bojkov, R.D., Ozone changes at the surface and in the troposphere, in *Tropospheric Ozone: Proceedings of the NATO Workshop*, edited by I.S.A. Isaksen, pp. 83–96, D. Reidel, Boston, 1987a.

Bojkov, R.D., Ozone variations in the Northern polar region, *Meteorol. Atmos. Phys., 38*, 117–130, 1988a.

Bojkov, R.D., Spring ozone change in the Antarctic and the role of the polar vortex, *Adv. Space Res., 136*, 89–98, 1986b.

Bojkov, R.D., Surface ozone during the second half of the nineteenth century, *J. Clim. Appl. Meteor., 25*, 343–352, 1986c.

REFERENCES

Bojkov, R.D., and W. Attmannspacher, Ozone variability and trends from ozone soundings at Hohenpeissenberg, paper presented at the Quadrennial Ozone Symposium, Göttingen, August 8–17, 1988.

Bojkov, R.D., and C.L. Mateer, On the relative quality and performance of the Global Ozone Observing System total ozone measurements, in *Atmospheric Ozone, Proceedings of the Quadrennial Ozone Symposium*, Halkidiki, Greece, September 3–7, 1984, edited by C.S. Zerefos and A. Ghazi, pp. 335–340, D. Reidel, Dordrecht, The Netherlands, 1985.

Bojkov, R.D., and G.C. Reinsel, Trends in tropospheric ozone concentration, in *Atmospheric Ozone, Proceedings of the Quadrennial Ozone Symposium*, Halkidiki, Greece, September 3–7, 1984, edited by C.S. Zerefos and A. Ghazi, pp. 775–781, D. Reidel, Dordrecht, The Netherlands, 1985.

Bojkov, R.D., C.L. Mateer, and A.L. Hansson, Comparison of ground-based and Total Ozone Mapping Spectrometer measurements used in assessing the performance of the Global Ozone Observing System, *J. Geophys. Res., 93*, 9525–9533, 1988.

Borucki, W.J., and W.L. Chameides, Lightning: Estimates of the rates of energy dissipation of nitrogen fixation, *Rev. Geophys., 22*, 363–372, 1984.

Bowman, K.P., and A.J. Krueger, A global climatology of total ozone from the Nimbus–7 Total Ozone Mapping Spectrometer (TOMS), *J. Geophys. Res., 90*, 7967–7976, 1985.

Box, G.E.P., and G.M. Jenkins, *Time Series Analysis, Forecasting and Control*, 575 pp., Holden–Day, San Francisco, 1976.

Boyd, J.P., The noninteraction of waves with the zonally averaged flow on a spherical Earth and the interrelationships of eddy fluxes of energy, heat and momentum, *J. Atmos. Sci., 33*, 2285–2291, 1976.

Brasseur, G., and A. De Rudder, Theoretical prediction of perturbations in the middle atmosphere related to the increasing emission of greenhouse gases, *Adv. Space Res, 6*, 51–54, 1986.

Brasseur, G., and P.C. Simon, Stratospheric chemical and thermal response to long-term variability in solar UV irradiance, *J. Geophys. Res., 86*, 7343–7362, 1981.

Brasseur, G., and S. Solomon, *Aeronomy of the Middle Atmosphere*, D. Reidel, Boston, 441 pp., 1984.

Brewer, A.W., A replacement for the Dobson spectrophotometer? *Pure and Applied Geophys., 106–108*, 919–927, 1973.

Brewer, A.W., and J.R. Milford, The Oxford–Kew ozonesonde, *Proc. Roy. Soc. London, A256*, 470–495, 1960.

Brewer, A.W., and A.W. Wilson, The regions of formation of atmospheric ozone, *Quart. J. Roy. Meteorol. Soc., 94*, 249–265, 1968.

Bridges, J.M., and W.R. Ott, Vacuum ultraviolet radiometry. 3: The argon mini-arc as a new secondary standard of spectral radiance, *Appl. Opt., 16*, 367–376, 1977.

Brownscombe, J.L., J. Nash, G. Vaughan, and C.F. Rogers, Solar tides in the middle atmosphere. I: Description of satellite observations and comparison with theoretical calculations at equinox, *Quart. J. Roy. Meteorol. Soc., 111*, 677–689, 1985.

Bruhl, C., *Ein effizientes Model für global Klima- und Luftzusammensetzunganderungen durch menschlishe activäten*, Doctorate Thesis, University of Mainz, Federal Republic of Germany, 1987.

Bruhl, C., and P.J Crutzen, Scenarios of possible changes in atmospheric temperatures and ozone concentrations due to man's activities, estimated with a one-dimensional coupled photochemical climate model, *Climate Dynamics, 2*, 173–203, 1988.

Brune, W.H., and J.G. Anderson, In situ observations of midlatitude stratospheric ClO and BrO, *Geophys. Res. Lett., 13*, 1391–1394, 1986.

Brune, W.H., E.M. Weinstock, J.J. Schwab, R.M. Stimpfle, and J.G. Anderson, Stratospheric ClO: In situ detection with a new approach, *Geophys. Res. Lett., 12*, 441–444, 1985.

Brune, W.H., E.M. Weinstock, and J.G. Anderson, Midlatitude ClO below 22 km altitude: Measurements with a new aircraft-borne instrument, *Geophys. Res. Lett., 15*, 144–147, 1988.

Burnett, C.R., K.R. Minschwaner, and E.B. Burnett, Vertical column abundance measurements of atmospheric hydroxyl from 26°, 40°, and 65°N, *J. Geophys. Res., 93*, 5241–5254, 1988.

Cabannes, J., and J. Dufay, Les variations de la quantité d'ozone contenue dans l'atmosphere, *J. Phys. Rad., Ser. 6, 8*, 353–364, 1927.

Cadle, R.D., C.S. Kiang, and J.F. Louis, The global scale dispersion of the eruption clouds from major volcanic eruptions, *J. Geophys. Res., 81*, 3125–3132, 1976.

Cadle, R.D., F.G. Fernald, and C.I. Frush, Combined use of lidar and numerical diffusion models to estimate the quantity and dispersion of volcanic eruption clouds in the stratosphere: Vulcán Fuego, 1974, and Augustine, 1976, *J. Geophys. Res., 82*, 1783–1786, 1977.

Callis, L.B., and M. Natarajan, The Antarctic ozone minimum: Relationship to odd nitrogen, odd chlorine, the final warming and the 11-year solar cycle, *J. Geophys. Res., 91*, 10771–10796, 1986.

Callis, L.B., J.C. Alpert, and M.A. Geller, An assessment of thermal, wind, and planetary wave changes in the middle atmosphere due to 11-year in flux variations, *J. Geophys. Res., 90*, 2273–2282, 1985a.

Callis, L.B., M. Natarajan, and J.M. Russell, III, Estimates of the stratospheric distribution of odd nitrogen from the LIMS data, *Geophys. Res. Lett., 12*, 259–262, 1985b.

Callis, L.B., M. Natarajan, R.E. Boughner, J.M. Russell III, and J.D. Lambeth, Stratospheric photochemical studies using Nimbus 7 data 2. Development of inferred trace specie distributions, *J. Geophys. Res., 91*, 1167–1197, 1986.

Cebula, R.P., H. Park, and D.F. Heath, Characterization of the Nimbus–7 SBUV radiometer for the long term monitoring of stratospheric ozone, *J. Atm. Oceanic Technology, 5*, 215–227, 1988.

Chandra, S., Recent trends in stratospheric ozone inferred from Nimbus–7 SBUV spectrometer, National Workshop on Ozone, April 13–15, 1987, pp. 33–44, National Physical Laboratory, New Delhi, 1988.

Chandra, S., Solar-induced oscillations in the stratosphere: A myth or reality?, *J. Geophys. Res., 90*, 2331–2339, 1985.

Chang, J.S., W.H. Duewer, and D.J. Wuebbles, The atmospheric nuclear tests of the 1950's and 1960's: A possible test of ozone depletion theories, *J. Geophys. Res., 94*, 1755–1765, 1979.

Chemical Manufacturers Association (CMA), Production, sales and calculated release of CFC–11 and –12 through 1984, *Report of Fluorocarbon Program Panel*, Washington, D.C., 1985.

Chemical Manufactures Association (CMA), World production and release of chlorofluorocarbons 11 and 12 through 1981, *Report FPP 83–F*, Washington, D.C., 1982.

Chu, W.P., Inversion of SAGE II Measurements, in *Abstracts of the 6th AMS Conference on Atmospheric Radiation*, pp. J49–J51, Williamsburg, Virginia, May 13–16, 1986.

Chu, W.P., Inversion technique for SAGE II data, Workshop on Remote Sensing Retrieval Methods, Dec. 15–18, 1987, Williamsburg, Virginia, 1988.

Chu, W.P., SAGE II inversion algorithm, *J. Geophys. Res., 94*, 8339–8351, 1989.

Chu, W.P., and M.P. McCormick, Inversion of stratospheric aerosol and gaseous constituents from spacecraft solar extinction data in the 0.38–1.0μm wavelength region, *Appl. Opt., 18*, 1404–1413, 1979.

Chu, W.P., and M.P. McCormick, SAGE observations of stratospheric nitrogen dioxide, *J. Geophys. Res., 91*, 5465–5476, 1986.

Chu, W.P., M.P. McCormick, J. Lenoble, C. Brogniez, and P. Pruvost, SAGE II inversion algorithm, *J. Geophys. Res., 94*, 8339–8351, 1989.

Chubachi, S., On the cooling of stratospheric temperatures at Syowa, Antarctica, *Geophys. Res. Lett., 13*, 1221–1223, 1986.

REFERENCES

Chubachi, S., Preliminary results of ozone observations at Syowa Station from February 1982 to January 1983, *Mem. Natl. Inst. Polar Res., Spec. Issue No. 34, Proceedings of the Sixth Annual Symposium of Polar Meteorology and Glaciology*, National Institute of Polar Research, Tokyo, Japan, p. 13, 1984.

Chubachi, S., and R. Kajawara, Total ozone variations at Syowa, Antarctica, *Geophys. Res. Lett., 13*, 1197–1198, 1986.

Cicerone, R.J., How has the atmospheric concentration of CO changed? in *The Changing Atmosphere*, edited by F.S. Rowland and I.S.A. Isaksen, Dahlem Konferenzen, Berlin, November 1–6, 1987, pp. 49–61, John Wiley and Sons, Ltd., Chichester, England, 1988.

Cicerone, R.J., L.E. Heidt, and W.H. Pollock, Measurements of atmospheric methyl bromide (CH_3Br) and bromoform ($CHBr_3$), *J. Geophys. Res., 93*, 3745–3749, 1988.

Clancy, R.T., El Chichón and "mystery cloud" aerosols between 30 and 55 km: Global observations from the SME visible spectrometer, *Geophys. Res. Lett., 13*, 937–940, 1986.

Clavelin, J.L., and P. Mirabel, Determination des pressions partielles du melange eau–acide nitrique, *J. Chimie Phys., 76*, 533–537, 1979.

Clemesha, B.R., and D.M. Simonich, Lidar observations of the El Chichón dust cloud at 23°S, *Geophys. Res. Lett., 10*, 321–324, 1983.

Clyne, M.A.A., and R.T. Watson, Kinetic studies of diatomic free radicals using mass spectrometry, Part 4—The BrO + ClO and BrO + ClO reactions, *J. Chem. Soc., Faraday Trans. I., 73*, 1169–1187, 1977.

CMA: see Chemical Manufacturer's Association

Cochrane, D., and G.H. Orcutt, Applications of least-squares regression to relationships containing autocorrelated errors, *J. Amer. Statist. Assoc., 44*, 32–61, 1949.

Coffey, M., On the temporal change of stratospheric NO_2, *Geophys. Res. Lett., 15*, 331–334, 1988.

Connor, B.J., J.W. Barrett, A. Parish, P.M. Solomon, R.L. DeZafra, and M. Jaramillo, Ozone over McMurdo Station, Antarctica, austral spring 1986: Altitude profiles for the middle and upper stratosphere, *J. Geophys. Res., 92*, 13221–13230, 1987.

Conway, T.J., P. Tans, L.S. Waterman, K.W. Thoning, K.A. Masarie, and R.H. Gammon, Atmospheric carbon dioxide measurements in the remote global troposphere, 1981–1984, *Tellus, 40B*, 81–115, 1988.

Cowley, J.R., and G.M. Lawrence, Earth limb altitude determination for the Solar Mesosphere Explorer, paper presented at 21st AIAA Aerospace Sciences Meeting, January 10–13, Reno, Nevada, 1983.

Cox, R.A., and G.D. Hayman, Stability and photochemistry of ClO dimers formed at low temperature in the gas phase, Polar Ozone Workshop, *NASA Conf. Publ. 10014*, pp. 256–258, Snowmass, Colorado, 1988.

Coy, L., An unusually large westerly amplitude of the quasi-biennial oscillation, *J. Atmos. Sci., 36*, 174, 1979.

Craig, H., and C.C. Chou, Methane: The record in polar ice cores, *Geophys. Res. Lett., 9*, 1221–1224, 1982.

Craig, R.A., *The Upper Atmosphere—Meteorology and Physics*, 209 pp., Academic Press, New York, 1965.

Craig, R.A., J.J. DeLuisi, and I. Stuetzer, Comparison of chemiluminescent and Umkehr observations of ozone, *J. Geophys. Res., 72*, 1667–1671, 1967.

Crutzen, P.J., Tropospheric ozone: An overview, in *Tropospheric Ozone: Proceedings of the NATO Workshop*, edited by I.S.A. Isaksen, pp. 3–32, D. Reidel, Boston, 1987.

Crutzen, P.J., and F. Arnold, Nitric acid cloud formation in the cold Antarctic stratosphere: A major cause for the springtime "ozone hole," *Nature, 324*, 651–655, 1986.

Crutzen, P.J., I.S.A. Isaksen, and G.C. Reid, Solar proton events: Stratospheric sources of nitric oxide, *Science, 189*, 457–459, 1975.

Cunnold, D.M., R.G. Prinn, R.A. Rasmussen, P.G. Simmonds, F.N. Alyea, C.A. Cardelino, A.J. Crawford, P.J. Fraser, and R.D. Rosen, The Atmospheric Lifetime Experiment 3. Lifetime methodology and application to three years of CCl_3F data, *J. Geophys. Res., 88*, 8379–8400, 1983a.

Cunnold, D.M., R.G. Prinn, R.A. Rasmussen, P.G. Simmonds, F.N. Alyea, C.A. Cardelino, and A.J. Crawford, The Atmospheric Lifetime Experiment 4. Result for CCl_2F_2 based on three years of data, *J. Geophys. Res., 88*, 8401–8414, 1983b.

Cunnold, D.M., M.C. Pitts, and C.R. Trepte, An intercomparison of SAGE and SBUV ozone observations for March and April 1979, *J. Geophys. Res., 89*, 5249–5262, 1984.

Cunnold, D.M., R.G. Prinn, R.A. Rasmussen, P.G. Simmonds, F.N. Alyea, C.A. Cardelino, A.J. Crawford, P.J. Fraser, and R.D. Rosen, Atmospheric lifetime and annual release estimates for CCl_3F and CCl_2F_2 from five years of ALE data, *J. Geophys. Res., 91*, 10797–10817, 1986.

Cunnold, D.M., W.P. Chu, R.A. Barnes, M.P. McCormick, and R.E. Veiga, Validation of SAGE II ozone measurements, *J. Geophys. Res., 94*, 8447–8460, 1989.

Danielsen, E.F., and H. Houben, Dynamics of the Antarctic stratosphere and implications for the ozone hole, unpublished manuscript.

Dave, J.V., Effect of aerosol on estimation of total ozone in an atmospheric column from the measurement of its ultraviolet radiance, *J. Atmos. Sci., 35*, 899–911, 1978.

Dave, J.V., Multiple scattering in a non-homogeneous, Rayleigh atmosphere, *J. Atmos. Sci., 22*, 273–279, 1964.

Dave, J.V., and P.M. Furukawa, Scattered radiation in the ozone absorption bands at selected levels of a terrestrial, Rayleigh atmosphere, *Meteorol. Mon., 7 (29)*, 1966.

Dave, J.V., and C.L. Mateer, A preliminary study on the possibility of estimating total atmospheric ozone from satellite measurements, *J. Atmos. Sci., 24*, 414–427, 1967.

Dave, J.V., J.J. DeLuisi, and C.L. Mateer, Results of a comprehensive theoretical examination of the optical effects of aerosols on the Umkehr measurement, *Special Environmental Report 14*, pp. 15–22, World Meteorological Organization, Geneva, 1979.

Dave, J.V., C.L. Mateer, and J.J. DeLuisi, An examination of the effect of haze on the Short Umkehr method for deducing the vertical distribution of ozone, in *Proc. Quadr. Ozone Symp.*, pp. 222–229, National Center for Atmospheric Research, Boulder, Colorado, 1980.

Deirmendjian, D., On volcanic and other particulate turbidity anomalies, *Adv. Geophys., 16*, 267–296, 1973.

DeLuisi, J.J., A study of the effect of haze upon Umkehr measurements, *Quart. J. Roy. Meteorol. Soc., 95*, 181–187, 1969.

DeLuisi, J.J., Umkehr vertical ozone profile errors caused by the presence of stratospheric aerosols, *J. Geophys. Res., 84*, 1766–1770, 1979.

DeLuisi, J.J., and C.L. Mateer, On the application of the optimum statistical inversion technique to the evaluation of Umkehr observations, *J. Appl. Meteor., 10*, 328–334, 1971.

DeLuisi, J.J., and J. Nimira, Preliminary comparison of satellite BUV and surface-based Umkehr observations of the vertical distribution of ozone in the upper stratosphere, *J. Geophys. Res., 83*, 379–384, 1977.

DeLuisi, J.J., C.L. Mateer, and D.F. Heath, Comparison of seasonal variations of upper stratospheric ozone concentrations revealed by Umkehr and Nimbus 4 BUV observations, *J. Geophys. Res., 84*, 3728–3732, 1979.

DeLuisi, J.J., T. DeFoor, K. Coulson, F. Fernald, and K. Thorne, *Lidar Observations of Stratospheric Aerosol Over Mauna Loa Observatory: 1974–1981, NOAA Data Report ERL ARL–4*, 107 pp., NOAA Environmental Research Laboratories, Boulder, Colorado, 1982.

DeLuisi, J.J., E.G. Dutton, K.L. Coulson, T.E. DeFoor, and B.G. Mendonca, On some radiative features of the El Chichón volcanic stratospheric dust cloud and a cloud of unknown origin observed at Mauna Loa, *J. Geophys. Res., 88*, 6769–6772, 1983.

REFERENCES

DeLuisi, J.J., C.L. Mateer, and P.K. Bhartia, On the correspondence between standard, short Umkehr, and solar backscattered ultraviolet vertical ozone profiles, *J. Geophys. Res., 90,* 3845–3849, 1985.

DeMore, W.B., and M. Patapoff, Comparison of ozone determinations by ultraviolet photometry and gas phase titration, *Environ. Sci. Technol., 10,* 897–899, 1976.

DeMore, W.B., J.J. Margitan, M.J. Molina, R.T. Watson, D.M. Golden, R.F. Hampson, M.J. Kurylo, C.J. Howard, and A.R. Ravishankara, Chemical kinetics and photochemical data for use in stratospheric modeling, evaluation number 7, *JPL Publication 85–37,* 226 pp., Jet Propulsion Laboratory, Pasadena, California, 1985.

deZafra, R.L., A. Parrish, P.M. Solomon, and J.W. Barrett, Quantitative observations of stratospheric chlorine monoxide as a function of latitude and season during the period 1980–1983, in *Atmospheric Ozone, Proceedings of the Quadrennial Ozone Symposium,* Halkidiki, Greece, September 3–7, 1984, edited by C.S. Zerefos and A. Ghazi, pp. 206–209, D. Reidel, Dordrecht, The Netherlands, 1985.

deZafra, R.L., M. Jaramillo, A. Parrish, P.M. Solomon, B. Connor, and J. Barrett, High concentrations of chlorine monoxide at low altitudes in the Antarctic spring stratosphere, I, Diurnal variation, *Nature, 328,* 408–411, 1987.

Dianov-Klokov, V.I., and L.N. Yurganov, A spectroscopic study of the global spacetime distribution of atmospheric CO, *Tellus, 33,* 262–273, 1981.

Dobson, G.M.B., Adjustment and calibration of ozone spectrophotometer, *Ann. IGY, 5,* 90–114, 1957b.

Dobson, G.M.B., Annual variation of ozone in Antarctica, *Quart. J. Roy. Meteorol. Soc., 92,* 549–552, 1966.

Dobson, G.M.B., The development of instruments for measuring atmospheric ozone during the last fifty years, *J. Phys. E: Sci. Instrum., 6,* 938–939, 1973.

Dobson, G.M.B., Measurements of the amount of ozone in the Earth's atmosphere and its relation to other geophysical conditions, Part IV, *Proc. Roy. Soc. London, A 129,* 411–433, 1930.

Dobson, G.M.B., Observers handbook for the ozone spectrophotometer, *Ann. IGY, 5,* 46–89, 1957a.

Dobson, G.M.B., A photoelectric spectrophotometer for measuring the amount of atmospheric ozone, *Proc. Phys. Soc. London, 43,* 324–339, 1931.

Dobson, G.M.B., and D.N. Harrison, Measurements of the amount of ozone in the Earth's atmosphere and its relation to other geophysical conditions, *Proc. Roy. Soc. London, A 110,* 660–693, 1926.

Dobson, G.M.B., and C.W.B. Normand, Determination of the constants, etc., used in the calculation of the amount of ozone from spectrophotometer measurements and the accuracy of the results, *Ann. IGY, 16,* 161–191, 1962.

Dobson, G.M.B., D.N. Harrison, and J. Lawrence, Measurements of the amount of ozone in the Earth's atmosphere and its relation to other geophysical conditions, Part II, *Proc. Roy. Soc. London, A 114,* 521–541, 1927.

Dobson, G.M.B., D.N. Harrison, and J. Lawrence, Measurements of the amount of ozone in the Earth's atmosphere and its relation to other geophysical conditions, Part III, *Proc. Roy. Soc. London, A 122,* 456–486, 1929.

Douglass, A.R., and R.S. Stolarski, The use of atmospheric measurements to constrain model predictions of ozone change from chlorine perturbations, *J. Geophys. Res., 92,* 6662–6674, 1987.

Douglass, A.R., R.B. Rood, and R.S. Stolarski, Interpretation of ozone temperature correlations 2. Analysis of SBUV ozone data, *J. Geophys. Res., 90,* 10693–10708, 1985.

Drayson, S.R., P.L. Bailey, H. Fischer, J.C. Gille, A. Girard, L.L. Gordley, J.E. Harries, W.G. Planet, E.E. Remsberg, and J.M. Russell, Spectroscopy and transmittances for the LIMS experiment, *J. Geophys. Res., 89*, 5141, 1984.

Dreschhoff, G.A., E.J. Zeller, and B.C. Parker, Past solar activity variation reflected in nitrate concentrations in Antarctic ice, in *Weather and Climate Responses to Solar Variations*, edited by B.M. McCormac, pp. 225–236, Colorado University Press, Boulder, 1983.

Dunkerton, T.J., Body force circulation and the Antarctic ozone minimum, *J. Atmos. Sci., 45*, 427–438, 1988.

Dunkerton, T.J., On the mean meridional mass motions of the stratosphere and mesosphere, *J. Atmos. Sci., 35*, 2325–2333, 1978.

Dütsch, H.U., The ozone distribution in the atmosphere, *Can. J. Chem., 52*, 1491–1504, 1974.

Dütsch, H.U., Total ozone trend in the light of ozone soundings: The impact of El Chichón, in *Atmospheric Ozone, Proceedings of the Quadrennial Ozone Symposium*, Halkidiki, Greece, September 3–7, 1984, edited by C.S. Zerefos and A. Ghazi, pp. 263–268, D. Reidel, Dordrecht, The Netherlands, 1984a.

Dütsch, H.U., An update of the Arosa ozone series to the present using a statistical instrument calibration, *Quart. J. Roy. Meteorol. Soc., 110*, 1079–1096, 1984b.

Dutton, E.G., and J. DeLuisi, Spectral extinction of direct solar radiation by the El Chichón cloud during December, 1982, *Geophys. Res. Lett., 10*, 1013–1016, 1983.

Dvoryashina, E.V., V.I. Dianov-Klokov, and L.N. Yurganov, Variations of the content of carbon monoxide in the atmosphere in the period from 1970 to 1982, *Journal of the Academy of Sciences USSR, Atmospheric and Oceanic Physics, 20*, 27–33, 1984.

Dziewulska-Losiowa, A., M. Degorska, and B. Rajewska-Wiech, The normalized total ozone data record, Belsk, 1963–1981, *Publ. Inst. Geophys., Ser. D, Pol. Acad. Sci., 18 (169)*, 23–73, 1983.

Eck, T.F., P.K Bhartia, P.H. Hwang, and L.L. Stowe, Reflectivity of the Earth's surface and clouds in ultraviolet from satellite observations, *J. Geophys. Res., 92*, 4287–4296, 1987.

Eckerle, K.L., Modification of an NBS reference spectrophotometer, *Natl. Bur. Stand. (U.S.) Tech. Note 913*, 43 pp., 1976.

Eckman, R.S., J.D. Haigh, and J.A. Pyle, An important uncertainty in coupled chlorine-carbon dioxide studies of atmospheric ozone modification, *Nature, 329*, 616–619, 1987.

Edmon, H.J., B.J. Hoskins, and M.E. McIntyre, Eliassen-Palm cross sections for the troposphere, *J. Atmos. Sci., 37*, 2600–2616, 1980. (See also *Corrigendum, 38*, 1115, 1981, esp. the second-to-last item.)

Ehhalt, D.H., R.J. Zander, and R.A. Lamontagne, On the temporal increase of tropospheric CH_4, *J. Geophys. Res., 88*, 8442–8446, 1983.

Elansky, N.R., A. Ya Arabov, A.S. Elokhov, and I.A. Senik, Spatial and temporal variability of the NO_2 total content based on annual observation data, in *Atmospheric Ozone, Proceedings of the Quadrennial Ozone Symposium*, Halkidiki, Greece, September 3–7, 1984, edited by C.S. Zerefos and A. Ghazi, pp. 157–162, D. Reidel, Dordrecht, The Netherlands, 1985.

Etheridge, D.M., G.I. Pearman, and F. de Silva, Atmospheric trace gas variations as revealed by air trapped in an ice-core from Law Dome, Antarctica, *Annals of Glaciology, 10*, 28–33, 1987.

Evans, W.F.J., Depletion of the Arctic ozone hole by the notching mechanism during spring 1986, Paper A12-02, Spring AGU Meeting, *EOS, 68*, 272, 1987.

Evans, W.F.J., and J.B. Kerr, Estimates of the amount of sulphur dioxide injected into the stratosphere by the explosive volcanic eruptions: El Chichón, mystery volcano, Mt. St. Helens, *Geophys. Res. Lett., 10*, 1049–1051, 1983.

Evans, W.F.J., I.A. Asbridge, J.B. Kerr, C.L. Mateer, and R.A. Olafson, The effects of SO_2 on Dobson and Brewer total ozone measurements, in *Proc. Quadrennial Ozone Symposium*, edited by J. London, pp. 48–56, International Ozone Commission, Boulder, Colorado, 1980.

Fabian, P., R. Borchers, S.A. Penkett, and N.J.D. Prosser, Halocarbons in the stratosphere, *Nature, 216*, 135–136, 1981.

Fabry, C., and M. Buisson, L'absorption de l'ultraviolet par l'ozone et la limite du spectre solaire, *J. Phys. Rad., Ser. 5, 3*, 196–226, 1913.

Fabry, C., and M. Buisson, Etude de l'extremité ultraviolette du spectre solaire, *J. Phys. Rad., Ser. 6, 2*, 197–226, 1921.

Fahey, D.W., C.S. Eubank, G. Hubler, and F.C. Fehsenfeld, Evaluation of a catalytic reduction technique for the measurement of total reactive odd-nitrogen, NO_y, in the atmosphere, *J. Atmos. Chem., 3*, 435–468, 1985.

Fairchild, C.E., E.J. Stone, and G.M. Lawrence, Photofragment spectroscopy of ozone in the UV region 270–310 nm and at 600 nm, *J. Chem. Phys., 69*, 3632, 1978.

Farkas, E., *Proc. Quadr. Ozone Symposium—1988*, Göttingen, edited by R.J. Bojkov and P. Fabian, Deepak Publ., USA, in press.

Farman, J.C., and B.G. Gardiner, Ozone depletion over Antarctica, *Nature, 329*, 574, 1987.

Farman, J.C., B.G. Gardiner, and J.D. Shanklin, Large losses of ozone in Antarctica reveal seasonal ClO_x/NO_x interaction, *Nature, 315*, 207–210, 1985.

Farmer, C.B., G.C. Toon, P.W. Schaper, J.F. Blavier, and L.L. Lowes, Stratospheric trace gases in the spring 1986 Antarctic atmosphere, *Nature, 329*, 126, 1987.

Farrara, J.D., and C.R. Mechoso, An observational study of the final warming in the Southern Hemisphere stratosphere, *Geophys. Res. Lett., 13*, 1232–1235, 1986.

Federal Coordinator for Meteorological Services and Supporting Research, *The National Plan for Stratospheric Monitoring 1987–1997*, Department of Commerce, NOAA, Washington, D.C., 1988.

Feister, U., and W. Warmbt, Long-term surface ozone increase at Arkona, in *Atmospheric Ozone, Proceedings of the Quadrennial Ozone Symposium*, Halkidiki, Greece, September 3–7, 1984, edited by C.S. Zerefos and A. Ghazi, pp. 782–787, D. Reidel, Dordrecht, The Netherlands, 1985.

Fels, S.B., and M.D. Schwarzkopf, The simplified exchange approximation: A new method for radiative transfer calculations, *J. Atmos. Sci., 32*, 1475–1488, 1975.

Fels, S.B., J.D. Mahlman, M.D. Schwarzkopf, and R.W. Sinclair, Stratospheric sensitivity to perturbations in ozone and carbon dioxide: Radiative and dynamical response, *J. Atmos. Sci., 37*, 2265–2297, 1980.

Findlay, F.D., and D.R. Snelling, Collisional deactivation of $O_2(^1\Delta g)$, *J. Chem. Phys., 55*, 545–551, 1971.

Finger, F.G., H.M. Woolf, and C.E. Anderson, A method for objective analysis of stratospheric constant-pressure charts, *Mon. Weather Rev., 93*, 619–638, 1965.

Finger, F.G., M.E. Gelman, F.J. Schmidlin, R. Leviton, and B.W. Kennedy, Compatibility of meteorological rocketsonde data as indicated by international comparison tests, *J. Atmos. Sci., 32*, 1705–1714, 1975.

Fiocco, G., and G. Grams, Observations of the aerosol layer at 20 km by optical radar, *J. Atmos. Sci., 21*, 323–324, 1964.

Fleig, A.J., K.F. Klenk, P.K. Bhartia, K.D. Lee, C.G. Wellemeyer, and V.G. Kaveeshwar, Vertical ozone profile results from Nimbus–4 data, in *Proc. Fourth Conference on Atmospheric Radiation*, pp. 20–26, AMS, Toronto, Ontario, June 16–18, 1981.

Fleig, A.J., P.K. Bhartia, C.K. Wong, and C.L. Mateer, Comparison of Nimbus–7 TOMS and ground-station total ozone measurements, *Index 17, XV–XVII*, World Meteorol. Organ. World Ozone Data Cent., Toronto, Canada, 1982.

Fleig, A.J., P.K. Bhartia, C.G. Wellemeyer, and D.S. Silberstein, Seven years of total ozone from the TOMS instrument—A report on data quality, *Geophys. Res. Lett., 13*, 1355–1358, 1986a.

Fleig, A.J., P.K. Bhartia, and D.S. Silberstein, An assessment of the long-term drift in SBUV total ozone data, based on comparison with the Dobson network, *Geophys. Res. Lett., 13,* 1359–1362, 1986b.

Fleig, A.J., D.S. Silberstein, C.G. Wellemeyer, R.P. Cebula, and P.K. Bhartia, An assessment of the long-term drift in TOMS total ozone data, based on comparison with the Dobson network, in *Proc. Quadr. Ozone Symposium—1988,* Göttingen, edited by R.D. Bojkov and P. Fabian, Deepak Publ., USA, in press.

Fogle, B., and B. Haurwitz, Noctilucent clouds, *Space Sci. Rev., 6,* 278–340, 1966.

Folland, C.K., D.E. Parker, and F.E. Kates, Worldwide marine temperature fluctuations 1856–1981, *Nature, 310,* 670–673, 1984.

Foot, J.S., Aircraft measurements of the humidity in the lower stratosphere from 1977 to 1980 between 45°N and 65°N, *Quart. J. Roy. Meteorol. Soc., 110,* 303–319, 1984.

Fowle, F.E., Atmospheric ozone: Its relation to some solar and terrestrial phenomena, *Smith's. Misc. Coll., 81, No. 11,* 1929.

Fox, R.J., G.W. Grams, B.G. Schuster, and J.A. Weinman, Measurements of stratospheric aerosols by airborne laser radar, *J. Geophys. Res., 78,* 7789–7801, 1973.

Fraser, P.J., and N. Derek, Atmospheric halocarbons and nitrous oxide, 1982–1985, in *Baseline 85, Baseline Atmospheric Program (Australia) 1985,* edited by B.W. Forgan and P.J. Fraser, pp. 44–47, Bureau of Meteorology/CSIRO, 1987.

Fraser, P.J., G.I. Pearman, and P. Hyson, The global distribution of atmospheric carbon dioxide 2. A review of provisional background observations, 1978–1980, *J. Geophys. Res., 88,* 3591–3598, 1983.

Fraser, P.J., P. Hyson, R.A. Rasmussen, A.J. Crawford, and M.A.K. Khalil, Methane, carbon monoxide and methylchloroform in the Southern Hemisphere, *J. Atmos. Chem., 4,* 3–42, 1986a.

Fraser, P.J., N. Derek, R. O'Brien, R. Shepherd, R.A. Rasmussen, and A.J. Crawford, Atmospheric halocarbons and nitrous oxide, 1976–1984, in *Baseline 83–84, Baseline Atmospheric Program (Australia) 1983–1984,* edited by R.J. Francey and B.W. Forgan, pp. 43–49, Bureau of Meteorology/CSIRO, 1986b.

Fraser, P.J., P. Hyson, S. Coram, R.A. Rasmussen, A.J. Crawford, and M.A.K. Khalil, Carbon monoxide in the Southern Hemisphere, in *Proceedings of the 7th World Clean Air Congress, 2,* pp. 341–352, Sydney, Australia, August 1986, 1986c.

Fraser, P.J., R.A. Rasmussen, and M.A.K. Khalil, Atmospheric observations of chlorocarbons, nitrous oxide, methane and carbon monoxide from the Oregon Graduate Center (OGC) flask sampling program, 1984–1985, in *Baseline 85, Baseline Atmospheric Program (Australia) 1985,* edited by B.W. Forgan and P.J. Fraser, pp. 57–55, Bureau of Meteorology/CSIRO, 1987a.

Fraser, P.J., S. Coram, and N. Derek, Atmospheric methane, carbon monoxide and carbon dioxide by gas chromatography, 1978–1985, in *Baseline 85, Baseline Atmospheric Program (Australia) 1985,* edited by B.W. Forgan and P.J. Fraser, pp. 48–50, Bureau of Meteorology/CSIRO, 1987b.

Frederick, J.E., G.N. Seraphino, and A.R. Douglass, An analysis of the annual cycle in upper stratospheric ozone, *J. Geophys. Res., 89,* 9547–9555, 1984.

Frederick, J.E., R.P. Cebula, and D.F. Heath, Instrument characterization for the detection of long-term changes in stratospheric ozone: An analysis of the SBUV/2 radiometer, *J. Atmos. Ocean. Tech., 3,* 472, 1986.

Friedl, R.R., and S.P. Sander, Kinetic and product studies of the reaction ClO + BrO using discharge flow-mass spectroscopy, Paper delivered at the Eighteenth International Symposium on Free Radicals, Oxford, England, 1987.

Gandin, L.S., Objective analysis of meteorological fields, *GIMIZ Gidrometeorologicheskoe Izdatel'stvo,* Leningrad, 1963.

Gandrud, B.W., M.A. Kritz, and A.L. Lazrus, Balloon and aircraft measurements of stratospheric sulfate mixing ratio following the El Chichón eruption, *Geophys. Res. Lett., 10*, 1037–1040, 1983.

Garcia, R., and S. Solomon, A possible relationship between interannual variability in Antarctic ozone and the quasi-biennial oscillation, *Geophys. Res. Lett., 14*, 848–851, 1987.

Garcia, R.R., S. Solomon, R.G. Roble, and D.W. Rusch, A numerical study of the response of the middle atmosphere to the 11 year solar cycle, *Planet. Space Sci., 32*, 411–423, 1984.

Gardiner, B.G., Comparative morphology of the vertical ozone profile in the Antarctic spring, *Geophys. Res. Lett., 8*, 901–904, 1988.

Geller, M.A., M.-F. Wu, M.E. Gelman, Troposphere–stratosphere (surface—55 km) monthly winter general circulation statistics for the Northern Hemisphere—Four year averages, *J. Atmos. Res., 40*, 334–342, 1983.

Gelman, M.E., and R.M. Nagatani, Objectives analyses of height and temperature at the 5, 2, and 0.4 mb levels using meteorological rocketsonde and satellite radiation data, *Space Research XVII, 17*, 122, 1977.

Gelman, M.E., A.J. Miller, R.M. Nagatani, and H.D. Bowman II, Mean zonal wind and temperature structure during the PMP–1 winter periods, *Adv. Space Res., 2*, 159–162, 1983.

Gelman, M.E., A.J. Miller, K.W. Johnson, and R.M. Nagatani, Detection of long-term trends in global stratospheric temperature from NMC analyses derived from NOAA satellite data, *Adv. Space Res., 6*, 17–25, 1986.

Gernandt, H., The vertical ozone distribution above the GDR-research base, Antarctica in 1985, *Geophys. Res. Lett., 14*, 84–86, 1987.

Gille, J.C., and L.V. Lyjak, Radiative heating and cooling rates in the middle atmosphere, *J. Atmos. Sci., 43*, 2215–2229, 1986.

Gille, J.C., and J.M. Russell, III, The limb infrared monitor of the stratosphere: Experiment description, performance, and results, *J. Geophys. Res., 89*, 5125–5140, 1984.

Gille, J.C., P.L. Bailey, and J.M. Russell III, Temperature and composition measurements from the LRIR and LIMS experiments on Nimbus 6 and 7, *Phil. Trans. Roy. Soc. London Ser. A, 296*, 205–218, 1980.

Gille, J.C., J.M. Russell, P.L. Bailey, L.L. Gordley, E.E. Remsberg, J.H. Lienesch, W.G. Planet, F.B. House, L.V. Lyjak, and S.A. Beck, Validation of temperature retrievals obtained by the Limb Infrared Monitoring of the Stratosphere (LIMS) experiment on Nimbus–7, *J. Geophys. Res., 89*, 5147–5160, 1984a.

Gille, J.C., J.M. Russell, III, P.L. Bailey, E.E. Remsberg, L.L. Gordley, W.F.J. Evans, H. Fischer, B.W. Gandrud, A. Girard, J.E. Harries, and S.A. Beck, Accuracy and precision of the nitric acid concentrations determined by the Limb Infrared Monitor of the Stratosphere experiment on Nimbus–7, *J. Geophys. Res., 89*, 5179–5190, 1984b.

Gille, J.C., C.M. Smythe, and D.F. Heath, Observed ozone response to variations in solar ultraviolet radiation, *Science, 225*, 315–317, 1984c.

Gille, J.C., L. Lyjak, and A.K. Smith, The global residual mean circulation in the middle atmosphere for the northern winter period, *J. Atmos. Sci., 44*, 1437, 1987.

GMCC, 1986a, see Schnell, R.C.

GMCC, 1986b, see Schnell, R.C., and R.M. Rosson.

Goldman, A., F.J. Murcray, R.D. Blatherwick, and D.G. Murcray, Quantification of HCl from high-resolution, ground-based infrared solar spectra in the 3000 cm^{-1} region, *J. Quant. Spec. Rad. Trans. 30*, 385–387, 1986.

Gooding, J.L., D.S. Clanton, E.M. Gabel, and J.L. Warren, El Chichón volcanic ash in the stratosphere: Particle abundance and size distribution after the 1982 eruption, *Geophys. Res. Lett., 10*, 1033–1036, 1983.

Gordley, L.L., and J.M. Russell, Rapid inversion of limb radiance data using an emissivity growth approximation, *Appl. Opt., 20*, 807, 1981.

Götz, F.W.P., A.R. Meetham, and G.M.B. Dobson, The vertical distribution of ozone in the atmosphere, *Proc. Roy. Soc. London, A145*, 416–446, 1934.

Graedel, T.E., and J.E. McRae, On the possible increase of the atmospheric methane and carbon monoxide concentrations during the last decade, *Geophys. Res. Letts., 7*, 977–979, 1980.

Grant, K.E., P.S. Connell, and D.J. Wuebbles, Monte Carlo uncertainty analysis of change in atmospheric ozone concentrations from large trace gas perturbations, *EOS, 66*, 838, 1985.

Gray, L.J., and J.A. Pyle, A two dimensional model of the quasi-biennial oscillation of ozone, Polar Ozone Workshop, *NASA Conf. Publ. 10014*, 306 pp., Snowmass, Colorado, 1988.

Grenander, U., On the estimation of regression coefficients in the case of an autocorrelated disturbance, *Ann. Math. Statist., 25*, 252–272, 1954.

Gustin, G.P., On the methodology of total ozone measurements in the global network, *Proc. Main Geophys. Obs. Leningrad, 406*, 63–75, 1978.

Gustin, G.P., Universal ozonometer, *Proc. Main Geophys. Obs. Leningrad, 141*, 83–98, 1963.

Gustin, G.P., S.A. Sokolenko, and V.A. Kovalyov, Total-ozone measuring instruments used at the USSR station network, in *Atmospheric Ozone, Proceedings of the Quadrennial Ozone Symposium*, Halkidiki, Greece, September 3–7, 1984, edited by C.S. Zerefos and A. Ghazi, pp. 543–546, D. Reidel, Dordrecht, The Netherlands, 1985.

Haigh, J.D., Radiative heating in the lower stratosphere and the distribution of ozone in a two-dimensional model, *Quart. J. Roy. Meteorol. Soc., 110*, 167–185, 1984.

Hamill, P., The time dependent growth of H_2O–H_2SO_4 aerosols by heteromolecular condensation, *J. Aerosol Sci., 6*, 475–482, 1975.

Hamill, P., and L.R. McMaster (Eds.), *Polar Stratospheric Clouds: Their Role in Atmospheric Processes, NASA CP–2318*, 72 pp., Hampton, VA, 1984.

Hamill, P., O.B. Toon, and R.P. Turco, Characteristics of polar stratospheric clouds during the formation of the Antarctic ozone hole, *Geophys. Res. Lett., 13*, 1288–1291, 1986.

Hamill, P., R.P. Turco, and O.B. Toon, Formation and properties of nitric acid polar stratospheric clouds, *J. Atmos Chem., 7*, 287–315, 1988.

Hamilton, K.P., *Stratospheric Circulation Statistics, NCAR Tech. Note TN–191–STR*, National Center for Atmospheric Research, Boulder, Colorado, 1982.

Hansen, J.E., W.C. Wang, and A.A. Lacis, Mt. Agung provides best of a global climate perturbation, *Science, 199*, 1065–1068, 1978.

Hanson, D., and K. Mauersberger, Precision ozone vapor pressure measurements, *J. Chem. Phys., 83*, 326–328, 1985.

Hanson, D., and K. Mauersberger, The vapor pressure of solid and liquid ozone, *J. Chem. Phys., 85*, 4669–4672, 1986.

Hao, W.M., S.C. Wofsy, M.B. McElroy, J.M. Beer, and M.A. Toqan, Sources of atmospheric nitrous oxide from combustion, *J. Geophys. Res., 92*, 3098–3104, 1987.

Harris, N.R.P., and F.S. Rowland, Trends in total ozone measurements at Arosa, *EOS, 67*, 875, 1986.

Harris, N.R.P., and F.S. Rowland, *Trends in Total Ozone Measurements at Arosa*, American Geophys. Union, San Francisco, 1988.

Harris, O.D., and G.W. Adams, Where does the $O(^1D)$ energy go? *J. Geophys. Res., 88*, 4918–4928, 1983.

Hartley, W.N., On the absorption of solar rays by atmospheric ozone, *J. Chem. Soc., 39*, 111–128, 1881b.

Hartley, W.N., On the absorption spectrum of ozone, *J. Chem. Soc., 39*, 57–61, 1881a.

Hartmann, D.L., The dynamical climatology of the stratosphere in the Southern Hemisphere during late winter 1973, *J. Atmos. Sci., 33*, 1789–1802, 1976b.

Hartmann, D.L., Some aspects of stratospheric dynamics, in *Advances in Geophysics, 28A*, edited by B. Saltzman, vol. ed. S. Manabe, pp. 219–247, Academic Press, Orlando, Florida, 1985.

Hartmann, D.L., The structure of the stratosphere in the Southern Hemisphere during late winter 1973 as observed by satellite, *J. Atmos. Sci., 33*, 1141–1154, 1976a.

Hartmann, D.L., C.R. Mechoso, and K. Yamazaki, Observations of wave mean-flow interaction in the Southern Hemisphere, *J. Atmos. Sci., 41*, 351–362, 1984.

Harwood, R.S., The temperature structure of the Southern Hemisphere stratosphere August–October 1971, *Quart. J. Roy. Meteorol. Soc., 101*, 75–91, 1975.

Harwood, R.S., and J.A. Pyle, a two-dimensional mean circulation model for the atmosphere below 80 km, *Quart. J. Roy. Meteorol. Soc., 101*, 723–747, 1975.

Hasebe, F., The global structure of the total ozone fluctuations observed on the time scales of two to several years, in *Dynamics of the Middle Atmosphere*, edited by J.R. Holton and T. Matsuno, pp. 445–464, Terra Publishers, Tokyo, 1984.

Hasebe, F., Interannual variations of global total ozone revealed from Nimbus IV BUV and ground-based observations, *J.Geophys. Res., 88*, 6819, 1983.

Hayman, G.D., J.M. Davies, and R.A. Cox, Kinetics of the reaction ClO + ClO $\rightarrow$ products and its potential relevance to Antarctic ozone, *Geophys. Res. Lett., 13*, 1347, 1986.

Hearn, A.G., The absorption of ozone in the ultra-violet and visible regions of the spectrum, *Proc. Phys. Soc. (London), 78*, 932–940, 1961.

Heath, D.F., Non-seasonal changes in total column ozone from satellite observations, 1970–1986, *Nature, 332*, 219–227, 1988.

Heath, D.F., Testimony before the Subcommittee on Health and the Environment of the House Committee on Energy and Commerce, 1986.

Heath, D.F., and B.M. Schlesinger, The Mg 280-nm doublet as a monitor of changes in solar ultraviolet irradiance, *J. Geophys. Res., 91*, 8672–8682, 1986.

Heath, D.F., and B.M. Schlesinger, Temporal variability of UV solar spectral irradiance from 160–400 nm over periods of the evolution and rotation regions from maximum to minimum phases of the sunspot cycle, in *IRS 84: Current Problems in Atmospheric Radiation, Proceedings of the International Radiation Symposium*, Perugia, Italy, edited by G. Fiocco, pp. 315–319, A. Deepak, Hampton, Virginia, 1984.

Heath, D., A.J. Krueger, and C.L. Mateer, The Backscatter Ultraviolet (BUV) Spectrometer experiment, in *The Nimbus IV User's Guide*, edited by R.R. Sabatini, pp. 149–171, NASA, Greenbelt, Maryland, 1970.

Heath, D.F., C.L. Mateer, and A.J. Krueger, The Nimbus–4 Backscatter Ultraviolet (BUV) atmospheric ozone experiment—Two years' operation, *PAGEOPH, 106–108*, 1238–1252, 1973.

Heath, D.F., A.J. Krueger, H.A. Roeder, and B.D. Henderson, The Solar Backscatter Ultraviolet and Total Ozone Mapping Spectrometer (SBUV/TOMS) for Nimbus G, *Opt. Eng., 14*, 323–331, 1975.

Heath, D.F., A.J. Krueger, and H. Park, The Solar Backscatter Ultraviolet (SBUV) and Total Ozone Mapping Spectrometer (TOMS) experiment, in *The Nimbus–7 User's Guide*, edited by C.R. Madrid, NASA Goddard Space Flight Center, Greenbelt, MD., 175–211, 1978.

Herron, M.M., Impurities sources of F, Cl, NO_3, and SO_4 in Greenland and Antarctic precipitation, *J. Geophys. Res., 87*, 3052–3060, 1982.

Heymsfield, A.J., Ice particles observed in a cirriform cloud at −83°C and implications for polar stratospheric clouds, *J. Atmos. Sci., 43*, 851–855, 1986.

Hill, W.J., P.N. Sheldon, and J.J. Tiede, Analyzing world-wide ozone for trends, *Geophys. Res. Lett., 4*, 21–24, 1977.

Hill, W.J., G.W. Oehlert, and G.C. Reinsel, Trend analysis sensitivity studies of Dobson total ozone data through 1984, *J. Geophys. Res., 91*, 14515–14520, 1986.

Hilsenrath, E., and B.M. Schlesinger, Total ozone seasonal and interannual variations derived from the 7 year Nimbus–4 BUV data set, *J. Geophys. Res., 86*, 12087–12096, 1981.

Hilsenrath, E., P.J. Dunn, and C.L. Mateer, Standard ozone profiles from balloon and rocket data for satellite and theoretical model input, Presented at IAGA/IAMAP Joint Assembly, Seattle, 1977.

Hilsenrath, E., W. Attmannspacher, A. Bass, W. Evans, R. Hagemeyer, R.A. Barnes, W. Komhyr, K. Mauersberger, J. Mentall, M. Proffitt, D. Robbins, S. Taylor, A. Torres, and E. Weinstock, Results from the balloon ozone inter-comparison campaign (BOIC), *J. Geophys. Res. 91*, 13137–13152, 1986.

Hofmann, D.J., Perturbations to the global atmosphere associated with El Chichón volcanic eruption of 1982, *Rev. Geophys., 25*, 743–759, 1987.

Hofmann, D.J., and J.M. Rosen, Antarctic observations of stratospheric aerosol and high altitude condensation nuclei following the El Chichón eruption, *Geophys. Res. Lett., 12*, 13–16, 1985.

Hofmann, D.J., and J.M. Rosen, On the temporal variation of stratospheric aerosol size and mass during the first 18 months following the 1982 eruption of El Chichón, *J. Geophys. Res., 89*, 4883–4890, 1984.

Hofmann, D.J., and J.M. Rosen, Stratospheric sulfuric acid fraction and mass estimate for the 1982 volcanic eruption of El Chichón, *Geophys. Res. Lett., 10*, 313–316, 1983b.

Hofmann, D.J., and J.M. Rosen, Sulfuric acid droplet formation and growth in the stratosphere after the 1982 eruption of El Chichón, *Science, 222*, 325–327, 1983, 1983a.

Hofmann, D.J., J.M. Rosen, T.J. Pepin, and R.G. Pinnick, Stratospheric aerosol measurements I: Time variations at northern mid-latitudes, *J. Atmos. Sci., 32*, 1446–1456, 1975.

Hofmann, D.J., J.M. Rosen, J.W. Harder, and S.R. Rolf, Ozone and aerosol measurements in the springtime Antarctic stratosphere in 1985, *Geophys. Res. Lett., 13*, 1252–1255, 1986.

Hofmann, D.J., J.W. Harder, S.R. Rolf, and J.M. Rosen, Balloon-borne observations of the development and vertical structure of the Antarctic ozone hole in 1986, *Nature, 326*, 59–62, 1987a.

Hofmann, D.J., J.M. Rosen, J.W. Harder, and S.R. Rolf, Observations of the decay of the El Chichón stratospheric aerosol cloud in Antarctica, *Geophys. Res. Lett., 14*, 614–617, 1987b.

Hofmann, D.J., J.M. Rosen, and J.W. Harder, Aerosol measurements in the winter/spring Antarctic stratosphere: I. Correlative measurements with ozone, *J. Geophys. Res., 93*, 665–676, 1988.

Hofmann, D.J., J.W. Harder, J.M. Rosen, J.V. Hereford, and J.R. Carpenter, Ozone profile measurements at McMurdo Station, Antarctica, during spring 1987, *J. Geophys. Res.*, 1989, in press.

Holland, A.C., R.A. Barnes, and H.S. Lee, Improved rocket ozonesonde (ROCOZ–A) 1. Demonstration of precision, *Appl. Opt., 24*, 3286–3295, 1985.

Holton, J.R., and W.M. Wehrbein, A numerical model of the zonal mean circulation of the middle atmosphere, *Pure Appl. Geophys., 118*, 284–306, 1980b.

Holton, J.R., and W.M. Wehrbein, The role of forced planetary waves in the annual cycle of the zonal mean circulation of the middle atmosphere, *J. Atm. Sci., 37*, 1968–1983, 1980a.

Hood, L.L., The temporal behavior of upper stratospheric ozone at low latitudes: Evidence from Nimbus 4 BUV data for short-term responses to solar ultraviolet variability, *J. Geophys. Res., 89*, 9557–9568, 1984.

Hoskins, B.J., M.E. McIntyre, and A.W. Robertson, On the use and significance of isentropic potential vorticity maps, *Quart. J. Roy. Meteorol. Soc., 111*, 877–946, 1985.

Houghton, J.T., Absorption and emission by carbon dioxide in the mesosphere, *Quart. J. Roy. Meteorol. Soc., 95*, 1–20, 1969.

Howard, C.J., and K.M. Evenson, Kinetics of the reaction of HO_2 with NO, *Geophys. Res. Lett., 4*, 437–441, 1977.

Hunter, W.R., Optical contamination: Its prevention in the XUV spectrographs flown by the Naval Research Observatory in the Apollo telescope mount, *Appl. Opt., 16*, 909–916, 1977.

Hyson, P., Stratospheric water vapour over Australia, *Quart. J. R. Meteorol. Soc., 109*, 285–294, 1983.

Isaksen, I.S.A., and O. Hov, Calculations of trends in the tropospheric ozone concentrations of O_3, OH, CO, CH_4 and NO_x. *Tellus, 39B*, 271–283, 1987.

Isaksen, I.S.A., and F. Stordal, Antarctic ozone depletion: 2-D model studies, *Geophys. Res. Lett., 13*, 1327–1330, 1986a.

Isaksen, I.S.A., and F. Stordal, Ozone perturbations by enhanced levels of CFCs, N_2O and CH_4: A two-dimensional model study including uncertainty estimates, *J. Geophys. Res., 91*, 5249–5263, 1986b.

Iwasaka, Y., Non-spherical particles in the Antarctic polar stratosphere—Increase in particulate content and stratospheric water vapor budget, *Tellus, 38B*, 364–374, 1986.

Iwasaka, Y., and K. Kondoh, Depletion of Antarctic ozone: Height of ozone loss and its temporal changes, *Geophys. Res. Lett., 14*, 87–90, 1987.

Iwasaka, Y., T. Ono, and A. Nonura, Changes in aerosol content and temperature in the Antarctic spring stratosphere: Lidar measurement at Syowa station (69° 00′ S, 30° 35′ E) in 1883, 1984, and 1985, *Geophys. Res. Lett., 13*, 1407–1410, 1985a.

Iwasaka, Y., A. Ono, and A. Saitoh, Measurements of water vapor content in the polar stratosphere: Syowa Station, Spring 1983, *Mem. Nat. Inst. Polar Research, Tokyo, Spec. Issue No. 39*, 51–55, 1985b.

Iwasaka, Y., T. Hirasawa, and H. Fukunishi, Lidar measurement on the Antarctic stratospheric aerosol layer (II) The changes of layer, height, and thickness in winter, *J. Geomag. Geoelectr., 38*, 99–109, 1986.

Iwasaka, Y., T. Ono, and A. Nonura, Lidar measurements of Antarctic stratospheric aerosols during 1983, 1984, and 1985: Effect of volcanic eruption of El Chichón, *Mem. Natl. Inst. Polar Res., Spec. Issue No. 47*, 56–61, 1987.

Jackman, C.H., J.E. Frederick, and R.S. Stolarski, Production of odd nitrogen in the stratosphere and mesosphere: An intercomparison of source strengths, *J. Geophys. Res., 85*, 7495–7505, 1980.

Jackman, C.H., R.S. Stolarski, and J.A. Kaye, Two-dimensional monthly average ozone balance from Limb Infrared Monitor of the stratosphere and stratospheric and mesospheric sounder data, *J. Geophys. Res., 91*, 1103–1116, 1986.

Jager, H., R. Reiter, W. Carnuth, and S. Jian, Stratospheric aerosol layers during 1982 and 1983 as observed by lidar at Garmisch–Partenkirchen, 12th International Laser Radar Conference, Aix-en-Provence, France, August 13–17, 1984, *Abstracts*, pp. 207–210, 1984.

Jakosky, B.M., G.E. Thomas, D.W. Rusch, C.A. Barth, G.M. Lawrence, J.J. Olivero, R.T. Clancy, R.W. Sanders, and B.G. Knapp, Solar Mesosphere Explorer observations of stratospheric and mesospheric water vapor, *MECA Workshop on Atmospheric H–b2–sO Observations of Earth and Mars: Physical Processes, Measurements, and Interpretations*, Houston, Texas, edited by S.M. Clifford and R.M. Haberle, Lunar and Planetary Inst., Houston, Texas, 1988.

Johnson, K.W., and M.E. Gelman, Trends in the upper stratospheric temperatures as observed by rocketsondes (1965–1983), in *Handbook for MAP*, edited by S. Kato, SCOSTEP, Urbana, Illinois, 18, 24–27, 1985.

Johnston, P.V., and R.L. McKenzie, NO_2 observations at 45° during the decreasing phase of solar cycle 21, from 1980 to 1987, *J. Geophys. Res., 94*, 3473–3486, 1989.

Juckes, M.N., and M.E. McIntyre, A high-resolution one-layer model of breaking planetary waves in the stratosphere, *Nature, 328*, 590–596, 1987.

Junge, C.E., C.W. Chagnon, and J.E. Mason, Stratospheric aerosols, *J. Meteorol., 18*, 81–108, 1961.

Keating, G.M., The response of ozone to solar activity variations. A review, *Solar Physics, 74*, 321–347, 1981.

Keating, G.M., G.P. Brasseur, J.Y. Nicholson III, and A. De Rudder, Detection of the response of ozone in the middle atmosphere to short-term solar ultraviolet variations, *Geophys. Res. Lett., 12*, 449–452, 1985.

Kent, G.S., Dispersion characteristics of volcanically injected aerosol as seen by SAGE I, SAM II and SAGE II, Conference on Atmospheric Radiation, Williamsburg, Virginia, May 13–16, 1986, *Abstracts*, pp. 54–55, 1986.

Kent, G.S., and M.P. McCormick, SAGE and SAM II measurements of global stratospheric aerosol optical depth and mass loading, *J. Geophys. Res., 89*, 5303–5314, 1984.

Kent, G.S., C.R. Trepte, U.O. Farrukh, and M.P. McCormick, Variation in the stratospheric aerosol associated with the north cyclonic polar vortex as measured by the SAM II satellite sensor, *J. Atmos. Sci., 42*, 1536–1551, 1985a.

Kent, G.S., P.H. Wang, U.O. Farrukh, A. Deepak, and E.M. Patterson, Development of a global model for atmospheric backscatter at CO_2 wavelengths, *NASA Final Report*, Contract NAS8–35594, 1985b.

Kent, G.S., L.R. Poole, and M.P. McCormick, Characteristics of Arctic polar stratospheric clouds as measured by airborne lidar, *J. Atmos. Sci., 43*, 2149–2161, 1986.

Kerr, J.B., I.A. Asbridge, and W.F.J. Evans, Intercomparison of total ozone measured by the Brewer and Dobson spectrophotometers at Toronto, *J. Geophys. Res., 93*, 11129–11140, 1988a.

Kerr, J.B., I.A. Asbridge, and W.F.J. Evans, Long-term intercomparison between the Brewer and Dobson spectrophotometers at Canadian network stations, in *Proc. Quadr. Ozone Symposium—1988*, Göttingen, edited by R.D. Bojkov and P. Fabian, Deepak Publ., USA, in press.

Khalil, M.A.K., and R.A. Rasmussen, The atmospheric lifetime of methylchloroform (CH_3CCl_3), *Tellus, 36B*, 317–332, 1984a.

Khalil, M.A.K., and R.A. Rasmussen, Atmospheric methane: Trends over the last 10,000 years, *Atmos. Environ., 21*, 2445–2452, 1987c.

Khalil, M.A.K., and R.A. Rasmussen, Carbon monoxide in the Earth's atmosphere: Increasing trend, *Science, 224*, 54–56, 1984b.

Khalil, M.A.K., and R.A. Rasmussen, Carbon monoxide in the Earth's atmosphere: Indications of a global increase, *Nature, 332*, 242–245, 1988.

Khalil, M.A.K., and R.A. Rasmussen, Chlorocarbons in the Southern Hemisphere: Concentrations and temporal trends, in *Baseline 85, Baseline Atmospheric Program (Australia) 1985*, edited by B.W. Forgan and P.J. Fraser, pp. 26–29, Bureau of Meteorology/CSIRO, 1987a.

Khalil, M.A.K., and R.A. Rasmussen, Increase and seasonal cycles of nitrous oxide in the Earth's atmosphere, *Tellus*, 35B, 161–169, 1983a.

Khalil, M.A.K., and R.A. Rasmussen, Increase of $CHClF_2$ in the Earth's atmosphere, *Nature, 292*, 823–824, 1981.

Khalil, M.A.K., and R.A. Rasmussen, Interannual variability of atmospheric methane: Possible effects of the El Niño–Southern Oscillation, *Science, 232*, 56–58, 1986.

Khalil, M.A.K., and R.A. Rasmussen, Nitrous oxide: Trends and global mass balance over the last 3,000 years, *Annals of Glaciology, 10*, 73–79, 1987b.

Khalil, M.A.K., and R.A. Rasmussen, Secular trends of atmospheric methane, *Chemosphere, 11*, 877–883, 1982.

Khalil, M.A.K., and R.A. Rasmussen, Sources, sinks and seasonal cycles of atmospheric methane, *J. Geophys. Res., 88,* 5131–5144, 1983b.

Khalil, M.A.K., and R.A. Rasmussen, The trend of bromochlorodifluoromethane (CB_rClF_2) and the concentrations of other bromine containing gases at the South Pole, *Antarctic Journal of the United States: 1985 Review,* pp. 206–207, 1985.

Khalil, M.A.K., R.A. Rasmussen, and R. Gunawardena, Atmospheric bromine in the polar regions, in *Geophysical Monitoring for Climatic Change No. 15 Summary Report 1986,* edited by R. Schnell, pp. 123–125, NOAA, Boulder, Colorado, 1986.

Kiang, C.S., and P. Hamill, H_2SO_4–HNO_3–H_2O ternary system in the stratosphere, *Nature, 250,* 401–402, 1974.

Kiehl, J.T., and B.A. Boville, The radiative–dynamical response of a stratospheric–tropospheric general circulation model to changes in ozone, *J. Atmos. Sci., 45,* 1798–1817, 1988.

Kiehl, J.T., B.A. Boville, and B.P. Briegleb, Response of a general circulation model to a prescribed Antarctic ozone hole, *Nature, 332,* 522–525, 1988.

Klenk, K.F., Absorption coefficients of ozone for the backscatter U.V. experiment, *Appl. Opt., 19,* 236–242, 1980.

Klenk, K.F., P.K. Bhartia, A.J. Fleig, V.G. Kaveeshwar, R.D. McPeters, and P.M. Smith, Total ozone determination from the Backscatter UV Experiment (BUV), *J. Appl. Meteorol., 21,* 1672–1684, 1982.

Kley, D., A. Volz, and F. Mülheims, Ozone measurements in historic perspective: Tropospheric ozone, regional and global scale interactions, edited by I.S.A. Isaksen, *NATO ASI Series C, Vol. 227,* pp. 63–72, D. Reidel, Dordrecht, The Netherlands, 1988.

Knollenberg, R.G., and D. Huffman, Measurements of the aerosol size distributions in the El Chichón cloud, *Geophys. Res. Lett., 10,* 1025–1028, 1983.

Ko, M.K.W., K.K. Tung, D.K. Weinstein, and N.D. Sze, A zonal-mean model of stratospheric tracer transport in isentropic coordinates: Numerical solutions for nitrous oxide and nitric acid, *J. Geophys. Res., 90,* 2313–2329, 1985.

Ko, M.K.W., M.B. McElroy, D.K. Weisenstein, and N.D. Sze, Lightning: A possible source of stratospheric odd nitrogen, *J. Geophys. Res., 91,* 5395–5404, 1986.

Kobayashi, J., and Y. Toyama, On various methods of measuring the vertical distribution of atmospheric ozone 2, *Papers in Meteor. and Geoph., 17,* 97–112, 1966.

Köhler, U., and W. Attmannspacher, Long time intercomparison between Brewer and Dobson spectrophotometer at the Hohenpeissenberg, *Beitr. Phys. Atmosph., 59,* 85–96, 1986.

Komhyr, W.D., A carbon–iodine sensor for atmospheric soundings, *Proc. Ozone Symp.,* Albuquerque, New Mexico, pp. 26–30, 1965.

Komhyr, W.D., Electrochemical concentration cells for gas analysis, *Ann. Geophys., 25,* 203–210, 1969.

Komhyr, W.D., Operations handbook: Ozone observations with the Dobson spectrophotometer, *WMO Ozone Report #6,* 125 pp., 1980.

Komhyr, W.D., and R.D. Evans, Dobson spectrophotometer total ozone measurement errors caused by interfering absorbing species such as SO_2, NO_2, and photochemically produced O_3 in polluted air, *Geophys. Res. Lett. 7,* 157–160, 1980.

Komhyr, W.D., and T.B. Harris, Development of an ECC ozonesonde, *NOAA Tech. Rep. ERL 200–APCL 18,* 54 pp., Natl. Oceanic and Atmos. Admin., Boulder, Colorado, 1971.

Komhyr, W.D., S.J. Oltmans, A.N. Chopra, R.K. Leonard, T.E. Garcia, and C. McFee, Results of Umkehr, ozonesonde, total ozone, and sulfur dioxide observations in Hawaii following the eruption of El Chichón volcano in 1982, in *Atmospheric Ozone, Proceedings of the Quadrennial Ozone Symposium,* Halkidiki, Greece, September 3–7, 1984, edited by C.S. Zerefos and A. Ghazi, pp. 305–310, D. Reidel, Dordrecht, The Netherlands, 1985.

Komhyr, W.D., R.D. Grass, and R.K. Leonard, Total ozone decrease at South Pole, Antarctica, 1964–1985, *Geophys. Res. Lett., 13*, 1248–1251, 1986.

Komhyr, W.D., R.D. Grass, and R.K. Leonard, Dobson spectrophotometer No. 83: A standard for total ozone measurements, manuscript of the NOAA Air Resources Laboratory, Boulder, Colorado, 36 pp., 1987.

Komhyr, W.D., R.D. Grass, and R.K. Leonard, Calibration history of world standard Dobson spectrophotometer 83 and total ozone trends at Mauna Loa Observatory, Hawaii, and at American Samoa, South Pacific, *Proc. Quadr. Ozone Symposium—1988*, Göttingen, edited by R.D.Bojkov and P. Fabian, A. Deepak, USA, in press.

Komhyr, W.D., P.R. Franchois, S.E. Kuester, P.J. Reitelbach, and M.L. Fanning, ECC ozonesonde observations at South Pole, Antarctica, during 1987, *NOAA Data Report ERL ARL–15*, Boulder, CO, 319 pp., 1988a.

Komhyr, W.D., S.J. Oltmans, and R.D. Grass, Atmospheric ozone at South Pole, Antarctica, in 1986, *J. Geophys. Res., 93*, 5167–5184, 1988b.

Komhyr, W.D., R.D. Grass, and R.K. Leonard, Total ozone, ozone vertical distribution, and stratospheric temperatures at South Pole, Antarctica, in 1986 and 1987, *J. Geophys. Res., 94*, 11429–11436, 1989.

Krueger, A.J., Sighting of El Chichón sulfur dioxide clouds with the Nimbus 7 total ozone mapping spectrometer, *Science, 220*, 1377–1379, 1983.

Krueger, A.J., and R.A. Minzner, A mid-latitude ozone model for the 1976 U.S. Standard Atmosphere, *J. Geophys. Res., 81*, 4477, 1976.

Krueger, A.J., and M.R. Schoeberl, TOMS observations of total ozone in the 1986 Arctic spring, *Geophys. Res. Lett., 14*, 527–530, 1987.

Krueger, A.J., P.E. Ardanuy, F.S. Sechrist, L.M. Penn, D.E. Larko, S.D. Doiron, and R.N. Galimore, The 1987 airborne Antarctic ozone experiment, *NASA Ref. Pub. 1201*, 252 pp., NASA/Goddard Space Flight Center, Greenbelt, MD, 1988.

Krumins, M.V., and W.C. Lyons, Corrections for the upper atmosphere temperatures using a thin film loop mount, *NOLTR 72–152*, Naval Ordnance Laboratory, White Oak, Silver Spring, Maryland, 1972.

Labitzke, K., Sunspots, the QBO, and the stratospheric temperature in the north polar region, *Geophys. Res. Lett., 14*, 535–537, 1987.

Labitzke, K., and H. van Loon, Associations between the 11-year solar cycle, the QBO and the atmosphere. Part I: The troposphere and stratosphere in the Northern Hemisphere in winter, *J. Atm. Terr. Phys., 50, 3*, 197–206, 1988.

Labitzke, K., J.J. Barnett, and B. Edwards, Atmospheric structure and its variation in the region 20 to 120 km, Draft of a new reference middle atmosphere, *Handbook for MAP, Vol. 16*, 318 pp., SCOSTEP, Urbana, Illinois, 1985.

Labitzke, K., G. Brasseur, B. Naujokat, and A. De Rudder, Long-term temperature trends in the stratosphere: Possible influence of anthropogenic gases, *Geophys. Res. Lett., 12*, 52–55, 1986a.

Labitzke, K., B. Naujokat, and J.K. Angell, Long-term temperature trends in the middle stratosphere of the Northern Hemisphere, *Adv. Space Res., 6*, 7–16, 1986b.

Labs, D., and H. Neckel, The radiation of the solar photosphere from 2000Å to 100 microns, *Z. Astrophy., 69*, 1–73, 1968.

Lacis, A.A., and J.E. Hansen, A parameterization for the absorption of solar radiation in the Earth's atmosphere, *J. Atmos. Sci., 31*, 118–133, 1974.

Laird, C.M., Solar particle flux and nitrate in South Pole snow, in *Weather and Climate Responses to Solar Variations*, edited by B.M. McCormac, pp. 237–242, Colorado, Assoc. Univ. Press, Boulder, 1983.

Lait, L.R., M.R. Schoeberl, and P.A. Newman, Quasi-biennial modulation of the Antarctic ozone depletion, *J. Geophys. Res., 94*, 11559–11571, 1989.

REFERENCES

Lal, S., R. Borchers, P. Fabian, and B.C. Kruger, Increasing abundance of $CBrClF_2$ in the atmosphere, *Nature, 216*, 135–136, 1985.

Larsen, J.C., M.P. McCormick, L.R. McMaster, and W.P. Chu, Observations of atmospheric water vapor with the SAGE II instrument, MECA Workshop on Atmospheric H_2O Observations of Earth and Mars, Houston, Texas, July 1986.

Lau, N.–C., Circulation statistics based on FGGE level III–B analyses produced by GFDL, *NOAA Data Report, ERL GFDL–5*, 427 pp., NOAA Fluid Dynamics Laboratory, Princeton, NJ, 1984.

Lazrus, A.L., R.D. Cadle, B.W. Gandrud, J.P. Greenberg, B.J. Huebert, and W.I. Rose, Jr., Sulfur and halogen chemistry of the stratosphere and of volcanic eruption plumes, *J. Geophys. Res., 84*, 7869–7875, 1979.

Lean, J., Solar ultraviolet irradiance variations: A review, *J. Geophys. Res., 92*, 839–868, 1987.

Legrand, M.R., and R.J. Delmas, The ionic balance of Antarctic snow: A 10-year detailed record, *Atmos. Environ., 18*, 1867–1874, 1984.

Legrand, M.R., and R.J. Delmas, Relative contributions of tropospheric and stratospheric sources to nitrate in Antarctic snow, *Tellus, 38*, 236–249, 1986.

Leovy, C.B., and P.J. Webster, Stratospheric long waves: Comparison of thermal structure in the Northern and Southern Hemispheres, *J. Atmos. Sci., 33*, 1624–1638, 1976.

List, R.J., *Smithsonian Meteorological Tables, 6th Edition*, 527 pp., Smithsonian Institution Press, Washington, D.C., 1951.

Lockwood, G.W., N.M. White, D.T. Thompson, and H. Tug, Spectrally resolved measurements of the El Chichón cloud, May 1982–August 1983, *Geof. Int., 23–3*, 351–362, 1984.

Logan, J.A., Tropospheric ozone—Seasonal behaviour, trends and anthropogenic influence, J. *Geophys. Res., 90*, 10463–10482, 1985.

London, J., Radiative energy sources and sinks in the stratosphere and mesosphere, in *Proceedings of the NATO Advanced Study Institute on Atmospheric Ozone: Its Variations and Human Influence*, edited by Nicolet and Aiken, pp. 703–721, U.S. Department of Transportation, Washington, D.C., 1980.

London, J., R.D. Bojkov, S. Oltmans, and J.I. Kelley, Atlas of the global distribution of total ozone, July 1957–June 1967, *NCAR Technical Note NCAR/TN/113 STR*, National Center for Atmospheric Research, Boulder, Colorado, 1976.

Lovelock, J.E., Methylchloroform in the troposphere as an indicator of OH radical abundance, *Nature, 267*, 32, 1977.

Luther, F.M., Monthly values of eddy diffusion coefficients in the lower stratosphere, *UCRL Report No. 74616, AIAA Paper No. 73–498*, presented to the AIAA/AMS Conference on the Environmental Impact of Aerospace Operations in the High Atmosphere, Denver, 1973.

Madden, R.P., Reflecting films for the vacuum ultraviolet, in *Physics of Thin Films*, Vol. 1, edited by G. Hass, pp. 123–186, Academic Press, New York, 1963.

Mahlman, J.D., and S.B. Fels, Antarctic ozone decreases: A dynamical cause?, *Geophys. Res. Lett., 13*, 1316–1319, 1986.

Mahlman, J.D., and L.J. Umscheid, Comprehensive modeling of the middle atmosphere: The influence of horizontal resolution, *Trans. Processes in Middle Atmos.*, edited by G. Visconti and Rolando Garcia, pp. 251–266, 1987.

Mahlman, J.D., and L.J. Umscheid, Dynamics of the middle atmosphere: Successes and problems of the GFDL "SKYHI" general circulation model, in *Dynamics of the Middle Atmosphere*, edited by J.R. Holton and T. Matsuno, pp. 501–525, Terra Sci. Publ. Co., Tokyo, 1984.

Mahlman, J.D., H.B. Levy II, and W.J. Moxim, Three-dimensional tracer structure and behavior as simulated in two ozone precursor experiments, *J. Atmos. Sci., 37*, 655–685, 1980.

Mahlman, J.D., D.G. Andrews, H.U. Dütsch, D.L. Hartmann, T. Matsuno, R.J. Murgatroyd, and J.F. Noxon, Transport of trace constituents in the stratosphere, *Handbook for MAP, Vol. 3*, edited by C.F. Sechrist, J., 14–43, SCOSTEP, Urbana, Illinois, 1981.

Mahlman, J.D., D.G. Andrews, D.L. Hartmann, T. Matsuno, and R.G. Murgatroyd, Transport of trace constituents in the stratosphere, in *Dynamics of the Middle Atmosphere*, edited by J.R. Holton and T. Matsuno, pp. 387–416, Terrapub, Tokyo, 1984.

Makide, Y., and F.S. Rowland, Tropospheric concentrations of methylchloroform, CH_3CCl_3, in January 1978 and estimates of atmospheric residence times for hydrocarbons, *Proc. Nat. Acad. Sci., USA, 78*, 5933–5937, 1981.

Makide, Y., A. Yokohata, Y. Kubo, and T. Tominaga, Atmospheric concentrations of halocarbons in Japan in 1979–1986, *Bull. Chem. Soc. Japan, 60*, 571–524, 1987a.

Makide, Y., Y. Kubo, Y. Tojima, and T. Tominaga, The increase of the atmospheric concentration of CFC–113 (CCl_2FCClF_2), 54th Annual Meeting, Chemical Society of Japan, Tokyo, 1–4 April 1987, *Abstracts, 1*, R8, 1987b.

Manabe, S., and R.W. Weatherald, Thermal equilibrium of the atmosphere with a given distribution of relative humidity, *J. Atmos. Sci., 24*, 241–259, 1967.

Mankin, W.G., and M.T. Coffey, Increased stratospheric hydrogen chloride in the El Chichón cloud, *Science, 226*, 170–172, 1984.

Mankin, W.G., and M.T. Coffey, Latitudinal distributions and temporal changes of stratospheric HCl and HF, *J. Geophys. Res., 88*, 10776–10784, 1983.

Marche, P., and C. Meunier, Atmospheric trace species measured above Haute-Provence observatory, *Planet. Space Sci., 31*, 731–733, 1983.

Marche, P., A. Barbe, C. Secroun, J. Corr, and P. Jouve, Ground-based spectroscopic measurement of HCl, *Geophys. Res. Lett., 7*, 869–872, 1980.

Martin, L.R., H.S. Judeikis, and M. Wu, Heterogeneous reactions of Cl and ClO in the stratosphere, *J. Geophys. Res., 85*, 5511–5518, 1980.

Massie, S.T., J.A. Davidson, C.A. Cantrell, A.H. McDaniel, J.C. Gille, V.G. Kunde, J.C. Brasunas, W.C. Maguire, A. Goldman, and M.M. Abbas, Atmospheric infrared emission of $ClONO_2$ observed by a balloon-borne Fourier spectrometer, *J. Geophys. Res., 92*, 14806–14814, 1987.

Mastenbrook, H.J., and S.J. Oltmans, Stratospheric water vapor variability for Washington, DC/Boulder, Colorado: 1964–82, *J. Atmos. Sci., 40*, 2157–2165, 1983.

Mateer, C.L., On the information content of Umkehr observations, *J. Atmos. Sci., 21*, 370–381, 1964.

Mateer, C.L., A review of some aspects of inferring the ozone profile from inversion of ultraviolet radiance measurements, in *Mathematics of Profile Inversion*, edited by L. Colin, pp. 1–2 to 1–25, *NASA Tech. Memo. TM X–62*, 150 pp., Greenbelt, Maryland, 1972.

Mateer, C.L., and H.U. Dütsch, *Uniform Evaluation of Umkehr Observations From the World Ozone Network, Part I. Proposed Standard Umkehr Evaluation Technique*, 105 pp., National Center for Atmospheric Research, Boulder, Colorado, 1964.

Mateer, C.L., J.J. DeLuisi, and C.C. Porco, The short Umkehr method, part I: Standard ozone profiles for use in the estimation of ozone profiles by the inversion of short Umkehr observations, *NOAA Tech. Memo. ERL ARL–86*, 20 pp., NOAA Air Resources Laboratories, Silver Spring, MD, 1980.

Mateer, C.L., D.F. Heath, and A.J. Krueger, Estimation of total ozone from satellite measurements of backscattered ultraviolet Earth radiances, *J. Atmos. Sci., 28*, 1307–1311, 1971.

Mauersberger, K., D. Hanson, J. Barnes, and J. Morton, Ozone vapor pressure and absorption cross section measurements: Introduction of an ozone standard, *J. Geophys. Res., 92*, 8480–8482, 1987.

Mauldin, L.E., III, and W.P. Chu, Optical degradation due to contamination on the SAGE/SAGE II spaceflight instruments, in *Proc. Society of Photo-optical Instrumentation Engineers*, Arlington, Virginia, May 4–6, 1982.

Mauldin, L.E., III, N.H. Zaun, M.P. McCormick, J.H. Guy, and W.R. Vaughn, Stratospheric Aerosol and Gas Experiment II instrument: A functional description, *Opt. Eng., 24*, 307–321, 1985a.

Mauldin, L.E., III, M.P. McCormick, L.R. McMaster, and W.R. Vaughn, The Stratospheric Aerosol and Gas Experiment II (SAGE II) design and in-orbit performance, in *Proc. Society of Photo-optical Instrumentation Engineers, Arlington, Virginia, Vol. 589, Instrumentation for Remote Sensing From Space*, pp. 104–111, 1985b.

McClatchey, R.A., R.W. Fenn, J.E.A. Selby, F.E. Volz, and J.S. Garind, Optical properties of the atmosphere, *Environ. Res. Papers, AFCRL–71–0279*, Air Force Cambridge Research Laboratories, Bedford, Massachusetts, 1971.

McCormick, M.P., El Chichón: Lidar and satellite measurements versus time and latitude, Topical Meeting on Optical Remote Sensing of the Atmosphere, January 15–18, 1985, Incline Village, Nevada, *Technical Digest*, pp. TuA2–1 to TuA2–5, 1985.

McCormick, M.P., Lidar measurements of the El Chichón stratospheric aerosol climatology, 12th International Laser Radar Conference, Aix-en-Provence, France, August 13–17, 1984, *Abstracts*, pp. 207–210, 1984.

McCormick, M.P., and J.C. Larsen, Antarctic springtime measurements of ozone, nitrogen dioxide, and aerosol extinction by SAM II, SAGE, and SAGE II, *Geophys. Res. Lett., 13*, 1280–1283, 1986.

McCormick, M.P., and T.J. Swissler, Stratospheric aerosol mass and latitudinal distribution of the El Chichón eruption cloud for October, 1982, *Geophys. Res. Lett., 10*, 877–880, 1983.

McCormick, M.P., and C.R. Trepte, Polar stratospheric optical depth observed between 1978 and 1985, *J. Geophys. Res., 92*, 4297–4307, 1987.

McCormick, M.P., and C.R. Trepte, SAM II measurements of Antarctic PSC's and aerosols, *Geophys. Res. Lett., 13*, 1276–1279, 1986.

McCormick, M.P., P. Hamill, T.J. Pepin, W.P. Chu, T.J. Swissler, and L.R. McMaster, Satellite studies of the stratospheric aerosol, *Bull. Amer. Meteorol. Soc., 60*, 1038–1046, 1979.

McCormick, M.P., G.S. Kent, G.K. Yue, and D.M. Cunnold, SAGE measurements of the stratospheric aerosol dispersion and loading from the Soufriere volcano, *NASA Tech. Paper 1922*, 23 pp., NASA/Langley Research Center, Hampton, VA, 1981.

McCormick, M.P., H.M. Steele, P. Hamill, W.P. Chu, and T.J. Swissler, Polar stratospheric cloud sightings by SAM II, *J. Atmos. Sci., 39*, 1387–1397, 1982.

McCormick, M.P., C.R. Trepte, and G.S. Kent, Spatial changes in the stratospheric aerosol associated with the north polar vortex, *Geophys. Res. Lett., 10*, 941–944, 1983.

McCormick, M.P., T.J. Swissler, E. Hilsenrath, A.J. Krueger, and M.T. Osborn, Satellite and correlative measurements of stratospheric ozone: Comparison of measurements made by SAGE, ECC balloons, chemiluminescent, and optical rocketsondes, *J. Geophys. Res., 89*, 5315–5320, 1984a.

McCormick, M.P., T.J. Swissler, W.H. Fuller, W.H. Hunt, and M.T. Osborn, Airborne and ground-based lidar measurements of the El Chichón stratospheric aerosol from 90°N to 56°S, *Geof. Int., 23–2*, 187–221, 1984b.

McElroy, M.B., R.J. Salawitch, and S.C. Wofsy, Antarctic ozone: Chemical mechanisms for the spring decrease, *Geophys. Res. Lett., 13*, 1296–1299, 1986a.

McElroy, M.B., R.J. Salawitch, S.C. Wofsy, and J.A. Logan, Reductions of Antarctic ozone due to synergistic interactions of chlorine and bromine, *Nature, 321*, 759–762, 1986b.

McIntyre, M.E., and T.N. Palmer, Breaking planetary waves in the stratosphere, *Nature, 305*, 593–600, 1983.

McIntyre, M.E., and T.N. Palmer, A note on the concept of wave breaking for Rossby and gravity waves, *PAGEOPH, 123*, 964–975, 1985.

McIntyre, M.E., and T.N. Palmer, The "surf-zone" in the stratosphere, *J. Atmos. Terr. Phys., 46*, 825–850, 1984.

McKenzie, R.L., and P.V. Johnston, Springtime stratospheric NO_2 in Antarctica, *Geophys. Res. Lett., 11*, 73–75, 1984.

McMaster, L.R., Stratospheric Aerosol and Gas Experiment (SAGE II), in *Abstracts of the 6th AMS Conference on Atmospheric Radiation*, pp. J46–J48, Williamsburg, Virginia, 1986.

McPeters, R.D., The climatology of nitric oxide in the upper stratosphere and mesosphere as measured by SBUV, in *Abstracts of the 19th General Assembly of the IUGG*, pp. 7–13, Vancouver, Canada, 1987.

McPeters, R.D., The climatology of nitric oxide in the upper stratosphere, mesosphere, and thermosphere from 1979 through 1986, *J. Geophys. Res., 94*, 3461–3472, 1989.

McPeters, R.D., A nitric oxide increase observed following the July 1982 solar proton event, *Geophys. Res. Lett., 13*, 667–670, 1986.

McPeters, R.D., and A. Bass, Anomalous atmospheric spectral features between 300 and 310 nm interpreted in light of new ozone absorption coefficients measurements, *Geophys. Res. Lett., 9*, 227–230, 1982.

McPeters, R.D., and W.D. Komhyr, Long-term changes in SBUV/TOMS relative to the world primary standard Dobson instrument, *Proc. Quadr. Ozone Symposium—1988*, Göttingen, edited by R.D. Bojkov and P. Fabian, A. Deepak, USA, in press.

McPeters, R.D., D.F. Heath, and P.K. Bhartia, Average ozone profiles for 1979 from Nimbus 7 SBUV instrument, *J. Geophys. Res., 89*, 5199–5214, 1984.

McPeters, R.D., R.D. Hudson, P.K. Bhartia, and S.L. Taylor, The vertical ozone distribution in the Antarctic ozone minimum measured by SBUV, *Geophys. Res. Lett. 13*, 1213–1216, 1986.

Mechoso, C.R., D.L. Hartmann, and J.D. Farrara, Climatology and interannual variability of wave, mean-flow interaction in the Southern Hemisphere, *J. Atmos. Sci., 42*, 2189–2206, 1985.

Mechoso, C.R., A. O'Neill, V.D. Pope, and J.D. Farrara, A study of the stratospheric final warming of 1982 in the Southern Hemisphere, *Quart. J. Roy. Meteorol. Soc., 114*, 1365–1384, 1988.

Meeks, M.L., and A.E. Lilley, The microwave spectrum of oxygen in the Earth's atmosphere, *J. Geophys. Res., 68*, 1683–1703, 1963.

Meetham, A.R., Correlation of atmospheric ozone with other geophysical phenomena, *Quart. J. Roy. Meteorol. Soc., Suppl. to 62*, 59–66, 1936.

Meetham, A.R., The correlation of the amount of ozone with other characteristics of the atmosphere, *Quart. J. Roy. Meteorol. Soc., 63*, 289–307, 1937.

Megie, G., G. Aucellar, and J. Pelon, Lidar measurements of ozone vertical profiles, *Appl. Opt., 24*, 3453–3463, 1985.

Menzies, T., A re-evaluation of laser heterodyne radiometer ClO measurements, *Geophys. Res. Lett., 10*, 729–732, 1983.

Mielenz, K.D., K.L. Eckerle, R.P. Madden, and J. Reader, New reference spectrophotometer, *Appl. Opt., 12*, 1630–1641, 1973.

Miller, A.J., and F.J. Schmidlin, Rocketsonde repeatability and stratospheric variability, *J. Appl. Meteor., 10*, 320–327, 1971.

Molina, L.T., and M.J. Molina, Absolute absorption cross sections of ozone in the 185- to 350-nm wavelength range, *J. Geophys. Res., 91*, 14501–14508, 1986.

Molina, L.T., and M.J. Molina, Production of Cl_2O_2 from the self-reaction of the ClO radical, *J. Phys. Chem., 91*, 433–436, 1987.

Molina, M.J., T.–L. Tso, L.T. Molina, and F.C.–Y. Wang, Antarctic stratospheric chemistry of chlorine nitrate, hydrogen chloride, and ice: Release of active chlorine, *Science, 238*, 1253–1257, 1987.

Mount, G.H., *The SME Ultraviolet Ozone Spectrometer—A Users Guide*, Laboratory for Atmospheric and Space Physics Internal Report, University of Colorado, Boulder, 50 pp., 1982.

Mount, G.H., D.W. Rusch, J.F. Noxon, J.M. Zandony, and C.A. Barth, Measurements of stratospheric NO_2 from the Solar Mesosphere Explorer satellite, 1. An overview of the results, *J. Geophys. Res., 89*, 1327–1340, 1984.

Mount, G., R. Sanders, A. Schmeltekopf, and S. Solomon, Visible spectroscopy at McMurdo Station, Antarctica: 1. Overview and daily variations of NO_2 and O_3, austral spring, 1986, *J. Geophys. Res., 92*, 8320–8328, 1987.

Mroz, E.J., A.S. Mason, and W.A. Sedlacek, Stratospheric sulfate from El Chichón and the mystery volcano, *Geophys. Res. Lett., 10*, 873–876, 1983.

Murcray, F.J., F.H. Murcray, A. Goldman, D.G. Murcray, and C.P. Rinsland, Infrared measurements of several nitrogen species above the South Pole in December 1980 and November–December 1986, *J. Geophys. Res., 92*, 13373–13376, 1987.

Murgatroyd, R.J., and F. Singleton, Possible meridional circulations in the stratosphere and mesosphere, *Quart. J. Roy. Meteorol. Soc., 84*, 225–234, 1958.

Muzio, L.J., and J.C. Kramuch, An artifact in the measurement of N_2O from combustion sources, *Geophys. Res. Lett., 15*, 1369–1372, 1988.

Nagatani, R.M., and A.J. Miller, The influence of lower stratospheric forcing on the October Antarctic ozone decrease, *Geophys. Res. Lett., 14*, 202–205, 1987.

Nash, J., Extension of explicit radiance observations by the stratospheric sounding unit into the lower stratosphere and lower mesosphere, *Quart. J. Roy. Meteorol. Soc., 114*, 1153–1171, 1988.

Nash, J., and J.L. Brownscombe, Validation of the stratospheric sounding unit, *Adv. Space Res., 2, 6*, 59–62, 1983.

Nash, J., and G.F. Forrester, Long-term monitoring of stratospheric temperature trends using radiance measurements obtained by the TIROS–N series of NOAA spacecraft, *Adv. Space Res., 6*, 37–43, 1986.

Nash, J., and F.J. Schmidlin, *Final Report of the WMO International Radiosonde Intercomparison, Report 30*, WMO, 120 pp., 1987.

Nastrom, G.D., and A.D. Belmont, Periodic variations in stratospheric–mesospheric temperatures from 20–65 km at 80° N to 30° S, *J. Atmos. Sci., 32*, 1715–1722, 1975.

Natarajan, M., L.B. Callis, and J.E. Nealy, Solar UV variability: Effects on stratospheric ozone, trace constituents and thermal structure, *Pure Appl. Geophys., 119*, 750–779, 1980/81.

National Research Council (NRC), *The Effects on the Atmosphere of a Major Nuclear Exchange*, 193 pp., National Academy Press, Washington, D.C., 1985.

Naujokat, B., Long-term variations in the stratosphere of the Northern Hemisphere during the last two sunspot cycles, *J. Geophys. Res., 86*, 9811–9816, 1981.

Naujokat, B., An update of the observed quasi-biennial oscillation of the stratospheric winds over the tropics, *J. Atmos. Sci., 43*, 1873, 1986.

Naylor, J.A., Error evaluation of a rocket meteorological temperature sounding system, *Contractor Report*, University of Utah to NASA/Wallops Flight Center, Virginia, 1976.

Neftel, A., J. Beer, H. Oeschger, F. Zurcher, and R.C. Finkel, Sulphate and nitrate concentrations in snow from South Greenland 1895–1978, *Nature, 314*, 611–614, 1985.

Newman, P.A., The final warming and polar vortex disappearance during the Southern Hemisphere spring, *Geophys. Res. Lett., 13*, 1228–1231, 1986.

Newman, P.A., and W.J. Randel, Coherent ozone-dynamical changes during the Southern Hemisphere spring, 1979–1986, *J. Geophys. Res., 93*, 12585–12606, 1988.

Newman, P.A., and M.R. Schoeberl, October Antarctic temperature and total ozone trends from 1979–1985, *Geophys. Res. Lett., 13*, 1206–1209, 1986.

Noxon, J.F., E.C. Whipple, Jr., and R.S. Hyde, Stratospheric NO_2, 1. Observational method and behavior at mid-latitude, *J. Geophys. Res., 84*, 5047–5065, 1979.

NRC: See National Research Council

Ny, T.–Z., and Choong S.P., L'absorption de la lumiere par l'ozone entre 3050 et 2150 Å, *C.R. Acad. Sci. Paris, 196*, 916–918, 1933.

Ny, T.–Z., and Choong S.P., L'absorption de la lumiere par l'ozone entre 3050 et 3400 Å (region des bandes de Huggins), *C.R. Acad. Sci. Paris, 195*, 309–311, 1932.

Oberbeck, V.R., E.F. Danielsen, K.G. Snetsinger, G.V. Ferry, W. Fong, and D.M. Hayes, Effect of the eruption of El Chichón on stratospheric aerosol size and composition, *Geophys. Res. Lett., 10*, 1021–1024, 1983.

Oehlert, G., Trends in Dobson total ozone: An update through 1983, *J. Geophys. Res., 91, D2*, 2675–2679, 1986.

Ohring, G., K. Gallo, A. Gruber, W. Planet, L. Stowe, and J.D. Tarpley, Climate and Global Change: Chapter 6 of NOAA Satellite Data, *EOS, 70*, 41, p. 889, 1989.

Olsen, R.O., F.J. Schmidlin, D.U. Wright, and J.K. Luers, Comparison of atmospheric temperatures derived from falling sphere and grenade experiments conducted at Wallops Island in 1975, in *COSPAR Space Research, XIX*, 111–114, 1979.

Oltmans, S.J., Water vapor profiles for Washington, DC; Boulder, CO; Palestine, TX; Laramie, Wy; and Fairbanks, AK; during the period 1974 to 1985, *NOAA Data Report ERL ARL–7*, NOAA, Silver Spring, Maryland, 1986.

Osantowski, J.F., Contamination sensitivity of typical mirror coatings—A parametric study, *Proc. SPIE 338*, 80–86, 1983.

Oslik, N., *Solar Backscattered Ultraviolet Radiometer Version 2 User's Guide, SASC Document No. SASC–T–5–5085–017–84*, ST Systems Corp., Lanham, Maryland, 1984.

Owens, A.J., C.H. Hales, D.L. Filkin, C. Miller, and M. McFarland, Multiple scenario ozone change calculations: The subtractive perturbation approach, in *Atmospheric Ozone, Proceedings of the Quadrennial Ozone Symposium*, Halkidiki, Greece, September 3–7, 1984, edited by C.S. Zerefos and A. Ghazi, pp. 82–86, D. Reidel, Dordrecht, The Netherlands, 1985.

Ozone Data for the World, Atmospheric Environment Service, Department of the Environment in cooperation with the World Meteorological Organization, Downsview, Ontario.

Palmer, K.F., and D. Williams, Optical constants of sulfuric acid; application to the clouds of Venus?, *Appl. Opt., 14*, 208–219, 1975.

Park, H., and D.F. Heath, Nimbus 7 SBUV/TOMS calibration for the ozone measurement, in *Atmospheric Ozone, Proceedings of the Quadrennial Ozone Symposium*, Halkidiki, Greece, September 3–7, 1984, edited by C.S. Zerefos and A. Ghazi, pp. 412–416, D. Reidel, Dordrecht, The Netherlands, 1985.

Parrish, A., P. Solomon, L. deZafra, M. Jaramillo, B. Connor, and J. Barrett, Extremely low N_2O concentration in the springtime stratosphere at McMurdo Station, Antarctica, 1988, *Nature, 332*, 53, 1988.

Parsons, C.L., J.C. Gerlach, and M.E. Williams, An intercomparison of ground-based total ozone instruments, *J. Appl. Meteorol., 21*, 708–724, 1982.

Paur, R.J., and A.M. Bass, The ultraviolet cross-sections of ozone: II. Results and temperature dependence, in *Atmospheric Ozone, Proceedings of the Quadrennial Ozone Symposium*, Halkidiki, Greece, September 3–7, 1984, edited by C.S. Zerefos and A. Ghazi, pp. 611–616, D. Reidel, Dordrecht, The Netherlands, 1985.

Pearman, G.I., D. Etheridge, F. de Silva, and P.J. Fraser, Evidence of changing concentrations of atmospheric CO_2, N_2O and CH_4 from air bubbles in Antarctic ice, *Nature, 320*, 248–250, 1986.

Penndorf, R.B., Tables of the refractive index for standard air and the Rayleigh scattering coefficient for the spectral region between 0.2mu and 20.0mu and their application to atmospheric optics, *J. Opt. Soc. Am., 47*, 176, 1957.

Penney, C.M., Study of temperature dependence of the Chappuis band absorption of ozone, *NASA CR 158977*, 1979.

Perry, R.A., Kinetics of the reactions of the NCO radicals with H_2 and NO using photolysis-laser induced fluorescence, *J. Chem. Phys., 82*, 5485–5488, 1985.

Peterson, K.R., An empirical model for estimating world-wide deposition from atmospheric nuclear detonations, *Health Physics, 18*, 357–378, 1970.

Pick, D.R., and J.L. Brownscombe, Early results based on the stratospheric channels of TOVS on the TIROS–N series of operational satellites, *Adv. Space Res., 1*, 247–260, 1981.

Pickering, S.U., Isolation of two predicted hydrates of nitric acid, *J. Chem. Soc., 63*, 436–443, 1893.

Pinnick, R.G., and D.J. Hofmann, Efficiency of light-scattering aerosol particle counters, *Appl. Optics, 12*, 2593–2597, 1973.

Pinnick, R.G., J.M. Rosen, and D.J. Hofmann, Measured light scattering properties of individual aerosol particles compared to Mie scattering theory, *Appl. Optics, 12*, 37–41, 1973.

Pitari, G., and G. Visconti, Two-dimensional tracer transport: Derivation of residual mean circulation and eddy transport tensor from a 3-D model data set, *J. Geophys. Res., 90*, 8019–8032, 1985.

Pitari, G., M. Verdecchia, and G. Visconti, A transformed Eulerian model to study possible effects of the El Chichón eruption on the stratospheric circulation, *J. Geophys. Res., 92*, 10961–10975, 1987.

Plumb, R.A., and J.D. Mahlman, The zonally averaged transport characteristics of the GFDL general circulation/transport model, *J. Atmos. Sci., 44*, 298–327, 1987.

Pollack, J.B., and T.P. Ackerman, Possible effects of the El Chichón cloud on the radiation budget of the northern tropics, *Geophys. Res. Lett., 10*, 1057–1060, 1983.

Pollack, J.B., and C.P. McKay, The impact of polar stratospheric clouds on the heating rates of the polar winter stratosphere, *J. Atmos. Sci., 42*, 245–262, 1985.

Pollack, J.B., O.B. Toon, C. Sagan, A. Summers, B. Baldwin, and W. VanCamp, Volcanic explosions and climate change: A theoretical assessment, *J. Geophys. Res., 81*, 1071–1083, 1976.

Poole, L.R., *Airborne Lidar Studies of Arctic Polar Stratospheric Clouds*, Ph.D. Dissertation, University of Arizona, Tuscon, 1987.

Poole, L.R., and M.P. McCormick, Airborne lidar observations of Arctic polar stratospheric clouds: Indications of two distinct growth modes, *Geophys. Res. Lett., 15*, 21–23, 1988.

Post, M.J., Atmospheric infrared backscattering profiles: Interpretation of statistical and temporal properties, *NOAA Tech. Memorandum ERL WPL–122*, 113 pp., NOAA, Boulder, CO, 1985.

Prather, M.J., Continental sources of halocarbons and nitrous oxide, *Nature, 317*, 221–225, 1985.

Prather, M.J., European sources of halocarbons and nitrous oxide: Update 1986, *J. Atmos. Chem., 6*, 375–406, 1988.

Prather, M.J., M.B. McElroy, and S.C. Wofsy, Reductions in ozone at high concentrations of stratospheric halogens, *Nature, 312*, 227–231, 1984.

Prinn, R.G., P.G. Simmonds, R.A. Rasmussen, R.D. Rosen, F.N. Alyea, C.A. Cardelino, A.J. Crawford, D.M. Cunnold, P.J. Fraser, and J.E. Lovelock, The Atmospheric Lifetime Experiment 1. Introduction, instrumentation and overview, *J. Geophys. Res., 88*, 8353–8367, 1983a.

Prinn, R.G., R.A. Rasmussen, P.G. Simmonds, F.N. Alyea, D.M. Cunnold, B.C. Lane, C.A. Cardelino, and A.J. Crawford, The Atmospheric Lifetime Experiment 5. Results for CH_3CCl_3 based on three years of data, *J. Geophys. Research, 88*, 8415–8426, 1983b.

Prinn, R.G., D. Cunnold, R. Rasmussen, P. Simmonds, F. Alyea, A. Crawford, P. Fraser, and R. Rosen, Atmospheric trends in methylchloroform during 1978–1985 and the global-average OH concentration, *Science, 238*, 945–950, 1987.

Prinn, R.G., D. Cunnold, R. Rasmussen, P. Simmonds, F. Alyea, A. Crawford, P. Fraser, and R. Rosen, Atmospheric trends and emissions of nitrous oxide deduced from nine years of ALE–GAGE data, 1988, in preparation.

Pruppacher, H.R., and J.D. Klett, *Microphysics of Clouds and Precipitation*, D. Reidel, Dordrecht, The Netherlands, 1978.

Pyle, J.A., A calculation of the possible depletion of ozone by chlorofluorocarbons using a two-dimensional model, *PAGEOPH, 118*, 355–377, 1980.

Ramaswamy, V., and J.T. Kiehl, Sensitivities of the radiative forcing due to large loadings of smoke and dust aerosols, *J. Geophys. Res., 90*, 5597–5613, 1985.

Ramaswamy, V., and V. Ramanathan, Solar absorption by cirrus clouds and the maintenance of the upper troposphere thermal structure, *J. Atmos. Sci., 46*, 2293–2310, 1989.

Raper, O.F., C.B. Farmer, R. Zander, and J.H. Park, Infrared spectroscopic measurements of halogenated sink and reservoir gases in the stratosphere with the ATMOS instrument, *J. Geophys. Res., 92*, 9851–9858, 1987.

Rasmussen, R.A., and M.A.K. Khalil, Atmospheric methane (CH_4): Trends and seasonal cycles, *J. Geophys. Res., 86*, 9826–9832, 1981.

Rasmussen, R.A., and M.A.K. Khalil, Atmospheric methane in recent and ancient atmospheres: Concentrations, trends and interhemispheric gradients, *J. Geophys. Res., 89*, 11599–11605, 1984.

Rasmussen, R.A., and M.A.K. Khalil, Atmospheric trace gases: Trends and distributions over the last decade, *Science, 232*, 1623–1624, 1986.

Rasmussen, R.A., and J.E. Lovelock, The Atmospheric Lifetime Experiment 2. Calibration, *J. Geophys. Res., 88*, 8369–8378, 1983.

Reed, R.J., The role of vertical motions in ozone-weather relationships, *J. Meteorology, 1*, 263–267, 1950.

Reed, R.J., The structure and dynamics of the 26-month oscillation, Paper presented at the 40th anniversary meeting of the Amer. Met. Soc., Boston, 1960.

Reed, R.J., W.J. Campbell, L.A. Rasmussen, and D.G. Rogers, Evidence of downward-propagating annual wind reversal in the equatorial stratosphere, *J. Geophys. Res., 66*, 813–818, 1961.

Reinsel, G.C., Analysis of total ozone data for the detection of recent trends and the effects of nuclear testing during the 1960's, *Geophys. Res. Lett., 8*, 1227–1230, 1981.

Reinsel, G.C., and G.C. Tiao, Impact of chlorofluoromethanes on stratospheric ozone: A statistical analysis of ozone data for trends, *J. Am. Stat. Assoc., 82*, 20–30, 1987.

Reinsel, G.C., G.C. Tiao, M.N. Wang, R. Lewis, and D. Nychka, Statistical analysis of stratospheric ozone data for the detection trend, *Atmos. Environ., 15*, 1569–1577, 1981.

Reinsel, G.C., G.C. Tiao, J.J. DeLuisi, C.L. Mateer, A.J. Miller, and J.E. Frederick, An analysis of upper stratospheric Umkehr ozone profile data for trends and the effects of stratospheric aerosols, *J. Geophys. Res., 89*, 4833–4840, 1984.

Reinsel, G.C., G.C. Tiao, A.J. Miller, D.J. Wuebbles, P.S. Connell, C.L. Mateer, and J. Deluisi, Statistical analysis of total ozone and stratospheric Umkehr data for trends and solar cycle relationship, *J. Geophys. Res., 92*, 2201–2209, 1987.

Reinsel, G.C., G.C. Tiao, S.K. Ahn, M. Pugh, S. Basu, J.J. Deluisi, C.L. Mateer, A.J. Miller, P.S. Connell, and D.J. Wuebbles, An analysis of the 7 year record of SBUV satellite ozone data: Global profile features and trends in total ozone, *J. Geophys. Res., 93*, 1689–1703, 1988.

Reiter, R., H. Jager, W. Carnuth, and W. Funk, The El Chichón cloud over central Europe, observed by lidar at Garmisch–Partenkirchen during 1982, *Geophys. Res. Lett., 10*, 1001–1004, 1983.

Remsberg, E.E., J.M. Russell III, L.L. Gordley, P.L. Bailey, W.G. Planet, and J.E. Harries, The validation of Nimbus 7 LIMS measurements of ozone, *J. Geophys. Res., 89*, 5161–5178, 1984.

Rinsland, C.P., and J.S. Levine, Free tropospheric carbon monoxide concentrations in 1950 and 1951 deduced from infrared total column amount measurements, *Nature, 318*, 250–254, 1985.

Rinsland, C.P., J.S. Levine, and T. Miles, Concentration of methane in the troposphere deduced from 1951 infrared solar spectra, *Nature, 318*, 245–249, 1985.

Robbins, R.C., L.A. Cavanagh, L.J. Salas, and E. Robinson, Analysis of ancient atmospheres, *J. Geophys. Res., 78*, 5341–5344, 1973.

Robock, A., and M. Matson, Circumglobal transport of the El Chichón volcanic dust cloud, *Science, 221*, 195–197, 1983.

Rodgers, C.D., A General Error Analysis for Profile Retrieval, 1988, in preparation.

Rodgers, C.D., Retrieval of atmospheric temperature and composition from remote measurements of thermal radiation, *Rev. Geophys. and Space Phys. 14*, 609–624, 1976.

Rodriguez, J.M., M.K.W. Ko, and N.D. Sze, Chlorine chemistry in the Antarctic stratosphere: Impact of OClO and Cl_2O_2 and implications for observations, *Geophys. Res. Lett., 13*, 1292–1295, 1986.

Rodriguez, J.M., M.K.W. Ko, and N.D. Sze, Antarctic chlorine chemistry: Possible global implications, *Geophys. Res. Lett., 15*, 257–260, 1988.

Roewe, D.A., J.C. Gille, and P.L. Bailey, Infrared limb scanning in the presence of horizontal temperature gradients: An operational approach, *Appl. Opt., 21*, 3775–3783, 1982.

Rood, R.B., and A.R. Douglass, Interpretation of ozone temperature correlations—Theory, *J. Geophys. Res., 90*, 5733–5743, 1985.

Rosen, J.M., Correlation of dust and ozone in the stratosphere, *Nature, 209*, 1342, 1966.

Rosen, J.M, The vertical distribution of dust to 30 kilometers, *J. Geophys. Res., 69*, 4673–4676, 1964.

Rosen, J.M., The boiling point of stratospheric aerosols, *J. Appl. Meteorol., 10*, 1044–1046, 1971.

Rosen, J.M., Simultaneous dust and ozone soundings over North and Central America, *J. Geophys. Res., 73*, 479–486, 1968.

Rosen, J.M., and D.J. Hofmann, Balloon-borne measurements of condensation nuclei, *J. Appl. Meteorol., 16*, 56–62, 1977.

Rosen, J.M., and D.J. Hofmann, Optical model of stratospheric aerosol: Present status, *Appl. Optics, 25*, 410–419, 1986.

Rosen, J.M., and D.J. Hofmann, Unusual behavior in the condensation nuclei concentration at 30 km, *J. Geophys. Res., 88*, 3725–3731, 1983.

Rosen, J.M., D.J. Hofmann, and J.W. Harder, Aerosol measurements in the winter/spring Antarctic stratosphere 2: Impact on polar stratospheric cloud theories, *J. Geophys. Res., 93*, 677–686, 1988.

Rosenfield, J.E., and M.R. Schoeberl, A computation of stratospheric heating rates and diabatic circulation for the Antarctic spring, *Geophys. Res. Lett., 13*, 1339–1342, 1986.

Rosenfield, J.E., M.R. Schoeberl, and P.A. Newman, Antarctic springtime ozone depletion computed from temperature observations, *J. Geophys. Res., 93*, 3833–3849, 1988.

Rossi, M.J., R. Malhotra, and D.M. Golden, Heterogeneous chemical reaction of chlorine nitrate and water on sulfuric-acid surfaces at room temperature, *Geophys. Res. Lett., 14*, 127–130, 1987.

Rottman G.J., C.A. Barth, R.J. Thomas, G.H. Mount, G.M. Lawrence, D.W. Rusch, R.W. Sanders, G.E. Thomas, and J. London, Solar spectral irradiance 120 to 190 nm, October 13, 1981–January 3, 1982, *Geophys. Res. Lett. 9*, 587–590, 1982.

Rowland, F.S., Some aspects of chemistry in the springtime Antarctic stratosphere, edited by F.S. Rowland and I.S.A. Isaksen, in *The Changing Atmosphere*, Dahlem Konferenzen, November 1–6, 1987, pp. 121–140, John Wiley and Sons, Ltd., Chichester, England, 1988.

Rowland, F.S., N.R.P. Harris, R.D. Bojkov, and P. Bloomfield, Statistical error analysis of ozone trends Winter depletion in the Northern Hemisphere, in *Proc. Quadr. Ozone Symposium—1988*, Göttingen, edited by R.D. Bojkov and P. Fabian, A. Deepak, USA, in press.

Rusch, D.W., and R.T. Clancy, A comparison of ozone trends from SME and SBUV satellite observations and model calculations, *Geophys. Res. Lett., 15*, 776–779, 1988.

Rusch, D.W., G.H. Mount, C.A. Barth, R.J. Thomas, and M.T. Callan, Solar Mesosphere Explorer Ultraviolet Spectrometer: Measurements of ozone in the 1.0–0.1 mbar region, *J. Geophys. Res., 89*, 11677–11687, 1984.

Russell, J.M., and S.R. Drayson, The inference of atmospheric ozone using satellite observations in the 1042 cm^{-1} band, *J. Atmos. Sci., 29*, 376–390, 1972.

Russell, J.M., III, and J.C. Gille, The Limb Infrared Monitor of the Stratosphere (LIMS) experiment, in *The Nimbus 7 Users' Guide*, edited by C.R. Madrid, pp. 71–103, NASA/Goddard Space Flight Center, Greenbelt, MD, 1978.

Russell, P.B., M.P. McCormick, T.J. Swissler, W.P. Chu, J.M. Livingston, W.H. Fuller, J.M. Rosen, D.J. Hofmann, L.R. McMaster, D.C. Woods, and T.J. Pepin, Satellite and correlative measurements of the stratospheric aerosol. II: Comparison of measurements made by SAM II, dustsondes and airborne lidar, *J. Atmos. Sci., 38*, 1295–1312, 1981.

Russell, J.M., III, C.B. Farmer, C.P. Rinsland, R. Zander, L. Froidevaux, G.C. Toon, B. Gao, J. Shaw, and M. Gunson, Measurements of odd nitrogen compounds in the stratosphere by the ATMOS experiment on Spacelab 3, *J. Geophys. Res., 93*, 1718–1736, 1988.

Salawitch, R.J., S.C. Wofsy, and M.B. McElroy, Chemistry of OClO in the Antarctic stratosphere: Implications for bromine, *Planet. Space Sci., 36*, 213–224, 1988a.

Salawitch, R.J., S.C. Wofsy, and M.B. McElroy, Influence of polar stratospheric clouds on the depletion of ozone over Antarctica, *Geophys. Res. Lett., 15*, 871–874, 1988b.

Sander, S.P., and R.R. Friedl, Kinetics and product studies of the BrO + ClO reaction: Implications for Antarctic chemistry, *Geophys. Res. Lett., 15*, 887–890, 1988

Sander, S.P., and R.R. Friedl, Kinetic studies of the reaction BrO + ClO: Products by flash photolysis, Paper delivered at the Eighteenth International Symposium of Free Radicals, Oxford, England, 1987.

Sanford, J.L., On the nature of persistent stratospheric clouds in the Antarctic, *Tellus, 29*, 530–534, 1977.

Sargan, J.D., Wages and prices in the United Kingdom: A study in econometric methodology, in *Econometric Analysis for National Economic Planning*, edited by P.E. Hart, G. Mills, and J.K. Whittaker, pp. 25–54, Butterworth, London, 1964.

Schlesinger, M.E., and J.F.B. Mitchell, Climate model simulations of the equilibrium response to increased carbon dioxide, *Rev. Geophys., 25*, 760–798, 1987.

Schmidlin, F.J., Intercomparison of temperature, density, and wind measurements from in situ and satellite techniques, *Adv. Space Res., 4*, 101–110, 1984.

Schmidlin, F.J., Repeatability and measurement uncertainty of the United States meteorological rocketsonde, *J. Geophys. Res., 86*, 9599–9603, 1981.

Schnell, R.C. (Ed.), *Geophysical Monitoring for Climatic Change, No. 14, Summary Report 1985*, NOAA, Air Resources Laboratory, Boulder, CO, pp. 57–60, 1986a.

Schnell, R.C. (Ed.), *Geophysical Monitoring for Climatic Change, No. 14, Summary Report 1985*, NOAA, Air Resources Laboratory, Boulder, CO, pp. 37–42, 1986b.

Schoeberl, M.R., and R.S. Stolarski, Reply to Elliott and Rowland, *Geophys. Res. Lett., 15*, 198–199, 1988.

Schoeberl, M.R., and D.F. Strobel, The response of the zonally averaged circulation to stratospheric ozone reductions, *J. Atmos. Sci., 35*, 1751–1757, 1978.

Schoeberl, M.R., A.J. Krueger, and P.A. Newman, The morphology of Antarctica total ozone as seen by TOMS, *Geophys. Res. Lett., 13*, 1217–1220, 1986.

Schuster, G., R. Rood, and M. Schoeberl, Quasi-biennial and inter-annual variability in high resolution Total Ozone Data (TOMS), in *Proc. Quadr. Ozone Symposium—1988*, Göttingen, edited by R.D. Bojkov and P. Fabian, Deepak Publ., USA, in press.

Schwarzkopf, M.D., and S.B. Fels, Improvements to the algorithm for computing CO_2 transmissivities and cooling rates, *J. Geophys. Res., 90*, 10541–10550, 1985.

Seiler, W., H. Giehl, E.G. Brunke, and E. Halliday, The seasonality of CO abundance in the Southern Hemisphere, *Tellus, 36B*, 250–254, 1984.

Sekiguchi, Y., Antarctic ozone change correlated to the stratospheric temperature field, *Geophys. Res. Lett., 13*, 1202–1205, 1986.

Self, S., M.R. Rampino, and J.J. Barbera, The possible effects of large 19th and 20th century volcanic eruptions on zonal and hemispheric surface temperatures, *J. Volcan. Geotherm. Res., 11*, 41–60, 1981.

Shah, G.M., and W.F.J. Evans, Latitude survey of aerosol optical thickness of the El Chichón eruption cloud in May 1983, *Geophys. Res. Lett., 12*, 255–258, 1985.

Shapiro, M.A., R.C. Schnell, F.P. Parungo, S.J. Oltmans, and B.A. Bodhaine, El Chichón volcanic debris in an Arctic tropopause fold, *Geophys. Res. Lett., 11*, 421–424, 1984.

Shettle, E.P., and R.W. Fenn, Models for the aerosols of the lower atmosphere and the effects of humidity variations on their optical properties, *Rep. AFGL–TR–79–0214*, 94 pp., 1979.

Shi, G.Y., W.C. Wang, M.K.W. Ko, and M. Tanaka, Radiative heating due to stratospheric aerosols over Antarctica, *Geophys. Res. Lett., 13*, 1335–1338, 1986.

Shibasaki, K., N. Iwagami, and T. Ogawa, Stratospheric nitrogen dioxide observed by ground-based and balloonborne techniques at Syowa Station (69.0°S, 39.6°E), *Geophys. Res. Lett., 13*, 1268–1271, 1986.

Shibata, T., M. Fujiwara, and M. Hirono, The El Chichón volcanic cloud in the stratosphere: Lidar observations at Fukuoka and numerical simulation, *J. Atmos. Terr. Phys., 46*, 1121–1146, 1984.

Shine, K.P., The middle atmosphere in the absence of dynamical heat fluxes, *Quart. J. Roy. Meteorol. Soc., 113*, 603–633, 1987.

Shine, K.P., On the modelled thermal response of the Antarctic stratosphere to a depletion of ozone, *Geophys. Res. Lett., 13*, 1331–1334, 1986.

Shiotani, M., and J.C. Gille, Dynamical factors affecting ozone mixing ratios in the Antarctic lower stratosphere, *J. Geophys. Res., 92*, 9811–9824, 1987.

Shumway, R.H., *Applied Statistical Time Series Analysis*, Prentice–Hall, Englewood Cliffs, New Jersey, 1988.

Simkin, T., L. Siebert, L. McClelland, D. Bridge, C. Newhall, and J.H. Latter, *Volcanoes of the World*, 232 pp., Smithsonian Institution, Washington, D.C., 1981.

Simmonds, P.G., F.N. Alyea, C.A. Cardelino, A.J. Crawford, D.M. Cunnold, B.C. Lane, J.E. Lovelock, R.G. Prinn, and R.A. Rasmussen, The Atmospheric Lifetime Experiment 6. Results for carbon tetrachloride based on three years of data, *J. Geophys. Res., 88*, 8427–8441, 1983.

Simmonds, P.G., D.M. Cunnold, F.N. Alyea, C.A. Cardelino, A.J. Crawford, R.G. Prinn, P.J. Fraser, R.A. Rasmussen, and R.D. Rosen, Carbon tetrachloride lifetimes and emissions determined from daily global measurements during 1978–1985, *J. Atmos. Chem., 7*, 35–58, 1988.

Singer, S.F., and R.C. Wentworth, A method for the determination of the vertical ozone distribution from a satellite, *J. Geophys. Res., 62*, 299–308, 1957.

Singh, H.B., Preliminary estimates of average tropospheric OH concentrations in the Northern and Southern Hemispheres, *Geophys. Res. Lett., 4*, 453–456, 1977.

Smith, D.Y., E. Shiles, and M. Inokuti, The optical properties of metallic aluminum, in *Handbook of Optical Constants of Solids*, edited by E.D. Palik, pp. 369–406, Academic Press, Orlando, Florida, 1985.

Smith, W.L., H.M. Woolf, C. Hayden, D.Q. Wark, and L.M. McMillan, TIROS–N operational vertical sounder, *Bull. Amer. Meteor. Soc., 60*, 1177–1197, 1979.

Solomon, S., The mystery of the Antarctic ozone hole, *Rev. Geophysics, 26*, 131–148, 1988.

Solomon, S., and R.R. Garcia, On the distributions of long-lived tracers and chlorine species in the middle atmosphere, *J. Geophys. Res., 89*, 11633–11644, 1984a.

Solomon, S., and R.R. Garcia, Transport of thermospheric NO to the upper stratosphere?, *Planet. Space Sci., 32*, 399–409, 1984b.

Solomon, S., R.R. Garcia, F.S. Rowland, and D.J. Wuebbles, On the depletion of Antarctic ozone, *Nature, 321*, 755–758, 1986a.

Solomon, S., J.T. Keihl, B.J. Kerridge, E.E. Remsberg, and J.M. Russell III, Evidence for nonlocal thermodynamic equilibrium in the v_3 mode of mesospheric ozone, *J. Geophys. Res., 91*, 9865–9876, 1986b.

Solomon, P.M., B. Connor, R. deZafra, A. Parrish, J. Barrett, and M. Jaramillo, Observations of high concentrations of chlorine monoxide in the lower stratosphere during the Antarctic spring, II, Secular variation, *Nature, 328*, 411–413, 1987.

Solomon, S., G.H. Mount, R.W. Sanders, and A.L. Schmeltekopf, Visible spectroscopy at McMurdo Station, Antarctica: 2 Observations of OClO, *J. Geophys. Res., 92*, 8329–8338, 1987.

Spinhirne, J.D., El Chichón eruption cloud: Latitudinal variation of the spectral optical thickness for October 1982, *Geophys. Res. Lett., 10*, 881–884, 1983.

St. John, D.S., S.P. Bailey, W.H. Fellner, J.M. Minor, and R.D. Snee, Time series search for trend in total ozone measurements, *J. Geophys. Res., 86*, 7299–7311, 1981.

St. John, D.S., S.P. Bailey, W.H. Fellner, J.M. Minor, and R.D. Snee, Time series analysis of stratospheric ozone, *Commun. Statist. Theory Methods, 11*, 1293–1333, 1982.

Stauffer, B., G. Fischer, A. Neftel, and H. Oeschger, Increase of atmospheric methane recorded in Antarctic ice, *Science, 229*, 1386–1388, 1985.

Steele, H.M., and P. Hamill, Effects of temperature and humidity on the growth and optical properties of sulphuric acid water droplets in the stratosphere, *J. Aerosol Sci., 12*, 515–527, 1981.

Steele, H.M., P. Hamill, M.P. McCormick, and T.J. Swissler, The formation of polar stratospheric clouds, *J. Atmos. Sci., 40*, 2055–2067, 1983.

Steele, L.P., P.J. Fraser, R.A. Rasmussen, M.A.K. Khalil, T.J. Conway, A.J. Crawford, R.H. Gammon, K.A. Masarie, and K.W. Thoning, The global distribution of methane in the troposphere, *J. Atmos. Chem., 5*, 125–171, 1987.

Stolarski, R.S., The Antarctic ozone hole, *Sci. Am., 258*, 20–26, 1988.

Stolarski, R.S., Changes in ozone over the Antarctic, in *The Changing Atmosphere*, Dahlem Konferenzen, edited by F.S. Rowland and I.S.A. Isaksen, pp. 105–120, John Wiley and Sons Ltd., Chichester, England, 1988.

Stolarski, R.S., and A.R. Douglass, Sensitivity of an atmospheric photochemistry model to chlorine perturbations including consideration of uncertainty propagation, *J. Geophys. Res., 91*, 7853–7864, 1986.

Stolarski, R.S., and M.R. Schoeberl, Further interpretation of satellite measurements of Antarctic total ozone, *Geophys. Res. Lett. 13*, 1210–1212, 1986.

Stolarski, R.S., A.J. Krueger, M.R. Schoeberl, R.D. Peters, P.A. Newman, and J.C. Alpert, Nimbus 7 SBUV/TOMS measurements of the springtime Antarctic ozone decrease, *Nature, 322*, 808–811, 1986.

Stolarski, R.S., A.J. Krueger, and M.R. Schoeberl, Total ozone trends from TOMS data, in *Proc. Quadr. Ozone Symp.—88*, Göttingen, Deepak Publ., USA, in press.

Stordal, F., Isaksen, I.S.A., and Hornveth, K., 1985, A diabatic circulation two-dimensional model with photochemistry simulations of ozone and long-lived tracers with surface sources, *J. Geophys. Res., 90*, 5757–5776, 1985.

Strand, O.N., and E.R. Westwater, Statistical estimation of the numerical solution of a Fredholm integral equation of the first kind, *J. Assoc. Comp. Mach., 15*, 100–114, 1968.

Streit, G.E., C.J. Howard, A.L. Schmeltekopf, J.A. Davidson, and H.I. Schiff, Temperature dependence of the $O(^1D)$ rate constants for reactions with O_2, N_2, CO_2, O_3 and H_2O, *J. Chem. Phys., 65*, 4761–4764, 1976.

Strong, A.E., Monitoring El Chichón aerosol distribution using NOAA–7 satellite AVHRR sea surface temperature, *Geof. Int., 23–2*, 129–142, 1984.

Swissler, T.J., M.P. McCormick, and J.D. Spinhirne, El Chichón eruption cloud, comparison of lidar and optical thickness measurements for October 1982, *Geophys. Res. Lett., 10*, 885–888, 1983.

Sze, N.D., Anthropogenic CO emissions: Implications for the atmospheric CO–OH–CH_4 cycle, *Science, 195*, 673–675, 1977.

Taylor, S L., P.K. Bhartia, V.G. Kaveeshwar, K.F. Klenk, A.J. Fleig, and C.L. Mateer, Role of multiple scattering in ozone profile retrieval from satellite measurements in the ultraviolet, in *Remote Sensing of Atmospheres and Oceans*, edited by A. Deepak, pp. 219–231, Academic Press, New York, 1980.

Thomas, G.E., Solar Mesosphere Explorer measurements of polar mesospheric clouds (noctilucent clouds), *J. Atmos. Terr. Phys., 46*, 819–824, 1984.

Thomas, G.E., B.M. Jakosky, R.A. West, and R.W. Sanders, Satellite limb-scanning thermal infrared observations of the El Chichón stratospheric aerosols: First results, *Geophys. Res. Lett., 10*, 997–1000, 1983.

Thomas, R.J., C.A. Barth, D.W. Rusch, and R.W. Sanders, Solar Mesosphere Explorer Near-Infrared Spectrometer: Measurements of 1.27μ radiances and the inference of mesospheric ozone, *J. Geophys. Res., 89*, 9569–9580, 1984.

Thomas, R.W.L., and A.C. Holland, Simple relationship between UV radiation backscattered by the Earth's atmosphere and the vertical ozone profile, *Appl. Opt. 16*, 2581–2583, 1977.

Thompson, A.M., and R.J. Cicerone, Possible perturbations to atmospheric CO, CH_4 and OH, *J. Geophys. Res., 91*, 10853–10864, 1986.

Tiao, G.C., G.C. Reinsel, J.H. Frederick, G.M. Allenby, C.L. Mateer, A.J. Miller, and J.J. DeLuisi, A statistical trend analysis of ozonesonde data, *J. Geophys. Res., 91*, 13121–13136, 1986.

Tolbert, M.A., M.J. Rossi, R. Malhotra, and D.M. Golden, Reaction of chlorine nitrate with hydrogen chloride and water at Antarctic stratospheric temperatures, *Science, 238*, 1258–1260, 1987.

Tolson, R.H., Spatial and temporal variations of monthly mean total columnar ozone derived from 7 years of BUV data, *J. Geophys. Res., 86*, 4788–4796, 1981.

Toohey, D.W., and J.G. Anderson, Formation of BrCl ($3\pi o+$) in the reaction of BrO with ClO, *J. Phys. Chem., 92*, 1705, 1988.

Toon, O.B., and J.B. Pollack, A global average model of atmospheric aerosols for radiative transfer calculations, *J. Appl. Meteor., 15*, 225–246, 1976.

Toon, O.B., P. Hamill, R.P. Turco, and J. Pinto, Condensation of HNO_3 and HCl in the winter polar stratosphere, *Geophys. Res. Lett., 13*, 1284–1287, 1986.

Torres, A.L., and A.R. Bandy, Performance characteristics of the electrochemical concentration cell ozonesonde, *J. Geophys. Res., 83*, 5501–5504, 1978.

Torres, A.L., and G. Brothers, Ozone measurements above Palmer Station, Antarctica, Polar Ozone Workshop, *NASA Conf. Publ. 10014*, pp. 42–44, Snowmass, Colorado, 1988.

Tung, K.K., On the relationship between the thermal structure of the stratosphere and the seasonal distribution of ozone, *Geophys. Res. Lett., 13*, 1308–1311, 1986.

Tung, K.K., and H. Yang, Dynamic variability of column ozone, *J. Geophys. Res., 93*, 11123–11128, 1988.

Tung, K.K., and H. Yang, Dynamical component of seasonal and year-to-year changes in Antarctic and global ozone, *J. Geophys. Res., 93*, 12537–12559, 1989.

Tung, K.K., M.K.W. Ko, J.M. Rodriguez, and N.D. Sze, Are Antarctic ozone variations a manifestation of dynamics or chemistry?, *Nature, 322*, 811–814, 1986.

Turco, R.P., R.C. Whitten, and O.B. Toon, Stratospheric aerosols: Observation and theory, *Rev. Geophys. Space Phys., 20*, 233–279, 1982.

Turco, R.P., O.B. Toon, and P. Hamill, Heterogeneous physicochemistry of the polar ozone hole, *J. Geophys. Res., Special Issue*, 1989, in press.

Twomey, S., *Atmospheric Aerosols*, 302 pp., Elsevier, Amsterdam, The Netherlands, 1977.

Twomey, S., On the numerical solution of Fredholm integral equations of the first kind by the inversion of the linear systems produced by quadrature, *J. Assoc. Comp. Mach., 10*, 97–101, 1963.

Twomey, S., B. Herman, and R. Rabinoff, An extension to the Chahine method of inverting the radiative transfer equation, *J. Atmos. Sci., 34*, 1085–1096, 1977.

Uchino, O., On dispersion processes of the El Chichón dust particles in the lower stratosphere, *J. Meteor. Soc. Japan, 63*, 288–293, 1985.

Valentini, J.J., D.P. Gerrity, D.L. Phillips, J.C. Neih, and K.D. Tabor, CARS spectroscopy of $O_2(^1\Delta/g)$ from the Hartley band photodissociation of O_3: Dynamics of the dissociation, *J. Chem. Phys., 86*, 6745–6756, 1987.

van Loon, H., and K. Labitzke, The Southern Oscillation, Part V: The anomalies in the lower stratosphere of the Northern Hemisphere in winter and a comparison with the Quasi-Biennial Oscillation, *Mon. Weather Rev., 115*, 357–369, 1987.

Vassey, A., and E. Vassey, Effect of temperature on the absorption spectrum of ozone: Chappuis bands, *J. Chem. Phys., 16*, 1163–1164, 1948.

Vedder, J.F., E.P. Condon, E.C.Y. Inn, K.D. Tabor, and M.A. Kritz, Measurements of stratospheric SO_2 after the El Chichón eruptions, *Geophys. Res. Lett., 10*, 1045–1048, 1983.

Veryard, R.G., and Ebdon, R.A., Fluctuations in tropical stratospheric winds, *Meteor. Mag., 90*, 125–143, 1961.

Vierkorn-Rudolph, B., K. Bachmann, B. Schwarz, and F.X. Meixner, Vertical profiles of hydrogen chloride in the troposphere, *J. Atmos. Chem., 2*, 47–63, 1984.

Vigroux, E., Contribution a l'étude experimentale de l'absorption de l'ozone, *Ann. Phys., 8*, 709–762, 1953.

Vigroux, E., Determination des coefficients moyens d'absorption de l'ozone en vue des observations concernant l'ozone atmospherique a l'aide du spectrometre Dobson, *Ann. Phys., 2*, 209–215, 1967.

Vupputuri, R.K.R., Potential effects of anthropogenic trace gas emissions on atmospheric ozone, temperature structure and surface climate, in *Measuring the Greenhouse Effect, Report ARD87-2*, edited by W.F.J. Evans, A.J. Forester, and D.I. Wardle, pp. 147–156, Atmospheric Environment Service, Canada, 1987.

Wagner, N.K., Theoretical accuracy of a meteorological thermistor, *J. Appl. Meteor., 3*, 461–469, 1964.

Wallace, J.M, General circulation of the tropical lower stratosphere, *Rev. Geophys. Space Phys., 11*, 191–222, 1973.

Wang, W-C, D.J. Wuebbles, W.M. Washington, R.G. Isaacs, and G. Molnar, Trace gases and other potential perturbations to global climate, *Rev. Geophys., 24*, 110–140, 1986.

Wardle, D.J., C.D. Walshaw, and T.W. Wormell, A new instrument for atmospheric ozone, *Nature, 199*, 1177–1178, 1983.

Waters, J.W., J.C. Hardy, R.F. Jarnot, and H.M. Pickett, Chlorine monoxide radical, ozone, and hydrogen peroxide: Stratospheric measurements by microwave limb sounding, *Science, 214*, 61–64, 1981.

Watson, R.T., M.A. Geller, R.S. Stolarski, and R.F. Hampson, Present state of knowledge of the upper atmosphere: An assessment, *NASA Reference Publication RP 1162*, NASA/Goddard Space Flight Center, Greenbelt, MD, 1986.

Wayne, R.P., Reactions of singlet molecular oxygen in the gas phase, in *Singlet O_2, Vol 1, Physical–Chemical Aspects*, edited by A.A. Frimer, pp. 81–175, CRC Press, Boca Raton, Florida, 1985.

Weinstock, E.M., M.J. Phillips, and J.G. Anderson, In situ observation of ClO in the stratosphere: A review of recent results, *J. Geophys. Res., 86*, 7273–7278, 1981.

Weiss, R.F., The temporal and spatial distribution of tropospheric nitrous oxide, *J. Geophys. Res., 86*, 7185–7195, 1981.

Wellemeyer, C.G., A.J. Fleig, and P.K. Bhartia, Internal comparisons at SBUV and TOMS total ozone measurements, *Proc. Quadr. Ozone Symposium—1988*, Göttingen, edited by R.D. Bojkov and P. Fabian, Deepak Publ., USA, in press.

Witteborn, F.C., K. O'Brien, H.W. Crean, J.B. Pollack, and K.H. Bilski, Spectroscopic measurements of the 8- to 13-micrometer transmission of the upper atmosphere following the El Chichón eruptions, *Geophys. Res. Lett., 10*, 1009–1012, 1983.

WMO, Report of the meeting of experts on the assessment of performance characteristics of various ozone observing systems, World Meteorological Organization Ozone Project, *Report No. 9*, WMO, Boulder, Colorado, 1980.

WMO, Report of the meeting of experts on sources of errors in detection of ozone trends, World Meteorological Organization Ozone Project, *Report No. 12*, WMO, Toronto, 48 pp., 1982.

WMO, Atmospheric Ozone, Assessment of Our Understanding of the Processes Controlling its Present Distribution and Change, Report No. 16, World Meteorological Organization Global Ozone Research and Monitoring Project, in three volumes, Washington D.C., 1986.

Wofsy, S.C., M. Molina, R.J. Salawitch, L.E. Fox, and M.B. McElroy, Interactions between HCl, NO_x, and H_2O ice in the Antarctic stratosphere: Implications for ozone, *J. Geophys. Res., 93*, 2442–2450, 1988.

Woodgate, B.R., E.A. Tandberg–Hanssen, E.C. Bruner, J.M. Beckers, J.C. Brandt, W. Henze, C.L. Hyder, M.W. Kalet, P.J. Kenny, E.D. Knox, A.G. Michalitsianos, R. Rehse, R.A. Shine, and H.D. Tinsley, The ultraviolet spectrometer and polarimeter on the Solar Maximum Mission, *Sol. Phys., 65*, 73–90, 1980.

Woods, D.C., and R.L. Chuan, Size-specific composition of aerosols in the El Chichón volcanic cloud, *Geophys. Res. Lett., 10*, 1041–1044, 1983.

Worsnop, D.R., M.S. Zahniser, P. Davidovits, C.C. Kolb, Heterogeneous reaction kinetics of importance to stratospheric chemistry, *Report No. ARIRR #613*, 1987.

Wuebbles, D.J., A theoretical analysis of the past variations in global atmospheric composition and temperature structure, *UCRL–53423*, Lawrence Livermore National Laboratory, Livermore, CA, 1983a.

Wuebbles, D.J., *A Theoretical Analysis of the Past Variations in Global Atmospheric Composition and Temperature Structure*, Ph.D. Thesis, University of California, Livermore, 1983b.

Wuebbles, D.J., Trends in ozone and temperature structure: Comparison of theory and measurement, in *Atmospheric Ozone, Proc. Quadrennial Ozone Symposium*, Halkidiki, Greece, September 3–7, 1984, edited by C.S. Zerefos and A. Ghazi, pp. 87–91, D. Reidel, Dordrecht, The Netherlands, 1985.

Wuebbles, D.J., M.C. MacCracken, and F.M. Luther, A proposed reference set of scenarios for radiatively active atmospheric constituents, U.S. Department of Energy, Carbon Dioxide Research Division, *Technical Report 015*, 54 pp., Washington, DC, 1984.

Wuebbles, D.J., P.S. Cornell, K.E. Grant, R. Tarp, and K.E. Taylor, Initial results with the LLNL 2-D chemical-radiative-transport model of the troposphere and stratosphere, Lawrence Livermore National Laboratory Report, *CID–21145*, 14 pp., Livermore, California, 1987.

Yue, G.K., M.P. McCormick, and W.P. Chu, A comparative study of aerosol extinction measurements made by the SAM II and SAGE satellite experiments, *J. Geophys. Res., 89*, 5321–5327, 1984.

Yue, G.K., M.P. McCormick, W.P. Chu, P. Wang, and M.T. Osborn, Comparative studies of aerosol extinction measurements made by the SAM II and SAGE II satellite experiments, *J. Geophys. Res., 94*, 8412–8424, 1989.

Zander, R., and Ph. de Moulin, Spectroscopic evidence for the presence of the ν_4–Q branch of chlorine nitrate ($ClONO_2$) in ground-based infrared solar spectra, *J. Atmos. Chem., 6*, 191–200, 1988.

Zander, R., G. Roland, L. Delbouille, A. Sauval, C.B. Farmer, and R.H. Norton, Column abundance and long-term trend of hydrogen chloride (HCl) above the Jungfraujoch station, *J. Atmos. Chem., 5*, 395–404, 1987a.

Zander, R., G. Roland, L. Delbouille, A. Sauval, C.B. Farmer, and R.H. Norton, Monitoring of the integrated column of hydrogen fluoride above the Jungfraujoch station since 1977—The HF/HCl column ratio, *J. Atmos. Chem., 5*, 385–394, 1987b.

Zander, R., G. Roland, L. Delbouille, A.J. Sauval, P. Marche, F. Karcher, M. Amoudei, and B. Dufour, Concentrations of hydrogen chloride and hydrogen fluoride during the MAP/GLOBUS comparison of September 1983, *Planet. Space Sci., 35*, 665–672, 1987c.

Zander, R., Ph. de Moulin, D.H. Ehhalt, and U. Schmidt, Secular increase of the column abundance of methane above the Jungfraujoch station, 1989, in preparation.